Remote measurements of volcanic gases : applications of open-path Fourier transform infra-red spectroscopy (OP-FTIR) and Correlation spectroscopy (COSPEC)

Thesis

The Open University

Remote measurements of volcanic gases: Applications of Open-path Fourier transform infra-red spectroscopy (OP-FTIR) and Correlation spectroscopy (COSPEC)

A thesis presented on

Tuesday, June 30th, 1998

for the degree of

Doctor of Philosophy

by

Adam John Henry Maciejewski

B.Sc (hons.) ***RHBNC (Lond.)*** **1993**

The Department of Earth Sciences

The Open University

Milton Keynes, MK7 6AA, UK

RESEARCH DEGREES CENTRE

LIBRARY AUTHORISATION FORM

Please return this form to the The Research Degrees Centre with the two bound copies of your thesis to be deposited with the University Library.
All students should complete Part 1. Part 2 only applies to PhD students.

Student: Adam J. H. MACIEJEWSKI PI: M71683546

Degree: Ph. D.

Thesis title: Remote measurments of volcanic gases: Applications of OP-FTIR and COSPEC

Part 1 Open University Library Authorisation [to be completed by all students]

I confirm that I am willing for my thesis to be made available to readers by the Open University Library, and that it may be photocopied, subject to the discretion of the Librarian.

Signed: [signature] Date: 7-11-99

Part 2 British Library Authorisation [to be completed by PhD students only]

If you want a copy of your PhD thesis to be available on loan to the British Library Thesis Service as and when it is requested, you must sign a British Library Doctoral Thesis Agreement Form. Please return it to the Research Degrees Centre with this form. The British Library will publicise the details of your thesis and may request a copy on loan from the University Library. Information on the presentation of the thesis is given in the Agreement Form.

Please note the British Library have requested that theses should be printed on one side only to enable them to produce a clear microfilm. The Open University Library sends the fully bound copy of theses to the British Library.

The University has agreed that your participation in the British Library Thesis Service should be voluntary. Please tick either (a) or (b) to indicate your intentions.

[a] ☑ I am willing for the Open University to loan the British Library a copy of my thesis. A signed Agreement Form is attached.

[b] ☐ I do not wish the Open University to loan the British Library a copy of my thesis.

Signed: [signature] Date: 8-11-99

Remote measurements of volcanic gases

Abstract

The composition of volcanic gas plumes depends largely on the chemistry of the degassing magma, the depth of volatile exsolution, and the level of volcanic activity. The ratios between the most common volcanic gases: CO_2, H_2O, SO_2, HCl and HF, as measured at the surface, can be used to provide information on the evolution of the magma body. My research on volcanic gases has centred on the use of open-path Fourier transform IR spectroscopy (OP-FTIR) and correlation spectroscopy (COSPEC). I have also used data collected using other direct and remote-sensing techniques.

Remote-sensing techniques rely on the characteristic IR or UV absorbances of natural and/or artificial radiation by different gases. The longer range of these techniques enables the analysis of gases in inaccessible plumes; thus reducing the need for operators to enter hazardous areas. As the instruments do not interact with the analysed gases there is no contamination, condensation or secondary reactions. However, the instruments tend to be heavy, expensive, and complex. Environmental factors can complicate analyses; clouds can dissolve and remove analyte rapidly, and variations in wind speed can result in gas fluxes having high errors. It is also much more difficult to analyse specific gas sources remotely as mixing of gases from different sources can occur.

Direct-sampling techniques rely on gases being trapped, dissolved or adsorbed before being analysed by traditional methods, e.g. wet-chemistry, colourimetry, and gas chromatography. The capture of gases is best achieved as close to the source as possible, thus increasing the risk to the operator, and may only be possible during periods of low activity. The physical interaction of gases with instrument and collection vessels can lead to contamination and initiation of secondary reactions. Direct-sampling techniques are labour intensive and thus are capable of only generating a relatively small amount of data compared to the more automated remote-sensing techniques. The suitability of an individual technique therefore depends greatly on: the type of gas to be measured; the location of vent or fumarole; the level of volcanic activity; and the environment in which data are collected.

I used OP-FTIR on La Fossa di Vulcano to measure the SO_2:HCl mass ratios of gases emitted from the rim and central crater fumaroles, ~4.3 - 6.1 and 0.9 - 2.6 respectively. I attributed the higher crater rim gas ratios to the interaction of the gases with shallow

hydrothermal reservoirs, causing scrubbing of the more soluble HCl. At Mt. Etna, my OP-FTIR analysis of gases emitted from the central craters showed that, in 1994, SO_2:HCl mass ratios were ~4.9 - 5.8. These values lie between those reported for eruptive degassing, >10, and background degassing, <1, and probably relate to refilling of the magma system prior to the 1997 eruption. A comparative study of lava effusion rates and COSPEC-derived SO_2 fluxes for the 1991 - 1993 Etna eruption showed that variations were generally synchronous; small scale differences relating to the drainage of degassed magma from beneath the summit craters into the eruptive fissure. I also conducted OP-FTIR and COSPEC analyses on Montserrat in June 1996 to show the gas plume to be relatively SO_2 poor, with SO_2:HCl mass ratios of <0.5. The OP-FTIR technique enabled the first remote measurements of SiF_4 in volcanic plumes to be made. I have also used HF–SiF_4 ratios to estimate gas equilibrium temperatures at La Fossa and Mt. Etna to be ~200°C and ~250 - 290°C respectively.

I have also investigated the structural evolution of the Masaya Volcanic Complex. The visible complex has formed over ~1000 years; with average rates of effusion of $\sim 0.2 \times 10^6$ m^3/y, much lower than those required to provide the estimated volume of caldera infill, $\sim 2 \times 10^6$ m^3/y. Historic activity has centred on the twin massifs of Volcán Masaya and Volcán Santiago and is dominated by pit-crater collapses. I propose that the degassing episodes, which occur with no increase in eruptive activity, are related to the convective overturn of magma beneath the craters.

Acknowledgements

This Ph.D. thesis is the cumulation of almost five years work during which time I have encountered many people and organisations who have, in their own way, made this thesis possible.

Individuals

Peter Francis - my supervisor, who gave me many invaluable comments about my work (I was even able to decipher some of them with help from Marilyn, Jo and Rita, Peter's various secretaries) and advice about jobs and the state of research throughout the world. Geoff Wadge and Dave Rothery who had to read my thesis before examining me in my *viva* (the poor things..). Clive Oppenheimer, for the wonderful warthog impression in Don Mauricio's (he's quite mad!). Helen Durrant who made things seem much brighter whilst I wrote my thesis and Debbie Adams who helped keep my mind off corrections. Louise Thomas, Jane Wares, Liz Kennedy, Kirsta Thumm and Cheryl Best for being there when I needed them (and when they didn't need me) which helped to keep me sane (well almost). Andrew "H" Harris for being so inspirational in anything not connected with my thesis work; be it contributing to papers on Stromboli or leading OUGS septuagenarians up a 1000 m volcano in the searing heat! "H" and Nicki Stevens who read chunks of thesis and provided valuable comments. All the staff at the MVO especially Pierre Delmelle, Billy Daroux, Jim McMahon the pilot and George Skerrit as well as Laurance Donelly, Rod Stuart and Simon Young from the BGS. John Smellie at BAS, Phil Kyle, Mike O'Keeffe, Kurt Panter, Ray Dibble (who discovered "Pringles" on the summit of Mt. Erebus at 70 years old). Matt from the BFC at McMurdo for teaching me how to "become one with my machine", Sam Tysdell of the Antarctica Sun Times for raising my testosterone levels in the icy south. Bob of "34 Quebec"; "Stereo", "Sparrow" and "Jimbo", the crew of "Kiwi 3" who went ice caving with me on the Summit Plateau of Mt. Erebus. Bill McGuire and Jane Moss at C&GCHE who helped me enjoy Mt. Etna. Nicki S. for pies and much alcohol! Louise T. and Georg Zellmer for being great office mates. Babs Bruno for showing me how to play "Ultimate". All the "Mad Kows" at the OU for being such a likeable bunch of people. Charles "T" Chaffin (KSU) for teaching me how to use the OP-FTIR. Russ Gill who was at Spectro Service for teaching me how to only

break the cheap bits. Hazel Rymer, Ben Van Wyk de Vries, Glyn Williams-Jones and John Murray at the OU and Helman Telena, Wilfried Strauch and Orlando at INETER for helping with the Masaya work. Dick Carlton, Dave Rothery and Steve Blake at the OU for putting up with all my questions. Mark Davies (TV personality/model extraordinaire) for making me laugh. Many other people at the OU especially Geraint "Taff" Morgan and Owen Howells who put up with me living with them for years. And last, but not least, Robin Gill at RHBNC for getting me interested in those hot, smelly, dusty, noisy things that throw out hot rocks and red runny stuff - cheers!

Organisations

Natural Environment Research Council (NERC); British Antarctic Survey (BAS); British Geological Survey (BGS); United States Antarctic Program (USAP) Overseas Development Administration (ODA); Commission to the European Community; The Open University (OU); The New Mexico Institute for Mining and Technology (NMIMT); The Italian Civil Defence (Protezione Civile); Instituto Nicaragüense de Estudios Territoriales (INETER); Ministrio d'Ambiente e Recources Naturales (MARENA); Montserrat Volcano Observatory (MVO) and the Government of Montserrat all of which have in some way helped with, contributed to, or funded fieldwork. Thanks also go to Spectro Service Ltd., the Midac Corporation and the 3M Corporation for donating technical and IR data as well as IR reference spectra.

Two atoms are walking down the street and they run in to each other.

One says to the other, "Are you all right?"

"No, I lost an electron."

"Are you sure?"

"Yeah, I'm positive!"

(- Off the Internet - well something has got to keep me (almost) sane...)

Adam J. H. Maciejewski

This thesis is dedicated to the people of Montserrat, W.I.

Table of Contents

List of Figures

Chapter 1.

Chapter 2.

Chapter 3.

Chapter 4.

Chapter 5.

Chapter 6.

List of Tables

Chapter 4

Chapter 5.

Chapter 6.

Chapter 1.

Remote measurements of volcanic gases: An introduction to aims, locations and techniques

1.1 Introduction

This thesis revolves around the use of terrestrial remote-sensing techniques to analyse volcanic gases emitted from active volcanoes. For this, I have used two techniques, Open-path Fourier transform infra-red spectroscopy (OP-FTIR) and Correlation spectroscopy (COSPEC). I have compared the data acquired using these techniques with data acquired by authors using other remote-sensing and traditional gas analysis techniques.

This thesis brings together my observations and data I have collected from four volcanoes. These are:

- The Masaya Volcanic Complex, Nicaragua. (March 1994)
- Mt. Etna, Sicily, Italy. (September 1994)
- La Fossa di Vulcano, Aeolian Isles, Italy. (September 1994)
- Soufrière Hills Volcano, Montserrat, West Indies. (May - June 1996)

In my research I have investigated how the compositions of volcanic plumes of Mt. Etna, La Fossa and Soufrière Hills relate to levels and styles of volcanic activity as well as explored how hydrothermal and atmospheric processes affect the observed gas compositions. I have also studied the composition of the hydrothermal system at La Fossa and how the Masaya Volcanic Complex has evolved through time.

1.2 Why measure volcanic gases?

The measurement of volcanic gases provides a useful way of monitoring the level of activity of a particular volcanic system. It has been demonstrated by numerous authors (Malinconico, 1987; Caltabiano et al., 1994; Hirabayashi et al., 1995; and MVO's "Team COSPEC" and "Team Volume") that effusion rates and the level of eruptive activity can be closely correlated with the flux of volcanic gases. The study of gases can therefore be used as a tool to monitor, and in some cases predict, changes in the state of a volcanic system. More recently, investigations into changes in the relative amounts of different volcanic gases, namely CO_2, SO_2, HCl and HF, have elucidated processes occurring deep within the volcano including the styles of volatile exsolution and the importance of magma convection. In the following chapters I have also used changes in gas compositions to show how both the hydrothermal system and the atmosphere can act to modify the original magmatic gas compositions. This can have important repercussions, both in using gases to monitor volcanic activity and in the local affect of the volcano on the environment.

In the following sections I will briefly outline the thesis layout; my main aims; and discuss a general gas model in which I relate volatile exsolution to magma chemistry and depth. I also give a brief review of the four volcanoes I have investigated and the techniques I have used, and include a note on the units used in this thesis.

1.3 Layout of thesis

I have separated this thesis into seven chapters. These are:

1. Remote measurements of volcanic gases: An introduction to aims, locations and techniques and discussion of a general gas model.

2. Gas analysis techniques used for monitoring volcanic activity.

3. The evolution and present-day activity of the Masaya Volcanic Complex.

4. The hydrothermal system at the La Fossa cone, Vulcano, Italy.

5. The use of OP-FTIR and COSPEC in determining the relationship between gas and magma fluxes at Mt. Etna, Italy.

6. The Soufrière Hills volcano, Montserrat, W.I.

7. Remote measurements of volcanic gases: General conclusions.

1.4 Main aims of thesis

The three main aims of my research have been:

- To develop the OP-FTIR technique and to understand how variations in the collected data relate to magmatic, hydrothermal and atmospheric processes.

- To use COSPEC data and observations relating to effusion rates to try and determine the relationship between gas and magma fluxes. To understand what the perturbations/discrepancies within such a relationship tell us about volcanic/eruptive processes.

- To describe the evolution of the Masaya Volcanic Complex and understand how degassing occurs without any eruption.

Each of the above aims has been achieved with a moderate degree of success. Minor aims and specific scientific problems relating to each volcano are discussed within each chapter.

1.5 A Generic gas model: The "ideal" volcano

In this thesis I have described how the specific situations on a number of volcanoes have affected the measured compositions of volcanic gases - in effect how the observed gas emission differs from that of an "ideal" volcano. In this section I therefore describe how an "ideal" volcano should behave with respect to its emission of volcanic gas. In order to do this I

first describe the effects of volatile solubility and magma viscosity on gas exsolution and then use two volcanoes, Kilauea and Mt. Etna, as case studies to illustrate how styles of volatile degassing affect the final composition of the gas plume.

1.5.1 Solubility of volatiles in magma

Giggenbach (1996) has compiled and reported the average volatile compositions within magmas from several volcanoes around the world for basaltic, andesitic and rhyolitic compositions. The proportions of different volatiles (mainly H_2O, CO_2, SO_2, HCl and HF) show a consistent variation between the different magma compositions. **Table 1.1** shows the averaged concentrations of these five gases in different magma compositions.

	Volatile concentration (ppmm)				
Magma type	H_2O	CO_2	S	Cl	F
Non-arc basalt	2770	1440	1010	100	165
Arc basalts	n/a	n/a	~*3300 - #300	~*2600 - #300	~*900
Andesite	17000	–	105	1500	460
Rhyolite	45000	~120	~100	1500	500

Table 1.1*. Summary of average volatile concentrations measured in four different magma types as collected from submarine basalts or melt inclusions in lavas (from: Giggenbach, 1996) Additional data from #Stolber et al. (1986) for Masaya and *Metrich et al. (1993) for Mt. Etna.*

The volatile concentrations reported in **table 1.1** were collected either from submarine samples or from melt inclusions in an attempt to determine undegassed compositions. This may, however, not be entirely successful for CO_2, as a significant proportion of this may have exsolved at depth prior to entrapment in melt inclusions, see below. **Table 1.1** shows that the volatiles in all three sampled magma types are primarily H_2O, with subordinate CO_2 and SO_2, the halogens representing <5% of the total volatile content. In this thesis I concentrate mainly on volcanoes which have recently erupted basaltic/hawaiitic (Masaya and Mt. Etna), andesitic (Montserrat) and trachytic (La Fossa di Vulcano) lavas. Generally non-arc basaltic lavas are far more sulphur-rich and halogen-poor than arc-based volcanoes, which appear to have similar

levels of halogens to other arc magmas but exhibit sulphur concentrations similar to non-arc basalts.

Solubilities of CO_2 and H_2O

Giggenbach (1996) and others have reported that the solubility of CO_2 with respect to pressure for all magmas is low, ~0.5 - 0.65 mg/kg.bar. The little variation in solubility with different magma chemistry is probably a reflection of the relative chemical inertness of CO_2 compared to H_2O and the halogens. Giggenbach (1996) used the data of Javoy & Pineau (1991) to estimate a pre-degassing concentration for CO_2 in the Mid-Atlantic Ridge "popping rock" of ~14,000 mg/kg. This value is much higher than those reported in **table 1.1** suggesting that most of the "pristine" samples are, in fact, considerably depleted in CO_2 relative to initial magmatic values.

The solubility behaviour of H_2O is more complicated than CO_2 due to its presence as both chemically incorporated hydroxyl and as free water. Giggenbach (1996) suggested that a combined solubility for both bound and free water was ~30 mg/kg.bar. By combining the calculated solubilities of CO_2 and H_2O with a theoretical initial magmatic concentration of CO_2 of 1 wt%, Giggenbach (1996), suggested that the depth of saturation for CO_2 may be >80 km, which is usually regarded as the level of initial melt generation. It is therefore highly probable that many samples analysed for CO_2 do not accurately reflect the initial magma source composition. The higher solubility and chemical compatibility of H_2O prevents it being exsolved until a much shallower depth, ~10 km.

Solubilities of sulphur and halogens

The solubility behaviour of S-, Cl- and F- bearing gases is further complicated by their incorporation into non-volatile compounds such as sulphides, sulphates and halide compounds. Investigations into the effects of pressure, temperature, and oxygen and sulphur fugacity on volatile solubility behaviour are reviewed in Carroll & Webster (1994). The complexity of the magma chemistry and difficulties of simulating magmatic conditions have

meant results are limited; the following sections however summarise the general solubility behaviour of S-Cl and F species.

Sulphur

The behaviour of sulphur is closely linked with the oxidation state of the magma, sulphur being capable of existing readily in both oxidised, i.e. SO_4^{2-} and reduced, i.e. H_2S, states. In most melts sulphur is predominantly carried as sulphide (Carroll & Webster, 1994). The differences in the ionic size and bonding characteristics of reduced and oxidised sulphur species affects their solubilities. The main chemical reactions which control sulphur solubilities are described by **equations 1.1** and **1.2** (Carroll & Webster, 1994).

$$S_{2(g)} + 2O^{2-}{}_{(m)} \rightleftharpoons O_{2(g)} + 2S^{2-}{}_{(m)} \qquad \textbf{(1.1)}$$

$$S_{2(g)} + 3O_{2(g)} + 2O^{2-}{}_{(m)} \rightleftharpoons 2SO_4^{2-}{}_{(m)} \qquad \textbf{(1.2)}$$

where (g) indicates gas species and (m) refers to ionic species dissolved in the melt. Depending on the oxygen fugacity of the melt, sulphur will either be stored as a sulphide (**equation 1.1**) or as a sulphate (**equation 1.2**). The larger size of the S^{2-} ion than the O^{2-} ion prevents it replacing tetrahedrally bonded oxygen; instead S^{2-} replaces the free, non tetrahedral oxygen in the melt, thus increasing the overall solubility of sulphur (Hess, 1977: in Carroll & Webster, 1994). In basaltic magmas the presence of FeO strongly increases the solubility of sulphur by enabling it to form an iron sulphide, see **equation 1.3**.

$$2FeO_{(m)} + S_{2(g)} \rightleftharpoons 2FeS_{(m)} + O_{2(g)} \qquad \textbf{(1.3)}$$

In hydrous magmas, however, the predominant sulphide in the vapour phase may be H_2S (after Burnham 1979: in Carroll & Webster, 1994) although again sulphur's affinity for iron will cause the following reaction, see **equation 1.4**, which suggests a negative correlation between magmatic H_2O content and sulphur solubility, because both volatiles will compete for any free iron in the melt.

$$H_2S_{(g)} + FeO_{(m)} \rightleftharpoons FeS_{(m)} + H_2O_{(g)} \qquad \textbf{(1.4)}$$

In natural systems the main controls on sulphur solubility are the oxidation state and FeO concentration of the magma. In mid-ocean ridge magmas sulphur concentrations may be ~800 - 1000 ppm (Carroll & Webster, 1994). In iron rich ferrobasalts this may be increased to >2500 ppm sulphur. At higher iron contents the precipitation of magnetite effectively reduces the magmatic iron content, and with it the magmatic sulphur concentration. In evolved, oxidising, magmas sulphur is carried as either SO_2 or SO_4^{2-} in the gas phase rather than in the melt; thus giving very low magmatic sulphur concentrations (<200 ppm) (Carroll & Webster, 1994). The recent eruptions of Mt. Pinatubo and Lascar exhibited very high rates of SO_2 emission and were accompanied by the eruption of anhydrite-bearing magma with estimated pre-degassed sulphur concentrations of ~0.1 - 1 wt%. Typically the volcanic glass from such evolved lavas contains <100 ppm of sulphur, supporting the suggestion of Carroll & Webster (1994) that much of the sulphur is not transported in the magmatic phase but in a gas phase. Katsura & Nagashima (1974 in Giggenbach, 1994) suggested that an average solubility of sulphur in magmas was ~480 mg/kg.bar, although this is strongly dependent on the magma composition.

Chlorine

The speciation of chlorine in comparison to sulphur is not well known (Carroll & Webster, 1994). Symonds et al. (1992) reported the complexing of chlorine with alkaline and alkaline earth metals, i.e. potassium, sodium and calcium from inclusion studies and inferences based on thermochemical calculations. In fluid-saturated aluminosilicate melts, under normal conditions, chlorine concentrations may range from ~1000 - 20,000 ppm (Carroll & Webster, 1994). The solubility of HCl is strongly dependent on the melt composition. Iwasaki & Katsura (1967 in Giggenbach, 1994) reported that at low pressures, close to 1 atm, the solubility of HCl was ~14,500 mg/kg.bar for non-arc basalts and ~4000 mg/kg.bar for andesites. At lower pressures chlorine favours the aqueous to magmatic phases. Giggenbach (1994) suggested that at depth the stable chlorine phase changed from HCl to MCl_n - alkali/alkaline earth chlorides which are more soluble in magma than HCl; possibly as in **equation 1.5** where (m) and (g) denote melt and gas phases respectively.

$$2HCl_{(g)} + Na_2O_{(m)} \overset{\text{pressure}}{\rightleftharpoons} 2NaCl_{(m)} + H_2O_{(g)} \qquad (1.5)$$

Shinohara (1989 in Giggenbach, 1994) reported that the solubility of alkali chlorides increased ten-fold with a pressure increase from 1 to 2 kbar; forming a significant part of any "vapour" phase and possibly even a separate fluid phase. This is the basis for the two-stage degassing model of Pennisi & Le Cloarec (1998) which I describe later in this chapter and Chapter 5.

Fluorine

The solubility behaviour of fluorine is not well known. The small ionic radius and high electronegativity of fluorine enable it to bond chemically to a range of magmatic components, including free silica, see Section 4.2.5, to give Al_nF_n, NaF_n, CaF_n and SiF_n complexes (Symonds et al., 1993). In felsic melts fluorine actively partitions into the magmatic phase where it readily forms alkali complexes. In more mafic melts, however, where the availability of alkaline/alkaline earth elements is lower, it is possible that the solubility of fluorine is also lower, being more liable to partition into the gas phase. Fluorine's high solubility in magma therefore means that a high degree of the original magmatic concentration is retained on eruption, hence emission rates of fluorine-bearing gas species are relatively small compared to chlorine and sulphur species. The high solubility of HF and HCl in aqueous fluids also influences the composition of gaseous emissions which have passed through water-rich hydrothermal areas, see Chapter 4.

Figure 1.1, adapted from Giggenbach (1994), shows the relationship between X_m, the fraction of a gas remaining in the melt, and R_v, the total vapour/melt volume ratio - loosely analogous to pressure. This summarises the differences in solubility between the various gas species as described above, with the larger, inert, noble gases being the first to exsolve, followed by CO_2 and H_2O with the smaller, chemically reactive, chlorine and fluorine being the last to be exsolved.

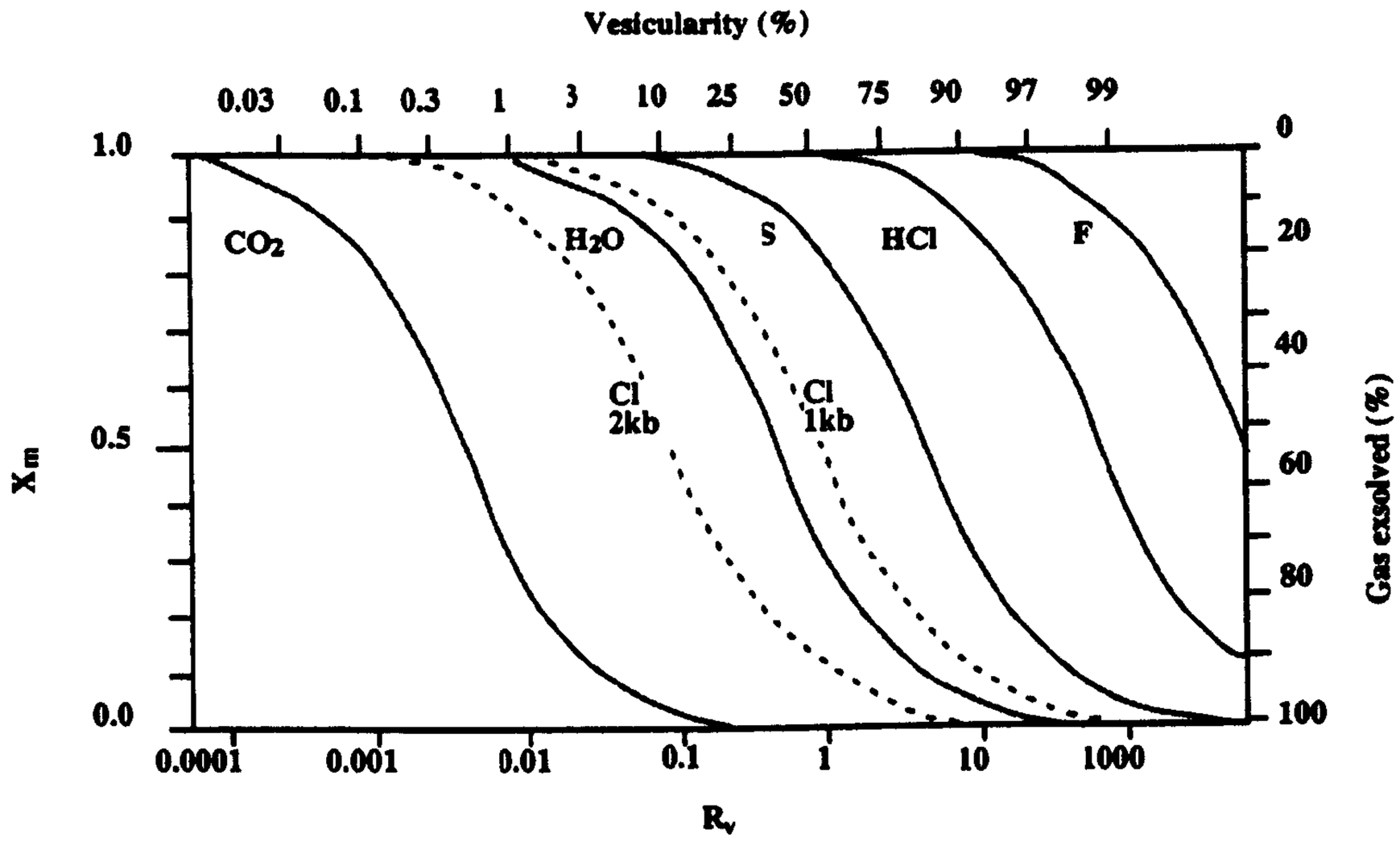

Figure 1.1. *The relationship of different volatile species as a function of vapour-melt volume ratio, R_v, and magma-vapour partitioning, X_m (after Giggenbach, 1996). This shows that the more insoluble gases, i.e. CO_2 and the noble gases, are exsolved fully at very low vapour-melt volume ratios, whilst the most soluble volatile, fluorine, is only partially exsolved even at very high vapour-melt ratios.*

The effects of magma viscosity on volatile exsolution

The previous sections have discussed the solubility of different volatiles within magmas. Once a gas has begun to exsolve, it is the physical, rather than chemical, properties of the magma which control the degassing process. In viscous magmas, such as dacites and rhyolites, H_2O, which is the major pressure-generating phase, interupts the chains of silica tetrahedra, thus depolymerising the melt. The high viscosities in these melts inhibit the diffusion and thus growth of gas pockets (bubbles). In slow moving, low viscosity basaltic magmas, bubbles can migrate through the melt enabling large volumes of gases to rise with relative ease towards the surface where they escape; either through passive degassing or during strombolian and fire fountaining events. Thus gases exsolved from depth are able to rise up and mix with volatiles exsolved closer to the surface. In dacitic and rhyolitic melts the migration of gas bubbles is severely inhibited (Sparks, 1978) resulting in the melt containing a much higher proportion of its initial volatile content as it nears the surface. The sudden fragmentation of this overpressurised magma may lead to an explosion and rapid release of volatiles. In the following two case-studies I will only deal with gas exsolution from low

viscosity basaltic magmas (Hawaii and Mt. Etna) as it is in these that preferential exsolution due to differing solubilities is most apparent.

1.5.2 Volcano case-studies

In the following sections I use Kilauea and Mt. Etna to describe how the differences in depths of volatile exsolution affect the final composition of gases measured at the surface. As magma rises from depth, >80 km, volatiles will begin to nucleate and form a separate gas phase, the composition of which will change constantly as the magma rises towards the surface. If the magma moves slowly enough the volatile phases, due to their lower density, will rise independently towards the surface, mixing with volatiles exsolved from other depths. The final composition of the gases thus emitted from the surface of the lava will therefore relate to an average of both deep and shallow exsolution processes. Kilauea and Mt. Etna volcanoes illustrate two different processes for separating out and identifying those volatiles exsolved at depth and those from shallow levels.

Kilauea, Hawaii

Magma rising beneath the summit of Kilauea volcano can either erupt, be ponded beneath the summit craters until it erupts, or drain down into one or both of the large volcanic rift systems. The rift zones at Kilauea volcano enable shallow degassing magma to be separated from the main body of deep degassing magma, see **figure 1.2**. Differences in the exsolved gas compositions from deep and shallow magmas can therefore be determined by comparing summit and rift gas emissions.

Table 1.2 shows the results of Gerlach & Graeber (1985) who restored the 1917 gas analyses of Jaggar, correcting for condensation and oxidation, and analysed melt inclusions and spatter from Kilauea to estimate the average volatile compositions in three gas sources. These were:

1). A theoretical "parental" magma containing all volatiles prior to onset of degassing.

2). Magmatic volatiles "stored" beneath the summit and east rift which have experienced some degree of adiabatic exsolution of the most insoluble gases.

3). Glasses from erupted lavas which contain only "residual" amounts of gas from the more soluble species.

In **table 1.2** I have compared these with gas emissions from the summit and east rift zone. The amounts of CO_2 emitted differs substantially between the summit and east rift zone, 54.3 wt% and 9.7 wt% respectively. This can be explained as most CO_2 being exsolved at depth and lost to the atmosphere via the main volcanic vent at the summit, rather than migrating to the surface via the rift zone. By comparison H_2O and sulphur, which both exsolve at shallower levels are increased by >50% during the shallow degassing processes in the rift zones. The lower part of **table 1.2** shows the amounts of volatiles lost from the magma between a theoretical undegassed "parent" magma and a fully degassed "residual" magma. CO_2 shows the greatest percentage loss, ~98% - again indicating its greater solubility, whilst fluorine shows almost no loss, ~1%.

	CO_2	H_2O	S	Cl	F
Gas source	Wt% gases in plume				
Summit	54.3	44.8	0.6	0.3	0.0
East rift zone	9.7	88.9	0.9	0.3	0.2
Volatile class	Wt% volatiles in magma/lava				
"Parental"	0.656	0.30	0.130	0.009	0.0354
"Stored"	0.034	0.27	0.070	0.009	0.0354
"Residual"	0.015	0.10	0.015	0.008	0.0350
Percentage loss	98	67	88	11	1

Table 1.2. *Relative proportions of degassed volatiles in gas plumes from the summit and east rift zone as well as from "parental" (calculated), "stored" (using inclusions) and "residual" (from spatter) magmas at Kilauea and the east rift zone, Hawaii, from samples collected by Jaggar and corrected by Gerlach & Graeber (1985).*

On the basis of the above and similar observations and other data, Gerlach & Graeber (1985) proposed a two-stage degassing model. In this they proposed that a "parental" magma carries melt and volatiles into Kilauea's summit magma chamber; with the exception of CO_2 which saturates and exsolves at depths of ~40 km. Either the "parental" melt was erupted or was ponded in the chamber from where it fed into the rift zones. During sustained summit eruptions, volatiles are exsolved from the magma prior to or during the eruption - leading to Type I degassing; characterised by a high CO_2:H_2O and S:Cl mass ratios. If there was no eruption at the summit, degassing occurred in two stages - Type II degassing, see **figure 1.2**. In the first stage "parental" magma re-equilibrates to summit chamber pressures and loses most of the CO_2 and ~50% of parental sulphur, but without major loss of H_2O, chlorine or fluorine. In the second stage of Type II degassing, volatile exsolution occurs when the magma is finally erupted from the summit or from the rift zone. Here it loses most of the remaining CO_2, H_2O, sulphur and chlorine and some of the fluorine due to the much lower confining pressures.

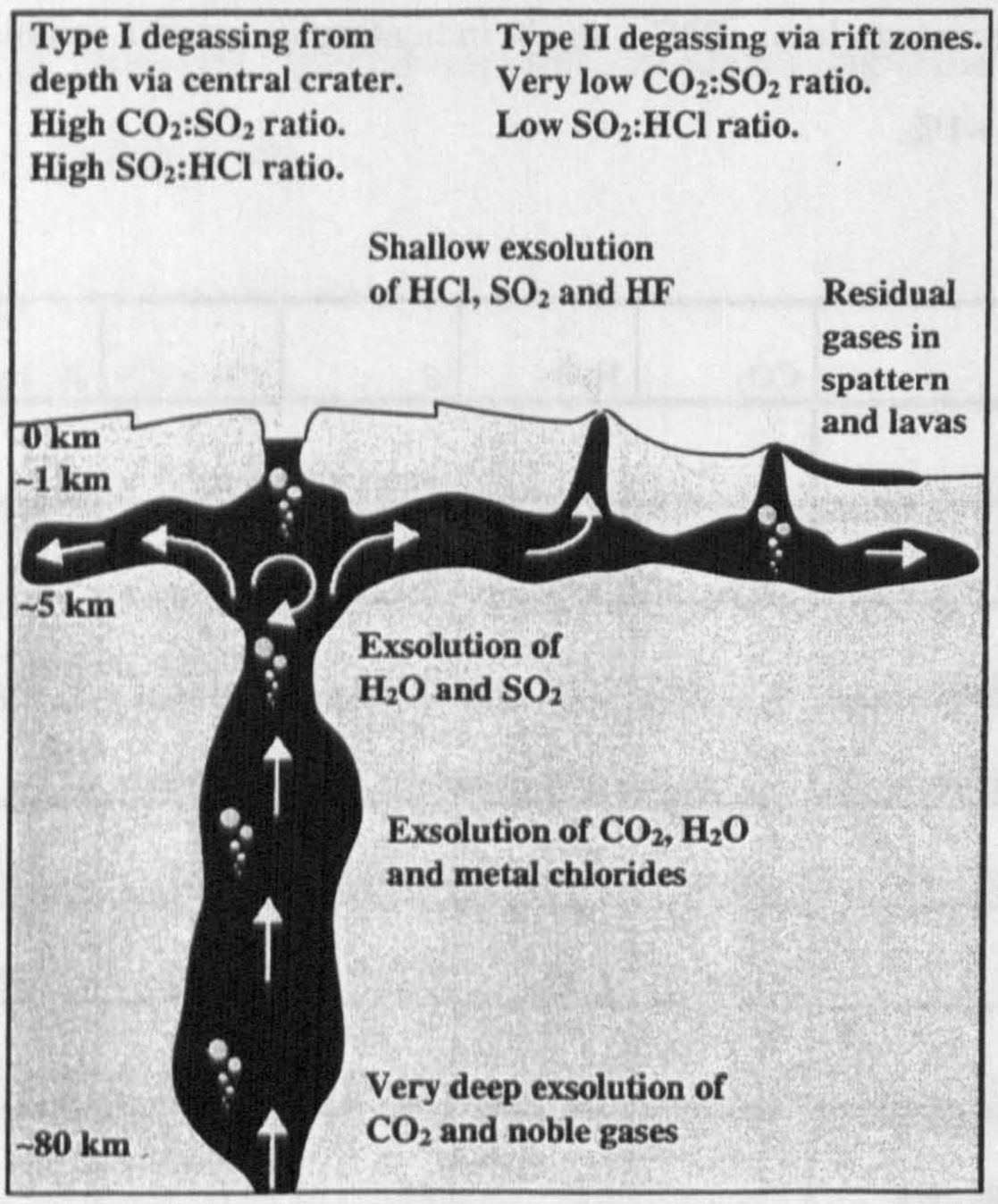

***Figure 1.2**. Schematic of the magmatic plumbing beneath Kilauea volcano, Hawaii, showing the levels where different gasses may exsolve (after Gerlach & Graeber, 1985).*

At volcanoes without such a well defined rift zone it can be difficult to differentiate between the differing styles of degassing. Mt. Etna, although having two well defined rift zones, degasses almost exclusively through the summit craters and by pervasive soil gas emission (see Chapter 5). Pennisi & Le Cloarec (1998) measured the relative proportions of sulphur, chlorine and fluorine emitted from the summit craters, the Bocca Nuova, SE Crater and La Voragine, during periods of activity and inactivity between 1992 and 1995 to relate different gas compositions to levels of eruptive/effusive activity.

Figure 1.3. A. Plot of SO_2:HCl ratio against sample date. B. Plot of HCl:HF ratio against sample date. A third order polynomial has been fitted to the data to show the trends in gas ratios. These show the changes in composition of gas emissions from the summit craters at Mt. Etna during and after the 1991 -1993 eruption, see Chapter 5.

The resulting data gave a range of HCl:HF mass ratios of ~5 - ~20, with an average of ~5 over the period studied, see **figure 1.3A**. The SO_2:HCl mass ratios were more variable,

ranging from <1 to >10 with an average of ~2.6. Both gas ratios show a similar variation over time; with values decreasing sharply after the end of the 1991 - 1993 eruption and then remaining relatively low. The HCl:HF ratio also shows a gradual climb as the summit craters began to be more active prior to the 1997 - 1998 effusive events, see **figures 1.3 A-B.**

Comparison of Cl:F and S:Cl mass ratios in the plume and in deep olivine inclusions, as analysed by Metrich et al. (1993) indicates the relative solubilities of the volatiles involved. Metrich et al. (1993) reported average Cl:F ratios in olivine inclusions of ~3, with average S:Cl ratios in the inclusions being ~1.2. The range in Cl:F and S:Cl ratios in the plume, were reported by Pennisi & Le Cloarec (1998) to be ~4 - 20 and ~0.1 - 4 respectively. The disparity between magmatic and plume ratios is indicative of the volatile's partition coefficient, with fluorine being ~1 - ~7 times more soluble in magma than chlorine. By the same argument, sulphur appears to be both 3 times more soluble, and 10 times less soluble than chlorine. This contradiction is due to the behaviour of sulphur with pressure being much different to that of chlorine, see earlier.

Pennisi & Le Cloarec (1998) have interpreted the differences in the SO_2:HCl gas ratios and their relative partition coefficients as relating to different styles of degassing - as a first approximation they related high SO_2:HCl ratios to eruptive or strombolian degassing; whilst low SO_2:HCl ratios were related to quiet, passive, degassing. After the end of the 1991 - 1993 eruption at Mt. Etna the rates of SO_2 emission decreased substantially. This was coupled with a decrease in the SO_2:HCl ratio to leave a generally Chlorine-rich plume, see Chapter 5. Pennisi & Le Cloarec (1998) inferred from this that the higher rates of exsolution of the more volatile sulphur enabled the relative concentrations of the more soluble chlorine to increase, thus altering the plume's composition. The lowering in SO_2 flux and SO_2:HCl ratio after an eruption has also been observed at the Central American volcano Masaya, see Chapter 3. Pennisi & Le Cloarec (1998) interpreted the gradual increase in gas ratios and level of activity at Mt. Etna in 1994 and onwards as the degassing of a new magma pulse as it gradually neared the surface, the amounts of sulphur exsolved increasing relative to that of chlorine.

Pennisi & Le Cloarec (1998) and Clocchiatti (1996) have therefore proposed a two-stage degassing model for Mt. Etna, based on volatile compositions of inclusions and the levels of volatile fluxes from the summit craters:

1). Deep or "non-eruptive" degassing which occurs at the transition from basalt to hawaiite at depths of over 4 km, >1 kbar, during which ~50% of chlorine and ~30% of sulphur are exsolved along with much of the CO_2 and H_2O. At Mt. Etna this is equivalent to an SO_2:HCl mass ratio of <1, see **figure 1.4**.

2). Shallow, or "eruptive" degassing which occurs at depths of less than 1 km, <25 kbar, where ~90% of sulphur is exsolved compared with ~10% of chlorine. At Mt. Etna this would be equivalent to an SO_2:HCl mass ratio of ~10.

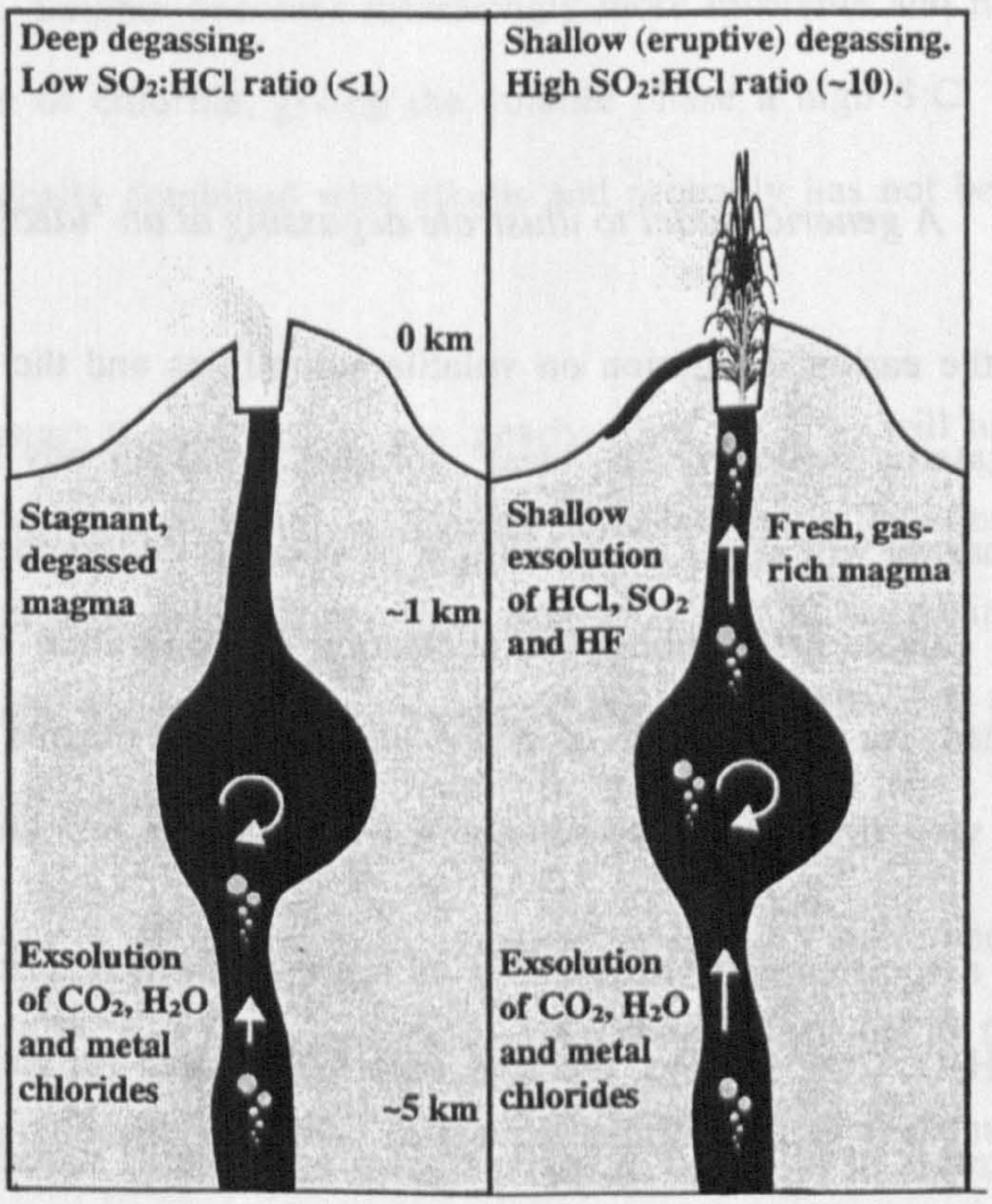

***Figure 1.4**. Schematic of the plumbing system beneath the summit craters at Mt. Etna illustrating the different styles of degassing during eruptive and quiescent periods (after Pennisi & Le Cloarec, 1998).*

This model is very similar to that described by Gerlach & Graeber (1985) for degassing at the summit of Kilauea and along its rift zones; although rather than gas

compositions being differentiated according to eruptive activity over a lateral distance, they have been differentiated according to variations in eruptive activity over time. Both models rely on the difference in solubilities of each volatile compound with depth and magma composition.

Several authors (i.e. Stoiber et al., 1986) have been observed short-term variations in SO_2:HCl gas ratios at basaltic volcanoes over periods of minutes to hours. This has been attributed to the convection of magma within a conduit. As a fresh batch nears the surface the less soluble water and sulphur are exsolved first, giving an initial high SO_2:HCl ratio. As the magma batch resides at the surface for increasing lengths of time, more chlorine and fluorine will exsolve relative to the now depleted SO_2. Once the majority of volatiles have been degassed and the magma has cooled it sinks to be replaced by less dense more volatile rich material from below (Kazahaya et al., 1994).

1.5.3 A generic model to illustrate degassing at an "ideal" volcano

I have used the earlier discussion on volatile solubilities and the two case-studies to derive a generic degassing model for an "ideal" volcano. It has already been noted that the composition of the magma will affect the exsolution of volatiles due to chemical reactions and that higher viscosity silicate melts inhibit the nucleation and migration of volatile phases. I have therefore assumed, for the purposes of this model, an "ideal magma" of typical basaltic composition, i.e: low viscosity; low silica and alkalis; with moderate iron and magnesium.

The volatiles associated with this melt on its formation will be principally, in order of relative abundance: H_2O, CO_2, sulphur, chlorine, fluorine, oxygen (in some form), hydrogen (in some form) and traces of inert and radiogenic gases and volatile metals. As the melt rises from its source to a depth of possibly ~80 km the most insoluble volatiles will begin to exsolve. These include the inert gases, i.e. helium and radiogenic argon, but mainly CO_2, see **figure 1.5**. The amount of non-tetrahedrally bound oxygen will control the chemistry of the volatile phases; sulphur being partitioned into either a reduced compound such as H_2S or FeS, or oxidised to SO_2 or SO_4^{2-} . Chlorine and fluorine, depending on melt composition, will have complexed with available alkalis and alkali earths to form a range of salts, i.e. NaCl, MgF_2 and

CaF_2. Those volatiles exsolved will have nucleated and formed small bubbles which grow slowly due to further nucleation and diffusion and to adiabatic expansion as the melt nears the surface. Only the larger bubbles (>1 cm) have enough buoyancy to overcome the melt's viscosity and migrate through the melt towards the surface (Vergniolle & Jaupart, 1986).

At depths of ~10 km the confining pressure will be low enough for H_2O to begin to supersaturate and exsolve from the melt. At these and shallower depths H_2O is the dominant volatile in the gas phase. Sulphur and chloride may also begin to exsolve at these depths with chloride more so than sulphur; giving the vapour a low S:Cl ratio.

As the melt reaches depths of ~4 km depth, the increasingly more immiscible chloride compounds begin to become unstable and chlorine combines with hydrogen to give HCl. This can combine with both the H_2O-rich volatile phase and melt and thus increasing the overall solubility of chlorine. Sulphur becomes increasingly more insoluble and its rate of exsolution begins to exceed that of chlorine: giving the volatile phase a high S:Cl ratio. At this depth fluorine is still chemically combined with alkalis and probably has not begun to exsolve, see **figure 1.5**.

As the melt nears the surface, <1 km, nearly all of the CO_2 will have been lost, along with most of the H_2O which forms the bulk of the volatiles lost to the atmosphere. The rate of SO_2 exsolution, although much lower than that of H_2O, is approximately an order of magnitude greater than that of HCl. At this depth, fluorine, as HF, will just be beginning to supersaturate and enter the volatile phase.

During periods of increased volcanic activity, enhanced convection and eruptive/effusive activity can bring magma rapidly from depth up to the surface. In such circumstances, dissolved volatiles may either not equilibrate to the changing pressures, or exsolved volatiles may remain with the melt rather than rising ahead of it. When this happens the observed gas compositions will relate to a system in disequilibrium, with gases which normally exsolve at different depths being suddenly forcibly exsolved close to the magma surface. It was this style of disequilibrium which enabled Pennisi & Le Cloarec (1998) to propose a model for the degassing at Mt. Etna.

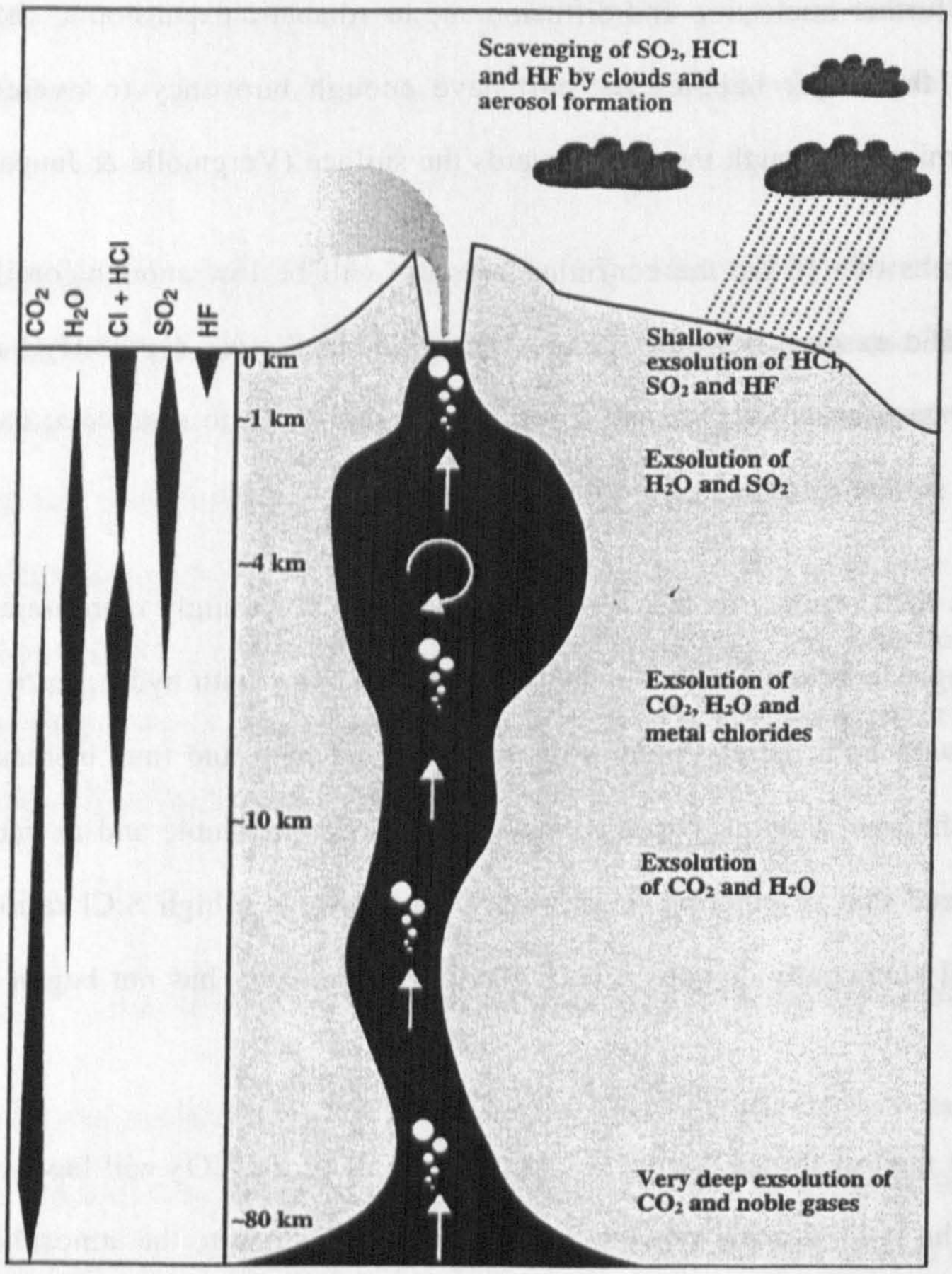

***Figure 1.5**. Schematic diagram of the approximate depths of volatile exsolution at the "ideal basaltic volcano". Chlorine forms two different phases, alkali chlorides and HCl, which exsolve at depths of >4 km and <4 km respectively (after: Gerlach & Graeber, 1985; Giggenbach, 1996; Pennisi & Le Cloarec, 1998).*

Once the volatiles have left the melt and either directly entered the atmosphere or have been injected into the base of a hydrothermal/fumarole system it is temperature and chemistry, rather than pressure, which governs the final composition of gases. In hydrothermal and fumarolic systems where the environment may either be reducing or oxidising, most compounds have a limited temperature range in which they are chemically stable. Outside of this range they will be oxidised or reduced. This is especially pertinent to sulphur and carbon species which both have a wide range of stable oxidation states. The aqueous solubility and acidity of gas species can also play an important role in whether they are absorbed into a fluid

reservoir or pass through it to be vented at the surface. These, and atmospheric interactions, are discussed in detail elsewhere in the thesis.

1.6 A brief review of localities

1.6.1 Masaya Volcanic Complex, Nicaragua

The volcanic complex is composed of basaltic lava flows and tephra deposits and lies within the recent (6.4 - 2.25 ka) dumbbell-shaped Masaya Caldera, along the line of the Central American Volcanic Front. The eruptive vents and fissures are located in a circular formation within the NW half of the caldera. A major regional fault, the Cofradía Fault, also passes through the caldera and may control the orientation of the most recent effusive activity which occurred in 1772. At present, the active Santiago Crater is emitting up to ~7000 t/d of SO_2 and has done so episodically since the crater's formation in ~1859.

1.6.2 La Fossa di Vulcano, Aeolian Isles, Sicily, Italy

La Fossa is a small, ~300 - 400 m high, cone formed during the last eruptive episode at Vulcano in 1888. This is the type-example for vulcanian eruptions, having ejected large bombs and pyroclastics which mantle the present cone. The present activity is solely fumarolic; with a rim and central fumarole field and minor fumarolic activity located along a fault line that extends northwards away from the cone through the small town of Porto di Levante at its foot. The use of D and ^{18}O isotopes has enabled three distinct types of fluid reservoir to be identified: magmatic, marine-hydrothermal and meteoric.

1.6.3 Mt. Etna, Sicily, Italy

Mt Etna is a ~3400 m high composite volcano of hawaiite (~basaltic andesite) composition which dominates the skyline of eastern Sicily. It has been the source of many historic eruptions, both from the summit craters and from lateral vents. The last major eruption was in 1991 - 1993 when a fissure opened into the Valle del Bove collapse scar, erupting

~231 ± 19 × 10^6 m^3 of lava. It produces prodigious quantities of volcanic gas; ~30 × 10^6 t/y of CO_2; ~1.8 × 10^6 t/y of SO_2, and ~0.4 × 10^6 t/y of HCl. This is equivalent to ~10% of the global volcanic SO_2 output and ~21% of the global anthropogenic output for HCl.

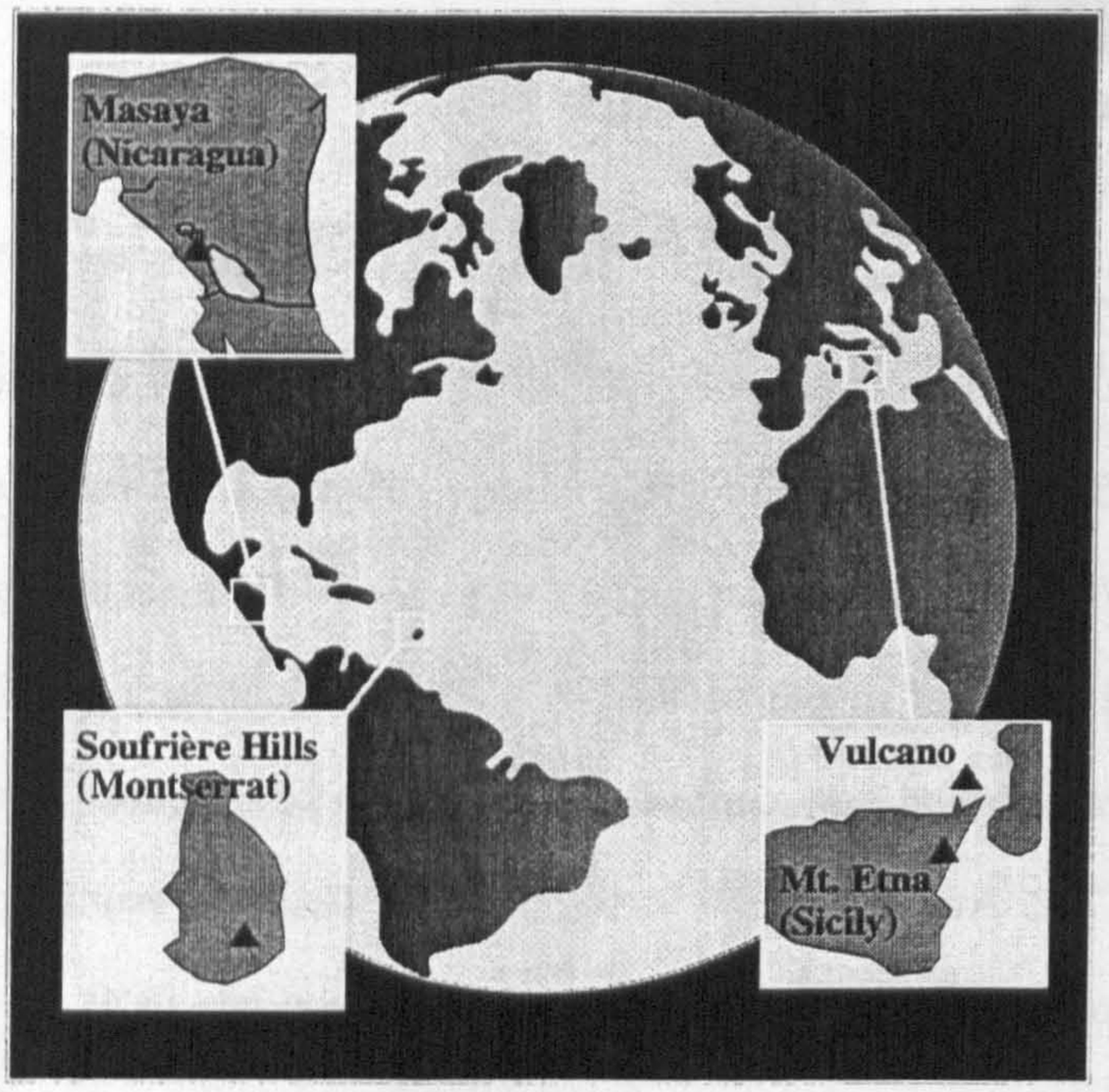

***Figure 1.6**. Locations of: the Masaya Volcanic Complex, Nicaragua; Soufrière Hills volcano, Montserrat; La Fossa di Vulcano, Aeolian Isles, Italy; and Mt. Etna, Sicily which are discussed in this thesis.*

1.6.4 Soufrière Hills volcano, Montserrat, W.I.

The dormant Soufrière Hills volcano in southern Montserrat began to show signs of activity in November 1994 after a two year period of increased seismicity. In July 1995 initial steam and ash venting from English's Crater, a large collapse scar at the summit, and a subsequent series of large phreatic eruptions prompted the evacuation of Plymouth, the island's capital which lies at the foot of the volcano. Escalation of activity, the formation of a large andesitic dome and the production of numerous pyroclastic flows have devastated the southern half of the island. Gas analyses using COSPEC and OP-FTIR have shown the plume to be relatively SO_2 poor and HCl rich.

1.7 Techniques used

I have mainly used the terrestrial remote-sensing techniques, OP-FTIR and COSPEC, as well as grab- and filter-sampling as sources of data relating to gas compositions. The remote-sensing techniques rely on the absorption of specific frequencies of radiation (either IR or UV) by molecular bonds. Climatic conditions, especially cloud, can affect the amounts of individual gases detected. Grab sampling, although relatively free from the effects of weather, suffer from problems relating to condensation, contamination and secondary reactions. As the operator has to get close to the gas source these techniques are inherently more dangerous than the remote techniques.

1.8 A brief note on units - the inter-comparison of data-sets

Many scientists have worked on volcanic gases using a wide range of techniques. It is unfortunate that different authors have used different units to convey their data; e.g: μmol/mol, ppm, %, mol%, mg/kg, % of dry gases, % of wet gases, vol%, t/d, wt%, $\mu g/m^3$, mg/m^3 and ppm.m. This has made the inter-comparison of different data-sets rather arduous, especially when ambiguous units, such as ppm or %, have been used. All analyses in this thesis have been converted to either on wt%, ppmm (parts per million by mass) or t/d; the exception being OP-FTIR data which are left as ppmv.m (parts per million by volume per metre path length) as these relate to partial analyses of the optical path and so cannot be converted accurately to mass units. I have, however, converted gas volume ratios derived from OP-FTIR data into mass ratios so that these can be easily compared with gas mass ratios derived using other techniques. To do this I used the conversion factor in **equation 1.6**:

$$\frac{SO_2}{HCl} \text{ by volume (or molar ratio)} \times 1.756 = \frac{SO_2}{HCl} \text{ by mass} \qquad \textbf{(1.6)}$$

A glossary of the units used and discussed in this thesis is located in the Appendix.

Chapter 2.

Gas analysis techniques used for monitoring volcanic activity

2.1 Introduction

2.1.1 Layout of chapter

In this chapter I review some of the techniques used for analysing volcanic gases and discuss their strengths and weaknesses and how they work in order to compare and contrast their effectiveness. I have used the first two techniques described, Open-path Fourier Transform Infrared Spectroscopy (OP-FTIR) and Correlation Spectroscopy (COSPEC), to collect some of the data used in this thesis. The other techniques have not been used by the author but are incorporated for evaluative and comparative purposes as they have been used by others to analyse volcanic gases from the volcanoes I have studied. The layout of the chapter and the individual techniques covered are as follows:

2.1 Introduction to chapter, where the use of gas analyses as part of the volcano monitoring effort is discussed.

2.2 Open-path Fourier transform infra-red spectroscopy (OP-FTIR).

2.3 Correlation spectroscopy (COSPEC).

2.4 Differential absorption LIDAR (DIAL).

2.5 Differential optical absorption spectroscopy (DOAS).

2.6 Direct-sampling using portable infra-red spectrometers.

2.7 "Grab-sampling" using evacuated flasks.

2.8 The use of filter packs for "grab-sampling".

2.9 Conclusions to Techniques Chapter. These can be summarised as:

- The measurement of volcanic fluxes and compositions, by any technique, is important as these can provide information on the state of the magmatic system beneath the volcano.

- Remote techniques enable gases in hazardous or inaccessible areas to be analysed with the minimum of risk to the operators.

- The simultaneous analysis of more than one gas by systems such as DOAS or OP-FTIR allow volume mixing ratios of gases, which are generally independent of atmospheric dilution, to be determined.

- The OP-FTIR technique discussed fulfils most of the above parameters, although the difficulties of utilising warm ground as an IR source detract from its overall good performance.

2.1.2 Types of gas sampling and analyses

There are three main approaches to the analysis of volcanic gases, be it from fumaroles, soil seepage or in volcanic plumes. These are:

1). Grab- or direct-sampling, where gases are physically trapped and collected for analysis, either in the field or in a laboratory.

2). Terrestrial remote-sensing, where the instrument operating platform is either static or in a vehicle or aircraft or on a boat. Because the gases are analysed without interacting with the instrument, the risk of contamination and secondary reactions is eliminated.

3). Satellite-based remote-sensing, where the instruments are located in a low orbit. Two different systems exist for measuring volcanic SO_2 from space: the Total Ozone Mapping Spectrometer (TOMS); and the Advanced

Spaceborne Thermal Emission and Reflectance Radiometer (ASTER) which is to be launched in 1998 and is the evolution of the airborne Thermal Infra-red Multispectral Scanner (TIMS). I will however only discuss the use of terrestrial techniques in this thesis as the collection and use of satellite data has been discussed extensively elsewhere (Krueger et al., 1990; Bluth et al., 1994; Schneltzer et al., 1994; Realmuto et al., 1994; Realmuto et al., 1997).

2.1.3 The use of gas analyses as part of the volcano monitoring effort

The emission of hot gases from volcanic areas has been known since antiquity and has long been linked with the level of volcanic activity. Volcanic gases are "messengers" from the earth's interior (Francis et al., 1995) and as such have proved useful in determining the states of activity at many volcanoes. The volcanological information provided by gas analysis techniques has been increasingly incorporated into the more geophysical-based monitoring efforts of volcano observatories and related organisations in an attempt to help predict changes in activity.

The following chapters will discuss examples of how gas compositions and fluxes have been used to determine the levels of volcanic activity, rates of lava effusion and the magmatic volatile content. Gas analyses are also used to measure the by-products of volcanic activity: soil-gas, volcanic plume, volcanic smog and the high ambient background levels of asphyxiant and toxic gases such as CO_2, SO_2, HCl and HF which can be introduced into the atmosphere in quantities measured in thousands of tonnes per day. The various techniques of gas analysis described in this chapter have been used on various volcanoes around the world to identify and quantify the gaseous products associated with volcanic activity.

2.1.4 *Gas analysis techniques - a quick guide*

In Sections 2.2 and 2.3 I describe two techniques, OP-FTIR and COSPEC that I have personally used to collect data. In Sections 2.4 to 2.9 I will describe some of the other terrestrial techniques used for gas analyses. I have not used these techniques but have used data acquired by other scientists who have. These techniques therefore merit inclusion in this thesis for comparative purposes and to evaluate their usefulness for gas analysis in a volcanological context. **Table 2.1** lists the different volcanic gases reported to have been detected, qualitatively or quantitatively, using each of the techniques described below; see appropriate section for details and references.

Technique	H_2O	CO_2	CO	SO_2	H_2S	HF	HCl	SiF_4	N_2O	H_2	CH_4	Noble gases
OP-FTIR	√	√	√	√	√	√	√	√	√	×	×	×
COSPEC	×	×	×	√	×	×	×	×	×	×	×	×
DIAL	×	×	×	√	×	×	×	×	×	×	×	×
DOAS	×	×	×	√	×	×	×	×	×	×	×	×
IR spectrophotometer	√	√	×	×	×	×	×	×	×	×	×	×
Direct sampling	√	√	√	√	√	√	√	×	√	×	√	√
Filter sampling	×	×	×	√	×	√	√	×	×	×	×	×

Table 2.1. *Summary of volcanic gases reported using each technique - √ = reported; × = not reported. Analyses may be either qualitative or quantitative. See text for details.*

2.2 Open-path Fourier transform infra-red spectroscopy (OP-FTIR)

2.2.1 Introduction to OP-FTIR

FTIR spectroscopy is a well known laboratory technique which has been used for a wide range of analytical studies. OP-FTIR has been used in industry for the environmental monitoring of smoke stacks in industrial complexes and for air quality; it is only as a by-product of this that OP-FTIR has found its way onto the slopes of active volcanoes. Over the years research for commercial gain has allowed development of smaller and better FTIR units for environmental monitoring. Long-path IR spectroscopy has also played an important role in identifying and determining concentrations of atmospheric pollutants since the 1950s (Hanst, 1993). Other studies have included photochemical reactions and the measuring of exhaust gases from jet engines (Herget & Brasher, 1979). The technique was first applied to volcanic gas plumes in 1991 by Notsu et al. (1993) at Asama volcano, Japan. Since then it has been used on volcanoes in Italy (Francis et al., 1995); Japan (Notsu et al., 1993); Montserrat (Oppenheimer et al., 1998), Mt. Erebus and Popocatepetl (Love et al., 1997). The details in this section refer to a portable Air Monitoring System (AMS™) FTIR spectrometer built by the Midac Corporation in California, although the principles apply to spectrometers produced by other manufacturers.

A rationale for the use of OP-FTIR in volcanology

The tragic deaths of several volcanologists in the last few years have highlighted the risk to life that volcanoes pose. The use of a remote Open-Path FTIR technique can clearly be seen as a safer alternative to "on-site" monitoring and "grab-sampling". The ability of FTIR spectrometers to simultaneously record absorbances over a wide frequency range, >4500 - <600 cm^{-1}, allows a large data set to be collected both quickly and easily. With a range of up to 4 km (Notsu et al., 1993) the danger of volcanologists being injured by a sudden explosion is minimised. The use of the sun as an IR source also enables analyses to be safely conducted far from the volcano and out of the gas plume (Love et al., 1998). The

quantitative analysis of volcanic gases allows an insight into magma chamber processes and the effects of the interaction of the magmatic-hydrothermal system on the gas species emitted.

2.2.2 *Principles and terminology of IR spectroscopy*

Principles

Infra-red radiation is an energy source that can be utilised by molecular bonds to change to another energy state. Molecular bonds vibrate. The speed of the vibration depends on two main factors: the mass of the atoms at each end of the bond and the strength of the bond itself. Each bond has a natural resonance frequency. Energy of a frequency that can be utilised by the bond will be absorbed. This is the Fundamental frequency and is unique to a particular bond and the atoms around it. It is this principle which allows infra-red spectroscopy to be the useful analytical tool it is.

For a molecule to be "infra-red active", i.e. be able to absorb infra-red radiation and convert it into mechanical energy (vibrations) the molecule must posses an electric dipole moment; produced when oscillations of atoms cause the centres of positive and negative charge to change position relative to each other (Hollas, 1987), see **figure 2.1**. Atoms without a dipole such as homonuclear diatomic molecules and monatomic species are "infra-red inactive"; such compounds include: oxygen, nitrogen and the noble gases. The main atmospheric gases that are infra-red active are H_2O and CO_2. Most of the pollutant gases such as NO_x, SO_x, hydrogen halides and methane are all infra-red active.

Multi-frequency IR radiation, emitted from a hot source, is detected by an IR detector. Gases in the optical path between the IR source and the detector will, if infra-red-active, absorb radiation at characteristic frequencies - the fundamental frequencies, leaving gaps, or absorbance bands, in the IR spectrum. Conversely hot infra-red-active gases can emit IR radiation as they change their vibrational states; this can be detected as peaks in the IR spectrum.

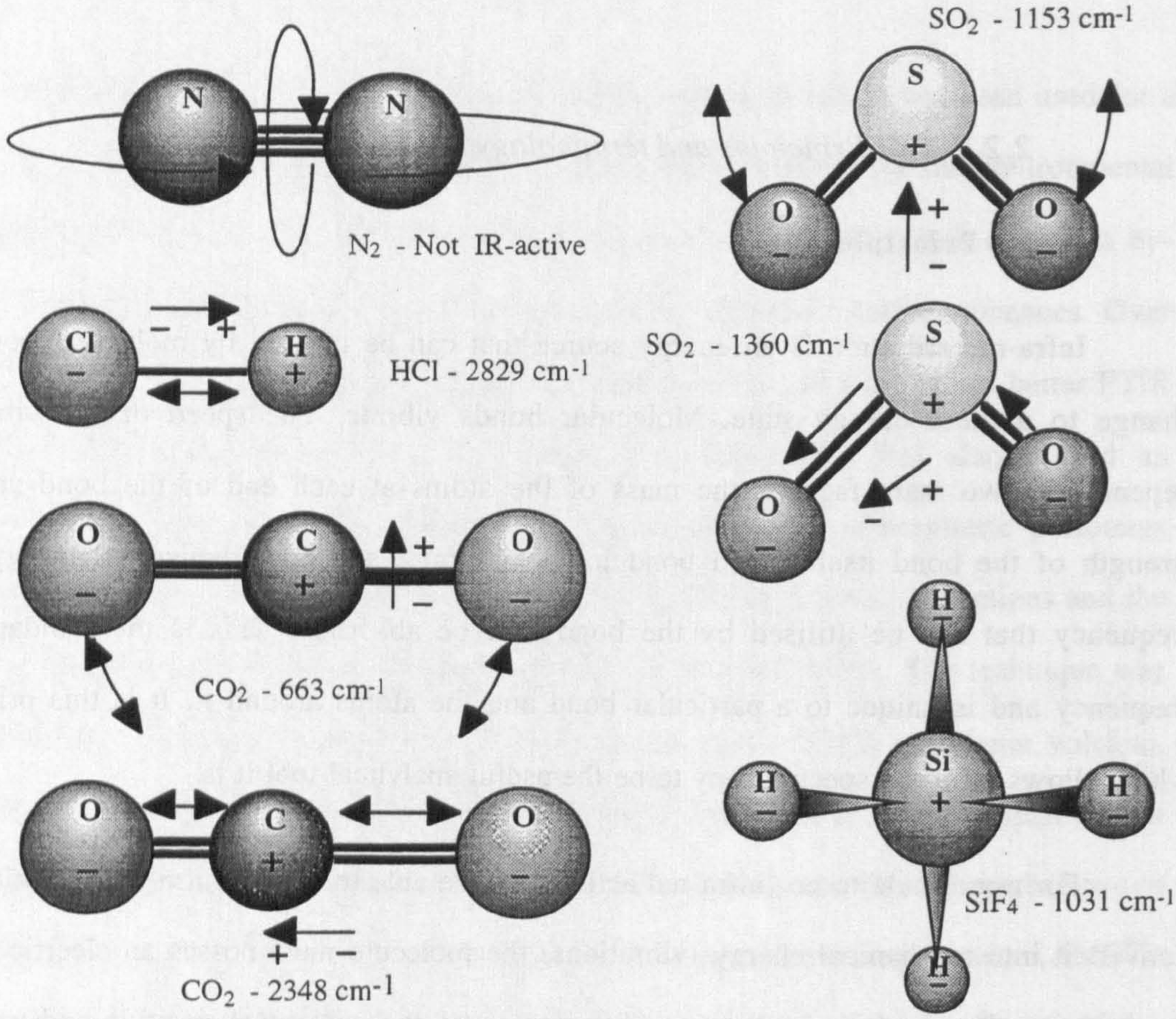

Rules for being IR-active

IR radiation is absorbed/radiated by covalent bonds during a transition to a higher/lower energy level. This requires the presence of an electric dipole moment:

$$\mu = \sum_i q_i r_i$$

where: q_i = charge of the ith particle and r_i = position vector of ith particle.

$$R_v = \psi'^*_v \, \mu \, \psi''^*_v \, dx$$

where: ψ'^*_v and ψ''^*_v are eigenfunctions of the IR radiation waveform and μ = electric dipole moment.

For vibrational spectroscopy:
During transition between energy levels $R_v \neq 0$. i.e. the electric dipole must change.

For rotational spectroscopy:
This can only happen if there is there is a permanent electric dipole moment, $\mu \neq 0$ and there is a transition between energy levels.

Rule for maximum number of normal modes of vibration

$$Nv = 3N - (6 - k)$$

where: N_a = number of atoms; k=1 for a linear molecule and k=0 for a non-linear molecule.

***Figure 2.1**. Schematic diagram for a selection of gas species showing the various vibrational states associated with absorption of IR radiation. The basic rules governing whether molecules are IR active are also shown for both rotational and vibrational states (after Hollas, 1987).*

The intensity of an absorbance band can be related to the concentration of the gas, or analyte, by the Beer-Lambert Law, see **equation 2.1** (Alberty, 1955).

$$I_\lambda = I_{0\lambda} e^{(\varepsilon_\lambda c l)} \qquad \textbf{(2.1)}$$

where: $I_{0\lambda}$ is the initial intensity at frequency λ; I_λ is the measured intensity of the radiation at the same frequency λ; ε is the molar absorption coefficient - a measure of how strongly a particular analyte absorbs IR radiation; c is the concentration of analyte within the optical path and l is the path length. Rearrangement of this equation gives **equation 2.2**:

$$\log\left(\frac{I_\lambda}{I^{0\lambda}}\right) = \varepsilon_\lambda c l \qquad \textbf{(2.2)}$$

which, in practical terms, is equivalent to:

$$\log\left(\frac{\text{Sample}}{\text{Background}}\right) = \text{Absorbance} \qquad \textbf{(2.3)}$$

It can therefore be seen in **equation 2.3** that the amplitude of the fundamental absorbance, derived by dividing an IR sample spectrum by its background spectrum, can be related to the concentration of an analyte if the length of the optical path and absorbance coefficient, ε, are known. If ε is not known, the concentration can be calculated by comparing the height of the unquantified absorbance peak with that of a reference of known concentration. In open-path spectroscopy, where the path length is often not accurately known, concentrations are recorded as ppmv.m – the path-averaged concentration (by volume) measured over the entire path length. The path-averaged concentration is simply the total concentration averaged over the entire optical path and is expressed in ppmv.m; e.g. 400 ppmv.m = 4 ppmv over 100 m or 20 ppmv over 20 m.

Terminology

Open-path FTIR spectroscopy can be carried out in two major ways: either by analysing the radiation absorbed by cold analyte species, called absorbance spectroscopy; or by analysing the radiation emitted from hot analyte species, called Emission Spectroscopy. Volcanic gases normally cool down rapidly on mixing with the atmosphere

and so the spectroscopy discussed here will be absorbance spectroscopy. The radiation absorbed by the analyte species needs to be generated from a hot body, either naturally by warm ground, fires or lava or artificially using an IR lamp. Analyses conducted using a pre-existing IR source are termed Passive; those using an artificial IR source, such as a portable IR lamp, are termed Active.

Types of infra-red spectra

All the IR data dealt with in this thesis have been represented graphically as a plot, or spectrum, of absorbance versus wavenumber. Wavenumber is the reciprocal of the wavelength of the IR radiation in cm and as such can be converted to μm by **equation 2.4** below.

$$\mu m = \left(\frac{1}{WN}\right) \times 10{,}000 \qquad (2.4)$$

where WN is the wavenumber value in cm^{-1}. Data are initially recorded by the FTIR spectrometer as an interferogram which relates the intensity of radiation to the position of a moving mirror within the instrument, see Section 2.2.3 and **figures 2.2A** and **2.5**. Fast Fourier Transformation of the interferogram converts the data into an intensity against frequency format, termed a single-beam spectrum, see **figure 2.2A**. This displays the intensity of radiation detected at any particular frequency with a resolution of between 16 cm^{-1} and 0.5 cm^{-1} for the Midac AMS™ FTIR spectrometer. The intensity of radiation detected is determined by the varying amount of atmospheric absorbance, the temperature of the IR source and the sensitivity of the IR detector used, see Section 2.2.3. Background noise caused by the predominance of CO_2, H_2O and the non-linear response of the IR detector swamps much of the data held in a single-beam spectrum. The noise caused by the background CO_2 and H_2O and the bias caused by the varying sensitivity of the IR detector can be overcome by dividing the intensities of one single-beam spectrum by another. If the log of such a division is taken the ensuing intensities thus become the absorbance, as indicated by **equation 2.5**. Such a spectrum, see **figure 2.2C**, is termed an absorbance spectrum; here the peak height of an analyte is proportional to its concentration within the

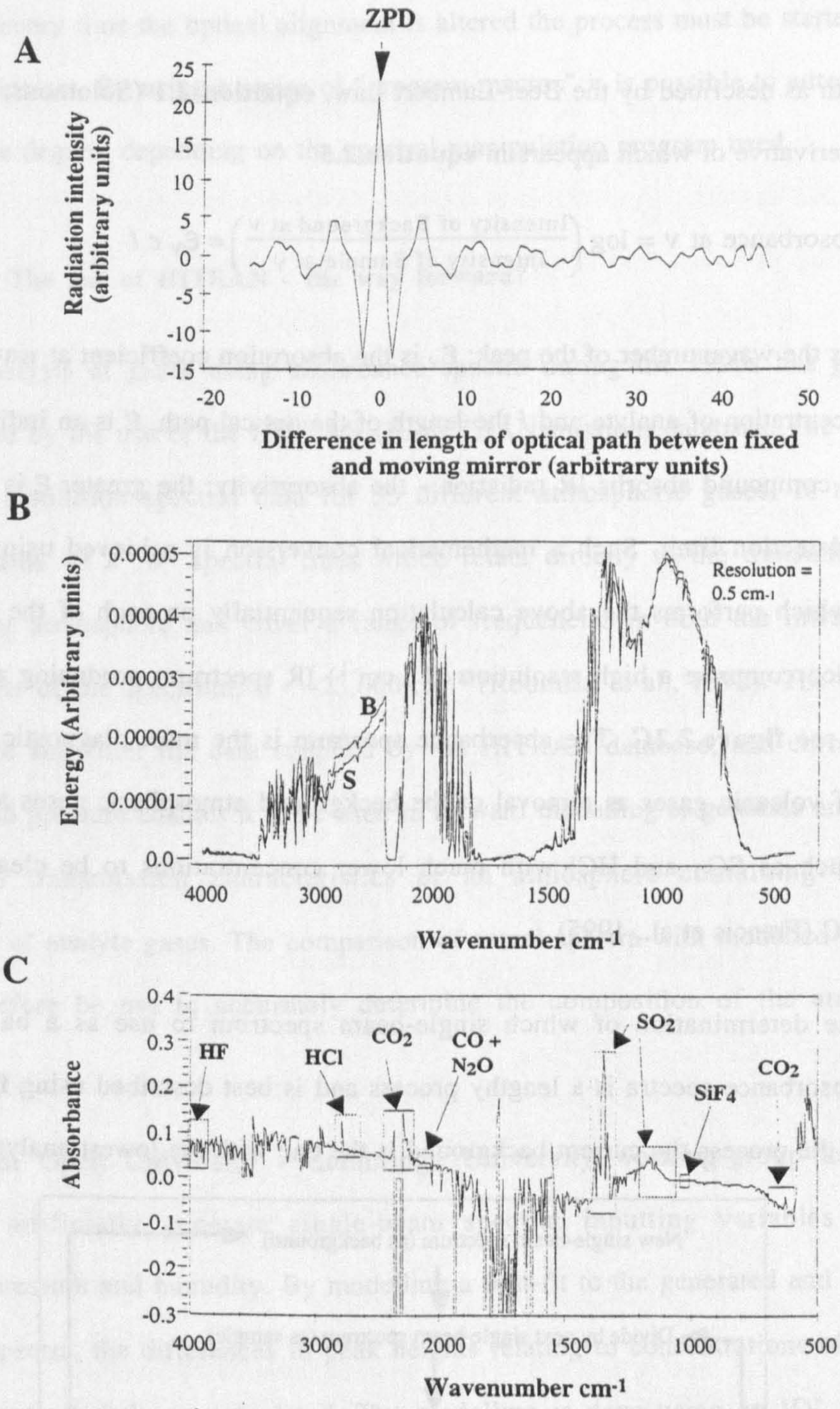

Figure 2.2 A. *An example of an interferogram. The arrow ZPD marks the position where the path-lengths to both mirrors within the interferometer are identical, therefore allowing all frequencies to recombine constructively giving the maximum peak seen.* ***B.*** *An example of two single-beam spectra used to create the absorbance spectrum in* ***C****; B = background and S = sample spectrum. The shape of the spectrum is due to the response of the MCT (Hg-Cd-Te) detector used to different frequencies of IR radiation.* ***C.*** *Absorbance spectrum created using the single-beam spectra in* ***B****. The noisy regions are due to the attenuation of IR radiation caused by atmospheric CO_2 and H_2O. The regions used for analysing different analytes can also be seen.*

optical path as described by the Beer-Lambert Law, **equation 2.1** (Solomons, 1976; Hollas, 1987), a derivative of which appears in **equation 2.5**.

$$\text{Absorbance at } \nu = \log\left(\frac{\text{Intensity of Background at } \nu}{\text{Intensity of Sample at } \nu}\right) = \varepsilon_\nu \, c \, l \qquad \textbf{(2.5)}$$

where: ν is the wavenumber of the peak; ε_ν is the absorption coefficient at wavenumber ν; c is the concentration of analyte and l the length of the optical path. ε is an indication of how strongly a compound absorbs IR radiation - the absorptivity; the greater ε is the lower the analyte's detection limit. Such a mathematical conversion is achieved using a computer program which performs the above calculation sequentially on each of the ~14,000 data points which comprise a high resolution (0.5 cm^{-1}) IR spectrum; producing an absorbance spectrum, see **figure 2.2C**. The absorbance spectrum is the most diagnostic spectrum for analysis of volcanic gases as removal of the background atmospheric gases allows analyte species, such as SO_2 and HCl with much lower concentrations to be clearly seen, see **figure 2.2C** (Francis et al., 1995).

The determination of which single-beam spectrum to use as a background for creating absorbance spectra is a lengthy process and is best described using **figure 2.3**. At the end of the process the current background is the one with the lowest analyte.

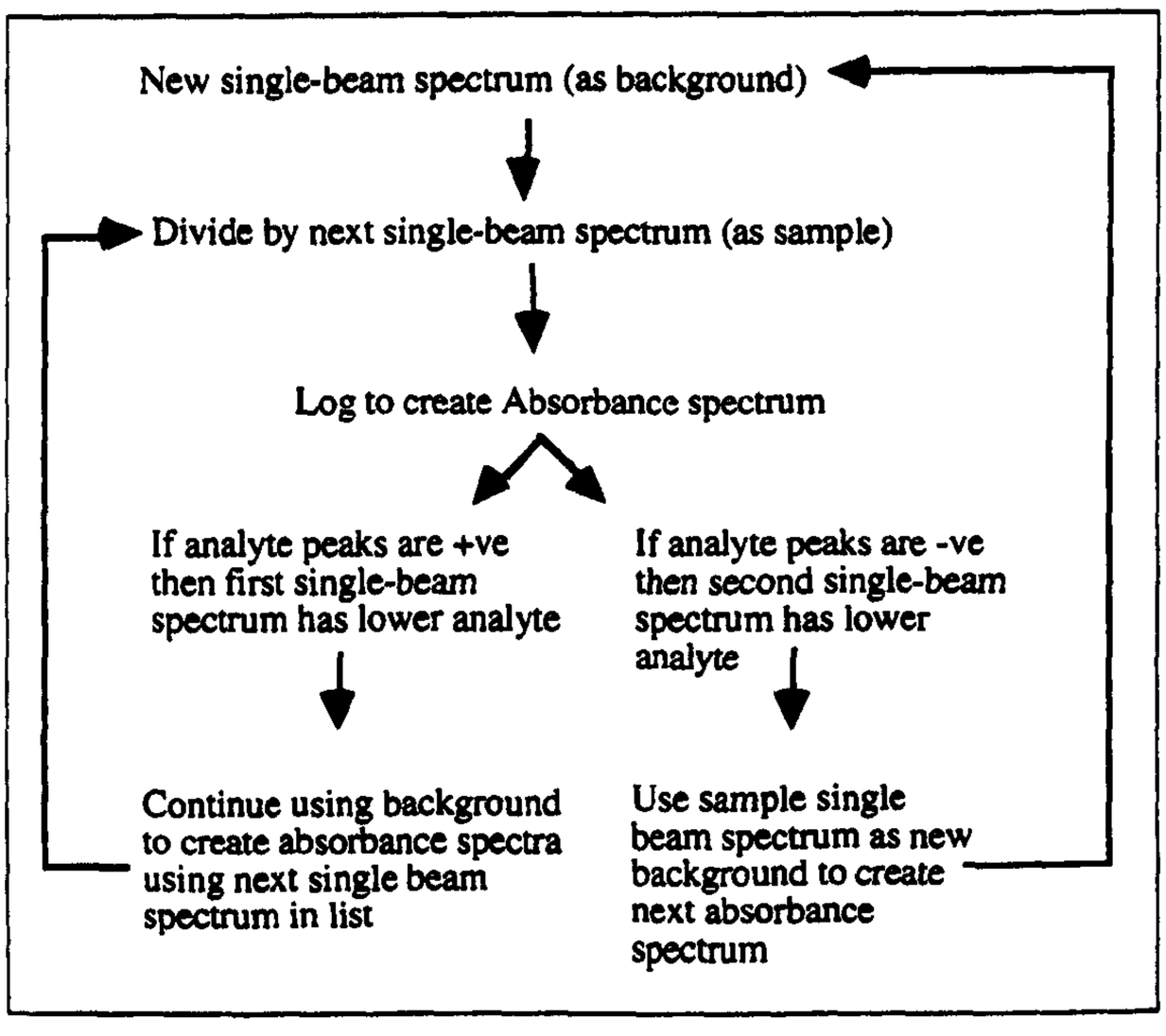

***Figure 2.3**. Flow chart showing the process of determining which sample spectrum to use as the background or reference spectrum, see text for further details*

Unfortunately, every time the optical alignment is altered the process must be started afresh with the new data-set. By using a series of "program macros" it is possible to automate the process to some degree, depending on the spectral manipulation program used.

The use of HITRAN - the way forward?

The analysis of gases using absorbance spectra during the 1990s has gradually been superseded by the use of the HITRAN (HIgh TRANsmission) database. The database contains high resolution spectral data for 35 different atmospheric gases. In total, the database contains ~1×10^6 spectral lines which relate directly to the transmittance of radiation in the atmosphere and cover a range of frequencies in both the infra-red and ultra-violet parts of the spectrum, 0 - ~23,000 cm^{-1} (Rothman et al., 1992). The ability to use, manipulate and filter the data supplied by the HITRAN database, and correct it for temperature and pressure enables it to be used in forward modelling to generate an accurate model of the transmission characteristics of an atmosphere containing specified concentrations of analyte gases. The comparison of actual spectra with modelled HITRAN data can therefore be use to accurately determine the composition of the atmosphere analysed.

A joint Open University - Cambridge University working-group have used HITRAN to artificially generate single-beam spectra; inputting variables such as temperature, pressure and humidity. By modelling a best-fit to the generated and measured single-beam spectra, the differences in peak heights relating to concentrations of volcanic gases in the optical path are calculated. The modelling is done using an IDL computer programme, allowing gas concentration data to be derived much faster and more objectively than by using absorbance spectra and manually comparing sample with laboratory reference spectra. The use of a modelled HITRAN background, rather than a sample spectrum, reduces the amounts of analyte present in the background/reference spectrum. This enables lower concentrations of analyte to be detected and thus increases the overall sensitivity of the system. All the IR data reported in this thesis have, however, been determined manually by the author using IR absorbance data and laboratory reference spectra.

Identification of analytes using IR spectra

There are four main factors that determine how effectively an analyte can be identified and its concentration determined. These are:

1). Path-averaged analyte concentration. According to **equation 2.5** the absorbance is the product of $\varepsilon \times c \times l$ - the absorptivity × concentration × path length. The higher the path-averaged concentration the more analyte there is to absorb IR radiation and the easier it is to detect it.

2). The level of background noise in the spectrum. Signal-to-noise ratios in my OP-FTIR studies were commonly below 10:1; defined as the ratio of analyte peak height to the noise trough-to-peak height. This is very low compared with laboratory-based FTIR spectra which may have signal-to-noise ratios in excess of ~10,000 (Hanst & Hanst, 1994). As ratios get even lower, the difficulty in identifying fundamental peaks causes problems in the identification and quantification of analytes. The causes of such high levels of background noise probably relate to the constantly changing composition of the optical path, atmospheric scintillations due the presence of heat-haze, and slight movements of instrument in the wind and dust/ash on the optics.

3). The absorptivity ε. Low signal-to-noise ratios can be made even more problematic by analytes having a low absorptivity. This reduces the physical size of the absorbance peak, sometimes burying it within the background noise of the absorbance spectrum and preventing the detection of the analyte.

4). Peak-shape. The absorbance peak can be further hidden by being a smooth, broad shape, caused by the analyte having a high mass and/or complex structure, such as SO_2 or SiF_4. Light analytes with a simple structure, such as HF and HCl, by comparison have sharp peaks.

The use of "Atmospheric windows"

The areas that can be studied with the IR part of the spectrum are controlled by two main factors. The first is the restricted frequency range of the individual IR detector, see Section 2.2.3. The second is due to the intense absorptions of H_2O and CO_2 which occur in the atmosphere in relatively high concentrations. The attenuation of IR radiation due to these two gases occurs in three ranges: 3900 cm^{-1} to 3550 cm^{-1}; 1800 cm^{-1} to 1400 cm^{-1} and 630 cm^{-1} to 450 cm^{-1} (Gosz et al., 1990; Hanst & Hanst, 1994). Two main windows therefore are left open for atmospheric spectroscopy: one from 3200 cm^{-1} to 1800 cm^{-1} and the other from 1400 cm^{-1} to 630 cm^{-1} (Gosz et al., 1990; Chaffin et al., 1995). I have used these two windows to identify several volcanic gases from their fundamental absorbances. A third window above ~4000 cm^{-1} can be used to detect lighter, high energy molecules, such as HF.

2.2.3 OP-FTIR instrumentation

I have divided the following section into five parts, in which I will discuss the theoretical and practical requirements for using a Midac AMS™ FTIR system.

1). IR source

I used a Midac portable IR source, mounted on a Quickset™ tripod to conduct active analyses. This was comprised of a 12V 1275°C SiC Globar housed within a 20" (50.8 cm) metal parabolic reflector, see **figure 2.8**. To protect the highly polished, diamond turned aluminium surface of the reflector it was coated with inert CaF_2 to reduce corrosion by acidic gases.

The temperature of the IR source governs the frequency range of the radiation emitted; hotter sources emitting higher frequencies. Gases with strong bonds and lighter atoms, such as HF, absorb energy at high frequencies and thus require a hotter IR source if

they are to be detected using absorbance spectroscopy. Hence the ~1275°C temperature of the Midac artificial source. I found passive analyses, using natural sources of IR radiation, produced poor quality data, see Chapters 4, 5 and 6. Generally ground temperatures expected during passive analyses will only reach a maximum of ~1100°C; temperatures experienced by the author ranged between <50°C to <600°C for analyses reported later in this thesis, see **table 2.4**. The main disadvantage of using a natural IR source is that not enough high frequency radiation is emitted to excite lighter molecules due to the lower source temperature. The relative proportions of low and high frequency radiation that are emitted are governed by the Planck Law, the results of which can be displayed graphically as a Planck Curve, see **equation 2.5** and **figure 2.4A** (Alberty, 1955).

$$M_\lambda = \left(\frac{c}{4}\right)\rho_\lambda = \left[\frac{2\pi hc^2\lambda^{-5}}{e^{\left(\frac{hc}{\lambda kT}\right)}-1}\right] \qquad \textbf{(2.6)}$$

where: h = the Planck constant (6.62176×10^{-34} Js); c = the speed of light (2.998×10^{8} ms^{-1}); λ = wavelength of radiation; k = the Boltzmann constant (1.306×10^{-23} JK^{-1}); T = temperature in Kelvin; ρ_λ = the energy density, ~frequency population at wavelength λ; and M_λ = the rate of energy emission in Wm^{-2} (Alberty, 1955). **Figure 2.4A** shows that at 600°C, the radiance is at its maximum at 3012 cm^{-1}. At 1000°C, the radiance at 3012 cm^{-1} is below its maximum, but is still higher than it was at 600°C; indicating that the radiation emitted increases at all wavelengths as the temperature of the IR source increases. It is therefore advantageous to use as hot an IR source as possible.

Cooler IR sources emit less intense radiation, with the maximum emission being located at lower frequencies; as defined by the Wein Displacement Law which gives the frequency, and therefore wavelength λ, for the maximum value of the Planck Curve for a given temperature, see **equation 2.7**.

$$\lambda_{\max T} = 1\times10^{6}\times\left(\frac{0.002898}{T}\right) \qquad \textbf{(2.7)}$$

Rearrangement of **equation 2.7** enables the temperature of the maximum on the curve to be determined for a given wavenumber - i.e. that of an analyte's fundamental absorbance, i.e. **equation 2.8** where WN is in μm.

$$WN = \left(\frac{1}{0.002898 T^{-1} \times 100} \right) \tag{2.8}$$

Figure 2.4A shows that although high temperature sources do emit low frequency radiation, most of the radiation is of a higher frequency. However the low temperature sources cannot produce the high frequencies of radiation required to excite the lighter molecules.

A

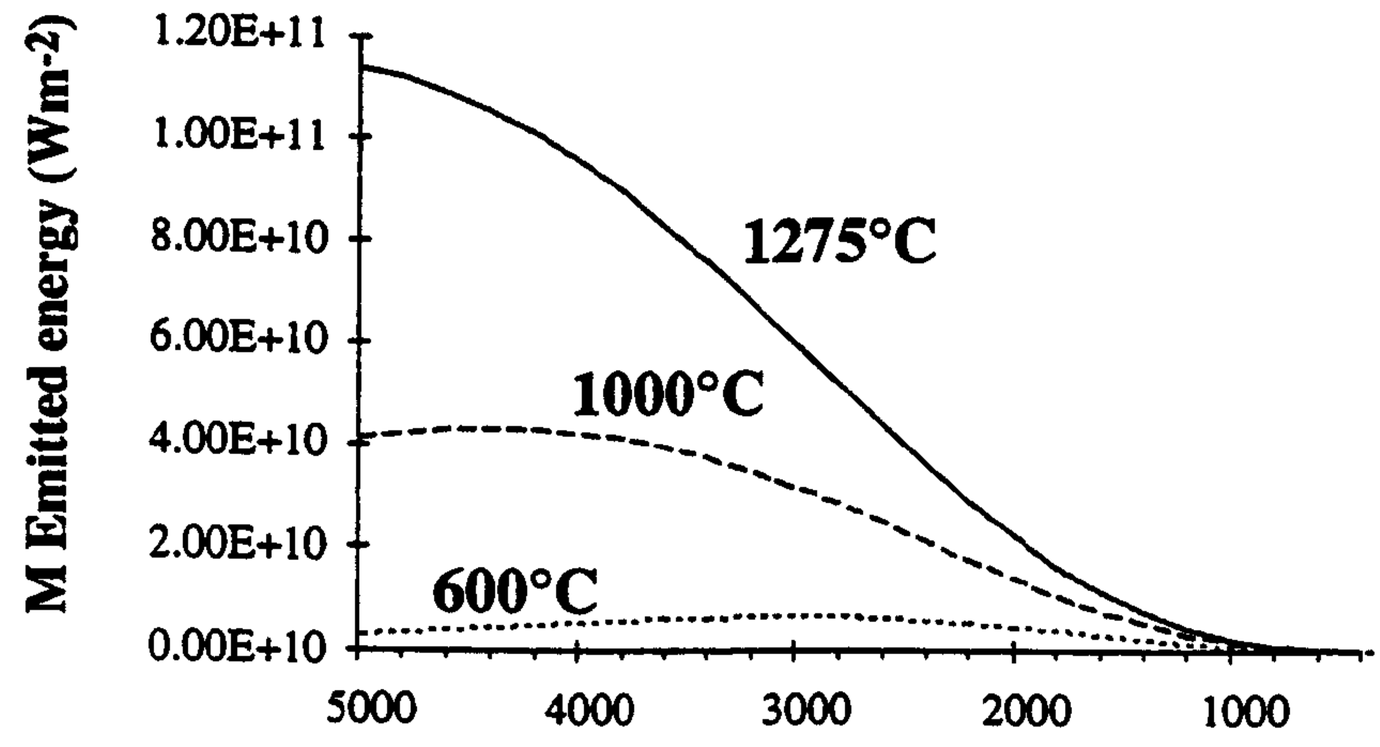

B

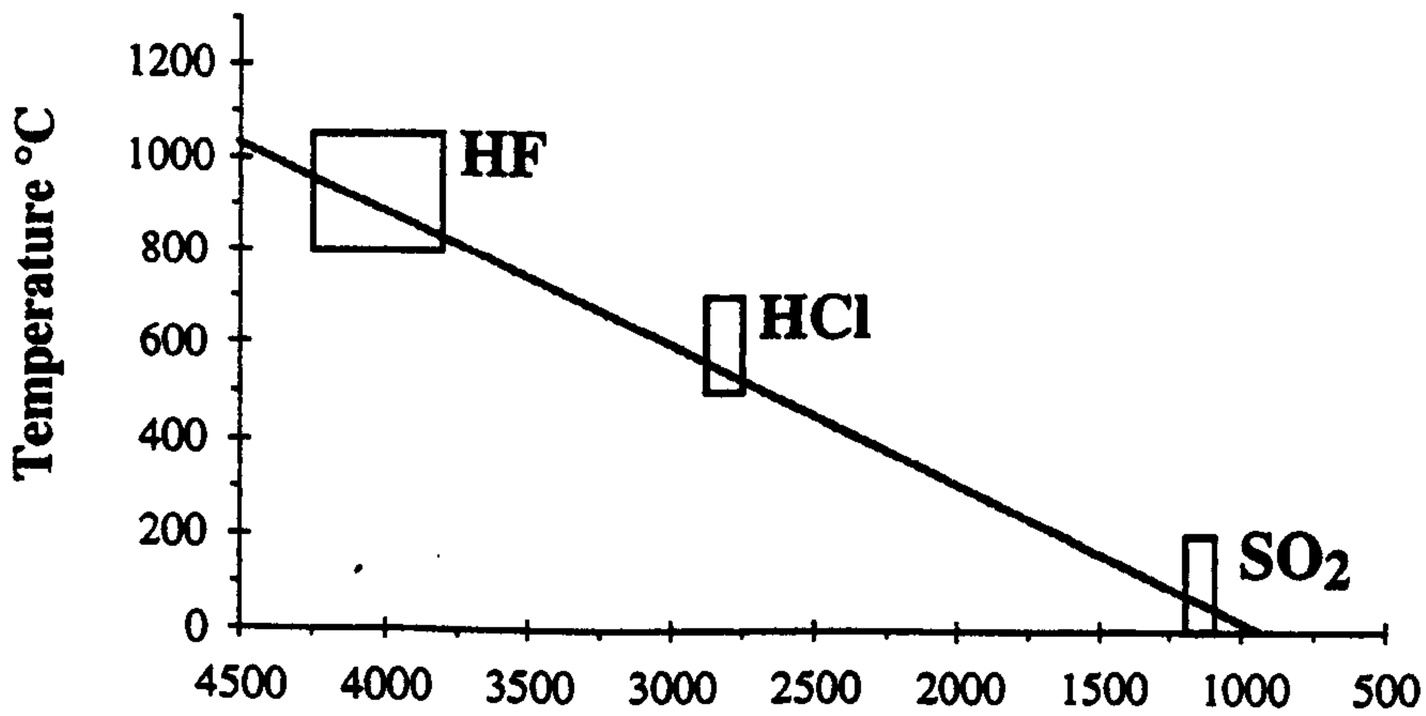

Figure 2.4A. *The Planck energy distribution at different frequencies; as determined for a black-body emitter at three temperatures: 600° and 1000°C and 1275°C - the temperature of the portable IR source.* ***B.*** *The Wein Displacement Law predicts the frequency of the maximum value on the Planck curve for a given temperature. I have used this temperature as an estimate for the minimum workable temperature of the IR source. The need for a much higher temperature for the excitement, and therefore detection, of HF relative to SO_2 can be clearly seen.*

This explains why the relatively heavy SO_2 can be detected using a hot artificial IR source, but light HCl cannot be detected using a cool natural source. To avoid the problem of low temperature IR sources providing insufficient high frequency radiation, I estimated minimum workable temperatures for the IR source and tried to only use IR sources above this temperature. I have based my estimates for minimum workable temperatures on the temperature at which the Wein Displacement Law gives a maximum radiance at the frequency of the measured analyte's fundamental absorbance, see **figures 2.4A** and **2.4B**. These are: SiF_4 (1050 cm^{-1}) ~30°C; SO_2 (1150 cm^{-1}) ~60°C; HCl (2880 cm^{-1}) ~565°C; HF (3800 cm^{-1}) ~830°C. I have derived SO_2:HCl ratios from my OP-FTIR data and so have had to use an IR source with a temperature far above the minimum workable temperature that would be required for solely investigating the presence of SO_2.

2). Telescope

The telescope used was a Midac f/3 Newtonian telescope with a diameter of 10" (25.4 cm). In the field it is mounted on a heavy-duty QuickSet™ tripod and provides a stable base onto which the spectrometer is mounted piggy-back style. The telescope has a field-of-view (FOV) of 3 mrad.

Range (m)	Radius of FOV (m)	Area of FOV (m^2)	% of FOV filled by 20" (50.8 cm) diameter IR source
50	0.08	0.02	100
100	0.15	0.07	100
170	0.26 (~10")	0.20	100
250	0.38	0.44	46
500	0.75	1.8	11
1000	1.5	7.1	3
2000	3.0	28	0.7

Table 2.2. *Relationship between path length and size of the 3 mrad field of view using the Midac telescope. At ranges >170 m, the 20" (50.8 cm) diameter portable IR lamp only partially filled the FOV. The signal from this however was clearly detectable at ranges of ~2000 m, although at these ranges fine adjustments to the aim of the telescope proved difficult.*

At a range of ~170 m the FOV is just filled by the 20" (50.8 cm) diameter portable Midac IR source used. At increasing distances the IR source fills less and less of the FOV; doubling the distance quarters the area the IR source fills in the FOV, see **table 2.2**. At 1000 m the IR source fills only 2.9% of the FOV and, at 2000 m, only 0.7%. Even so, enough of the high energy IR radiation from the source can reach the detector to provide high quality analyses. At these ranges, aiming the telescope is difficult; especially during windy periods which can cause misalignment of the telescope and consequent loss of IR signal.

3). Spectrometer

The Midac AMS™ spectrometer is mounted piggy-back on top of the telescope; two mounting-pins ensuring that the telescope optics are accurately aligned with those of the spectrometer. The spectrometer is housed within a solid metal casing which, weighing ~14 kg, makes up most of the instrument's 17 kg total weight. The rigidity of the casing allows the optical components to be located directly on to this; the lack of flexing preventing perturbations, caused by the misalignment of mirrors, being introduced into the optical path. The mass and solidity of the casing also help prevent damage caused by accidental impacts, making it ideal for use in the field.

IR radiation is collected by the telescope and directed into the instrument where it enters the plane-mirror Michelson interferometer. Here a ZnSe beam-splitter directs the radiation to two mirrors at right angles; one fixed and the other moving orthogonal to the plane of the first mirror. Movement of the mirror alters the length of the optical path and thus the phase of the reflected light. The two light beams, after being reflected are then recombined by the beam splitter. The phase difference of the recombined radiation, which is dependent on the position of the moving mirror and the wavelengths of the combined radiation, causes constructive or destructive interference (Griffiths et al., 1975). The recombined beam is then focused on to an IR detector which detects the intensity of IR radiation. A HeNe laser also sends a beam through the interferometer to the IR detector. This is used to control and track the position of the moving mirror making it possible to

unscramble the IR interference pattern - an interferogram, using a mathematical process - Fast Fourier Transformation.

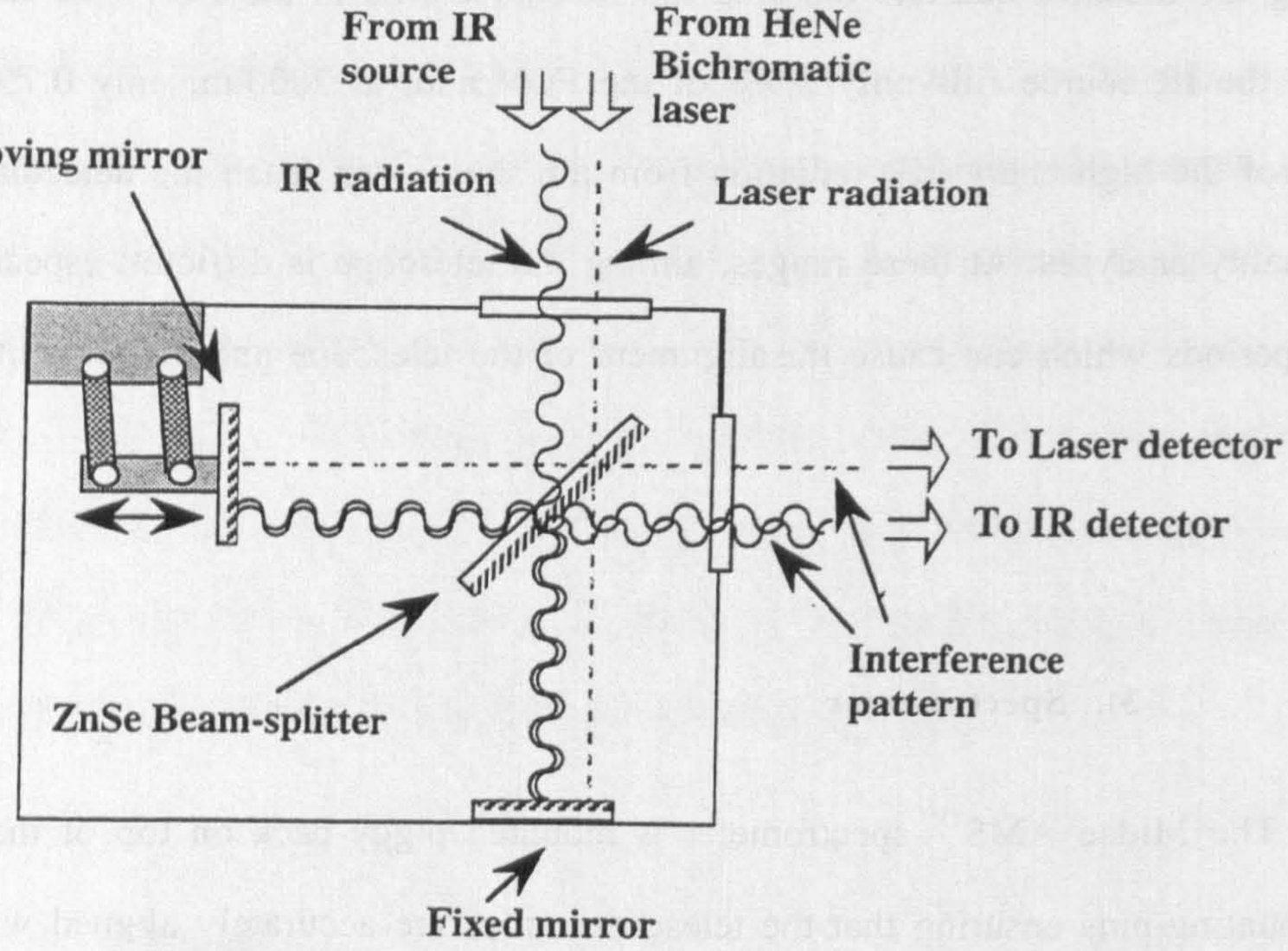

Figure 2.5. *Schematic set-up of a Michelson Interferometer showing moving and fixed mirrors and the phases of radiation as they pass through the instrument (after: Hollas, 1987; Midac operators manual). The laser beam used to control the moving mirror is shown as a dashed line.*

4). Detectors

The modular design of the Midac AMS™ spectrometer enables different detectors to be used in the instrument. Exchanges of detector are easily carried out in the field. Low noise levels can be attained by using a low-noise detector; these are cooled to prevent any radiation generated by the detector from interfering with that coming from the sample. I used a liquid-nitrogen-cooled Hg-Cd-Te (MCT) detector, reported by Hanst & Hanst (1994) to produce low noise levels of <0.0001 absorbance units. MCT detectors produce a noise level that is up to 100 times less than detectors which operate at ambient temperatures; such as deuterated triglycerine sulphate (DTGS) detectors (Hanst & Hanst, 1994). In the future it may be possible to cool the detector using a Stirling-cycle cryocooler, which

operates in a similar fashion to a refrigerator. At present, however, these units are too big and heavy to be used in a portable FTIR system.

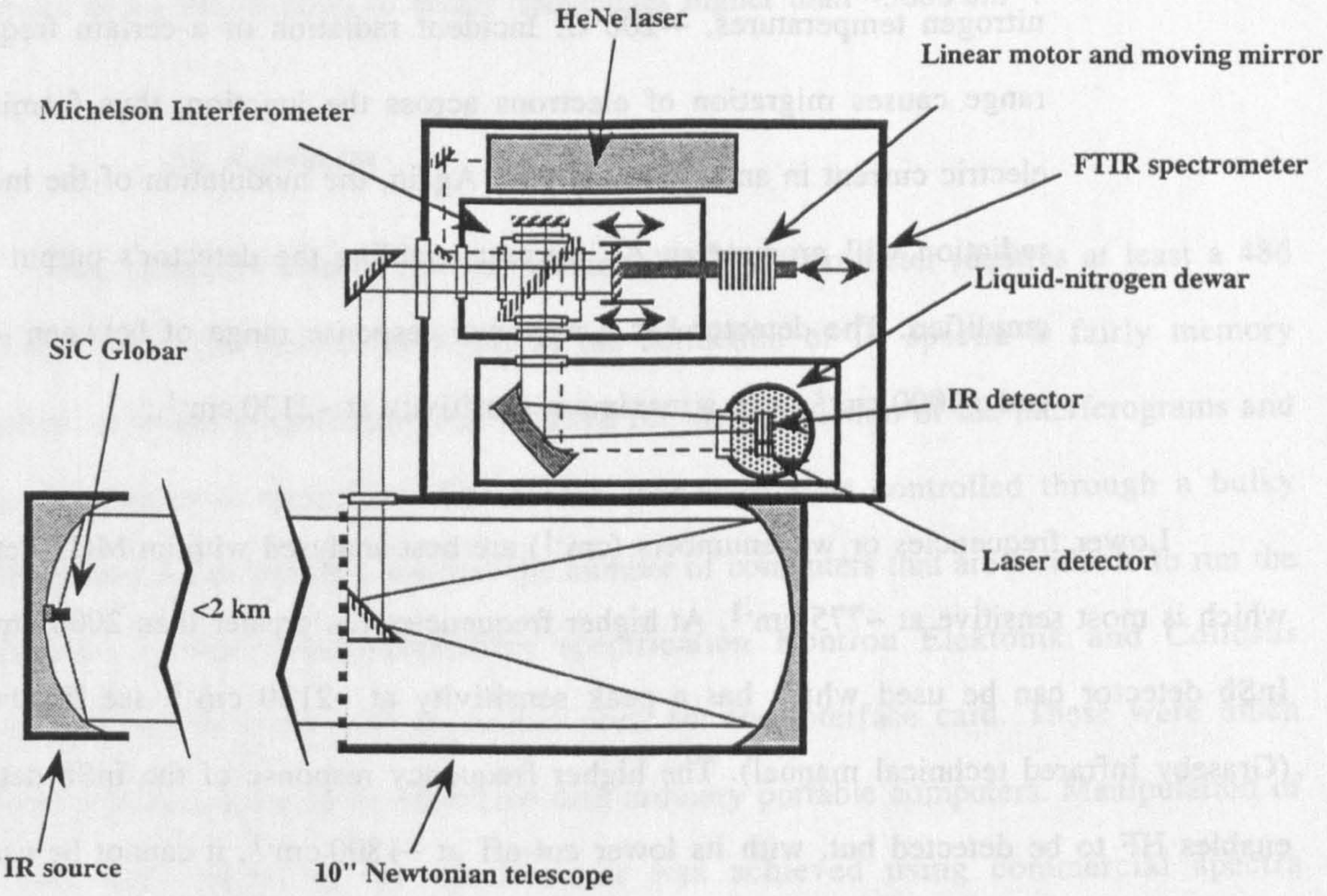

***Figure 2.6**. Schematic diagram illustrating the optical path through a Midac FTIR spectrometer used in a bistatic set-up. The modular design of the system can also be seen (after Schiff, 1992). Included in the figure are the laser and the linear motor for the moving mirror within the Michelson interferometer.*

The individual construction of the IR detector depends on its type. The MCT and InSb detectors I have used in this thesis are cooled by liquid nitrogen. Here the detector is housed within a liquid-nitrogen filled vacuum dewar with a ZnSe window. The particulars of the MCT and InSb detectors are summarised as follows (Graseby Infrared technical manual):

- The Hg-Cd-Te (MCT) detector is a 1 mm^2 photoconductive diode; the resistivity of which decreases when IR radiation within a certain frequency range is incident upon it. This causes a change in the voltage across the detector when a constant current is passed through it. Modulation of the incident radiation produces an AC current enabling the detector's output to

be amplified. The detector has a response range of between ~600 and >5000 cm^{-1}, with a maximum sensitivity at ~775 cm^{-1}.

- The InSb detector is a semiconductor, with a P-N junction, at liquid-nitrogen temperatures, ~-200°C. Incident radiation of a certain frequency range causes migration of electrons across the junction, thus forming an electric current in an external circuit. Again, the modulation of the incident radiation will produce an AC current enabling the detector's output to be amplified. The detector has a narrower response range of between ~1800 and >5000 cm^{-1}, with a maximum sensitivity at ~2130 cm^{-1}.

Lower frequencies or wavenumbers (cm^{-1}) are best analysed with an MCT detector which is most sensitive at ~775 cm^{-1}. At higher frequencies i.e. greater than 2000 cm^{-1} an InSb detector can be used which has a peak sensitivity at ~2130 cm^{-1}, see **figure 2.7** (Graseby Infrared technical manual). The higher frequency response of the InSb detector enables HF to be detected but, with its lower cut-off at ~1800 cm^{-1}, it cannot be used to analyse any analyte in the 1400 cm^{-1} to 1800 cm^{-1} atmospheric window.

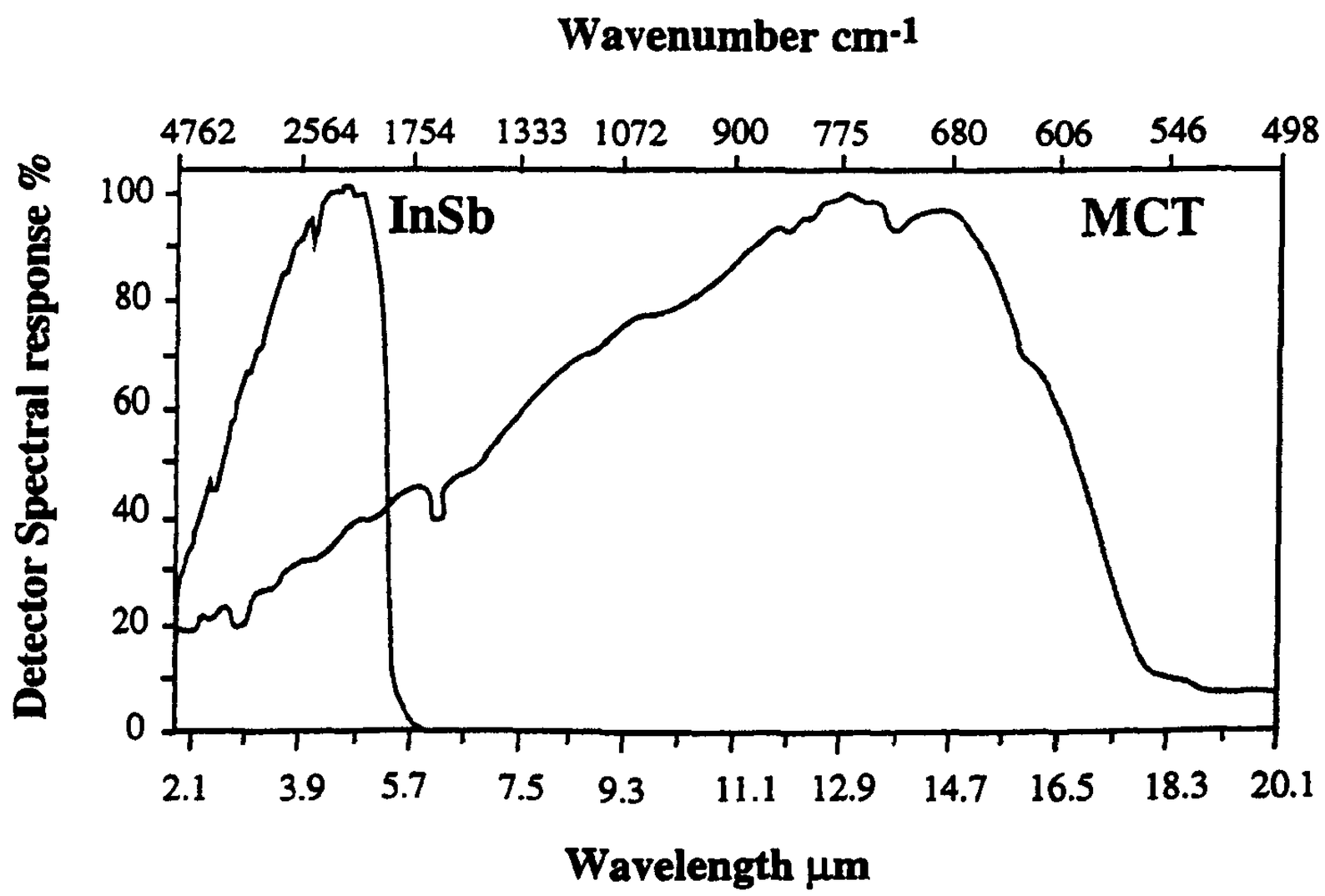

Figure 2.7. *The varying responses of the MCT and InSb detectors with wavelength/ wavenumber (Graseby Infrared technical manual).*

It is in this region that volatile organic carbon compounds, nitrogen and sulphur oxides and other heavier analytes are found. The MCT detector has its peak sensitivity in this area and therefore is much more suitable for measuring these analyte species; the only drawback being the inability to detect frequencies higher than ~5000 cm^{-1}.

5). Computer

The computer used to run the Midac AMS™ spectrometer requires at least a 486 processor with ~16 Mbytes of RAM as the collection of IR spectra is fairly memory intensive. A maths co-processor was required for the calculation of the interferograms and other mathematical operations. The Midac spectrometer is controlled through a bulky interface card which severely restricts the number of computers that are available to run the instrument. I used industrial/military specification Kontron Elektonik and Collosus Computers, which come with expansion ports for the interface card. These were much heavier, bulkier and far more expensive than ordinary portable computers. Manipulation of the data and control of the spectrometer was achieved using commercial spectra manipulation packages. In this thesis I used the DOS-based SpectraCalc™ (Galactic Software Inc.) and Windows 3.11-based Spectacle™ (LabControl GmbH).

2.2.4 Instrumental set-up and usage

System specifications

FTIR spectroscope	11.3 kg
Telescope	13.6 kg
Source	11.3 kg
2 Tripods	11 kg each
2 Car batteries	8 kg each
Portable computer.	4 kg
TOTAL	~78 kg

Table 2.3. *Equipment weights for Midac AMS™ OP-FTIR set-up (Midac technical brochure, 1992; Chaffin et al., 1995). This is a minimum weight. A portable generator, fuel, tools, and a liquid-nitrogen dewar all add to the overall weight of the set-up.*

The Midac OP-FTIR set up is one of the most portable that is commercially available; **table 2.3** lists the weights for the equipment needed to run the system in an active mode. Extra equipment can include spare car batteries and a 25 l liquid-nitrogen dewar, though a 2 l steel vacuum flask is normally sufficient for a day's analyses.

Field set-up

I have divided the Midac AMS™ system into two units:

- The IR source, one tripod and a battery - the "mobile unit".
- The spectrometer, telescope, a tripod, computer and liquid nitrogen - the "static unit", see **figure 2.8**.

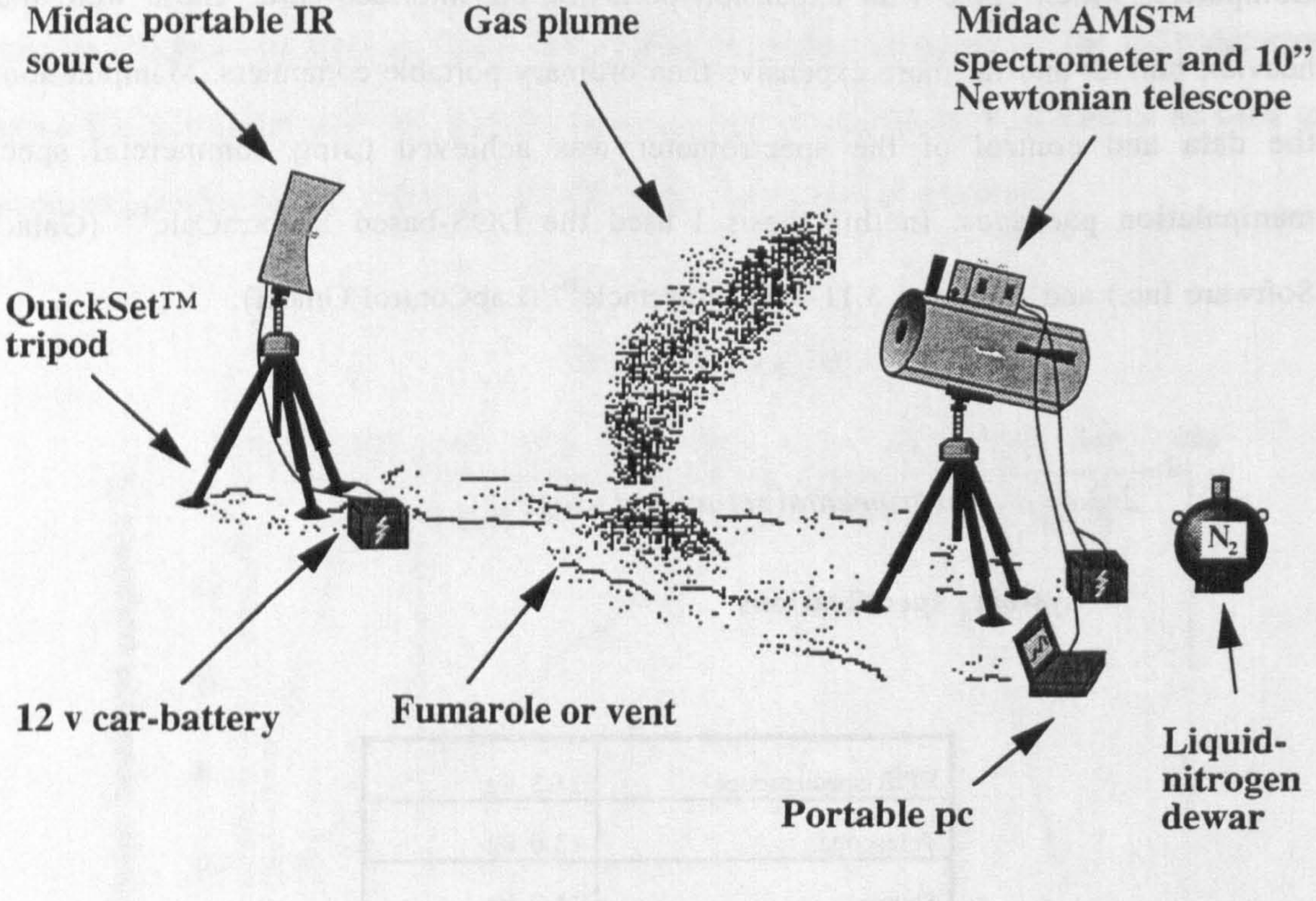

***Figure 2.8**. Schematic of the set up of the OP-FTIR system in the field. This shows the components of the mobile unit and the static unit.*

Transport of equipment in the field is best accomplished using a van, or large four-wheel-drive vehicle as the equipment is bulky; for less accessible areas the equipment can be heliported to the required site. Once the static unit with the spectrometer is in place, the

mobile unit can be manhandled around the volcano to obtain the best position which is still in line-of-sight of the static unit.

Instrument positioning

The location of the spectrometer has to take into account the site's accessibility, how exposed to wind and ash it is and whether or not it is in the plume. The quality of the data collected depends strongly on the length of the optical path and the amount of plume incorporated within it. Once the spectrometer is set-up (normally on the downwind side of the vent or fumarole, although this may depend on the terrain) a good site for the IR source can be found. This is normally located closest to the vent or fumarole as the unit is more portable and is less sensitive to corrosion.

The IR source and spectrometer both have a rifle-sight which is used to locate the other unit. The alignment of each can then be fine-tuned by using the calibration facility, built into the computer package used for controlling the spectrometer, whilst alternately adjusting the orientations of the IR source and spectrometer until the best signal from the IR source is detected. This is aided greatly by the use of two-way radios. The calibration facility displays a rapidly acquired and constantly updated interferogram; changing the instrument's alignment alters the interferogram's peak height. At extended distances the low peak height, relating to low amounts of IR radiation detected, can be increased by changing the manual gain on the detector within the spectrometer. This is a fiddly operation at the best of times and can be detrimental to the instrument if conducted in the wet or during periods of ash-fall. The correct alignment of the detector and telescope is extremely important. At distances above a few hundred metres, even a fraction of a degree can make the difference between the radiation from the IR source being detected or missed completely. This is achieved by using the calibration feature as above. It is important to try and locate the detector in a sheltered position away from strong winds as these can cause slight alterations in the instrument's alignment during data collection, reducing data quality. Occasionally, if very windy, it may be necessary to tie-down the lighter and more bulky IR source as this is usually located in a more exposed position.

Passive analyses

Passive analyses do not require the use of an artificial IR source, naturally occurring hot ground being used instead and so are slightly simpler to conduct. This is also a preferred set-up if the target area is in a dangerous location. As discussed previously, and in future chapters, the temperature of the natural source used directly affects the quality of the data collected. I have earlier estimated that, for high quality analyses of SO_2 and HCl, ground temperatures should ideally be >500°C. I have indicated the ranges of temperatures experienced from different natural volcanic IR sources in **table 2.4**, based on personal observations and reported measurements. Optimal thermal conditions for passive OP-FTIR analyses would exist if the IR source was incandescent or very fresh lava. Surfaces with visible condensates, sulphur or anhydrite, indicate a lower temperature surface which would give poorer quality data if used as an IR source. The size of the IR source has been shown from active analyses to be less important than the temperature. I used a 20" (50.8 cm) diameter 1275°C IR source on La Fossa di Vulcano; this filled <1% of the telescope's field of view but still provided high quality analyses, see Chapter 4.

Visual appearance	Approximate temperature range (°C)
Warm fumarolic ground (Stromboli)	~35 - 65°C
Black ash/scoria at midday (Etna)	~45 - 70°C
Fumarole field with white sublimates (possibly $CaSO_4$)	<100°C
Fumarole with yellow sulphurous sublimate	≤112 - 140°C (Sharp, 1986)
Fumarole with black sulphur	~160 - 400°C (Sharp, 1986)
Fumaroles with no apparent sublimates	>450°C
Active andesitic dome (Soufrière Hills volcano)	~100 - >800°C (Donelly, 1996)
Cooling Pahoehoe lobe < 6 hrs old (Kilauea)	100 - 400°C (Harris, pers. com.)
Active Pahoehoe lobe (Kilauea)	≥900 (Harris, pers. com)
Incandescent vent (Stromboli volcano, 19/9/94)	~930°C (Harris et al., 1996)
Active lava lake or channel (Hawaiian)	~500 - 1150°C (Flynn et al., 1993)

Table 2.4. *The relationship between the visual appearance and the approximate temperature of natural IR sources found in volcanic areas; based on the author's and other's temperature measurements.*

Passive solar analyses

Love et al. (1997) conducted passive OP-FTIR analyses, using a solar IR source, during February 1997 as part of investigations into the gas plume from Popocatepetl, Mexico. At the time, explosive eruptions had prevented any access to the summit areas for traditional gas and filter sampling. They were able to detect SO_2, HCl, HF, SiF_4 and H_2O, with the OP-FTIR located at ranges of ~5 - 10 km from the summit. A working-group based jointly at the Open and Cambridge Universities has also managed to acquire solar OP-FTIR data at Mt. Etna in 1997 and at Masaya volcano in 1998 (Burton & Horrocks, pers. com.).

The sun is an ample source of high frequency IR radiation; however its use poses several technical problems. The intensity of sunlight entering the telescope must be reduced; Burton & Horrocks (pers. com.) placed a metal mesh over the telescope, thus reducing the amount of sunlight. Problems I have encountered whilst obtaining solar spectra relate to the steep angle at which the instrument must be inclined. Too high an angle may cause the partial emptying of the liquid-nitrogen dewar and/or failure of the linear motor which drives the Michelson Interferometer. The speed of the linear motor is controlled by switches on the circuit-board; a slower speed will enable the instrument to work at the steeper angles required for solar spectroscopy.

Airborne investigations

I have carried out experimental trials in using the OP-FTIR spectrometer mounted in a helicopter at La Fossa di Vulcano and Soufrière Hills volcanoes with limited success (Oppenheimer et al., 1998). These experiments were to investigate the feasibility of passively monitoring gas compositions from the safety of the air. During these experiments the spectrometer was either mounted on the telescope or pointed, without the telescope, at areas which appeared to be hot. Whilst mounted in a helicopter there is little or no fine control over the precise direction that the instrument is pointing in making target selection

very arbitrary and dependent on the actions of the helicopter pilot. So far no high quality data have been collected using airborne measurements, all the spectra collected having very low signal-to-noise ratios. This is due to the inability to keep the spectrometer pointed at a sufficiently hot (>500°C) IR source, either because the area being targeted was too cool or the movement of the helicopter prevented the instrument being trained on the selected target.

Effects of climatic extremes

The Midac AMS™ was taken to Ross Island, Antarctica, by a working party based jointly at the Open University and the New Mexico Institute of Mining and Technology with the aim of studying the gas emissions from Mt. Erebus. Gas analyses were conducted at an altitude of ~10,000 - 12,000 feet (3 - 3.5 km) a.s.l. during the austral summer. The temperatures experienced by the equipment ranged from ~+10°C in the hut at the field camp down to -25°C close to the rim of the crater. The low temperatures caused the metal casing to contract, thus shifting the optical alignment of the internal mirrors. This resulted in the almost total loss of any IR signal reaching the detector, which had to be corrected by the use of two adjusting screws which controlled the focusing of the IR radiation into the interferometer.

The extremely low temperatures had a more severe affect on the Kontron portable computer used to control the spectrometer and store the data. Even when insulated from the cold and heated with a number of portable hand-warmers, the metal-skinned computer could not withstand the low temperatures and shut itself off. When it was working, the extremely bright conditions made it very difficult, to read the LCD screen except when shaded by black polythene bags. For our main set-up on Mt. Erebus we positioned the portable IR source on the crater rim, locating the more bulky spectrometer ~100 m down the flank of the summit cone. The very bright sky background prevented the orange glow from the IR source being seen by the operator, greatly hindering the initial aiming of the telescope and spectrometer.

The extreme altitude and low temperatures greatly reduced the efficiency of the 12V car batteries and portable generator used to power the IR source, spectrometer and computer. Battery lives were reduced to <2 hours and problems with fuel mixtures meant that generators kept stalling. The combination of all these factors meant that a great deal of time was spent setting up and preparing the OP-FTIR system prior to being able to collect data. Eventually the extreme temperatures prevented the computer operating, and in the process of recovering the equipment the hard drive was damaged beyond repair. The initial design specification of the Midac spectrometer was for it to be laboratory-based. The Midac AMS™ still has a bench-top architecture - including a bulky spectrometer-computer interface card which fits in bench-top computers but not in standard portable models. The breakdown of the only Midac-compatible portable computer in Antarctica therefore meant the effective ending of OP-FTIR data collection programme.

Future work in such harsh conditions would require the use of a much more robust computer, preferably thermally insulated or internally heated, along with a more reliable source of power for the equipment. Problems with reading the computer screen can be overcome simply by shading the screen with a heavy black cloth or similar. Once the system can be operated easily with some degree of reliability, problems associated with aiming the equipment and the collection of data can be addressed.

2.2.5 Processing of OP-FTIR data

I used commercial spectra manipulation packages: SpectraCalc™ (Galactic Software Inc.); and Spectacle™ (LabControl GmbH) to carry out spectra acquisition and processing. Background spectra were chosen by determining which single-beam spectrum had the lowest volcanic signature - represented by the presence of SO_2. For data collected at Soufrière Hills I used the spectrum with lowest HCl as a background as SO_2 was generally below the limits of detection for all data collected.

I determined the analyte concentrations manually by subtracting, point for point, a laboratory reference spectrum, multiplied by a scaling factor F, from the sample

absorbance spectrum. When I could see neither a positive or negative peak due to the analyte I deemed the sample to contain the reference gas concentration × the scaling factor F, in ppmv.m. The precise amount of analyte removed is however very subjective; and tends to rely on the amount of spectral noise and resolution of the monitor; although in tests I carried out, it proved more accurate than the in-built computer programme. Difficulties with the process occur if the spectra are shifted, normally ±0.5 cm^{-1}, due to perturbations in the optics. Problems can also occur when the resolution of the data, converted to ~0.24113 cm^{-1} by the Spectacle™ programme, does not match that of the reference spectrum, ~0.24107 cm^{-1}. The mismatching of the resolution and spacing of data points between sample and reference cause difficulty for determination of concentrations of analytes with fundamental absorbances composed of an array of narrow peaks, e.g. HCl and HF. This is due to "spiking" of the data during the subtraction process.

The main difficulty in manually processing spectral data results from the very low signal-to-noise ratios encountered; commonly below 5:1; defined as the ratio of analyte peak height to the noise trough-to-peak height. At low ratios, I encountered difficulty in identifying fundamental peaks and estimating when they had been fully subtracted. This, and the shape of the absorbance peak, were the main constraints on the detection limits of the analytes; generally <10 ppmv.m, see later chapters.

2.2.6 Sources of error in OP-FTIR spectroscopy

I have reported the results of OP-FTIR studies in this thesis mainly as average gas ratios, rather than as gas concentrations. This is due to the uncertainty involved in atmospheric dilution of the plume and the amount of plume contained in the optical path. The average gas ratios derived from the collected data were an average of between 10 and 160 individual ratios. Gas concentrations cannot be used due to the dilution of gas by the atmosphere as it mixes and uncertainties in the length of the optical path.

Errors in OP-FTIR can occur due to a variety of factors; this section will discuss the main errors and their causes, and attempt to quantify them. This has been difficult because

it is almost impossible to differentiate between natural variation and the combined effects of instrumental and data processing errors.

Error versus natural processes and variations

I conducted OP-FTIR analyses at Soufrière Hills, La Fossa di Vulcano and Mt. Etna volcanoes, and noted that the variation in gas ratios could be partially attributed to natural processes. These include the scavenging of analytes by solution/oxidation processes in clouds and oxidation/aerosol formation within the plume. Other causes of variation may be the incorporation of gases with different compositions from different fumaroles/vents, depending on the wind direction, or gas puffing and magma convection processes. These are discussed in the relevant chapters. Whilst all are natural processes which tell us about the evolution of gases, both within the volcano and once they have entered the atmosphere, they can all give rise to significant variations in the gas ratios detected. The contributions of each individual process to the final gas ratio can only be estimated, unless significant variation can be directly attributable to an observed change in volcanic activity or the weather.

Total variation in data

Any variations in gas ratio will detract from the true average. I have calculated 1σ standard deviations for the gas ratios I derived from analyses at Mt. Etna and La Fossa di Vulcano; these are ~17 - 21% of the average values. This "error" reflects the combination of all types of error and natural variation. Although these variations are responsible for increasing the range of values about the average, they can be used to elucidate the processes governing volatile degassing and, as such, are in themselves a useful source of information.

Problems associated with non-zero backgrounds

The single-beam background spectra I have used for deriving absorbance spectra may contain low levels of analyte gases which can ultimately affect the values of any gas ratios determined. I have attempted to quantify the levels of analytes in the background spectra by comparing them with instrumental blanks collected by Chaffin (pers. com.) using laboratory air or nitrogen blanks. By creating absorbance spectra using the nitrogen blank as background it was possible to estimate the SO_2 concentrations within the background spectra. The difference in the optical configurations of the spectrometer and path lengths whilst collecting blanks in the laboratory and sample spectra in the field resulted in the derived absorbance spectrum having large amounts of spectral noise. This introduced large errors into my estimation of background HCl and SO_2 concentration, approximately <15 and <40 ppmv.m respectively. This is equivalent to an error in the average measured SO_2 and HCl path-averaged concentrations of ~8 - 27% and 5 - 12% respectively for data collected at La Fossa di Vulcano and Mt. Etna.

Instrumental and data processing errors

As stated previously, I have not been able to quantify the magnitude of the instrumental errors. The Midac Corporation, who manufactured the spectrometer used by the author, suggest that instrumental errors are <0.5% and due mainly to the misalignment of optics within the spectrometer. Some of the errors discussed above are, as yet, unquantifiable due to lack of data. By using a long-path calibration cell it should be possible to compare known analyte concentrations with those determined by the Midac Corporation. Only then will some of instrumental errors be quantified with any accuracy. Calibration of the Midac spectrometer by the Open and Cambridge Universities working-group is scheduled for later in 1998 to determine the errors involved with optical misalignment and the differences between the InSb and MCT detectors used. Once instrumental and data processing errors are accurately quantified it should be possible to determine the actual magnitude of the natural variation in gas ratios.

Errors and loss of data during collection can occur if the gain on the detector, set manually, is incorrect. A measure of the signal intensity is the signal "peak-to-peak" value (PP%), displayed during signal calibration, which ranges between 0% and 100%. Optimum PP% values are ~70% - 90% and relate directly to the intensity of radiation detected. Too low a gain results in a low PP% value and a poor SNR with consequent loss of data. Too high a gain can result in the PP% reaching 100% causing detector saturation and clipping of the interferogram collected, resulting in severe data loss.

I experienced difficulties in manually subtracting the laboratory reference spectrum from the sample spectra if the these has been shifted, normally $\pm$ <0.5 cm^{-1}, due to perturbations in the optics. For data collected at Montserrat, the resolution of the data, converted to ~0.24107 cm^{-1} by the computer, did not match that of the reference spectra. The mismatching of the resolution and spacing of data points between sample and analyte reference spectra can also cause difficulty in the determination of concentrations of analytes with fundamental absorbances composed of an array of narrow peaks, e.g. HCl and HF. On subtraction of the reference spectrum, the mismatch between the position of sample and reference data points, normally <0.5 cm^{-1}, results in only half of the width of analyte peak being fully subtracted. This can, to some extent, be overcome by spectrally shifting the data.

I estimated a Standard Error, $\left(\frac{\sqrt{\sigma}}{(n-1)}\right)$, for the spectral manipulation by reanalysing the same sample spectrum 10 times. To see how errors varied with analyte concentration, and therefore signal-to-noise ratio (SNR), I analysed spectra with high, medium, and low analyte concentrations, see **table 2.5**. The results indicate that processing errors are

Relative analyte concentration	HCl Standard error % (n=10)	HCl SNR	SO_2 Standard error % (n=10)	SiF_4 Standard error %	SiF_4 SNR
High	**2.3**	22	**0.6**	**1.2** (n=10)	3.7
Medium	**1.0**	9.4	**0.9**	**57** (n=7)	0.4
Low	**3.5**	1.5	**3.3**	**45** (n=3)	<0.4

Table 2.5. *Showing standard errors,* $\left(\frac{\sqrt{\sigma}}{(n-1)}\right)$, *for manual analysis of active spectra conducted by the author for* SO_2, *HCl and* SiF_4 *fundamental absorbance peaks with differing SNRs. Errors are the variation determined from the repeated reanalysis of individual spectra.*

dependent on the shape of the analyte's fundamental peak and the SNR and range from <1% for high concentrations of HCl (sharp peaks) to >45% for very low levels of SiF_4 (smooth broad peak). In general, data processing errors were found to be in the range ~1 - 4% for spectra with reasonable SNR.

Summary of errors

Quantification of the errors associated with OP-FTIR has been difficult. Several natural processes cause variation in the data, including: gas mixing; puffing; scavenging; and aerosol formation. These are all of interest as they provide information on the processes within the magma chamber and the volcanic plume. Unfortunately it is not always possible to identify and separate the variations due to these processes from the errors due to instrumental and data processing. Data processing errors can be done by repeated analyses of spectra to determine the error on the derived values. The values for instrumental error tend to manifest themselves as noise within the spectra, thus contributing to processing errors; here I have used Midac Corporation's error values as the spectrometer used by the author has yet to be independently calibrated. The combined errors are summarised in **table 2.6**.

Error source	Minimum error %	Maximum error %	Mean error %
Non-zero Background	5	27	16
Instrumental (estimate)	0.5	0.5	0.5
#Data Processing	1	3.5	2.3
Total Error % (RMS)	**5**	**27**	**16**

Table 2.6 *Error values for OP-FTIR spectroscopy conducted by the author using a Midac AMS™ FTIR system.* $RMS = \sqrt{\left(\frac{\Sigma(error^2)}{N^o \text{ of errors}}\right)}$. *#Data Processing based on errors associated with calculating HCl and* SO_2.

2.2.7 *Summary of OP-FTIR technique*

OP-FTIR is a remote technique that utilises the characteristic frequencies of absorbance in the infra-red exhibited by many gas species. Using either natural (hot rocks), or artificial (IR lamp) sources of IR radiation, the spectrometer can detect a wide variety of gases in the line-of-sight optical path between itself and the IR source. Gases detected on volcanoes by OP-FTIR include: H_2O, SO_2, HCl, HF, CO_2, SiF_4, N_2O and CO. For lighter molecules to be detected, IR radiation must be of a higher frequency than is required for heavy molecules; necessitating using a hotter IR source, in accordance with Planck's Law. Other factors, such as background spectral noise, peak-shape and the analyte's absorptivity all contribute to the detectability of an analyte. Gas ratios, being independent of the level of atmospheric dilution, were used instead of gas concentrations. Analyses in this thesis were conducted at ranges of <2 km. At such distances atmospheric processes, solution, oxidation and aerosol formation, may play a significant role in determining how close to the original exsolved gas composition the measured plume is.

2.3 Correlation Spectroscopy (COSPEC)

The Correlation Spectrometer (COSPEC) has been used since 1971 for research on volcanic SO_2 fluxes. The instrument was originally developed by Barringer Research, Canada, for environmental ozone and SO_2 monitoring and was first used on volcanoes in 1971 at Mount Mihara, Japan (Stoiber et al., 1983). Since then many active volcanoes have had their SO_2 flux measured by COSPEC including Mt. Etna where the technique was first used in 1975 (Haulet et al., 1977).

The ultimate aim of COSPEC analyses is to determine the SO_2 flux - a measure of the gas productivity of the volcano. This relates to the level of volcanic activity, the magmatic volatile composition, and style of degassing, i.e. deep or shallow, see Chapter 5. COSPEC can therefore be used as a premonitory tool to detect changes in the state of volcanic activity and possibly predict volcanic eruptions.

The system is compact and durable and capable of being used statically or from a vehicle, aircraft or boat (Stoiber et al., 1983). It has several advantages over more sophisticated systems: it is relatively portable and simple to use; it utilises the sun as a natural source of UV radiation; it does not require precise pointing; and it can operate even through overcast skies. However, as discussed later, the high level of error involved in the final values means that the technique may in some circumstances only be semi-quantitative. In the following sections I will describe the technique as pertaining to my use of it on Montserrat in 1996.

2.3.1 COSPEC instrumentation

COSPEC determines the amount of SO_2 in the optical path. This is usually a vertical air column situated between the detector and direct and indirect UV light sources; mainly sun, clouds and light-scattering particles. It is the specific absorbance of UV radiation with wavelengths of 300 - 316 nm by SO_2 that is detected by the instrument (Millán, 1985). Selective absorption by UV active analytes attenuates particular frequencies which can be

detected by the instrument, in a similar manner to the detection of fundamental absorbances in the IR part of the spectrum. To be UV active, compounds need to possess a delocalised electron, such as in double or triple molecular π-bonds, i.e.: N=O, S=O, C=C or C≡C, such as SO_x and NO_x (Solomons, 1976).

The COSPEC consists of four parts: peripheral optics; diffraction grating and correlator disk; calibration cells and instrument electronics, see **figure 2.9**. Solar radiation passes through the gas plume and is gathered by a Cassegrain-type telescope and focused into the instrument (Malinconico, 1979). The telescope's field of view is 23 mrad by 7 mrad and, by using a right-angled extension, UV radiation can be captured from vertically above the instrument when using a vehicle.

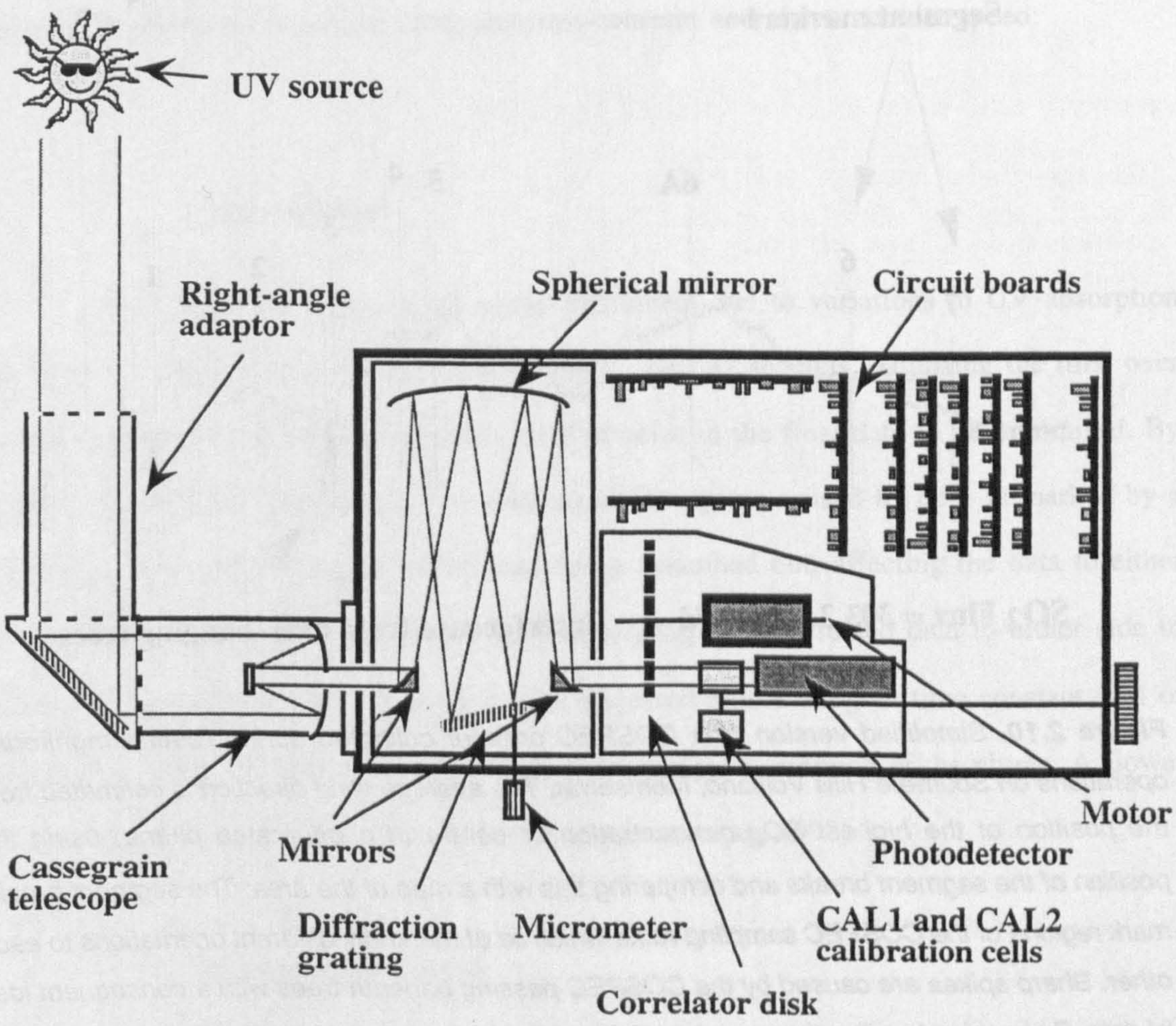

Figure 2.9 *Schematic of the inside of a COSPEC taken from photographs by the author and after Stoiber et al. (1983).*

Once inside the instrument, the light is focused on to a diffraction grating, the position of which is controlled by a micrometer, which separates the beam into individual wavelengths. These are then focused onto a rotating correlator disc in which slits have been etched to allow the passage of specific sets of UV radiation which correspond to peaks and troughs in the SO_2 absorption band between ~300 and 316 nm (Millán & Hoff, 1978). The modulated radiation passing through the correlator disc is converted into two voltages by a photomultiplier tube and processed by the instrument's electronics. As the level of atmospheric SO_2 increases so the ~300 nm radiation detected decreases causing a change in the voltage ratio which is proportional to the amount of SO_2 present.

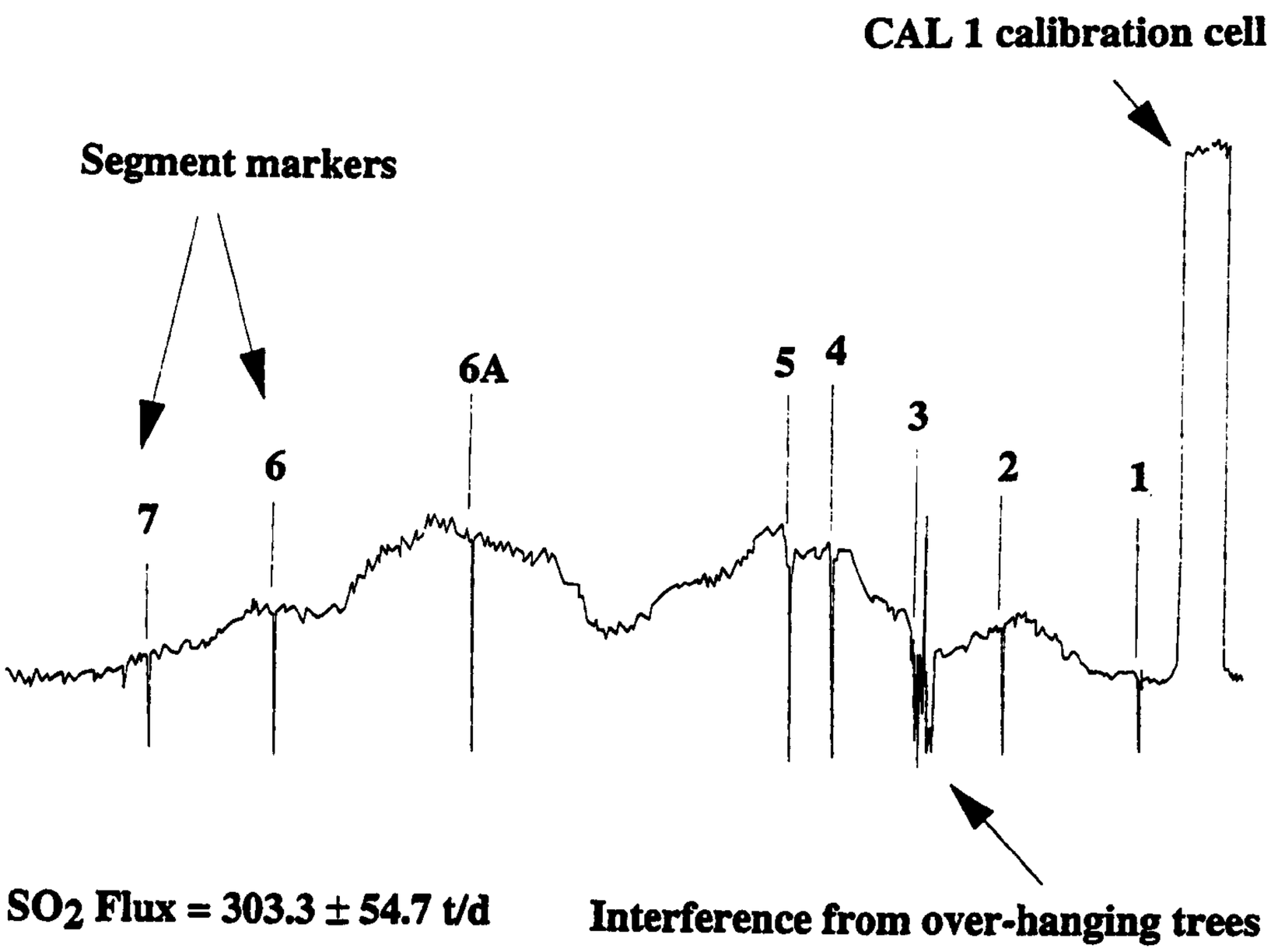

Figure 2.10. *Simplified version of a COSPEC printout collected during routine monitoring operations on Soufrière Hills Volcano, Montserrat. The average wind direction is estimated from the position of the highest SO_2 concentration or centre of a bifurcated plume, using the position of the segment breaks and comparing this with a map of the area. The segment breaks mark regions of the COSPEC sampling route which lie at markedly different orientations to each other. Sharp spikes are caused by the COSPEC passing beneath trees with a consequent loss of data. By keeping to a low time constant these spikes are sharp and can be simply interpolated across if the data is recorded using a chart-recorder.*

Calibration of the instrument is achieved by placing one of two internal gas calibration cells, with known concentrations of SO_2, into the instrument's optical path when this is directed away from the volcanic plume into clean air. For the particular instrument I used on Montserrat, the calibration concentrations, CAL1 and CAL2, were: 339.2 ppm.m and 64 ppm.m respectively, see Section 6.2. The output of the COSPEC is a voltage proportional to the concentration of SO_2 in the optical path. This is recorded either on a simple chart recorder or, by using an analogue to digital converter, inputted directly into a computer. The sensitive electronics within the instrument require a short period of warming-up, ~30 min; this can simply be done whilst moving the instrument from the field base to the sampling site.

There are several controls that can be used to adjust the input and output of the instrument; the most important being the time-constant and chart-recorder speed:

Time constant

The voltage ratios produced in the instrument due to variations in UV absorption by SO_2 are averaged over a set period of time - 1 to 32 seconds. Adjusting the time over which voltages are averaged allows the level of noise in the final data to be minimised. By using a shorter time period, e.g. 1 second, signal disruption caused by trees is marked by a strong, narrow, negative spike rather than being smoothed out, affecting the data to either side. This spike can then be ignored by interpolating the unaffected data to either side to fill in the gap, see **figure 2.10**. With a more dispersed plume a higher time constant (~ 4 or 8 sec.) may be used to increase the SNR to allow adequate sampling of the plume. A slower vehicle or scan speed is also required (Williams-Jones et al., 1998).

Chart-recorder speed

The rate at which the paper moves through the chart recorder can be set at a variety of speeds. The speed selected by the operator is dependent on the duration of a single traverse. For traverses at slow speeds, i.e. ~20 km/h, and ~30 min duration, chart speeds of

2 cm/min are optimal. For longer or more time consuming traverses a slower chart speed should be used; conversely for aerial traverses chart speeds of >6 cm/min should be used (Williams-Jones et al., 1998). For the purposes of data processing, any COSPEC print-out should really be no longer than ~0.5 m in length; beyond this length only increases the probability of simple numerical errors and wastes processing time and chart paper.

2.3.2 Description of vehicular operating platform for COSPEC analyses

COSPEC analyses can be undertaken using static, airborne, boat and vehicular platforms. I will describe only the use of a vehicular platform, as I used this technique on Montserrat, see Chapter 6.

When using a vehicle for carrying out COSPEC analyses it is important that the instrument is fitted securely so that it remains in a fixed position. To raise the instrument so that the right-angled telescope can project out of the vehicle's window, the instrument can be positioned on a crate or sturdy box. The right-angled adapter for the Cassegrain telescope is adjusted so that it points vertically upwards, see **figure 2.11**.

***Figure 2.11**. Photographs taken by the author of a COSPEC IV, owned by the University of Montreal, in operation on the Isle of Montserrat as part of the Montserrat Volcano Observatory's (MVO) monitoring effort. The vertical orientation of the right-angled telescope is essential for high quality data collection.*

I connected the COSPEC and chart recorder, which both utilise a ~12V supply, directly to the vehicle's battery. Watson (pers. com.) used a Mini-COSPEC™ on Montserrat and reported that changes in temperatures affected the instrument's response; he rectified the problem by using a sun-shade in hot conditions. A vehicular traverse may take over 30 minutes to complete making it essential to calibrate the instrument both before and after each run as changes in sun angle and instrumental drift can cause a shift in the baseline equivalent to >10 ppm.m SO_2. It is essential that the instrument is calibrated outside the SO_2 plume which may be wider than the visible plume (Stoiber et al., 1983) otherwise anomalous results may result in the analysis being of little use.

The SO_2 content of the plume is analysed by driving in a traverse beneath the plume in a direction as orthogonal to the wind direction as possible. The roads used in such traverses are rarely straight or lying in the required direction; the route is therefore divided into a series of sections, each with a known length and orientation. I estimated the wind direction from the plotted COSPEC data by assuming the highest measured SO_2 concentration is to be found directly downwind of the vent (Delmelle, pers. com.). On the occasions when I measured a bifurcated plume I assumed the average wind direction lay midway between the two maxima. The lengths and orientations of each section are corrected to give an orthogonal equivalent by using the sine of the angle that the segment makes with the wind direction. The choice of roads used for COSPEC analyses must take into consideration several factors, these include: the windiness of the road; the number of overhanging trees and bridges; as well as the steepness of the road and its camber; and the speed and amount of traffic on it. As previously discussed the windiness of the road can be corrected by simple trigonometry.

Objects such as trees and bridges which over-hang the road interrupt the supply of UV radiation into the instrument causing negative peaks and data loss. It is therefore necessary to find a route which is relatively free of trees. The steepness of the road affects the degree to which the right-angled telescope is out of vertical alignment. This has the most serious consequences when the sun is directly overhead as small movements of the vehicle cause the sun to directly enter the telescope, saturating the sensor and causing loss of data. Newer COSPEC models, COSPEC V and later, have an internal baffle in both the

telescope and spectrometer to reduce this problem which helps prolong the life of the photomultiplier tube. I had to suspended analyses using the COSPEC IV on Montserrat for the hour between 11:30 and 12:30 due to this problem. The high camber on some roads may also cause similar problems with the vehicle leaning towards the curb and therefore moving the telescope away from its vertical position.

In order to reduce noise and keep data collection consistent between different road sections it is necessary to drive at a constant speed. Faster vehicle speeds should be linked with an increased speed on the chart recorder to provide a reasonably sized print-out of the data.

2.3.3 Calculation of gas fluxes

Determination of gas fluxes

The instrument itself can only provide a direct measure of the total SO_2 in the air-column within the field of view, in ppm.m. In the case of a vehicle, boat or aerial traverse this is a vertical air-column. By traversing across the width of the plume it is possible to measure the total SO_2 within a vertical plane. In order the derive the flux it is necessary to know the speed at which the wind carries the gas through this plane. It is therefore essential that accurate wind speeds are determined if gas flux is to be of any real use.

Processing the data

Once the COSPEC data have been collected, they have to be processed; either manually, if data were collected using a chart recorder, or automatically, if data were collected using a computer. My use of the term "squares" in the following discussion relates to the squared paper used in most chart recorders - typically the squares used have sides of either 1 or 2 mm and make processing of the print-out far easier and more accurate. The following list summarises the calculations I had to use to convert the raw data from a chart recorder print-out into a flux value:

1). Measure the height of the calibration peak, CAL1. Divide CAL1 concentration by height to get SO_2 ppm.m per unit height (squares).

2). Count number of squares between base-line (background) and plume-trace for each segment. Count length of each segment and work out segment area and therefore average segment height in squares.

3). Work out average segment ppm.m by using (1) × (2).

4). Correct each segment for orientation to wind direction by using multiplication factor, f = sin (|wind° - road°|).

5). Estimate average wind speed from before-and-after measurements, see later.

6). Calculate flux by multiplying: (3) × (5) × actual length of each segment × a constant to convert units into t/d.

The main errors from the above calculations most likely relate to arithmetic errors which are trivial compared to the inaccuracies associated with estimating the wind speeds,.

Automation of data processing

The determination of a gas flux from data recorded by a chart recorder can be slow and laborious, taking up to 45 minutes per run. I developed a computer spreadsheet to reduce the amount of time taken to derive gas fluxes during the COSPEC monitoring campaign at Soufrière Hills Volcano, Montserrat, see **figure 2.12**. This was designed to minimise the amount of simple calculations required to derive a gas flux from the chart recorder print-out, thus saving time and reducing the chances of mistakes. The data required for the spreadsheet were:

AREA - the area beneath the printout for each road-segment, see Section 2.3.4

CAL1 - the start and finish peak heights for the calibration runs

SEG - the full or partial length of each road-segment

AZM - the wind direction, taken as location of maximum peak height on the traverse route

Wind CALC - the wind speed measurements taken before and after the COSPEC data was collected.

Montserrat Volcano Observatory COSPEC worksheet

Analysis Date 06/02/96 Run D

Step

1) Mark of individual segments and count number of squares in each segment between baseline and RED line.

Segment number	Area (squares)	Segment length (squares)
s -4 to -3		
s -3 to -2		
s-2 to -1		
s -1 to 0		
s 0 to 1	4.5	5
s 1 to 2	201	21.5
s 2 to 3	118	12.5
s 3 to 4	89.5	14
s 4 to 5	42.5	5
s 5 to 6a	53	19
s 6a to 6		
s 6 to 7		
s 7 to 8		
s 8 to 9		
s 9 to 10		
s 10 to 11		
s 11 to 12		
s 12 to 13		

2) Input the average height of calibration (CAL1) at start and end of run

Start CAL1	33.5
End CAL1	34

3) If plume does not coincide with start or end of plume calculate new segment

Sector	Normal distance	Corrected distance
s -4 to -3	150	150
s -3 to -2	420	420
s-2 to -1	280	280
s -1 to 0	410	410
s 0 to 1	450	128
s 1 to 2	560	560
s 2 to 3	380	380
s 3 to 4	380	380
s 4 to 5	180	180
s 5 to 6a	1180	533
s 6a to 6	760	760
s 6 to 7	480	480
s 7 to 8	840	840
s 8 to 9	440	440
s 9 to 10	450	450
s 10 to 11	200	200
s 11 to 12	840	840
s 12 to 13	400	400

4) Use maximum peak height to give plume azimuth or center if plume is split into two portions. Value in degrees from north (000).

Plume Azimuth 97 degrees

5) Input Windy Hills wind speed measurements after correcting for instrument error

Before COSPEC runs

Measurement	feet/minute
1	1083
2	1386
3	1406
4	1422
5	1223
6	1411
7	
8	
9	
10	

After COSPEC runs

1	1303
2	1227
3	1325
4	1355
5	1552
6	1270
7	
8	
9	
10	

SO2 flux (t/d)= 216.3 ± 19.7

Figure 2.12. *Part of the Montserrat Volcano Observatory spreadsheet used for calculating gas fluxes from raw COSPEC data. The section shown is the user interface requiring the input of the basic data: wind speeds and direction; calibration intensities; and segment lengths and areas.*

The terms: AREA, CAL1, SEG, AZM, Wind CALC, and ROAD, see below, refer to the various inputs needed. The errors associated with all these are discussed in Sections 2.3.4 and 6.2. The spreadsheet was designed to be only used on a selected route between two end-points. Application of the spreadsheet to a new route on the same or a different volcano would entail entering the actual length of the new road-segments (ROAD), taken from a map or from a vehicle odometer, and the average orientation of the road-segment into the spreadsheet.

Measurement of wind speeds

The accurate collection of wind speed data is fundamental to the determination of a gas flux; indeed it is the uncertainty in the wind speed that gives COSPEC its high error range, ~10 - >45%, see Section 2.3.4. Ideally, the wind speed should be measured at the same height as the volcanic plume. However, this may be inaccessible due to terrain and/or volcanic activity. Wind speeds are therefore often measured at some distance below the plume and thus are prone to variations induced by eddy currents and drag from the ground.

Because wind speeds generally increase with altitude, I measured wind speeds whilst on Montserrat from the highest point possible which was not in the wind-shadow of the volcano. This was done using a Davis ball-bearing wind flow-meter. It is important to be consistent in the manner that wind data is collected; i.e. from the same location with the same instrument and over a similar time period. I measured wind speeds before, half-way through and after the day's data collection so that any long-term change in the wind speed could be detected. Air turbulence and eddy currents cause gusts of wind so I collected multiple measurements and used the average value for the wind speed. On Montserrat I could compare my wind speeds with those measured at both the local airport and the one in nearby Antigua; which provided data for different altitudes allowing the difference between wind speeds at ground level and that of the plume to be estimated, see Chapter 6.

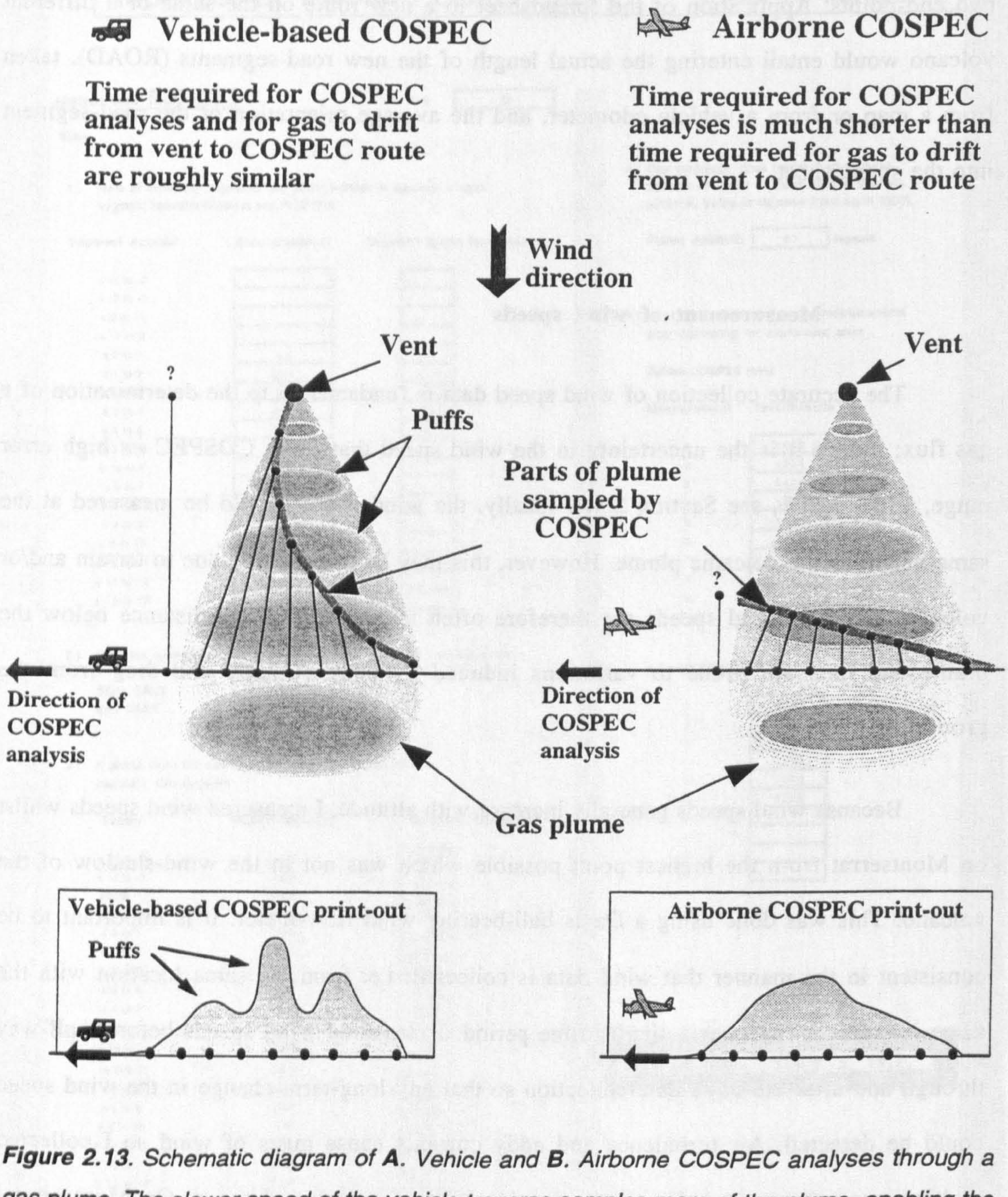

***Figure 2.13**. Schematic diagram of **A**. Vehicle and **B**. Airborne COSPEC analyses through a gas plume. The slower speed of the vehicle traverse samples more of the plume, enabling the temporal evolution of the plume to be elucidated. See text for discussion.*

The effects of plume drift and air turbulence

The speed of the COSPEC traverse beneath the plume in relation to its downwind-drift affects which parts of the plume are analysed. In **figure 2.13**, I have schematically illustrated two extreme situations:

A). Where plume drift is similar to the traverse speed, i.e. COSPEC from a slow-moving vehicle.

B). Where plume drift is negligible in relation to traverse speed, i.e. COSPEC from an aircraft

In **A**, the gases analysed towards the end of the traverse may not even have left the vent when the traverse began. Hence rather than simply sampling across the plume, a slow traverse speed samples obliquely along the plume, possibly through different levels of degassing, i.e. puffs. The resulting COSPEC-derived flux is therefore an average along the plume for a period of degassing equivalent to the duration of the traverse.

In **B**, the gases are analysed so rapidly that the plume may drift only a short distance during the traverse. Hence the plume is sampled across its width rather than along it. This will result in an almost "instantaneous" flux being derived by the COSPEC; without any considerations being given to short term fluctuations due to puffing. Successive traverses will therefore show variations in SO_2 flux due to puffing. This is evident from the airborne data of Allard et al. (1996) which shows variations between successive runs. They tested the effect of puffing on the measured gas flux by conducting several analysis runs along the line of the plume; these analyses showed sharp variations in flux consistent with puffing, see **figure 2.14**.

The speed of COSPEC traverse controls how much of the plume is analysed and whether real changes in flux may be detected. A slow traverse speed will give a better average of the gas flux and also highlight short-term variations. The effect of air turbulence will cause the gradual mixing of distinct portions of the plume, causing gradual homogenisation. Hence COSPEC traverses across the plume tend to show gradual changes,

rather than the sharp peaks due to puffing. The further from the vent, the greater the homogenisation and the less distinct individual puffs become, see **figure 2.14**.

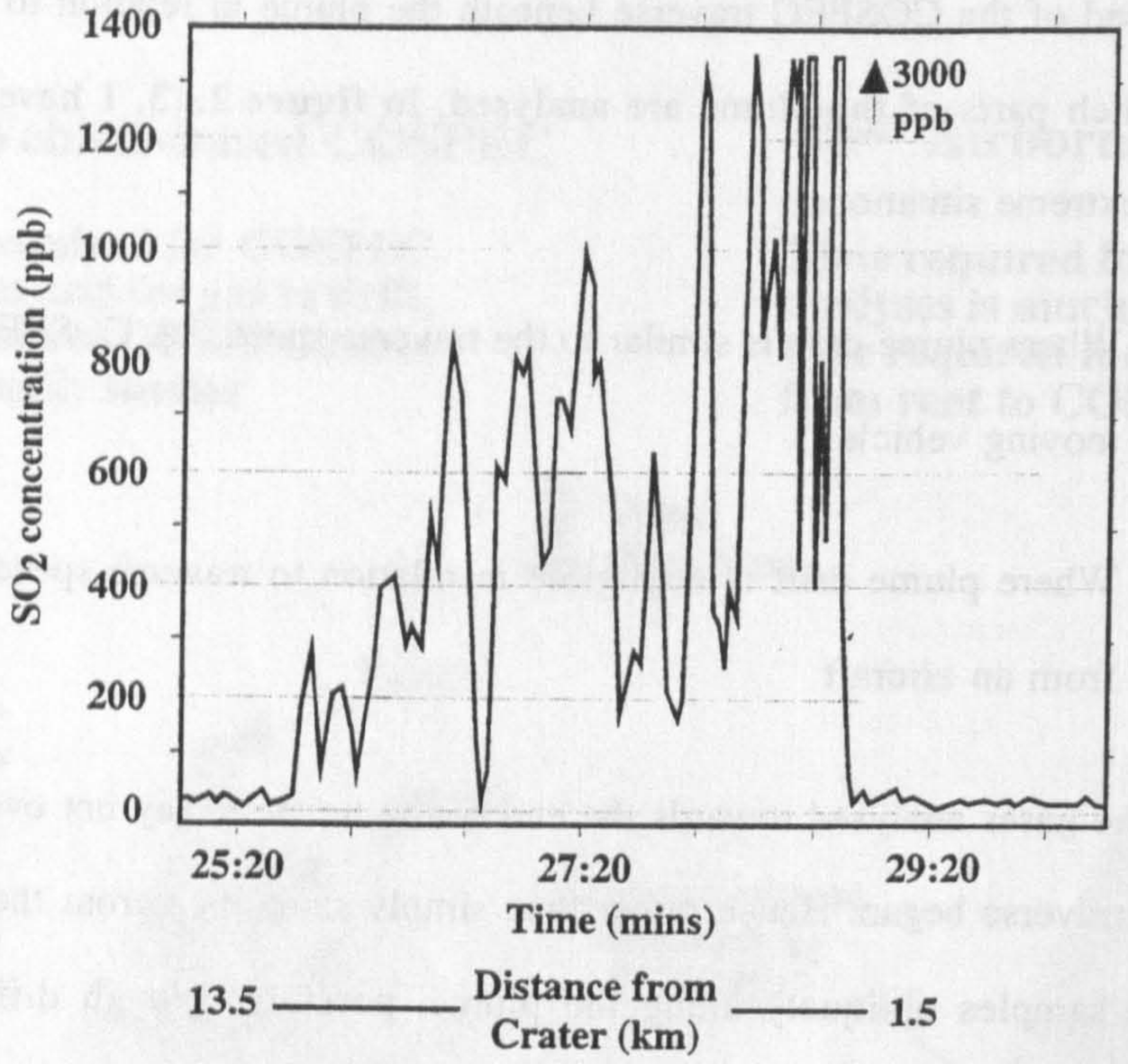

Figure 2.14. *Airborne COSPEC traverse along the length of the gas plume showing variations due to puffing (Allard et al., 1996). The gradual decrease in apparent flux is due to scavenging, see Chapters 5 and 6; whilst the progressive broadening of the peaks are due to the gradual homogenisation caused by air turbulence.*

2.3.4 Sources of COSPEC error

The calculation of an SO_2 flux using COSPEC is, in principle, a fairly simple procedure. The data required are the wind speed and the integrated absorbance of SO_2 across the plume. In this section I will have attempted to identify and quantify various errors that exist for COSPEC analyses, see **table 2.7** below. The errors are divided into three groups:

A). Data processing errors produced by a chart recorder.

B). Those associated with the instrument.

C). Those dependent on wind, clouds, and level of volcanic activity.

I have estimated the general ranges for error values associated with COSPEC analysis; these lie between ~8 and ~45%; depending on the weather conditions, see **table 2.7**. These errors relate to general COSPEC usage and are loosely based on work I carried out at Montserrat; see Chapter 6 for a more specific description of the errors associated with this work. Codes in parentheses i.e. (SEG) relate to individual errors reported in **table 2.7** and described below.

A - Data processing errors

These errors mainly concern the calculating of the integrated area beneath the plotted line produced by the chart recorder, used to record the output voltage of the COSPEC instrument. These are as follows:

- Errors relating to the accuracy of reading and counting the squares on the chart recorder print-out. I rounded these to the nearest $\frac{1}{2}$ square for each set of squares I counted. This relates to the recorded lengths of each road-segment (SEG); the area beneath the plotted line in each segment (AREA); and the peak height of the measured calibration peaks (CAL1).

- The wind direction (AZM), see **table 2.7**, is taken as being the orientation of the line from the degassing vent to the location within a road-segment, corresponding to the maximum SO_2 peak on the plotted chart; or midway between the two maxima if the plume is bifurcated. I estimated the uncertainty in transferring the position relating to wind direction from the chart print-out to a location map was approximately $\pm$ 2°.

- The actual lengths of each road segment (ROAD), see **table 2.7**, were measured using a combination of vehicle odometer and published 1:25,000 scale maps. I estimated the accuracy in determining these distances as ~$\pm$ 4%.

B - Instrumental errors

These may come from two sources: the COSPEC and the anemometer/wind flow-meter being used.

- Instrumental errors come from several sources. Instrumental drift due to temperature changes within the instrument; variations in the supply voltage; and vibrations of the operating platform which may affect the rotation of the correlator disc, can all contribute to small variations in the output voltage (INST). I have found no reference to the magnitude of this error and so I have assumed a maximum value of ~2% based on baseline drift (Millán & Hoff, 1977).

- Errors in the measurement of wind-speed (WINMES), see **table 2.7**, may be due to the errors in measuring the wind speed over a fixed time. On Montserrat I measured wind speeds using a wind flow-meter for 1 minute intervals; with the intervals being accurately timed to within ~1 s, or a ~2% variation in the averaged wind speed.

C - Natural errors

Natural errors are due to the obstruction of UV light entering the instrument caused either by solid objects, trees and buildings, or by diffuse objects, ash and vapour clouds. Other causes of error relates to the variation in wind, both at ground level and at altitude. These are described below.

- Interference caused by the instrument passing beneath trees and overhanging objects causes momentary data loss due to spiking. This though can be remedied by interpolating the unaffected data to either side.

- I measured wind speeds for COSPEC analyses before and after each series of runs on Montserrat. Collection of wind speed data was taken over several short periods and the average value taken as being representative. The variation in these wind-speed values and their relationship to the conditions immediately down-wind of the degassing vent are the main sources of error in COSPEC analyses. A further error inherent with measuring wind speeds is the effect that buildings, trees and the ground have on the wind speed. This error is highly variable due to convection and turbulence and is incorporated into the general variation in wind speed (WINVAR), see **table 2.7**.

- The difference in wind speeds as measured at ground level and at the altitude of the plume can cause the gas flux to be underestimated. This is due to the friction from the ground, vegetation and buildings acting to reduce wind speeds at ground level. I used the availability of wind-speed data at different altitudes on Montserrat to estimate an error for the variation of wind speeds with altitude (WINALT), see **table 2.7**. This error will, of course, vary substantially depending on location and altitudes of the vent and COSPEC instrument; on Montserrat I estimated it to be ~4%, see Chapter 6.

- Ash, clouds and condensation within the plume can also cause significant variations in the amount of SO_2 detected during traverses beneath the plume. The UV radiation collected and detected by the COSPEC comes from three sources: scattered solar radiation, scattered sky radiation, and radiation that has passed through the plume (Millán, 1980). The diffraction of each type of radiation is dependent on: the height of the sun above the horizon and thus also the instruments field of view relative to the horizon; the height of the plume; its thickness; and how close the detector is to the edge of it (Millán, 1980; Williams-Jones et al., 1998). Calculations by Millán (1980) have indicated that scattering effects will increase the

measured amount of SO_2 by ~10% in the centre of the plume, but will cause a similar decrease at the margins of the plume. The effects of ash, cloud and condensation will be to enhance diffraction which, if the detector is directly beneath the plume, can produce a further increase in the measured SO_2 of up to 30%.

Error type	Origin of Error	Variation/ Units	Best error %	Average error %	Worst error %
A	CAL 1	± 0.5 squares	1	2	2
A	AREA	± 0.5 squares	5	9	11
A	SEG	± 0.5 squares	2	3	4
A	AZM	± 2 degrees	1	1	1
A	ROAD	± 2 percent	2	3	5
B	INST	± 2 percent	2	2	2
B	WINMES	± 2 percent	1 *(M)*	2 *(M)*	2 *(M)*
C	WINVAR	variable	14 *(M)*	21 *(M)*	29 *(M)*
C	§WINALT (wind at 3000 ft)	variable	4 *(M)*	4 *(M)*	4 *(M)*
C	#Ash	variable	0	5	10
C	*Clouds	variable	0	15	30
Total error		**percent**	**~16**	**~29**	**~45**

Table 2.7. *The errors associated with COSPEC analyses can be divided into three types: A. data processing errors; B. instrumental errors; and C. variations due to atmospheric effects. The errors are: CAL1. height of CAL1 calibration peak; AREA. area beneath the plotted line for each segment; SEG. length of each plotted segment; AZM. wind direction - taken as the position on the road beneath the maximum SO_2 concentration detected; ROAD. length of each segment on the ground; INST. the errors involved with the concentrations of the calibration cells, and internal electronic variations; WINMES. instrumental error involved in measuring wind speed; WINVAR. variation in wind speed due to gusts, eddy currents and buildings/trees; WINALT. variation in wind speed with altitude; Ash and Clouds. the variations in UV scattering due to the presence of these between the sun and the COSPEC. Total error percentages are calculated as* $\sqrt{\Sigma(E^2)}$ *where E are the individual error values (after Stoiber et al., 1983).* *Millán (1980), #Delmelle (pers. com.),‡Williams-Jones et al. (1998), §D. C. Bird International Airport, Antigua, (M) magnitudes of errors relate specifically to analyses by the author on Montserrat, see Chapter 6.*

Summary of COSPEC errors

The errors in **table 2.7**, 16 - 28%, with a worst case of ~45%, relate to the COSPEC analyses I carried out on Montserrat and are similar to those of Stoiber et al. (1983) who reported errors as: generally 13% - 23% and worst case 42%. In both cases variations in wind speed is the major source of error. The main errors associated with COSPEC relate to atmospheric processes and so may vary greatly from location to location.

Stoiber et al. (1986) and Edner et al. (1994) have both reported that the SO_2 flux decreases with increasing distance from the vent. They suggested this was due to removal of SO_2 by oxidation and aerosol formation. The magnitude of this reduction in apparent SO_2 flux has been reported as <7% by Stoiber et al. (1986) and <20% by Edner et al. (1994). In Chapter 6, I suggest that <50% may be removed from the gas plume at Montserrat over distances of <20 km from the vent. Thus COSPEC analyses should be carried out as close to the vent as logistically possible.

2.3.5 Summary of COSPEC technique

The COSPEC technique utilises the differential absorbance of solar UV radiation by SO_2 at different wavelengths to determine the total amount of SO_2 in the optical path. This is normally a vertical air-column above the instrument when it is based in a vehicle, aircraft or boat. By traversing beneath the gas plume a snap-shot of the amount of SO_2 can be obtained. Combining this data with the wind speed gives a gas flux. **Table 2.7** summarises all the major COSPEC errors. Although cumulative errors range between ~16 and 45% and can be larger in adverse situations, the system is a quick and convenient method to make semi-quantitative estimates of the SO_2 output of a volcano. It must be realised, however, that smaller scale fluctuations can be due solely to the inaccuracies in wind speed, clouds and amount of ash in the atmosphere. It can be seen the COSPEC is not particularly suited for detecting the subtle variations in fluxes that can give an insight into the degassing mechanisms active beneath volcanoes. Its true role may well be as a monitoring tool to detect the substantial rise in gas fluxes that precedes a volcanic eruption.

2.4 Differential absorption LIDAR (DIAL)

DIAL is a technique that has been used since the mid 1960s to measure the compositions of a wide range of atmospheric pollutants. Edner et al. (1994) used the technique in 1992 to investigate the SO_2 concentrations in the volcanic plumes from Mt. Etna, Vulcano and Stromboli. In the following sections I will discuss the usefulness of DIAL as a remote volcanic monitoring system and compare the results obtained by Edner et al. (1994) with the COSPEC data of Caltabiano (pers com.).

2.4.1 DIAL instrumentation

The DIAL system uses two pulsed Nd:YAG (yttrium-aluminium-garnet) or Ti:Sapphire lasers as the source of UV radiation. Each laser is tuned to a specific frequency using a combination of temperature control and dispersing prisms (Lambda Photometrics Ltd. technical brochure). One laser is tuned to the absorption band of the analyte, e.g. 300.02 nm for SO_2; the other, acting as a reference beam, is tuned to a similar, but non-absorbed frequency, e.g. 299.30 nm (Grant et al., 1992; Edner et al., 1994). The lasers are directed through the collecting optics of the telescope into the volcanic plume, see **figure 2.15**. Laser radiation is back-scattered by plume and atmospheric aerosols, and collected by the telescope and focused into the instrument.

The difference in intensity of the back-scattered radiation from the two lasers is due to absorption by the analyte; this reflects the analyte concentration in the optical path. The pulsing of the lasers enables two-way travel times, and hence length of optical path to be calculated (Edner et al., 1994). This enables a two or three-dimensional concentration profile of analyte concentrations in the gas plume to be constructed. Mobile DIAL systems are reputed to be able to detect gases such as SO_2 and N_2O at levels of ~5 and 20 ppb respectively over ranges of ~3 - 4 km (Lambda Photometrics Ltd. technical brochure), making it a very sensitive system for monitoring background levels of volcanic gas.

However, there are several problems with the system. It is very expensive and very bulky, being housed in a lorry or large van, thus making close-in analyses of plumes difficult or impossible at many volcanoes. The narrow frequency range of emitted radiation only allows one analyte to be analysed at a time; thus making simultaneous measurements of different analytes impossible. The limited range of the smaller lasers of <5 km can also cause measurements of optically dense or high altitude plumes to be lower than they really are, since the back-scattered radiation may be totally absorbed at greater distances.

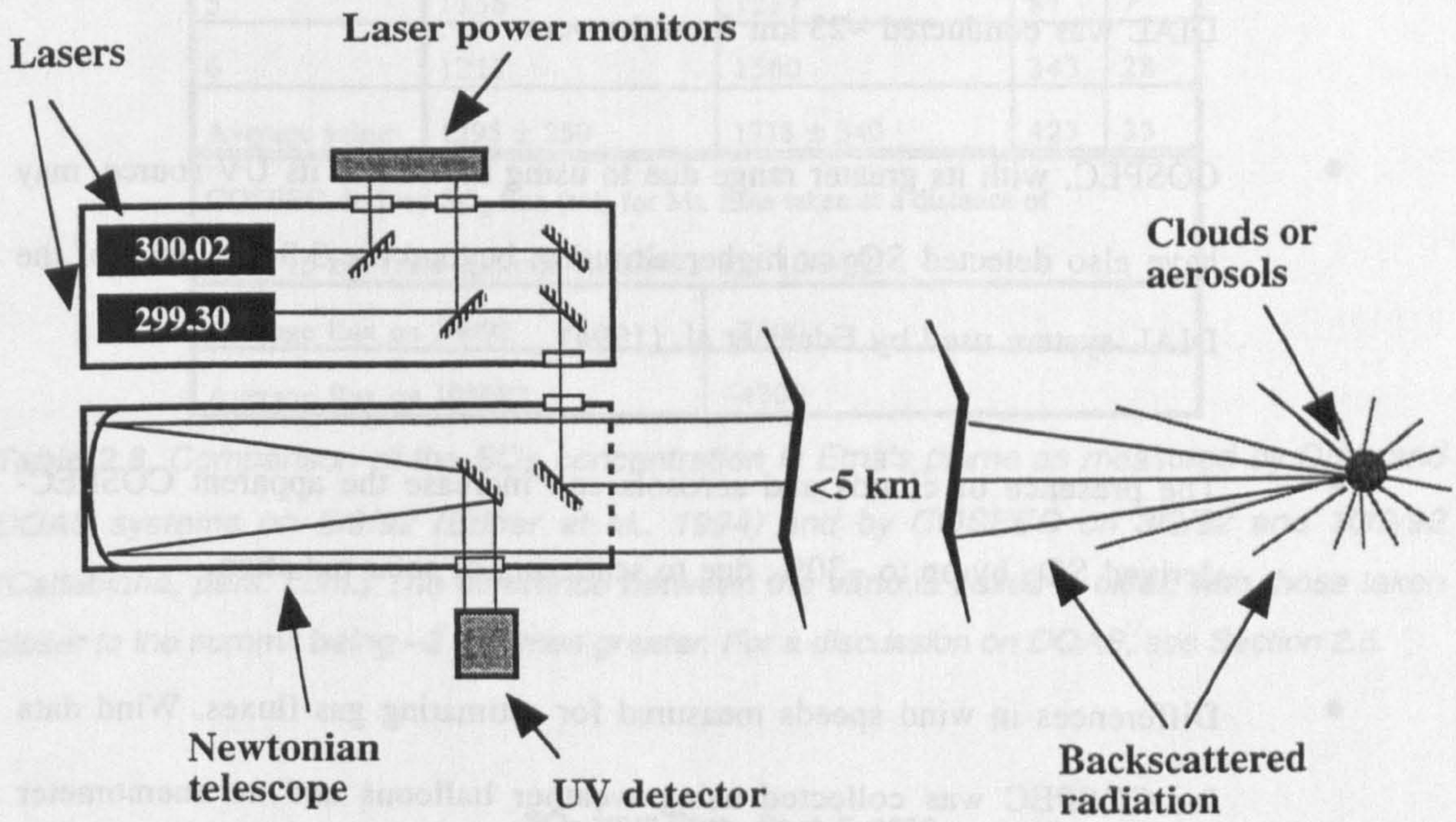

***Figure 2.15**. Schematic illustration of a DIAL system. The system has been used to determine the SO_2 composition of the gas plumes from Mt. Etna, Vulcano and Stromboli volcanoes in Italy (after: Grant et al., 1992; Edner et al., 1994).*

2.4.2 DIAL field applications - comparison with COSPEC

Edner et al. (1994) used a DIAL system set up in a truck parked on the rear of a ship for their 1992 experiment. Measurements of Mt. Etna's gas plume were conducted off-shore in the Golfo di Catania, at a distance of ~23 km from the summit vents. Results showed the plume, at this distance to be ~10 km wide and ~1.5 km thick at an altitude of ~2 km, see **figure 2.16** (Edner et al., 1994). They estimated an average SO_2 flux of ~1295 ± 250 t/d on 5/9/92. Caltabiano (pers. com.) used COSPEC to measure SO_2 fluxes of

~4700 - ~7700 t/d on 3/9/92 and 10/9/92 at distances of ~10 - 15 km from the summit, see **table 2.8**.

The large difference in fluxes recorded by DIAL and COSPEC may be due to the following:

- Scavenging of SO_2 by its oxidation to sulphate as the plume drifts away from the volcano; causing the measured SO_2 flux to be higher closer to the vent. As stated, COSPEC analyses were conducted at ~10 - 15 km, whilst DIAL was conducted ~23 km from the vent.

- COSPEC, with its greater range due to using the sun as its UV source, may have also detected SO_2 at higher altitudes; beyond the 3.5 km range of the DIAL system used by Edner et al. (1994).

- The presence of clouds and aerosols can increase the apparent COSPEC-derived SO_2 by up to ~30%, due to scattering of solar radiation.

- Differences in wind speeds measured for estimating gas fluxes. Wind data for COSPEC was collected using weather balloons and an anemometer located at the summit (Caltabiano et al., 1994). For DIAL, wind data were collected at ~500 m and ~1000 m below the summit. Lower wind speeds at these levels would result in a lower DIAL-derived flux.

- Natural short-term variations in the gas output from Mt. Etna. COSPEC analyses by Caltabiano et al. (1994) during the period 10/87 - 12/91, indicated that the SO_2 flux could vary by >4000 t/d over a one week period.

DIAL and DOAS-derived flux values for Mt. Etna taken at a distance of ~23 km from summit on 5/9/92.				
Traverse N°.	DIAL SO_2 flux (t/d)	DOAS SO_2 flux (t/d)	Difference (t/d) and %	
1	966	1622	656	68
2	1645	2122	477	29
3	1332	1756	424	32
4	1453	2010	557	38
5	1156	1237	81	7
6	1217	1560	343	28
Average value	1295 ± 250	1718 ± 340	423	33
COSPEC-derived SO_2 flux (t/d) for Mt. Etna taken at a distance of ~10 - 15 km from summit on 3/9/92 and 10/9/92.				
Average flux on 3/9/92		~7600		
Average flux on 10/9/92		~4700		

Table 2.8. *Comparison of the SO_2 concentration in Etna's plume as measured by DIAL and DOAS systems on 5/9/92 (Edner et al., 1994) and by COSPEC on 3/9/92 and 10/9/92 (Caltabiano, pers. com.) The difference between the various fluxes is clear; with those taken closer to the summit being ~3 - 8 times greater. For a discussion on DOAS, see Section 2.5.*

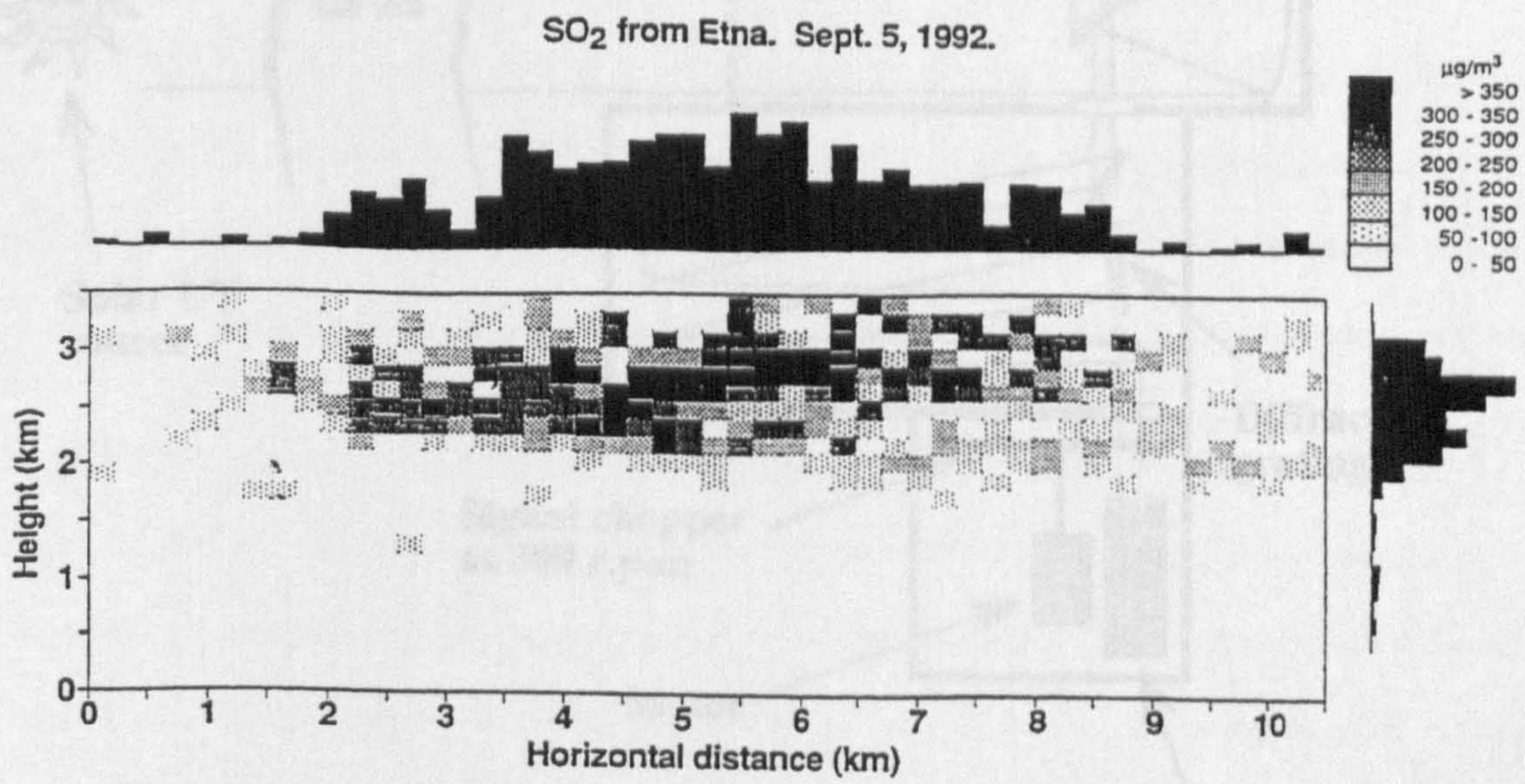

Figure 2.16*. Results of a DIAL investigation of the plume of Mt. Etna by Edner et al. (1994). The figure shows a DIAL traverse beneath the plume conducted, at a distance of ~23 km from the summit vents, from onboard a ship in the Golfo di Catania to the east of the volcano.*

Combining the maximum errors associated with the measurements of both techniques, as outlined above, still leaves a significant difference between the COSPEC and DIAL-derived fluxes. I believe this is probably due to a real difference in the volcano's gas output, coupled with the short range of the DIAL system and the differences in estimating wind speeds.

The ability of the DIAL technique to determine concentration profiles in two, or three, dimensions may prove invaluable for investigations into how volcanic plumes evolve as they travel downwind. However, the size of the equipment severely restricts its access to the summits of most volcanoes, although this, to some degree, is countered by its <5 km range. It is also reliant on the presence of aerosols (including oxidised SO_2) to scatter the laser radiation. The system can be used to detect a range of analytes, although not simultaneously, and can thus be used to complement techniques, such as OP-FTIR, which can simultaneously detect a multitude of analytes.

2.5 Differential optical absorption spectroscopy (DOAS)

2.5.1 History and instrumentation of the DOAS system

The DOAS system, like COSPEC, uses solar UV radiation as a light source. The technique was pioneered by Platt and Perner in the 1970s and is based on absorption by those analytes which will absorb UV radiation in the spectral range from 0.2 - 2 μm (50,000 - 5000 cm^{-1}) (Schiff, 1992). Edner et al. (1994) first used the technique to monitor volcanic gases in 1992 on Mt. Etna and Stromboli. This formed half of the comparative study which also used the DIAL technique, described in Section 2.4.

Ultraviolet radiation passes through the volcanic plume and is collected by a telescope and directed into the instrument; where it is focused onto a diffraction grating. This separates the radiation into individual frequencies which pass into a photomultiplier-tube detector, see **figure 2.17**.

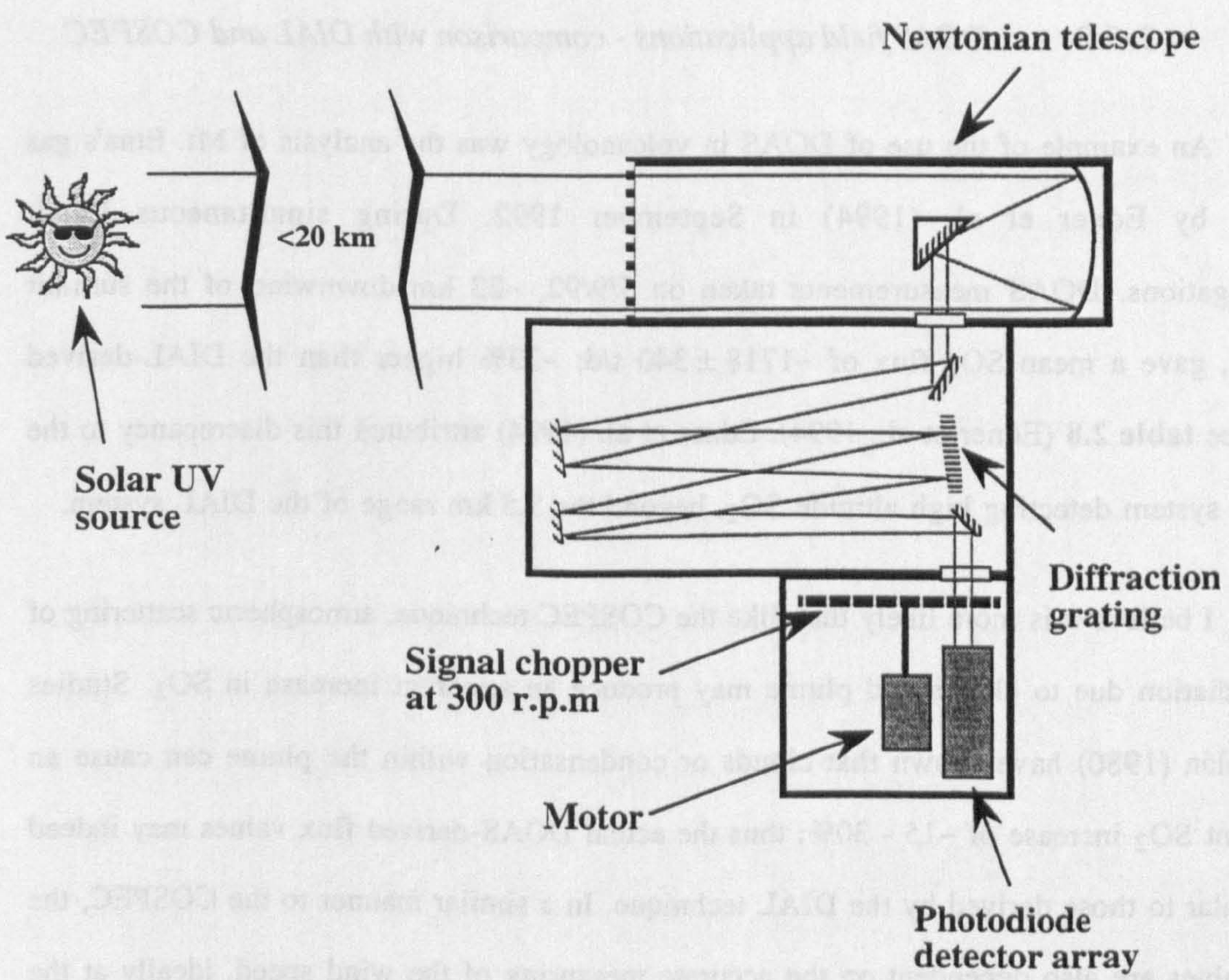

***Figure 2.17**. Schematic of the internal workings of a DOAS system (after Schiff, 1992).*

Rapid scanning through the spectral range enables the system to simultaneously analyse multiple analytes. Interference in the radiation by atmospheric scintillations is a major source of error. This typically occurs over time scales of between 0.1 to 1 Hz (Schiff, 1992). This can, however, be overcome by placing a rotating disk, which contains about 20 10 μm wide slits, between the diffraction grating and the photomultiplier tube. A mask ensures that only one slit at a time allows light into the detector. The rotational speed of the disc is ~300 r.p.m. allowing measurement of a selected part of the spectrum at a frequency of ~100 Hz (Schiff, 1992). Each scan produces a spectrum of frequency of absorption against intensity of absorption which can be used to analyse the gases in the plume. Several tens of thousands of scans are co-added to increase the signal-to-noise ratios of the resulting spectra (Schiff, 1992). A background spectrum is collected by directing the telescope away from the plume and used, along with laboratory reference spectra, in a similar fashion to FTIR background and reference spectra, see earlier.

2.5.2 DOAS field applications - comparison with DIAL and COSPEC

An example of the use of DOAS in volcanology was the analysis of Mt. Etna's gas plume by Edner et al. (1994) in September 1992. During simultaneous DIAL investigations, DOAS measurements taken on 5/9/92, ~23 km downwind of the summit craters, gave a mean SO_2 flux of ~1718 ± 340 t/d; ~33% higher than the DIAL-derived flux, see **table 2.8** (Edner et al., 1994). Edner et al. (1994) attributed this discrepancy to the DOAS system detecting high altitude SO_2, beyond the 3.5 km range of the DIAL system.

I believe it is more likely that, like the COSPEC technique, atmospheric scattering of UV radiation due to clouds and plume may produce an apparent increase in SO_2. Studies by Millán (1980) have shown that clouds or condensation within the plume can cause an apparent SO_2 increase of ~15 - 30%; thus the actual DOAS-derived flux values may indeed be similar to those derived by the DIAL technique. In a similar manner to the COSPEC, the flux values are also dependent on the accurate measuring of the wind speed, ideally at the same height as the plume. The DOAS-derived SO_2 fluxes are lower than those determined by COSPEC; again suggesting that the lower flux may be due to the poorer estimates of

wind speed and the greater distance from the vent; thus increasing the amount of SO_2 scavenged from the plume.

The bulky DOAS system is capable of simultaneously analysing a large number of gases. However, the number of volcanic gases exhibiting absorption bands in the UV is very small compared with the number that have absorbances in the infra-red (Schiff, 1992); making OP-FTIR spectrometry the more useful technique.

2.6 Field IR spectrophotometry

The gas analysis techniques in this and the following sections relate to "grab- or direct-sampling", where gases are physically collected prior to their being analysed. Direct-sampling reduces the amounts of atmospheric interaction and negates the variations introduced by ash and clouds. However, other problems exist, principally sample contamination, secondary reactions, and the re-equilibration of collected gases. These are described in the following sections.

Small hand-portable IR spectrophotometers have been designed by manufacturers such as Li-Cor or Dräger to measure a limited number of gases, such as CO_2 and H_2O. Newer models are capable of being battery powered and give a direct digital reading of the gas concentrations. The spectrophotometers work by drawing the sample gas into a gas cell through which a beam of IR radiation is passed. This is absorbed at specific frequencies, relating to the analyte's fundamental absorbances. The loss in intensity of radiation at these frequencies relates to the analyte concentration. By using diffraction gratings, multiple detectors, or tuning the detector to specific frequencies, different gases can be analysed. Two of the techniques used to sample volcanic gases using a spectrophotometer are:

- The use of a soil-probe. By pushing a hollow probe down into loose soil/ash to a depth of ~30 cm, soil-gases can be drawn up and into the instrument; this reduces the contamination of the sample with atmospheric CO_2 and H_2O.

- By using an accumulation chamber. This is an upturned airtight box of known volume firmly planted into the soil, see **figure 2.18**. Soil gas slowly fills the box and is pumped through the instrument, analysed, and returned to the chamber where a small fan mixes the trapped gases. The rate of change of gas concentrations inside the chamber relates to the emission rate of the soil gas. This technique has been used on Vulcano by Chiodini et al. (1996) and on Mt. Erebus by the author and O'Keeffe (pers. com.) to evaluate the flux of soil-gas.

Chiodini et al. (1996) estimated the accuracy of the accumulation chamber technique, with the variation in obtained results being <10% at any one site. The area covered by the chamber, generally «0.25 m^2, must be extrapolated to encompass a larger area, which may contain areas of high gas permeability, e.g. fissures and loose ash, or lower permeability, e.g. Tarmac and hard-packed soils. However, by using a dense network of sample sites this problem may be partially overcome, and by generating a map of gas permeable zones, may elucidate volcanic structures, see Chapter 4 and **figure 4.6** (Chiodini et al., 1996).

This technique is most widely used away from the main eruptive centres and so tends to be used in less hazardous conditions than other direct sampling techniques, see below, and provides an *in situ*, relatively low-tech, portable means for determining the levels of a limited number of gases.

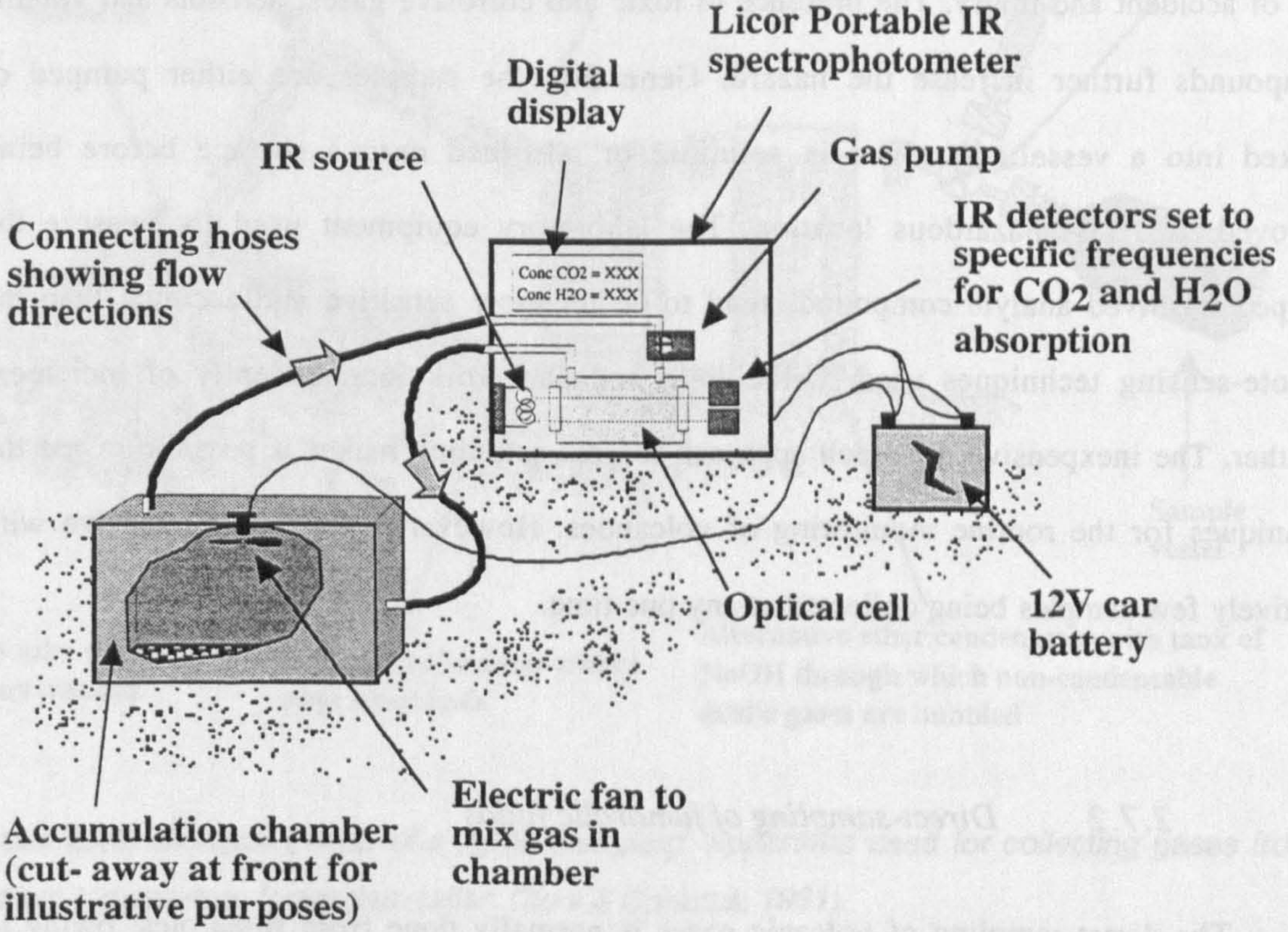

***Figure 2.18**. Schematic illustration of a portable IR spectrophotometer coupled to an accumulation chamber to determine the flux of CO_2 from diffuse soil emissions in "Warm-grounds" on Mt. Erebus, Antarctica during December 1996.*

2.7 "Grab-sampling" including the use of evacuated flasks and filter packs.

2.7.1 Introduction to grab-sampling

The standard method of chemically analysing volcanic gases has been to obtain a sample of gas from as close to the vent as possible. The techniques required to do this are extremely simple, portable and inexpensive; making their use as applicable today as in 1831 when Davies analysed the gases emitted from the emerging Graham Island (Francis, pers. com.). This section describes some of the reported techniques for physically collecting gases for analysis in the field or in a laboratory at a later date along with the advantages and disadvantages of the techniques discussed.

Normally gases are collected as close to the source as possible which may entail being close to hot fumarolic vents, active craters or crater walls; all of which increase the risk of accident and injury. The presence of toxic and corrosive gases, aerosols and volatile compounds further increase the hazard. Generally, the samples are either pumped or sucked into a vessel; dissolved in solution; or adsorbed onto a surface before being removed to a less hazardous location. The laboratory equipment used to measure the trapped/dissolved analyte compounds tend to be far more sensitive and accurate than the remote-sensing techniques used in the field and can work independently of inclement weather. The inexpensive, low-tech approach to grab-sampling makes it possible to use the techniques for the routine monitoring of volcanoes. However, it is labour intensive with relatively few samples being collected at any one time.

2.7.2 Direct-sampling of fumarolic fluids

The direct-sampling of volcanic gases is normally done from fumaroles; owing to the much higher temperatures and risk of explosions involved in collecting gas samples at open vents. A large range of gases can be collected and analysed including: SO_2, HF, HCl, H_2S, CO_2 and CO; as well as trace gases and isotopes, i.e. CH_4, N_2 Rn and ^3He, see

table 2.1. The compositions of the collected gases may reflect the ongoing hydrothermal processes rather than provide a direct source of magmatic volatiles, see Chapter 4.

Direct-sampling reduces the amount of dilution and interaction with the atmosphere. However, secondary reactions and the re-establishment of chemical equilibria do occur which can complicate the interpretation of the analyses. During collection, acid gases can react with pipes and vessels to produce hydrogen, metal oxides and fluorosilicates. Disproportionation of sulphur can also occur to give precipitation of insoluble metal sulphides, elemental sulphur and sulphates which are then lost from the analyses (Symonds et al., 1994; Le Guern, pers. com.).

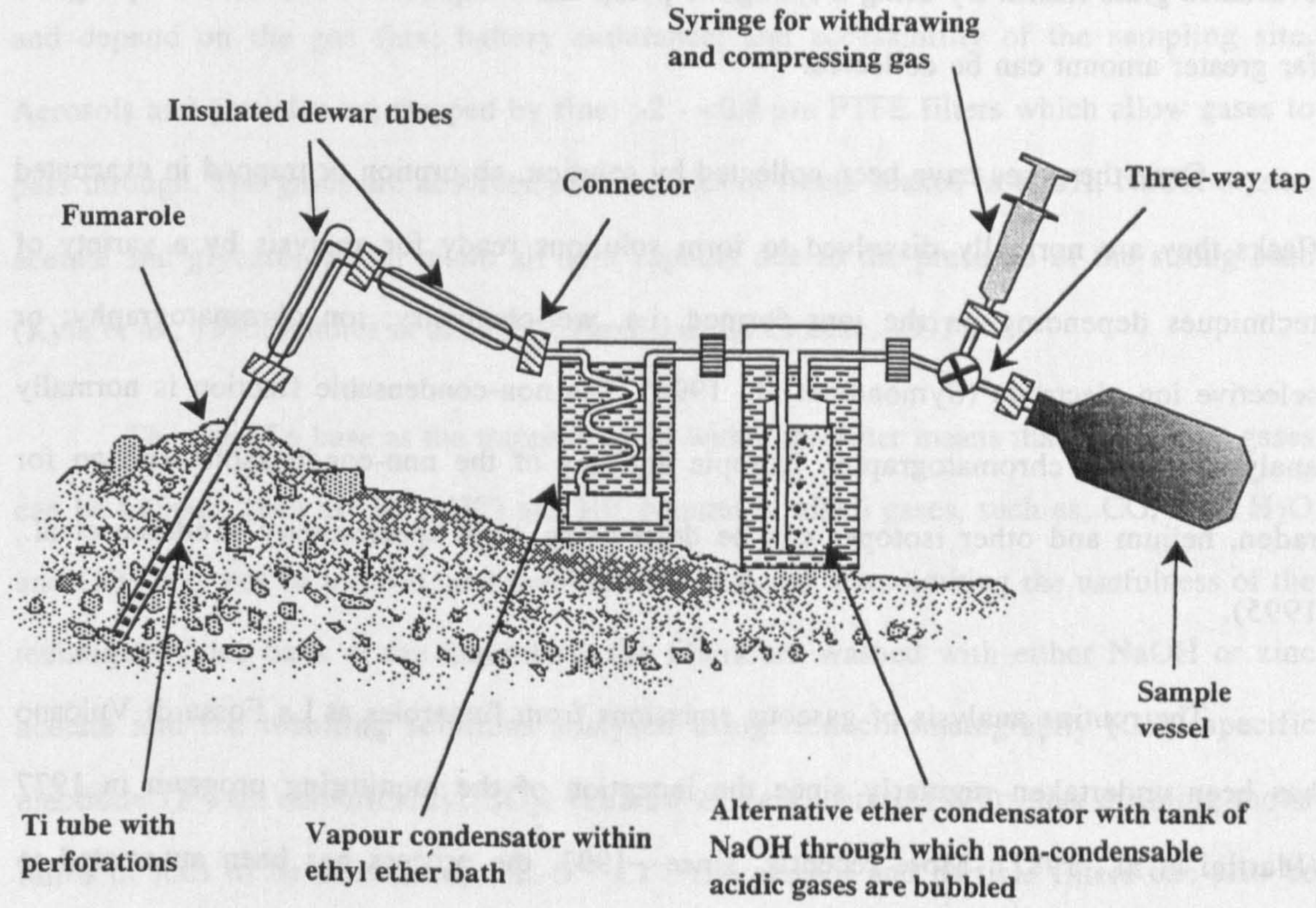

***Figure 2.19**. General set-up of a "grab sampling" apparatus used for collecting gases from medium temperature fumaroles. (after: Cioni & Corazza, 1981).*

The general principles behind gas collection are to insert an inert tube into the fumarole to a depth of ~60 cm below the surface (Cioni & Corazza, 1981), see **figure 2.19**. After insertion the pipe is left to heat up to the gas temperature and also to fill with gas thus lowering the chances of atmospheric contamination. Various fumarolic gases may react

with the material that the tube is made of, with acids reacting with metal to form hydrogen, and HF reacting with glass to form fluorosilicates. To maintain the gas temperatures and therefore the equilibrium between gas species the sample gases pass along insulated pipes. To freeze the equilibrium into the gas sample it can be chilled by being passed through an ether bath; this though can be extremely hazardous as ether has a very low flash-point and is highly flammable (Cioni & Corazza, 1981); a safer alternative would be a salted ice-bath. The sample can then either be pumped into a Teflon bag or passed into evacuated flasks or bubbled into flasks containing an alkali solution. By bubbling the sample gas slowly through a flask of strong NaOH solution, acid gases and condensable species can be removed and analysed by titration leaving the non-condensable gases to be collected in evacuated glass flasks. By using a syringe to pump and compress the collected sample gas a far greater amount can be collected.

Once the gases have been collected by solution, absorption or trapped in evacuated flasks they are normally dissolved to form solutions ready for analysis by a variety of techniques depending on the ions formed, i.e. wet-chemistry; ion chromatography; or selective ion electrode (Symonds et al., 1994). The non-condensable fraction is normally analysed by gas chromatography. Isotopic analysis of the non-condensable fraction for radon, helium and other isotopes can be done using mass spectrometry (Tedesco et al., 1995).

The routine analysis of gaseous emissions from fumaroles at La Fossa di Vulcano has been undertaken regularly since the inception of the monitoring program in 1977 (Martini et al., 1981). More recently, since ~1993, the process has been automated to measure a variety of parameters: temperature; reducing capacity; soil degassing of CO_2; radon emission and weather (Badalamenti et al., 1996). Tedesco et al. (1991; 1995) determined the chemical and isotopic compositions of a range of gases, for the period 1986 to 1990. This involved using a grab-sampling technique in which gases were directed up a pipe and trapped in evacuated flasks, or in solution, for laboratory analysis at a later date. I will discuss the analyses conducted at La Fossa in Chapter 4.

2.8 Use of filter packs for gas analyses

Filter packs provide a robust and lower risk approach to gas collection on volcanoes where fumaroles or vents are situated within a steep-sided crater making conventional grab-sampling difficult. The filters are set up close to the crater-edge downwind of the vent to allow the highest concentration of gases to be sampled. Mounting the filters ~1 - 2 m above ground-level reduces contamination by wind-blown dirt. A continuous through-flow of air is provided by a battery-powered pump which normally is set to pump air at a fixed rate. For different analyses this may vary between <1 and >50 l/min (Andres et al., 1993; Pennisi & Le Cloarec, 1998). Sampling times for filter-pack analyses range from less than an hour (Andres et al., 1993; Pennisi & Le Cloarec, 1998) to a couple of days (Kyle, pers. com.) and depend on the gas flux; battery endurance; and accessibility of the sampling site. Aerosols and particles are trapped by fine, >2 - <0.4 μm PTFE filters which allow gases to pass through. The gases are absorbed onto a series of filters soaked in LiOH, NaOH or zinc acetate and glycerol which retain all acid vapours due to the presence of the strong base (Kyle et al., 1990; Andres et al., 1993; Pennisi & Le Cloarec, 1997).

The use of a base as the trapping agent within the filter means that only acidic gases can be trapped, such as: SO_2, HCl and HF. Neutral or alkali gases, such as: CO, H_2S, H_2O and CO_2 may not be trapped, and therefore not detected; thus limiting the usefulness of the technique. Once back at the laboratory, the filters are washed with either NaOH or zinc acetate and the resulting solutions analysed using: ion chromatography (Cl^-); specific electrode (F^-) or colourimetry (SO_2) (Pennisi & Le Cloarec, 1997); thus enabling molar ratios of ions to be determined, i.e. S^{6+}:Cl^-. The aerosol and particle filters can also be analysed by INAA (Andres et al., 1993). The technique is a simple and convenient way of measuring the amounts of volatiles and particles present in the plume close to an inaccessible vent. However the analysis of the data is again labour intensive, with few samples being collected at any one time. The presence of eddy currents, variability in pumping speeds and yield of the eluted analytes may all incorporate errors into any derived flux. Andres et al. (1993) reported these to vary between ~5 and 30%.

2.9 Conclusions

This chapter has described a variety of different techniques for analysing volcanic gases, emitted from vents, fumaroles or by soil-seepage. The range of techniques, from trapping gas on a filter or in a flask through to using high power pulsed lasers, have all been designed for a specific purpose. Usually this has nothing to do with volcanology, most techniques originating from the chemist's laboratory or from the field of environmental science. The technique has had to be adapted, or used at the extreme range of its operating abilities for the purposes of investigating or monitoring volcanic emissions. As such, many of the techniques used are a compromise between what the instrument can detect; where it can be used; and how reliable the recorded data actually is. The techniques discussed in this chapter can be broadly divided into two groups:

- Remote-sensing techniques. These are all optical techniques which rely on the characteristic IR or UV absorbances of different gases. These techniques use either a natural source of radiation, such as the sun or hot ground, or an artificial source, such as a portable IR lamp or UV laser. These techniques have a long range and so can detect gases in inaccessible plumes; thus reducing the need for operators to enter hazardous areas. As the instruments do not interact with the species being analysed there is no contamination, condensing or secondary reactions which may affect the amounts of analyte measured. However, the instruments tend to be heavy, expensive, and complex. A major problem with remote-sensing can be the weather. Clouds can dissolve and remove analyte rapidly and rapid variations in wind speed can give extremely high amounts of error when trying to determine flux rates.

- Direct-sampling techniques. These rely on the gas being trapped, dissolved or adsorbed before being analysed by more traditional methods of analysis: e.g. wet-chemistry, colourimetry, selective ion electrode or gas chromatography. The capture of gases is best achieved as close to the source as possible, be it an active vent or fumarole field. This increases the

risk to the operator, and may only be possible during periods of low activity. The physical interaction of gases with instrument and collection vessels can lead to contamination and formation of secondary reactions including: disproportionation, redox, and reactions involving the collection vessel. The errors due to such problems may, however, be relatively minor when compared with the errors caused by changing climatic conditions, as experienced by remote-sensing techniques. Direct-sampling techniques are, however, labour intensive and thus are capable of only generating a relatively small amount of data compared to the more automated remote-sensing techniques, such as OP-FTIR. The direct sampling techniques also cannot give volumetric fluxes which relate to the overall gas output of a location.

The suitability of an individual technique will depend greatly on the type of gas to be measured, the location of vent or fumarole, the level of volcanic activity, the environment in which data is to be collected, the duration over which data are to be collected and the purpose behind the data collection. Other factors include the cost of the equipment and its reliability. At locations which are relatively inaccessible by vehicles or prone to long periods of bad weather, a remote-sensing technique would be of little use. Conversely, direct sampling of gases from a vent, situated at the base of a pit-crater and undergoing strombolian activity, would again be unfeasible.

I have summarised the observations into the merits and detriments of the direct and remote-sensing techniques as:

- Remoteness of operation. It has been highlighted throughout the chapter that techniques which enable the minimum amount of time to be spent in areas of danger, or allow sampling from otherwise inaccessible areas, are by their very nature better than those techniques which require scientists to spend long periods of time in hazardous localities. Such techniques such as filter and grab sampling and portable IR spectroscopy can therefore be limited in their use by volcanic hazards.

- Number of gases analysed. A gas analysis technique should be able to analyse a number of gases, simultaneously if possible. This will enable fluxes of many gas species to be determined to elucidate the various processes taking place within the magmatic-hydrothermal system. Examples of techniques capable of analysing many gases simultaneously are the OP-FTIR and DOAS techniques.

- The OP-FTIR, DOAS and LIDAR techniques can make a large number of measurements rapidly, producing a much larger data-set than that produced using grab-sampling.

- Speed of results. It is desirable for the routine monitoring of a volcano to be able to have the results of analyses within as short a time as possible. Techniques which output data directly to computer or plotter are far more useful than those which just collect samples for laboratory analysis; this includes all the optical techniques which can download all the data directly to a computer.

- Usefulness of data for scientific and monitoring purposes. Certain data are of more immediate importance during routine monitoring of a volcano. These include SO_2 flux and ratios of SO_2:CO_2, SO_2:HCl and HCl:HF which give information about the volatility and evolution of the degassing magma. These data can be obtained by the simultaneous use of COSPEC and OP-FTIR techniques (Francis et al., 1995) or by direct-sampling techniques; although the samples may take a long time to analyse.

- Instrument portability and reliability. Many sources of volcanic gas are in rough terrain which may only be accessible on foot or by helicopter or tracked/four-wheel-drive vehicle. In such circumstances the instrumentation has to be rugged enough to withstand rough treatment; be small enough to be almost hand-portable and be simple enough to be assembled in the field

within a short period of time. Resistance to ash, rain and the corrosive effects of acidic gases would also give the instrument a longer operating-life. Certain techniques such as LIDAR and DOAS are housed in mobile laboratories and so cannot be used in many locations.

- Environment. Techniques which rely on clear skies and/or good weather, such as COSPEC, OP-FTIR and other optical techniques may have a limited use in certain localities. In such situations, simple, direct sampling techniques which require the minimum amount of atmospheric interaction may be more appropriate.

Chapter 3.

The Evolution and Present-day activity of the Masaya Volcanic Complex

3.1 Introduction

3.1.1 Layout of chapter

In this chapter I describe the progressive evolution of the Masaya Volcanic Complex and the changes in the present-day pit-crater morphology, using my observations gained during a field excursion in March 1994. The chapter also includes observations on gas emission data collected by Correlation Spectroscopy (COSPEC) and the gas and magma fluxes obtained. The chapter is broken down into the following sections:

3.1 General introduction, discussion of previous work, and a brief volcanic history of the Masaya Volcanic Complex from ~135 ka onwards.

3.2 Description of the individual features within Masaya Caldera with the aim of elucidating the evolution of the Masaya Volcanic Complex including the formation of the pit-craters, cones and eruptive fissures.

3.3 Discussion of the degassing episodes at Santiago Crater. I use COSPEC measurements to infer volumes of degassed magma, which relate to the shallow plumbing system beneath Masaya Caldera. I also propose a model to explain the degassing episodes reported.

3.4 Conclusions. These can be summarised as:

- Locations of vents within the NW part of the caldera are related to the interaction between a postulated cone-sheet and the deep-seated Cofradía Fault which bisects the caldera.

- Degassing episodes are caused by the introduction of a large magma body to shallow depths beneath the caldera, where it degasses without replenishment. This is possibly caused by the convective overturn of a deeper magma chamber. The volumes convected govern both the length of increased degassing and the repose period before the next episode.

- The volume of magma degassed since the formation of Santiago Crater in ~1859 is estimated at ~10 - 20 km^3. The total volume erupted since the formation of Masaya Caldera ~2250 - 6400 years ago is estimated as ~13 km^3. The volume erupted during the last ~1000 years, forming the visible lava flows, is only ~0.2 km^3; suggesting a marked decrease in effusion rates over time.

3.1.2 General volcanological background

Masaya Caldera and the volcanic complex situated within it, lies on the Central American Volcanic Front, a NW - SE line of closely spaced volcanic centres lying ~20 km apart, which has formed as a result of the subduction of the Cocos Plate beneath the Caribbean Plate (Carr, 1984). The caldera marks the western edge of the Nicaraguan Depression; an area of low lying ground, situated between the coastal highlands to the west and the central highlands to the east, which follows the line of the volcanic front, see **figure 3.1**.

Masaya Caldera is encircled by the much larger, ~15 km by 15 km, Las Sierras Caldera. This may have formed ~135 ka ago and relates to eruptive activity within the Las Sierras shield volcano located to the west of Masaya (Walker et al., 1993). The deposits from the Las Sierras shield are predominantly basaltic, with basaltic ignimbrites covering an area of over 7000 km^2 (van Wyk de Vries, 1993). Close to Masaya Caldera these have been buried by the younger Masaya ignimbrites and tephra deposits (van Wyk de Vries, pers. com.).

The exact nature of the connection between the basaltic activity at Masaya and the Las Sierras shield is uncertain; they have both produced basaltic ignimbrites and one caldera lies within the other; strongly suggesting a well established, >135 ka old, pathway for the migration of volatile-rich basaltic magma to the surface. This may be associated with the regional Cofradía Fault system that passes beneath Masaya Caldera; see Sections 3.2.3 and 3.2.5.

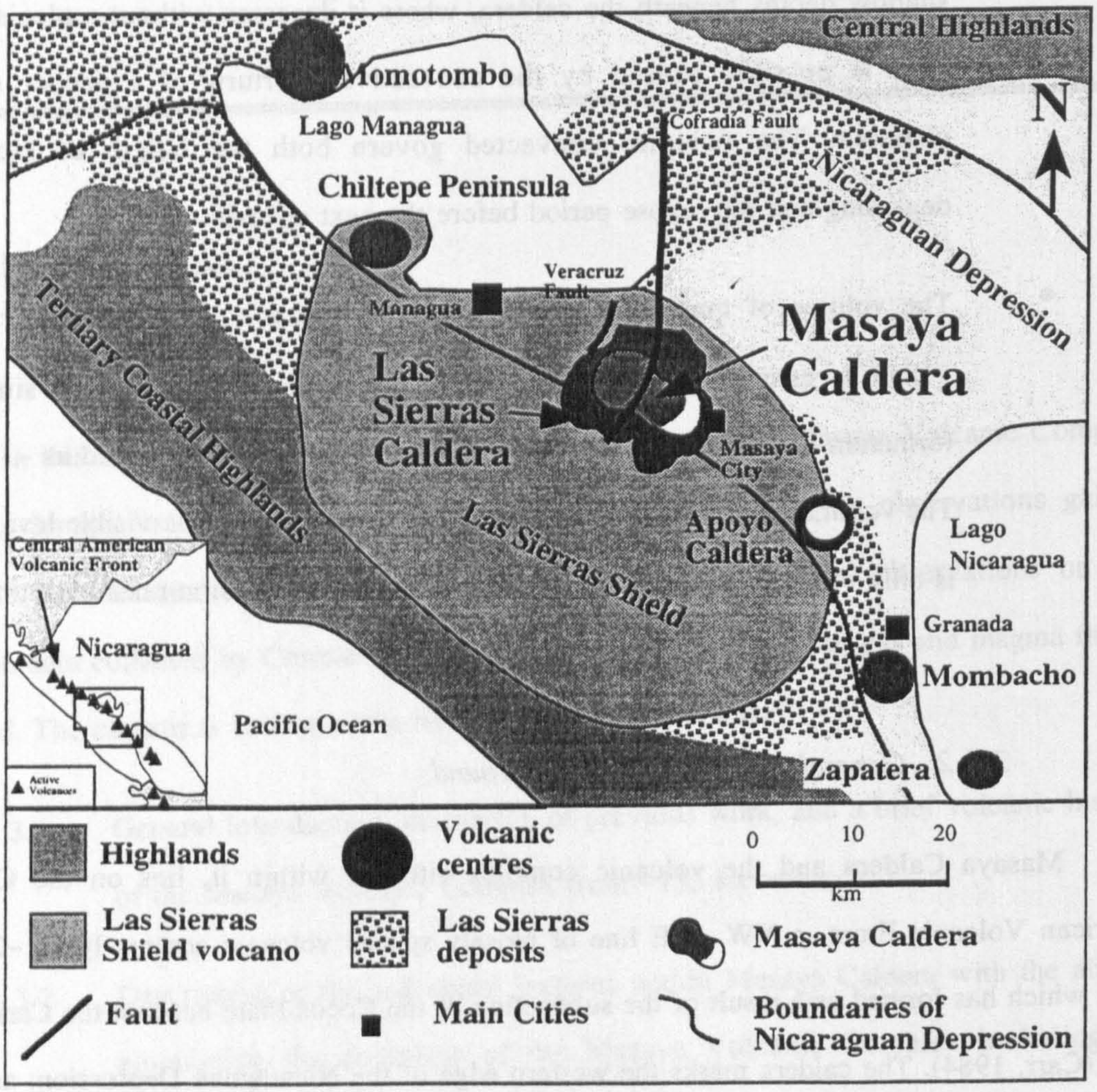

***Figure 3.1**. The general locations of volcanic and geographic features in the area surrounding Masaya Caldera (after: van Wyk de Vries, 1993; Metaxian, 1994). **Inset**. Map of Nicaragua showing the line of the Central American Volcanic Front (after: Walker et al., 1993; van Wyk de Vries, 1993).*

Masaya Caldera is a large dumbbell-shaped depression ~11.5 km by ~6 km in size, with its long axis oriented ~NW - SE parallel to the main volcanic line, see **figure 3.1**. The caldera formed between 2250 and 6400 years ago, as inferred from the ^{13}C-dating of archaeological relicts, and has been associated with the Masaya Tuff ignimbrite and pyroclastic surge deposits of that age (Bice, 1985; Walker et al., 1993). The Masaya Volcanic Complex is

situated within the western half of Masaya Caldera. Here it forms two connected massifs; Volcán Masaya and Volcán Santiago, associated with several eruptive fissures and smaller scoria/spatter cones. Santiago Crater in Volcán Santiago is the only active crater within the volcanic complex.

3.1.3 Previous studies of Masaya Caldera and associated volcanic complex

The Masaya Volcanic Complex and surrounding caldera have been studied by several authors using a variety of techniques; I have briefly summarised the work of some of these below. The earliest accounts of Masaya Caldera come from the Conquistador Oviedo y Valdes (1855, in McBirney, 1956) who visited the area in 1529. Later casual observations of volcanic activity at the volcanic complex come from early visitors and have been reported in McBirney (1956); these include: Fray Blas del Castillo in 1537; Stephens (1841) in 1840; Montessus de Ballore (1888) in the 1850s; and von Seebach (1892) in 1865. Later observations on the activity and shapes of the pit craters were reported by Sapper (in McBirney, 1956) between 1897 and ~1927.

McBirney (1956) investigated the formation of Masaya Caldera and conducted a review of the historical activity. This is the only "recent" work which has described the historical evolution of the volcanic complex; using the limited number of historical accounts, see Section 3.2. Bice (1980) conducted a detailed study of the pyroclastic deposits in the Managua area and determined that at least three: the Masaya Tuff; Masaya Triple Layer; and Masaya Lapilli Bed, originated from Masaya Caldera, based on isopach data. Williams (1983) investigated the formation of Masaya Caldera and mapped and analysed the lava flows within it. Crenshaw et al. (1983) used emission of Rn and Hg to investigate the postulated existence of coalescing calderas within the main caldera; their results proved inconclusive. Williams (1983b) investigated two of the plinian deposits associated with Masaya Caldera and estimated eruption rates and muzzle velocities. Stoiber et al. (1986) measured the SO_2 flux from the 1972 - 1986 degassing episode at Santiago Crater and discussed the periodicity of degassing episodes and the flux of unerupted magma; I will discuss their work in detail in Section 3.3.

Recent studies have tended to be based on the use of geophysical techniques. Connor & Williams (1990) conducted a gravity survey throughout Masaya Caldera and surrounding area and reported the presence of a large positive gravity anomaly immediately to the north of the caldera. Kieffer & Creusot-Eon (1992) proposed a new, phreatomagmatic origin for the caldera; forming a series of large coalescing maars. Walker et al. (1993) modelled the chemistry of the basaltic lavas at Masaya Caldera and suggested that fractional crystallisation and magma mixing were the dominant processes involved in determining magma compositions. Metaxian (1994) measured gravity and seismicity within Masaya Caldera to try and constrain the size and volume of the shallow magmatic system but results proved inconclusive due to the similarity in density between magma and surrounding country-rock. Rymer et al. (1998) studied the changes of gravity and gas emissions between 1993 and 1997 and inferred that both related to the possible convective overturn of magma within the system. I will address these issues later.

3.1.4 Volcanic history

Pre-caldera activity

The currently active Santiago Crater represents the latest episode in the complex volcanic history of the Masaya region. The area occupied by Masaya Caldera was originally part of the eastern flank of the basaltic Las Sierras ignimbrite shield; reported by Walker et al. (1993) to be of Plio-Pleistocene age. A violent collapse episode formed the Las Sierras Caldera on the eastern flank of the volcanic shield, see **figure 3.1**. The ensuing basaltic plinian eruption possibly deposited the "J1" marine tephra layer; dated by Ledbetter (1985, in Walker et al., 1993) at ~135 ka.

After formation of the Las Sierras Caldera, continued eruption of basaltic lava and tephra formed a small shield volcano, here called proto-Masaya volcano, situated where Masaya Caldera is now. The gradual upwards-slope of the ground towards the walls of Masaya Caldera is evidence for the existence of this edifice. Evidence for both explosive and effusive eruptive activity at proto-Masaya is supplied by the numerous tephra beds and lava flows that

outcrop in the caldera walls. The dominant north-easterly wind has concentrated the pyroclastic deposits in the SW caldera walls; with thick lava flows being found mainly in the north and eastern walls.

Walker et al. (1993) and Bice (1980) interpreted the more recent basaltic plinian eruptions, centred on proto-Masaya, as being smaller, possibly caldera-forming, eruptions. These include the Masaya Lapilli Bed (Fontana Lapilli of Williams, 1983) and the Masaya Triple Layer (San Judas Formation of Williams, 1983) which have approximate dates of 35 - 25 ka and 9 - 7 ka respectively (Walker et al., 1993). The much younger Masaya Tuff ignimbrite and proximal pyroclastic surge, dated at 6.4 to 2.25 ka (Bice, 1980 & 1985) was deposited as part of the eruption which formed the present caldera.

Post-caldera activity

The eruptive activity since the formation of Masaya Caldera has been predominantly effusive; with lava flows being produced either from the overspilling of lava lakes or from fissure eruptions (Walker et al., 1993). Fire-fountaining and minor strombolian activity have occurred forming small scoria and spatter cones throughout the western part of the caldera. No eruptive vents have been found by the author, or other scientists, in the eastern half of the caldera; thus marking an important divide, see later.

The Conquistador, Oviedo y Valdes (1855 in McBirney, 1956) was the first to record observations of the volcanic complex in 1525. At this time, Nindiri was a deep crater with a lava lake at the bottom, see **figure 3.10C**. Successive lava lakes infilled the crater until in 1670 the crater had filled up and overflowed; forming an ~3 km long lava flow to the north of the crater (Walker et al., 1993). Cooling of the layered lava lakes, contraction and faulting took place to leave the subsided level surface present today. The last major eruption occurred in 1772, when a large, almost N-S, fissure opened to erupt ~2.3×10^7 m^3 of basaltic lava, see **figure 3.2**. This flowed northwards, breaching the caldera wall to flow a total of ~7 km.

Montessus de Ballore (1888, in McBirney, 1956) reported that during the period 1850 - 1859 two pit-craters formed, one at either end of the subsided Nindiri lava lake; San Pedro to

the west and Santiago to the east, see **figures 3.3A-B**. The volcanic activity, since the formation of the pit-craters, has almost exclusively been centred on Santiago Crater. Here several lava lakes have formed and solidified to later collapse forming an inner-crater in 1988 (Rymer et al., 1997). Stoiber et al. (1986) reported that Santiago Crater has also been the site of at least five degassing episodes during the last 150 years, I will discuss these in Section 3.3.

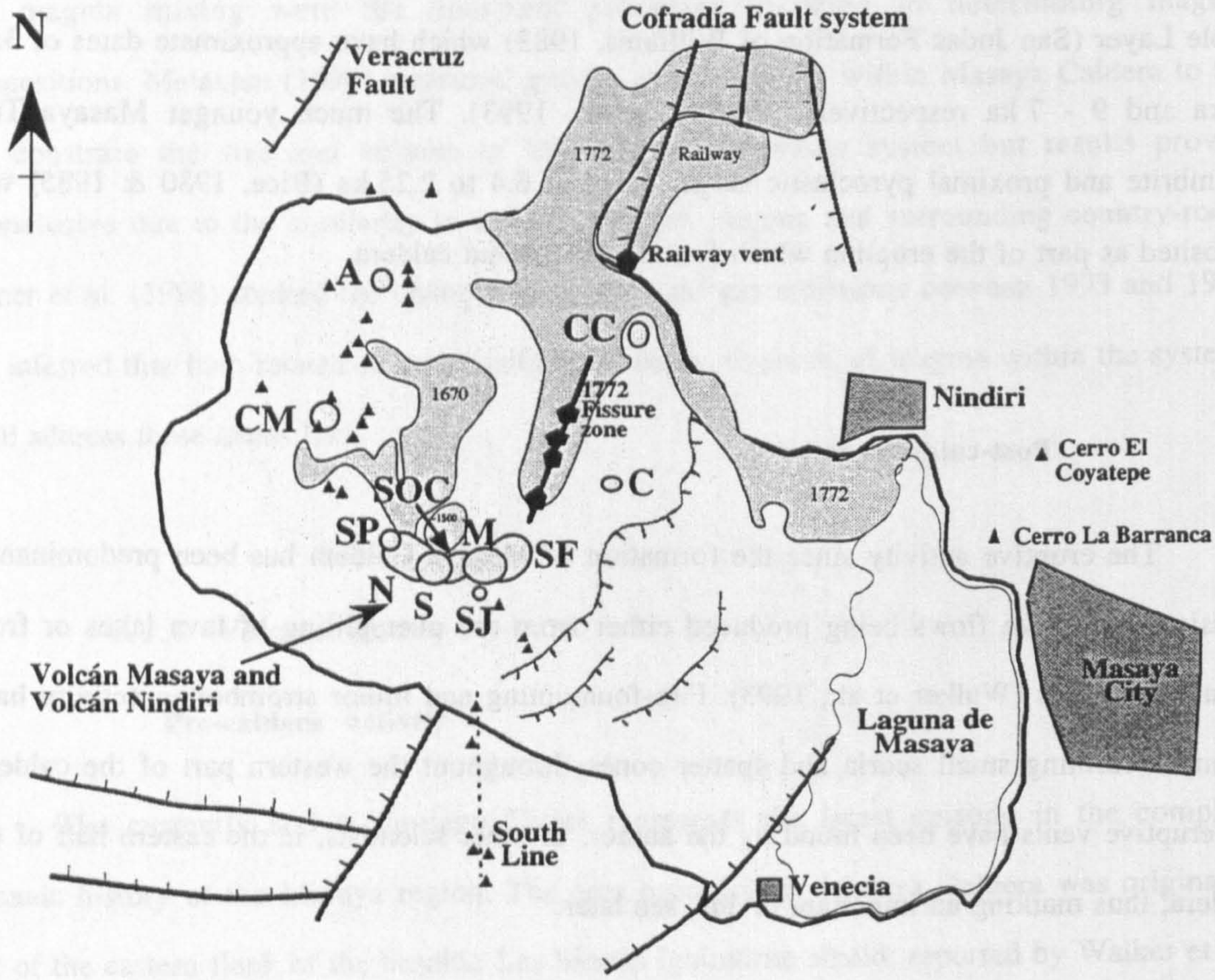

Figure 3.2. *Map of the main structures composing the Masaya Volcanic Complex showing the relationships between volcanic structures and local faults (after: McBirney, 1956; Walker et al.,1986; Metaxian, 1994). More detailed diagrams of volcanic features within the caldera can be found in the following sections.*

3.1.5 Summary of recent volcanic activity at Santiago Crater

Santiago Crater formed as a result of the collapse of the eastern end of the solidified and subsided Nindiri lava lake in 1859 (McBirney, 1956). After its formation, the pit-crater had a diameter of ~600 m with vertical walls and a depth of ~150 m. It was from the floor of the crater that volcanic gases were emitted in six degassing episodes: 1852 - 1859; 1902 - 1906; 1919 - 1927; 1947 - 1959; 1979 - 1988 and 1997 onwards (Stoiber et al., 1986). High gas fluxes occurring after 1995 may also represent a smaller degassing period, see Section 3.3. During the 1919 - 1927 degassing episode, ash was emitted until 1924; the cessation of degassing occurring in 1927 after blasting operations by Schönberg and Scharfenberg caused a collapse which blocked the degassing vents (McBirney, 1956). Lava lakes formed in the crater in both 1948 and 1964; solidification of the 1964 lava lake left a flat bottom to the pit crater. Collapse of the central portion of the solidified lava lake produced a hole ~80 m in diameter which was the source of gases during the 1979 - 1988 degassing episode (Stoiber et al., 1986).

The variations in the style and level of the recent volcanic activity within Santiago crater, as described below, reflected changes in the level of the magma beneath the floor of the pit-crater. Enlargement of the vent westwards in 1986 formed the inner-crater seen today and led to the undercutting of the SW wall, initiating a collapse. Rymer et al. (1997) reported the collapse was preceded by the opening up of two pits which became the centre for gas venting. They reported that during the first part of 1989 several new vents appeared within the inner-crater from which active degassing, strombolian activity and occasional fire fountaining took place. The heightened level of activity and the ejection of molten material indicates the proximity of the magma beneath the crater floor. Eruptive activity stopped in April 1989 and withdrawal of magma led to a further collapse, deepening the inner-crater which became the site for minor strombolian activity. In the latter part of 1989 fissures opened up above the southern wall close to Plaza Oviedo and the number of rockfalls increased until in November 1989 a large collapse with a volume of ~50,000 m^3 buried the crater floor and blocked the vents (Talena, pers. com.).

No activity was seen except for minor fumarolic activity until June 1993 when a vent appeared beneath the foot of the northern wall of the inner-crater. This was fed from a small lava lake and slowly built an ejecta cone. During a visit to the crater in March 1994, Murray and the author estimated the level of magma to be ~30 - 80 m beneath the level of the vent, situated in the NE wall of the inner-crater. In early 1997 the vent was degassing heavily and recorded temperatures were >1000°C (GVN Bulletin, Vol. 22, N°. 3, 1997). In April 1997, however, a small collapse partially blocked this vent; the gas still being able to escape by percolating up through the boulders.

3.1.6 Science issues associated with the Masaya Volcanic Complex and Masaya Caldera

Many aspects of Masaya Caldera have already been studied by authors described in Section 3.1.3. However, very little descriptive work on the evolution of Masaya Caldera and volcanic complex has been done. Sapper (1925: in McBirney, 1956); McBirney (1956); Williams (1983b); and Rymer et al. (1998) have been the only authors this century to observe and describe the changes occurring within the caldera. I have identified several issues that have only been touched upon and warrant further investigation. These can be summarised as follows:

- The Masaya Volcanic Complex contains a large number of vents illustrating almost every aspect of basaltic volcanism: scoria cones; spatter cones; eruptive fissures; agglutinated spatter from fire fountains and pit craters. All the features have formed in <6.5 ka. I will describe how the complex has evolved over this time.

- McBirney (1956) and others have remarked on the apparent circular occurrence of eruptive vents. Can this be attributed to the presence of cone-sheets or ring-dykes? All the visible eruptive vents lie within the western half of Masaya Crater. What is controlling this vent distribution? The positioning of the 1772 eruptive fissure, the most recent major eruptive feature, does not

follow the pattern of older features and crosses the ring. I will discuss the positioning of vents and the influence of faults in Section 3.2.

- Santiago Crater has undergone at least five major degassing episodes with minimal lava effusion. Stoiber et al. (1986) and others have proposed a 25 - 30 year periodicity to the degassing crises. Does such a periodicity exist, and what causes/controls it. What happens to the magma that degasses but does not erupt? Is it intruded; convected downwards or simply pooled? I will discuss this in Section 3.3.

3.2 Formation and evolution of the Masaya Volcanic Complex

3.2.1 Introduction to the Masaya Volcanic Complex

The Masaya volcanic Complex has evolved to its current state over a period of between 2250 - 6500 years (Bice, 1985; Walker et al., 1993). During this time the morphology of the volcanic complex has changed considerably. In this section I will describe in detail the

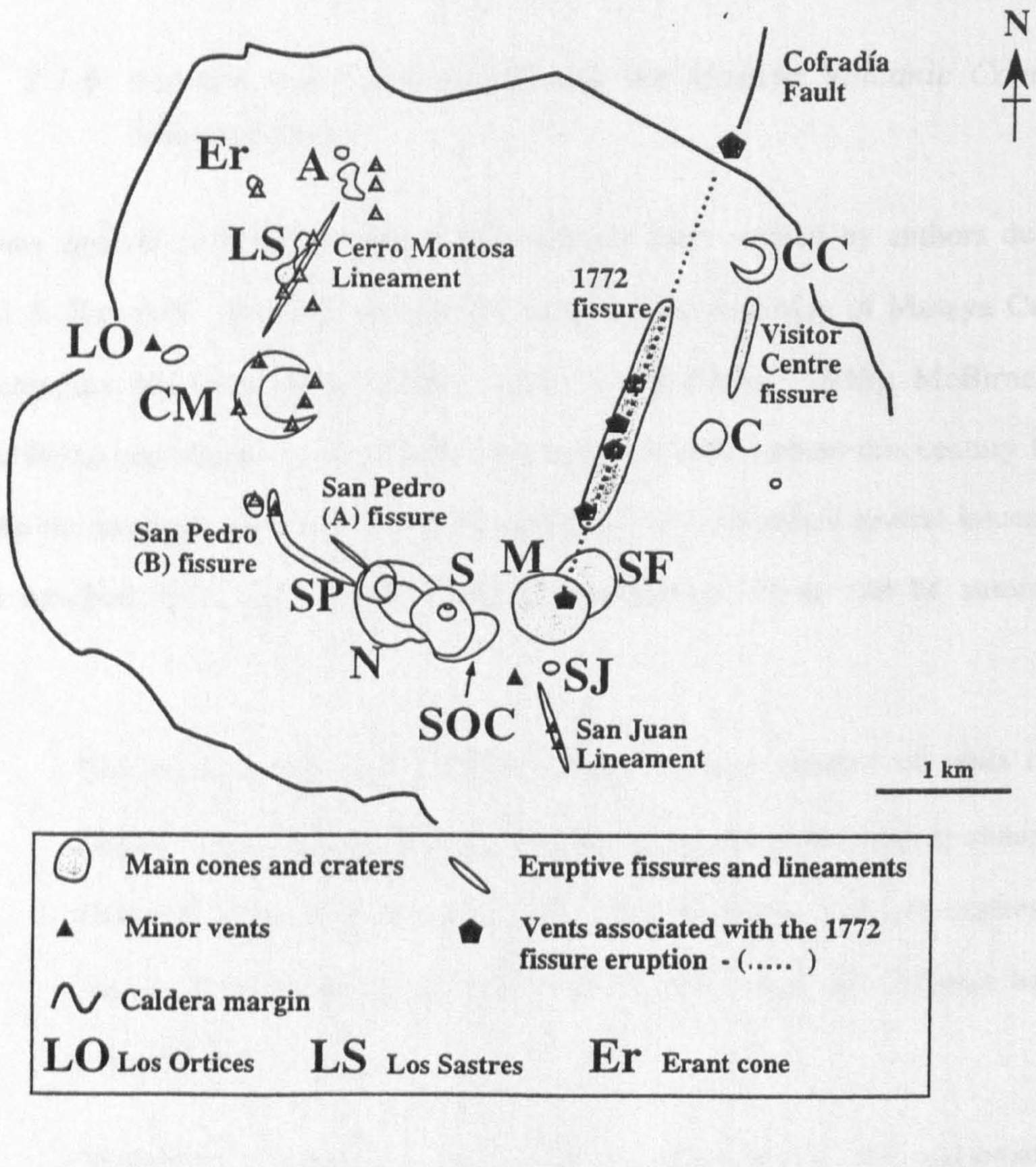

Figure 3.3. A. *Map showing the locations of all structures described in Section 3.2. Features of individual structures can be found elsewhere within the section. Abbreviations are as follows: A. Arenal, Er. Erant cone, LS. Los Sastres, LO. Los Ortices, CM. Cerro Montosa, SP. San Pedro Crater, N. Nindiri Crater (partially infilled), S. Santiago Crater, SOC. Sapper-Oviedo Complex (infilled), M. Masaya Crater, SJ San Juan Crater, SF. San Fernado Crater (infilled), C. Comalito, CC. "Casas" cone.*

structure of the complex, with the aim of determining how it has evolved over the last ~2250 - 6400 years and why the volcanic edifices are located where they are. The observations and conclusions discussed below are the results of field work by the author in March 1994.

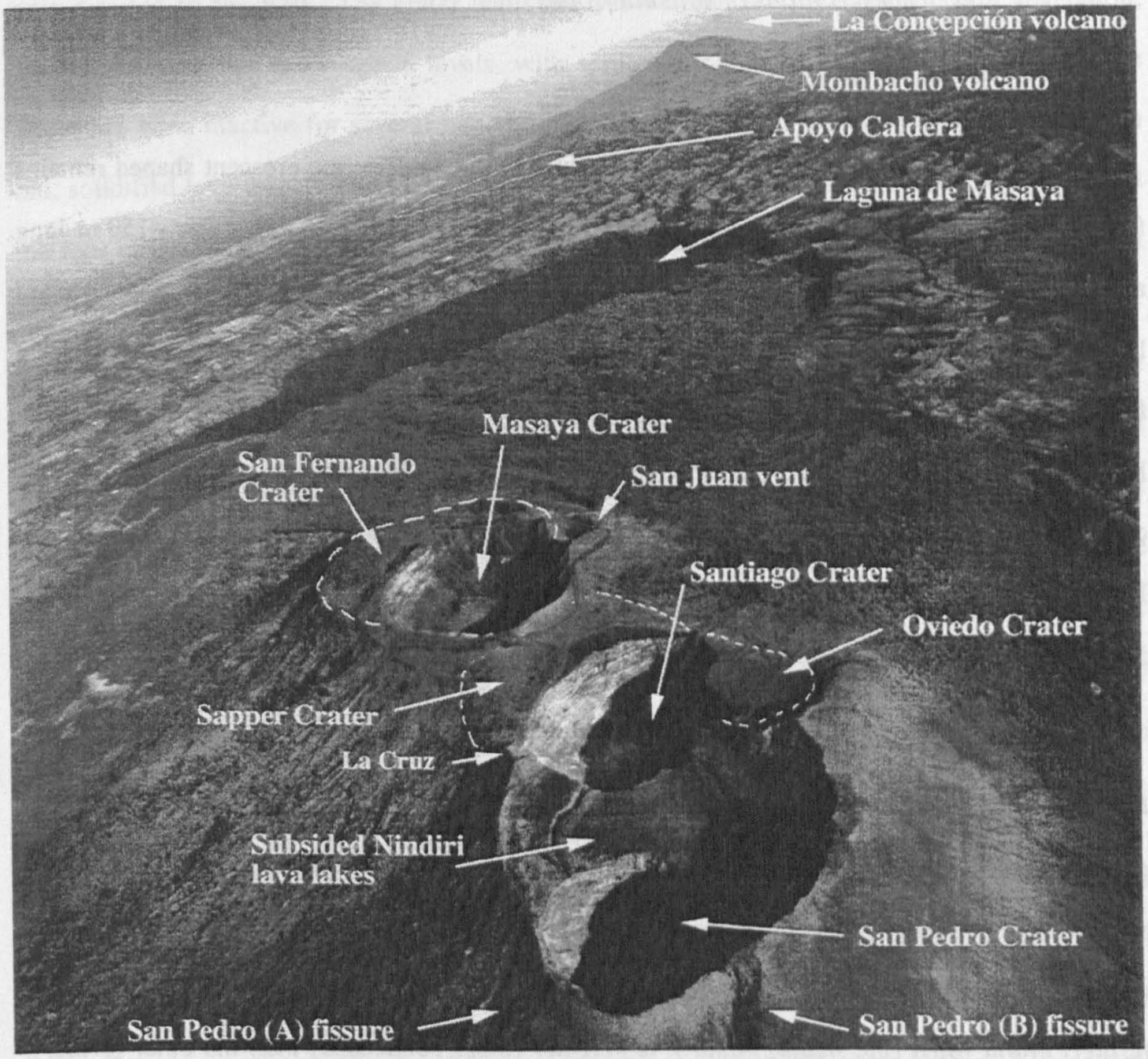

***Figure 3.3. B**. Aerial photograph of Volcán Masaya and Volcán Santiago within Masaya Caldera showing the main volcanic features discussed in the following sections (courtesy of INETER). The photograph is taken looking SE along the line of the volcanic front and illustrates the proximity of other volcanoes.*

I have divided the volcanic complex into three main areas: Volcán Masaya; Volcán Santiago and the remainder of the caldera floor. Volcán Masaya and Volcán Santiago together are composed of at least seven craters; two of which are exposed only in the walls of pit-craters. The five visible craters are: San Fernando, Masaya, Nindiri, Santiago and San Pedro, see **figures 3.2** and **3.3**. The main cones, found on the floor of the caldera, are: Cerro

Montosa, Arenal and Comalito. The formation of these and their relationships to each other are discussed below.

3.2.2 Descriptions of volcanic cones

San Fernando Crater

This is probably the oldest visible pit-crater in the caldera; the crescent shaped remains forming the flat area to the east of Masaya Crater. When whole, the crater was ~750 m long and ~600 m wide, with the long-axis oriented NE - SW and >100 m deep. Horizontally bedded lavas seen in the crater wall of Masaya Crater indicate that San Fernando underwent at least five cycles of lava lake formation and solidification, see **figure 3.4A-B**. The rim of San Fernando is approximately 30 m below the lip of Masaya Crater on the eastern side and is covered by channellised pahoehoe that has been erupted from the adjacent Masaya pit-crater. I have translated an excerpt of an account by the Conquistador, Oviedo y Valdes (1855, in McBirney, 1956) who described his visit to the Nindiri Crater in 1529.

"Continuing on from this crater (Nindiri) is a hill, the top of which is a ridge of hills leading towards the east, where a track lies, here another crater lies (San Fernando), as large as the other one which contains the smaller (vent at Nindiri?), this is higher towards the summit than the other (Nindiri). From this other crater (San Fernando) steam rises at night, and in the day although it is not so clearly seen, late at night it is clearer than the other (crater?); and when (the steam) mixes it is brighter (more condensed) than the other (crater); but at the bottom of this (San Fernando) there is no floor, rather having arrived at the wide rim the sides sloped downwards, closing-in to form a funnel, and at the bottom there was only ash."

This passage indicates that at the time of Oviedo's visit, San Fernando existed as a deep, funnel-shaped crater which was to some extent still active, as indicated by the emissions of gas, and possibly ash. The crater must have been filled by the lava lakes that outcrop in the walls of Masaya Crater prior to its collapse. Indeed, according to Oviedo (in McBirney, 1956) Masaya crater did not exist, a ridge of hills standing in its place.

Masaya Crater

Masaya is a large pit-crater ~150 m deep and 700 m by 600 m in size with the long-axis directed to the ENE. The crater walls are sub-vertical and over-grown with vegetation; mainly grass on the upper scoria levels, with scrub on the rockier parts; suggesting that the crater has been inactive for several hundred years. The flat, level crater floor appears to be an old, solidified lava lake. A short lava flow has issued from a small, ~10 m wide, vent located at the foot of the ENE wall to partially cover the crater floor. The position of the vent, along the line of the 1772 fissure, suggests that it may be connected with this eruptive fissure. Sub-vertical dykes in the SSE crater wall probably relate to the San Juan Lineament, a small fissure zone running SSE from Masaya, see **figures 3.4A-B**. A large scoria apron mantles the top of the western side of the crater; I have called this the Masaya Scoria Apron. This dips inwards at the crater lip, indicating the apron was formed after the pit-crater had initially formed. The lack of any scoria in the crater itself indicates that the crater floor was resurfaced after the eruption of the scoria blanket. The eastern third of the crater wall shows the dramatic change in lithology due to the incorporation of part of the lava-filled San Fernando pit-crater into the crater walls.

According to an account of Oviedo y Valdes (1855, in McBirney, 1956), the Masaya Crater did not exist in 1529. This enables the time of the collapse of Masaya Crater to be determined as after 1529, Oviedo's account, and before 1772, assuming the small vent in the crater floor is associated with the 1772 fissure eruption. In the 243 years before 1772, several events must have occurred: San Fernando Crater was infilled by successive lava lakes; this was then buried by a lava flow from the east side of Masaya; this eruption may have emptied the magma chamber below Masaya, forming a pit-crater; the formation and solidification of a lava lake in the bottom of the crater produced the flat crater-bottom. Only then was it possible for the tip of the dyke associated with the 1772 fissure eruption to form the vent situated in the NE corner of Masaya Crater.

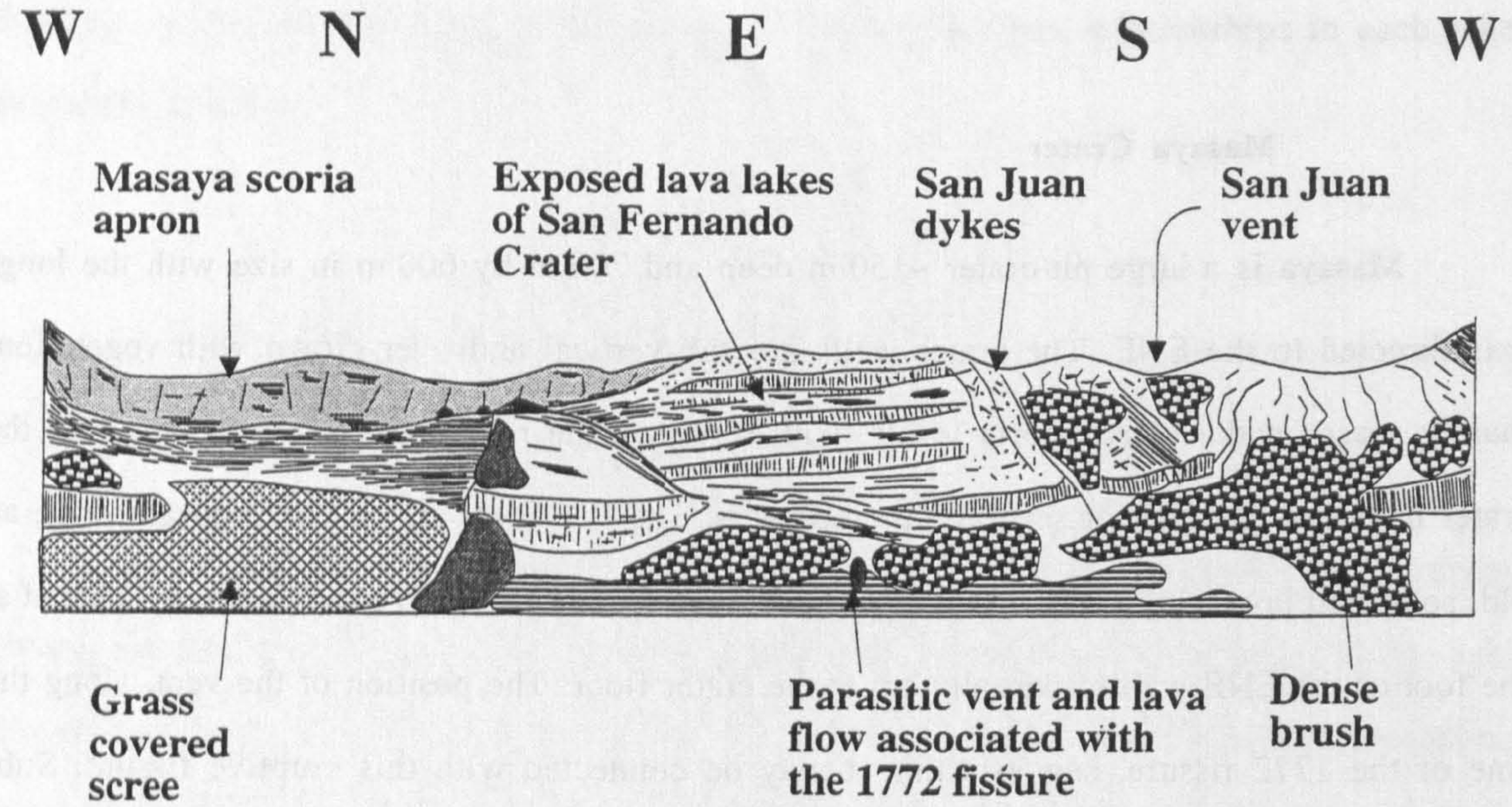

***Figure 3.4. A**. Sketch of the pit-walls of Masaya Crater showing the dykes associated with the San Juan Lineament and the lava lake layers which infill the adjoining San Fernando Crater. The eruptive vent possibly connected with the 1772 fissure eruption is also shown.*

San Juan Crater

San Juan is a small, parasitic vent ~60 m diameter high on the southern flank of Masaya Crater, see **figures 3.3A-B**. It appears free of scoria, the material round the lip being spatter that dips inwards indicating it was formed after the Masaya scoria apron was deposited. Walker et al. (1993) indicated that this vent may have been connected with the 1772 eruptive fissure. The crater is also on a short line of small scoria cones which lie almost due south; termed here, the San Juan Lineament.

Sapper and Oviedo pit-craters

These craters can only be seen in cross-section, outcropping in the walls of Santiago Crater and so have not been named in the literature. I have named them the Sapper and Oviedo Craters; after the two level areas to either side of Santiago Crater, Plaza Sapper and Plaza Oviedo, which mark their lateral extent, see **figure 3.3B**. Sapper Crater, estimated by the author to be ~600 m across, lies between the southern edge of the Masaya scoria apron and the

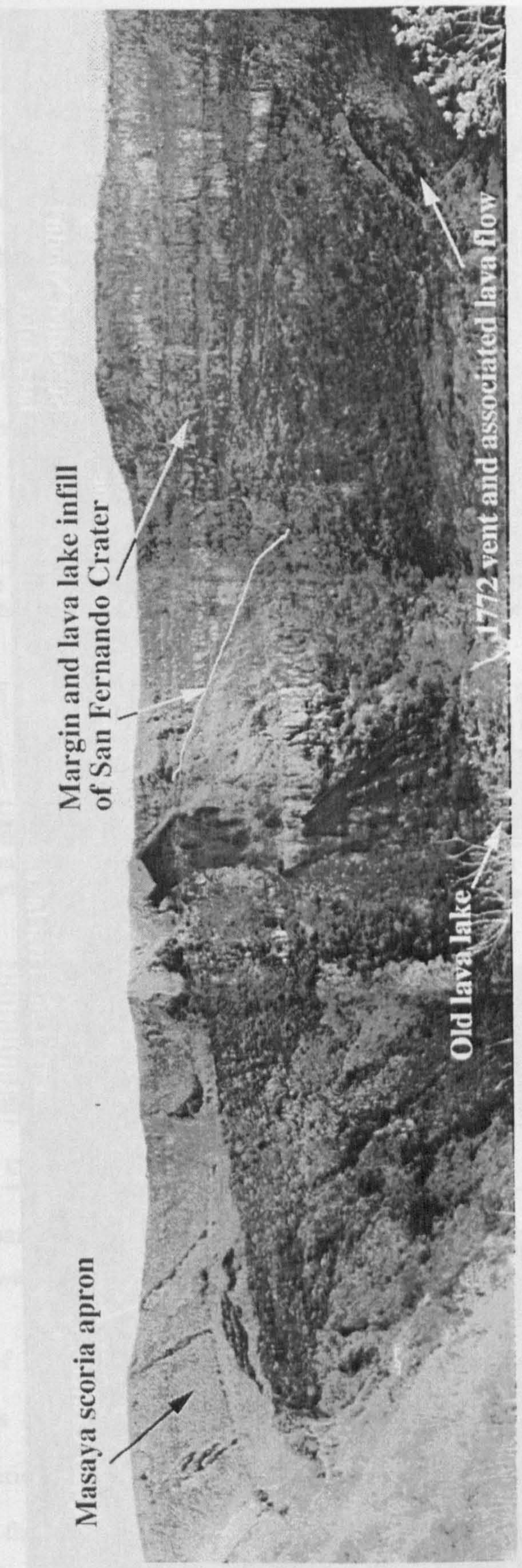

***Figure 3.4. B**. Photograph of Masaya Crater, taken looking ~NE. This shows the level lava lakes of San Fernando Crater and the vent possibly associated with the 1772 fissure eruption.*

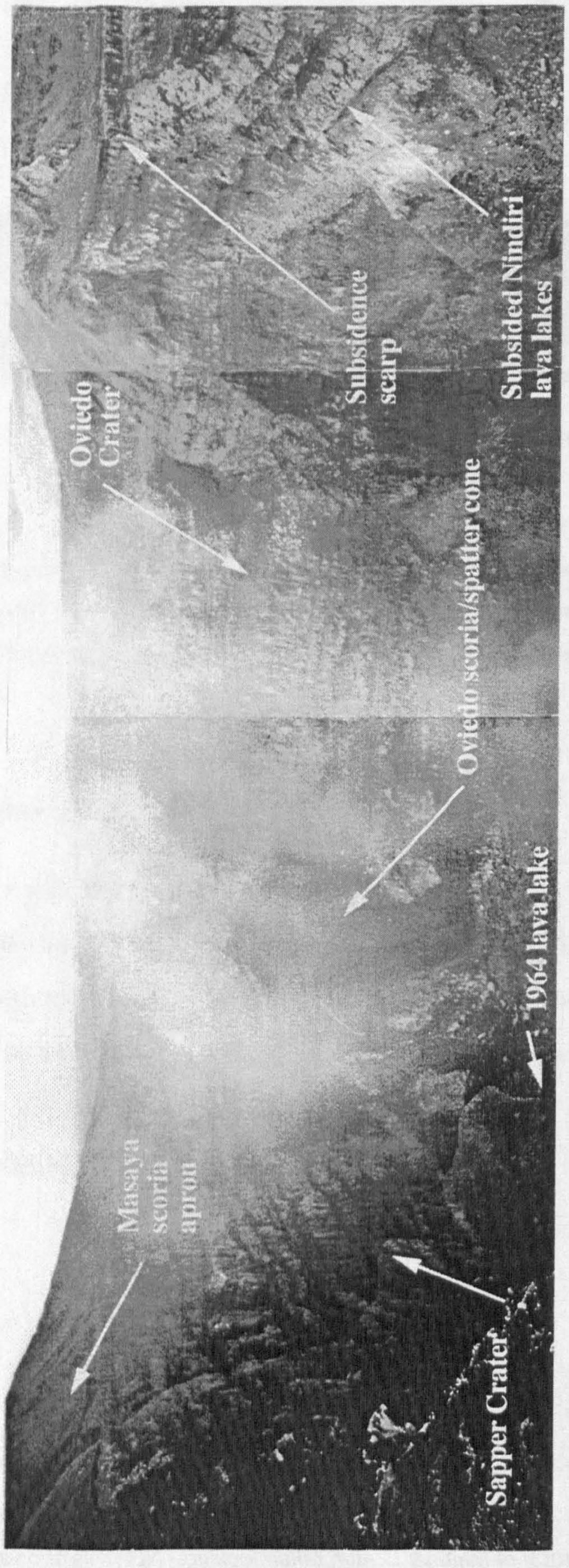

Figure 3.5. A. *Photograph of the southern half of Santiago Crater, showing the cross-sections through the Sapper and Oviedo Craters.*

La Cruz hill. It is infilled with a regular sequence of ~20 solidified lava lakes down to a depth of ~160 m; below this level is a mass of breccia which may represent the original debris from the collapse of the crater. At the southern end of the crater, lava lake layers interfinger with and have lapped on to the flank of a large scoria/spatter cone ~200 m in diameter and of similar height. A further series of ~20 layered lava lakes, as inferred from their horizontal nature, interfinger with the opposite flank of the scoria/spatter cone, see **figure 3.5A-B**. The concentration of lava lakes suggests that these have accumulated in a crater, called here the Oviedo crater. I have estimated its diameter at ~350 m and a depth, from the Plaza Oviedo, of over ~150 m.

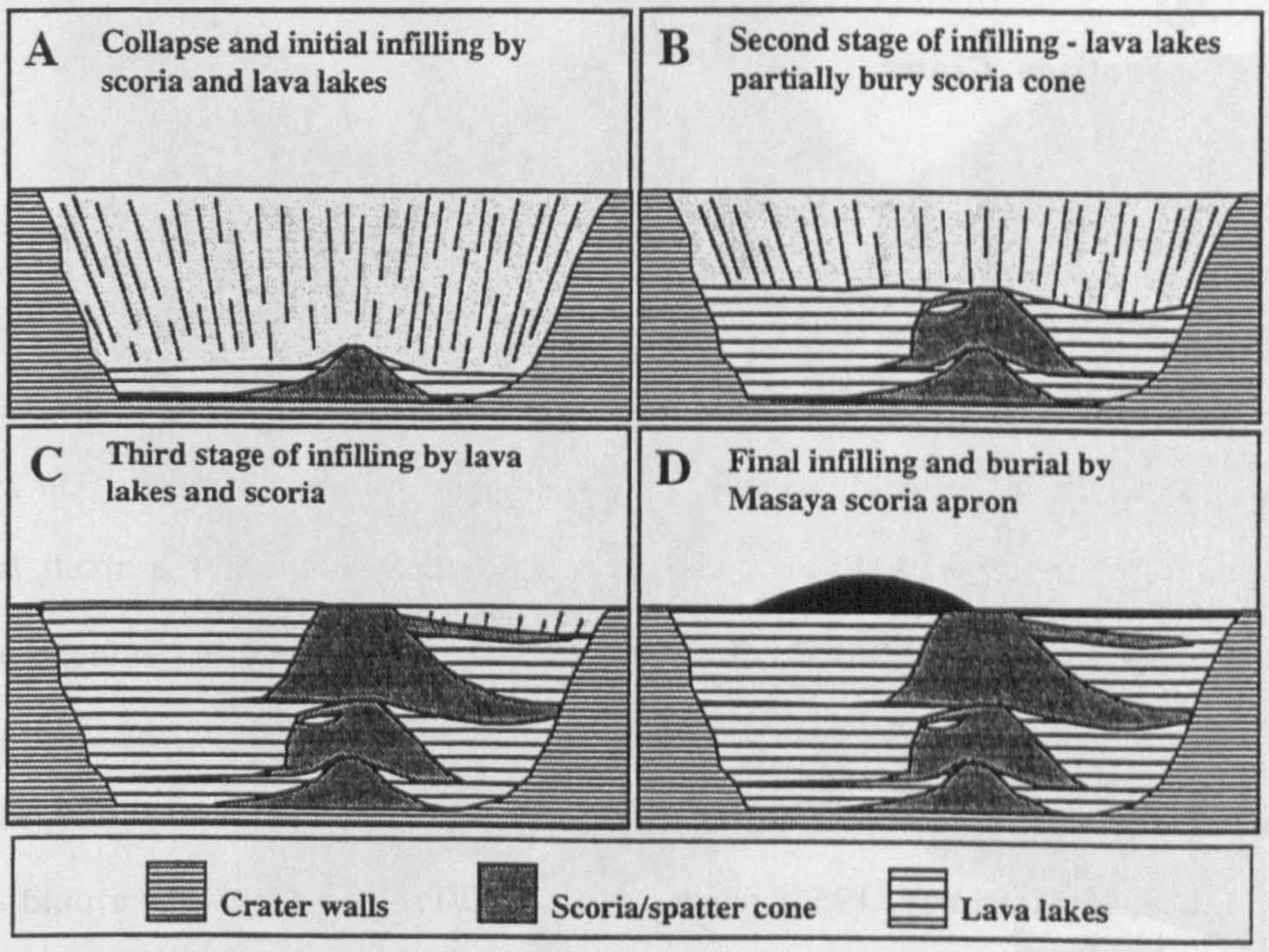

***Figure 3.5. B**. Schematic diagram illustrating the gradual evolution of the Sapper and Oviedo Craters in conjunction with the large Oviedo spatter/scoria cone that separates them.*

The number of lava layers in the Oviedo and Sapper craters is similar; however, the spacing and thickness of the layers are quite different with those in Oviedo crater being separated into three series. I have interpreted the interfingering between the scoria/spatter cone and the lava lakes of the Oviedo and Sapper Craters as indicating that there have been three phases of eruptive activity, see **figure 3.5B**. The presence of an almost continuous lava layer through the middle of the scoria cone appears to connect two lava lakes of approximately the

same thickness; suggesting both craters were linked to the same magma source for at least part of their existence. The construction of the scoria/spatter cone was contemporaneous with the infilling of the two craters to provide the delicate interfingering and interbedding seen in the walls of Santiago Crater. This implies that an elongate depression over 150 m deep and ~750 m in length formed with a NE - SW orientation; Sapper Crater was situated at the NE end of this depression with Oviedo Crater at the SW end. Subsequent strombolian activity in a vent located towards the SE end of the depression formed a septum, preventing the intermittent lava lakes that formed to either side from connecting; other than on one occasion half-way through the gradual in-filling of the craters.

Santiago Crater

The formation of Santiago Crater

The description of the formation of Santiago Crater comes through the accounts of Montessus de Ballore (1888, in McBirney, 1956). He reports that on 8/6/1852 Laguna de Masaya began to bubble, probably escape of CO_2 trapped in lake sediments. On 29/6/1852 "underground rumblings" were heard and he reported the presence of a small lava flow appearing three days later. On 9/5/1853 steam and gases rose from Volcán Santiago, indicating the presence of an open vent. McBirney (1956) inferred from the lack of any descriptions of ash eruptions that the magma level must have been at some depth below the vent. Montessus de Ballore (1888, in McBirney, 1956) reports that on 10/11/1858 there was a mild eruption. This was followed by strong "underground rumbling" and gas and ash venting on 27/1/1859. I have interpreted this account as the influx of new magma, and hence seismicity, which led to the gradual removal of material below the surface of the unformed pit-crater. Eventually, in 1853, the surface cap over a small vent/crater caved in, allowing gases to escape. The strong seismicity reported in early 1859 relates to the final formation of the pit-crater, possibly as a result of magma withdrawal. This is exactly the same as the formation of the Bocca Nuova at Mt. Etna, which initially formed by the collapse of a thin crust over a deep vent, before later collapsing to form a large pit-crater (Chester et al., 1985).

Recent changes

Santiago Crater contains the only active vent in the volcanic complex. It is also the deepest of the open craters, with the vent lying at 294 m below the Plaza Oviedo car park; as measured by Murray and the author using EDM. The main crater is ~500 m by 600 m across and ~150 m deep. At its centre lies an inner-crater, approximately 200 m by 130 m in size and ~150 m deep which formed in April 1989, see **figure 3.6A**.

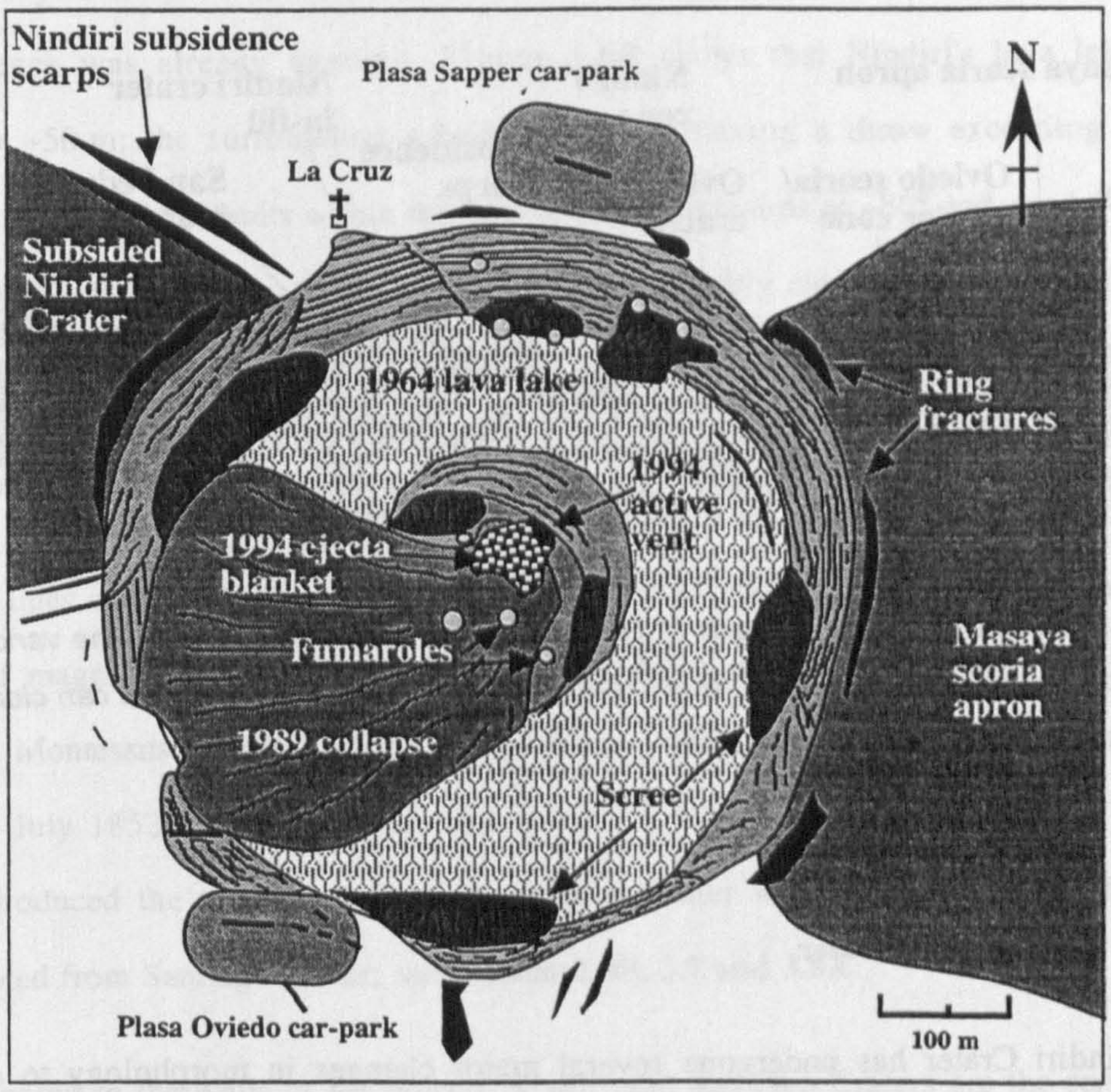

Figure 3.6. A. *Schematic diagram of Santiago Crater showing inner-crater, fumaroles and collapse debris, as seen in 1994 by the author. Also shown are the fissures relating to the slow inwards-collapse of the pit-crater.*

The walls of the both main crater and inner-crater are vertical; except for the southern quarter where a large collapse with a volume estimated at ~50,000 m^3 occurred in 1989 burying the active vent (Talena, pers. com.). Activity did not resume until June 1993 when strombolian activity formed a small ejecta blanket outside the vent located at the foot of the

northern inner-crater wall. Murray and the author measured the vent in March 1994 using EDM; this was ~12 m long E-W with a width of 3 m, see **figure 3.6A**, and was thought by Murray to dip beneath the crater wall at an angle of 80° to a depth of ~40 - 80 m. This was buried by a small collapse in April 1997; but had reopened in March 1998 slightly to the west of its earlier position (van Wyk de Vries, pers. com.). The remains of three pit-craters can be seen in the walls of the main crater: one to the NE, Sapper Crater; one to the south, Oviedo Crater; and one to the west, Nindiri Crater, see **figures 3.5A** and **3.6B**.

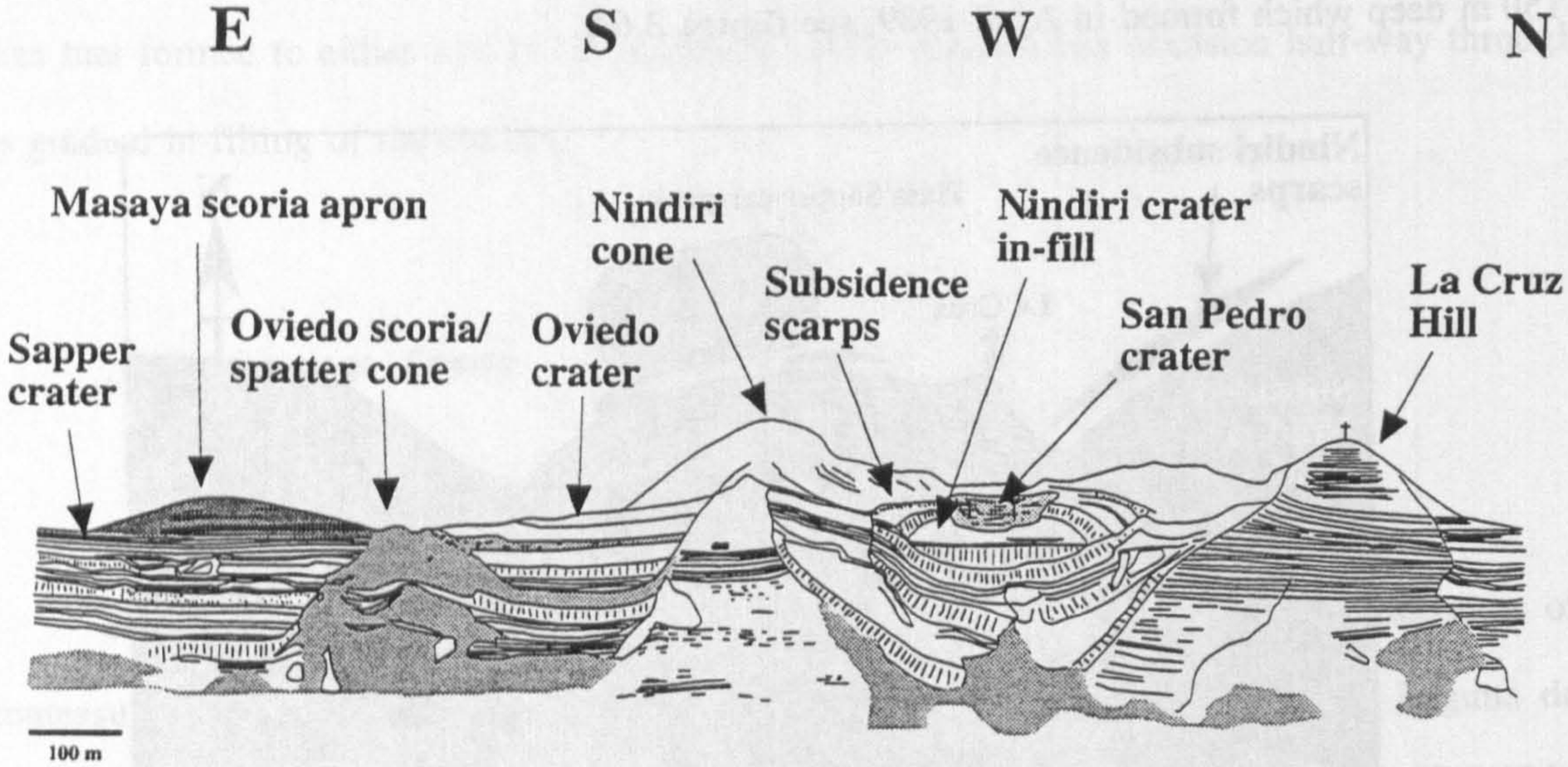

Figure 3.6. B. *Sketch of the pit-walls of Santiago crater in 1994 illustrating the various features that can be seen. Cross-sections through Nindiri, Oviedo and Sapper Craters can clearly be seen as well as the Oviedo scoria/spatter cone.*

Nindiri Crater

Nindiri Crater has undergone several major changes in morphology to achieve its present form; these are described below drawing on the field relations of various ash and lava layers and crater collapses, see **figures 3.3B**, **3.7** and **3.10A-E**. Nindiri was the active crater during visits by the Conquistadors in 1525 and 1529 (Oviedo, 1855, in McBirney 1956). Their earliest accounts, in 1525, describe Nindiri Crater as being ~216 m deep with a flat bottom with a vent ~12 m by ~15 m situated close to the southern side of the crater floor. This contained a lava lake, ~66 m below the level of the crater floor. They also reported the presence of a very fresh lava flow which had issued from Nindiri Crater, and now lies

immediately to the north of Santiago Crater. This suggests that the level of magma within Nindiri Crater was capable of rising and falling by almost 300 m over a period of a few years. Little is known about activity at Nindiri crater until 1670 when lava overflowed from the northern rim of Nindiri crater, forming a lava flow ~3 km long (Rymer et al., 1997). Between 1570 and 1840 Nindiri Crater filled up by repeated formation of lava lakes, see **figure 3.6B**.

Major subsidence occurred after the lava infilling Nindiri Crater had solidified; forming fault-bounded scarps on the NE and SW sides of Nindiri Crater and the downwarping of lava lake layers. Stephens (1841 in McBirney, 1956) visited the crater in 1840 and reported that subsidence was already ongoing. **Figure 3.6B** shows that Nindiri's lava lakes have subsided by ~50 m; the surrounding subsidence scarps having a throw exceeding 15 m in some places. Some of the faults within the lava lakes dip outwards at ~80° and can be traced in the crater walls to depths of >50 m. Subsidence was probably caused by magma withdrawal from beneath the central part of Nindiri. Walker et al. (1993) reported a volume for the 1670 lava flow of ~10.6×10^6 m^3. I have assumed that the diameter of the magma chamber beneath the Nindiri Crater is similar to that of lava lake subsidence, ~520 m, which extends ~40 m beyond the lines of the subsidence scarps. The eruption of 10.6×10^6 m^3 of lava would lower the level of magma remaining in the chamber by ~50 m; similar to the observed lava lake subsidence. Montessus de Ballore (1888, in McBirney, 1956) reported a further period of lava effusion in July 1852, after subsidence had stabilised. The ponding and cooling of this lava probably produced the level surface of the Nindiri Crater which has since been buried by tephra erupted from Santiago Crater, see **figures 3.6B, 3.7** and **3.8A**.

Exposed in the walls of the present Nindiri and Santiago Craters are the remains of a large tuff cone, centred over the subsided Nindiri Crater. I have called this the Nindiri Tuff Cone; the distal western edge of which outcrops in the western wall of the San Pedro pit-crater whilst the northern parts form the upper parts of the La Cruz hill. In both locations it lies above intercalated aa lava flows, breccia and spatter which probably relate to the initial cone building stage of Volcán Santiago, see **figures 3.7** and **3.10E**. The cone consists mainly of interbedded ash and fine scoria. A smaller, partially truncated tuff cone, separates the Oviedo and Nindiri pit craters and lies unconformably on the older Nindiri Tuff Cone.

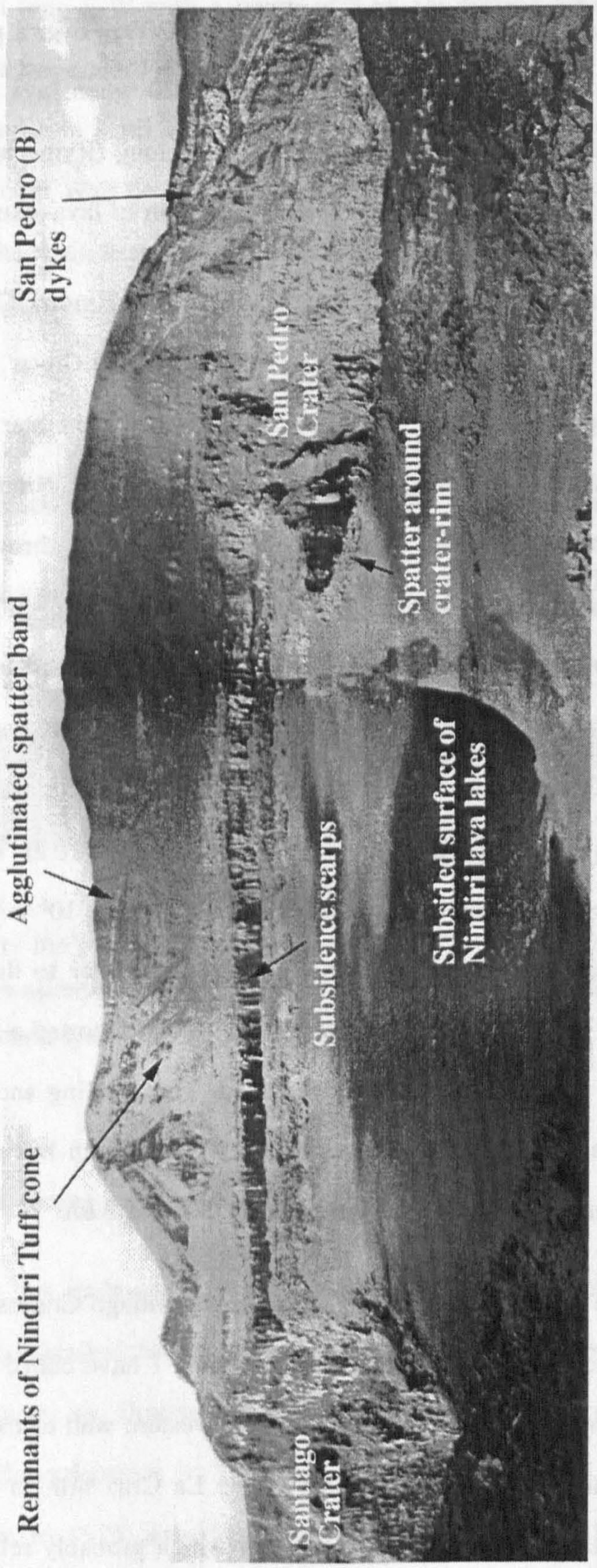

Figure 3.7. *Photograph of the SW crater wall of Nindiri Crater. taken from La Cruz hill, looking SW. This clearly shows the subsidence scarps and the pyroclastic nature of the southern portion of the Nindiri Crater. This also shows the rim of spatter around San Pedro Crater and the level nature of the subsided Nindiri lava lakes, now buried by tephra ejected from Santiago Crater.*

The dip of the ash layers indicate that the eruptive vent was probably close to the area occupied by the current Santiago inner-crater. The main edifice of Nindiri Crater takes the shape of a large, ~700 m in diameter, crater with sub-vertical slopes. The northern and western rims of this larger crater are low and comprised predominantly of basaltic lava flows. By contrast, the much higher southern rim is composed of ash at the base with agglutinated spatter and ash above, see **figure 3.7B**. Prior to collapse this edifice would have been the highest in the caldera.

San Pedro pit-crater

Montessus de Ballore (in McBirney, 1956) recorded a series of events at Masaya during the period January to March 1859. Initially there was a mild eruption, this was followed by ground tremors and finished with ash eruptions and the formation of a gas plume which damaged local vegetation. It was during this period that both the San Pedro and Santiago pit-craters formed. I have taken the short time between the formation of the Santiago and San Pedro pit-craters to suggest that storage of magma must have taken place over a wide area and at a shallow depth. San Pedro Crater currently is ~350 m in diameter and ~200 m deep and contains a small inner-crater ~130 m in diameter close to the eastern wall. I have interpreted the level bottom of the inner-crater as representing a solidified lava lake. A thick layer of agglutinated spatter immediately around the rim of the main crater suggests that strombolian activity has occurred since its formation, see **figure 3.7**. More recently a collapse of part of the western wall has formed a large scree slope that has partially buried the inner-crater.

Walker et al. (1993) described some of the flows emanating from Nindiri and flowing to the NW as being from San Pedro and its associated fissure; these may have occurred towards the end of the period of Nindiri lava lake formation and before the present crater formed in ~1859. There are several vertical dykes in the western wall of the pit-crater, one of which fed a small scoria cone and is linked to the now almost buried San Pedro (A) fissure which runs to the NW, see **figures 3.3B** and **3.8A-B**. A higher density of dykes to the SW of the scoria cone

mark the much deeper, and probably younger, San Pedro (B) fissure which runs parallel to the San Pedro (A) fissure and can be traced almost to the Cerro Montosa cone, ~1.5 km to the NW.

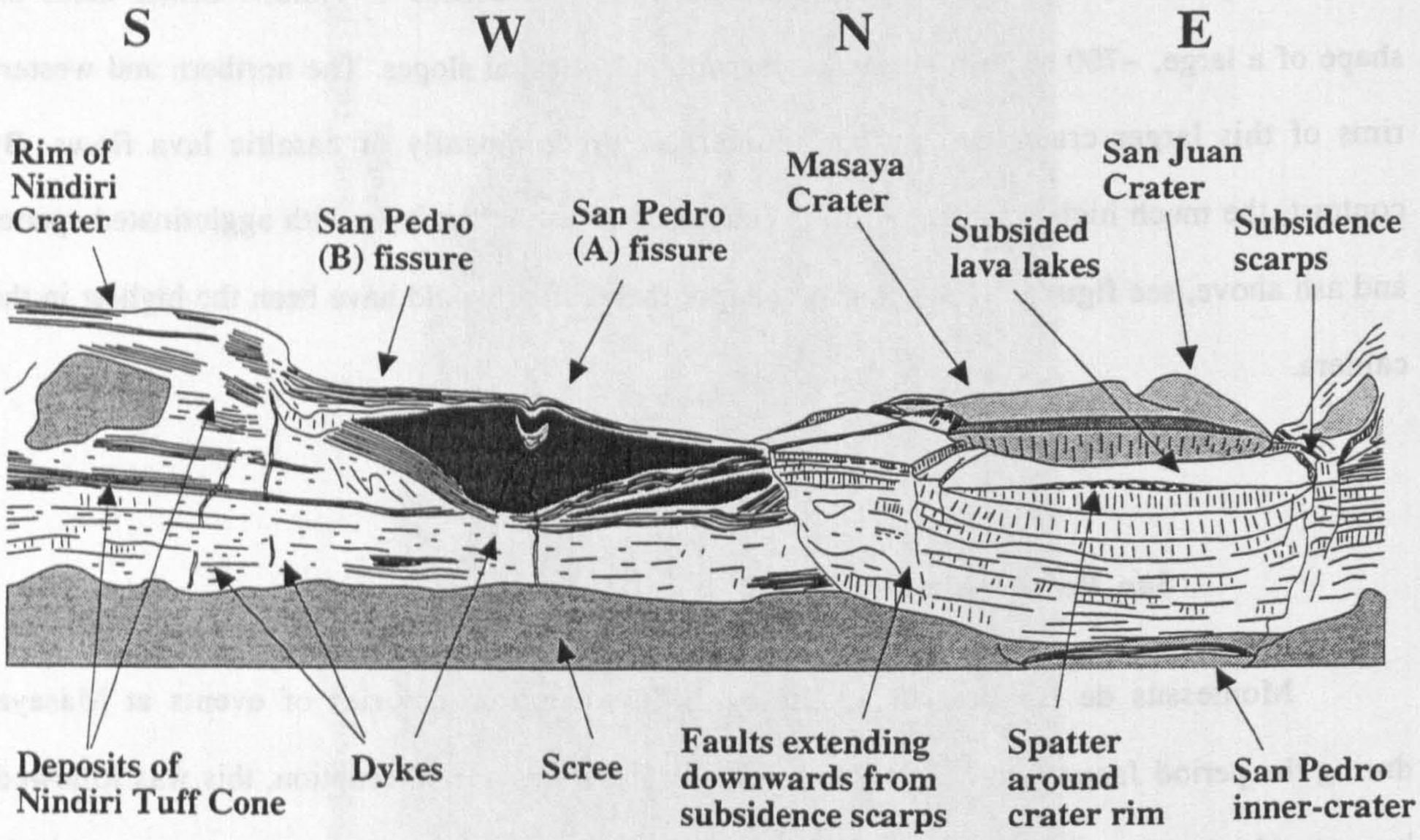

Figure 3.8. A. *Sketch of San Pedro Crater showing the main structures including the dykes associated with San Pedro (A) and (B) fissures and the subsided Nindiri lava lakes.*

Comalito cone

This is a breached scoria and spatter cone, open to the NE with a diameter of ~120 m. To the NNE is a succession of smaller spatter vents; the sizes of these craters range from ~10 m to ~40 m and generally have a <10 m deep pit in the centre. The series of vents was probably associated with the formation of the Visitor Centre fissure zone which has a similar strike and is located ~300 m to the NW, see **figure 3.3A-B**. A fumarole field lies between Comalito and the Visitor Centre fissure zone; I estimated temperatures here to be ~60° - 80°C in 1994.

Cerro Montosa, Arenal and other cones.

Cerro Montosa is a large scoria/spatter cone ~600 m in diameter. It is quite eroded and open to the NE; the SW rim being much higher due to deposition of scoria and ash blown by

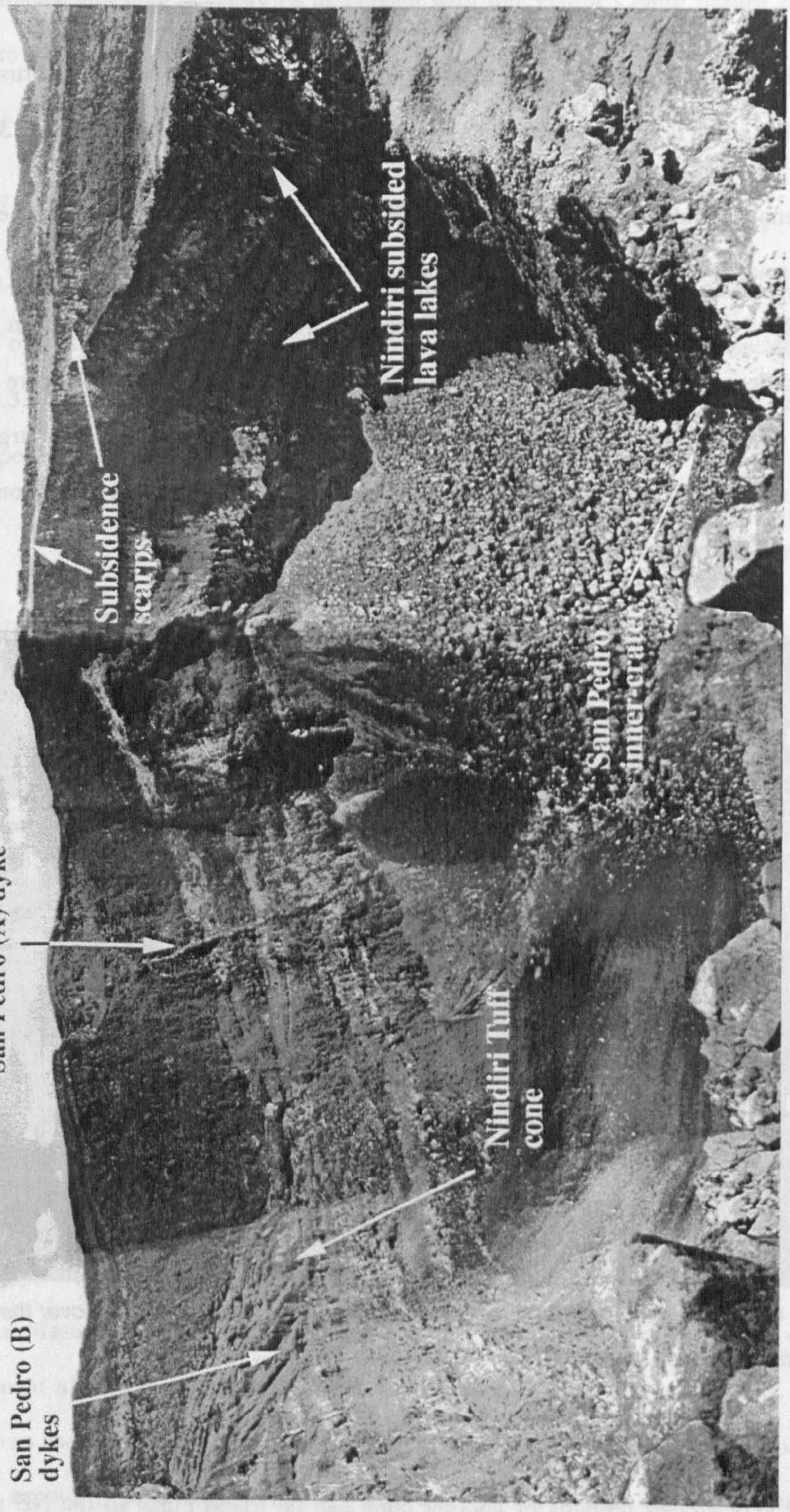

***Figure 3.8. B**. Photograph of the walls of San Pedro pit-crater, looking due north. Visible are the dykes in the western wall and the succession of lava lakes in the eastern wall which in-fill the Nindiri Crater.*

the prevailing NE winds. The cone is quite vegetated, being covered mainly in brush and small trees suggesting that it is one of the older structures in Masaya Caldera, see **figure 3.9**.

Arenal is probably older than Cerro Montosa, as it is considerably more eroded. It is also much smaller being ~200 m in diameter; the highest point again being on the SW side of the crater. It is composed almost entirely of scoria, with large bombs up to 50 cm in diameter being found deep within the excavated parts of the cone. Material close to the core of the cone is reddish; indicating prolonged oxidation caused by the rapid deposition of a large thickness of erupted material. I have therefore inferred that Arenal was a monogenetic cone, possibly formed over a period of a few weeks at most.

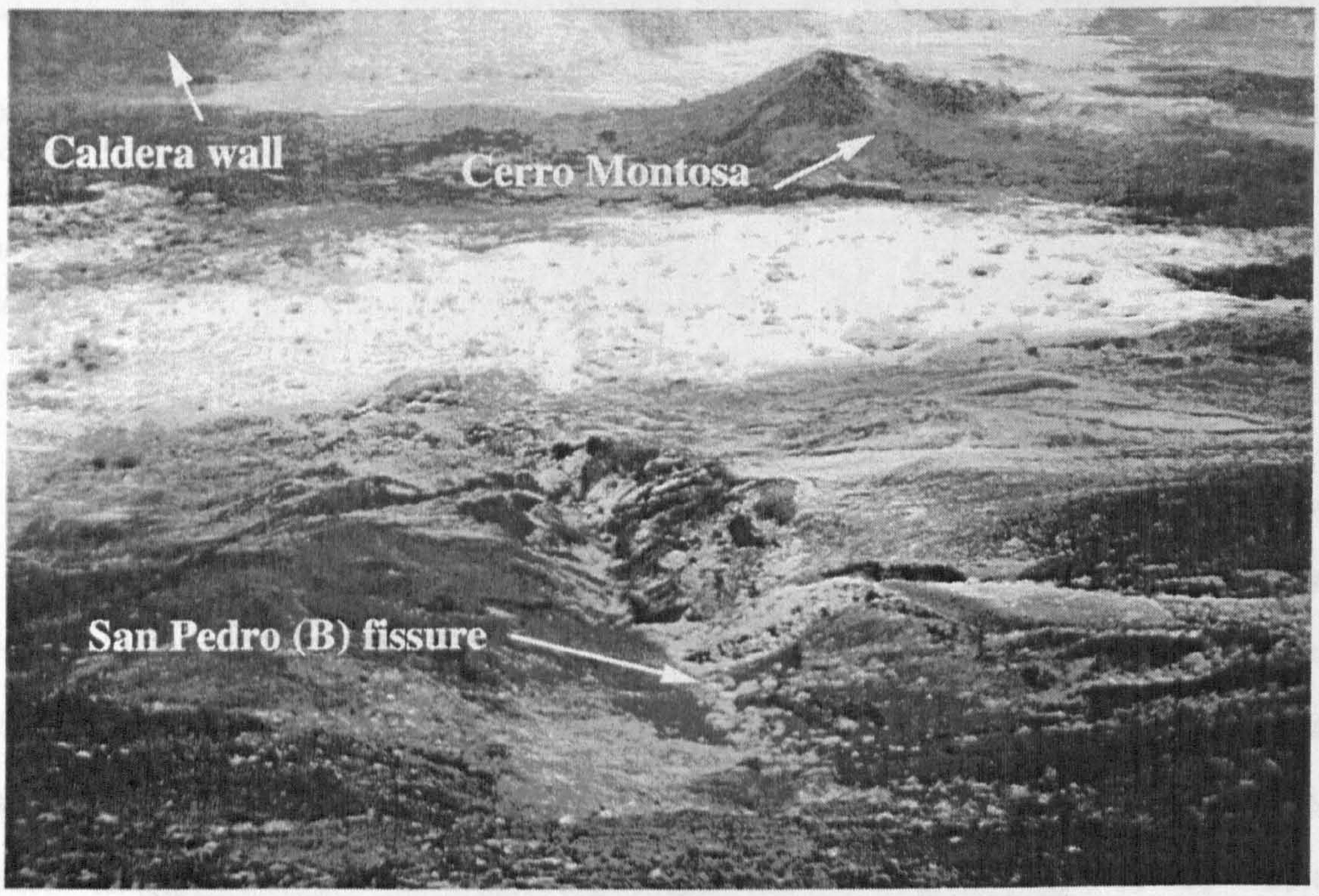

***Figure 3.9**. View from the western rim of San Pedro Crater looking to the NW over the San Pedro (A) and (B) fissure zones towards Cerro Montosa.*

The very eroded remains of another cone can be found close to the NE wall of the caldera; because of its location I have called it the "Casas" cone, see **figure 3.3**. This is ~250 -

300 m in diameter and may possibly be associated with the Visitor Centre fissure zone which lies directly to the SSW of it.

3.2.3 Fissure zones and lineaments

I have identified six fissure zones/lineaments using field mapping, aerial photography and the map of Williams (1983) - modified by Walker et al. (1993); these are described below, see **figure 3.3**. Previous authors (e.g. McBirney, 1956; Walker et al., 1993) have occasionally mentioned specific features; their observations are included below.

The 1772 fissure zone

This fissure was the site of the most recent effusive episode within the Masaya Volcanic Complex, occurring in 1772 (Walker et al., 1993); McBirney (1956) having erroneously confused the eruption dates of the 1772 fissure and 1670 Nindiri eruptions. Williams (1983 and references therein) reported that the eruption began after only two hours of earthquakes. After the opening of the fissure a large aa flow formed with a volume of ~2.3×10^7 m^3. This initially flowed northwards before diverging; part overtopping the lowest part of the northern caldera wall and flowing ~3 km northwards; the rest following the caldera wall eastwards into Laguna de Masaya. This is the only post-caldera flow that has managed to overtop the caldera wall on the northern side (Walker et al., 1993).

The 1772 fissure system lies directly between an eruptive vent on the northern caldera rim and Masaya crater and extends for ~2.5 km with a ~020° orientation, see **figure 3.3A**. The small vent in Masaya Crater; San Juan Crater and the most northern of the cones of the San Juan Lineament all lie along the line of the fissure if it is extended southwards. The 1772 fissure follows the line of the major regional Cofradía Fault, which lies buried beneath the caldera and, according to Williams (1983), marks an important crustal segment-break. The line of the 1772 fissure may also be extended northwards to the caldera wall, where the effusive vent associated with the "Railroad flow" of Williams (1983) is located. He proposed that this

lava flow erupted after caldera collapse, using a ring fracture as a conduit. I have inferred from the presence of extensional faults in the vicinity of the 1772 lava flow outside the caldera that this area is a small half graben, bounded by the Cofradía Fault system (Metaxian, 1994; van Wyk de Vries, pers. com.). The ensuing subsidence caused by the graben therefore enabled the 1772 lava to overflow the lowered northern part of the caldera wall; ponding alongside the earlier "Railway flow" which probably took advantage of the same topographic low.

Visitor Centre fissure zone

This fissure, oriented ~010°, runs almost parallel to the 1772 fissure and lies between the Comalito and "Casas" cones. I have called it the Visitor Centre fissure as the new visitor complex, which manages the Masaya National Park, is located on the highest part of the fissure system. The high level of vegetation on the fissure suggests that this is far older than the 1772 fissure; which is almost devoid of vegetation. The southern end of the fissure zone, close to the Comalito cone, is still an area of fumarolic activity. Van Wyk de Vries (pers. com.) recorded gas temperatures of ~68°C here in early 1997. The alignment of this fissure is probably controlled by the proximity of the Cofradía Fault, which has a strike of ~020°, and the possible presence of a cone-sheet, see Section 3.2.5.

South Line Lineament

This slightly segmented line of scoria and spatter cones runs at ~200° from the southern caldera wall for ~2.5 km. The low topographic relief tends to indicate that this fissure is much older than the 1772 fissure. Walker et al. (1993) have suggested the highly vegetated lava flow associated with this fissure is one of the oldest post caldera flows. The orientation of the lineament is almost parallel to the Visitor Centre fissure and again may be the surface expression of the buried Cofradía Fault.

San Pedro (A) and (B) fissure zones

I identified two fissure zones emanating from the western end of Volcán Santiago using aerial photographs kindly provided by INETER, see **figure 3.3B**. These originate from the region of the San Pedro pit-crater and, with similar orientations of ~135°, stretch for ~0.5 and ~1.0 km for (A) and (B) fissures respectively. I have assumed that fissure (A), which is the least distinct, is the older of the two. This fed the small scoria cone seen outcropping in the western wall of the San Pedro pit-crater. The wider fissure (B) lies ~200 m SW of fissure (A) and can also be seen outcropping in the western wall of the San Pedro pit-crater as a swarm of thin vertical dykes, see **figures 3.8A-B** and **3.9**. Fissure (B) has undergone fairly active strombolian eruptions as evidenced by the widespread spatter which mantles the southern portion of the fissure. I have inferred that eruptive activity on both fissures must have occurred prior to the collapse of the Nindiri pit-crater as the dykes relating to the fissures are exposed in part of the San Pedro/Nindiri crater-wall.

Cerro Montosa Lineament

This runs between the Cerro Montosa and Arenal cones and is oriented ~025°. It consists of a number of small spatter and scoria cones on a segmented ridge, the Los Sastres of McBirney (1956). The intense vegetation and poor topographic expression of the fissure suggests it is fairly old. Walker et al. (1993), based on the stratigraphy of Williams (1983), concur with this, suggesting that Arenal, its associated fissure and small flows were the oldest visible flows within Masaya Caldera.

San Juan Lineament

This can be seen as a rough line of 3 or 4 low spatter cones running ~160° from San Juan southwards for ~700 m. These may lie on a continuation of the San Pedro fissure system or possibly relate to part of the Cofradía Fault system, see **figure 3.3**. The cones are located in a ~1 km wide zone occupied by the 1772, Visitor Centre fissures and the South Line

Lineament which also runs along the probable strike of the Cofradía Fault and may therefore reflect a line of preferential magma migration to the surface.

3.2.4 Order of edifice formation

I have used my field observations and the historical accounts reported in McBirney (1956) to derive an approximate sequence of events which has governed the evolution of the Masaya Volcanic Complex, see **table 3.1**. The relationships of the volcanic centres which do not form part of the massifs of either Volcán Santiago or Volcán Masaya can not be accurately placed in this stratigraphy as they do not interact with any other edifice; these structures are in *italics*. Text in **bold** marks major events. None of the edifices or lavas have been dated and not all recent events may be noted in the historical records and so the stratigraphy is only a relative one. **Figure 3.10A-F** summarises the evolution of Volcán Santiago and Volcán Masaya in graphical form.

It is, at this stage, impossible to insert the formation of Cerro Montosa, Arenal and Cerro Montosa fissure zone into the time sequence with any degree of certainty. However, judging by the similar erosional states to Masaya Crater, they were probably formed only a few hundred years earlier. It is not possible to determine the nature of the volcanic structures within the caldera prior to ~1 ka ago. However, the large volume of caldera infill, ~12.8 km^3, and higher NW half of the caldera suggests that one or more vents were situated within it, possibly in similar locations to the current vents. The stratigraphy outlined above concurs with that of Walker et al. (1993) which details some of the main collapse and cone forming events.

***Table 3.1** (overleaf). Summary of list of events that contributed to form the visible parts of the Masaya Volcanic Complex taken from the author's field observations. Bold text refers to main events; italicised text to features whose age cannot be directly gauged from field relations. *Walker et al. (1993); #Rymer et al. (1997); §Bice (1980); ‡McBirney (1956).*

Structure or event	Date
Formation of Santiago crater inner-crater	1986 - 1989
Formation of current crater floor in Santiago Crater by a lava lake	#1965
Formation of San Pedro lava lake	
Collapse of San Pedro inner-crater	
Collapse of Santiago and San Pedro pit-craters	#*1859
Lava eruption and formation of flat area in Nindiri Crater	*1852
Eruption of 1772 Fissure and Masaya micro-vent	#1772
Nindiri lava-lake subsidence	‡pre-1840
Collapse of east wall of Nindiri Crater	‡pre-1840
Overflow from the Nindiri pit-crater	#1670
Formation of San Juan vent	
Infilling of Nindiri crater by successive lava lakes	
Partial infilling of Masaya pit-crater by successive lava lakes	
Formation of Masaya scoria apron	
Collapse of Masaya pit-crater	
Lava lake in bottom of Nindiri pit-crater	*1525
Collapse of Nindiri pit-crater	
Eruption of San Pedro (B) fissure-zone	
Eruption of San Pedro (A) fissure-zone and west Nindiri scoria cone	
Formation of peripheral scoria vents around edge of Nindiri	
Infilling of San Fernando Crater with lava lakes	
Eruption of San Juan lineament	
Formation of San Fernando crater	
Eruption of Visitor Centre fissure zone and Casas and Comalito cones	
Infilling of Oviedo and Sapper pit-craters	
Formation of the Oviedo - Sapper scoria cone	
Collapse of Oviedo and Sapper pit-craters	
Formation of Oviedo and Nindiri Tuff Cones	
Formation of pre-Nindiri and Masaya volcanic cones	
Eruption of Cerro Montosa fissure zone	
Formation of Cerro Montosa and Arenal cones	
Eruption of South Line Lineament	
Possible gap in observed eruptive activity of ~1200 - 5400 years	
Collapse of Masaya Caldera	§2.25 - 6.5 ka

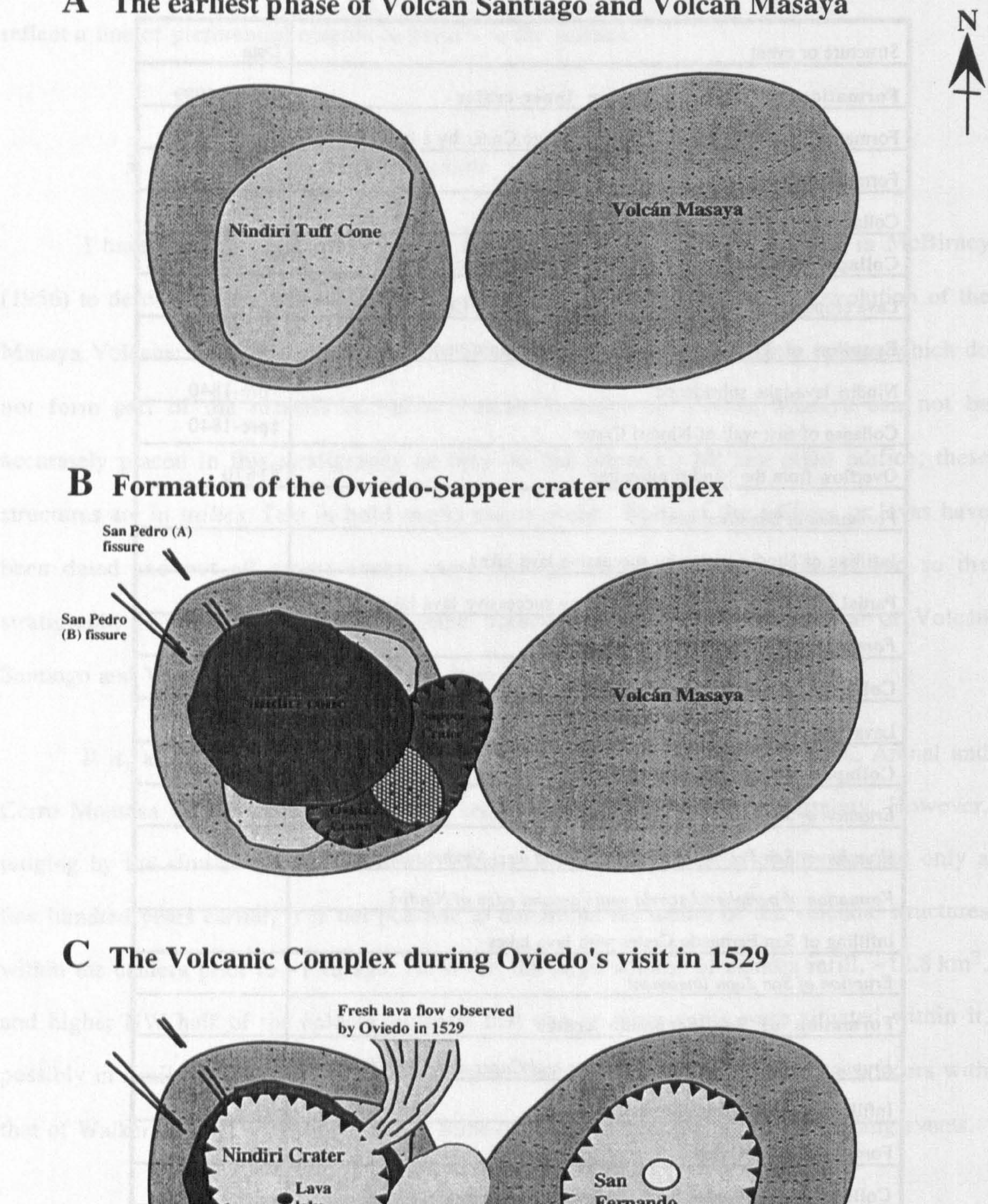

Figure 3.10. A-C. *See page 126 for figure caption.*

D The Volcanic Complex between 1529 and 1772

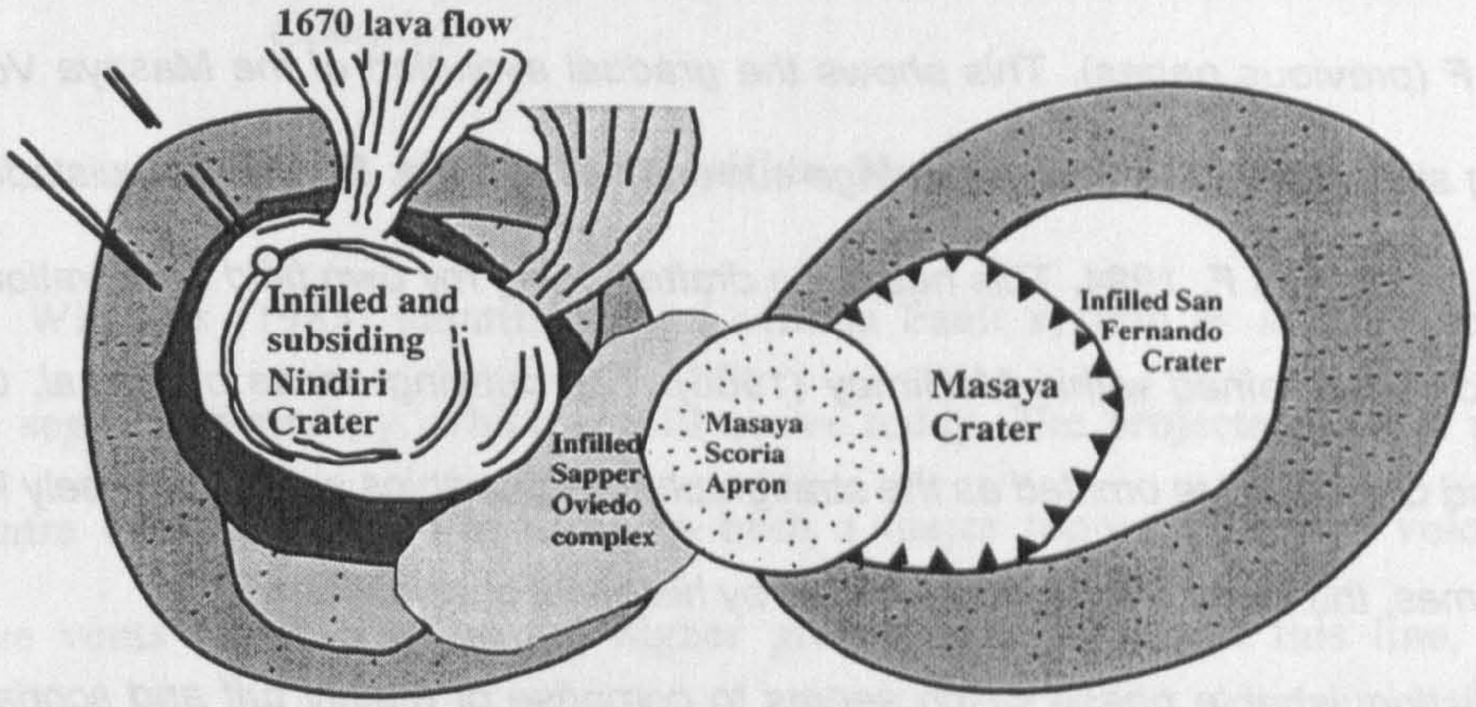

E The Masaya Volcanic Complex in 1859

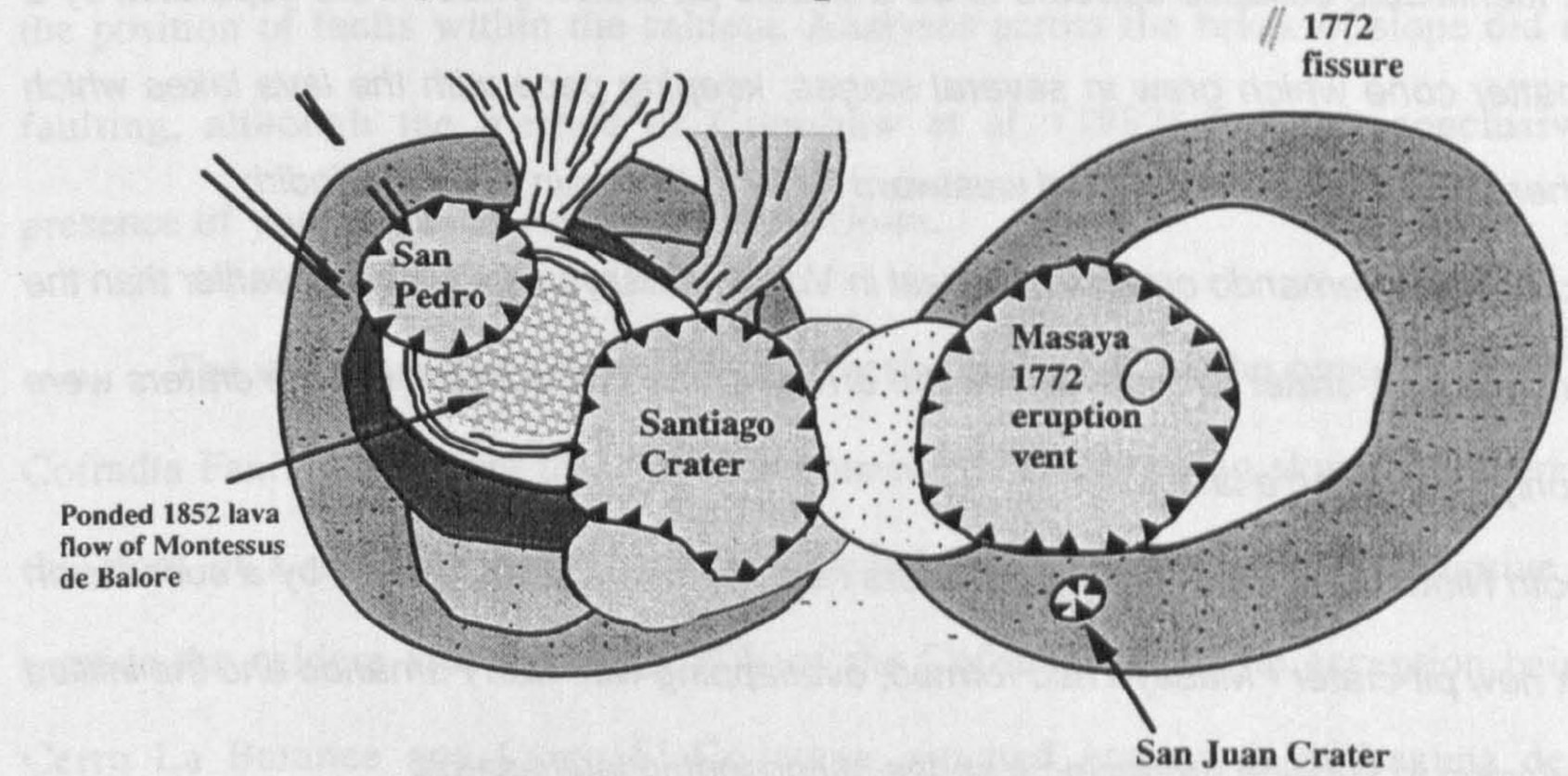

F The Masaya Volcanic Complex in 1994

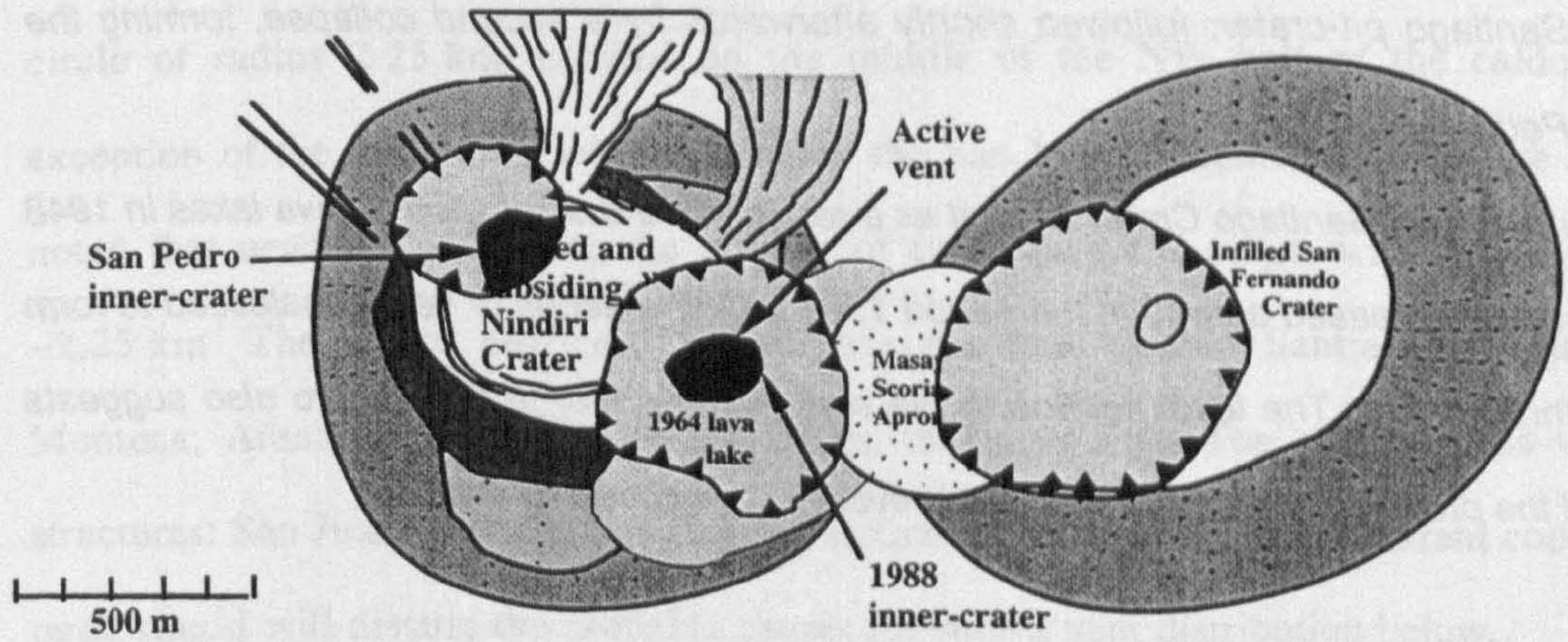

Figure 3.10. D-F. *See page 126 for figure caption.*

Figure 3.10. A - F *(previous pages). This shows the gradual evolution of the Masaya Volcanic Complex showing six stages:* ***A****. the earliest stage currently still visible;* ***B****. pre-Conquistadors;* ***C****. 1529;* ***D****. 1770;* ***E****. 1859; and* ***F****. 1994. This has been drafted using my own field observations and the historical records contained within McBirney (1956). The outlying cones of Arenal, Casas, Cerro Montosa and Comalito are omitted as the stratigraphic relationships are not precisely known. Of the six time frames, the latest four are constrained by historical observations.*

A*. The earliest distinguishable phase which seems to comprise of mainly tuff and scoriaceous material.*

B*. The earliest identifiable collapse appears to be a double pit-crater. These were separated by a large scoria/spatter cone which grew in several stages, keeping pace with the lava lakes which solidified to either side. Activity then shifted westward forming the main cone of Nindiri;*

C*. The formation of San Fernando crater to the east in Volcán Masaya was probably earlier than the collapse of the Nindiri pit-crater to the west. At the arrival of the Conquistadors both craters were degassing but only Nindiri had a lava lake.*

D*. By ~1770 both Nindiri and San Fernando Craters had been completely infilled by a succession of lava lakes. A new pit-crater - Masaya had formed, overlapping with San Fernando and the infilled Nindiri was beginning to subside producing a series of concentric fault scarps.*

E*. Two small vents, San Juan and one on the floor of Masaya Crater, may possibly have formed as a result of the 1772 Fissure eruption. After a period of quiescence, a small lava flow infilled the subsiding Nindiri Crater creating the level area within Nindiri Crater. In early 1859 a major collapse formed the Santiago pit-crater; followed shortly afterwards by a second collapse, forming the smaller San Pedro pit-crater.*

F*. The present floor of Santiago Crater formed as a result of the solidification of lava lakes in 1948 and 1964. During increased activity in the period 1986 - 1989 a series of vents coalesced to form the current inner-crater. The level surface in the small inner-crater in San Pedro also suggests collapse and the presence of a lava lake but this event has not been recorded.*

3.2.5 Discussion on the craters and fissures within the Masaya Volcanic Complex

Location of structures within Masaya Caldera

Williams (1983) identified the Cofradía Fault system as a major regional fault and crustal segment boundary, which is still active today. The projected line of the fault through the centre of the caldera lies close to both a major topographic and volcanic break with eruptive vents found only on the higher ground to the west of this line, see **figure 3.2**. Crenshaw et al. (1982) investigated the possibility of Masaya Caldera being composed of two or more overlapping calderas by using radon gas and mercury vapours as tracers to determine the position of faults within the caldera. Analyses across the break of slope did not detect any faulting, although the method of Crenshaw et al. (1982) was not conclusive due to the presence of young, gas impermeable, lava flows.

The easterly "downthrow" on the break of slope is of the opposite sense to the nearby Cofradía Fault; suggesting these are not connected. The break in slope may therefore represent the front of a thick flow that has been buried by more recent flows. Eruptive vents located outside the caldera also lie to the NW of the Cofradía Fault; the exception being two cones, Cerro La Baranca and Cerro El Coyatepe, situated just north of Laguna de Masaya, see **figure 3.2**. These probably lie along the continuation of a fault identified by Metaxian (1994) which passes along the western edge of Laguna de Masaya and to the SW.

The positions of all the visible craters and cones within the caldera are located within a circle of radius 2.25 km, centred on the middle of the NW half of the caldera with the exception of the few cones which comprise the San Juan Lineament, see **figure 3.11**. I have noted that nearly all the vents lie on one of two concentric rings, with radii of ~1.75 and ~2.25 km. The major edifices: Volcán Masaya and Volcán Santiago; Comalito; Cerro Montosa; Arenal and Los Sastres all lie on the inner ring. The smaller, less well defined structures: San Juan; Oviedo Tuff Cone; Los Ortices; and the Casas and Errant cones lie on the outer ring. I will discuss the probable causes for such a vent distribution below.

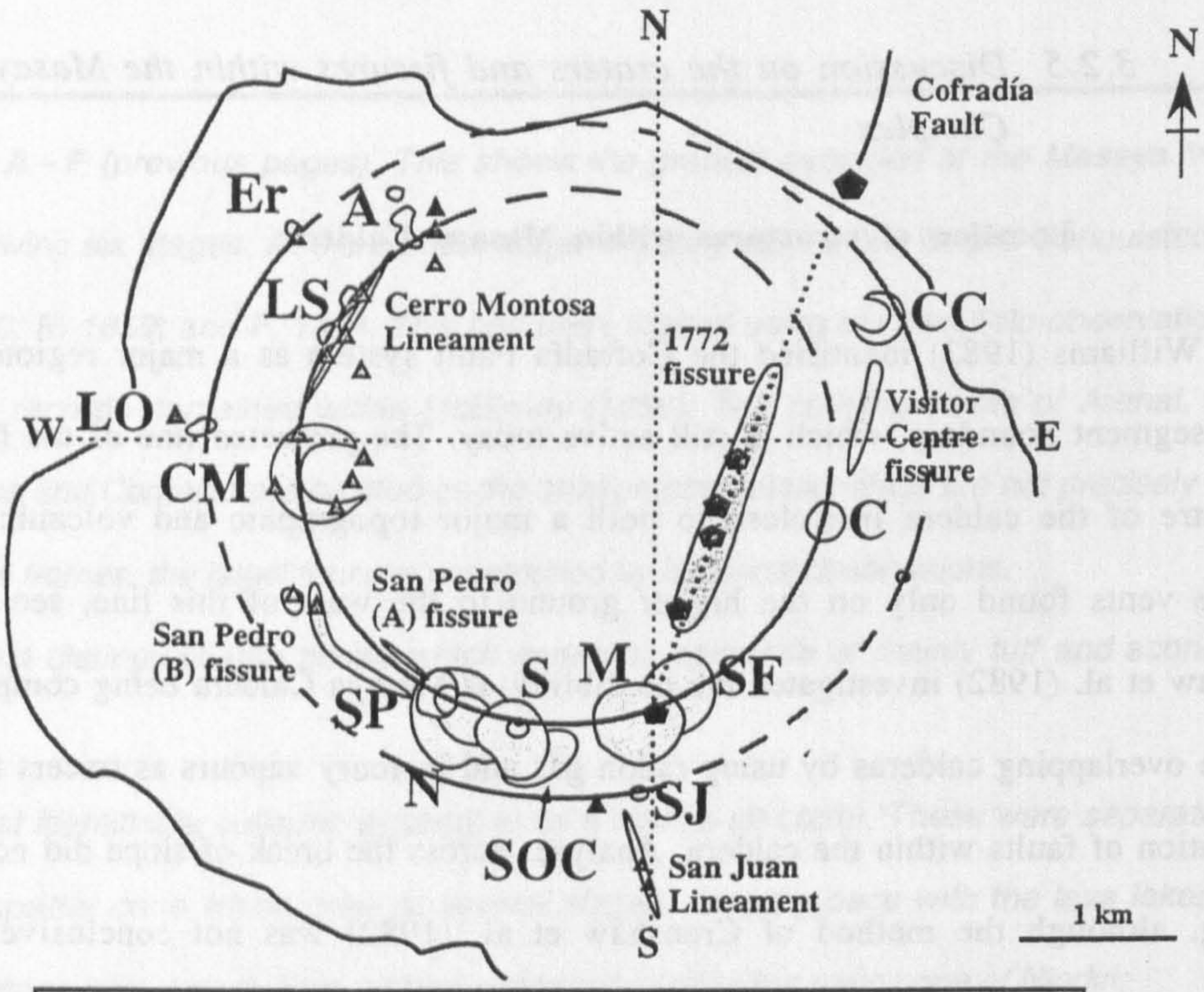

***Figure 3.11**. Map of the NW half of Masaya Caldera showing the positioning of all the main eruptive centres on one of two circles with radii of ~1.75 and ~2.25 km, centred on the middle of the NW half of the caldera. Dashed parts of the rings indicate where no vents are located. Abbreviations to eruptive vents are as follows: A. Arenal, Er. Erant cone, LS. Los Sastres, LO. Los Ortices, CM. Cerro Montosa, SP. San Pedro Crater, N. Nindiri Crater (partially infilled), S. Santiago Crater, SOC. Sapper-Oviedo Complex (infilled), M. Masaya Crater, SJ San Juan Crater, SF. San Fernado Crater (infilled), C. Comalito, CC. "Casas" cone.*

Evidence for presence of a cone-sheet within Masaya Caldera

McBirney (1956) also noted the circular pattern in the location of eruptive vents, proposing that this marked the boundary of an older, more central, collapse feature ~3.5 km in diameter which has since been buried by lava flows. He suggested that the formation of such a feature, by concentric faulting and subsidence following magma withdrawal, would

produce one or more outward-dipping ring dykes. However, the presence of an outwards-dipping ring-dyke would suggest a magma chamber of >4.5 km in diameter. There is no geophysical evidence for anything of this magnitude lying beneath the centre of the NW half of the caldera (Metaxian, 1994).

Alternatively, I propose the circular feature may be the surface representation of two swarms of cone-sheets; caused by the over-pressurisation of a magma chamber beneath the NW part of the caldera or by the injection of a sill-like body at a shallow depth (Walker, 1993). This would produce uplift within the central part of the caldera, and the intrusion of centrally-inclined-sheets (Walker, 1992) around the uplifted plug. The migration of magma along the cone-sheets to the surface would therefore result in an eruption of lava in an annular pattern (Walker, 1993). The inward dip of possibly between ~70° and 45° of the cone-sheets (Walker et al, 1992) would require a much smaller magma chamber, possibly <2 km in diameter, to act as the source of the overpressure required to raise the central plug.

Differentiation between the presence of cone-sheets or a ring dyke at Masaya Caldera is impossible using only the visible surface expression of the feature. Gravimetric studies by Connor and Williams (1990) and Metaxian (1994) were carried out over wide areas, >100 km^2, and therefore gave no indication of the presence of either feature, which may only be a few to tens of metres wide.

Due to the lack of any conclusive geophysical evidence for or against a swarm of cone-sheets, I have taken the positive topographic expression of the area north of Volcán Santiago and Volcán Masaya as indicative of uplift, rather than subsidence; and therefore postulated the annular pattern of vents to relate to a cone-sheet, rather than a ring dyke. Circumstantial evidence to support this arises from the following points relating to the topography of the volcanic complex:

- The low-lying edifice stands only a few hundred metres above the caldera floor.

- The depths of the pit-craters, <300 m, indicate that any accumulation of magma must be below the general level of the caldera floor; which is bounded by the steep caldera walls.

These two factors suggest that compression of the edifice, due to magma influx, will not result in lateral deformation and/or extension to form dykes and rifts (after Walker, 1992). Hence the physical confinement of the complex within the caldera will instead cause the vertical displacement of overburden and the intrusion of sills (after Walker, 1992). Williams (1983) suggested that the segments of the walls of Masaya Caldera were parallel to local and regional fault/fracture orientations; ~30° - 70°; ~110° - 135°; and ~160° - 180°, which had influenced the shape of the caldera. Assuming fractures with similar orientations exist at depth below the caldera, I suggest that the vertical displacement by intrusion of sills has been accommodated by movement along these pre-existing discontinuities; the presence of which has facilitated magma migration towards the surface.

In the previous sections I described the eruptive vents and fissures within the caldera. I have observed a pattern within the circular arrangement of vents, relating to their size, level of erosion and amount of vegetation; these are summarised in **table 3.2.**

Sector of ring	Features	Size	Eruptive style	Vegetation	Re-activation
North	Absent	None	None	Buried by 1772 flow	Inactive
NE and NW	Casas, Arenal, Errant	Small	Mainly scoria	Highly vegetated, trees and scrub	Monogenetic - very short-lived
East and West	Cerro Montosa, Comalito	Medium	Scoria, spatter and small lava flow	Well vegetated mainly scrub	Probably monogenetic but longer-lived
South	Volcán Santiago and Volcán Masaya	Large	Mainly lava with some tephra. Multiple pit-craters.	Barren over large areas, grass elsewhere	Polygenetic long-lived

Table 3.2. *Summary of differences between eruptive vents illustrating the differences from north to south around the postulated cone-sheet.*

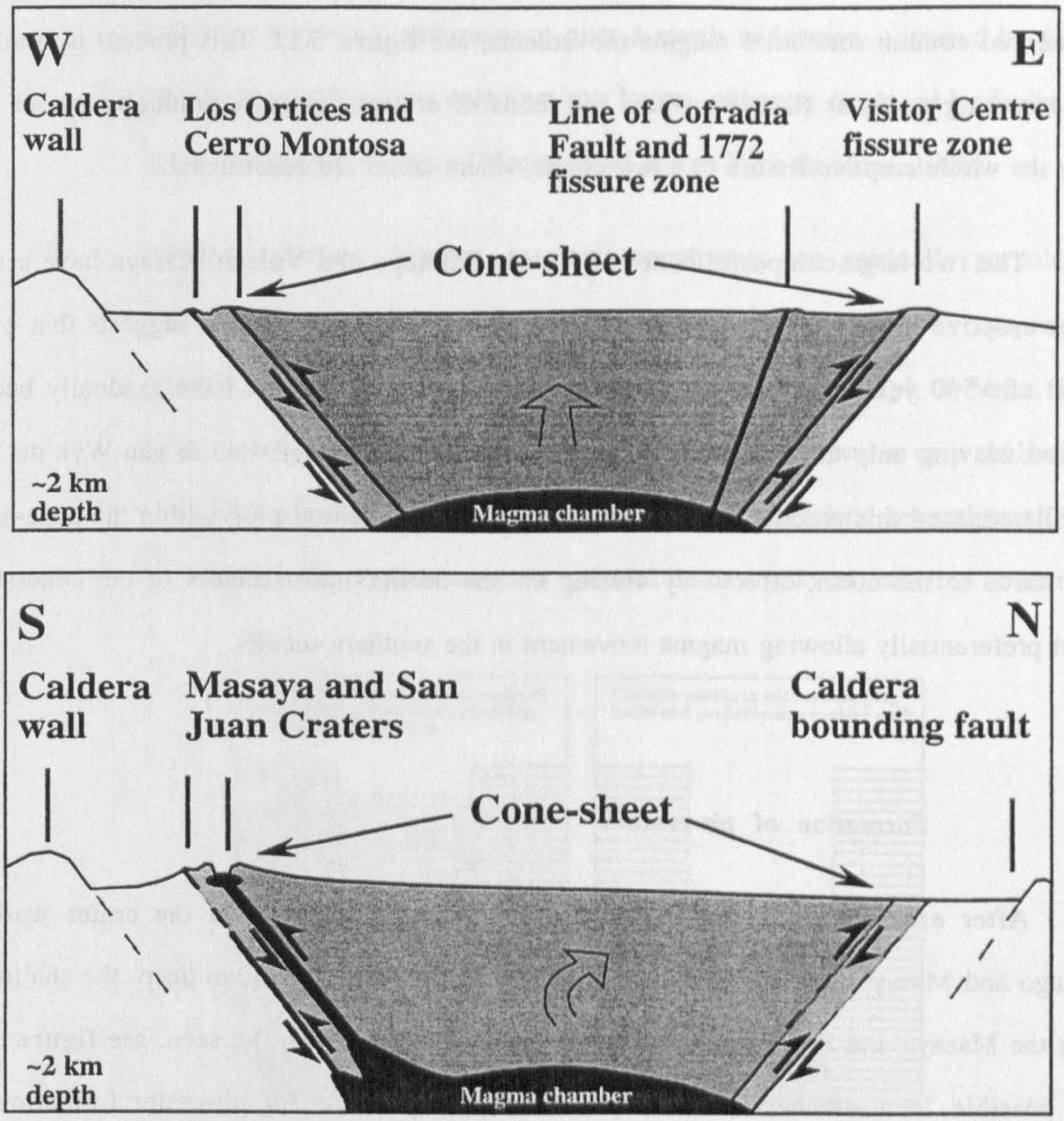

***Figure 3.12**. Schematic cross-sections through the Masaya Volcanic Complex in E-W and N-S directions illustrating the proposed rotation of the faulted central plug. The northwards rotation of the plug is supported by the general topography and also the results of a re-occupation of a levelling line across the caldera in 1994 by Murray, van Wyk de Vries and Maciejewski; which showed a gradual increase in height of the southern part of the caldera relative to the north. The dips of cone-sheets illustrated, ~45°, are consistent with those reported by Walker (1993b) for the cone-sheets complexes of the Cuillin Hills in Skye, where dips range from ~30° - 70°.*

The differences I observed in the eruptive vents, and summarised in **table 3.2**, may be explained by perturbations in the density of the inferred cone-sheet swarms. Maciejewski & van Wyk de Vries (1998) proposed that where it was lowest, magma would have cooled rapidly and solidified before reaching the surface, or possibly to erupt briefly - forming a monogenetic cone. Only in the thickest parts of the cone-sheet swarms would there be a high

enough magma flux; enabling the conduit to remain open for long periods, thus forming a preferential conduit for future magma movements, see **figure 3.12**. This process is similar to that occurring at linear fissures; where the focus of eruptive activity gradually moves from along the whole eruptive fissure to a few points, where cones are constructed.

The two large composite cones of Volcán Santiago and Volcán Masaya have a much longer eruptive history than the other, smaller, monogenetic cones. This suggests that over a period of >500 years the magmatic conduits forming the cone-sheet have gradually become blocked; leaving only the southern part of the system open. Maciejewski & van Wyk de Vries (1998) envisaged this process be as a tilting/rotation of the central plug within the cone-sheets downwards to the north; effectively closing off the northernmost sectors of the cone-sheets whilst preferentially allowing magma movement in the southern sectors.

Formation of pit-craters

After examining the present pit-craters and those situated in the crater walls of Santiago and Masaya Craters, I have estimated all to be >100 to ~300 m deep; the shallowest being the Masaya and San Fernando Craters where the base cannot be seen, see **figure 3.13**. Two possible "end-members" for the mechanisms responsible for pit-crater formation are outlined as follows:

- Magma withdrawal. This is probably the simplest process for creating a pit-crater. Withdrawal of magma from a shallow chamber beneath part of the edifice removes the buoyant support required to maintain the chamber roof. If the mechanical strength of the overlying rock is insufficient to hold up the chamber roof a collapse occurs. This is dependent on the diameter of the chamber and type and number of heterogeneities present. Collapse can occur either piecemeal, with the disruption of the overlying rock migrating upwards; or as a single block, moving downwards along axial fractures. The subsidence of the Nindiri lava lake pile appears to have been a combination of both styles. Thick debris located at the base of the lava lake pile suggests that initially

piecemeal collapse occurred at the centre of the pile. However, rather than this process continuing, deformation over a much wider area occurred by faulting and downwarping; thus enabling lava layers, although displaced by faults, to be traced across the collapse (Maciejewski & van Wyk de Vries, 1998).

- Magma injection. Magma, as small apophyses, can gradually percolate up through the overlying rock; which is gradually removed by stoping and thermal erosion (Rymer et al., 1998; Maciejewski & van Wyk de Vries, 1998). Such a process leads to the formation of a solid crust over a very shallow lava lake. The partial collapse of this thin crust may produce several small vents which gradually expand as other material is removed and remelted or carried

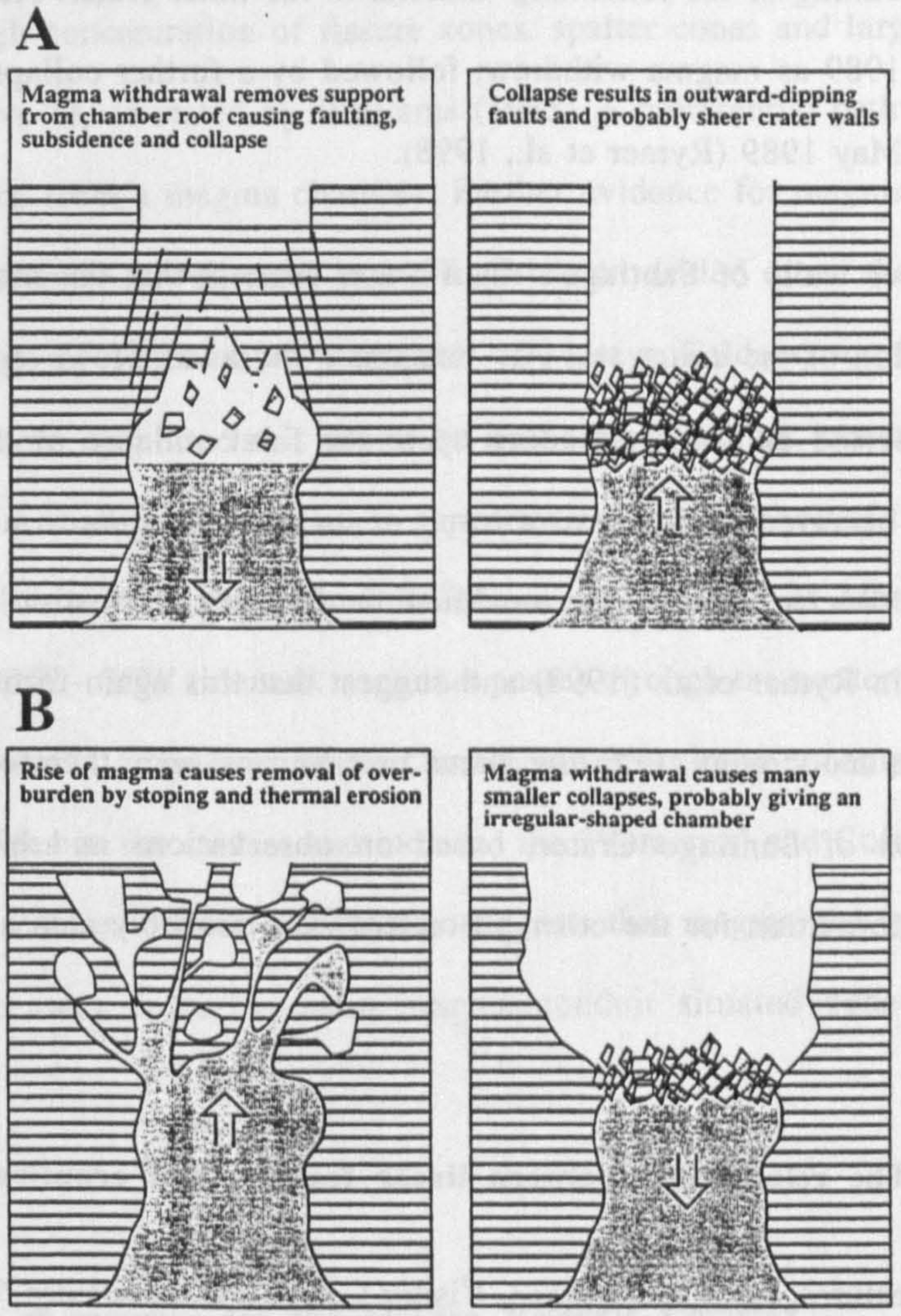

Figure 3.13. *Schematic illustration of two mechanisms for pit-crater formation.* ***A.*** *Collapse caused by magma withdrawal and collapse of chamber roof.* ***B.*** *Magma injection leads to stoping and thermal erosion. The ensuing cavities then collapse, possibly associated with a lowering of the magma level.*

deeper into the volcano. I have envisaged such a process happening to form the features observed in the Santiago inner-crater during the period 1986 - 1989. Rymer et al. (1998) described the changes in vent morphology for this period. In April 1986 a vent ~80 m wide existed in the crater floor. This gradually expanded to the SW by the apparent caving-in of several smaller hollows beneath the crater floor. Further collapses had blocked the vent by November 1986. In January 1989 two of the small hollows in the new inner-crater began to act as vents; by February several other small hollows had also formed, each either filled with or ejecting lava or glowing red (Rymer et al., 1998). The numerous small vents, each filled with magma, caused the under-cutting of the remaining material in the inner-crater. Activity stopped in April 1989 as magma withdrew; followed by a further collapses within the vents in May 1989 (Rymer et al., 1998).

The sheer walls of Santiago's main crater suggest that the main mechanism for the eventual formation of the crater was A. - magma withdrawal. However, I have inferred from the prolonged period of activity leading up to the final collapse of the crater (see Section 3.2.2), that this occurred gradually as a result of magma injection; in a similar manner to the formation of the Bocca Nuova Crater on Mt. Etna. The later formation of the inner-crater has been described in Rymer et al. (1998) and suggest that this again formed during a period of magma injection and stoping. Both the above mechanisms seem therefore to have contributed to the formation of Santiago Crater, based on observations and historical records. The mechanisms of formation for the other pit-craters were probably also a combination of these two processes.

The relationship between linear features and eruptive activity

Linear features, such as the 1772, Visitor Centre and San Pedro (B) fissure zones, have been noted by Bice (1980), Williams (1983) and Walker et al. (1993); but not described in any detail. Williams (1983) suggested, as a mechanism for their formation, that the fissures were aligned parallel to major faults, which govern the orientation of tensional stress within the area.

Tensional fractures provide a preferential pathway for magma to reach the surface where it forms an eruptive fissure. The main orientations of the fault systems, cited by Williams (1983) as responsible for both the shape of the caldera and formation of the fissure zones, were: ~30° - 70°; ~110° - 135°; and ~160° - 180°. Three of the fissure zones referred to by Williams (1980) lie along or are perfectly tangential to the cone-sheet of McBirney (1956). Only the largest fissure, the 1772 fissure, does not form a tangent to the cone-sheet. Instead the fissure lies along the line of the Cofradía Fault, which is lost under the northern wall of the caldera, see **figure 3.11**.

I have assumed from the size and regional importance of the Cofradía Fault that it penetrates the crust to a substantial depth; below the level to which Masaya Caldera affects the local geology. The high concentration of fissure zones, spatter cones and larger craters close to the fault is indicative of, as stated by Williams (1983), a preferential pathway for magma migration to the surface from a magma chamber. Further evidence for magma using faults as magma conduits comes from a well sunk in 1988. This was drilled down the line of a fault running near the village of Veracruz, ~7 km north of Masaya Caldera, see **figure 3.1**. Van Wyk de Vries (pers. com.) reported this produced hot, almost boiling, water; indicating the presence of magma at a shallow depth. This is supported by the presence of two maar craters ~1 km NE of the well site. The geothermal indicators ~7 km north of Masaya Caldera lie along a ~3 km wide, NNE - SSW oriented, zone that passes through the western half of Masaya Caldera and on southwards to the town of La Concepción. This zone encompasses almost all the volcanic features seen in the caldera and includes the "Veracruz" and Cofradía Faults. The presence of volcanic features outside the caldera suggests that magma has migrated laterally along the fault zone away from the main magma conduit situated beneath the Masaya Volcanic Complex.

Rates of eruption for the Masaya Volcanic Complex

Williams (1983) estimated that Cerro Montosa, Arenal and associated lava flows were the oldest visible eruptive products in the caldera. I have used the timing of the events and states of erosion and vegetation levels to infer that the evolution of the visible volcanic

complex has occurred within a period of less than ~1000 years. Williams (1983) estimated the volume of all the visible lava flows to be ~0.20 km^3; this is equivalent to an average eruption rate of $>2 \times 10^5$ m^3/y when averaged over 1000 years. I have estimated a volume of caldera in-fill of ~12.8 km^3; using topographic data and an original crater floor level of 30 m a.s.l, taken from bore-hole data close to Laguna de Masaya (Williams, 1983). Bice (1985) estimated that the age of Masaya Caldera to be ~2250 - 6400 years, based on ^{13}C dating of the Masaya Tuff. I therefore infer that, that prior to ~1000 A.D, the rate of lava and tephra eruption was far higher, with average eruption rates of between ~2.3×10^6 - 10.1×10^6 m^3/y. This order of magnitude difference may either reflect a real change in the magma flux at the Masaya Volcanic Complex, or possibly, to a poor estimation of the caldera volume and/or the volume of recently erupted material.

3.2.6 Summary of the evolution of the Masaya Volcanic Complex

In the previous sections I have described the cones, craters and fissures which comprise the Masaya Volcanic Complex and have proposed a sequence of events to describe the evolution of the complex. Nearly all the eruptive vents lie in two concentric rings, with radii of ~1.75 and 2.25 km. I have interpreted this as being due to the formation of two swarms of cone sheets produced by overpressure within the magma chamber. The northwards rotation of the central plug has restricted magma migration in the northern parts of the cone-sheet; whilst allowing magma to rise freely in the southern sector, producing the massifs of Volcán Santiago and Volcán Masaya. The pit craters formed within the two massifs have formed by the combination of magma withdrawal, thus destabilising the magma chamber roof, and by magma injection, causing stoping and thermal erosion. I have estimated from the level of erosion and vegetation that the visible parts of the complex have formed within ~1000 years. I have shown that the average effusion rate over the last ~1000 years is approximately an order of magnitude less that since the formation of the caldera ~2250 - 6400 years ago. This may therefore represent a fundamental change in the eruptive behaviour of the magmatic system beneath Masaya Caldera.

3.3 The use of SO_2 gas fluxes to investigate the magmatic system at Santiago Crater

3.3.1 Introduction to degassing at Santiago Crater

Santiago Crater has undergone several episodes of degassing since its formation in early 1859; these have been in: 1852-1859, 1902-1906, 1919-1927, 1947-1959 and 1979-1988 (Walker et al., 1993), with the latest phase of degassing commencing in 1997. Stoiber et al. (1986) used a Correlation Spectrometer (COSPEC) to measure the rates of SO_2 emission from Santiago Crater during the 1979 - 1988 degassing episode. High gas fluxes at most volcanoes relate to increased levels of volcanic activity; accompanied by explosive eruptions or lava effusion, see Chapter 5. The SO_2 flux recorded by Stoiber et al. (1986), with daily averages of <2100 t/d, falls within the range of other actively erupting basaltic volcanoes, such as Stromboli, ~320 - 1600 t/d (Allard et al., 1994), and Mt. Etna, <1000 - >15,000 t/d (Bruno et al., 1993 and Chapter 5). However, in contrast to these, the periods of elevated degassing at Santiago Crater occur with little or no increase in visible eruptive activity. In the following sections I will discuss the data and conclusions of Stoiber et al. (1986) and address the problems of whether degassing episodes occur periodically and what happens to the degassed magma that is not erupted.

3.3.2 Degassing at Santiago Crater

SO_2 fluxes recorded

Table 3.3 summarises the COSPEC-derived SO_2 fluxes measured between 1972 and 1998. This shows that the data are highly variable. Stoiber et al. (1986) measured the gas flux sporadically during the first three years of the 1979 - 1988 degassing episode and recorded a highly variable data-set, see **figure 3.14A**. This shows that there was a slight decrease in SO_2 flux with time; with daily averages ranging between ~540 t/d and ~2100 t/d for the measured period. The rate of decrease in gas flux is discussed below in more detail.

Stoiber et al. (1986) did not quote any errors for their COSPEC data; however Stoiber et al. (1983) reported that these could be up to ~45%. At this level of error, all the daily averaged values are indistinguishable. I have however assumed a lower level of error as much of the data was collected in the dry season when the interaction of plume gases with moist air is at a minimum, as is the number of clouds which may also affect the amount of SO_2 measured, see below and Section 2.3.

Short-term variations in SO_2 flux and S:Cl ratios

The large errors associated with COSPEC, <45%, make observations on anything more than the general overall trends difficult. During the period 7/1/82 - 9/1/82 Stoiber et al. (1986) made COSPEC traverses as rapidly as possible along the Llano Pacaya road to the SW of the

Degassing activity	Date	COSPEC-derived SO_2 flux (t/d)
Pre-degassing episode	September 1972	180
	October 1976	~700
	April 1978	~200 - 550 (average ≈380)
Degassing episode	February 1980	~1350 - 1700
	June 1980	~800 - 1600
	February - March 1981	~400 - 1500
	December 1981	~540 - 600
	February 1982	~600 - 900
	July 1982	~1000
	December 1982	~1100
Post degassing episode	March 1993	~25
	March 1996	~600
	March 1997	~350
Next degassing episode ?	March 1998	~2500

Table 3.3. *Summary of day-averaged COSPEC measurements carried out on the Santiago gas plume between 1972 and 1998. 1980 - 1982 data in Stoiber et al. (1986); 1993 - 1997 data in Rymer et al. (1998); 1998 data courtesy of G. Williams-Jones (pers. com.).*

caldera; enabling 36, 39 and 44 analyses to be carried out for these days respectively. The variation between consecutive analyses was sometimes >2000 t/d; making the determination of any pattern to the variation difficult.

The data of Stoiber et al. (1986) do, however, show a doubling of the flux over ~1 hour on five occasions during the three day analysis period; with a sampling rate of ~5 - 6 traverses an hour. For the rest of the period there was no distinctive short-term pattern, rather a general increase or decrease throughout the day; which Stoiber et al. (1986) attempted to relate to changes in the earth tide. They reported that there was "no obvious pulsation in the volume of the volcanic plume", i.e. no puffing, during the three day period. They also used filter-packs placed on the rim of Santiago Crater to recorded short-term variations in sulphur and chlorine fluxes on 7/1/82; with results indicating an oscillation in S:Cl mass ratios of between ~0.3 - 0.45 and ~0.55 - 0.65.

The variations in reported SO_2 flux and S:Cl ratio may be related to the convection of magma beneath Santiago Crater; bringing pockets of variably degassed magma to the surface. Stoiber et al. (1986) saw oscillations in the S:Cl ratios and fluctuations in SO_2 fluxes over periods of ~60 - 120 minutes; possibly indicating the periodicity of magma convection beneath the crater. They also collected sulphur and chlorine concentration data over a longer time-scale, 1980 - 1982. These data showed a gradual decrease in the average S:Cl mass ratios from ~1.14 in February 1980 down to 0.49 in November 1982. The gradual decrease in ratio is consistent with the degassing of a single body of magma; the more volatile sulphur being depleted at a faster rate than the more soluble chlorine (Giggenbach, 1996). Changes in gas ratios have also been observed at Mt. Etna during and after eruptive periods, see Chapter 5. Here the S:Cl mass ratios tend to be much higher, ~5 - 10 during eruptions dropping to ~0.1 - 1 afterwards. This is described by the two-stage degassing model of Pennisi & Le Cloarec (1998), see below.

Removal of SO_2 from the plume

Stoiber et al. (1986) also collected and analysed S:Cl ratios using a filter sampling technique, see Section 2.8. The S:Cl mass ratios determined varied depending on the sampling distance from Santiago Crater; from ~0.8 at the crater rim to ~1.6 on the Llano Pacaya ~16 km distant. A similar pattern could be seen in the average SO_2:SO_4 mass ratios for the period November 1980 - February 1981; ~91 at the crater but only ~11 on the Llano Pacaya. This indicates that a significant proportion, ~7%, of SO_2 is removed from the plume over a distance of ~16 km by atmospheric processes, i.e. oxidation and solution, see Chapters 5 and 6. The conversion of SO_2 to SO_3 and SO_4, will reduce the COSPEC-derived gas flux as COSPEC can detect only SO_2. The high degree of variability in the three-year Stoiber et al. (1986) data-set therefore represents a combination of variable SO_2 scavenging, cloud cover, and actual physical variations in the degassing at Santiago Crater.

Styles of magma degassing

The decrease in S:Cl ratios during and after eruptions has also been observed at other volcanoes; e.g. Mt. Etna, see Chapter 5. As a body of magma degasses close to the surface, the less soluble volatiles, such as H_2O and SO_2, exsolve more rapidly than the soluble species, HCl and HF (Giggenbach, 1996), see Section 1.5. This leads to the gradual decrease of volatile ratios such as S:Cl as both species gradually re-equilibrate to the depth of degassing. Pennisi & Le Cloarec (1998) proposed a two-stage degassing model to explain changes in S:Cl ratios at Mt. Etna, see Chapter 5. This consisted of the following:

- Deep ("background") degassing below ~4 km depth. At this level, chlorine complexes with alkali metals to form metal chlorides (Giggenbach, 1996); these are less soluble than sulphur and so ~50% of chlorine exsolves, compared to ~30% sulphur. This gives a very low, <0.4, S:Cl mass ratio.

- Shallow ("eruptive") degassing at less than ~4 km depth. At low pressures, HCl is the stable form of chlorine which is much more soluble than sulphur.

Therefore whilst ~90% of the remaining sulphur is exsolved, only a minimal amount of HCl is lost from the melt. This gives a much higher S:Cl mass ratio of ~10.

The model of Pennisi & Le Cloarec therefore predicts that during periods of low activity most of the outgassed volatiles will be sourced from depth and thus give a low S:Cl ratio. During periods of increased activity, mass magma migration through the system will bring volatile-rich magma to the surface which will degas, thus increasing the measured S:Cl ratios. The precise ratios relating to deep and shallow degassing will relate to the depths involved and the original volatile content and composition of the magma.

Stoiber et al. (1986) analysed residual glasses and melt inclusions in olivines to determine pre- and post-degassing volatile compositions at Santiago Crater; these were 320 ppm S, 300 ppm Cl and 80 ppm S, 100 ppm Cl respectively. These values are much lower than the volatile concentrations determined by Armienti et al. (1994) at Mt. Etna which ranged between 400 - 2520 ppm and 1400 - 3300 ppm for sulphur and chlorine respectively; and may therefore relate to an already partially degassed magma. This has implications for the volumes of degassed magma I have estimated using the inclusion data of Stoiber et al. (1986).

3.3.3 The exponential decay of the gas flux

Stoiber et al. (1986) attempted to use their COSPEC data to calculate the rate of decay of the gas flux. They suggested that the decreasing SO_2 flux was related to the degassing of a single, non-replenished, magma body; and thus the flux should decay exponentially with time, as in **equation 3.1**. I concur with their assumptions relating to the that exponential rate of decay of volatile exsolution; however their application of **equation 3.1** to such a scattered data-set will give an inaccurate value for k, the decay constant. This is compounded further by the lack of gas flux data for the remaining years of the degassing episode, which ended in ~1988. Without any constraint on the final SO_2 flux, their decay rate can only be an approximate estimation.

$$Q_T = Q_0 \, e^{(-k \times T)} \qquad \text{(Stoiber et al., 1986)} \qquad \textbf{(3.1)}$$

where Q_0 is the initial flux (t/y); T is the number of years since degassing began; Q_T is the flux (t/y) at time T; and k is the rate constant (y^{-1}). Stoiber et al. (1986) used a value of 1200 t/d for Q_0, defined as the flux in February 1980; a value of 380 t/d for the final Q_T at T= 25 y to achieve a decay rate (k) of 0.04 y^{-1}. They took the background level of SO_2 gas emission as ~380 t/d from the average level of degassing in the period 1972 - 1979.

I have re-evaluated the COSPEC data of Stoiber et al. (1986) and calculated a best-fit exponential curve through the data of Stoiber et al. (1986), see **equation 3.2**. The wide spread in the data produces an exponential regression curve with an extremely low R^2 value, ~0.06.

$$Q_T = 4 \times 10^{117} \, e^{(-0.1332 \times T)} \qquad \textbf{(3.2)}$$

To calculate **equation 3.2**, I have had to take the data of Stoiber et al. (1986) at face-value and accept it as being correct; even though errors on the COSPEC technique may be up to 45%. I fitted **equation 3.1** to the exponential regression curve given by **equation 3.2** by changing the variables Q_0, Q_T, and T; and therefore objectively determined the final flux Q_T at time T using the original value of k = 0.133 from **equation 3.2**. The values I have thus derived are found in **table 3.4**.

Q_0 = 1200 t/d	k = 0.133 y^{-1}
Q_T (t/d)	T (years)
25	29.0
180	14.25
380	8.6

Table 3.4. *The results of fitting the curve defined by* ***equation 3.1*** *to that defined by* ***equation 3.2*** *by varying Q_T and T; keeping Q_0 and k constant at 1200 t/d and 0.133 y^{-1} respectively. The background fluxes, Q_T, relate to: 25 t/d estimated by Williams (in Rymer et al., 1997) in April 1992; 180 t/d measured by Stoiber & Jepson (1973) in 1972; and 380 t/d measured by Stoiber et al. (1986) in 1978.*

I have determined T for a range of Q_T in **table 3.4**. Stoiber et al. (1986) used the average SO_2 flux collected in 1978, ~380 t/d, the year prior to the beginning of the degassing episode, for Q_T. I suggest this level of degassing to possibly be a much smaller degassing episode, see Section 3.3.4, and so have assumed the earlier, lower value of 180 t/d to be more representative of background degassing. This is supported by the very low fluxes estimated in 1993 - 1995 by Williams at ~25 t/d. In **figure 3.14B** I have extrapolated the decay curve, recalculated from **equation 3.1** of Stoiber et al. (1986), until it reaches the background levels for SO_2 flux defined in **table 3.4**. This shows that the SO_2 flux from the magma body beneath Santiago Crater should have dropped to 380 t/d after ~8.6 years; 180 t/d after ~14.25 years; and 25 t/d after ~29 years. The rate of gas emission, and its duration, should reflect qualitatively the size of the magma body, with larger bodies generally emitting more gas over longer periods.

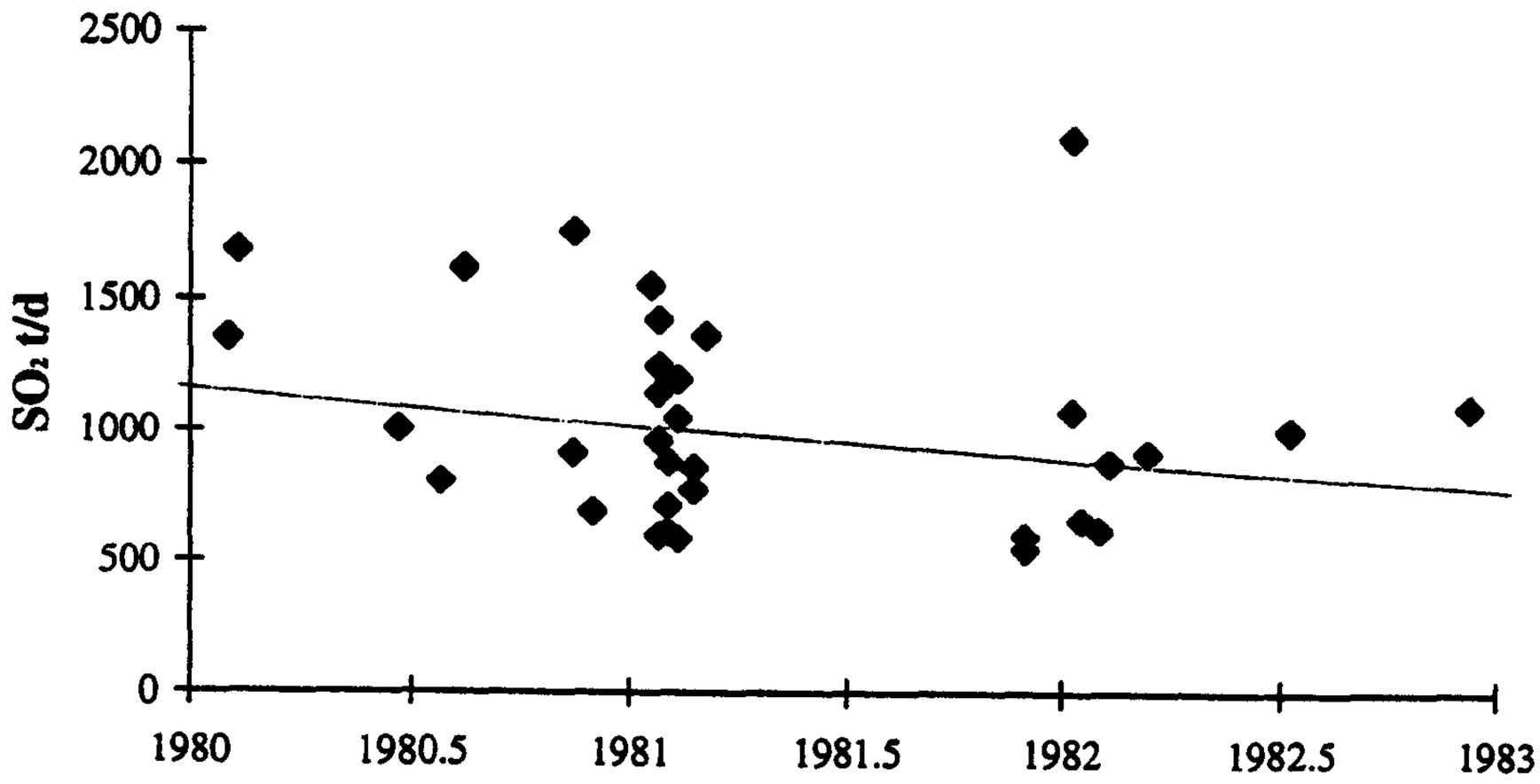

***Figure 3.14. A.** Results of the COSPEC survey undertaken by Stoiber et al. (1986) for the period 1980 - 1982. An exponential decay curve with Q_0 of 1200 t/d and a decay constant, k, = 0.133 y^{-1} has been fitted to the data.*

Rymer et al. (1998) have taken the increased SO_2 fluxes in ~1995 - 1998, see **figure 3.14B**, as indicative of the onset of a new degassing episode. This concurs with the high SO_2 fluxes measured by Williams-Jones (pers. com.) between 22/2/98 and 1/3/98, with a maximum flux of ~7390 t/d. **Figure 3.14B** shows that in 1974 - 1977 and 1994 - 1996, immediately prior to the last two degassing episodes, SO_2 fluxes reached maxima of ~1900 t/d and 1100 t/d respectively (Stoiber et al., 1986; Rymer et al., 1997). I suggest that these short

periods of increased flux represent minor degassing events as predicted by my numerical model in the next section.

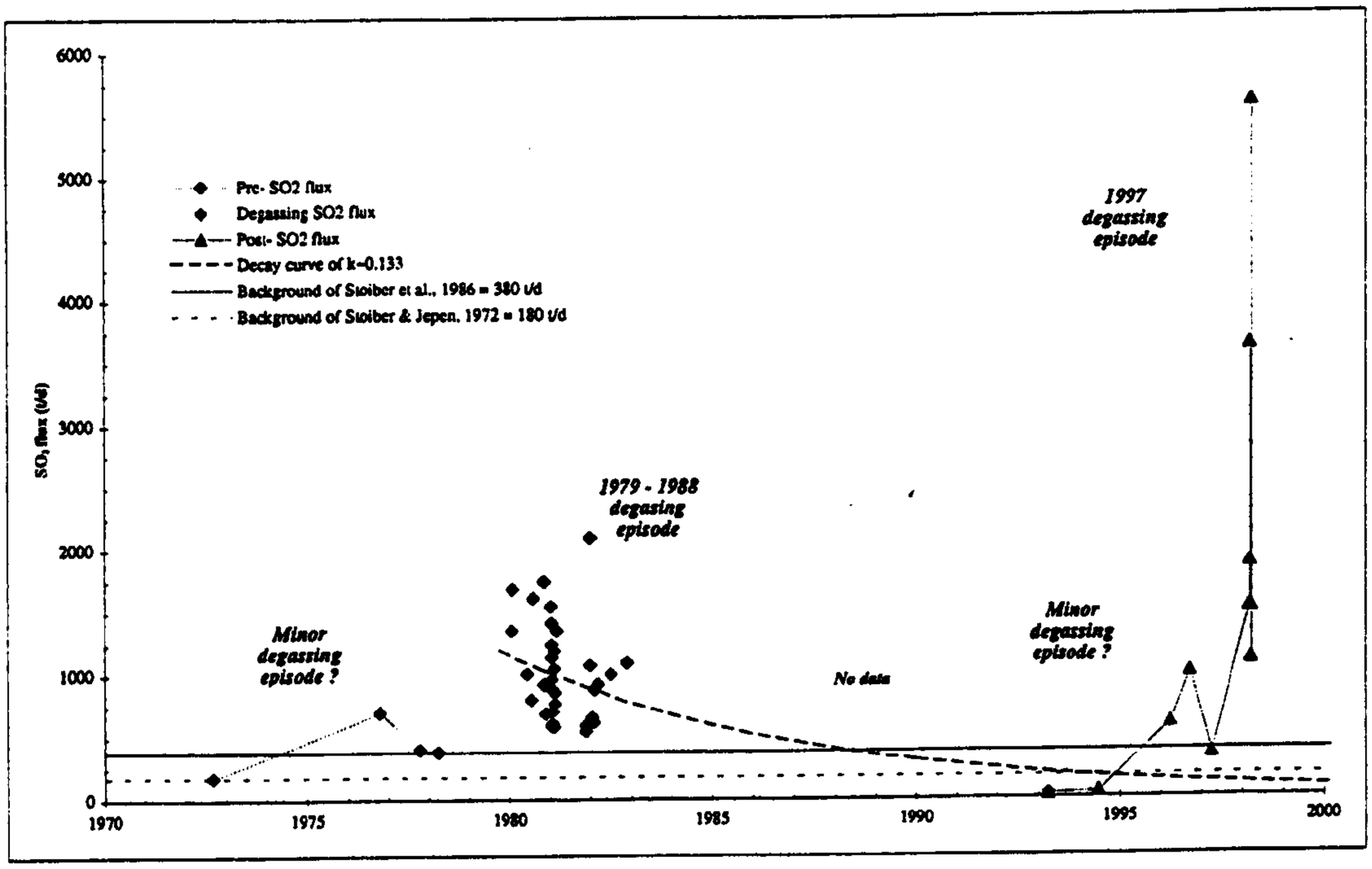

Figure 3.14. B. *Plot of COSPEC-derived SO_2 fluxes for the degassing at Santiago Crater between 1972 and 1998 (after: Stoiber & Jepson, 1973; Stoiber et al., 1986; Rymer et al., 1998; Williams-Jones, pers. com, 1998). I have highlighted two shorter periods of elevated degassing; I suggest these may relate to smaller degassing events as predicted by the degassing model in Section 3.3.5.*

3.3.4 Discussion of degassing at Santiago Crater

Periodicity of degassing

Stoiber et al. (1986) and Walker et al. (1993) have both described the degassing episodes at Santiago Crater as being "periodic". **Table 3.5** gives the dates of the degassing episodes, along with their duration and intervals; and shows that the degassing episodes have a recurrence interval of ~32 ± 17 years with a duration of ~9 ± 5 years (after Walker et al., 1986). The poor records of early volcanic activity within Masaya Caldera make it difficult to use the tabulated data with confidence; smaller degasing episodes may have been left unreported, or simply not observed and the accuracy of the reported start and finish dates is unknown. I have therefore assumed that: reported degassing must have been of a significant

magnitude, in terms of gas emitted and consequent effects on the environment, to have been reported; any episodes not reported must have been comparatively small and therefore of less significance.

The two earliest episodes have a wide variation in their values for duration and interval. The last two episodes however are very similar, having "cycle" lengths of ~36 and 32 years; similar to the average value. Rymer et al. (1998) and Williams-Jones (pers. com.) have both taken the post-1996 degassing, with SO_2 fluxes of up to ~7390 t/d (Williams-Jones, pers. com.), as being the next degassing episode, see earlier. This slightly reduces the average length of each "cycle" and duration of episode.

Start date	Finish date	Period degassing (years)	Length of interval (years)	Length of cycle (years)
1852	1859	7.0	43.0	50.0
1902	1906	4.0	5.0	9.0
1911	1927	16.0	20.0	36.0
1947	1959	12.0	20.0	32.0
1979	1988	9.0	8	~17 ?
1997	on-going ?	–	–	–
Average range of values		10 ± 5	22 ± 15	32 ± 17
Assuming new episode started in 1996		10 ± 5	19 ± 15	29 ± 16

Table 3.5. *The five, - possibly six, degassing episodes at Santiago Crater. Included are the length of each episode; the interval and duration of cycle. Also included are the average values for these (after Walker et al., 1994). According to the above "periodicity", the next degassing episode should start in ~2010; however, recent COSPEC measurements reported in Rymer et al. (1998) suggest another episode began in 1997, see* ***figure 3.14B*** *and text.*

Table 3.5 shows that the duration of each degassing episode is similar to the length of the interval immediately afterwards; the exception being the original period of degassing during the period immediately prior to the formation of Santiago and San Pedro pit-craters. I have inferred from this similarity that the amount of degassing, and hence volume of degassed magma, see **figure 3.15**, has an effect on the time taken to recharge the deep magma chamber prior to the next degassing episode.

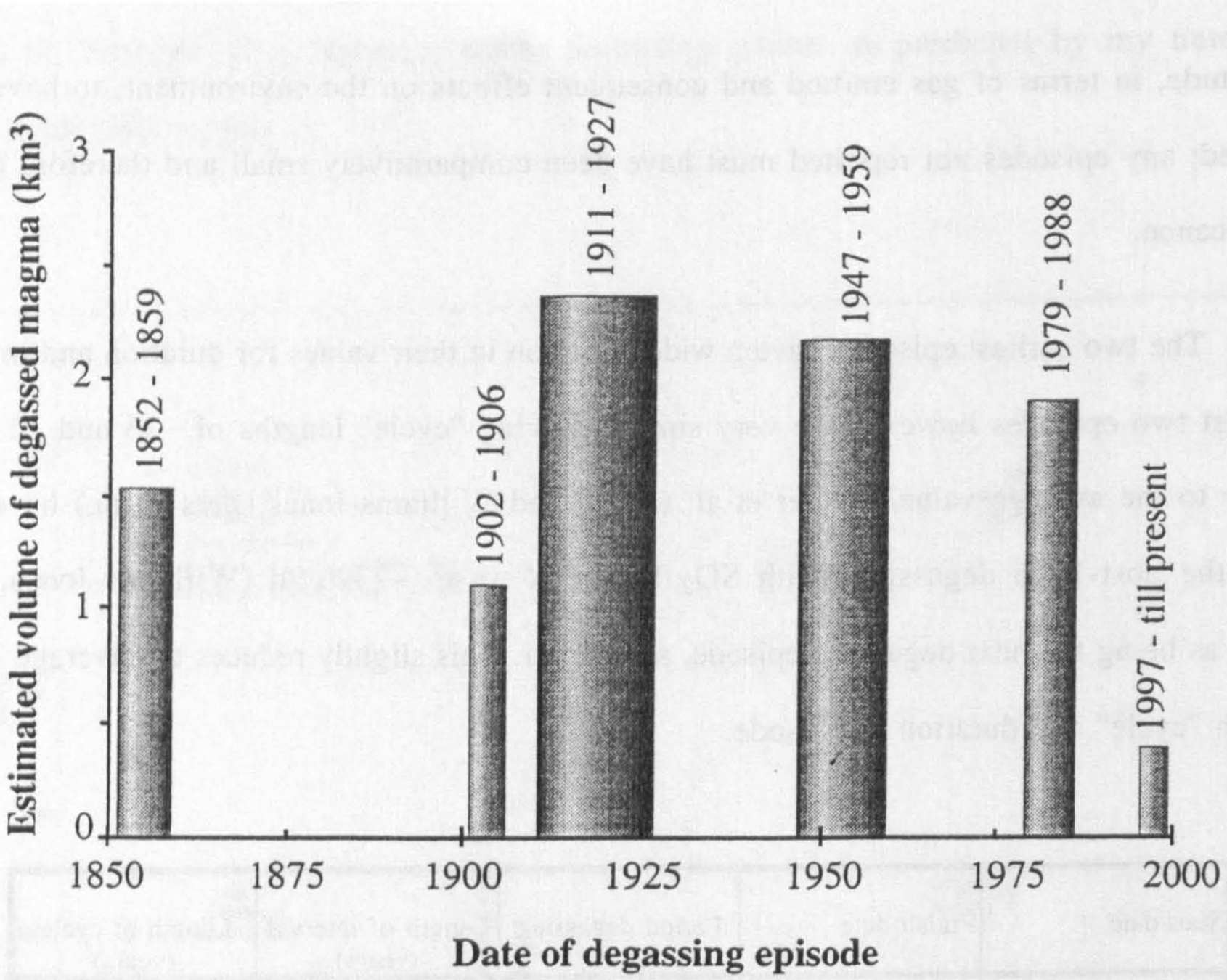

Figure 3.15. *Schematic illustration of the "periodicity" of degassing episodes at Santiago Crater (after Walker et al., 1993). I have estimated degassed volumes by assuming each degassing episode had a similar initial level of degassing, which decayed in a similar manner to the 1979 - 1988 episode. Degassing volumes are therefore related to the duration of the episode.*

Using the decay constant I have calculated from Section 3.3.3 and an average episode duration of ~32 years, see above, I estimated a total volume of magma degassed during a degassing episode, $\sim 2.4 \times 10^9$ m^3 or 2.4 km^3. Rymer et al. (1998) estimated a volume of magma directly beneath Santiago Crater of >0.1 km^3 from gravimetric studies. Clearly the volume of magma degassing is far greater than the volume of the shallow level magma chamber; therefore, if the degassing crisis is related to the degassing of a single body of magma, as suggested by the exponential decay of the gas flux, this must be stored at a greater depth. The magma from this deeper chamber must then convect upwards to the upper chamber, where it can degas, before returning to the lower chamber. The driving force behind the convection of the magmatic system is due to the increase in density of magma at the surface of the lava lake; caused by cooling and degassing (Kazahaya et al., 1994). The volume of the lower magma chamber must therefore be able to accommodate ~2.4 km^3 of magma, the volume expected to degas during a degassing cycle. In the model in Section 3.3.5, I have used

two magma chambers, rather than a single vertically elongated chamber with convective overturns, due to the requirement of a constriction of some form to prevent convection occurring until a certain threshold, relating to the critical volume, has been reached.

Volumes of magma degassed

Stoiber et al. (1986) calculated that after the first six years of degassing the amount of SO_2 degassed was ~2.3×10^6 t and reflected a magma injection of 1.2 km^3; using an exsolved sulphur concentration of ~240 ppm - the difference in sulphur concentrations between pristine melt inclusion (~320 ppm) and residual glass (~80 ppm). More recent analyses by Horrocks (pers. com., 1998) have confirmed that sulphur concentrations in plagioclase melt inclusions are <320 ppm; using samples from a recently erupted bomb. As previously mentioned, the very low levels of sulphur present in the melt inclusions suggest that the "pristine" inclusions may in fact be partially degassed. This would cause a gross over-estimation of degassing volumes of magma. In **table 1.1**, I summarised the ranges of initial volatile concentrations in different magmas; basaltic magmas typically having sulphur concentrations of >1000 ppm. The low sulphur concentrations reported in plagioclase inclusions may represent the formation of plagioclase at very shallow depths where sulphur has equilibrated to the low pressures and therefore already exsolved. Alternatively, as evidenced by inclusions of plagioclase in olivines (Horrocks, pers. com.), convection of magma between shallow and deeper parts of the plumbing system may effectively mix degassed with undegassed magmas, thus lowering the overall sulphur concentration within the melt.

If initial sulphur concentrations were similar to those reported for Mt. Etna, ~3000 ppm (Metrich et al., 1993), then the volumes degassed at Santiago Crater would be much smaller; ~0.1 - 0.2 km^3 for a degassing episode. It may be possible that the very low initial sulphur concentrations is due to sulphur being partitioned into either a non-immiscible sulphide or anhydrite phase. However no evidence of this has been reported. I have, therefore, had to use the low sulphur concentrations of Stoiber et al. (1986) and Horrocks (pers. com) to estimate degassing magma volumes.

In reanalysing the data of Stoiber et al. (1986) I estimated a higher value for the decay constant, k, of ~0.133 y^{-1}, see earlier. For the whole of the 1979 - 1988 degassing episode, I estimated a degassed volume of ~1.9 km^3, using a concentration of 240 ppm for exsolved sulphur as reported by Stoiber et al. (1986) as this is the only datum available. This approach to determining degassed volumes is not particularly accurate. This is due to the limited number of COSPEC analyses; the uncertainties in the final value of the gas decay constant; the actual duration of degassing; and the level of background degassing. These uncertainties allow only an approximation of the volume of degassed material to be derived. However, even this approach can give an insight into the magmatic processes beneath the volcanic complex and therefore merits discussion.

Stoiber et al. (1986) estimated the mass of SO_2 degassed during the last four degassing episodes to be ~1.1×10^7 t. In deriving this, they assumed a similar level of degassing in each episode; and, for the period 1900 - 1985, assumed a normal, background, level of degassing, equivalent to a total emission of SO_2 of ~7.7×10^6 t. The total combined SO_2 emission is equivalent to a total mass of degassed magma of ~3.3×10^{10} t, or a volume of ~10 km^3. I have used a magma density of 2600 kg/m^3, which is an average of basalts measured by Metaxian (1994) in Masaya Caldera. It is also unlikely that each degassing episode had a similar initial rate of SO_2 exsolution and rate of decay. However, as there are no data for these earlier episodes, the amounts of degassing can only be estimated using the assumptions of Stoiber et al. (1986).

I have recalculated the total amount of SO_2 degassed since 1900. To do this, I estimated the amount of SO_2 emitted during each degassing episode; assuming an initial flux of 1200 t/d; a decay constant of $k = 0.133\ y^{-1}$; and by determining how the cumulative amounts of gas emission related to the differing lengths of each episode. This gave a total SO_2 flux of ~9.3×10^6 t. For the same period I also estimate the amounts of SO_2 degassed during background degassing, estimated at a level of 180 t/d; this gave a total of ~3.5×10^6 t, see **table 3.6**. This is equivalent to a total amount of degassed magma of ~2.7×10^{10} t, or ~10.3 km^3.

If the first degassing episode in 1852 - 1859 is include in the calculations, the total amount of magma degassed to date is ~3.9×10^{10} t, ~15 km^3. The level of background flux can substantially affect the overall amount of SO_2 degassed and consequently the volume of degassed magma. For background SO_2 fluxes of 25 t/d and 380 t/d I have estimated volumes of magma degassed since 1852 of ~10.5 km^3 and 20.5 km^3 respectively.

Parameter	Stoiber et al. (1986)	This chapter
Background SO_2 flux	380 t/d	180 t/d
SO_2 degassed in last 4 episodes	1.08×10^7 t	~9.3×10^6 t
Background SO_2 degassed after 1900	7.7×10^6 t	3.5×10^6 t
Total amount of magma degassed	3.3×10^{10} t	~2.7×10^{10} t
Volume of degassed magma since 1900	~10 km^3	~10.3 km^3
Amount of degassed magma 1852 - 1998	—	~3.9×10^{10} t
Volume of degassed magma 1852 - 1998	—	~14.9 km^3
Volume of material erupted during the period 1852 - 1998	—	«0.1 km^3

Table 3.6. *Summary of amounts of SO_2 and magma degassed at Santiago Crater. The volume of magma degassed is dependent on the background SO_2 flux; for fluxes of 25, 180 and 380 t/d the volume degassed in the period 1852 - 1998 is ~10.5, 15 and 20.5 km^3 respectively, see text.*

The volume of magma erupted from Santiago Crater during the period 1852 - 1998 has been negligible, composed of a few lava lakes and possibly a metre of tephra over the immediate area, mainly covering the southern rim of Nindiri Crater and the subsided Nindiri lava lakes. The vast bulk of the magma, >10 km^3, see **table 3.6**, must therefore have been intruded beneath Masaya Caldera. This may have been at a shallow depth, possibly within the structure of the cone sheets, or at a greater depth, possibly as an intrusion or as cumulate pile. Below I have summarised the arguments and evidence for shallow and deep intrusion of the degassed magma.

- Shallow intrusion: The current topography in the area occupied by the postulated cone-sheet is ~40 m above the surrounding parts of the caldera. This is partly due to the built-up of successive lava flows on the north flanks of

Volcán Santiago and Volcán Masaya and partly due to the postulated inflation caused by the cone sheets. An inflation of ~20 m would only accommodate ~0.18 km^3 of dykes, assuming the cone sheet was inclined at 45°, since its formation, ~1000 years ago. The author, Murray and van Wyk de Vries measured ground deformation in March 1994 using a levelling line. This indicated deformation was centred along the line of the Cofradía Fault system (GNV Bulletin, 1994; Murray pers. com.). I have estimated a volume change relating to this deformation of ~1.6×10^6 m^3/y; this is ~0.6% of the annual volume of magma degassed during background degassing, based on an SO_2 flux of 180 t/d. Ground deformation can therefore not explain the high gas emissions and low eruption rates.

- Deep intrusion. Magma, once degassed may sink down to be intruded at depth, or crystallise *in situ*, forming a cumulate pile. Connor and Williams (1990) have undertaken gravimetric studies both within and outside Masaya Caldera and report no evidence of any intrusions; although, as reported by Metaxian (1994), density contrasts between magma and country rock might be insufficient to indicate the locations of magma and intrusions. Connor and Williams (1990) did however identify a large, ~200 km^3, anomalously dense intrusive body immediately to the north of Masaya Caldera; with a similar size and orientation to the caldera. They suggested, however, that the body must pre-date caldera collapse due to the perturbations in the Bouger anomaly contours where they cross the caldera walls. The intrusion may therefore relate to an earlier period in the evolution of Masaya Caldera, possibly associated with the proto-Masaya edifice.

No evidence has therefore been found of any significant volumes of magma intruded at shallow or deeper levels in recent times. This may be due to the similarity between lava/country rock and magma as reported by Metaxian or just to the paucity of geophysical investigations.

3.3.5 A proposed model for degassing at Santiago Crater

In the previous sections I have shown that the large magma volumes degassed in each episode could not be stored directly beneath the crater, and that the episode duration and ensuing repose period were of similar lengths. I have tried to explain this through the use of a simplistic numerical model which I describe below. In my model I have made the following assumptions:

- The supply of undegassed, and therefore buoyant, magma to a deep chamber is a steady, continuous flow. Within the deep chamber, hot, undegassed magma displaces any cooler, degassed magma, which is intruded or forms cumulates at depth.

- Once the chamber holds a critical volume of undegassed magma, a convective overturn occurs; resulting in a portion of the magma chamber emptying to form a body of magma which rises towards the surface.

- Rising magma is replaced by an equal volume of sinking degassed magma from a shallow-level chamber; this refills the deep chamber, thus maintaining its constant volume.

- Rising magma is pooled in a shallow-level chamber from which convection takes place, enabling magma to rise to beneath the crater, degas, cool and then sink back down.

The convective overturn within the deeper chamber will be caused by the amount of buoyant, undegassed, magma reaching a critical volume. At this point, the buoyancy of the magma will be able to overcome its viscosity and possibly lithostatic pressure to re-open a conduit to the shallow-level chamber. I suggest the volume convected will depend on its density, viscosity and density of the degassed magma replacing it. Convective overturn will cease once the buoyancy force, proportional to the volume of undegassed magma in the deep magma chamber, decreases. Hence magma bodies of varying volumes will sporadically rise

towards the surface to degas. Precisely when this occurs will be directly related to the undegassed magma volume remaining in the deep chamber; as described by **equation 3.3.**

$$R_V = (V_{crit} - O_V) + (Q_{mag} \times T) \qquad (3.3)$$

where: R_V = volume of undegassed magma in deep chamber; V_{crit} = Critical volume; O_V = volume of undegassed magma in last convective overturn; Q_{mag} = rate of steady-state influx of undegassed magma; T = time since last convective overturn. R_V is therefore controlled by the volume and time elapsed since the last convective overturn, see **table 3.7**.

In my numerical model I based the rate of steady-state influx on amount of magma degassed during background degassing; using the SO_2 fluxes and sulphur concentrations discussed earlier. I also specified that the critical volume was equal to the magma chamber volume. A modifier was used to control the maximum percentage of the magma chamber that could convect at any one time.

In **figure 3.16A** I compare the modelled data with the volumes I estimate for the degassing episodes described by Stoiber et al. (1986). This shows that by using the above assumptions the model can reproduce the periodicity of the actual degassing events. The smaller events predicted by the model are not recorded in the historical accounts. This may have been due to the events being too small to warrant recording or may have been assumed to be part of the previous or later degassing event. The model shows that the repose time between degassing episodes is proportional to the volume degassed in the previous episode. Larger amounts of magma convected relate to longer repose periods before the deep magma chamber is re-filled to the critical volume and the next cycle can begin. To match the frequency of modelled degassing episodes to those reported, I have set the maximum convected volume to 75% of the chamber volume. In **figure 3.16B** I have reduced the maximum volume of magma convected to 25% of the chamber volume. This shows that the smaller the volumes convected, the shorter the repose period between episodes. Such numerous degassing episodes are not reported at Santiago Crater; either they were too small to be of significance to be reported or they did not occur. To match the frequency of modelled degassing episodes to those observed, the volumes of convected magma must therefore be similar, i.e. <4 km^3, see **figure 3.15A**.

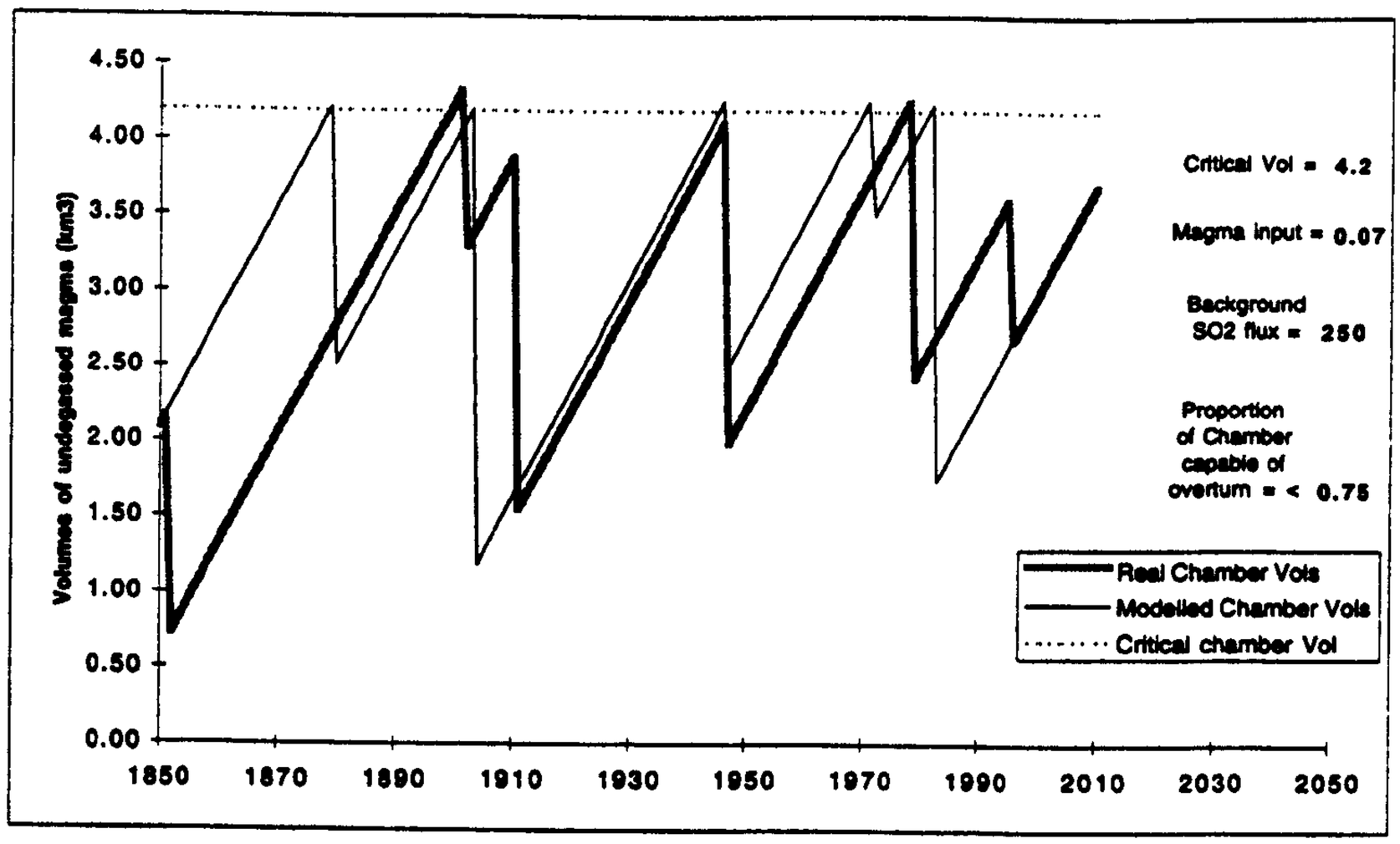

Figure 3.16.A. *The chaotic generation of convective overturns, based on parameters discussed in the text is fairly similar to the data I estimate from the dates of degassing episodes reported in Stoiber et al. (1986). The sudden reduction in chamber volume relates to the amount of undegassed magma that is removed from the chamber during periods of convective overturn, see text for discussion.*

I suggest the similarity between the observed degassing, **figure 3.15A**, and the calculated output supports the convective overturn model as an explanation of "cyclic" degassing. Rymer et al. (1998) have also inferred a magmatic convective overturn from the changes in gravity and rates of gas emission they observed between 1993 and 1997. Burt et al. (1994) modelled the eruption history of Nyamuragira volcano, Zaire, using a similar set of assumptions. These included: the rupture of the magma chamber occurred when a threshold value was reached; the volume of basaltic lava erupted was random; the volume of remaining magma was also random; and influx of magma into the chamber was at a constant rate. The Burt et al. (1994) model used 21 eruptions which were well constrained for eruptive volume and start and finish dates and so was much more accurate than my model which used six poorly constrained degassing episodes. However, the assumptions relating to the rupture and randomness of the magma volumes involved appears to be valid for both models when compared with the real data.

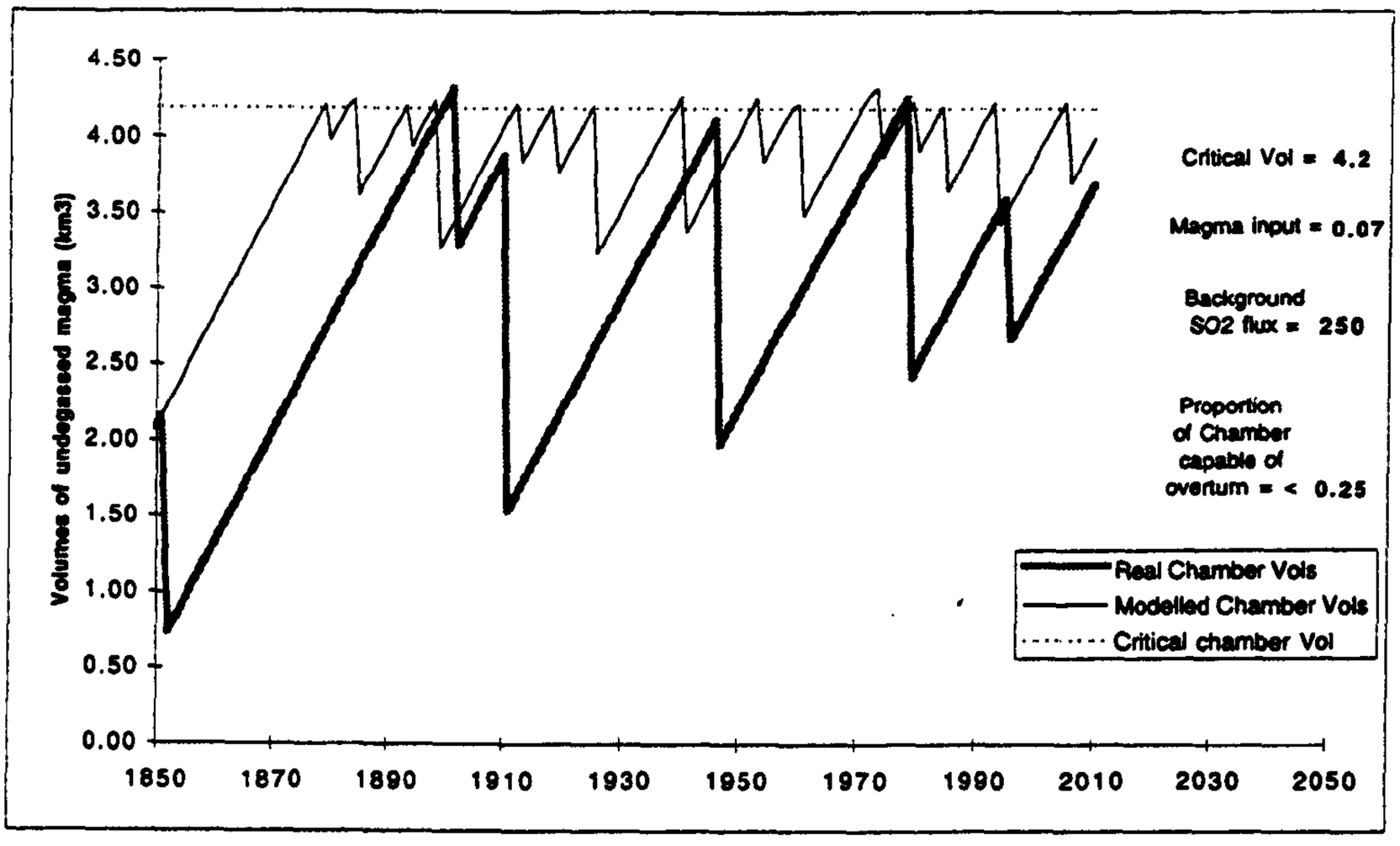

Figure 3.16.B. *A reduction in the maximum amount of convecting magma increases the frequency of degassing episodes, whilst reducing their duration. The matching of frequencies of modelled and reported episodes can therefore constrain the amounts of magma convected.*

The numerical model

I have used the assumptions discussed above to devise a simplistic numerical model to investigate whether degassing at Santiago Crater is controlled by the convection of a random volume of magma. The following three tables, **tables 3.7, 3.8** and **3.9**, relate to the model's controlling parameters; the initial parameters used; and the main body of the model respectively. I ran the model using a Microsoft Excel™ 4.0 spreadsheet with output displayed graphically using an X-Y scatter-graph. The model is divided into two parts, the hypothetical model (columns A-E) and a control based on data from Stoiber et al. (1986) (columns G-K). The model uses a random function (RAND) to simulate varying volumes of convecting magma. The logical (IF) statement is used to determine whether degassing is ongoing or the system is in a period of repose.

Factor name	Excel Row & Column	Factor symbol	Microsoft Excel value/equation	Value/equation
Parameters used to control model – taken principally from Stoiber et al. (1986)				
Chamber radius (km)	**D 3**	R	1	1
Chamber volume (km^3)	**D 4**	V_{chamb}	=((D3)^3)* 3.1415927*(4/3)	$=\frac{4}{3}\pi R^3$
Degassed sulphur (ppm)	**D 5**	XS_{degas}	*=320-80*	$= XS_{init} - XS_{resid}$ (= 320-80)
Initial Q_i SO_2 flux (t/d)	**D 6**	$QSO_{2(i)}$	1200	1200
Background SO_2 flux (t/d)	**D 7**	$QSO_{2(b)}$	250	250
Gas decay constant k (s^{-1})	**D 8**	k	0.133	0.133
Critical volume (km^3)	**D 9**	V_{crit}	=D4	$=V_{chamb}$
Initial chamber volume (km^3)	**D 10**	V_{init}	=D9-2.1	$=V_{crit}$-2.1
Magma supply (km^3)	**D 11**	Q_{mag}	=1*(D7*365.25)/(2*(D5/1000000)*D12*1000000000)	$=\left(\frac{(Q_{SO_2(b)}\times 365.25)}{\left(2\times\left(\frac{XS_{deg\,as}}{1\times10^6}\right)\times\rho\times1\times10^9\right)}\right)$
Magma density (t/m^3)	**D 12**	r	2.6	2.6
Overturn Control volume Factor	**D 13**	F	0.9	0.9

Table 3.7. *The parameters used to control and vary the numerical model. Chamber radius is estimated from the radius of the hypothetical chamber beneath the proposed cone-sheets. Chamber volume assumes a spherical chamber. The degassed sulphur concentration is taken as being the initial (undegassed) concentration taken from fluid inclusions, ~320 ppm, minus the residual sulphur concentration taken from glassy rinds on spatter, ~80 ppm (Stoiber et al., 1986). The initial SO_2 flux is assumed to be ~1200 t/d - similar to that measured by Stoiber et al. (1986) at the beginning of the 1978 - 1986 degassing event. I have used a value of 250~ t/d as a background gas flux - see text for discussion. A constant of 2.1 is used initially to regulate the chamber volume of the model to be within the critical volume. I have assumed that the magma supply rate is constant and is equivalent to the amount of magma required to provide the levels of background SO_2 flux. Magma density is taken as an average from numerous measurements conducted by Metaxian (1994) on basalts within Masaya Caldera. The "overturn control factor" is used to control the relative size of the convected magma volume - 1 = 100% of critical volume convected, 0 = 0% of critical volume convected.*

Excel Row & Column	Description	Microsoft Excel value/equation
First row in numerical model – sets up initial parameters to run.		
Hypothetical model		
A17	Date (years)	=1850
B17	Chamber Volume (km^3)	=$D$10-((IF(C16>=$D$9,1,0)*(RAND()*$D$9*$D$13)))
C17	Logical statement	=(IF(B17<$D$9,1,0))*((IF(B17>=$D$9,0,1))+C16)
D17	Degassing Volume (km^3)	=((IF(B17>=$D$9,1,0))*(B17-B18)) +((IF(C17=0,0,1))*D16)
E17	Gas decay (t/d)	=((IF(($D$6*EXP(-$D$8*C17))>=$D$7,1,0))*($D$6*EXP (-$D$8*C17)))+((IF(($D$6*EXP (-$D$8*C17))<$D$7,1,0))*$D$7)
Modelled data		
G17	Degassing episode logical True /False (1/0)	0
H17	Logical statement	=(IF(G17=1,1,0))*(1+H16)
I17	Gas flux decay (t/d)	=((IF(G17=1,1,0))*($D$6*EXP(-$D$8*H16)))
J17	Estimated degassed magma volumes (km^3)	left blank until convection event.
K17	Chamber volume (km^3)	=D10

Table 3.8. *The first row of the numerical model sets up the initial parameters to be run. These are controlled from* ***table 3.7.*** *The model is divided into two parts. The first is a purely theoretical model which uses random (RAND) functions to control the size of the convected volume. The second is based on the estimated magma volumes and dates reported in Stoiber et al. (1986) and elsewhere in this chapter.*

Excel Row & Column	Description	Microsoft Excel value/equation
Following rows in numerical model – controls the graphical output for **figure 3.16**		
	Hypothetical model	
A18	Date (years)	=A17+1
B18	Chamber Volume (km^3)	=(B17+$D$11)-((IF(B17>=$D$9,1,0)*(RAND()*$D$9*$D$13)))
C18	Logical statement	=(IF(B18<$D$9,1,0))*((IF(B18>=$D$9,0,1))+C17)
D18	Degassing Volume (km^3)	=((IF(B18>=$D$9,1,0))*(B18-B19))+((IF(C18=0,0,1))*D17)
E18	Gas decay (t/d)	=((IF(($D$6*EXP(-$D$8*C18))>=$D$7,1,0))*($D$6*EXP(-$D$8*C18)))+((IF(($D$6*EXP(-$D$8*C18))<$D$7,1,0))*$D$7)
	Modelled data	
G18	Degassing episode logical True /False (1/0)	0 - unless degassing is >D7 (= level of background degassing).
H18	Logical statement	=(IF(G18=1,1,0))*(1+H17)
I18	Gas flux decay (t/d)	=((IF(G18=1,1,0))*($D$6*EXP(-$D$8*H17)))
J18	Estimated degassed magma volumes (km^3)	Left blank until convection event. Then volumes estimated in **figure 3.15** used for dates indicated.
K18	Chamber volume (km^3)	=K17+$D$11-J18

Table 3.9. *Once the parameters for the general model and initial conditions have been set up using* ***tables 3.7*** *and* ***3.8****, this and successive rows copied directly from this one, relate to the main, functional, part of the model. Each new row relates to an increment of one year and shows how the levels of magma in the chamber build up until reaching the critical volume. Once reached a random volume convects, lowering the volume remaining in the chamber. This will then slowly refill at the steady-state rate prescribed in* ***table 3.7****.*

3.3.6 Summary of investigations into degassing at Santiago Crater

Stoiber et al. (1986) studied the degassing of Santiago Crater in 1980 - 1982 during the early stages of a degassing episode. From their sporadic and highly variable COSPEC measurements they estimated that SO_2 degassing decayed exponentially. I re-evaluated their data and confirmed this to be the case. Rymer et al. (1998) and others have attributed the recent increased levels of degassing to be the start of a new degassing episode. This is contrary to the periodicity proposed by Stoiber et al. (1986) and Walker et al. (1993). I propose that, rather than being periodic, the timing of each degassing episode is related to the duration of the previous episode. I have inferred a physical process controlling the release of each magma pulse; this I believe to be convective overturn of a deeper magma chamber once it contains a critical volume of undegassed, buoyant magma. I have estimated the volumes of magma degassed in each episode from the amount of SO_2 degassed during the early part of the 1979 - 1988 episode; assuming similar conditions existed for earlier degassing episodes. This resulted in a total volume of magma degassed, since 1852 of ~15 km^3, assuming a level of background SO_2 degassing of ~180 t/d. This amount cannot be stored within the edifice and has probably been stored at depth; although gravimetric investigations have yet to identify an intrusive body related to the current degassing. Connor and Williams (1990) identified an older intrusive body but inferred it related to a pre-caldera period of intrusive activity.

3.4 Conclusions

I have divided the conclusions to this chapter into two sections: those relating to the evolution of the Masaya Volcanic Complex; and those relating to the degassing episodes centred on Santiago Crater.

3.4.1 Evolution of the Masaya Volcanic Complex

The Masaya Volcanic Complex has evolved rapidly over the last ~450 years, with the earliest historical observations in 1529 describing a very different complex to that seen today. By using field relationships and historical accounts I have described the changes in the morphology of the complex. I have used the levels of erosion, vegetation and rates of change to estimate a total age for the visible complex of ~1000 years. Over this period all the eruptive activity has been either strombolian, fire-fountaining or lava effusion; markedly different from the plinian caldera-forming eruptions that have occurred at Masaya intermittently for ~135 ka. The locations of all the eruptive vents lie, with only a few exceptions, on two concentric rings, with radii ~1.75 and ~2.25 km. These are centred on the middle of the NW half of the caldera. Maciejewski & van Wyk de Vries proposed that this is due to the existence of a double cone-sheet in this part of the caldera. We explained the difference in age, size and style of eruptive products around the cone-sheet (symmetrical on a N–S line) as being due to the northwards rotation of the inner block of the cone-sheet. This has preferentially allowed magma migration around the southern parts of the cone-sheet and the construction of the twin massifs of Volcán Santiago and Volcán Masaya. The persistence of magma at very shallow depths beneath these massifs has resulted in the formation of several overlapping pit-craters. We suggested two possible mechanisms for pit-crater formation: the withdrawal of magma resulting in collapse of the magma chamber roof; or by rise in magma removing overburden by stoping and thermal erosion. Evidence for both styles of collapse has been observed during historical times.

All the eruptive vents lie in a ~3 km wide NNE-SSW oriented zone which lies along the active Cofradía Fault system. Williams (1983) suggested this was a regionally important fault which acted as a crustal-segment break. The depth of the fault enables magma to use it as a preferential pathway, hence all the activity is located close to it and along it to the north and south. The orientation of the eruptive fissures tend to be tangential to the surface expression of the cone-sheet, occasionally extending parallel to the Cofradía Fault. The only exception to this is the most recent 1772 eruptive fissure, which cuts across the cone-sheet along the line of the fault and was therefore probably directly influenced by it rather than the cone-sheet.

3.4.2 Episodic degassing at Santiago Crater

There have been several degassing episodes centred on Santiago Crater. The last was studied by Stoiber et al. (1986) using a COSPEC. I have estimated a rate of decay for the SO_2 flux of ~0.133 y^{-1} using their sporadic and variable COSPEC data. For my calculations I have assumed an initial maximum SO_2 flux of ~1200 t/d and average background flux of ~180 t/d. Stoiber et al. (1986) also reported sulphur contents of undegassed inclusions and residual glasses which has enabled the author to estimate volumes of degassing magma; based on the levels of degassing in the 1979 - 1988 degassing episode. This resulted in a total volume of magma degassed, since 1852 of ~10 - 20 km^3; the wide range being due to the uncertainty in level of background SO_2 degassing, between ~180 - 380 t/d. This value also assumes that degassing episodes were of similar intensity to the 1972 - 1988 episode. During the same period there has been a minimal amount of lava erupted; forming two lava lakes and several small ejecta blankets. Williams (1983) estimated the total volume of observed erupted material within the caldera to only be ~0.2 km^3; I estimate this to have been erupted in ~1000 years, a rate of ~2×10^5 m^3/y. I have also estimated the entire volume of caldera fill to be ~12.8 km^3. This has been erupted over a period of ~2250 - 6400 years; equivalent to a much higher eruption rate of ~2.3×10^6 - ~10.1×10^6 m^3/y. This suggests a fundamental change in recent eruption rates, or a gross overestimation of the volume of caldera in-fill, which is poorly constrained.

Rymer et al. (1998) interpreted the increased gas emissions since ~1996 as relating to a new degassing episode. Stoiber et al. (1986) and Walker et al. (1993) proposed a ~25 - 30 year cyclicity to degassing at Santiago. According to them, the next degassing episode should not have occurred until ~2005 - 2010. I have noted that, for the last four episodes, the duration has been of a similar length to the episode's repose period; suggesting a link between the two. I have inferred this to relate to the time taken to partially empty and refill a deeper magma chamber after a convective overturn of the system; assuming a steady-state replenishment of the chamber. I modelled this successfully using a very simplistic numerical model which showed the volume in a magma chamber through time with a steady-state influx and partial emptying once it had reached a critical volume. This demonstrated that the random removal (convective overturn) of magma could generate degassing episodes with an apparent periodicity - depending on the periods observed. It also suggested that the large volumes estimated to degas in each episode, ~1 - 2.5 km^3, are accommodated at depth rather than immediately beneath the craters. This is supported by several gravimetric surveys which have not found any recent shallow intrusions which can be attributed to the recent degassing activity.

The main points from my investigation into the morphological evolution and degassing history at the Masaya Volcanic Complex can therefore be summarised as follows:

- The locations of volcanic structures within Masaya Caldera are directly related to the presence of a cone-sheet and deep-seated Cofradía Fault system that form pathways for magma migration within the NW half of the caldera.

- The northwards rotation of the central faulted block within a postulated cone-sheet within this part of the caldera has facilitated the growth of the polygenetic massifs of Volcán Masaya and Volcán Santiago in the last ~1000 years and has given rise to the annular pattern of eruptive vents.

- The degassing episodes that have occurred are aperiodic. They are, however, possibly controlled by the steady-state influx of magma into a deeper chamber

which on reaching a critical volume triggers the convective overturn of the magmatic system.

- The volumes of magma degassed since the formation of Santiago Crater in ~1859 are estimated at >10 - 20 km^3.; the wide range being due to the uncertainties involved in the estimation. By contrast, the estimated volume of caldera-fill, which has been erupted over ~2250 - 6400 years, is ~12.8 km^3.

- The estimated rates of eruption of recent lavas (<1000 years) is ~2×10^5 m^3/y. This is much lower than the rates derived from the volume of caldera fill, ~2.3×10^6 - ~10.1×10^6 m^3/y.

Chapter 4.

Degassing at the La Fossa cone, Vulcano, Italy

4.1 Introduction

4.1.1 Layout of chapter

This chapter will expand on my collaborative work with Francis et al. (1995, 1996 and 1996b), Maciejewski et al. (1996) and Chaffin et al. (1995); detailing various aspects of Open-path Fourier transform infra-red spectroscopy (OP-FTIR) investigations on the gaseous emissions from the La Fossa cone, Vulcano. Comparison of the results with the analyses of other authors, using different techniques, will highlight important factors relating to the hydrothermal system on Vulcano. The chapter is divided into four sections:

4.1. A general review of the volcanic history of the La Fossa cone; the description of previous geochemical investigations into volcanic gases and the techniques used. This will provide the background gas-chemistry against which the author's own OP-FTIR results will be compared.

4.2. The gathering, analysis and interpretation of OP-FTIR data.

4.3 A review of the hydrothermal system and discussion of the geochemical and isotopic data previously published. The seasonal variation of fumarolic gases is also discussed.

4.4. Conclusions. These can be summarised as:

- Three distinct fluid types can be discerned within the hydrothermal system using isotopes and gas chemistry. These are: a deep magmatic fluid; a shallow

marine hydrothermal fluid that possibly may be replenished from the influx of sea water; and a shallow meteoric component.

- The compositions of fumarolic fluids depend strongly on the location of the fumarole with respect to the crater rim. Compositions with a more magmatic signature can be found in the central crater whilst fumaroles on the rim show evidence of mixing with shallow aquifers.

- Long-term studies of gas chemistry, using direct-sampling methods, show a "pseudo-seasonal" variation exists in gases emitted at most fumaroles. This may reflect changes in the relative proportions of the three hydrothermal reservoirs; caused by lower rainfall and increased demand on water from boreholes (Martini, 1983; Capasso et al., 1992; and Tedesco, 1995). This can cause major problems when comparing data sets collected at different times.

- OP-FTIR analysis of the gas plume using path-lengths of <2 km gave consistent SO_2:HCl mass ratios of ~0.9 - 2.6 for gases emitted from the crater fumaroles. Analyses of the rim fumaroles gave a higher SO_2:HCl mass ratios of ~4.3 - 6.1. This is due to removal of the more soluble HCl by a shallow hydrothermal reservoir, as inferred from isotopic analyses of Chiodini et al. (1995).

4.1.2 General volcanological description of Vulcano

Vulcano is the second largest island of the Aeolian Archipelago, in the Tyrrhenian Sea to the north of Sicily. The active centre, La Fossa di Vulcano, has been built up over the last ~6000 years with the last eruption taking place during the period August 1888 to March 1890 (Clocchiatti et al., 1994). During the eruption numerous vulcanian explosions produced rhyolitic phreatomagmatic breccias, trachytic and lattitic surge and fall deposits and rhyolitic tephras with large bread-crust bombs. Earlier eruptions in 1727 - 1739 and 1771 - 1775 had produced surges and lapilli falls. Since 1444 A.D. there have been ten eruptive episodes (Tedesco et al., 1995); averaging one every ~55 years. The smaller cone of Vulcanello at the

northern end of the island first formed during the 2nd century B.C., see **figure 4.1**. By the end the 16th century A.D. when eruptive activity ceased the cone had been connected to the mainland. The present activity in La Fossa di Vulcano is entirely from degassing through fissures and fumaroles; there is no open conduit to the magma-chamber.

Most of the rocks on Vulcano belong to a shoshonitic series from basalt to rhyolite, though potassic rocks belonging to a more undersaturated series also exist (Clocchiatti et al., 1994). Clocchiatti et al. (1994) have suggested that the rhyolites have evolved by fractional crystallisation, with the addition of minor assimilation for the more evolved magmas. The latitic and rhyolitic deposits produced during the 1888 - 1890 eruption probably reflect the current situation within the magma chamber and thus will affect any analyses related to it.

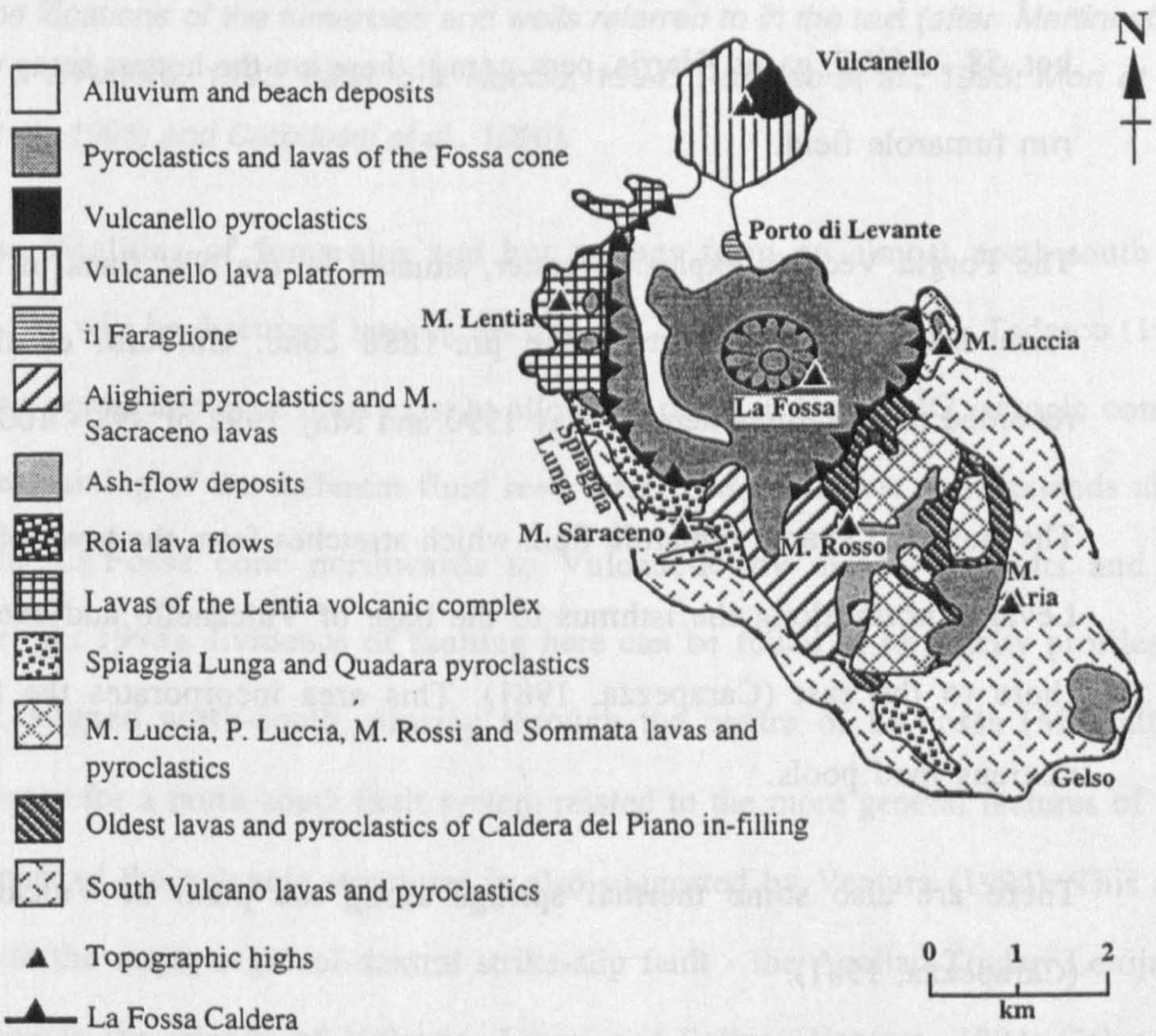

***Figure 4.1**. Map of the island of Vulcano, showing the locations of the main structural and volcanic features (after Ventura,1994).*

4.1.3 Locations of fumarolic activity on Vulcano

The current fumarolic/geothermal activity is centred on a north-south line between La Fossa and Vulcanello. Along this zone are four areas that have been active for many years and consequently contain fumaroles which have been designated identification codes, used throughout the literature; some of these can be seen in **figure 4.2**. The four fumarole fields are located as follows:

1). La Fossa di Vulcano, or the Gran Cratere, which was the site of the 1888 eruption. The fumaroles are found in two main areas; the NW edge of the central crater and the NE rim of the main crater. Thermal investigations by Harris & Stevenson (1997) in 1994, 1995 and 1997 have shown that the fumarole temperatures around the rim and towards the centre of the crater are quite different, having ranges of <50°C to >275°C and <176°C to >530°C respectively. Several large fissures cross the NE crater rim and vigorously emit hot, 58 - 348°C, gases (Harris, pers. com.); these are the hottest areas within the rim fumarole field.

2). The Forgia Vecchia explosion crater, situated on the NW flank of La Fossa, formed the northern part of the pre-1888 cone. Chiodini et al. (1995) recorded temperatures here in May 1990 and May 1992 of ~98 - 100°C.

3). The Baia di Levante fumarole field which stretches from the town of Porto di Levante north along the isthmus to the base of Vulcanello and extends off-shore to the east (Carapezza, 1981). This area incorporates the famously noxious mud pools.

4). There are also some thermal springs along the plain of Vulcano Porto (Carapezza, 1981).

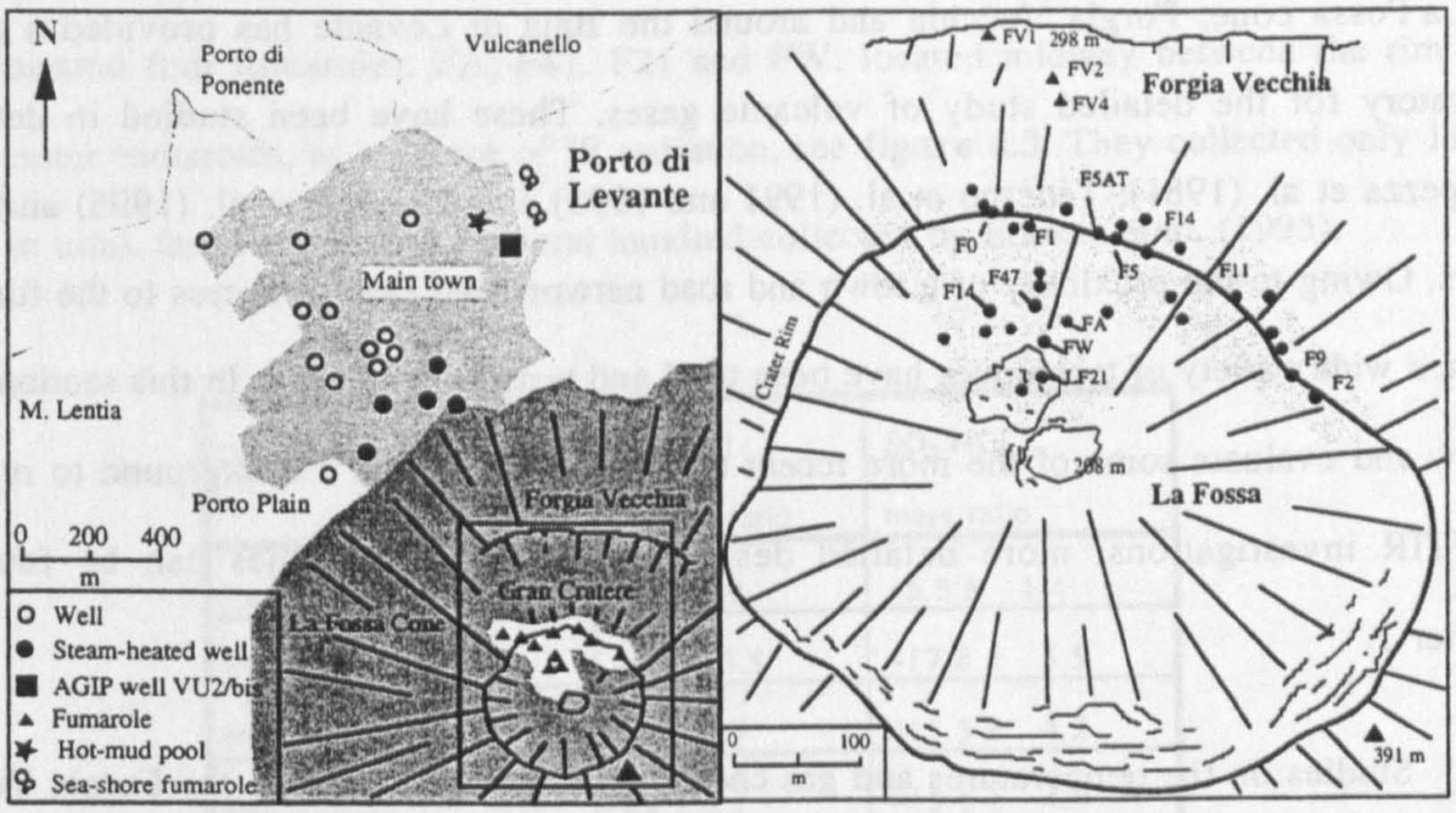

***Figure 4.2**. Map of the area around the La Fossa cone and the Gran Cratere (enlargement) showing the locations of the fumaroles and wells referred to in the text (after: Martini et al., 1981; Bolognesi & D'Amore, 1993; Italiano & Nuccio, 1994; Tedesco et al., 1995; Mori et al., 1995; Chiodini et al., 1995; and Carodossi et al., 1996).*

The localities of fumaroles and hot springs form an almost north-south line, see **figure 4.2**. As will be discussed later in Section 4.3, analysis of fluids by Tedesco (1995) have shown that a permeable zone must exist to allow the range in D and ^{18}O isotopic compositions observed by mixing of the different fluid reservoirs. The permeable zone extends along from beneath the La Fossa cone northwards to Vulcanello by means of faults and fractures (Tedesco et al., 1995). Evidence of faulting here can be found in seismicity profiles showing epicentres, aligned north-south, passing through the centre of La Fossa (Montalto, 1994). More evidence for a north-south fault system related to the more general features of the island and alignment of the volcanic structures is also suggested by Ventura (1994). This alignment is parallel to the major regional dextral strike-slip fault - the Aeolian-Tindari-Letojanni Fault which connects the islands of Vulcano, Lipari and Salina (Ventura, 1994; Calanchi et al., 1996).

4.1.4 Review of techniques used previously

The accessibility of the constantly degassing fumarole fields situated in and around the La Fossa cone, Forgia Vecchia and around the Baia di Levante has provided a natural laboratory for the detailed study of volcanic gases. These have been studied in detail by Carapezza et al. (1981); Tedesco et al. (1991 and 1995) and Chiodini et al. (1995) and many others. Owing to the proximity of a town and road network and ease of access to the fumarole fields, a wide variety of techniques have been tried and tested on Vulcano. In this section I will review and evaluate some of the more recent techniques to provide a background to my own OP-FTIR investigations; more detailed descriptions of the techniques can be found in Chapter 2.

Studies on the temperatures and gas chemistry of crater fumaroles, the Forgia Vecchia and around the Baia di Levante, have been carried out by number of authors since the earliest investigations in ~1855 by St. Claire de Ville and Fouquè (in Carapezza et al., 1981). Early studies of the fumaroles and volcanic gases on Vulcano initially took place in a haphazard way until 1978, when rapid temperature increases, related to the Patti M5.5 regional earthquake and volcanic seismic swarm (Tedesco, 1995), prompted the study of the volcano to intensify. Increasing fumarole temperatures led the Gruppo Nazionale di Vulcanologia (GNV) in 1988 - 1989 to organise two extensive field surveys and an increase in monitoring efforts (Tedesco et al., 1995). Since then, an almost constant monitoring effort has been kept up, co-ordinated locally from the observatory on Vulcano (Badalamenti et al., 1996).

Open-path Fourier transform infra-red spectroscopy (OP-FTIR)

OP-FTIR investigations of the fumaroles at La Fossa have been carried out by two working groups: Francis et al. (1995, 1996; 1996b and this chapter) and Mori et al. (1995). In this chapter, the use of "we" refers to collaborative work I have carried out as part of the Francis et al. (1995) working-group. I shall discuss mainly the work of Mori et al. (1995) in the following sections; the work of Francis et al. (1995) being discussed in detail in Section 4.2.

Mori et al. (1995) analysed volcanic gases in La Fossa in April 1993 using a Bomem FTIR spectrometer with a liquid-nitrogen cooled MCT (Hg-Cd-Te) IR detector, see Section 2.2. They positioned the spectrometer on the south side of the crater and used the hot ground around four fumaroles: FA, F47, F21 and FW, located midway between the rim and central crater fumaroles, as a source of IR radiation, see **figure 4.3**. They collected only 11 IR spectra in total, far fewer than the several hundred collected by Francis et al. (1995).

Fumarole name	SO_2:HCl volume ratio	SO_2:HCl mass ratio
F47	3.5 ± 0.9	~5.5 ± 1.4
FW	11.2 ± 3.5	~17.8 ± 5.5
FW	9.8 ± 2.7	~15.5 ± 4.2
FW	9.5 ± 2.5	~15.1 ± 4.0
FW	9.5 ± 2.5	~15.1 ± 4.0
FA	4.5 ± 1.2	~7.1 ± 1.9
FA	4.6 ± 1.2	~7.3 ± 1.9
FA	4.9 ± 1.3	~7.8 ± 2.1
FA	5.4 ± 1.5	~8.6 ± 2.3
FA	5.3 ± 1.4	~8.4 ± 2.3
Lower F21	5.8 ± 2.7	~9.2 ± 4.2
Average gas ratio	**~6.7 ± 2.7**	**~10.7 ± 4.2**

***Table 4.1.** Results of Mori et al (1995) for OP-FTIR investigation using a natural IR source at La Fossa crater on 24/4/93. The SO_2:HCl mass ratios are much higher than those determined by conventional direct-sampling methods, see **table 4.2** and the OP-FTIR analyses of Francis et al. (1995); see text below.*

Mori et al. (1993) derived SO_2:HCl volume ratios of ~3.5 - 11.2 by comparing the infra-red spectra collected with an artificial one generated from the HITRAN database, see **table 4.1**. I have assumed these are volume ratios (there is no definition of units) as Mori et al. (1995) have used the HITRAN database to derive their gas concentrations and compare their data with other volume-proportional data. I have used mass-ratios for my data and therefore have converted their data into similar units, see **table 4.1**, giving a range of SO_2:HCl mass ratios of ~5.5 - 17.8. Mori et al. (1995) reported that different fumaroles tens of metres apart gave different SO_2:HCl ratios and suggested this was due to compositional differences between

fumaroles; although they did recognise that atmospheric mixing may contribute to the variations detected.

As part of the Francis et al. (1995) working group, I used a Midac AMS™ OP-FTIR system; again with a liquid-nitrogen cooled MCT IR detector on Vulcano in late September 1994. We used warm fumarolic ground and a portable, 1275°C, IR lamp as sources of IR radiation. The portable IR source was positioned on the crater rim in the volcanic plume and the detector located in a variety of sites; including the far crater rim and Monte Lentia, ~1.9 km distant, see Section 4.2. Data from over 300 such active analyses gave average SO_2:HCl mass ratios of ~1.8 - 2.7 ± 0.4. A smaller set of 90 analyses through the rim fumaroles gave a higher ratio of ~4.9. This range of ratios is also higher than those collected by direct-sampling, see **table 4.2**, with an average mass ratio of ~1.4. The collection and interpretation of this data will be discussed in Section 4.2.

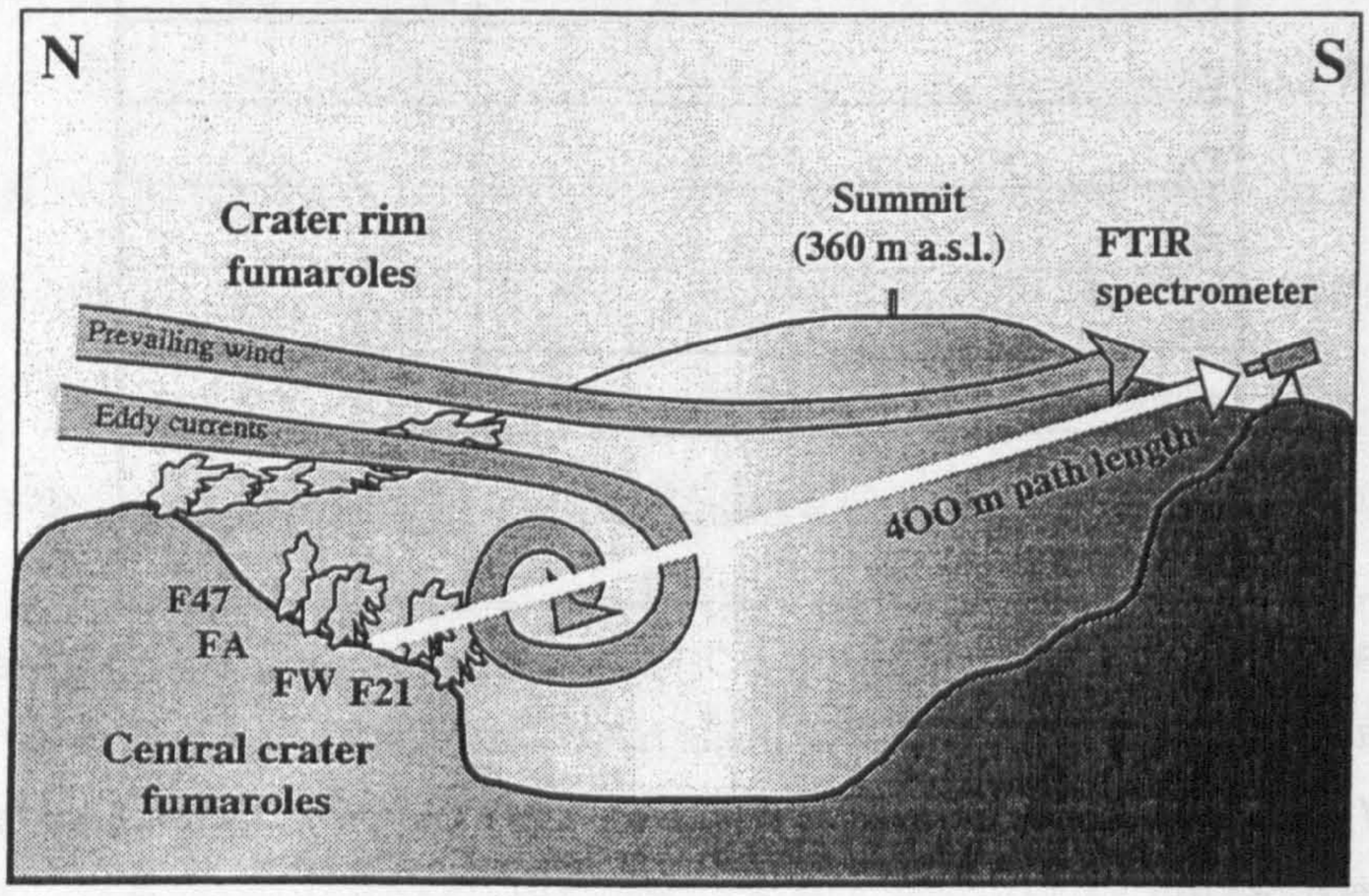

***Figure 4.3**. Schematic of set-up used by Mori et al. (1995) on Vulcano for OP-FTIR analysis of the fumarole gases. The central crater area targeted for passive analyses contains the hottest fumaroles; those on the crater rim being substantially cooler and therefore do not produce as much IR radiation. A schematic representation of the eddy currents that may form due to wind turbulence is also shown. As can be seen, this will cause a significant amount of mixing between gases from different fumaroles.*

The gas ratios detected by Mori et al. (1995) in April 1993 were far higher than those reported by Francis et al. (1995) for September 1994. This discrepancy may by due to the different times of year that the OP-FTIR studies were conducted and a real change in the

composition of volatiles degassed; or as a result of inaccuracies incurred by Mori et al. (1995) whilst using a cooler, natural, IR source, see later. They used the HITRAN database to derive an artificial background spectrum with which to compare their data. Errors in calculating this may have contributed to the high gas ratios reported.

The result of OP-FTIR analyses depends not on which fumarole is targeted, but on the composition of gases occupying the optical path between IR source and spectrometer. I used histograms of SO_2:HCl ratios from the Francis et al. (1995) data-set to separate out the different compositional signatures of rim and crater fumaroles as these had become partially homogenised by eddy currents. With the small data-set of Mori et al. (1995) it would not be possible to identify accurately individual fumaroles by their OP-FTIR-derived compositions.

Differential absorption LIDAR (DIAL)

Edner et al. (1994) used a boat-based DIAL system to determine the SO_2 flux from the La Fossa crater during traverses beneath the plume. The system uses a pair of monochromatic lasers; the back-scattered radiation from which are used to determine the concentration of SO_2 at precise points along the optical path, see Section 2.4. **Figure 4.4** shows the results of a traverse beneath the plume, showing possibly a bifurcated plume (Edner et al., 1994). The highest SO_2 concentrations in the plume, >1050 $\mu g/m^3$ (>0.4 ppmm), were at heights of 200 - 700 m with SO_2 fluxes for different traverses ranging between 17 and 26 t/d (Edner et al., 1994). Although the DIAL technique can provide accurate concentrations, the determination of gas fluxes requires the wind speed to be estimated. This was done using the instruments onboard the ship used by Edner et al. (1994); which measure wind speeds close to sea-level, rather than at the altitude of the plume, ~200 - 800 m. As with COSPEC, see Section 2.3, errors in accurately determining the wind speed may give error of <45% in any flux measurement.

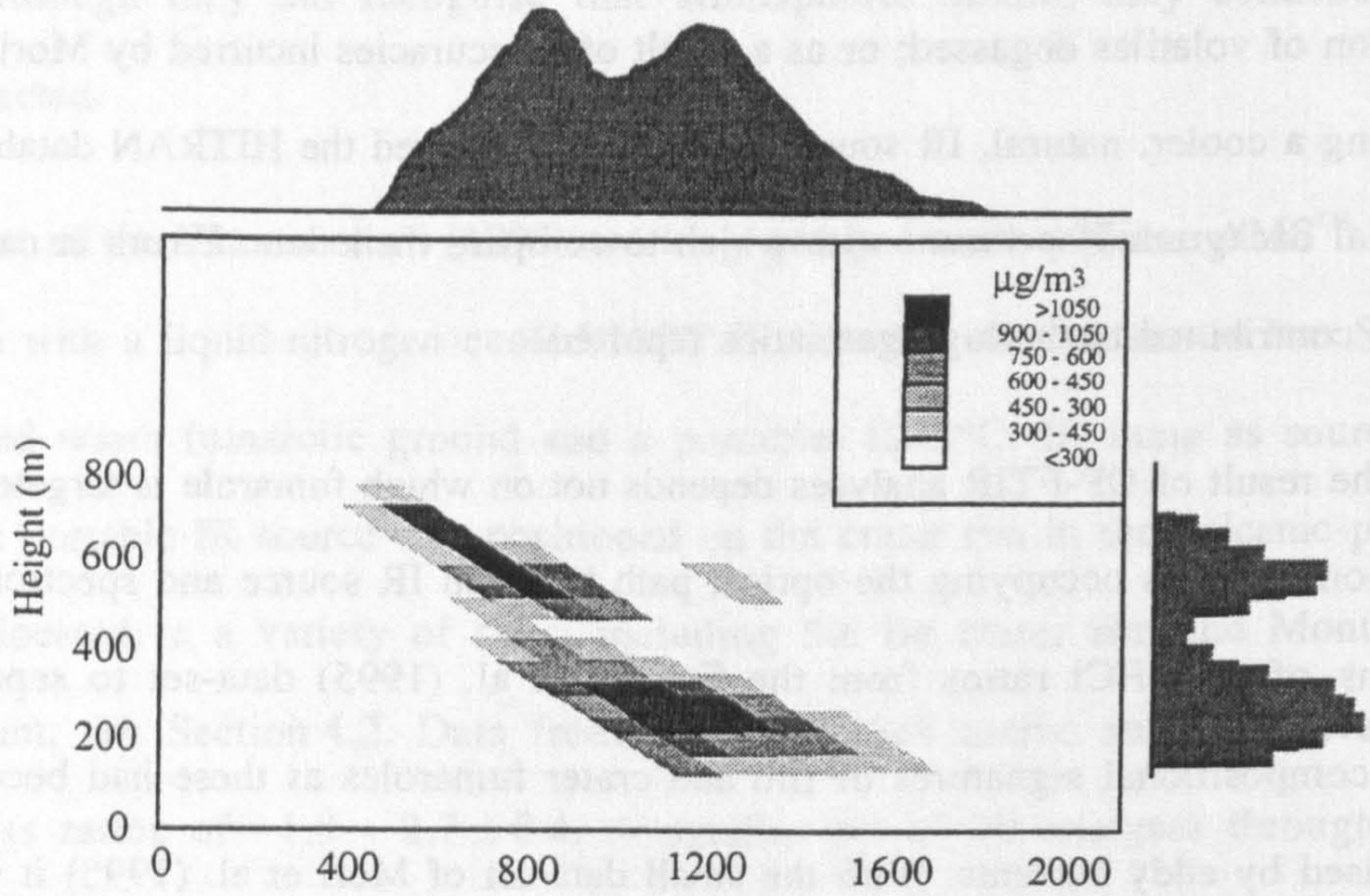

***Figure 4.4**. Diagram of the 2-dimensional and vertically and horizontally integrated SO_2 profiles measured by the DIAL system of Edner et al. (1994) on 3/9/92 showing a vertically bifurcated plume. The SO_2 flux from the traverse was estimated by Edner et al. (1994) to be ~26 t/d.*

Correlation spectroscopy (COSPEC)

The use of COSPEC as a technique for SO_2 flux measurements is well proven, see Section 2.3. I have estimated an average SO_2 flux from sporadic COSPEC measurements conducted between 1978 and 1995 of ~68 ± 64 t/d, see **figure 4.4**. This is much lower than the fluxes estimated for nearby Stromboli, ~320 - 1100 t/d (Allard et al., 1994) and Mt. Etna, <1000 - >25,000 t/d (Chapter 5 and references therein). The major disadvantage of COSPEC is the large error, <45%, associated with uncertainties in the wind speeds used to calculate the flux, see Section 2.3.2. The low gas flux at La Fossa relates to the present 110 years of solely fumarolic activity and the lack of a direct, open conduit to the magma chamber. **Figure 4.5** shows that between ~1978 and ~1991 the SO_2 flux rose steadily, related to the increase in fumarole temperatures which reached a maximum in 1993. After 1991 SO_2 fluxes decreased sharply. Tedesco (1995) and others have interpreted such variations as relating to changes in the amount of interaction between magmatic gases and other fluid reservoirs, see Section 4.3. Such trends can be studied only poorly using COSPEC due to paucity of previous data and

high errors associated with the technique; especially when measuring small gas plumes which can easily be dispersed by the wind.

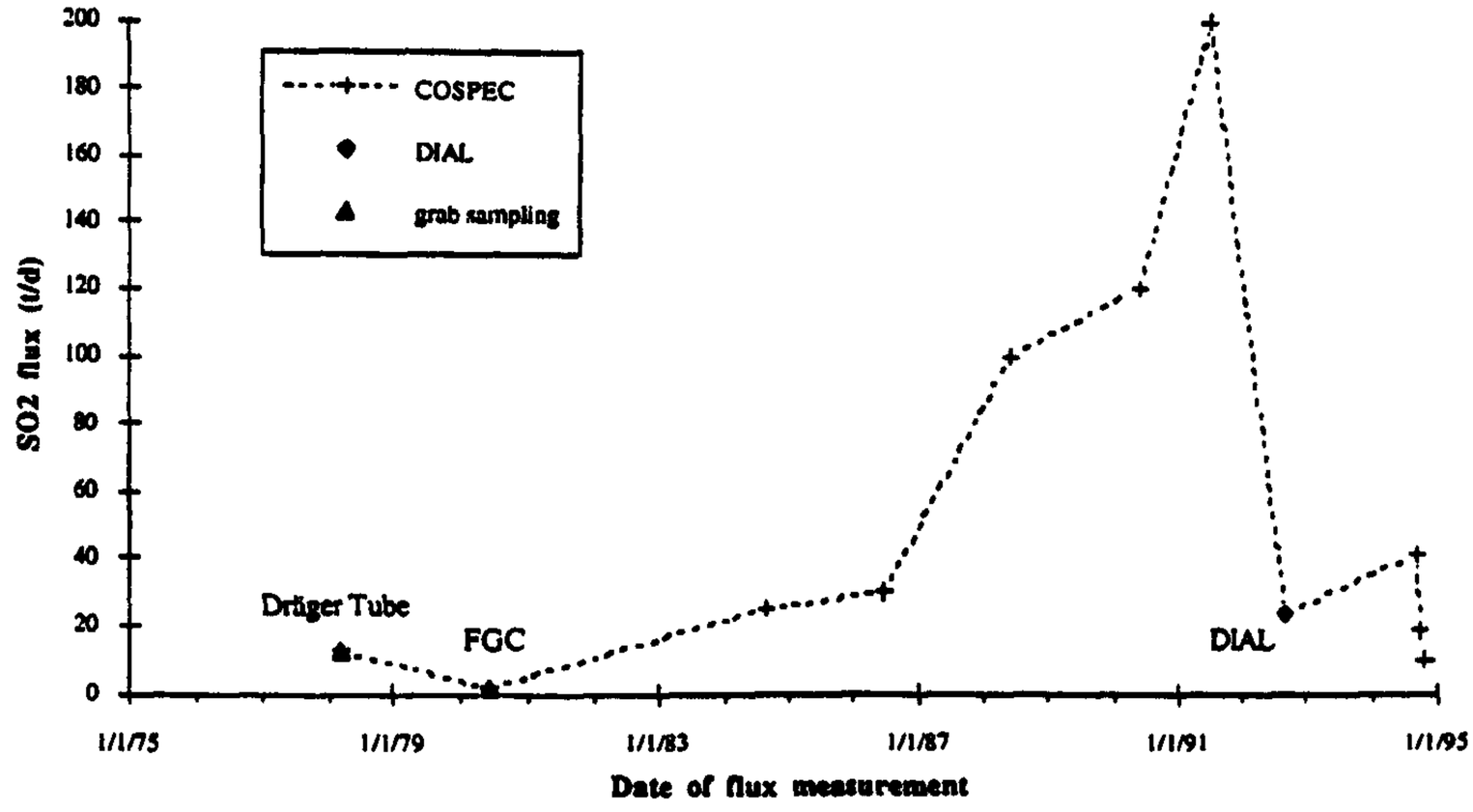

***Figure 4.5** Plot showing variations in SO_2 gas flux during the period 1978 - 1995; as determined by COSPEC analyses (crosses) and other techniques (labelled triangles and diamonds), (after: Sabroux ,1982; Faivre Pierret et al.,1982; Bruno et al., 1990; Allard et al., 1992; Edner et al.,1994 and Caltabiano, pers. com.).*

Direct sampling of fumarolic fluids

The accessibility of the fumarole fields on Vulcano has facilitated direct sampling of the fumaroles and many analyses have been published. The fumaroles have been analysed for a wide range of gases, including: H_2O, CO_2, SO_2, HF, Ar, N_2, CH_4 and He (Martini et al., 1981; Cioni & Corazza, 1981; Tedesco et al., 1991). Direct sampling has also allowed isotopic analyses of ^4He, D, T, ^{34}S and ^{18}O to be conducted (Bolognesi & D'Amore, 1993; Chiodini et al., 1995; Tedesco et al., 1995; and Cortecci et al., 1996).

The direct sampling of volcanic gases using pipes inserted into fumarole vents reduces the amount of atmospheric interaction, oxidation, solution or dilution of emitted gases. Higher concentrations of fumarolic gases can therefore be collected for analysis in the laboratory, see Section 2.7. Contamination and secondary reactions involving the collecting apparatus and re-establishment of chemical equilibria, due to temperature and pressure changes, will alter the original gas composition, thus complicating the interpretation of the analyses (Le Guern, pers. com.). Gases are drawn up the pipes and are either collected in evacuated flasks or by

bubbling them through a strong base, such as NaOH, to dissolve the acid gases. Analysis of the collected gas samples is then done using a variety of high precision laboratory techniques, see Section 2.7. The vagaries of atmospheric absorption, cloud and winds need not be considered, thus reducing the errors involved with the analyses. However, the hazard in collecting the samples and time taken to do the analyses can be major drawbacks in certain situations.

A review of the chemistry of the hydrothermal system at Vulcano, based on the direct sampling of fumaroles, is found in Section 4.1.5. I have compared the OP-FTIR analyses with direct-sampled data as these are probably the most accurate analyses and comprise the largest analytical data-set.

Field IR spectrophotometry

Chiodini et al. (1996) used a hand portable Dräger Polytron IR spectro-photometer to calculate real-time soil-gas fluxes from numerous localities within and surrounding the La Fossa cone in 1995, see Sections 2.6 and 4.2.4 and **figure 4.6**.

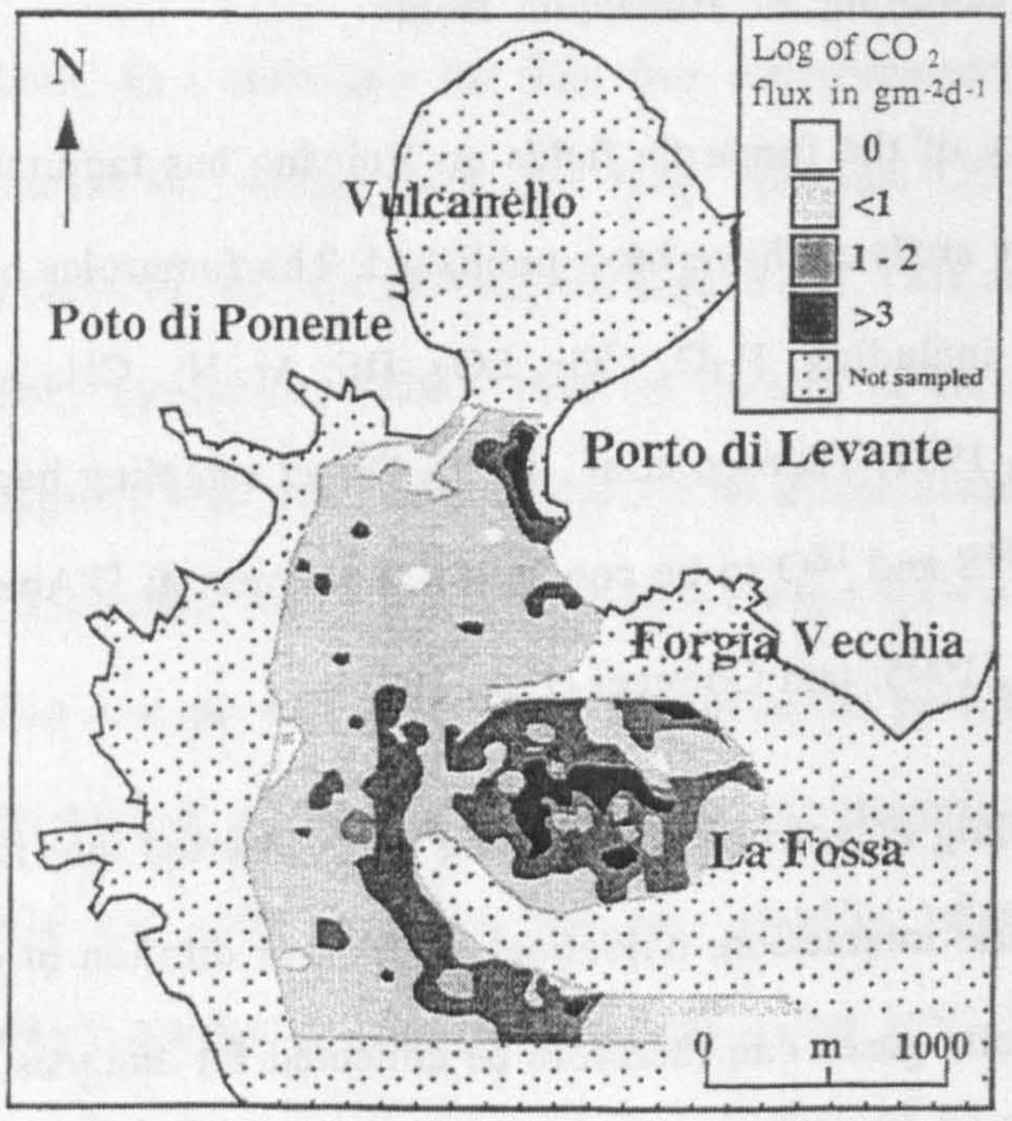

***Figure 4.6**. Map of the Porto plain and La Fossa cone showing areas of high and low soil-gas (CO_2) flux as recorded in April - July 1995 (April1993 for analyses on Porto plain). The highest areas of diffuse CO_2 emission are concentrated close to the rim of the Gran Cratere, (after Chiodini et al., 1996).*

Their data showed areas of high CO_2 flux existed on the NW and NE rims of the crater; with a total CO_2 flux from the upper flanks of La Fossa estimated at ~200 t/d; comparable to that emitted by the fumaroles (Baubron et al., 1990). Elevated levels of soil-degassing have also been found at other volcanoes, such as Mt. Erebus and Mt. Etna (Allard et al., 1991), where background levels of CO_2 are elevated for several metres above ground-level. In Section 4.2 I have proposed that increased background CO_2 levels, due to soil-gas emissions, may have detracted from the accurate quantification of CO_2 using the OP-FTIR technique.

4.1.5 The composition of the gas plume and fumaroles on Vulcano

Results of direct-sampling analyses

A large data-set has already been established by a number of different authors using several analytical techniques. **Table 4.2** summarises the gas compositions reported by Chiodini et al. (1995) for fumaroles at La Fossa, Baia di Levante beach and the Forgia Vecchia, for the period 1979 - 1992. Combined, H_2O and CO_2 form ~93 - 100% of the gases emitted; the remainder being mainly SO_2, H_2S and HCl. It is clear that the average composition of gases emitted from La Fossa is markedly different from fumaroles situated nearby at the Forgia Vecchia and on the beach.

The variation in the gas compositions emitted from the fumaroles can be attributed to the different sources of volatiles. Capasso et al. (1992), Bolognesi & D'Amore (1993) and Chiodini et al. (1995) have identified three different reservoirs by their chemical and isotopic compositions; see Section 4.3. Tedesco (1995) has described these as:

- A deep magmatic reservoir.
- An intermediate marine-hydrothermal reservoir.
- A shallow meteoric reservoir.

Fumarole name	Sampling period	Temp ℃	H_2O wt%	SO_2 wt%	H_2S wt%	S_{tot} wt%	HCl wt%	HF ppm	H_2 ppm	CO_2 wt%	$\frac{SO_2}{HCl}$ (by mass)	δD‰	$\delta^{18}O$‰
FO	88 - 89	304	84	0.7	0.8	1.1	0.6	355	3	13	1.2	9.2	5.7
F1	79 - 89	243	78	1.4	0.5	1.2	1.0	265	1	19	1.4	-1.0	4.7
F5	79 - 91	309	76	1.5	0.8	1.6	0.8	383	2	20	1.8	-0.3	5.2
F5AT	88 - 91	406	82	0.9	1.0	1.4	0.6	492	9	14	1.4	5.2	5.6
F11	88 - 91	345	78	1.3	1.1	1.7	0.8	684	5	17	1.8	1.5	5.3
FA	88 - 91	488	75	2.0	1.6	2.5	1.2	1765	45	18	1.6	4.4	6.5
Average	**79 - 91**	**349**	**79**	**1.3**	**1.0**	**1.6**	**0.9**	**657**	**11**	**17**	**1.5**	**3.2**	**5.5**
FV2	90 - 92	99	90	0.04	0.03	0.0	0.0	0.0	7	10	na	-2.8	1.7
VSF	91 - 92	99.5	79	0.0	0.4	0.4	0.0	0.0	10	21	na	-14.4	-2.9

***Table 4.2**. Gas concentrations and the isotopic compositions of various fumaroles analysed by Chiodini et al. (1995) using a direct-sampling technique. The average composition of the six fumaroles situated on La Fossa is also shown. The locations of fumaroles can be seen in **figure 4.2**. All fumaroles are situated in La Fossa except for FV2 in the Forgia Vecchia and VSF on the Baia di Levante beach. Here the gas emissions are mainly H_2O and CO_2 with minor SO_2, H_2S and H_2.*

Table 4.2 shows that acid gases: SO_2, HCl and HF are emitted almost exclusively from La Fossa, the main source of magmatic volatiles. Reduced gases, H_2S and H_2, if emitted from fumaroles at a high enough temperature, will oxidise to SO_2 and H_2O on contact with the atmosphere. A significant percentage, ~12% (Harris, unpublished data), of the fumaroles at La Fossa are close to or above a temperature of 290°C, the auto-inflammation temperature of H_2S where **reaction 4.1** occurs.

$$2H_2S + 3O_2 \rightleftharpoons 2SO_2 + 2H_2O \qquad \text{(Mori et al., 1995)} \qquad \textbf{(4.1)}$$

H_2S is therefore best detected by using a direct sampling technique which reduces atmospheric interaction. The composition of the beach fumaroles, by comparison, is almost entirely H_2O and CO_2, with an estimated total gas flux of ~30 t/d (after Nuccio, 1994). This is due to the magmatic reservoir only contributing minor amounts of fluids to a system dominated by the meteoric and marine-hydrothermal reservoirs, which may actively dissolve soluble gases. The high solubility of the acid gases causes them to be retained in the reservoirs rather than emitted from the fumaroles (Tedesco, 1995). As will be shown later, the interaction

of acid gases with aqueous reservoirs is, I believe, the fundamental control governing the amounts of SO_2, HCl and HF emitted from fumaroles. The differential solubilities of these gases may therefore tell us more about reservoir mixing than about the original degassing of the magma body. This will be discussed further in Section 4.3.

Comparison of the OP-FTIR data of Mori et al. (1995) with data collected using direct-sampling techniques

Mori et al. (1995) reported an average SO_2:HCl mass ratio of ~10.7 ± 4.2 for OP-FTIR analyses conducted in April 1993; far higher than that reported by Chiodini et al. (1995) of ~1.5 for the period 1979 to 1991, see **table 4.2**. **Table 4.3** compares the average SO_2:HCl mass ratios and the ratios of $SO_{2\ total}$:HCl, assuming all sulphur is oxidised to SO_2, for a number of different fumaroles (after: Martini et al., 1981; Chiodini et al., 1995). The results of this comparison show that, whilst the overall average SO_2:HCl mass ratio is ~2.1, depending on fumaroles investigated, the $SO_{2\ total}$:HCl ratio is higher, ~3.5. This is closer to the lower values of the study by Mori et al. (1995), see **table 4.1**, and highlights one of the differences in comparing the data-sets obtained by different techniques.

Relative position	Crater		Rim Fissure		Rim					
Fumarole name	FA	F14	F0	F1	F2	F5	F5AT	F9	F11	Average
SO_2:HCl mass ratio	#1.6	*2.1	#1.2	#1.4	*2.9	*3.1 - #1.8	#1.4	*2.8	*2.5 - #1.8	**~2.1**
$SO_{2\ total}$:HCl mass ratio	#4.0	*2.2	#3.5	#2.3	*4.4	*3.4 - #3.8	#4.2	*3.9	*2.8 - #4.5	**~3.5**

Mori et al. (1995)	Nearest central crater ⟷ Nearest crater rim				
OP-FTIR data	LF21	FW	FA	F47	Average
SO_2:HCl mass ratio	9.2	15.9	4.9	5.5	**~10.7**

Table 4.3. *This shows the average SO_2:HCl and $SO_{2\ total}$:HCl mass ratios for a range of crater fumaroles during the period #1979 to 1990 (after Chiodini et al. 1995), and *1978 to 1980 (after Martini et al. 1981). I have included the general location of each fumarole to show spatial variations. The SO_2:HCl mass ratios of Mori et al. (1995) are far higher than those reported using direct-sampling techniques.*

The SO_2:HCl ratios derived from the OP-FTIR technique of Mori et al. (1995) reflect more closely the total oxidised sulphur to HCl ratio ($SO_{2\ total}$:HCl), rather than just the

SO_2:HCl ratio, as derived from direct sampling techniques. The role of the atmosphere as a modifier of gas compositions therefore should not be neglected. This is discussed further in Section 4.3 and elsewhere in the thesis.

Mori et al (1995) have assumed that the only gas filling the optical path at the time of analysis was that emitted from the fumarole being targeted. The situation depicted in **figure 4.3** showing the wind eddy currents within the crater will, however, cause significant interaction between gases emitted from different fumaroles. It may therefore only be possible to differentiate between gases emitted from the rim area or crater, rather than from individual fumaroles. Further to this, low temperature IR sources, as used by Mori et al. (1995), do not emit the high frequency radiation required for accurate analysis of HCl leading to high errors in the derived gas ratios. The low IR radiance reported by Mori et al. (Fig. 4, 1995) for their analyses of fumarole FA shows this to be the case. I have therefore concluded that the SO_2:HCl ratios reported by Mori et al. (1995) are too high to be to be assumed representative of the gas emissions of La Fossa. This view is supported by the much lower OP-FTIR analyses of Francis et al. (1995) and the direct-sampling of Chiodini et al. (1995) and others.

4.2 The use of OP-FTIR at La Fossa by Francis et al. (1995)

The data in this chapter relates to an experimental field campaign with the aim of evaluating the potential of the OP-FTIR technique as a tool for investigating volcanic gases. Data were collected using a Midac AMS™ FTIR spectrometer at La Fossa during the period 27/9/94 - 30/9/94 by the author and P. Francis, C. Oppenheimer and C. & T. Chaffin. Simultaneous COSPEC SO_2 flux data were also gathered by T. Caltabiano enabling fluxes of HCl and other gases to be derived. The fumarole fields at La Fossa provided a suitable, and comparatively safe, testing-ground to experiment with a variety of different OP-FTIR sampling methods; some of which were proved to be far more successful than others. A discussion on a variety of techniques tried, and reasons for success or failure, can be found in the following sections.

4.2.1 Perceived problems with gas analysis at Vulcano: A rationale for OP-FTIR

Investigations into the gas emissions of La Fossa have been summarised in the previous sections. The effects of the hydrothermal system and the atmosphere combine to significantly alter the composition of the gas plume from that initially exsolved in the magma chamber. This OP-FTIR study, with results already reported in Francis et al. (1995 and 1996), will discuss the techniques, observations and implications of using remote-sensing to investigate the composition of the plume at La Fossa. The compositions of individual fumaroles cannot be determined using OP-FTIR; neither can the concentrations of IR-inactive gases, such as N_2, H_2 or He. In some circumstances it may not be possible to determine the levels of reduced gases, such as H_2S, which may oxidise on entering the atmosphere. OP-FTIR can, however, detect highly reactive gases, such as HF, and their derivatives, such as SiF_4. These gases are difficult to measure by direct sampling techniques as they are normally associated with secondary reactions involving the collecting apparatus. The processes of condensation and re-equilibration, which act to change the gas composition during direct-sampling are avoided using remote techniques. One of the main advantages of remote techniques is the

ability to measure gases in inaccessible or hazardous areas. Remote techniques may therefore be seen to complement direct sampling methods, rather than be an alternative to them.

4.2.2 OP-FTIR techniques used on Vulcano

Instrumentation

Data were collected using a Midac AMS™ FTIR spectrometer incorporating a liquid-nitrogen cooled MCT detector. The spectrometer was mounted piggy-back on a 10" (25.4 cm) diameter telescope with a 3 mrad field of view. This enabled the IR source to be precisely targeted and allowed a greater amount of IR radiation to be gathered and focused on the detector. We used a portable 1275°C IR lamp and hot, <540°C, fumarolic ground as an IR source for the OP-FTIR analyses. The specifications of the Midac AMS™ system are covered in detail in Section 2.2. Optical path-lengths ranged between ~5 m and ~1875 m, with the spectrometer situated so that as much of the plume lay within the sampling path as possible.

Active measurements using the portable IR source were best achieved by placing the spectrometer directly downwind of the fumarole field with the IR source situated upwind on the crater rim. A maximum path-length of ~1875 m was achieved by locating the portable IR source at the summit of La Fossa and by positioning the spectrometer downwind on Monte Lentia, see **figure 4.7**. Passive analyses were conducted as an experiment to see whether it was possible to use fumarolic ground as a suitable source of IR radiation. Other set-ups were tried on a purely experimental basis to see whether data could be collected using a variety of sources and techniques. Optical path-lengths were determined using a local large-scale map to pin-point the positions of IR source and spectrometer. We collected over 650 active and passive analyses during the course of the study; producing one of the largest, short-term, analytical data-sets for gas chemistry at La Fossa. We achieved this using the set-ups described below.

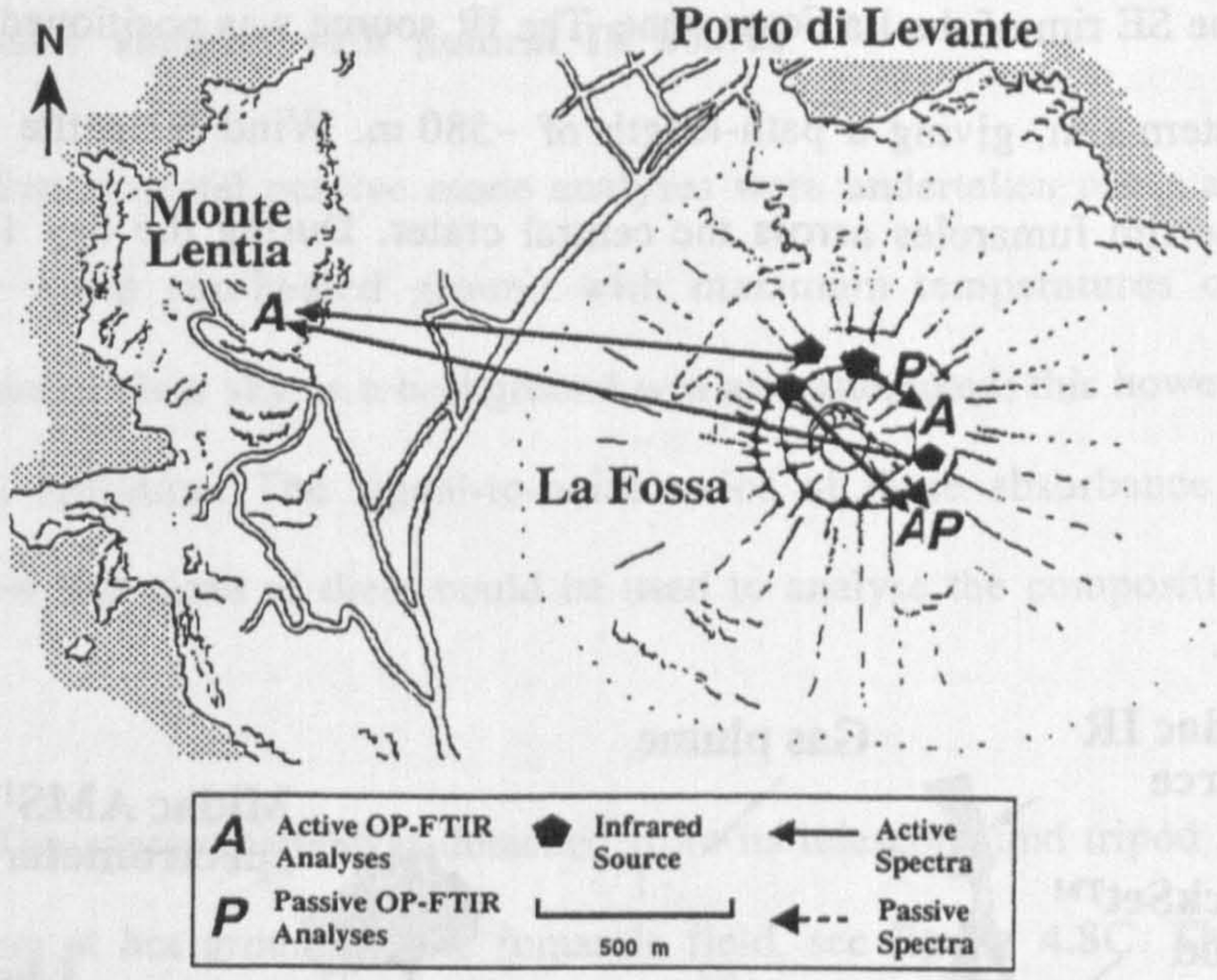

Figure 4.7. *Locations of Midac FTIR spectrometer, portable IR source and optical paths used for OP-FTIR analyses by Francis et al. (1995 & 1996a), and for this thesis, during the period 27/9/94 - 30/9/94. Active and passive refer to the use of artificial and natural IR sources respectively, see text and Section 2.2.*

Active analyses with artificial IR source

27/9/94:- The spectrometer was located at the summit of Monte Lentia on the western rim of the Fossa Caldera. The IR source was placed on the western rim of the Gran Cratere giving a path length of ~1300 m. At the time the wind was from the ESE which allowed the optical path to be completely filled by plume for most of the analyses. The IR source was then carried to the opposite side of the crater close to the summit (~360 m a.s.l.) which increased the path-length to ~1875 m. During the day 160 active spectra were collected. During the four days on Vulcano the weather was hot and sunny with light winds, the direction of which changed from day to day. **Figure 4.8A** shows a schematic of the active OP-FTIR set-up used.

28/9/94:- The spectrometer was detached from its tripod and telescope; positioned on a boulder and aimed at the IR source, which was situated ~100 m away on the northern face of the La Fossa cone. The optical path was usually filled with dense fumes from the rim fumarole field allowing 80 spectra to be collected.

29/9/94:- The spectrometer, telescope and tripod, were transported by helicopter to the summit above the SE rim of the La Fossa cone. The IR source was positioned below and inside the crater's western rim, giving a path-length of ~580 m. Wind from the NNE blew gases emitted from the rim fumaroles across the central crater. During the day 150 active spectra were collected.

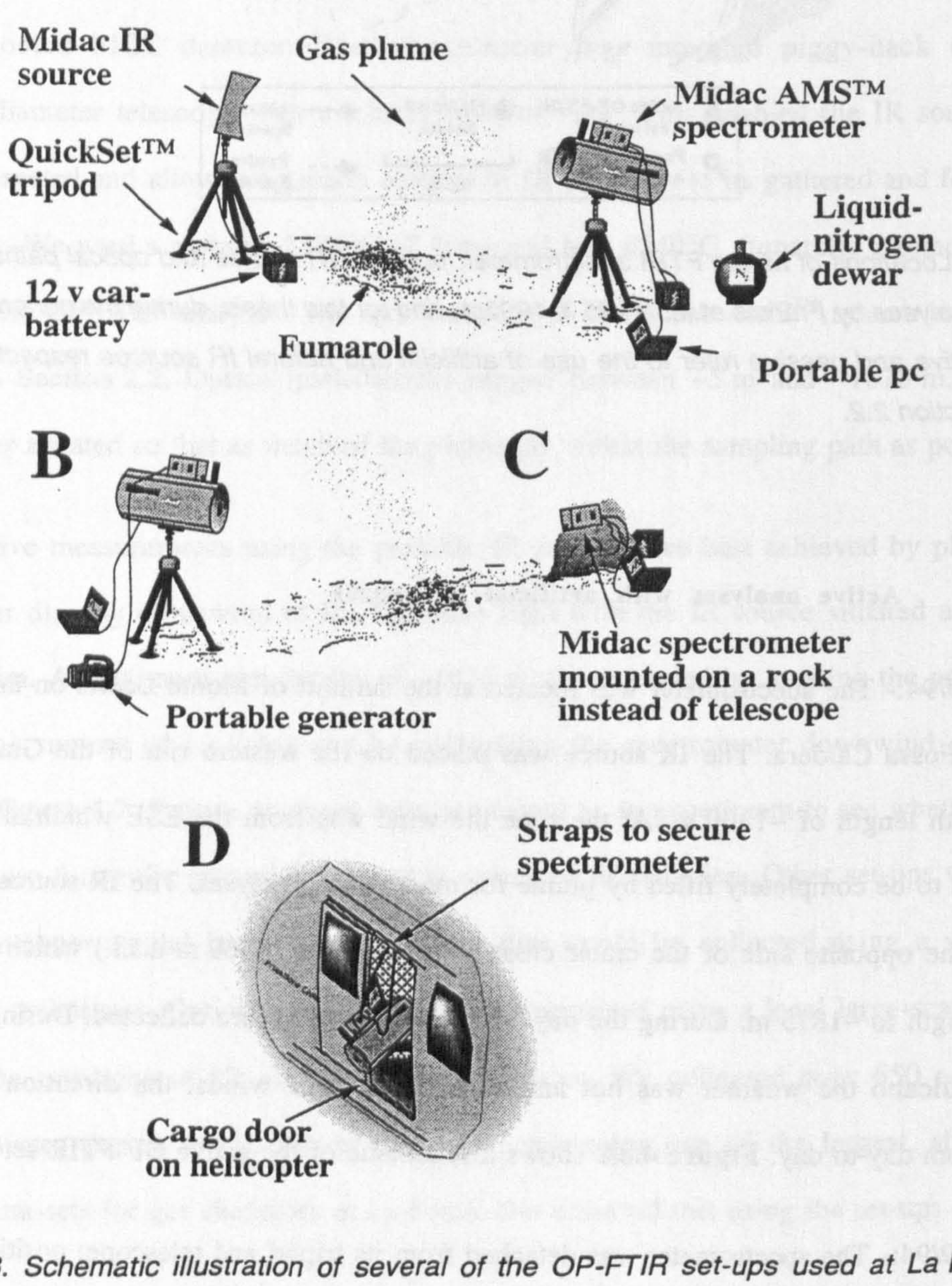

***Figure 4.8**. Schematic illustration of several of the OP-FTIR set-ups used at La Fossa. **A**. Standard active set-up with portable IR source and spectrometer-telescope combination. **B**. Standard passive set-up using spectrometer and telescope, aimed at hot ground. **C**. Short-range passive set up using solely spectrometer. **D**. Airborne set-up.*

Passive analyses with natural IR source

27/9/94:- Experimental passive mode analyses were undertaken using a variety of IR sources including warm sun-heated ground with maximum temperatures of <60°C, see **figure 4.8B**. The use of clear sky as a background was also attempted; this however was a very poor source of IR radiation. The signal-to-noise ratios of these absorbance and emission spectra were so low that none of them could be used to analyse the compositions of the gas plume.

28/9/94:- The spectrometer was detached from its telescope and tripod and was hand-held whilst pointing at hot ground in the fumarole field, see **figure 4.8C**. This enabled the optical path to be ~5 m and for the field-of-view to be completely filled by hot ground of between 125°C and 275°C. The disadvantage of this approach was that a totally analyte-free background could not be collected and any small movements introduced perturbations into the interferogram due to changes in the focusing of IR radiation on the detector. At such short distances, the small differences in temperature between emitted gas and IR source were too small to clearly show the amounts of radiation absorbed by the gases (Chaffin et al., 1995). This produced a very noisy spectrum, especially at shorter wavelengths from which no consistent gas ratios could be determined

29/9/94:- The spectrometer with tripod and telescope were heliported to the top of the SE rim of the Gran Cratere which forms the summit of the volcano. From this vantage-point the instrument could target the hottest fumaroles situated in the centre of the crater. These had been measured on 27/9/94 by Warenbergen (pers. com.) using a thermocouple and by Harris (pers. com.) on 27/9/94 and 11/10/94 using a Minolta-Land Compac 3 radiometer, giving temperatures of ~275 - 540°C. The OP-FTIR set-up was similar to that of Mori et al. (1996) and used a ~400 m optical path. The high temperatures and increased stability of the tripod mounting enabled the signal-to-noise ratio to be increased.

An attempt was made to use the instrument from the air. For this the spectrometer was detached from the tripod and held balanced on the seat-edge in the back of an Italian Civil Defence Augusta 109 helicopter, see **figure 4.8D**. Problems encountered with aiming the

instrument and the constantly changing optical parameters due to movement of the aircraft meant that analyses were very poor (Chaffin, pers. com.). The experiment was opportunist, owing to the limited flight-time; little more than an idea of what an aerial OP-FTIR technique entails could be gained. To optimise the technique, the spectrometer would need to be mounted within the helicopter so that it could be aimed accurately at a hot source and compensated for the movement of the aircraft during a scan. It would also be advisable to fully brief the pilot into exactly what was required for the exercise.

30/9/94:- A further attempt was made to try to record some passive airborne analyses of the gases in the Gran Cratere, again with poor results (Chaffin pers. com.).

4.2.3 General results of the OP-FTIR study

Active analyses

The results from the OP-FTIR study conducted by Francis et al. (1995) during the period 27/9/94 - 31/9/94 at La Fossa di Vulcano are shown in **table 4.4**. The table relates to those gases, SO_2, HCl and SiF_4, that were quantifiable from the study. Other gases, such as N_2O, CO and CO_2 were detected but in insufficient quantities to be accurately reported; estimates for the concentrations of these gases can be found in the discussion below.

It should be noted that the concentration values quoted are only relative. The units of ppmv.m refer to the path-averaged concentration of the analyte and are described by **equation 4.2**.

$$\text{ppmv.m} = \frac{\text{average concentration of analyte in plume}}{\text{length of optical path in plume + length of optical path not in plume}} \qquad \textbf{(4.2)}$$

In our analyses, we tried to maximise the amount of plume in the optical path, however, the capricious nature of the wind sometimes caused only a fraction of the plume to be analysed. Single-beam spectra containing little or no analyte were used as background spectra to create absorbance spectra required for deriving analyte concentrations, see Section 2.2.2. Our concentration data, as ppmv.m, represents a path averaged value, as defined in **equation 4.2**, and incorporated gases of different compositions which have drifted into the optical path

causing a range of gas ratios to be derived. I have determined the average gas ratio by using a regression line drawn through the origin of a plot of SO_2 against HCl, see **table 4.4.**

Date	N° of Spectra	Path length (m)	Mean Value SO_2 ppmv·m	Mean Value HCl ppmv·m	Mean Value SiF_4 ppmv·m	$\frac{SO_2}{HCl}$ (mass ratio)
27/9/94	40	~1400	97 ± 26	91 ± 23	0.5 ± 0.01	1.9 ± 0.2
27/9/94	120	1875	121 ± 14	120 ± 11	0.6 ± 0.004	1.6 ± 0.2
28/9/94	90	100	21 ± 1.5	7.7 ± 0.4	0.07	*~4.7 ± 2.6
29/9/94	150	580	133 ± 12	96 ± 7.87	0.8	2.4 ± 0.4

Table 4.4. *A summary of the data from active mode OP-FTIR analyses at La Fossa, Vulcano. Concentrations of analyte are measured in ppmv.m , see text. Gas mass ratios are derived from the gradient of regression lines used in* ***figures 4.9 A-C****. Noise and variation in the data are due to gases from different parts of the fumarole field being incorporated in the optical path in varying proportions. The optical paths used for analyses can be seen in* ***figure 4.7****. *The gas ratios determined on 28/9/94 are the result of variable mixing between the rim and crater fumaroles, thus producing a high standard deviation for the average gas ratio. This is discussed in the text.*

The results from our active OP-FTIR analyses are plotted in **figures 4.9A-C**. The derived SO_2:HCl ratios for 27/9/94 and 29/9/94 are fairly similar, ~1.6 - 1.9 and ~2.4 respectively, with only a minor amount of variation. This is greatest for the ~1875 m path-length analyses, conducted on 27/9/94, with the shorter 580 m data collected on 29/9/94 having the least variation, see **figures 4.9A** and **C**. This is due to the longer path data recording a greater variety of gas compositions from both the rim and central crater fumarole fields. The greater consistency in gas mass ratios derived from data collected on 29/9/94, 4.8 ± 0.7, using a ~580 m path-length suggests the homogenisation of the plume within the crater; the higher concentrations of gases detected also increased the signal-to-noise ratio and therefore accuracy of the analyses.

The ACT 451-557 data-set in **figure 4.9A** exhibits a non-linear correlation between the OP-FTIR derived SO_2 and HCl concentrations, with the regression line through the data intersecting the HCl axis rather than passing through the origin. This may be due to the differences in detectability of the two analytes at low concentrations, with HCl being quantifiable at lower concentrations than SO_2, see Chapter 2. The data in **figure 4.9A** were collected over the longest path lengths, ~1.85 km. At such ranges it is possible that the effects

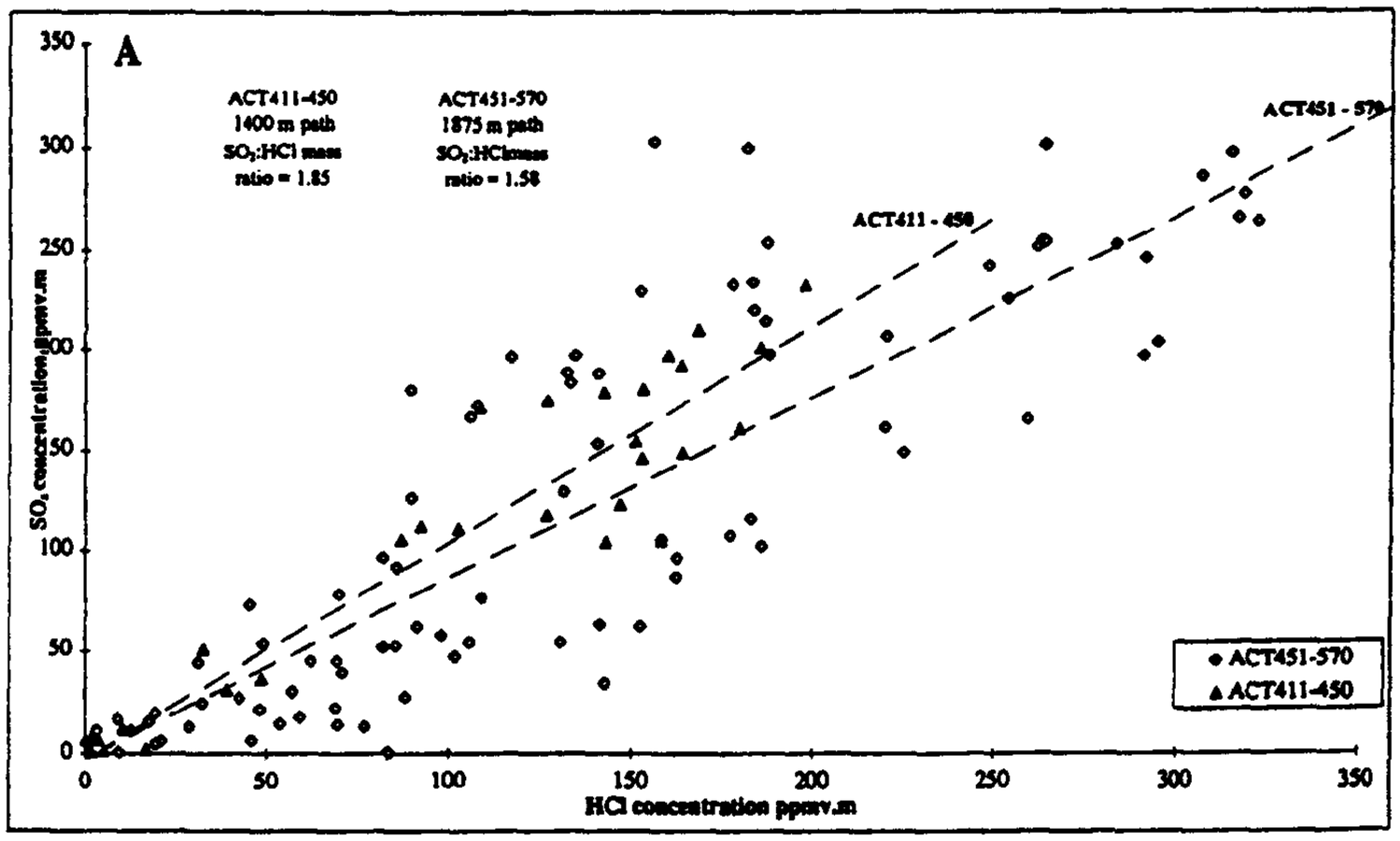

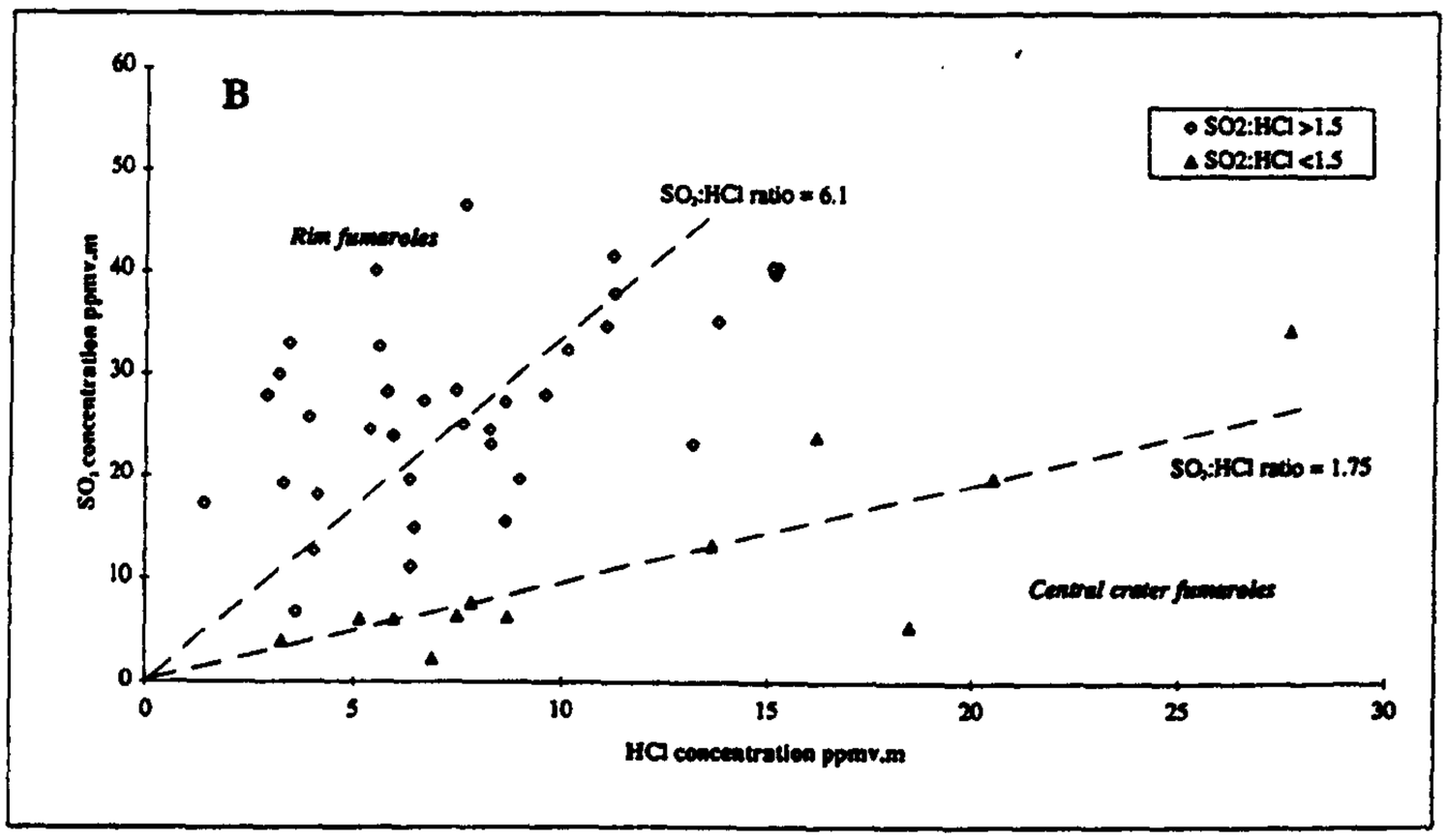

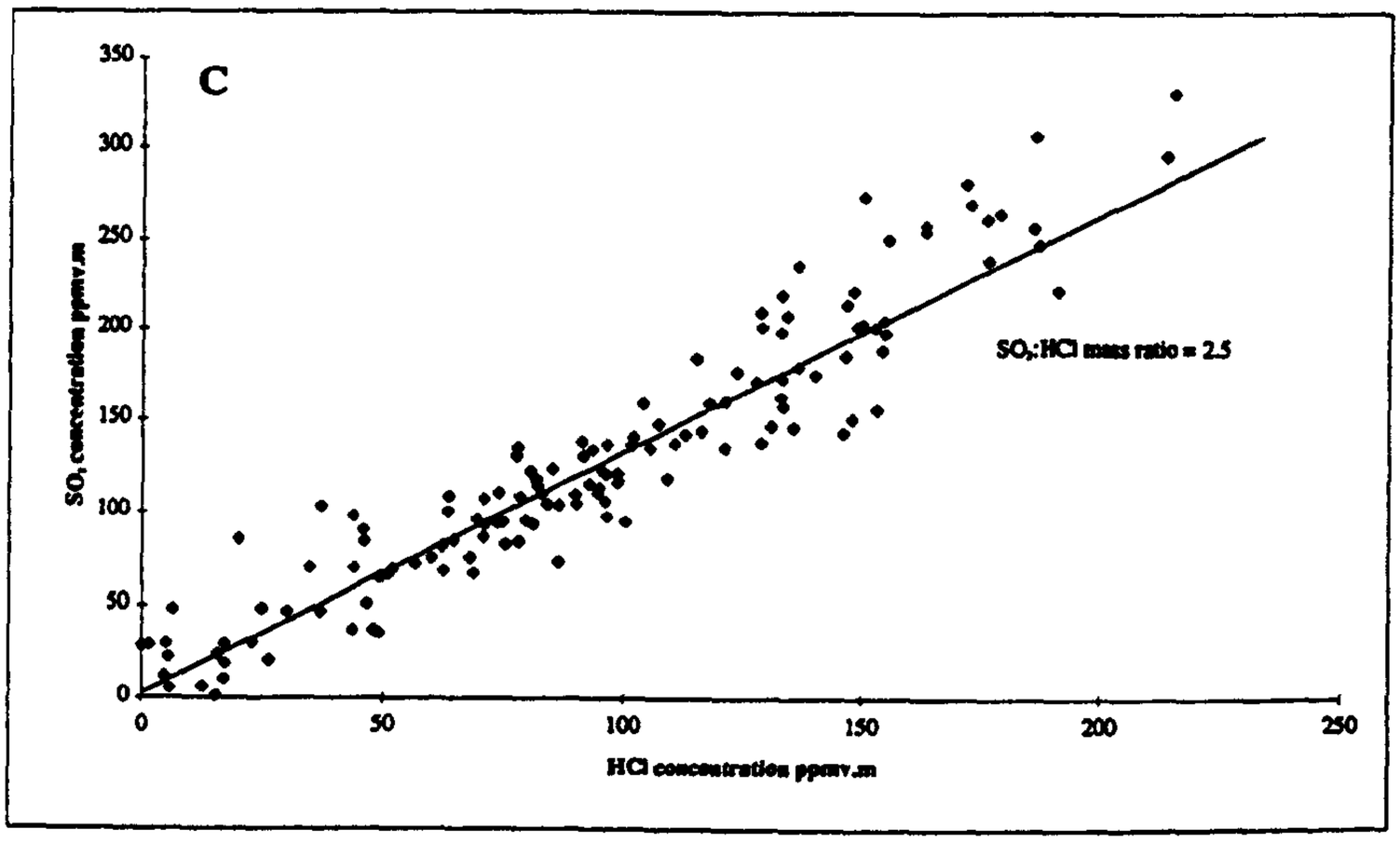

Figure 4.9. A. *Plot of active OP-FTIR data on 27/9/94 using two path lengths: 1400 m and 1875 m between the Gran Cratere and Monte Lentia.* ***B.*** *Plot of data from the 28/9/94 showing OP-FTIR data collected through the rim fumaroles with a short, ~100 m, optical path-length.* ***C.*** *Active data acquired on 29/9/94 using a path length of 580 m across the Gran Cratere.*

of SO_2 scavenging within the gas plume were becoming apparent, thus reducing the SO_2 concentrations detected. Alternatively this may relate to an, as yet, unquantified effect or process within the fumarolic system.

Data collected on 28/9/94 in the rim fumarole field using a shorter, 100 m, path-length exhibits a much wider range in gas mass ratios; from <2 to >15. I have determined two general ranges for the gas ratios for data from 28/9/94 using the frequency distribution of gas ratios when plotted as a histogram; these are ~0.5 - 3.1 and ~4.0 - 6.6, see **figure 4.9B**. Variation in observed gas ratios on different dates is due to the atmospheric mixing between three gas sources: the hot central crater fumaroles; the hot rim fissures; and the warm rim fumaroles, see **table 4.3**. The compositions of gases from these three sources will be discussed in Section 4.2.4 below.

Passive analyses

Many of the passive set-ups we used at La Fossa were experimental and failed to provide any quality data; mainly due to the IR source used being too cool to provide sufficient IR radiation at the frequencies needed for HCl and SO_2 analysis, see Section 2.2.3. Only one data-set enabled us to derive usable SO_2:HCl ratios; this was recorded on 29/9/94 and used the hottest fumaroles, <540°C (Warenbergen, pers. com.), in the central fumarole field.

Date	N° of spectra	Path length (m)	Mean Value SO_2 ppmv·m	Mean Value HCl ppmv·m	Mean Value SiF_4 ppmv·m	$\frac{SO_2}{HCl}$ mass ratio
29/9/94	20	~400	113 ± 6	51 ± 16	1.4 ± 0.1	4.1

Table 4.5. *This shows the average values for the only high quality passive analyses conducted at La Fossa. We used the hottest fumaroles in the central crater as an IR source for the analyses. The average SO_2:HCl mass ratio was again derived using a regression line rather than a mean due to the spread of the data .*

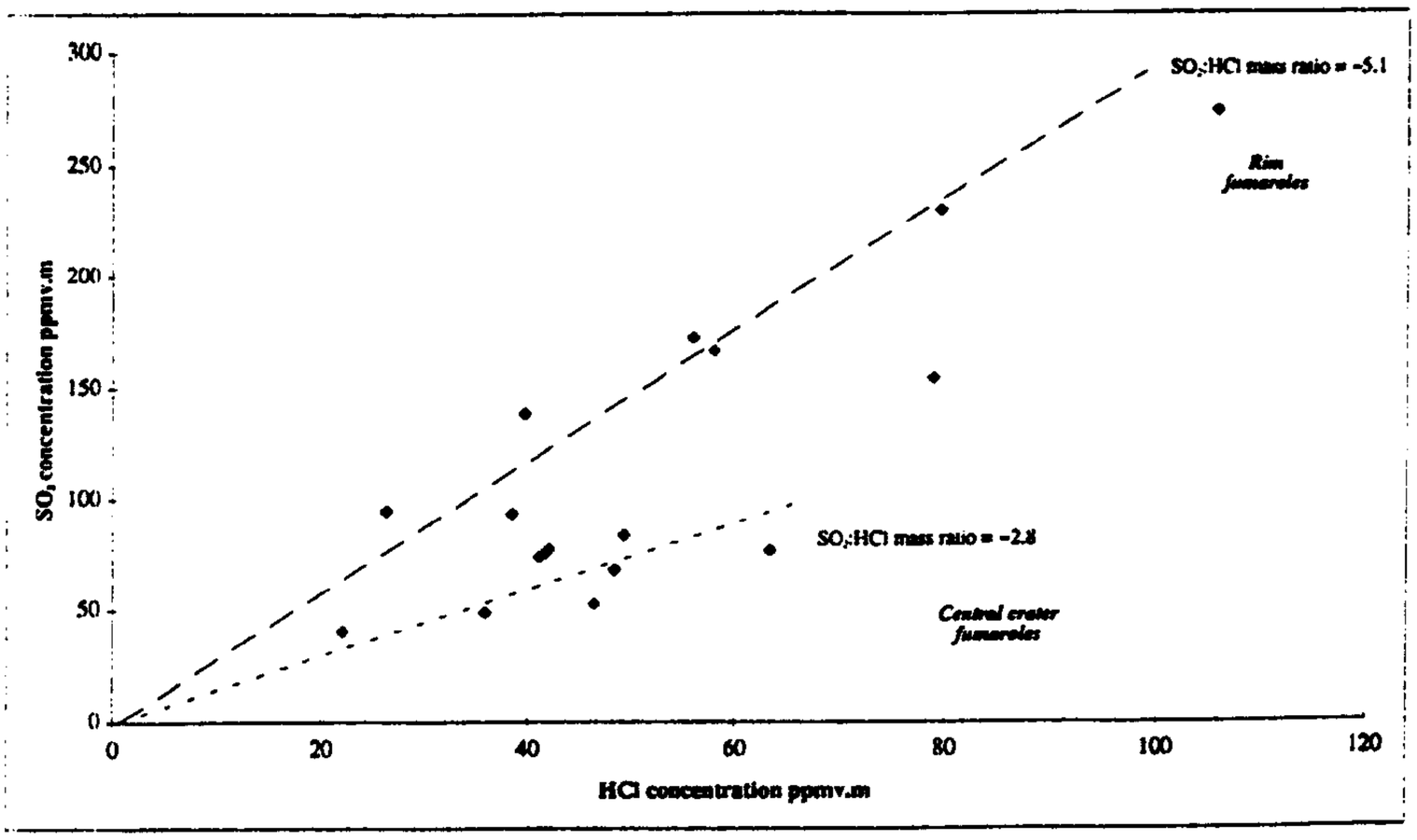

Figure 4.10. *Plot of passive OP-FTIR data for 29/9/94. The SO_2:HCl gas ratios for these data lie between the gas ratios calculated for the active data acquired on 28/9/94 and 29/9/94; indicating that mixing of fumarolic gases may be occurring. Gas mass ratios relate to the slope of the regression line after conversion from initial volume ratios. The spread in data is due to the mixing of gases from the rim and central crater fumaroles or to the lower IR temperature of the natural IR source introducing noise into the spectra, thus increasing errors during calculation of analyte concentrations, see text.*

Data from these analyses are presented in **table 4.5** and **figure 4.10**. Although the errors were higher due to the increased spectral noise, the data are similar to the higher quality active analyses. On this day the wind was blowing across the line of the optical path. It is therefore likely that a majority of the optical path was filled with gas emitted from the crater-rim, rather than the targeted central fumaroles; with variations in the SO_2:HCl ratios occurring due to changes in the proportions of gases rim or crater gases. The differences in the compositions of the gases emitted from central crater and rim fumaroles must therefore relate to fundamental differences in magmatic-hydrothermal processes that affect these areas.

4.2.4 Discussion of results

The results from our OP-FTIR investigations show that there are two general ranges of SO_2:HCl ratio: ~0.9 - 2.6 and ~4.3 - 6.1, see **table 4.6**. Higher gas ratios were always present during analyses when gases from the rim fumarole field were blowing through the optical path. I have therefore inferred that the higher SO_2:HCl ratios represent the rim fumarole field,

with the lower gas ratios relating to the central crater fumaroles. This concurs with the averaged analyses of Chiodini et al. (1995) and Martini et al. (1981), see **table 4.3**. Similarly, the total S, as SO_2, to HCl mass ratios I have calculated from the direct-sampled data of Chiodini et al. (1995) are also lowest for the central crater fumaroles.

Date	SO_2:HCl mass ratio	Inferred gas source
27/9/94	~0.5 - 1.9	central - scavenge
27/9/94	~1.1 - 2.3	central - scavenge
28/9/94	~0.5 - 3.1	mainly central
28/9/94	~4.0 - 6.6	rim
29/9/94	~1.6 - 2.6	mainly central
29/9/94	~4.8 - 5.2	rim
29/9/94 (Passive)	~1.7 - 3.2	centre + rim
29/9/94 (Passive)	~4.4 - 6.1	mainly rim

***Table 4.6**. This shows the ranges of the dominant gas ratios in each of the active data-sets; the passive data-set is included for comparison. As can be seen there are two overall ranges: ~0.9 - 2.6 and ~4.3- 6.1 which I have inferred to represent the SO_2:HCl mass ratios of the central crater and rim fumarole fields respectively; based on the positions of optical path and wind direction during periods of analysis. This is also supported by the direct-sampling data in **table 4.3**.*

Pennisi & Le Cloarec (1998) have proposed a model for degassing at Mt. Etna where high SO_2:HCl mass ratios, ~10, represent active, shallow level, degassing; whereas lower ratios, ~1, represent background. deeper, degassing, see Chapter 5. I have measured SO_2:HCl ratios of generally >3 at Mt. Etna using OP-FTIR, and therefore inferred that high SO_2:HCl ratios are indicative of high temperature, magmatic degassing. The gas SO_2:HCl mass ratios I have estimated at La Fossa, are generally lower; especially for the hottest fumaroles situated in the centre of the crater. I have assumed the fumes from these, having the highest temperatures, have the most direct link to the cooling magma body and are therefore the least altered in composition. The low SO_2:HCl mss ratios of these, ~2, therefore most closely reflect the volatile composition within the magma chamber. As discussed in Giggenbach (1996) and Chapter 5, the differential magmatic solubility of SO_2 and HCl causes the SO_2:HCl ratio to decrease as the magma body degasses. I have interpreted this as probably being due to the degassing of an older, cooler magma of rhyolitic, rather than basaltic, composition; based on

the rhyolitic/latitic compositions of the last eruption, in 1888 (after: Clocchiatti et al., 1994; Giggenbach, 1996) and **table 1.1**.

Gases emitted from the lower temperature fumaroles around the crater rim have taken a less direct route to the surface and have interacted with shallow level meteoric and marine-hydrothermal reservoirs (Tedesco et al., 1991 & 1995). It is in these reservoirs that I believe the highly soluble HCl has been dissolved preferentially, relative to SO_2, thus increasing the SO_2:HCl ratio observed; HCl being ~10^6 times as soluble in H_2O as SO_2 at 25°C (Mori et al., 1995). The less soluble SO_2, rather than remaining in solution, may precipitate out as anhydrite and form impermeable barriers between the different fluid reservoirs, see Section 4.3 (after Oskarsson, in Cioni & D'Amore, 1984).

We also measured low concentrations, <1.5 ppmv.m, of the gas SiF_4 in our active and passive OP-FTIR data at La Fossa. This gas is the product of the reaction of HF with SiO_2 which takes place within the hydrothermal system, see **equation 4.4**. The reaction also takes place in the glassware used for the direct-sampling of gases. SiF_4 has therefore been poorly studied in a volcanological context due to its formation by secondary reaction and its relative unimportance as an indicator of volcanic activity. I have, as part of Francis et al. (1996), developed a technique for using SiF_4 to remotely estimate the temperature of the hydrothermal system. This technique, its applications and limitations is discussed in Section 4.2.5.

I also detected trace amounts, <20 ppm.m, of N_2O in several spectra collected on 29/9/94 when winds were blowing from the nearby town of Porto di Levante. I have therefore assumed that these were probably of anthropogenic origin; possibly fumes from vehicle exhausts; although the possibility of an agricultural/natural source can not be dismissed.

CO_2 in OP-FTIR spectra at Vulcano

The results of analyses by Chiodini et al. (1995) of fumarolic emissions from La Fossa showed that, after H_2O, CO_2 is the most abundant gas emitted, ~13 - 20 wt%. I therefore attempted to quantify CO_2 emissions from La Fossa using OP-FTIR data. I initially used the

small absorbance peak at ~668 cm^{-1}; the main fundamental absorbance between ~2280 and 2380 cm^{-1} being truncated due to the total attenuation of IR radiation by atmospheric CO_2. I estimated variations in CO_2 levels of <30 ppmv.m above background using this method; far lower than I expected, based on the direct-sampled data of Chiodini et al. (1995), see **table 4.2**.

Mori & Notsu (1997) analysed gases at Aso volcano, Japan, on 26/6/97 using an InSb detector and an area of hot fumaroles as a natural IR source. They used the weak absorbance peak at ~2077 cm^{-1} to derive CO_2 concentration data from absorbance spectra created in a similar fashion to that used by the author. I re-calculated the CO_2 concentrations in the Francis et al. (1995) 27/9/94 OP-FTIR data-set using the 2077 cm^{-1} peak of Mori & Notsu (1997). My preliminary results indicate that, although there is a wide variation in the CO_2 concentration data, ~200 - 10,000 ppm.m, the SO_2:CO_2 mass ratios are ~0.02 - 0.05, with an average mass ratio of ~0.033 ± 0.016. This average value discounts the small number of data giving ratios of ~0.005 which appear to belong to a separate population; possibly related to soil degassing, see below, or the extreme mixing of plume and atmosphere, see **figure 4.11**. Derivation of CO_2 concentrations is difficult as the 2077 cm^{-1} absorbance peak used is relatively small, even at high analyte concentrations. The peak also lies close to a water absorbance line (Mori & Notsu, 1997) making accurate CO_2 subtraction even harder; hence the ~50% variation in SO_2:CO_2 gas ratios. The SO_2:CO_2 mass ratio of ~0.033 is lower than the average ratio I derived from the data of Chiodini et al., (1995), ~0.05 - ~0.1. This may also be due to either atmospheric CO_2 or soil-gas emissions being incorporated into the IR spectra or, a fundamental change in the SO_2:CO_2 ratio since Chiodini et al. (1995) analysed fumarole emissions, 1979 - 1992.

I have previously suggested that gases with low SO_2:HCl ratios are emitted from the central crater fumaroles. From CO_2 data I can also infer that emissions from the central craters have lower SO_2:CO_2 ratios. Analyses of Tedesco (1995) suggest that both SO_2 and CO_2 originate from a deep, magmatic, source. It may be possible that CO_2 is concentrated by the fractures which facilitate the passage of hotter gases to the central crater fumarole field; thus producing a lower SO_2:CO_2 ratio.

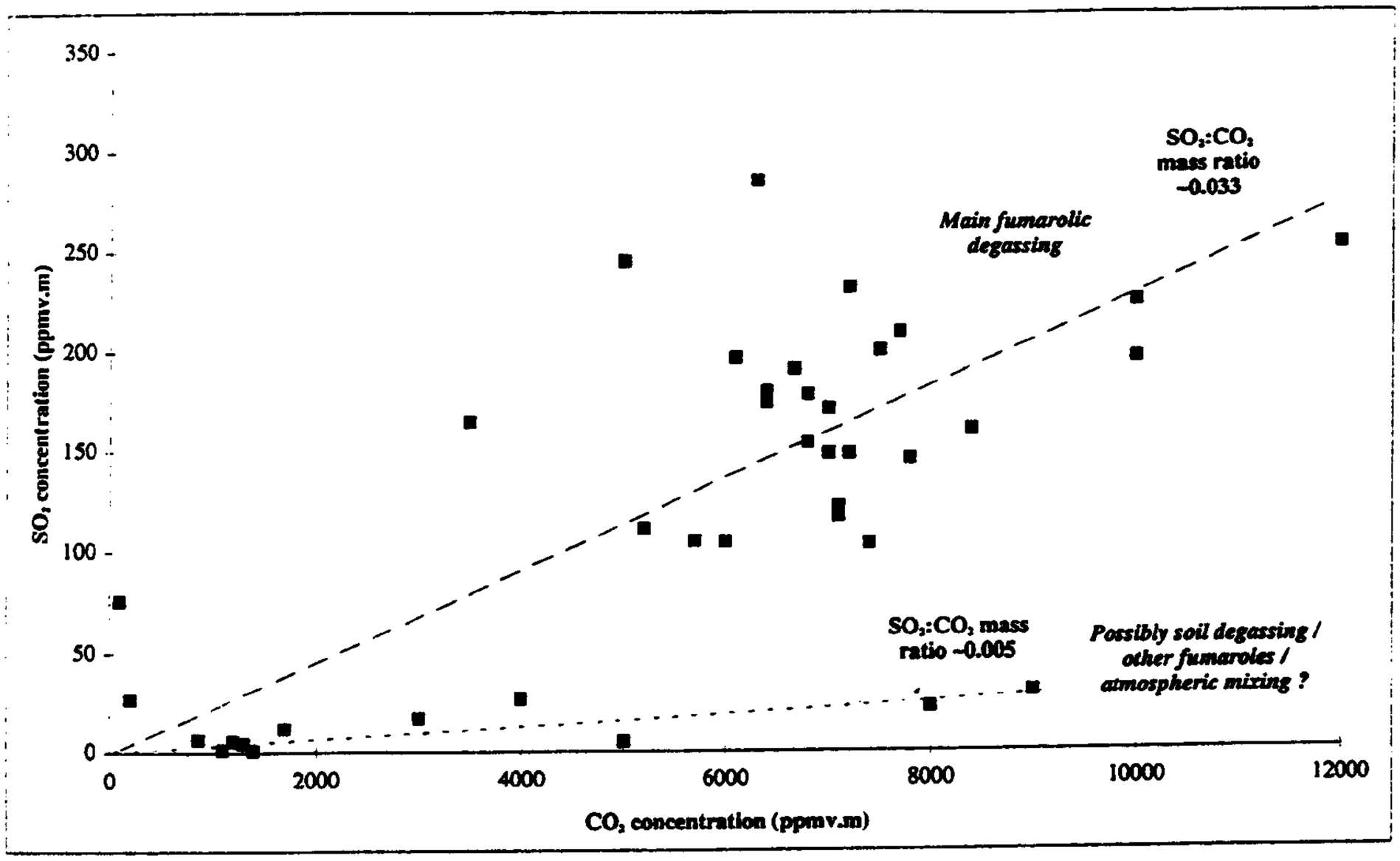

Figure 4.11. *Plot of SO_2 against CO_2 for OP-FTIR data collected by Francis et al. (1995) on 27/9/94. Two populations of data can be seen, one with a mass ratio of ~0.033, the other with a mass ratio of ~0.005. I have attributed the low SO_2, high CO_2 gas composition to possibly soil degassing and/or extreme mixing with the atmosphere.*

Explanation for variation in OP-FTIR-derived SO_2:CO_2 ratios

I have not been able to explain the disparity between gas concentrations derived using different parts of the same CO_2 laboratory reference spectrum; i.e. 668 and 2077 cm^{-1} peaks. As the data derived from the 2077 cm^{-1} peak is similar to that expected, I have assumed these results to be valid. The large variation in the data is probably due to how absorbance spectra are derived. These are the log of the ratio between background and sample single-beam spectra; as derived from the Beer-Lambert Law, a derivative of which appears in **equation 4.3** (Solomons, 1976; Hollas, 1987).

$$\text{Absorbance at } \nu = \log\left(\frac{\text{Intensity of Background at } \nu}{\text{Intensity of Sample at } \nu}\right) = \varepsilon_\nu \, c \, l \qquad (4.3)$$

where: ν is the wavenumber of the peak; ε_ν is the absorption coefficient at wavenumber ν; c is the concentration of analyte; and l the length of the optical path. For high background analyte concentrations, such as CO_2, the sample concentration must be proportionally higher to give

the same intensity of absorbance; consequently the detection limits of that analyte will be raised leading to higher errors on derived concentrations. During analyses eddy currents can carry either fumarolic gases or clean air into the optical path leading to the variations observed. The high ambient level of CO_2 is also increased by the high flux of soil-gas from the La Fossa cone and surrounding area, see below.

CO_2 emissions from La Fossa

CO_2 is not only produced by degassing in the fumarole fields, but through diffuse soil-gas emission from both the Gran Cratere and Porto Plain (Chiodini et al., 1996). Baubron et al. (1990) and Chiodini et al. (1996) measured CO_2 fluxes from the fumaroles at La Fossa in 1984 and 1988 and estimated fluxes of 180 ± 10 t/d and ~20 - 150 t/d respectively. Chiodini et al. (1996) and Baubron et al. (1991) have also estimated the CO_2 flux from the Porto plain to be ~75 - 115 t/d. Italiano & Nuccio (1994) estimated the CO_2 flux from the fumaroles at Baia di Levante was considerably lower, being only ~6.5 t/d.

Chiodini et al. (1996) investigated diffuse soil-gas emissions from the La Fossa cone and immediate vicinity in 1995 and estimated a CO_2 discharge rate of 180 - 230 t/d. Their results show two obvious areas of high CO_2 productivity: the western rim of La Fossa and the area immediately to the south east of the crater, see **figure 4.6**. These were, coincidentally, the two areas used by Francis et al. (1995) to locate the FTIR spectrometer and portable IR source during OP-FTIR analyses, see **figure 4.8**.

Comparison of the OP-FTIR data of Francis et al. (1995) with that of Mori et al. (1995) and other direct-sampled data-sets

Comparison with Mori et al. (1995)

Mori et al. (1995) conducted the first OP-FTIR investigation into fumarolic emissions at La Fossa on 24/4/93. Their results gave an average SO_2:HCl mass ratio of $\sim 11.8 \pm 4.7$. Ratios obtained by Francis et al. (1995) in September 1994 were ~1.0 - 3.0 over the whole

fumarole field, see **tables 4.2** and **4.4**. Measurements of fumarole chemistry and temperature during the periods 1979 to 1992 (Chiodini et al., 1995) and 1986 to 1990 (Tedesco et al., 1995) showed that over time the SO_2:HCl mass ratio has varied between ~0.3 - 2.9. Mori et al. (1995) argued that high SO_2:HCl ratios of the OP-FTIR data were due to H_2S oxidation. It is unlikely that there were major changes in levels of H_2S oxidation between April 1993 and September 1994 as fumarole temperatures remained relatively constant (Badalamenti et al., 1996).

Differences may therefore relate to the pseudo-seasonal variation of gases (Martini et al., 1981). Data from Tedesco et al. (1991) indicated that concentrations of SO_2 and H_2O were lower in the autumn. In contrast HCl and CO_2 were lower in the spring. High SO_2 and H_2O concentrations, combined with lower soluble HCl in spring, would result in higher SO_2:HCl ratios when compared to autumn data collected in a drier environment with lower SO_2 and relatively higher HCl. It is also possible that, as Mori et al. (1995) were conducting a passive OP-FTIR investigation, the temperature of the natural IR source used was not sufficient to allow the accurate detection of HCl; the increase in signal-to-noise ratio causing the HCl detection limits to be raised and thus possibly leading to an overestimate of their reported SO_2:HCl ratios. Thus the combination of seasonal variation and lower detectability of HCl may explain the differences between the Mori et al. (1995) and Francis et al. (1995) data-sets.

Comparison of Francis et al. (1995 & 1996a) data-sets to the analyses of Chiodini et al. (1995) and Tedesco et al. (1995)

The SO_2:HCl ratios I have estimated for the rim and central fumaroles using OP-FTIR show the same trend as that of the conventional data of Chiodini et al. (1995); with rim fumaroles having a higher average mass ratio than the central fumaroles, ~2.3 and 1.7 respectively. A similar trend is observed for the average S_{tot}:HCl mass ratios; ~4 and ~3 for rim and central fumaroles respectively. I have not identified H_2S in any OP-FTIR spectra; this is due to the very weak H_2S fundamental absorbance being obscured by H_2O lines, and its partial/total oxidation to SO_2. Many of the rim fumaroles were below the autoinflammation temperature of 290°C for H_2S (Mori et al., 1995); suggesting H_2S could be present in the

atmosphere at La Fossa. I smelled a strong odour, similar to rotten eggs - characteristic of H_2S, whilst at La Fossa; supporting the suggestion that not all the emitted H_2S was oxidised. This is supported by the analyses of Chiodini et al. (1995) and Tedesco (1995) who both detected H_2S using direct-sampling techniques. The similarity between OP-FTIR and directly-sampled gas mass ratios suggests that the OP-FTIR technique can, within certain limits, reproduce gas analyses derived using conventional direct-sampling methods. Limitations to the OP-FTIR technique include the following, which will all play a part in the overall success of an OP-FTIR investigation:

- The suitability of different analytes to IR analysis - i.e. whether a gas is IR-active and has a large enough fundamental absorbance in an atmospheric "window" for it to be detected at the concentration levels experienced on a volcano.

- Analyte oxidation - reduced gases, such as H_2S, CH_4 and even CO may oxidise on emission, if at a high enough temperature, and therefore not be detected by OP-FTIR.

- Climatic effects - solution of HCl and HF by clouds and rain can alter the composition of the gas plume. UV and particle induced oxidation of SO_2 can also occur, forming SO_3 and SO_4^{2-} aerosols.

- The pseudo-seasonal variation of gas compositions from La Fossa, although not specifically affecting OP-FTIR analyses, will cause analyses from different time periods to vary significantly, see Section 4.3.3.

4.2.5 SiF_4 in volcanic emissions

The occurrence of SiF_4 in volcanoes

Silicon tetrafluoride, SiF_4, should be the tenth most common volcanic gas species found in volcanic plumes; based on the gas thermodynamic calculations carried out at 870°C by Symonds et al. (1992, 1994). Its presence has, however, never been reported in previous

conventional studies of volcanic gas chemistry; owing to SiF_4 being a product of secondary reactions caused by magmatic HF reacting with sampling and laboratory glassware, see **equation 4.4**. We reported in Francis et al. (1996) low, but significant, levels of SiF_4 at La Fossa using an OP-FTIR technique, see **figure 4.12**. This is the first time SiF_4 had been quantified in a volcanic plume.

$$SiO_2 + 4HF \rightleftharpoons SiF_4 + 2H_2O \qquad \text{(Rosenberg, 1973)} \qquad \textbf{(4.4)}$$

The equilibrium of **equation 4.4** is strongly pressure and temperature dependant; SiF_4 being produced preferentially at lower temperatures or higher pressures (Symonds & Reed, 1993; Honda & Mizutani, 1968). I have found little data relating to the thermal stability of SiF_4. Rosenberg (1973) and Symonds et al. (1992) have modelled its chemical equilibrium at temperatures of >800°C; I have therefore assumed it is thermally stable at temperatures found at La Fossa, <600°C. The main reagents for **equation 4.4**, fluorine and silica are both present in magma. In the conduit and hydrothermal system fluorine may be present as HF or as a salt e.g. CaF_2 or NaF; silica may be found as amorphous quartz (Symonds & Reed, 1993). Once the gas has been emitted from the vent/fumarole the ensuing decrease in pressure and/or drop in temperature effectively "freezes" the hot equilibrium into the cold gas (Mueller, 1970). I have used this principle to gain an insight into the hydrothermal environment beneath the vent.

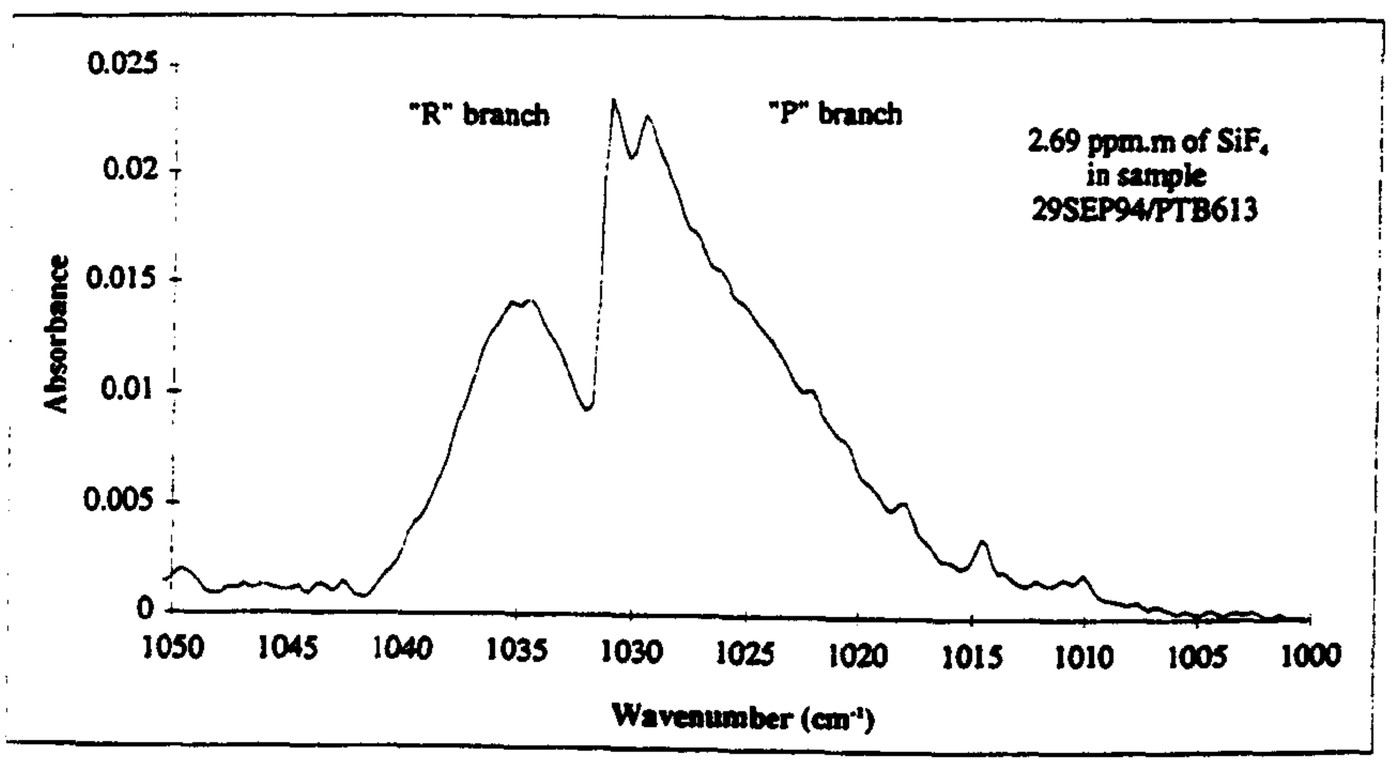

Figure 4.12. *IR absorbance spectrum showing ~3 ppm.m of SiF_4 in passive sample PTB613 collected on 29/9/94 at La Fossa using a 400 m path length. The smooth shape of the absorbance peak is due to the fine structure not being resolvable at the resolution of 0.5 cm^{-1} used for the analysis.*

Thermodynamics of the $HF\text{-}SiF_4$ reaction

The equilibrium position of **equation 4.4**, which governs the relative amounts of reagents and products, is not temperature dependant (Morgan, pers. com.); however the equilibrium constant, K_{eq}, is. This relates to the rate at which a reaction takes place. Honda & Mizutani (1988) have determined K_{eq} for **equation 4.4** for a range of temperatures. At higher temperatures the rate of reaction is far slower; with K_{eq} ~1×10^2 at 600°C but ~1×10^{11} at 100°C (Honda & Mizutani, 1988). This is probably due to a rate-limiting intermediate species being less thermodynamically stable at higher temperatures - i.e. it doesn't form for long enough for the next step of the reaction to take place. Therefore, as a general rule, hotter fumaroles produce less SiF_4 than cool fumaroles.

Fumarole temperatures inferred from SiF_4 data

The temperatures of volcanic gases can be related to the depth, and state, of the magma chamber beneath the volcano. Monitoring temperature changes are therefore important in determining the overall level of activity at a volcano. Gas equilibrium temperatures enable us to monitor subsurface temperatures and "see" deeper into a volcano than is possible using just gas emission temperatures. Francis et al. (1996) therefore developed a technique to study equilibrium temperatures remotely, thus reducing the risks involved in data collection. We used the relationship between temperature, pressure, HF fugacity and the $HF:SiF_4$ ratio to estimate equilibrium temperatures within the hydrothermal system at La Fossa, see **figures 4.13A-B** to **4.15** (Rosenberg 1973; Francis et al., 1996; Maciejewski et al., 1996). This is the first time that the $HF–SiF_4$ system has been used to estimate the equilibrium temperatures of fumarolic gases and thus, by its very nature, is an experimental technique. Rosenberg (1973), Honda & Mizutani (1988) and White & Hochella (1992) have modelled the theoretical behaviour of the $HF–SiF_4$ system. We have used their modelled data to estimate the temperatures from our OP-FTIR-derived concentration data. The following sections describe how this was achieved and the assumptions made.

Calculating fumarole/equilibrium temperatures

According to Rosenberg (1973) and White & Hochella (1992) the equilibrium temperature, T_{eq}, of the HF–SiF_4 system can be determined if the HF:SiF_4 molar ratio; HF fugacity (fHF) and pressure are known. We estimated average SiF_4 concentrations for gases emitted from La Fossa from OP-FTIR data. To determine fumarole equilibrium temperatures, T_{eq}, at least semi-quantitatively requires the concentrations of both SiF_4 and HF. However, the calibration used for the OP-FTIR system prevented measurement of HF absorbance spectra. To circumvent this, we used the OP-FTIR derived HCl:SiF_4 ratio and an HF:HCl ratio derived from data collected using conventional sampling methods, see **figure 4.14**. This is a circuitous route to get the data required. The number of wavenumbers scanned by the FTIR spectrometer can be adjusted to enable both HF and SiF_4 to be detected using an MCT detector; this has recently been done successfully at Masaya volcano, Nicaragua (Horrocks, pers. com). HF concentrations can also be measured using an InSb detector which is more sensitive at higher frequencies than the MCT detector; however the low-wavenumber cut-off for the InSb detector of ~1850 cm^{-1} prevents detection of SiF_4, see Section 2.2. The technique of using HCl as a substitute for HF leads to uncertainties being incorporated into the final estimated equilibrium temperature.

Two methods of calculating equilibrium temperatures using SiF_4 have been attempted; one by Francis et al (1996) and one by the author.

Francis et al. (1996) - the White & Hochella (1992) model

Francis et al. (1996) remotely determined the temperature of fumaroles at La Fossa using the following method. The OP-FTIR derived HCl:SiF_4 volume ratios were combined with the HF:HCl ratios of Chiodini et al (1995) to give an approximate HF:SiF_4 molar ratio of ~10. The HF fugacity in the fumarolic emissions, log fHF, as measured by direct sampling (Chiodini et al., 1995), ranges between -3.6 and -2.6. The above HF:SiF_4 molar ratio and the general range of fHF were incorporated into the model in **figure 4.13A** (White & Hochella,

1992) which graphically describes the relationship between *f*HF, temperature and the log of the SiF_4:HF molar ratio. Using the OP-FTIR data from the gas plume, Francis et al. (1996) derived a temperature of ~200 - 450°C for the fumaroles at La Fossa.

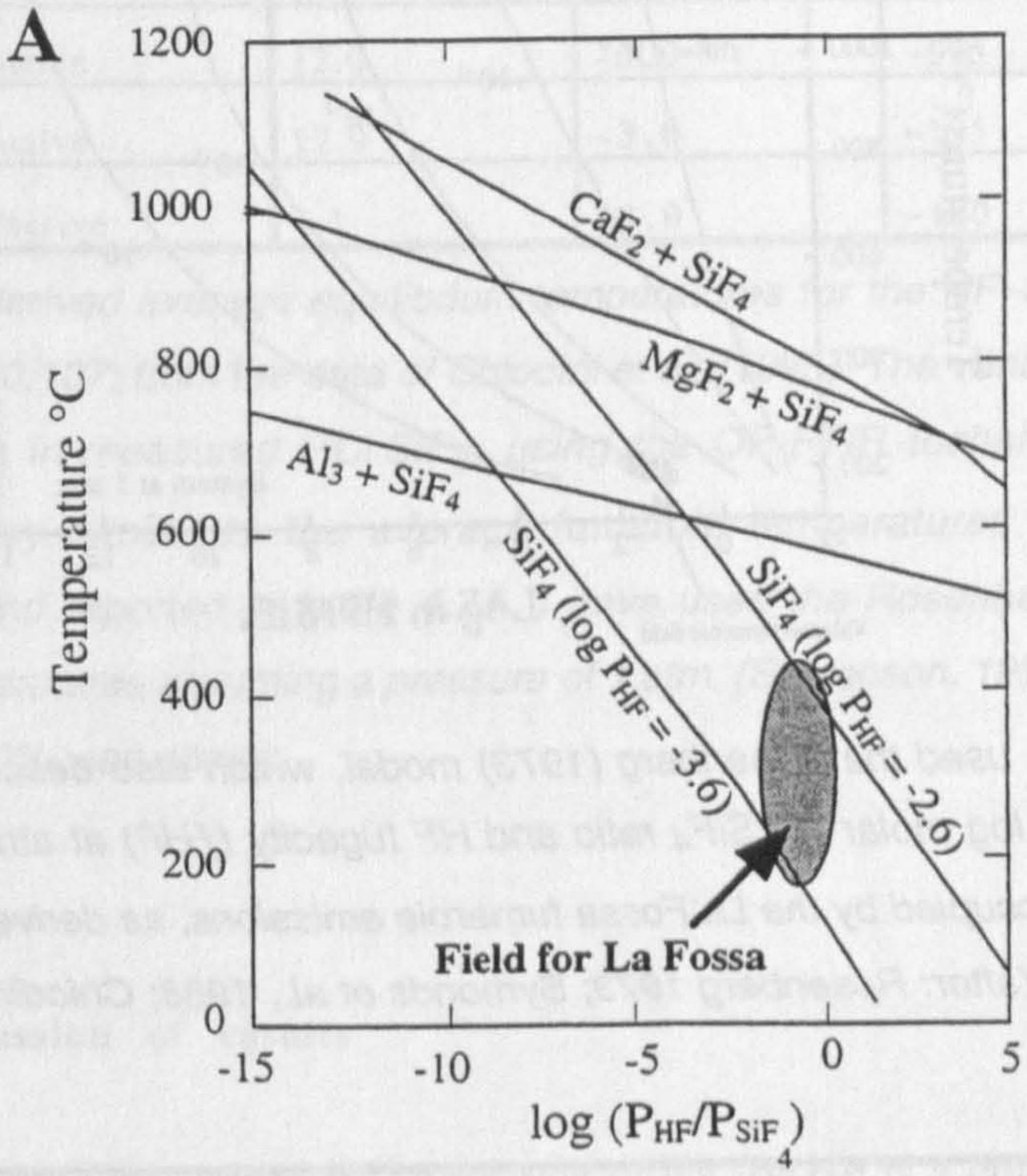

***Figure 4.13. A**. The White & Hochella (1992) model for the relationship between temperature; log molar HF:SiF_4 ratio and HF fugacity (ƒHF) as used by Francis et al. (1996).*

This thesis - the Rosenberg (1973) model

The methodology of estimating temperatures from HCl:SiF_4 ratios that I have developed is similar to that used by Francis et al. (1996). I have used average HF:HCl ratios for each of the fumaroles analysed by Chiodini et al. (1995) and OP-FTIR-derived HCl:SiF_4 ratios to determine a range of HF:SiF_4 molar ratios. I have also used the analyses of Chiodini et al. (1995) to derive log *f*HF values, see **table 4.7A** and **figure 4.13B**. I have used a model of the exponential relationship between temperature and the SiF_4:HF molar ratio reported in Rosenberg (1973) rather than the linear model (White & Hochella, 1992) used by Francis et al. (1996); due to the non-linear relationship between K_{eq} and temperature, as described in the equations of Honda & Mizutani (1988), see **figure 4.15**. Since the log of the SiF_4:HF molar

ratio is used, the model is insensitive to the minor variations caused by using a linear or exponential relationship or molar or mass SiF_4:HF ratios.

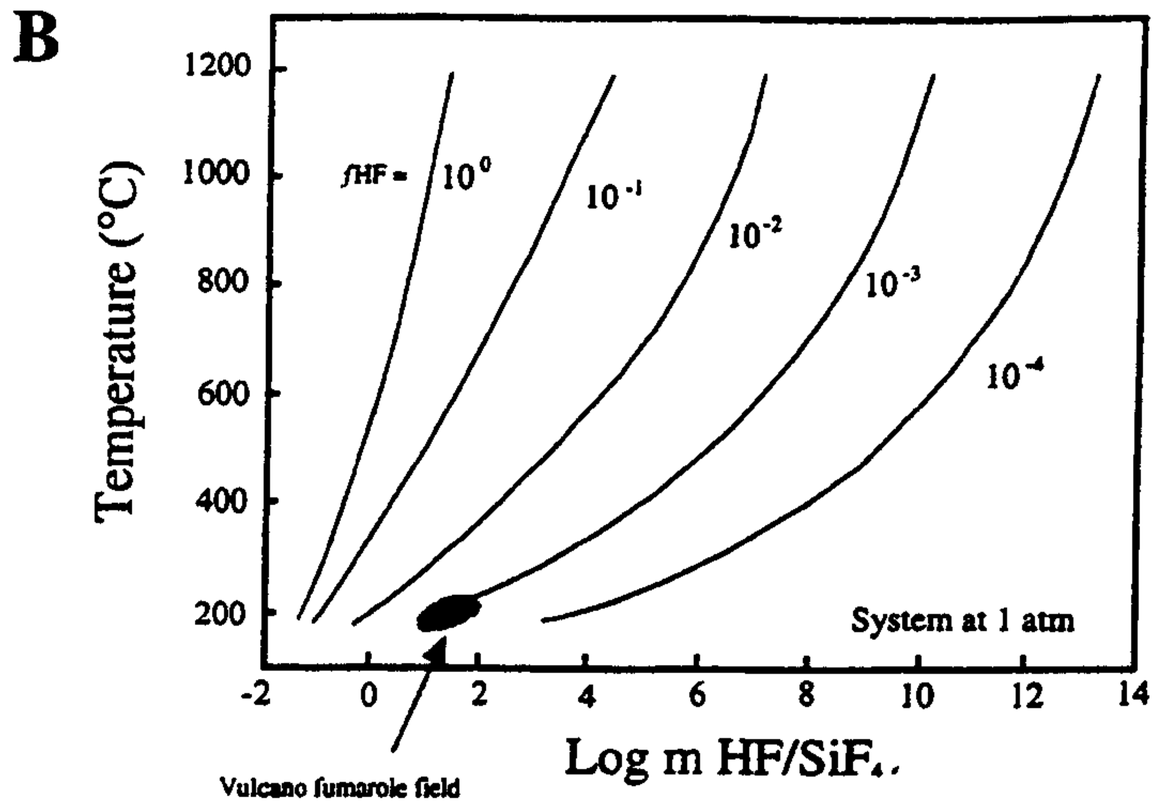

Figure 4.13. B. *I have used the Rosenberg (1973) model, which also describes the relationship between temperature; log molar HF:SiF_4 ratio and HF fugacity (ƒHF) at atmospheric pressure. I have shown the field occupied by the La Fossa fumarole emissions, as derived from OP-FTIR and conventional analyses (after: Rosenberg 1973; Symonds et al., 1988; Chiodini et al., 1995).*

Fumarole name	Measured temperature	Measured log ƒHF	Derived fumarole equilibrium temperature			1994 temperatures (Harris, pers. com.)
			log ƒHF = -2	log ƒHF = -3	log ƒHF = -4	*Area averages °C
F0	304	-3.4	300	**195**	130	260 ± 55
F1	243	-3.5	280	**180**	120	260 ± 55
F5	309	-3.4	295	**190**	130	171 ± 63
F5AT	406	-3.3	310	**200**	130	171 ± 63
F11	345	-3.1	320	**200**	135	171 ± 63
FA	488	-2.7	335	**210**	140	284 ± 105
Average	~336	~ -3.2	310	**200**	130	214 ± 88

Table 4.7. A *The measured temperatures of six fumaroles analysed by Chiodini et al. (1995) along with their HF fugacities (log ƒHF). Using HF:SiF_4 molar ratios derived from combined OP-FTIR analyses and the conventional analyses of Chiodini et al. (1995) I have estimated equilibrium temperatures for a range of log ƒHF of -2 to -4. The HF:SiF_4 molar ratios have been adjusted for the loss of HCl and HF, due to solution of the gases in the marine-hydrothermal reservoir. I have estimated this to be ~50%, based on the difference in SO_2:HCl ratio between rim and central crater fumaroles. *Area averages of Harris (unpublished data) represent the average temperature of fumaroles within the rim (171°C); rim fissure (260°C); central crater (284°C); and entire fumarole field (214°C) for October 1994.*

Sample date	Analysis type	Estimated molar $HF:SiF_4$ ratio	Estimated molar log *f*HF value	Equilibrium temperature in °C
27/9/94	Active	20.2	**-3.0**	~205
28/9/94	Active	12.0	**-3.0**	~195
29/9/94	Active	12.9	**-3.0**	~195
29/9/94	Passive	4.1	**-3.0**	~180

Table 4.7 B. *I have derived average equilibrium temperatures for the HF–SiF_4 system using an HCl:HF molar ratio of 0.107; from the data of Chiodini et al. (1995). The variation in HF:SiF_4 ratios are due to variations in measured HCl:SiF_4, using the OP-FTIR technique. The equilibrium temperatures are very similar to the average fumarole temperatures measured by Harris (unpublished data) and reported in* ***table 4.7A.*** *I have used the Rosenberg (1973) model and have calculated temperatures assuming a pressure of 1 atm. (Stevenson, 1993) and again a loss of HCl by solution of ~50%, see above.*

Discussion of results

My use of OP-FTIR-derived HCl data as a proxy for HF is a circuitous route to get to the final equilibrium temperatures, however, future use of OP-FTIR-derived HF data will greatly improve the reliability and versatility of this technique. **Tables 4.7A** and **4.7B** show the results of my application of the La Fossa OP-FTIR and Chiodini et al. (1995) data-sets to the Rosenberg (1973) HF–SiF_4 model, see **figure 4.13B**. A comparison of the temperatures measured by Chiodini et al. (1995) and the equilibrium temperatures in **table 4.7A**, shows there is a difference of ~100 - 300°C between the two techniques , assuming a log *f*FH value of -3. In contrast, the fumarole temperatures measured by Harris (unpublished data) in October 1994, soon after the OP-FTIR investigation, show very similar temperatures to the gas equilibrium temperatures I have derived. In comparing the different temperatures there are several factors which need to be discussed.

- The compositions and temperatures reported by Chiodini et al (1995) relate to specific fumaroles whereas the HCl:SiF_4 ratios used to determine the equilibrium temperatures relate to the average output of the whole fumarole field.

- The very low levels of SiF_4 produced from small volcanoes such as La Fossa, ~0.1 t/d, are close to the detection limits of the OP-FTIR technique used. The SiF_4 concentration decreases as the temperature of the magmatic system increases; therefore there will be a point at which it can no longer be detected. The low SiF_4 concentration signature of hot fumaroles will be hidden by the much higher SiF_4 concentration of the cool fumaroles. The hottest fumaroles would only emit levels of SiF_4 below the detection limit of the OP-FTIR instrument.

- The temperature measurements and gases analysed by Chiodini et al. (1995) were collected between October 1979 and February 1992, several years before the September 1994 OP-FTIR analyses of Francis et al. (1995) used in this thesis. During this period fumarole temperatures, measured at fumarole FA, steadily increased to a maximum in January 1993 before slowly decreasing (Capasso et al., 1996).

The very low levels of SiF_4 emitted from the hottest fumaroles on Vulcano, cannot be detected by OP-FTIR, preventing the determination of T_{eq} within a hot system. For lower temperature fumaroles the technique appears to work; the coolest fumaroles in **table 4.7A** exhibiting temperatures closer to those I have estimated. According to Rosenberg (1973), the $HF:SiF_4$ ratios of a fumarole at ~400°C are ~1×10^4 times greater than an equivalent fumarole at ~200°C. Hence one cool fumarole will drown out the SiF_4 signature from a large number of hot fumaroles. The technique of estimating K_{eq} using OP-FTIR may therefore be best used in determining the lowest - or base temperature of the system. In a monitoring role, SiF_4 telethermometry can be used for determining the fumarole field's base temperature. Any increase in this would relate to an overall increase in the temperature of the hydrothermal system, indicating the presence of hotter fluids migrating towards the surface.

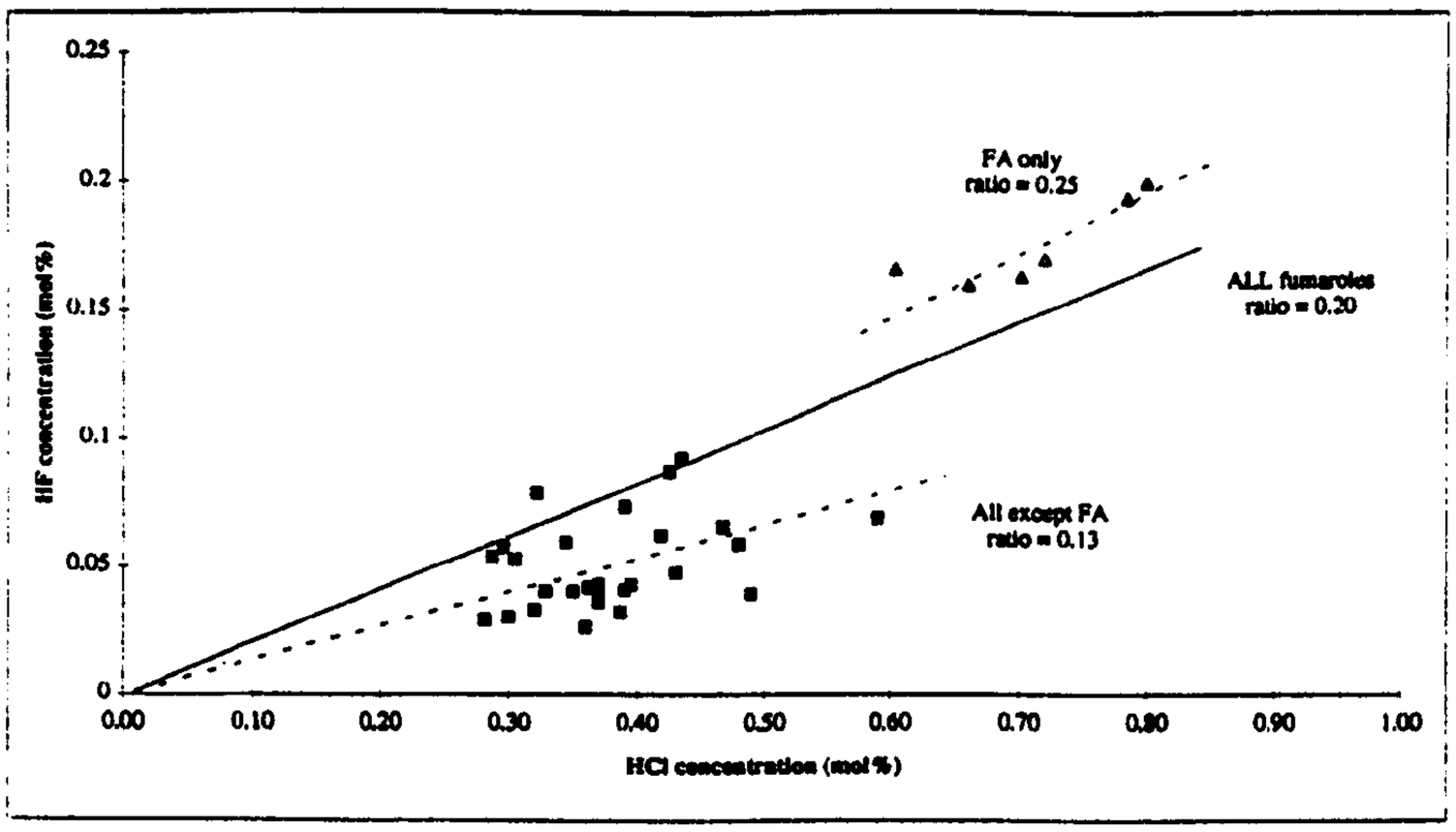

Figure 4.14. *Plot showing the relationship between HF and HCl used to allow HCl measured by OP-FTIR techniques to be used as a proxy for HF, (Chiodini et al., 1995).*

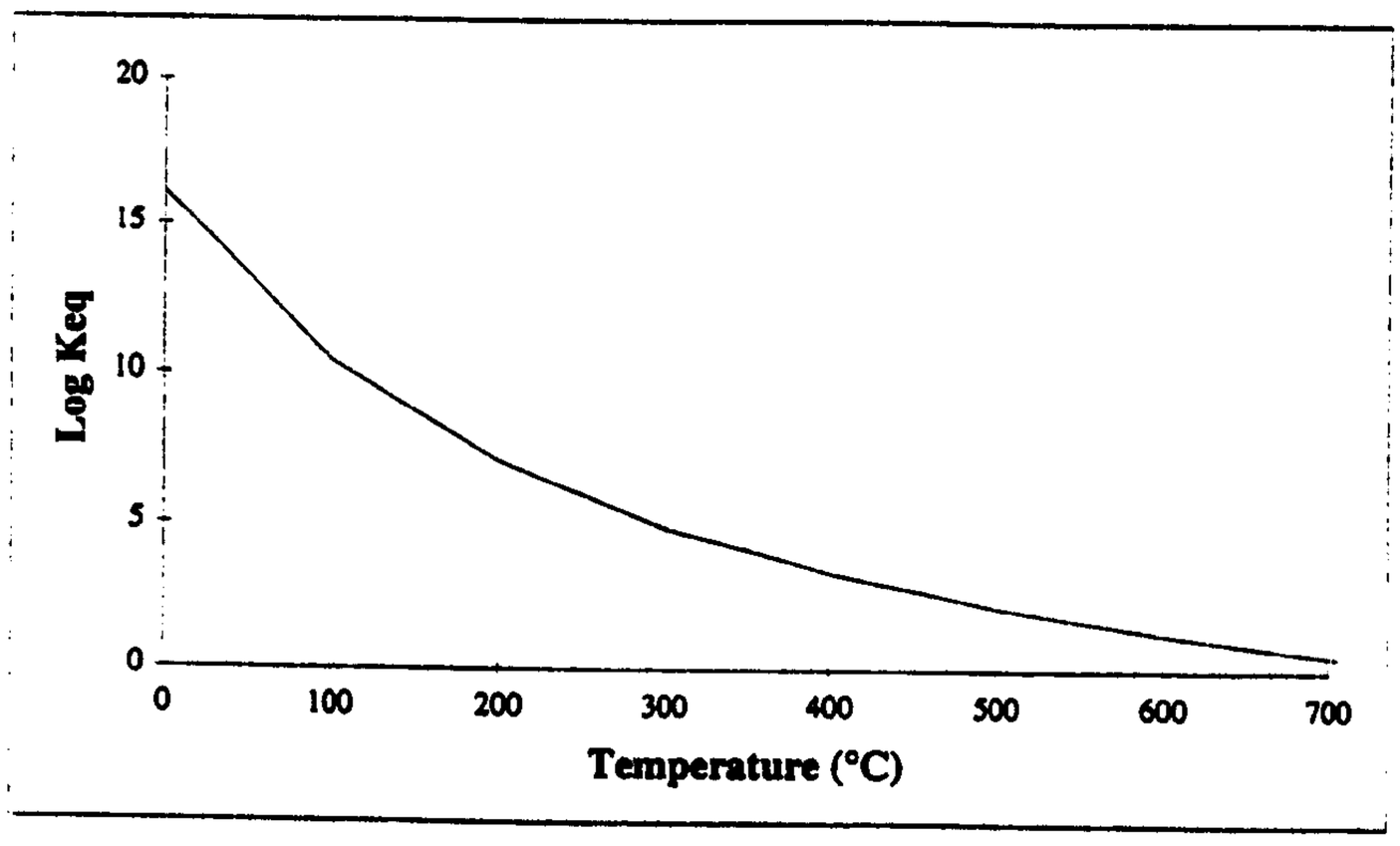

Figure 4.15. *Plot showing how K_{eq} for* ***equation 4.4*** *changes with temperature enabling it to be used to calculate T_{eq}, (after Honda & Mizutani, 1968).*

Comparison of SiF_4 derived by both models to measured temperatures

Francis et al. (1996) reported a range of T_{eq} between 200°C and 450°C; using a range of log *f*HF between -3.6 and -2.6. My method gave a much narrower, lower range for T_{eq}, ~180 - ~205°C, for log *f*HF = -3. This temperature is similar to that measured by Harris & Stevenson (1997) in October 1994 who reported a mean surface temperature of 214 ± 88°C for 504 fumaroles; with a maximum temperature measured of ~530°C. The differences between the two models are greatest at low temperatures, <400°C; which is the temperature range needed to produce sufficiently high levels of SiF_4 to be detected. At locations, such as

Mt. Etna, where gas fluxes are significantly higher, »1000 t/d, hotter temperatures may be determined using the HF–SiF_4 relationship, see Chapter 5.

4.2.6 The use of other gas equilibria-systems for thermometry

Other gas equilibrium systems have been used by Tedesco (1995) and Italiano & Nuccio (1994) to calculate equilibrium temperatures within fumarolic systems. These are outlined in **equations 4.5 - 4.8** below. These systems contain either H_2O, which totally absorbs the IR signal, or H_2, which is IR-inactive, and so cannot be measured using OP-FTIR techniques.

$$H_2S + 2H_2O \rightleftharpoons SO_2 + 3H_2 \qquad \text{(Tedesco et al., 1991)} \qquad \textbf{(4.5)}$$

$$CO_2 + H_2 \rightleftharpoons CO + H_2O \qquad \text{(Tedesco et al., 1991)} \qquad \textbf{(4.6)}$$

and also

$$2CO + O_2 \rightleftharpoons 2CO_2 \qquad \text{(Italiano \& Nuccio, 1994)} \qquad \textbf{(4.7)}$$

$$CH_4 + 2O_2 \rightleftharpoons CO_2 + 2H_2O \qquad \text{(Italiano \& Nuccio, 1994)} \qquad \textbf{(4.8)}$$

Tedesco (1995) used the sulphur–carbon systems in **equations 4.5** and **4.6** to derive equilibrium temperatures of ~315 - 440°C for the F5 fumarole at La Fossa during the period 1987 - 1988. Italiano & Nuccio (1994) used the carbon system outlined in **equations 4.7** and **4.8** to derive a range of T_{eq} for the Baia di Levante, mudpools and isthmus of ~183 - 222°C in 1990. The average fumarole temperatures which have been measured at La Fossa and in the Baia di Levante areas are ~200 - 300°C and ~100°C respectively, see **table 4.2**. The difference of ~20 - 80°C between T_{eq} and measured temperatures indicates that the hydrothermal fluids lose this much heat to the country rock between their last re-equilibration and being emitted at the surface (Carapezza et al., 1981; Tedesco et al., 1991).

The difference between equilibrium temperatures and emission temperatures has implications for determining the validity of the HF–SiF_4 system. If the HF–SiF_4 system equilibrates at depth, the higher temperatures recorded would be similar to those estimated by

Francis et al. (1996). If, however the system equilibrates close to the vents, T_{eq} may reflect actual emission temperatures, supporting the author's own model. Rosenberg (1973), based on experimental data, reported that at lower temperatures the system would be relatively insensitive to minor pressure changes; I estimated T_{eq} of ~250 - 300°C for depths of equilibration of ~4 km, ~1 kbar, the minimum estimated depth of the magma chamber (Tedesco et al., 1995). However, as there is nothing in the literature relating to the depth of final equilibration of the HF–SiF_4 system, I can only infer from the two models that the average T_{eq} is >180°C. This temperature must be a minimum as the coolest fumaroles, <150°C, will emit enough SiF_4 to obscure the much lower SiF_4 concentrations emitted from the hotter fumaroles.

4.2.7 Summary of OP-FTIR investigations

The author and Francis et al. (1995) used an experimental OP-FTIR to investigate the fumarolic emissions from La Fossa, Vulcano; with the aim of appraising the suitability of the technique to monitoring volcanic gases. This is a remote technique, thus enabling the analysis of gases at safe distances from potentially hazardous locations and facilitating the monitoring of volcanic activity through detecting changes in plume compositions.

The results from the trial have shown that SO_2:HCl mass ratios range between <2 and >7 over periods of a few hours to a day. I have ascribed this variation, not to changing magmatic processes, but rather to the optical path of the OP-FTIR being filled with different proportions of fumes from the crater rim and central fumarole fields. The highest SO_2:HCl ratios occurred when gases from the rim blew through the optical path, with the lowest ratios occurring over the longest path-lengths. I used histograms to analyse the frequency distribution of SO_2:HCl ratios in different data-sets to estimate the mass ratios of fumes emitted from the rim and central fumarole fields; these are ~4.3 - 6.1 and ~0.9 - 2.6 respectively. Gases emitted from the rim fumaroles have interacted with a cooler, marine-hydrothermal fluid reservoir and have lost HCl. By contrast, the hotter central fumaroles have reached the surface by a more direct route and thus are more likely to retain their original composition.

I have used the presence of SiF_4 to estimate gas equilibrium temperatures; using HCl as a proxy for HF. The concentration of SiF_4 is inversely proportional to the gas temperature. The hottest fumaroles emit very little SiF_4. These are swamped by the far higher concentrations of SiF_4 emitted from cooler fumaroles. Using SiF_4 to estimate equilibrium temperatures therefore only gives an average temperature for the coolest fumaroles – an approximate minimum temperature for the overall fumarole field. I have estimated an equilibrium temperature of ~180 - 205°C, similar to the average fumarole (i.e. gas emission) temperatures measured by Harris & Stevenson (1997).

4.3 The hydrothermal system at La Fossa, Vulcano

4.3.1 Introduction

The hydrothermal system at La Fossa, Vulcano, has so far only been discussed in the light of how it has affected the SO_2:HCl ratios in fumes emitted from the rim and central fumarole fields at La Fossa. The following section will provide a review of the system, based on results from earlier direct-sampling techniques by other authors, and elaborate on statements made in earlier sections. I will demonstrate that the hydrothermal system is composed of three separate components and show how they differ and govern the compositions of emitted fumes, and that pseudo-seasonal variations in level of ground-water can affect the interactions of these hydrothermal reservoirs.

Various models have been used to describe the hydrothermal system operating beneath the La Fossa and Vulcanello cones. These can be divided into two basic types, as described by Cioni & D'Amore (1984) below.

- Wet Model: - The fluids originate from a deep boiling aquifer, which may possibly by recharged by sea water. The fluids gradually rise up to the surface and absorb heat from the surrounding rocks as they pass through them. Any contributions to the deep boiling aquifer by rising magmatic fluids are buffered by overlying shallow aquifers of a mainly meteoric origin.

- Dry Model: - Fluids emitted from the fumaroles in the crater are composed of a mixture of deep and shallow fluids. The deeper fluids are a direct result of degassing from the magma chamber; these have then interacted with shallower fluids produced by the total evaporation of saline aquifers that have encroached on the hotter fluids rising from below. The mixing of fluids therefore always takes place above the boiling point of the aquifer at that depth.

Chiodini et al. (1995; and papers cited therein) have investigated the D and ^{18}O isotopic compositions of the La Fossa fumaroles. Their results support the "dry" model of

Cioni & D'Amore (1984). Here, the hydrothermal system has two components: a deeper central magmatic reservoir enveloped by a shallower one formed by the total evaporation of hydrothermal fluids of marine origin, see **figure 4.17**. The marine hydrothermal reservoir infringes on and is incorporated into the rising magmatic fluids (Chiodini et al., 1995). Panichi & Noto (1992 in Chiodini et al., 1995) interpreted the isotopic data as mixing of waters from an andesitic source with sea water that had been modified to reflect the $\delta^{18}O$ isotopic composition of the surrounding rocks with which it had (partially) equilibrated.

When data from fumaroles and mudpools on the Baia di Levante and Isthmus are included in D and ^{18}O isotopic studies, a third component becomes obvious, see **figure 4.17**. This is a shallow meteoric reservoir, which, although not directly interacting with the fluids emitted from La Fossa does have an effect on their compositions. This is discussed further below.

4.3.2 Description of the hydrothermal system

Chemistry

Tedesco et al. (1991) analysed the rim-fumarole "FA" (**figure 4.2**) frequently between July 1987 and December 1988. Their data show that CO_2, as well as the soluble acidic gases, HF, HCl and SO_2, vary inversely with the H_2O content. I have taken this to show that, as demonstrated with the OP-FTIR data, fumaroles which interact with non-magmatic reservoirs lose a proportion of their soluble gases by solution. The preferential solution of the more soluble HCl relative to that of SO_2 can be clearly seen in the Tedesco et al. (1991) 1987 - 1988 data-set for the crater-rim fumarole, "F5", see **figure 4.16**. Tedesco (1995) observed the same trend and explained it as addition of water vapour at a shallow level to the hydrothermal system thus diluting the magmatic SO_2 and H_2S already present. The positive correlations of SO_2 to N_2 and CO_2 when contrasted with the negative correlation of SO_2 to H_2O indicate that the water vapour is the only component with a dominantly shallow origin, the others having a deeper magmatic source (Tedesco, 1995).

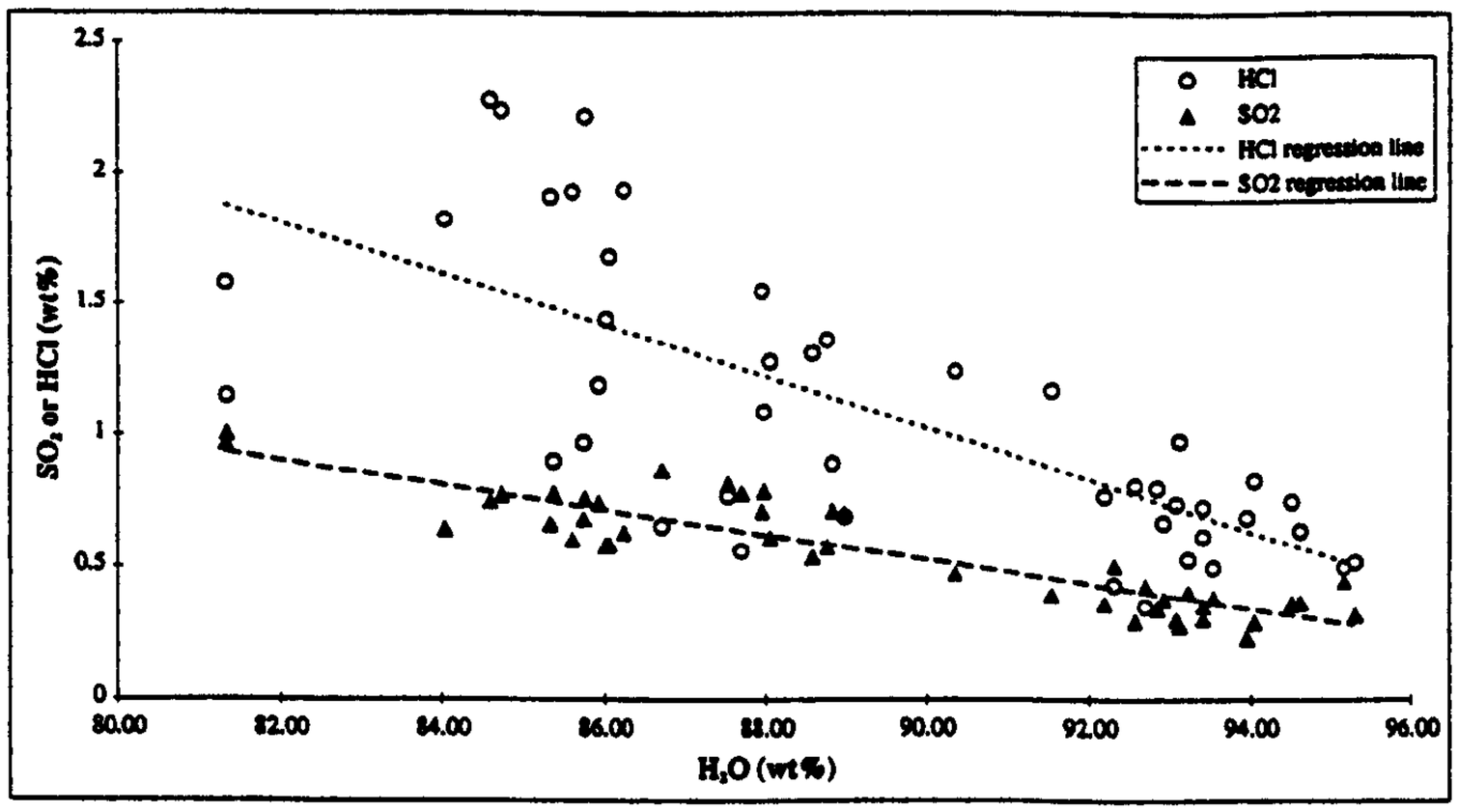

Figure 4.16. *This shows the relationship of SO_2 and HCl concentration against H_2O content for fumarolic emissions analysed by Tedesco et al. (1991) for the period July 1987 - December 1988. The greater loss of HCl at higher water contents is due to the preferential removal of the more soluble HCl in those fluids which have interacted with non-magmatic reservoirs.*

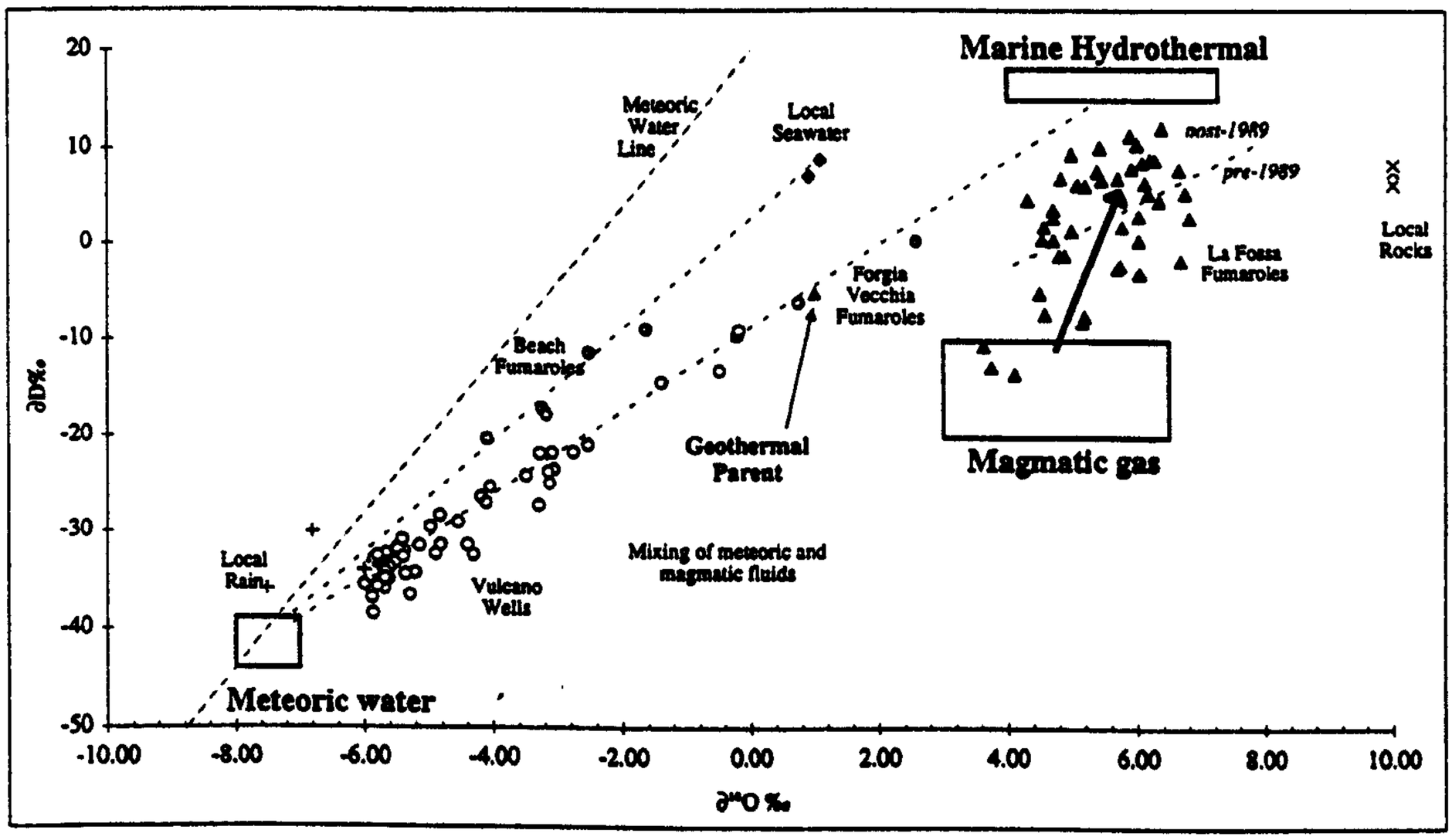

Figure 4.17. *Plot of δD against $\delta^{18}O$ for various components in the La Fossa hydrothermal system. The main body of the crater fumaroles can be seen to lie on a mixing line between magmatic and marine-hydrothermal fluids. The fumaroles located near the beach indicate that mixing also occurs between the sea water and meteoric water as well as between marine-hydrothermal and meteoric fluids (after: Ellam & Harmon, 1990; Capasso et al., 1992; Bolognesi et al., 1993; Chiodini et al., 1995). The large arrow shows the gradual trend from 1979 to 1991 of less and less magmatic fluids being incorporated into the emissions from the La Fossa fumaroles.*

D and ^{18}O isotopic analysis of the La Fossa hydrothermal system

Isotopic analysis of steam, geothermal aquifers and well waters have been carried out by several working groups (Chiodini et al., 1995; Bolognesi & D'Amore, 1993; Capasso et al., 1992) to try and constrain the characteristics of some of the various reservoirs found on Vulcano. I have summarised the results of these investigations in **figure 4.17** to highlight the mixing trends between the three reservoirs and to put the inferences drawn from my OP-FTIR investigations into context.

The D and ^{18}O analyses of Chiodini et al. (1995) have demonstrated the existence of three fluid reservoirs: magmatic, marine-hydrothermal and meteoric. The compositions of these are summarised in **table 4.8** along with other factors which have an effect on the isotopic composition of the hydrothermal system.

Fluid and rock	δD‰ values	$\delta^{18}O$‰ values
*Marine hydrothermal	+6 to +12	>+2 to +7
*Magmatic	-10 to -22	+3 to +6.5
*Meteoric	-40 to -42	-7 to -8
*Sea water	+10	+1
‡Rock	-	+6.3 to +8.4
#Geothermal water	-5	+1
§Rain water (averaged)	-33.3	-6.7

***Table 4.8**. Showing the isotopic composition of various fluids related to the hydrothermal system on Vulcano. *Chiodini et al. (1995), #Bolognesi & D'Amore (1993), §Capasso et al., (1992), ‡Ellam & Harmon (1990).*

Figure 4.17 indicates that mixing occurs between three chemically distinct fluid reservoirs. Carapezza et al. (1981) and Voltaggio et al. (1997) have suggested that the deposition of impermeable silica, calcite and anhydrite at the margins of the hydrothermal reservoirs inhibits mass mixing between them, thus allowing them to keep their own chemical identities. It is only after periods of enhanced local seismicity, leading to the formation of fresh fractures, that enhanced localised mixing between the aquifers occurs (Voltaggio et al., 1997; Bolognesi , 1996). Chiodini et al. (1995) reported that for the period 1979 - 1990, $\delta^{18}O$ values changed little; except in 1988 when there was a significant change which

coincided with a period of intense localised seismicity and an M2.5 earthquake beneath La Fossa (Bolognesi & D'Amore, 1993). Chiodini et al. (1995) suggested that the changes in $\delta^{18}O$ values were caused by degassing of a more volatile rich portion of the magma chamber accessed by fracturing in the seismic crises. Similarly, the increased temperatures after the 1978 Patti earthquake may be related the release of magmatic volatiles by the propagation of new fractures through impermeable areas.

Figure 4.17 shows the isotopic analyses for fumaroles, wells and ground waters from the areas around La Fossa. Several things are noticeable:

- The beach fumaroles, which are <100°C, show mixing between the meteoric reservoir and sea water with little input from either the marine-hydrothermal or magmatic reservoirs.
- The isotopic composition of the water wells at Vulcano all lie along the mixing line between the meteoric and marine-hydrothermal reservoirs. The fumaroles of the Forgia Vecchia lie along this line close to the hypothetical geothermal parent composition of Bolognesi & D'Amore (1993).
- The δD data of Chiodini et al. (1995) show a well defined mixing trend between a magmatic end-member and a marine hydrothermal end-member which has formed by water-rock isotopic exchange of sea water with the volcanic pile.

Chiodini et al. (1995) and Bolognesi & D'Amore (1993) have both reported a gradual change in the D and ^{18}O isotopic compositions at La Fossa. Prior to the M5.5 Patti Earthquake on 15/4/78, with its epicentre close to Vulcano, fumarole temperatures were relatively low, <250°C (Bolognesi & D'Amore, 1993). After the earthquake fumarole temperatures suddenly increased and have since remained fairly steady with occasional increases related to periods of seismic activity (Bolognesi & D'Amore, 1993). The D and ^{18}O isotopic compositions of fumarolic fluids collected in 1979 by Bolognesi & D'Amore (1993) and Chiodini et al. (1995) indicated that fluids were mainly of magmatic origin, with minor amounts of marine-hydrothermal and meteoric water. Since ~1980, the isotopic composition

of fumarole emissions has gradually changed, with the contribution from both the magmatic and meteoric reservoirs decreasing over time, see **figure 4.17**.

I have explained the decrease in the contribution of the meteoric fluids by the gradual heating up and boiling off of the local meteoric reservoir beneath La Fossa; based on the change in $\partial^{18}O$ and gradual increase in fumarole temperatures between ~1980 and 1993 (Chiodini et al., 1995). The increase in the marine-hydrothermal signature with time, based on the ∂D values of Chiodini et al. (1995), may possibly be due to the increased heat flux gradually establishing a convective hydrothermal cell beneath La Fossa; whilst at the same time gradually isolating the magmatic reservoir by deposition of silica, calcite and sulphate.

Summary review of the hydrothermal system at La Fossa di Vulcano

The above review has shown that the hydrothermal system is composed of three isotopically distinct reservoirs. These are: a shallow meteoric reservoir, and deeper marine-hydrothermal and magmatic reservoirs. Carapezza et al. (1981) and Voltaggio et al. (1997) have both suggested that impermeable precipitations of silicate, calcite and sulphate effectively prevent mass mixing of the reservoirs, thus enabling them to keep their own characteristic isotopic identity. However, mixing does occur in a major permeable zone that runs between La Fossa and Vulcanello (Tedesco et al, 1995); giving rise to the fumarolic activity observed. Sudden changes in fumarole temperature, gas chemistry and isotopic composition have been noted by Bolognesi & D'Amore (1993) and Chiodini et al. (1995) to correlate with increased periods of seismicity. The changes have been attributed to the formation of new fractures allowing the mixing of fluids from different reservoirs, thus changing the composition of the fumes emitted from La Fossa. More regular changes have also been noted by Tedesco (1995) and Martini (1981), see below.

4.3.3 Temporal variations in the degassing on Vulcano

Analyses of the fumarolic emissions have been carried out at La Fossa by many different authors on many different dates. It is essential to establish if there are temporal or

of fumarole emissions has gradually changed, with the contribution from both the magmatic and meteoric reservoirs decreasing over time, see **figure 4.17**.

I have explained the decrease in the contribution of the meteoric fluids by the gradual heating up and boiling off of the local meteoric reservoir beneath La Fossa; based on the change in $\partial^{18}O$ and gradual increase in fumarole temperatures between ~1980 and 1993 (Chiodini et al., 1995). The increase in the marine-hydrothermal signature with time, based on the ∂D values of Chiodini et al. (1995), may possibly be due to the increased heat flux gradually establishing a convective hydrothermal cell beneath La Fossa; whilst at the same time gradually isolating the magmatic reservoir by deposition of silica, calcite and sulphate.

Summary review of the hydrothermal system at La Fossa di Vulcano

The above review has shown that the hydrothermal system is composed of three isotopically distinct reservoirs. These are: a shallow meteoric reservoir, and deeper marine-hydrothermal and magmatic reservoirs. Carapezza et al. (1981) and Voltaggio et al. (1997) have both suggested that impermeable precipitations of silicate, calcite and sulphate effectively prevent mass mixing of the reservoirs, thus enabling them to keep their own characteristic isotopic identity. However, mixing does occur in a major permeable zone that runs between La Fossa and Vulcanello (Tedesco et al, 1995); giving rise to the fumarolic activity observed. Sudden changes in fumarole temperature, gas chemistry and isotopic composition have been noted by Bolognesi & D'Amore (1993) and Chiodini et al. (1995) to correlate with increased periods of seismicity. The changes have been attributed to the formation of new fractures allowing the mixing of fluids from different reservoirs, thus changing the composition of the fumes emitted from La Fossa. More regular changes have also been noted by Tedesco (1995) and Martini (1981), see below.

4.3.3 Temporal variations in the degassing on Vulcano

Analyses of the fumarolic emissions have been carried out at La Fossa by many different authors on many different dates. It is essential to establish if there are temporal or

seasonal variations in fumarole compositions before comparing data collected at different times of the year. Only once this variation is quantified can compositional changes related to magmatic degassing be identified. This section will review the existence of such temporal variations.

Data collected since the late 1970s by Martini et al. (1981); Capasso et al. (1992); Chiodini et al. (1995) and Tedesco, (1995) have all indicated that the fluid compositions observed in fumaroles, beach fluids and well waters undergo a systematic variation - "pseudo-seasonal" as described by Capasso (1992). Tedesco (1995) noted that fumarolic emission data could be divided into two groups: gases that follow the variations in H_2O such as H_2 and H_2S; and those that show an inverse variation, such as CO_2, SO_2, N_2, HCl and the S/C ratio, see **figure 4.18**. The main component in the emissions is H_2O, which ranges in proportion from <83 to >96%. Tedesco (1995) observed that fumarolic H_2O concentration reaches a maximum in about April and a minimum in October-November. Variations in fumarolic components, illustrating the pseudo-seasonal variation can be seen in **figure 4.18**.

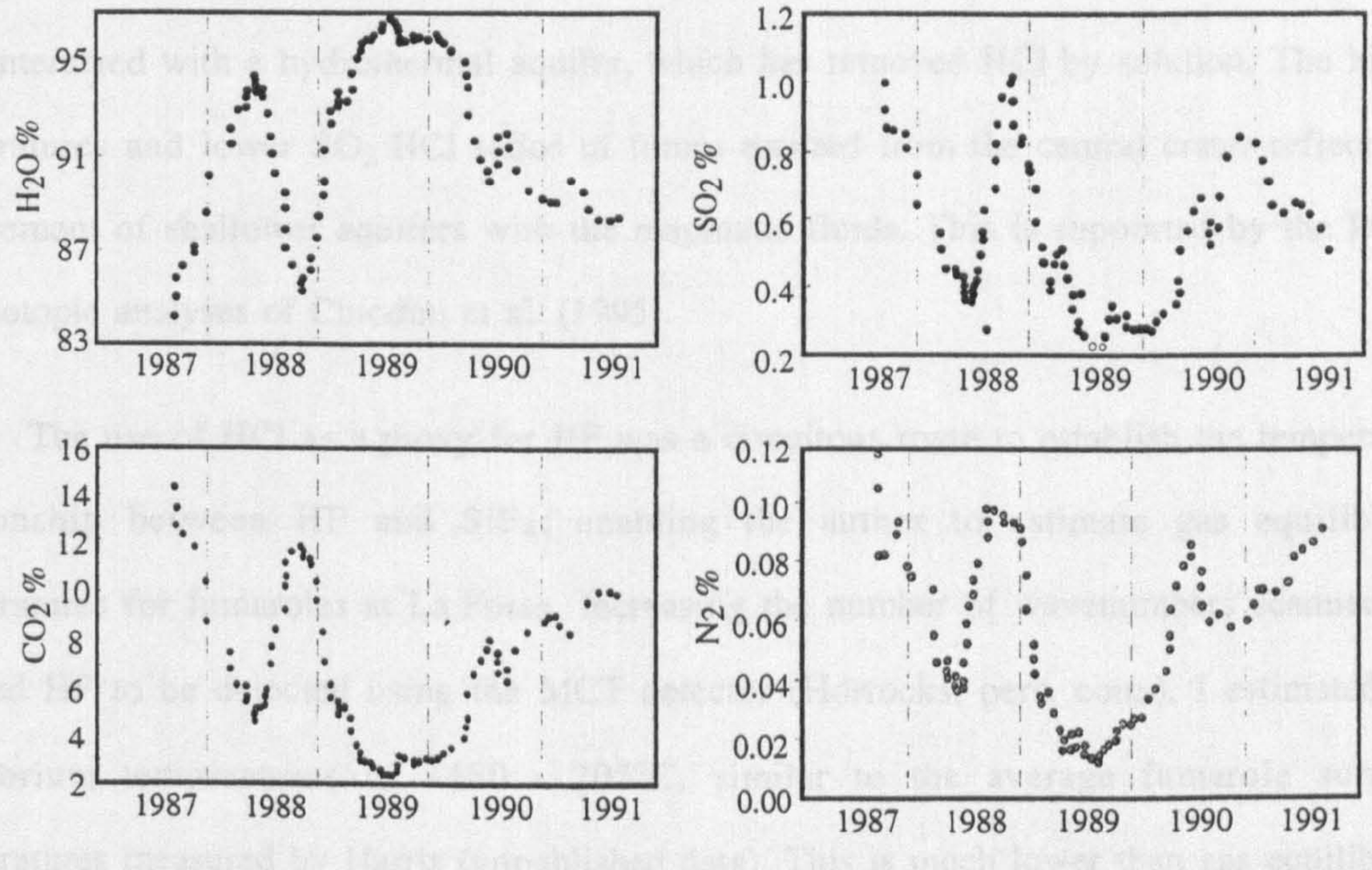

***Figure 4.18**. Plots showing the temporal variations of various gases from the "F5" fumarole in La Fossa for the period 1987 - 1991: H_2O, CO_2, SO_2, and N_2, (after Tedesco, 1995). Note that the variation in CO_2, SO_2 and N_2 is opposite to that of H_2O. Tedesco (1995) has inferred this to indicate that H_2O originates from a predominantly shallow source, the other components rising up from deeper sources.*

This variation has been assigned to seasonal differences in rainfall (0 - 150 mm in summer and 300 - 500 mm in winter) by Martini (1983) and Tedesco (1995). Capasso et al. (1992) stated that it was more likely to be the increased demand on well waters in the summer months that influenced fumarole compositions than the amount of rainfall. Whatever the cause, pseudo-seasonal variations in the chemical (Martini, 1983; Tedesco, 1995) and isotopic (Capasso et al., 1992) compositions of fumarolic gases are evident. This will prevent different data sets being closely compared; which may only be possible with modification of the data-sets to allow for any variation. However, this can only really be done when a full understanding of what causes the variations has been developed.

4.4 Conclusions

I have divided the conclusions for this chapter into two sections. The first summarises the scientific implications of the OP-FTIR results and conclusions drawn from the conventional analyses of others. The second summarises the technical implications of the OP-FTIR technique, and its use on volcanoes.

4.4.1 Scientific implications

The OP-FTIR analyses of fumarolic gases by the author and Francis et al. (1995, 1996) have supported conclusions drawn from isotopic analyses, suggesting mixing of different fluid reservoirs beneath La Fossa governs the compositions of emitted gases. Our data has shown that the SO_2:HCl mass ratios of the fumes emitted from the central and rim fumarole fields are different, ~0.9 - 2.6 and ~4.3 - 6.1 respectively. I have inferred from the higher SO_2:HCl ratios, and lower emission temperatures, of the rim fumaroles that these fluids have interacted with a hydrothermal aquifer, which has removed HCl by solution. The higher temperatures and lower SO_2:HCl ratios of fumes emitted from the central crater reflect less involvement of shallower aquifers with the magmatic fluids. This is supported by the D and ^{18}O isotopic analyses of Chiodini et al. (1995).

The use of HCl as a proxy for HF was a circuitous route to establish the temperature relationship between HF and SiF_4; enabling the author to estimate gas equilibrium temperatures for fumaroles at La Fossa. Increasing the number of wavenumbers scanned has enabled HF to be detected using the MCT detector (Horrocks, pers. com.). I estimated gas equilibrium temperatures of ~180 - 205°C, similar to the average fumarole surface-temperatures measured by Harris (unpublished data). This is much lower than gas equilibrium temperatures estimated by Tedesco (1995) for sulphur and carbon equilibrium systems, ~315 - 440°C. This is due to the HF–SiF_4 system being biased towards the detection of the cooler fumaroles.

The OP-FTIR technique has enabled a very large data-set to be collected in a short period of time. Our data has not only supplemented and complemented conventional investigations, but enabled Francis et al. (1996) to devise a new method for telethermometry using the ratios of emitted fumarolic gases. The combination of the various techniques has enabled the author to draw these main conclusions together for the hydrothermal system at La Fossa di Vulcano:

- Fumarolic compositions are strongly dependant on the fumarole sampled. Fluid flow outside the central crater facilitates mixing of deeper magmatic fluids with shallower aquifers of either a meteoric or altered marine component; causing soluble acid gases to remain in the reservoirs, rather than be emitted. I have inferred that SO_2:HCl mass ratios of ~0.9 - 2.3 relate to the central crater fumarole field; whilst ratios of ~4.3 - 6.1 relate to the rim fumarole field.

- The compositions of the fumaroles have varied in time demonstrating "pseudo-seasonal" cycles and, over a longer period, the progressive reduction of amounts of magmatic fluids reaching the surface. Thus the time of gas sampling can have a profound effect on the composition of analysed fluids; as is evident in the differences between the OP-FTIR data of Mori et al. (1995) and Francis et al. (1995), measured in April 1993 and September 1994 respectively. The use of a natural IR source by Mori et al. (1995) and problems associated with accurate quantification of HCl also contributed to the high gas ratios they reported.

- Three distinct fluid reservoirs have been identified using D and ^{18}O isotopes. These are: a magmatic reservoir; a marine-hydrothermal reservoir; and a meteoric reservoir. The precipitation of impermeable calcite, silica and anhydrite effectively partitions the reservoirs, thus retaining their chemical identities. During periods of increased seismicity new fractures facilitate reservoir mixing; as expressed in sudden changes of fumarole chemistry and isotopic composition. The mixing of the three fluid reservoirs as discussed

above takes place continuously to provide the fumarole compositions reported. This is inferred to occur along a fracture zone running north-south between La Fossa and Vulcanello and probably relates to the regional Aeolian-Tindari-Letojanni fault system that passes beneath Vulcano.

- The HF–SiF_4 system can be used to estimate equilibria temperatures, rather than just the emission temperatures of fumarolic gases. This can therefore be used to monitor the level of subsurface volcanic activity. There is a wide distribution of vent temperatures at La Fossa due to gases interacting with shallow aquifers in a complex way. Cooler fumaroles emit far higher SiF_4 concentrations than hot fumaroles; effectively drowning out the hot fumarole signature, which is expected to be close to the detection limits of the OP-FTIR system. Only an average equilibrium temperature for the cooler fumaroles can be recorded. Any change in the equilibrium temperatures of the cool fumaroles will therefore relate to a significant change in the temperature of the overall fumarole system.

4.4.2 Technique aspects

OP-FTIR is an experimental technique for using IR spectrometry to analyse volcanic gases in the field; and as such, Francis et al. (1996) had to develop the technique on an almost location-by-location basis. This chapter has reported the initial success of the technique and discussed the systems limitations. OP-FTIR investigations of the gases emitted from La Fossa were carried out using both active (artificial) and passive (natural) IR sources. We found that the use of sun-heated ground and warm fumarolic ground did not emit a sufficient intensity of IR radiation for analysis of lighter gases, such as HCl and HF; only using the hottest, ~500 - 540°C, fumaroles was HCl detected. The 1275°C artificial IR source, however, enabled high quality data to be collected at path lengths of up to 1875 m. The use of SiF_4 and HCl enabled gas equilibrium temperatures to be estimated for the HF–SiF_4 system. The re-adjustment of the spectrometer, enabling a greater number of wavenumbers to be scanned, can now allow HF

and SiF_4 to be measured simultaneously, thus avoiding the use of HCl as a proxy for HF. Observations on the use of the OP-FTIR technique may be summarised as follows:

- The best data with the highest signal-to-noise ratios were generated using the 1275°C artificial IR source. Sun-heated ash and cooler fumarolic ground were too cold to emit the high frequency IR radiation required to analyse gases such as HCl and HF. The only passive measurements that proved to be useful for determining SO_2:HCl ratios were obtained using the hottest fumaroles in the central fumarole field.

- OP-FTIR analyses require the IR source to be located within line-of-sight of the spectrometer. On Vulcano, this was done by positioning the portable IR source on the rim of the crater for active analyses; for conducting passive analyses the spectrometer was positioned at the summit to look down onto the hottest fumaroles. This would not be possible during periods of volcanic crisis and so a solar source would have to be utilised. OP-FTIR investigations by Love et al. (1998) and the Cambridge and Open University working group have both successfully analysed plume gases using a solar source.

- The use of airborne OP-FTIR has yet to be perfected. A hot natural IR source must be targeted from a stationary (hovering) aircraft. This requires the full understanding of the aircrew and the correct volcanic and atmospheric conditions. The technique may be possible using a large IR source, such as a lava lake; but probably will remain of little use.

Chapter 5.

The use of OP-FTIR and COSPEC in determining the relationship between gas and magma fluxes at Mt. Etna, Italy

5.1 Introduction

5.1.1 Layout of chapter

This chapter will discuss the use of COSPEC to monitor the 1991 - 1993 eruption of Mt. Etna and the later experimental use of an Open-path FTIR system to investigate gas emissions from the Bocca Nuova and NE Crater. The chapter will also discuss how gas emissions relate to eruptive activity and the state of the shallow magmatic plumbing system beneath the summit of Mt. Etna. The chapter is divided into four main sections:

5.1 A review of the volcanic activity and previous techniques used for investigating gas emissions at Mt. Etna.

5.2 An investigation into the relationship between lava effusion and gas emission and how these relate to the levels and styles of magmatic degassing. I use the 1991 - 1993 eruption as a case-study to illustrate how gas emissions can be used to elucidate volcanic plumbing and magma migration.

5.3 Methodology, results and discussion of OP-FTIR investigations carried out at Mt. Etna by Francis et al. (1995). The use of SiF_4 in estimating gas equilibrium temperatures will be discussed; as will the fluxes of various gas species, determined by simultaneous COSPEC and OP-FTIR analyses.

5.4 Conclusions to the chapter relating to the scientific and technical implications of gas analysis at Mt. Etna. These can be summarised as:

- The use of natural IR sources for passive OP-FTIR analyses is entirely dependant on their temperature. If the IR source is too cool it will not radiate enough high frequency radiation to enable lighter gases, such as HCl and HF, to be detected. OP-FTIR analyses of soluble gases cannot be performed during periods of heavy cloud or rain as these analytes are rapidly scavenged from the plume.

- Inclusion data, filter analyses and our OP-FTIR analyses all support the two-stage degassing model of Pennisi & Le Cloarec (1998); which suggests that chlorine is principally exsolved at >4 km during deep degassing, whilst SO_2 is exsolved much closer to the surface during shallow degassing. The non-eruptive/background gas flux is provided by deep degassing with shallow degassing occurring during eruptive periods.

- Average OP-FTIR-derived SO_2:HCl mass ratios are ~4.9 - 5.8 at the NE Crater. Heavy cloud may have removed ~50% of the HCl from the Bocca Nuova's plume giving a higher ratio of ~7.4; an estimated original gas ratio being ~3.5. The lower ratio at the Bocca Nuova is consistent with gases being primarily sourced from deep degassing.

- The use of the SiF_4–HF system for telethermometry gave an estimated equilibrium temperature of ~290°C at both the Bocca Nuova and NE Crater. This is higher than vent temperatures recorded by radiometer indicating that the gas equilibrium is set before the gas has been emitted, but still lower than expected for open vent degassing.

5.1.2 Introduction to Mt. Etna volcano

General geology

Mt Etna is a large, 3340 m high, stratovolcano situated on the eastern coast of Sicily. It has been active for over 300 ka, during which at least 10 eruptive phases have occurred; each sited in a different locality forming the present edifice (Chester et al., 1985). During the last

200 ka Mt. Etna has almost exclusively erupted alkali basalts of a hawaiite - mugearite composition, termed etnaites (Chester et al., 1985). Condomines et al. (1995) reported that true basalts are absent from the historical record, the most basic eruptive products being potassic trachybasalts erupted after 1970. Several of the older eruptive centres outcrop in the walls of the Valle del Bove, a 5 km wide horse-shoe shaped multiple-collapse scar high on the eastern flank of the volcano (Calvari & Groppelli, 1996). Calvari & Groppelli (1996) inferred this had formed by a series of collapses between ~80 ka and ~15 ka ago. The debris from the collapses has been largely reworked, forming the ~12 km^3 Chiancone deposit which outcrops on the coast to the east of Mt. Etna, see **figure 5.1** (Calvari & Groppelli, 1996).

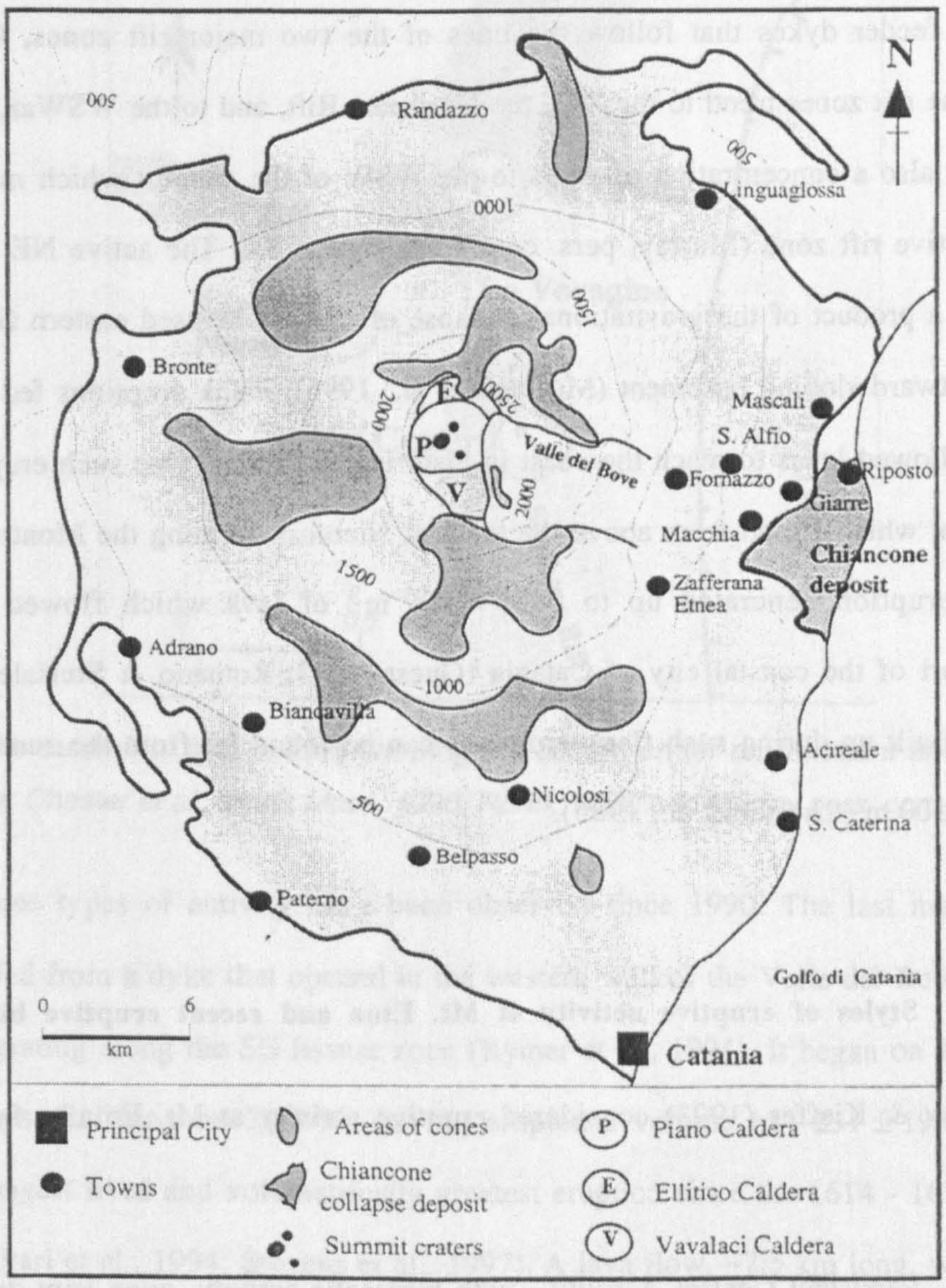

***Figure 5.1**. Schematic map of Mt. Etna, Sicily. The horse-shoe shape of the Valle del Bove collapse structure is clearly visible on the eastern flank; the deposits of which form the Chiancone outcropping along the coast. The older infilled calderas relating to the Ellittico and Piano collapses are also shown (after Calvari & Groppelli, 1994; Chester et al., 1985).*

Mt. Etna's craters and rift zones

The present summit of Mt. Etna consists of a ~400 m high cone situated in the middle of a wide platform, the infilled Cratere del Piano caldera, lying at an altitude of 2940 m a.s.l (Guest, 1973). The four craters currently active at the summit of Mt. Etna have all formed since 1911 (Chester et al., 1985). These are: the eccentric NE Crater; La Voragine or "The Chasm"; The Bocca Nuova and the SE Crater, see **figure 5.2**.

Lava effusions from Mt. Etna are not confined solely to the summit area. Many have issued from feeder dykes that follow the lines of the two major rift zones, forming flank eruptions. The rift zones trend to the: NE, the Northeast Rift, and to the WSWaz, the Southern rift. There is also a concentration of vents to the WSW of the summit which may relate to a third, less active rift zone (Murray, pers. com.), see **figure 5.2**. The active NE and Southern rifts and are a product of the gravitational collapse of the unbutressed eastern flank aided by the steep eastward sloping basement (McGuire et al., 1996). Flank eruptions fed from the rift zones have allowed lavas to reach the coast in historical eruptions. One such eruption was the 1669 eruption, which issued from above the town of Nicolosi, forming the Monte Rossi scoria cones. The eruption generated up to ~936×10^6 m^3 of lava which flowed southwards, destroying part of the coastal city of Catania (Guest, 1973; Romano & Sturiale, 1982). The scoria cones built up during such flank eruptions can be found far from the summit, down to altitudes of <500 m (Chester et al., 1985).

Styles of eruptive activity at Mt. Etna and recent eruptive history

Tanguy & Kieffer (1993) considered eruptive activity at Mt. Etna to fall into three distinct types:

- Persistent Central Activity - with fumarolic activity, open vent degassing and minor strombolian explosions associated with the formation of small ash clouds.

- Central Paroxysmal Activity - with large strombolian explosions and lava fountains. Pyroclastic material may be ejected to heights of >1000 m with material being scattered over a wide area. Lava flows may also issue from the summit and extend for several kilometres.
- Flank fissure-eruptions - which follow the lines of the three fissure zones can bring erupted lava close to built-up areas. Opening of eruptive fissures tends to be preceded by intense seismicity and increased activity at the summit craters.

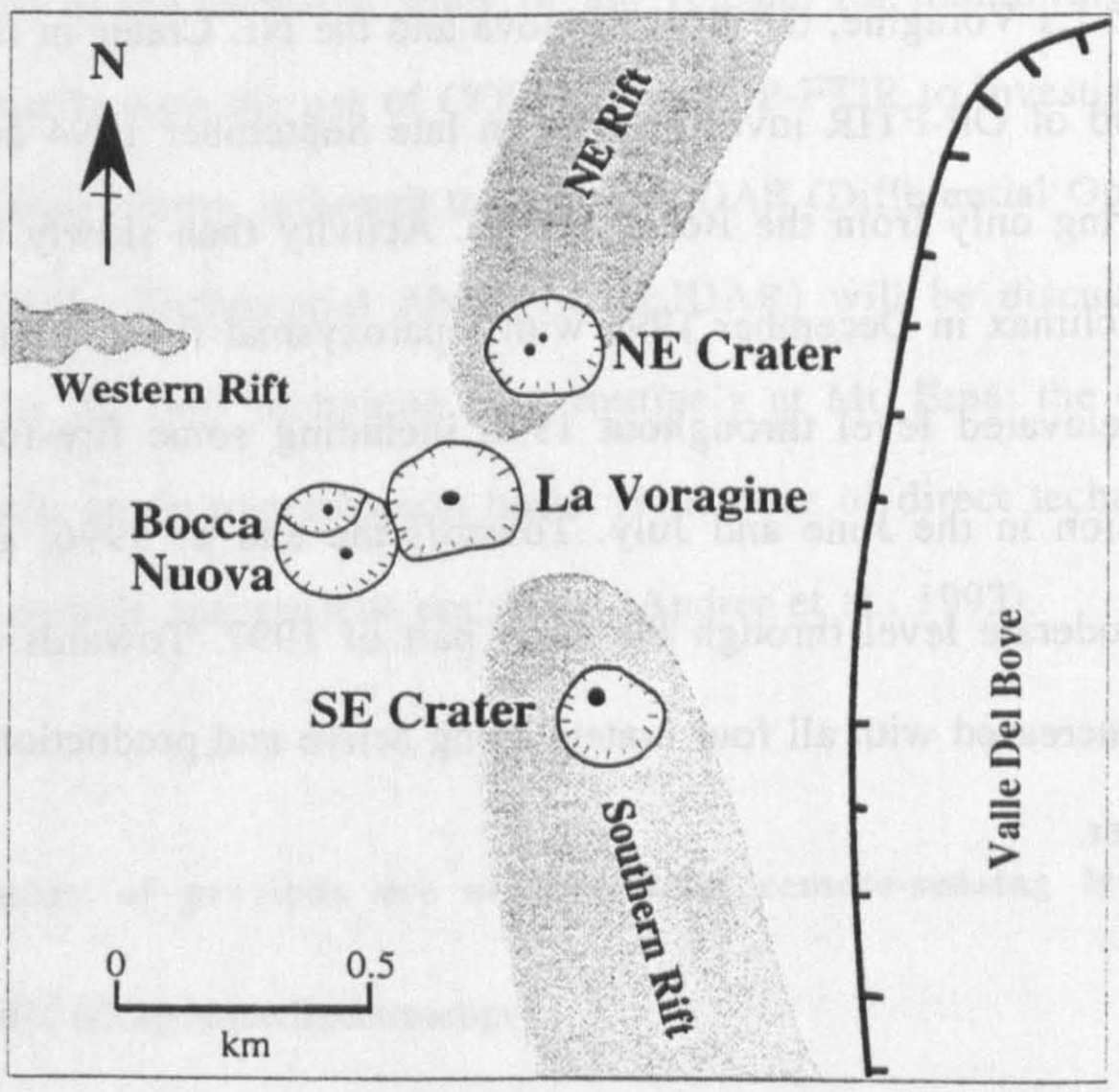

***Figure 5.2**. The summit of Mount Etna showing the current crater environment and associated rift zones (after: Chester et al., 1985; Moss, 1996; Röllin, 1996; and Murray pers. com.).*

All three types of activity have been observed since 1990. The last major effusive eruption was fed from a dyke that opened in the western wall of the Valle del Bove as a result of magma migrating along the SE fissure zone (Rymer et al., 1994). It began on 14/12/91 and lasted 473 days, finishing on 29/3/93, having erupted a volume of ~231 ± 19 × 10^6 m^3 to become the longest lived and volumetrically greatest eruption since the 1614 - 1624 and 1669 eruptions (Calvari et al., 1994; Stevens et al., 1997). A lava flow, ~7.5 km long, was produced which destroyed several houses and threatened the town of Zafferana; only by the redirecting of the lava flow into the upper parts of the Valle del Bove was the town saved (Barberi &

Villari, 1994, Harris et al., 1997). After the eruption ceased little activity was observed at the summit, mainly passive degassing and occasional explosions.

Eruptive activity since the 1991 - 1993 eruption

The gradual re-activation of the volcano after the 1991 - 1993 eruption is well documented elsewhere (GVN Bulletins 1994 - 1997) and so has only been briefly summarised in this section. There was very little activity during the first half of 1994 with small explosions being heard from La Voragine, the Bocca Nuova and the NE Crater in the later half of 1994. During the period of OP-FTIR investigations in late September 1994 activity was low with degassing occurring only from the Bocca Nuova. Activity then slowly increased throughout 1995 reaching a climax in December 1995 with a paroxysmal fire-fountaining event. Activity remained at àn elevated level throughout 1996 including some fire-fountaining and some minor lava effusion in the June and July. Towards the end of 1996, activity lessened and remained at a moderate level through the early part of 1997. Towards the end of 1997 the level of activity increased with all four craters being active and production of small lava flows from the SE Crater.

Gas output

Mt. Etna is one of the largest producers of volcanic SO_2 and CO_2 (Gerlach, 1991; Allard et al., 1991; Maciejewski et al., 1996). Allard et al. (1991) estimated its average annual SO_2 production as $\sim 1.8 \times 10^6$ t/y; which approaches ~10% of the global volcanic output and ~1% of the anthropogenic output. They also estimated a CO_2 flux of $\sim 30 \times 10^6$ t/y from combined crater and diffuse soil emissions. I have estimated an annual HCl emission rate from Mt. Etna of $\sim 0.4 \times 10^6$ t/y, using average COSPEC and OP-FTIR data, see Section 5.3. This is equivalent to ~21% of global anthropogenic chlorine emissions and is similar to the ~27% estimated by Andres et al. (1993) for all chlorine species. The prodigious gas production of Mt. Etna coupled with its almost constant state of activity at the central craters and its accessibility make the volcano an ideal natural laboratory for the testing of new techniques,

with a view to using them for future monitoring at Mt. Etna and other volcanoes. Hence Francis et al. (1995) chose Mt. Etna as the site for their experimental OP-FTIR investigations of volcanic gases.

5.1.3 Previous investigations of gas emissions at Mt. Etna

The proximity of the city of Catania and towns such as Belpasso, Nicolosi, Randazzo and Zafferana (see **figure 5.1**) to an active volcano which has undergone numerous, historic, flank eruptions has led to the intensive study of the volcano for monitoring purposes. This chapter will deal primarily with the use of COSPEC and OP-FTIR to investigate the flux and composition of Mt. Etna's plume, although the use of DOAS (Differential Optical Absorption Spectroscopy) and DIAL (Differential Absorption LIDAR) will be discussed briefly, see Chapter 2. COSPEC is the only technique used routinely at Mt. Etna; the other techniques being used infrequently on an experimental basis. A number of direct techniques have also been used to analyse particle and gaseous emissions (Andres et al., 1993).

Summary of previous use of terrestrial remote-sensing techniques

COSPEC (Correlation Spectroscopy)

The COSPEC system utilises the absorption of solar-UV radiation by SO_2 to determine the amount of gas in a column of air or across a traverse of the plume. By combining this value with an estimate for wind speed, the amount of SO_2 emitted from a volcano can be derived. Although the instrument can only analyse one volcanic gas, SO_2, and analytical errors can range between <15 and >40%, the system provides a quick and convenient method to make quantitative estimates of the volcanic SO_2 output, see Section 2.3. It is the most portable and cheapest of the readily accessible terrestrial remote-sensing techniques and thus has been used on many volcanoes worldwide. This, combined with its ease of use and ruggedness make it extremely suitable for volcanological applications.

Haulet et al. (1977) first used COSPEC on Etna in 1975 and recorded a gas flux of 3740 t/d. Since then COSPEC has been used to estimate the total SO_2 flux and its variation

over time, see **figure 5.3**. Regular investigations by Malinconico (1987), Caltabiano et al. (1994) and others have shown that the gas emissions can be correlated with the level of eruptive activity; making it a useful monitoring technique. Bruno et al. (1994) used COSPEC extensively during the 1991 - 1993 eruption to built up a detailed picture of the changes in SO_2 flux during the eruption. I will discuss the observations and the conclusions drawn from these measurements in Section 5.2.

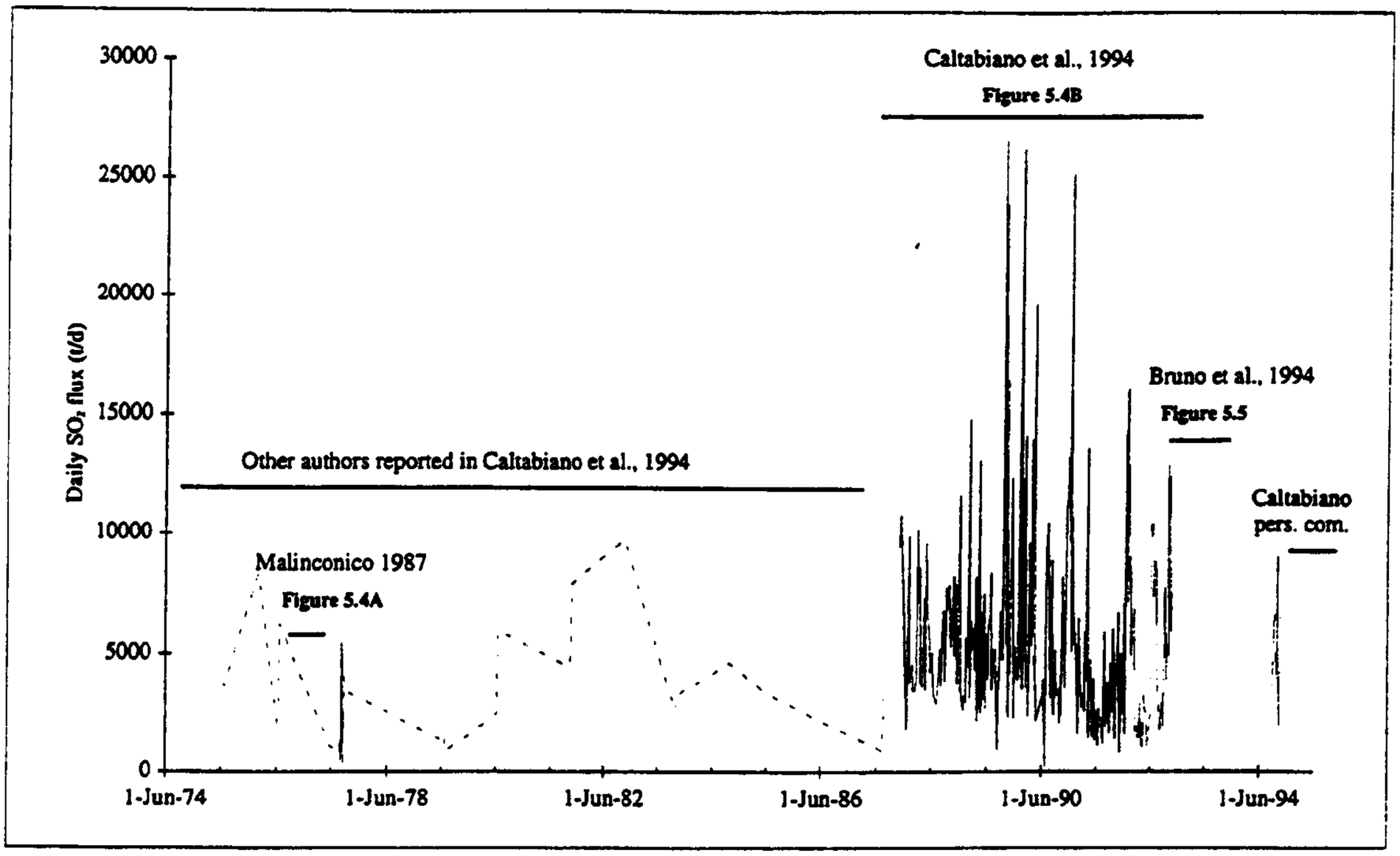

***Figure 5.3**. Summary of COSPEC results collected after 1975 (after Bruno et al., 1994; Caltabiano et al., 1994; Malinconico, 1987; Caltabiano pers. com., Andres et al., 1993). The highlighted portions of this figure are enlarged in later figures.*

DIAL (Differential Absorption LIDAR)

Edner et al. (1994) used DIAL for the first time on Mt. Etna on 5/9/92. The technique used two pulsed UV lasers to provide range-resolved concentration data; enabling 2-dimensional concentration profiles to be constructed through the plume, see Section 2.4. DIAL, although highly sensitive, is only capable of analysing one compound at a time and is an extremely bulky and expensive technique. Edner et al. (1994) conducted their measurements from a mobile laboratory aboard a ship in the Golfo di Catania, ~23 km downwind of the summit vents. Their results, at this distance from the vent, indicated the

plume was ~10 km wide and at a height of ~2 km with a thickness of ~1.5 km, see **figure 2.15** and **table 5.1** (Edner et al., 1994). They estimated an SO_2 flux of ~1295 ± 250 t/d; with the highest SO_2 concentrations, >350 $\mu g/m^3$, ~0.3 ppmm, located in the centre of the plume where atmospheric dilution and dissipation rates were at their lowest.

Bruno et al. (1994) used a COSPEC to record SO_2 fluxes of ~8000 t/d on ~3/9/92 at ranges of ~10 - 15 km from the vent; far greater than the DIAL-derived flux. It is possible that the limited range, <3.5 km, of the DIAL system used by Edner et al. (1994) prevented higher-level volcanic SO_2 being analysed, thus reducing the observed flux.

	SO_2 flux (t/d)	
Traverse N°.	DIAL	DOAS
1	966	1622
2	1645	2122
3	1332	1756
4	1553	2010
5	1156	1237
6	1217	1560
Average values	1295 ± 250	1718 ± 340

Table 5.1. *Comparison of the SO_2 concentration in Etna's plume as measured by DIAL and DOAS systems on 5/9/92, (Edner et al., 1994). Edner et al. (1994) attributed the disparity between the two systems to the limited range, <3.5 km, of the DIAL system.*

I have attributed the large difference in the SO_2 fluxes to the scavenging of SO_2 and its conversion to SO_3 and SO_4 aerosols. Edner et al. (1994) reported that the rate constant for the conversion of SO_2 to SO_4 was ~10^{-4} - 10^{-5} s^{-1}; far lower than Oppenheimer et al. (1998, in prep) and I estimate for scavenging of SO_2 on Montserrat, see Chapter 6. The amount of SO_2 removed from the plume will increase with distance, and therefore travel-time, from the vent. Oppenheimer et al. (1998, in prep) proposed the amount of material removed by scavenging decreases exponentially; relating to a first-order rate constant for SO_2 oxidation, see Chapter 6. This suggests that most of the SO_2 will be removed in the proximal, rather than distal parts of volcanic plumes. Edner et al. (1994) suggested that ~3 - 20% of the SO_2 had been removed by the time the plume had drifted to the Golfo di Catania, ~23 km from the

craters. By comparison, COSPEC analyses, generally conducted on roads that lie between ~3 and ~15 km from the vent, are affected much less by scavenging.

The DIAL system, by merit of being able to derive 2- and 3-dimensional concentration profiles accurately, may prove useful in determining how volcanic plumes interact with the atmosphere. However, the bulkiness of the system prevents it from getting close to the degassing vents and analysing gas compositions prior to being altered by atmospheric oxidation and solution processes.

DOAS (Differential Optical Absorption Spectroscopy)

The DOAS system, like COSPEC, uses solar UV radiation as a light source. Edner et al. (1994) were the first the to use the technique at Mt. Etna, on 5/9/92, during simultaneous DIAL investigations, see above. Their DOAS measurements, taken ~23 km downwind of the summit craters, gave a mean SO_2 flux of ~1718 ± 340 t/d; ~33% higher than the simultaneous DIAL-derived flux stated earlier, see **table 5.1**. Edner et al. (1994) attributed this discrepancy to the DOAS system detecting high altitude SO_2, beyond the ~3.5 km range of the DIAL system. The DOAS-derived SO_2 fluxes are still lower than those determined by Bruno et al. (1994) using COSPEC; again indicating that the removal of SO_2 by solution or oxidation may modify the composition of the volcanic plume.

The DOAS system, unlike COSPEC, can simultaneously analyse a wide frequency range and thus detect a number of gases; although Edner et al. (1994) only reported the detection of SO_2. The system is bulky and may be of little use in volcanology, the COSPEC generally being a better and more portable technique to study SO_2 fluxes.

OP-FTIR (Open-path Fourier Transform Infra-red Spectroscopy)

FTIR spectroscopy is a long-established laboratory technique. Notsu et al. (1993) were the first to use an open-path technique to analyse volcanic gases at Asama volcano, Japan, in 1991; using a Bomem FTIR spectrometer. I, as part of Francis et al. (1995), investigated the

experimental technique at Mt. Etna in 1994 using a field-portable Midac AMS™ FTIR spectrometer. We experimented with a variety of different techniques, both in the vicinity of the Valle de Leone (Pizzi Deneri) and the Bocca Nuova, close to the summit, and further down the flanks of the volcano, in the towns of Nicolosi and Zafferana-Etnea. We used a range of natural IR sources including warm ground and the sun. A portable artificial IR lamp was also used during analyses as this provided a more intense source of high frequency IR radiation. The technique enabled the detection of a number of gases, including SO_2, HCl, SiF_4 and CO_2 which, when combined with simultaneous COSPEC data, enabled gas fluxes to be determined. A more detailed discussion of the techniques used and results obtained can be found in Section 5.3.

5.2 The relationship between magmatic volatiles and eruptive activity at Mt. Etna

In this section I will review some of the previous investigations into the volatile content of Mt. Etna's magmas and volcanic plume to establish the relationship between eruptive activity and SO_2 flux. I will then discuss the shallow magmatic plumbing system beneath Mt. Etna, and how gas fluxes can be used to infer magma movement, using the 1991 - 1993 eruption as a case history.

5.2.1 The composition of Mt. Etna's plume and the variation in S:Cl ratios

The composition of Mt. Etna's volcanic plume

The presence of a permanent open conduit at Mt. Etna allows exsolved gas to be expelled from the summit craters with little or no interaction with a hydrothermal system. The collection of gas samples at Mt. Etna is hampered by the sheer crater walls and sporadic explosive activity; hence gases tend to be collected either from fumaroles outside the main craters or once they have mixed with the atmosphere (Chester et al., 1985).

I have summarised five sets of gas analyses in **table 5.2**. These have all been converted from their original units into wt%, assuming that only the reported gases were present in the analysed gas sample/plume. This approach has effectively given "dry gas" concentrations for those analyses where H_2O was not reported (i.e. Carbonelle et al., 1982; Allard et al., 1991; and this chapter) and enables gas mass ratios to be derived. The wide variety between analyses is, in part, due to different gases being analysed at different times, but mainly due to the different techniques used, OP-FTIR, direct-sampling and filter pack analysis, and the amounts of atmospheric interaction that occurred. Chapter 2 describes the problems relating to each type of analysis.

The paucity of complete, and accurate, gas data-sets has provided little to compare the OP-FTIR data of Francis et al. (1995) against; these data are discussed in Section 5.3. Depending on the technique used, a wide range of gases have been detected at Mt. Etna;

including a number of trace gases: N_2 and CH_4 (Edner et al., 1994); SiF_4 (Francis et al., 1996); CO and N_2O (this chapter). **Table 5.2** shows that H_2O and CO_2 are the most abundant gases, generally followed by SO_2, HCl and HF.

Author	Analysis date	H_2O	CO_2	SO_2	HCl	CO	H_2S	HF	$\frac{C}{S}$	$\frac{SO_2}{HCl}$
Chester et al., 1985	~1970	26.5	27.8	44.7	–	0.4	0.2	–	~0.3	–
Edner et al., 1994	pre 1973	14.5	29.3	46.8	0.2	2.0	4.8	–	~0.3	274
Carbonelle et al., 1982	May 1977	–	95.8	3.5	0.7	–	–	0.05	15	5
Allard et al., 1991	1975 - 1985	–	90	10	–	–	–	–	4.8	–
This chapter (OP-FTIR)	22/9/94	–	~89	~9	~2	–	–	*~0.2	~5.4	~5.3

Table 5.2. *Summary of gas compositions reported after being converted into wt% from: t/d (Carbonelle et al., 1982); Mol% (Chester et al., 1985); Vol% (Edner et al., 1994); Gg/y (Allard et al., 1991) and ppmv.m (Francis et al., 1995). Analyses are reported as wt% for only those analytes tabulated, hence the high CO_2 values for analyses which do not take H_2O into consideration; these are effectively reported as "dry gases". *Analyses for OP-FTIR-derived HF by Horrocks (pers. com.) for data collected in October 1997 .*

SO_2:HCl gas ratios measured at Mt. Etna

To understand how magmatic degassing and the plumbing system at Mt. Etna affect the S:Cl mass ratios measured at different craters, I shall briefly review the work of Andres et al. (1993); Le Cloarec et al., (1988) and Pennisi & Le Cloarec (1998) before discussing the two-stage degassing model proposed by Pennisi & Le Cloarec (1998).

S:Cl ratios estimated in 1987

Andres et al. (1993) used filter packs to estimate elemental and particulate fluxes at the Bocca Nuova and SE Crater in July 1987; see Section 2.8 for a description of the technique. They determined S:Cl mass ratios for the Bocca Nuova and SE Crater of ~0.3 and ~2.4 respectively; equivalent to an SO_2:HCl ratio of ~0.5 and ~4.7. They derived estimates for elemental fluxes by using simultaneous COSPEC data, ~1120 t/d, and scaling this to the element:sulphur ratio, see **table 5.3**. Andres et al. (1993) assumed all the sulphur was expelled

as, or oxidised to, SO_2 as the majority was trapped using the alkali-treated filters; rather than existing in a more reduced form, such as H_2S or S_8.

The large difference in the S:Cl ratios and gas fluxes recorded by Andres et al. (1993) from the Bocca Nuova and SE Crater relate to the different degassing environments present within these craters. At the time of filter sampling, both craters were degassing heavily; with the Bocca Nuova undergoing strombolian activity. Le Cloarec et al. (1988) have suggested that the Bocca Nuova has a direct connection to the magma chamber whilst the SE Crater does not. The Bocca Nuova should therefore have a higher gas flux, especially during periods of explosive activity. I have explained the lower S:Cl ratios measured at the Bocca Nuova using the two-stage degassing model of Pennisi & Le Cloarec discussed below and in Section 1.5.2 in which degassing is described as a continuous process; with two end-members: "deep" and "shallow" degassing. Deep degassing from the Bocca Nuova consists mainly of Cl and CO_2 exsolution. Shallower degassing, which will occur at both craters releases mainly H_2O and SO_2. The deep connection of the Bocca Nuova to the magma chamber therefore channels volatiles exsolved at deep and shallow depths, giving a generally low S:Cl ratio; the SE crater by comparison, has no deep connection, being supplied by magma moving along the Southern rift zone, and only undergoes shallow degassing, giving a much higher S:Cl ratio.

	Elemental flux (t/d)			Bocca Nuova	SE Crater
Element	Bocca Nuova	SE Crater	Total	S:Cl mass ratio	
S	370	200	~560	0.3	2.4
Cl	1200	82	~1300	SO_2:HCl mass ratio	
F	140	21	~160	0.6	4.7

Table 5.3. *Elemental fluxes and S:Cl and SO_2:HCl mass ratios estimated by Andres et al. (1993) for the Bocca Nuova and SE Craters; based on a COSPEC-derived SO_2 flux of 1120 t/d measured in July 1987 .*

The use of short-lived isotopes to determine degassing processes

Le Cloarec et al. (1988) investigated the degassing processes of the Bocca Nuova, La Voragine and SE Craters in 1986, during a period of strong degassing and strombolian

explosions. They used short lived isotopes of volatile elements: ^{210}Bi, ^{210}Pb and ^{210}Po to determine the rates of outgassing and the relative proportions of fresh magma present. Using the ratios of ^{210}Bi:^{210}Pb they estimated that magma outgassing at all three craters occurred over periods of ~1.5 - 2.7 days; indicating that the size of the magma conduits and convective cells were all similar. The variation in ^{210}Po:^{210}Pb ratios, however, indicated substantial differences between the amounts of undegassed magma present below each crater. Le Cloarec et al. (1988) estimated the proportions of deep, undegassed, magma in the degassing cells to be <50% for La Voragine, ~29% for the Bocca Nuova and ~19% for the SE Crater. They interpreted this to show that, unlike the Bocca Nuova and La Voragine, the SE Crater had no direct connection to the main magma chamber but was a secondary degassing vent, linked to the Southern rift zone.

S:Cl ratios estimated after the 1991- 1993 eruption

Pennisi & Le Cloarec (1998) collected gas samples during the period 1992 to 1995, using an air filtration system with a strong alkali to trap acid gases, see Section 2.8, to determine how the compositions of degassed volatiles from different craters varied with time. They reported that gases expelled from the Bocca Nuova had generally higher S:Cl mass ratios than those expelled from the SE Crater or La Voragine.

I have estimated SO_2:HCl mass ratios for the latter parts of the 1991 - 1993 eruption; using the assumption based on the Andres et al. (1993) data that all sulphur was emitted as SO_2. These ratios averaged ~8.4 for the Bocca Nuova with single analyses for the La Voragine and SE Craters giving ratios of ~10.8 and ~1.4 respectively. I have interpreted the high gas ratios at the Bocca Nuova and La Voragine craters to be indicative of the shallow degassing of volatiles prior to injection into the 1991 - 1993 eruptive fissure. The very low gas ratio reported for the SE Crater, which lies along the Southern rift zone, suggests that magma, rather than rising to the summit and then passing down along the rift, used a direct route from the magma chamber to the eruptive fissure; thus by-passing the rift zone.

Filter samples collected by Pennisi & Le Cloarec (1998) in June 1993, after the eruption ceased, indicated that the SO_2:HCl ratios had dropped to <0.3 - ~2, see **table 5.4.**

Pennisi & Le Cloarec (1998) suggested this low ratio was due to the final degassing of magma that had not been erupted but had already "lost" most of its sulphur. Over the next two years, for samples collected in June 1994 and September 1995, the SO_2:HCl ratios slowly rose to ~2.5 - ~3.8. The gradual increase in gas ratios from 1993 to 1995 was matched by an increase in the observed level of volcanic activity within the summit craters (GVN Bulletins, 1994 - 1996). I have interpreted the steady rise in gas ratios to indicate the influx and gradual rise of a fresh body of magma into the system beneath Mt. Etna.

Period of analyses	SO_2:HCl mass ratios derived from filter data	
	Bocca Nuova	SE Crater
16/1/92 - 25/10/92	~6 - ~11	~1.4
7/6/93 - 18/6/93	~0.5 - ~2	~0.5
18/6/94 - 23/6/94	~2.5 - ~3	~1.3
15/9/95 - 16/9/95	~3.4 - ~3.8	~2.5 - ~3.3

***Table 5.4**. Summary of the results of Pennisi & Le Cloarec (1998) showing the gradual change in SO_2:HCl mass ratios of gases emitted from the Bocca Nuova and SE Crater; assuming all sulphur is emitted as SO_2 and all chlorine as HCl.*

A two-stage degassing model

Giggenbach (1996) and Pennisi & Le Cloarec (1998) reported that the S:Cl ratios of degassed volatiles are dependant on the depth of volatile exsolution and the solubility of sulphur and chlorine species within the melt. Giggenbach (1996) suggested that chlorine, as alkali chlorides, is less soluble than sulphur at pressures greater than ~1 kbar. Below 1 kbar, HCl is the more stable chlorine compound, see Section 1.5. This is more soluble in magma than SO_2 and thus will exsolve at a later, shallower, stage (Carroll & Webster, 1994; Giggenbach, 1996). Pennisi & Le Cloarec (1998) and Clocchiatti (1996) proposed a two-stage degassing model for Mt. Etna:

1). Deep or "non-eruptive" degassing occurs at the transition from basalt to hawaiite at depths of over 4 km, >1 kbar, during which ~50% of chlorine and

30% of sulphur are exsolved along with much of the CO_2 and H_2O. At Mt. Etna this is equivalent to an SO_2:HCl mass ratio of <1.

2). Shallow, or "eruptive" degassing at depths of less than 1 km, <0.25 kbar, where ~90% of sulphur is exsolved compared with ~10% of chlorine. At Mt. Etna this would be equivalent to an SO_2:HCl mass ratio of ~10.

The above model seems counter-intuitive, with the more soluble HCl seeming to degas at a deeper level. This is due to the solubility of chlorine changing markedly with depth (Giggenbach, 1996). At deeper levels, >1 kbar, chlorine forms relatively insoluble complexes with alkali metals, which exsolve with shallowing due to oversaturation and immiscibility with precipitating crystals (Carroll & Webster, 1994). At lower pressures, <1 kbar, chlorine is more stable as HCl. This is a relatively soluble compound in magma, especially one containing an aqueous phase, and so will not reach saturation until very close to the surface (Carroll & Webster, 1994; Johnson et al., 1994). The two stage degassing model of Pennisi & Le Cloarec (1998) therefore utilises the depth-dependant solubility of chlorine. They proposed that the deeper degassing feeds the steady-state degassing at Mt. Etna giving lower SO_2:HCl ratios, as observed in 1993 - 1994; with shallower degassing, and hence higher SO_2:HCl ratios, occurring once a fresh batch of magma begins to rise up within the volcano (Le Cloarec et al., 1996).

5.2.2 Variation of SO_2 gas flux with the level of volcanic activity

Malinconico (1987) and Caltabiano et al. (1994) demonstrated, both on a day-to-day basis and over a period of several years, that the SO_2 flux is markedly higher during eruptive periods than during times of relative quiescence, see **figures 5.4A-B**. Malinconico (1987) suggested that if a background SO_2 flux could be determined, any rise in the flux above this level would relate to an increase in the activity of the volcano. The SO_2 flux associated with quiescent degassing on Mt. Etna varies between <500 and >6000 t/d, making it difficult to determine the background flux. Caltabiano et al. (1994) conducted regular COSPEC analyses over the period 29/10/87 to 30/12/91. They suggested the wide variation in levels of background SO_2 flux was due to a long-period variation in magma supply, over months or

years; due to the sporadic rise of new magma into the magmatic system beneath the volcano. Malinconico (1987) suggested three states of degassing activity:

- "Active" degassing which relates to the general background level of degassing.
- "Premonitory" degassing which relates to an increase in level of degassing of ~2 - 3 times that of the background level. This would be indicative of a possible eruption.
- "Eruptive" degassing which relates to at least a five-fold increase in degassing above the background level.

Figure 5.4B shows the prolonged study of Caltabiano et al. (1994). The periods of eruptive and increased seismic activity generally exhibit gas fluxes ~5 times the general background level. Bruno et al. (1994) and Caltabiano et al. (1994) also noted that COSPEC-derived SO_2 fluxes tended to dip sharply below the background level ~4 - 6 weeks prior to an eruption, see **figures 5.4A-B** and **5.5**. Caltabiano et al. (1994) attributed this decrease to the possible sealing-up of the magmatic system caused by a withdrawal of high-level magma in response to dyke propagation prior to an eruptive episode. Rymer et al. (1993) reported gravity changes between June 1990 and June 1991 which they inferred related to magma filling a fissure. This may have been related to the two periods of decreased gas flux which

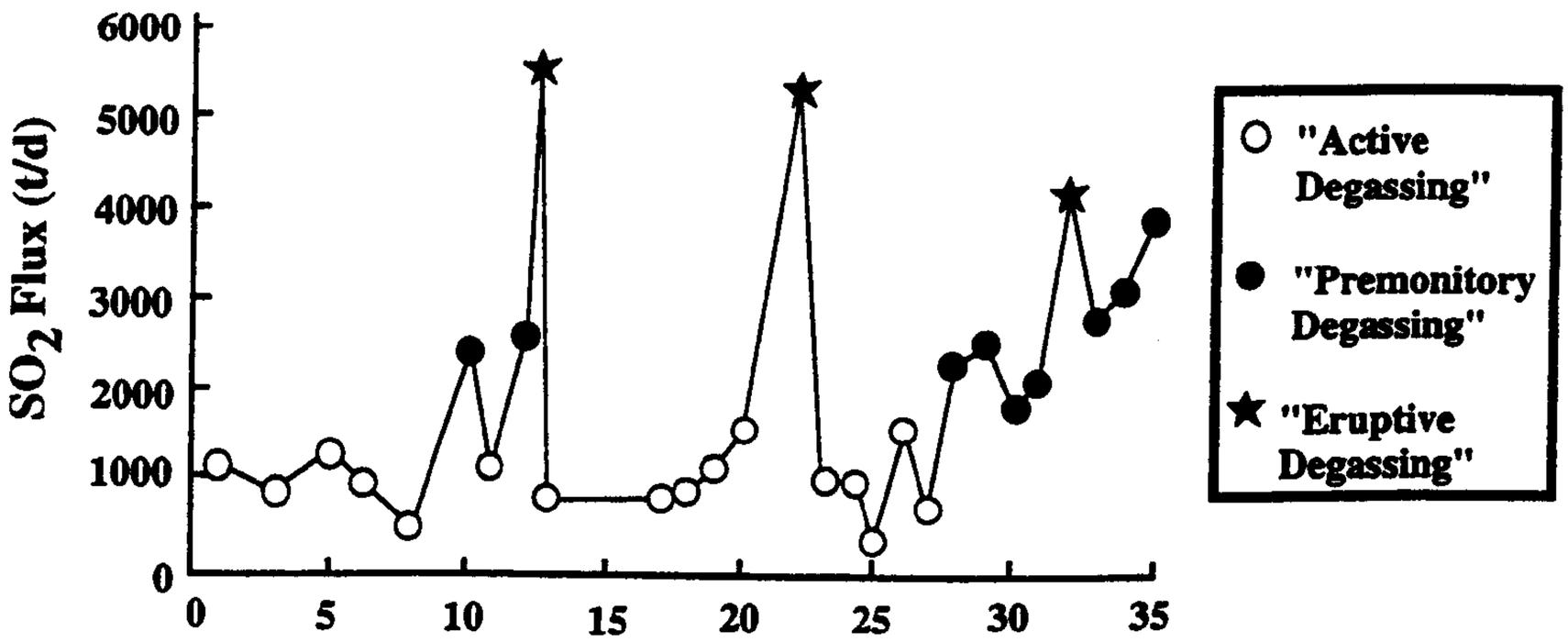

Figure 5.4. A. *COSPEC-derived SO_2 fluxes collected by Malinconico (1987) for a one month period in 1977. This shows three degassing levels related to: "Active degassing"; "Premonitory degassing" and "Eruptive degassing", see text.*

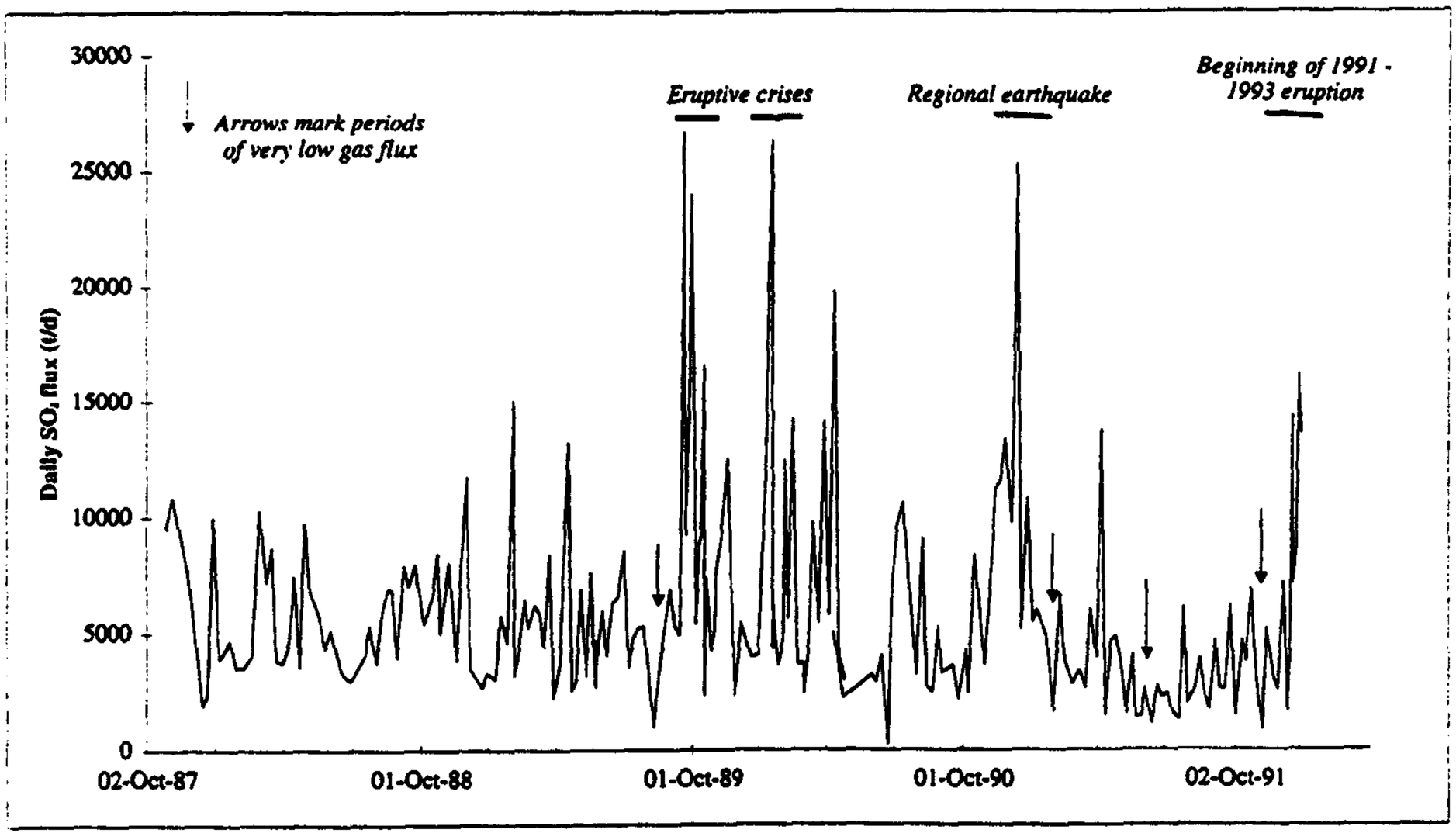

Figure 5.4. B. Caltabiano et al. (1994) collected SO_2 fluxes using COSPEC over a period of 4 years. Marked are periods of eruptive or seismic activity. Arrows indicate periods of flux below the background level. These may possibly relate to periods of magma drainage, see text.

occurred on 31/1/91 and in May - June 1991. A further flux decrease, on 8/11/91, was the lowest recorded since ~1977 and may possibly relate to a further extension of the magma-filled fissure.

5.2.3 COSPEC investigation of magmatic activity associated with the 1991 - 1993 eruption

Geophysical precursors to the 1991 - 1993 eruption

This section describes the phases of magma migration that occurred beneath the summit areas prior to the 1991 - 1993 eruption, as interpreted by Rymer et al. (1993) from microgravity data, in order to establish the role of rift zone and feeder dyke in the eruption. They reported that an increase in mass in the summer and autumn of 1989 had preceded the eruption; this, they inferred, was related to the influx of magma into the upper parts of the volcano. A large pyroclastic eruption in January 1990 led to a mass decrease between November 1989 and June 1990, associated with a progressive deflation of the summit area.

Between June 1990 and June 1991 Rymer et al. (1993) detected microgravity increases in the summit area and in a zone extending to the SSE. They inferred this to have been caused by magma migrating away from the summit area and filling a pre-existing subsurface fissure, probably formed during the 1989 eruption. The infilling of the fissure was essentially passive as no seismicity was evident at a shallow level. They interpreted inflation along the line of the fissure, associated with a gravity decrease and deep, 4 - 5 km, seismicity as indicating expansion of vesicular magma and the downwards propagation of the fissure. Intense seismic activity at depths of ~1 - 3 km immediately prior to the eruption on 14/12/91 was associated with a widening of the fissure and eruption close to the summit at 2900 m a.s.l. By 15/12/91 the eruptive activity had migrated along the fissure to the SSE until it reached an altitude of 2400 m a.s.l where the fissure intersected the wall of the Valle del Bove - the main vent for the 1991 - 1993 eruption.

Exsolved S:Cl ratios determined from melt-inclusion studies of the 1991 - 1993 lavas

To determine how the measured fluxes of degassed volatiles relate to the flux of degassing magma/lava, it is necessary to establish the concentrations of magmatic volatiles, both prior to, and after degassing has occurred. This is best done by analysing volatiles trapped within fluid inclusions and in residual glasses.

Armienti et al. (1994) analysed the element and volatile compositions of lavas and melt inclusions from the 1991 - 1993 eruption. They reported that the main body of the eruption was of hawaiite composition; except for lavas emitted in the first few days. These exhibited a wide range of compositions, attributed by Armienti et al. (1994) to the mixing of fresh hawaiite magma with pooled magmas from previous eruptions, mainly the more primitive alkali basalt from the 1989-eruption, and the magma initially residing in the feeder dyke.

Armienti et al. (1994) analysed olivine melt inclusions from the 1991 -1993 eruption. They reported average sulphur and chlorine concentrations within "undegassed" melt inclusions of ~1180 and 2290 ppm respectively. For "residual", degassed, glasses, they

reported sulphur and chlorine concentrations of ~400 and 1710 ppm respectively. The difference in volatile concentrations between "undegassed" and "residual" samples relates to the amount of volatiles exsolved. I have estimated an exsolved S:Cl mass ratio of ~1.3, using the average exsolved sulphur and chlorine concentrations.

I estimated exsolved S:Cl mass ratios for individual samples analysed by Armienti et al. (1994). For samples collected on 17/3/92 and 25/5/92, S:Cl mass ratios are ~0.5 and ~1.1 respectively and relate to periods of low and high lava effusion, see **figure 5.5**. I have interpreted the low S:Cl ratios, relating to low magma effusion, as possible being due to degassed magma from beneath the summit craters draining down into the rift zone and being erupted. The higher S:Cl ratios relate to the second magma pulse being erupted. This was fed directly into the rift zone and therefore probably had degassed to a lesser extent.

Monitoring the 1991 - 1993 eruption using COSPEC

Bruno et al. (1994) took advantage of the 1991- 1993 eruption to monitor the variation in SO_2 flux during a long-lasting eruption using the COSPEC technique. They compared variations in the combined gas flux, measured at the summit craters and eruptive fissure, to tilt and seismic measurements. They suggested that the observed changes were caused by the lateral emptying of a shallow, central magma supply system; followed by two magma pulses which rose up and drained away through the fissure system to be erupted into the Valle del Bove. Bruno et al. (1994) divided the eruption up into four parts, based on gas emission:

I).	Influx of first magma pulse.	11/91 - 2/92
II)	Draining of magma.	3/92 - 5/92
III).	Influx of second magma pulse.	6/92 - 7/92
IV).	Influx of third magma pulse.	8/92 - 10/92 (and onwards)

I have used **equation 5.1** (adapted from Bruno et al., 1994) to compare the COSPEC data of Bruno et al. (1994) with a theoretical SO_2 flux based on lava effusion data I have derived from cumulative lava effusion volumes of Calvari et al. (1994) and Harris (1996).

$$\Phi_{SO_2} = \left(\frac{\rho_m \times (CV_2 - CV_1) \times S_m \times S_\Delta}{(T_2 - T_1)} \right) \times (2 \times 10^{-8}) \qquad \textbf{(5.1)}$$

where: ΦSO_2 = the sulphur flux (t/d); ρ_m = lava density (2.8 t/m^3); CV_1 and CV_2 = cumulative lava volumes at times T_1 and T_2; S_m = sulphur content of lavas (1560 ppm); and S_Δ = percentage of S degassed (~74%). The sulphur content used in **equation 5.1**, 1560 ppm, is the maximum sulphur content reported by Armienti et al. (1994) for the main body of the 1991 - 1993 lavas. I have used a degassed sulphur concentration of 400 ppm, as reported by Armienti et al. (1994); this gives a magmatic degassing percentage of ~74%; similar to the 73% reported in Bruno et al. (1994).

To establish if the parameters I have used in **equation 5.1** were accurate, I used a simple root-means-squared test to determine the best-fit between the measured and calculated data. For my calculations, I have assumed that SO_2 is degassed only from the volumes of lava erupted, either prior to eruption, as summit degassing, or from the fissure and lava flows; and that the magmatic composition remains relatively constant through the main body of the eruption; as suggested by the analyses of Armienti et al. (1994).

Figure 5.5 shows the measured and calculated SO_2 fluxes as well as the observed lava effusion rates, derived from the cumulative volumes of Calvari et al. (1994) which were based on the mapping of flows at a scale of 1:10,000. There is generally a good correlation between measured and calculated SO_2 fluxes, as expected; however, in places there are notable disparities. These are outside the ~20% error quoted for both COSPEC and volume measurements by Bruno et al. (1994) and Calvari et al. (1994) respectively. I will discuss the probable causes for the disparities in the following sections.

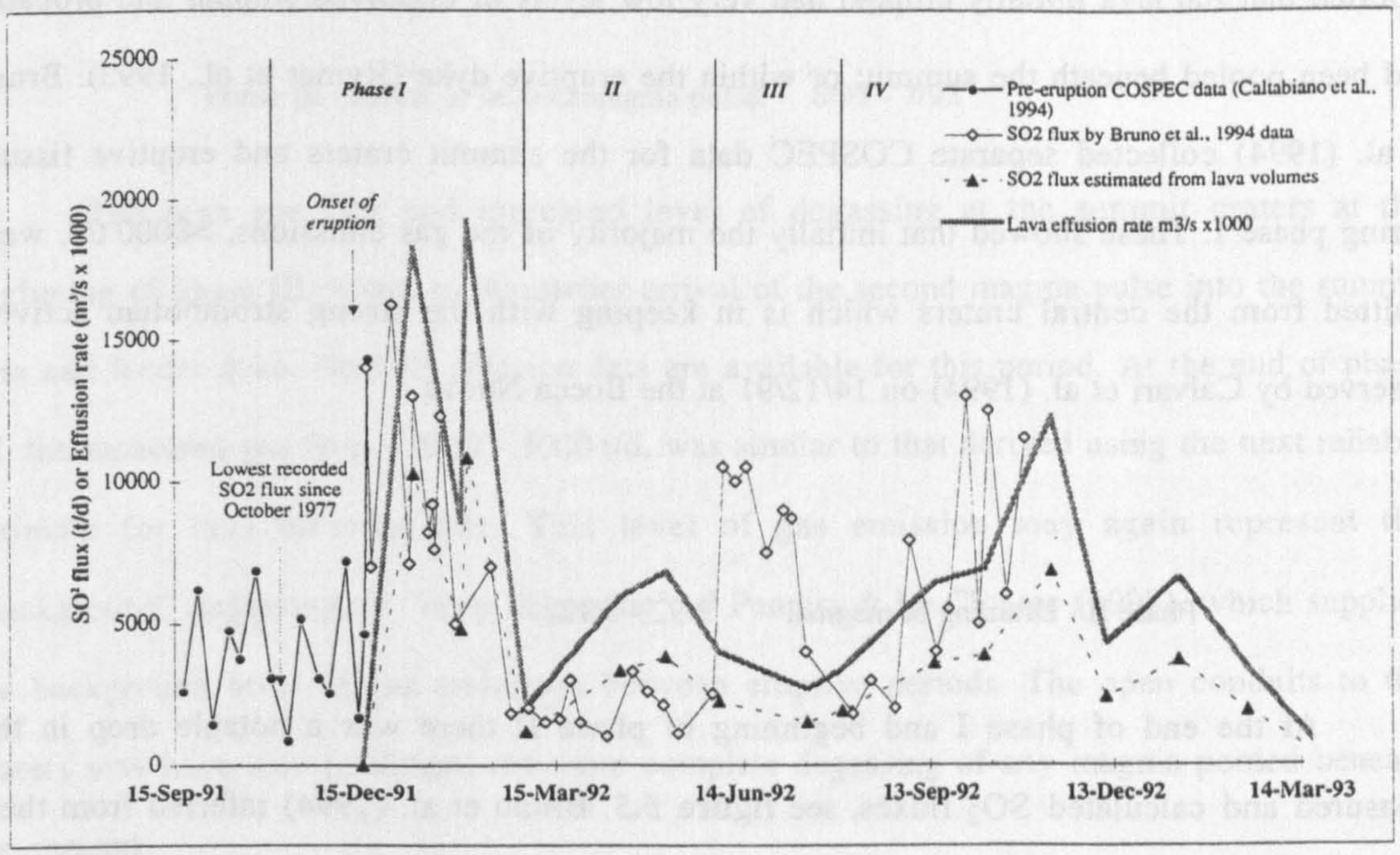

***Figure 5.5**. Comparison of SO_2 fluxes measured by COSPEC (Bruno et al., 1994) with those I calculate using lava effusion rates (after Calvari et al., 1994) and **equation 5.1.** A plot of lava effusion rate is also included for comparative purposes to show that both measured and calculated SO_2 fluxes generally correlate well with lava effusion rates. The periods in which gas and effusion rates do not correlate are discussed in the text.*

The interpretation of magma-movements using COSPEC

The following sections are based around the relationships between measured and calculated SO_2 fluxes portrayed in **figure 5.5** and based on **equation 5.1**.

Phase I - Influx of first magma pulse. 11/91 - 2/92

During phase I, the SO_2 fluxes I have derived from reported lava volumes are similar to those determined using COSPEC; suggesting the erupted magma was relatively undegassed and probably had entered directly into the main feeder-dyke; rather than migrating via the summit craters. There is not enough effusion-rate data for the first few days of the eruption to be able to compare the difference in volatile content between the magma stored in the fissure and the body of magma which was erupted directly afterwards. Armienti et al (1994), however,

reported that the lava initially erupted had very low levels of dissolved sulphur and probably had been pooled beneath the summit; or within the eruptive dyke (Rymer et al., 1993). Bruno et al. (1994) collected separate COSPEC data for the summit craters and eruptive fissure during phase I. These showed that initially the majority of the gas emissions, >8000 *t/d*, were emitted from the central craters which is in keeping with the strong strombolian activity observed by Calvari et al. (1994) on 14/12/91 at the Bocca Nuova.

Phase II - Draining of magma. 3/92 - 5/92

At the end of phase I and beginning of phase II there was a notable drop in the measured and calculated SO_2 fluxes, see **figure 5.5**. Bruno et al. (1994) inferred from their COSPEC data that, at this point, the magmatic system may have been partially emptied. I suggest the observed decrease in gas flux, towards "background" levels of ~2000 *t/d*, see **figure 5.4B**, was caused by lowering of the magma levels within the system after the first magma pulse; resulting in the draining of the magma from the summit and fissure areas. The withdrawal of magma from below the summit is also supported by the reduction in crater activity during this period and the lowering of the floor of the NE Crater by ~70 m (Calvari et al., 1994).

Ground deformation, as recorded by tilt stations in Bruno et al. (1994), also showed a gradual deflation of the edifice during February to May 1992. The rise in observed effusion rates towards the middle of phase II and the increase in radial tilt at Casa del Vescovo, ~6 km SSE of the summit, possibly heralded the influx of a second body of magma. This was reflected in a small rise in the COSPEC measurements of Bruno et al. (1994).

Bruno et al. (1994) interpreted the sharp increase in COSPEC-derived SO_2 flux in early June to relate to the arrival of a second magma pulse. This corresponded with a period of wide variation in the estimated rates of lava effusion as observed in the field (Calvari et al., 1994; Harris, 1996). I have therefore used the much lower rate derived by Harris (1996) from AVHRR-satellite data; which is itself limited by the paucity of cloud-free images for the period in question. Thus the period of high gas emission reported by Bruno et al. (1994) is not reflected in the calculated data.

Phase III - Influx of second magma pulse. 6/92 - 7/92

The high gas flux and increased level of degassing at the summit craters at the beginning of phase III relates to the earlier arrival of the second magma pulse into the summit area and feeder dyke. No lava effusion data are available for this period. At the end of phase III, the measured gas flux, ~2000 - 3000 t/d, was similar to that derived using the next reliable estimate for lava effusion rate. This level of gas emission may again represent the "background" degassing, or "deep degassing" of Pennisi & Le Cloarec (1998), which supplies the background level of gas emissions between eruptive periods. The open conduits to the craters may have also facilitated the more complete degassing of any magma pooled beneath the summit.

Phase IV - Influx of third magma pulse. 8/92 - 10/92 (and onwards)

The very low SO_2 fluxes, both calculated and measured, at the beginning of phase IV in July and August 1992 correspond to a period of low effusion rates. I have inferred a partial withdrawal of magma from the summit area at this time as there was another lowering of the floor of the NE Crater (Calvari et al., 1994). In September and October 1992, effusion rates once again increased; this was reflected in the increased SO_2 flux and increased activity in the Bocca Nuova (Harris et al., 1997: Bruno et al., 1994; Calvari et al., 1994). The SO_2 fluxes measured by Bruno et al., (1994) during phase IV were similar to the author's calculated fluxes, except for several short periods when the measured flux was much higher. I attributed these short-term deviations to collapses and changes in the activity of the summit craters which temporarily increased the amount of summit degassing (Calvari et al., 1994; Caltabiano et al., 1994).

Bruno et al. (1994) reported COSPEC observations only until the end of October 1992. In November and December 1992 the rate of lava effusion decreased rapidly. I inferred that the collapses and lowering of the floor of the NE Crater related to magma beneath the summit being drawn down into the feeder dyke. Calvari et al. (1994) reported further

collapses in the summit region occurred at the end of March 1993 when the main eruption stopped.

Summary of the 1991 - 1993 eruption

The chain of events, summarised earlier from Rymer et al. (1993), show the progressive rise of fresh magma up into the summit areas which initiated the January 1990 eruption. Partially degassed magma then entered a pre-existing fissure and migrated along the Southern rift zone. A rise in the level of magma prior to eruption led to the formation of the spatter cone at 2900 m a.s.l (Rymer et al., 1995) and strong strombolian activity in the Bocca Nuova (Calvari et al., 1994) before dyke migration and the onset of the main eruption in the wall of the Valle del Bove.

I have demonstrated above that the combined use of SO_2 flux and effusion rate data can be used to infer the amounts of sulphur degassed and the interaction between fresh and degassed magmas. I have used the observations of Calvari et al. (1994) on volcanic activity at the summit craters to demonstrate that three episodes of magma influx and drainage have occurred. This is supported by the COSPEC measurements of Bruno et al. (1994) and the SO_2 fluxes I have derived from the volume data of Calvari et al. (1994) and Harris (1996); which show successive magma pulses being reflected in the level of degassing. Marked differences between gas emission and lava effusion occurred when an influx of fresh, volatile rich, magma displaced older, degassed, magma. This caused an apparent increase in the gas fluxes calculated from volumes of lava erupted when compared to the measured SO_2 flux. After the influx of each magma pulse the effusion rate and level of degassing fell sharply. The ensuing drainage of magma away from the summit areas then led to a series of crater collapses.

5.3 The use of OP-FTIR on Mt. Etna

Francis et al. (1995) and Chaffin et al. (1995) conducted experimental OP-FTIR investigations into the gas emissions from Mt. Etna September 1994. This chapter is an expansion of that work in which I will discuss in detail the methods used and results obtained from the investigation, carried out between 20/9/94 and 25/9/94. The aim of the investigation was to determine whether the OP-FTIR technique was suitable for analysing volcanic gases and to develop a robust methodology for the application of the technique, if suitable, at other volcanoes. In the following, I have used "we" to refer to OP-FTIR work I carried out as part of Francis et al. (1995); who were A. Maciejewski, P. Francis, C. Oppenheimer and C. Chaffin; T. Caltabiano was a key figure in the collection of COSPEC data.

5.3.1 Perceived problems with analysis of gases at Mt. Etna: A rationale for OP-FTIR investigations

The reason for using an OP-FTIR system to analyse volcanic gases lay in the problems encountered by other scientists using conventional gas analysis techniques. The dangers associated with sudden strombolian activity and collapse of the sheer walls of the summit craters makes direct sampling of volcanic gases at Mt. Etna difficult and dangerous. We hoped that by developing a remote technique, an accurate analysis of Mt. Etna's volcanic plume could be achieved in relative safety. Our use of the OP-FTIR technique highlighted problems experienced by other terrestrial remote-sensing techniques, see Chapter 2. These included the portability of the other systems, with only the COSPEC being a lighter and more compact unit than the OP-FTIR. The OP-FTIR, however, is the only "portable" technique available which is capable of analysing many different gases simultaneously, and thus being able to provide accurate gas ratios which are independent of atmospheric dilution. The presence of dirt-tracks close to the summit craters along with the large volumes of gas emitted ensured that analyses could be carried out close to the gas source with high chances of detecting a range of analyte species. This made Mt. Etna an ideal choice as a natural laboratory for a field trial for the OP-FTIR technique.

5.3.2 OP-FTIR methodology

OP-FTIR instrumentation

This was the first time that a Midac AMS™ FTIR had been used for monitoring volcanic gases. We therefore experimented with a wide variety of different methods to determine which gave the best data. I have described some of these variations in the next section. The following summarises the basic set-up, a more detailed description of the OP-FTIR system can be found in Section 2.2.

The Midac AMS™ spectrometer, using a mercury-cadmium-telluride (MCT) IR detector, was mounted piggy-back on top of a 10" (25.4 cm) Newtonian telescope set on a heavy-duty Quickset™ tripod, see **figure 5.6**. The IR source and spectrometer were positioned so that volcanic gases passed through the optical path between them. We conducted both "active" analyses, using a portable artificial IR lamp; and "passive" analyses, using a natural IR source - such as warm ground or lava.

***Figure 5.6**. Photograph of the Midac AMS™ spectrometer being used at Pizzi Deneri below the NE Crater on Mt. Etna by C. Chaffin. The numerous tracks that cross the volcano enabled us to transport the instrument using a 4-wheel-drive Land-Rover .*

As an experiment, we also collected IR spectra using clear skies and clouds as a background to investigate the radiation emitted by volcanic gases. The temperature of the

natural IR sources we used on Mt. Etna proved too cool to emit enough of the high energy IR radiation required for high quality gas analyses. The majority of the data analysed was therefore collected using the portable IR lamp. This was a 1275°C SiC Globar with a large, 20" (50.8 cm), parabolic reflector mounted on a Quickset™ tripod. The 12V Globar was powered using a car battery, or a vehicle's electric supply. The portability of the IR source enabled us to position it directly in line with the gas emissions and detector, thus ensuring that the analyte gas filled the optical path as much as possible. The individual set-ups for active and passive OP-FTIR analyses are described below; sample localities and optical paths can be seen in **figure 5.7**.

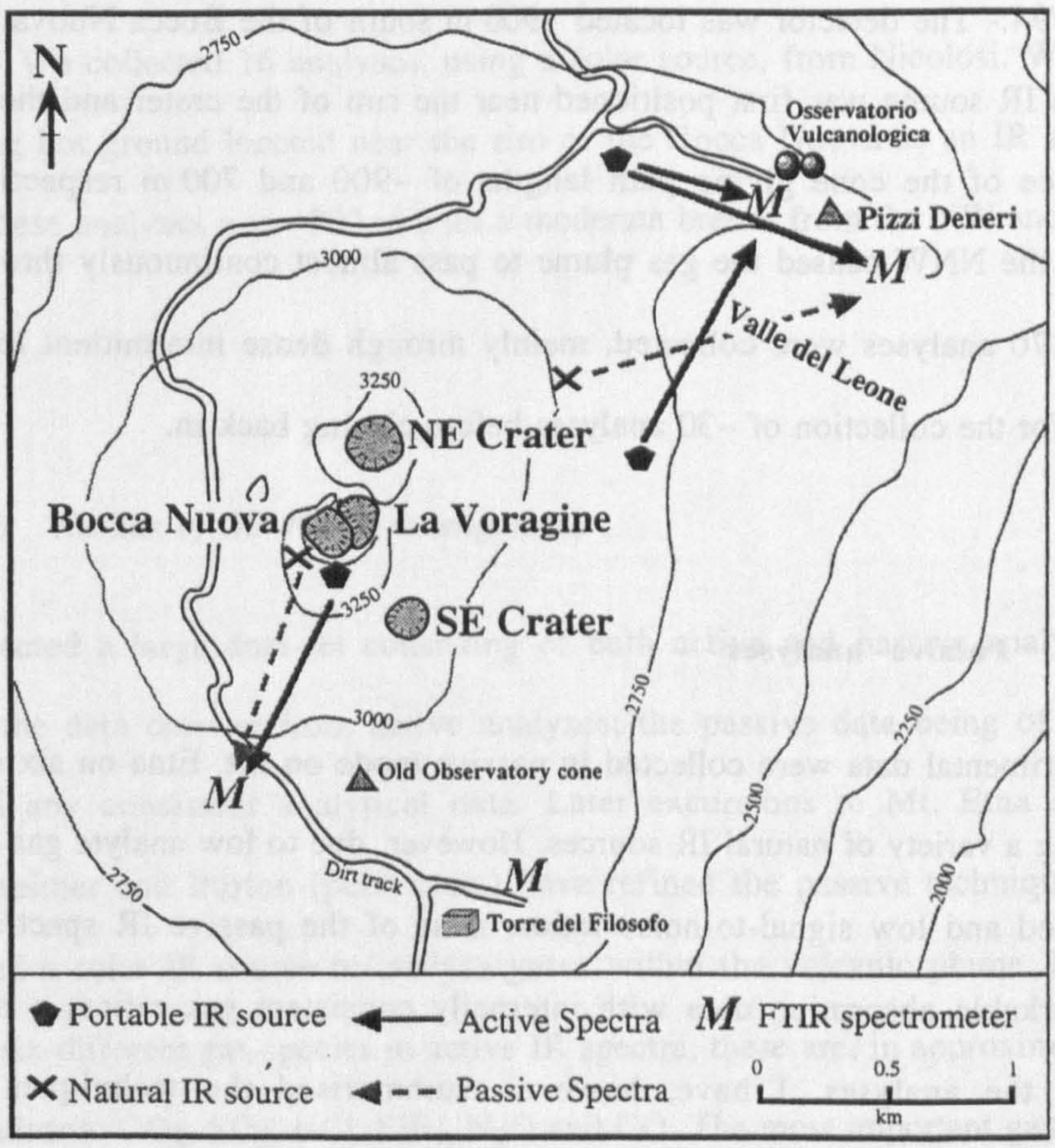

Figure 5.7 *Map of the summit area of Mt. Etna showing the locations of active and passive OP-FTIR analyses conducted by Francis et al. (1995).*

Active analyses

21/9/94:- Analyses were conducted with the detector placed at the centre of the ridge at Pizzi Deneri overlooking the Valle de Leone ~1250 m NE of the NE Crater. The portable IR

source was positioned on the face of the Valle del Leone 750 - 1000 m away and then moved to the western end of the ridge, giving a ~250 m path length. The wind was from the WSW with gases passing intermittently through the optical path. 46 analyses were collected.

22/9/94:- Analyses were again conducted at the Pizzi Deneri, this time at the east end of the ridge overlooking the Valle del Leone, ~1500 m NE of the NE Crater. The portable IR source was positioned ~500 m away at the west end of the ridge. The wind was again from the WSW, with Caltabiano (pers. com.) measuring a wind speed of ~5 m/s. Volcanic plume passed intermittently through optical path whilst ~100 analyses were collected.

25/9/94:- The detector was located ~900 m south of the Bocca Nuova on a dirt-track. The portable IR source was first positioned near the rim of the crater and then further down the south face of the cone giving path lengths of ~900 and 700 m respectively. A strong breeze from the NNW caused the gas plume to pass almost continuously through the optical path. Over 170 analyses were collected, mainly through dense intermittent low-lying cloud; this cleared for the collection of ~30 analyses before closing back in.

Passive analyses

Experimental data were collected in passive mode on Mt. Etna on six days, 20/9/94 - 25/9/94, using a variety of natural IR sources. However, due to low analyte gas concentrations, technique used and low signal-to-noise ratios, none of the passive IR spectra we collected provided workable absorption data with internally consistent gas ratios; a measure of the accuracy of the analyses. I have, however, summarised the techniques we used for completeness.

21/9/94:- We used sun-heated ash as an IR source at Torro del Filosofo or the collection of 40 IR spectra. We then moved to Pizzi Deneri, ~1250 m NE of the NE Crater where we used ash and old lava as an IR source to collect 81 analyses. The wind was generally from the NW.

22/9/94:- We again used ash and old lava close to Pizzi Deneri as an IR source; collecting 25 analyses through dense plume. Clear sky and clouds were used as a background

for emission spectroscopy. We also tried using the sun as an IR source. A total of 74 passive spectra were collected. The wind was from the WSW.

23/9/94:- We collected 90 experimental spectra using a solar source from two localities: Randazzo, ~10.5 km NNW of the summit and Nicolosi, ~12 km south of the summit during which time the wind shifted from SSE to SW.

24/9/94:- We collected 64 experimental spectra, again using a solar source, from the town of Zafferana, 9 km SE of the summit. The wind was from the NW and the weather generally good.

25/9/94:- We collected 16 analyses, using a solar source, from Nicolosi. We collected 12 analyses using hot ground located near the rim of the Bocca Nuova as an IR source. The path length for these analyses was ~900 m with a moderate breeze from the NW and dense low lying cloud.

5.3.3 Results of OP-FTIR investigations

We collected a large data-set consisting of both active and passive analyses. I will discuss mainly the data derived from active analyses; the passive data being of too poor a quality to yield any consistent analytical data. Later excursions to Mt. Etna in 1997 by Francis, Oppenheimer and Burton (pers. com.) have refined the passive technique and have successfully used a solar IR source to analyse gases within the volcanic plume. I have been able to identify six different gas species in active IR spectra; these are, in approximate order of decreasing abundance: CO_2, SO_2, HCl. SiF_4, N_2O and CO. The most important gases, HCl and SO_2, will be discussed first; with CO_2 and trace gases discussed later.

Analysis of SO_2 and HCl

The quantification of SO_2 and HCl allows an SO_2:HCl ratio to be derived which relates to the degassing history and processes on-going within the volcano's magmatic system.

Variations in gas ratios may be due to atmospheric interactions or secondary processes, possibly in the hydrothermal system.

The signal-to-noise ratios of absorbance spectra derived from IR spectra collected using an active IR source varied between ~20:1 to less than 2:1 which are extremely low. This was however generally sufficient to provide high quality analyses for SO_2 and HCl. Absorbance data created using passive IR data had much lower signal-to-noise ratios, <2, and so could not be used to derive any accurate concentration data. The errors associated with the quantification of SO_2 and HCl are similar to those I estimated for spectra collected at La Fossa, ~6 - 13%. A full description of errors appears in Section 2.2.6.

I have summarised the active OP-FTIR data we collected at Pizzi Deneri and the Bocca Nuova in **table 5.5**. I have omitted CO and N_2O in the table as these were found in only a few spectra; their occurrence is discussed in the text. Analyte concentrations are reported in ppmv.m; a function of the total concentration of analyte over the length of the optical path, see Section 2.2.

Date of analysis	Location	N° of spectra	Path length (m)	Mean analyte concentration (ppmv.m)				$\frac{SO_2}{HCl}$
				CO_2	SO_2	HCl	SiF_4	mass ratios
21/9/94	Pizzi Deneri	46	~750	nd	18.0 ± 4	17.5 ± 4	nd	*~4.9
22/9/94	Pizzi Deneri	99	~900	~4000 ±1300	280 ± 69	93 ± 23	0.04 ± 0.02	5.8
25/9/94	Bocca Nuova	130	~900	~7100 ± 4700	260 ± 64	76 ± 19	0.2 ± 0.05	#*7.4

***Table 5.5**. Summary of our results for active OP-FTIR analyses collected at Pizzi Deneri, close to the NE Crater, and at the Bocca Nuova during September 1994. *Some analyses were omitted from the average calculations as they were considered erroneous due to instrumental problems. I have derived SO_2:HCl mass ratios by using a best-fit line through the data in **figures 5.8A-C** and converting these using the relative molecular masses of SO_2 and HCl. CO_2 data are preliminary and vary greatly depending on atmospheric conditions, see text. #The SO_2:HCl mass ratio estimated for 25/9/94 may also be interpreted as being ~3.5, assuming thick cloud has scavenged ~50% of the HCl emitted, see text.*

I have recorded a variation in concentration for SO_2 and HCl of almost two orders of magnitude; <10 - >1000 ppmv.m and <5 - >300 ppmv.m for SO_2 and HCl respectively. This variation is due mainly to volcanic gases filling the optical path to differing degrees during the

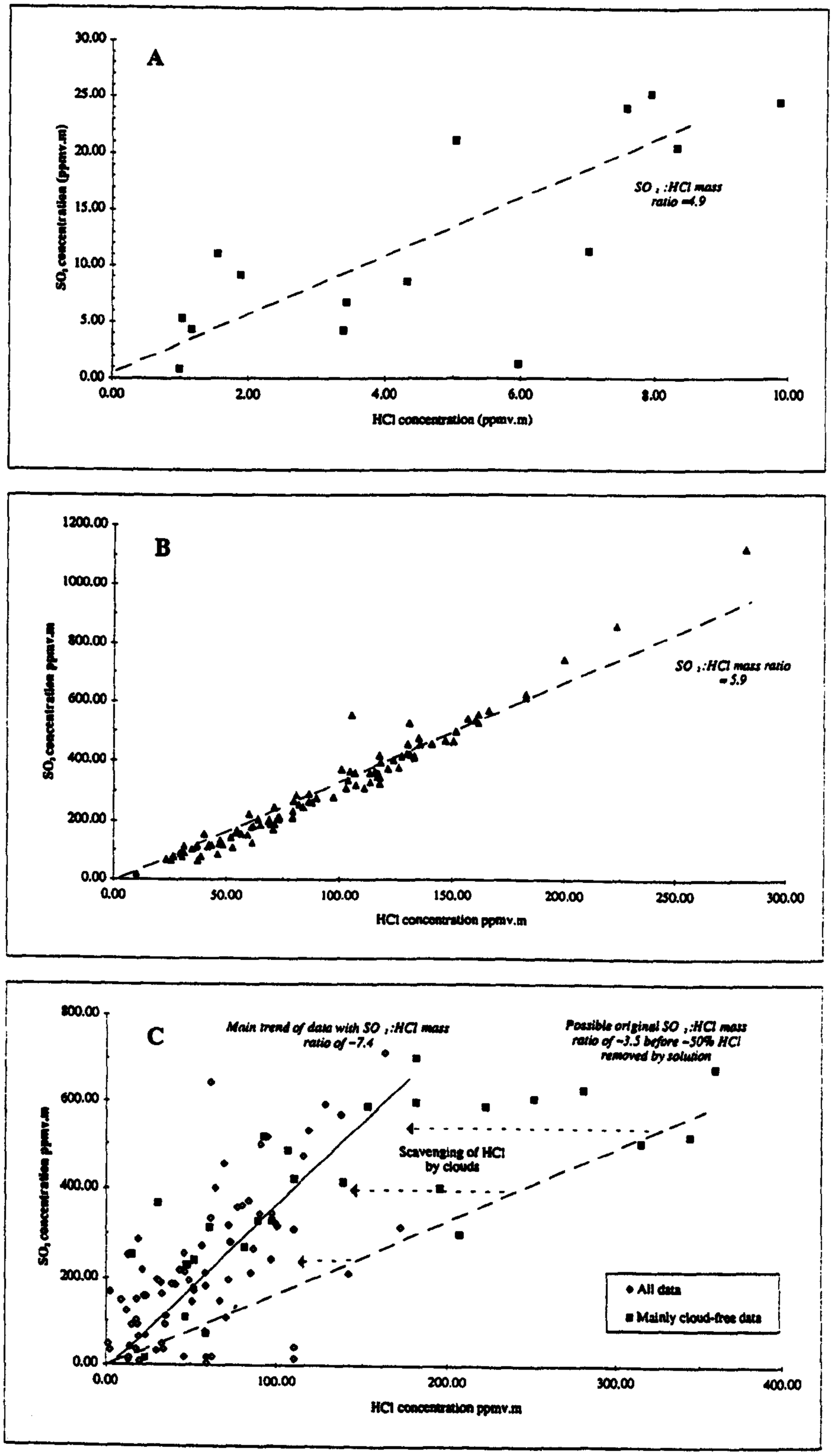

Figure 5.8. A. *Results of active OP-FTIR analyses collected on 21/9/94 using path lengths of 250 and 750 m at Pizzi Deneri.* ***B.*** *Active analyses collected on 22/9/94 at Pizzi Deneri using a 900 m path length.* ***C.*** *Active analyses collected on 25/9/94 with a path length of 700 - 900 m at the Bocca Nuova. Two gas ratios lines have been fitted to the data. One marks the ratios as they were recorded; the other indicates an approximate initial gas ratio before the removal of ~50% of the HCl by solution in thick cloud, see text for discussion.*

periods of analysis. Francis et al. (1995) only used concentrations >100 ppmv.m to generate gas volume ratios; taken as the average value of the reduced data-set. I have used the whole data-set and derived gas mass ratios by converting the volume ratios I have determined from regression lines through the plotted data, see **figures 5.8A-C**.

Gas analyses conducted close to the NE Crater exhibit SO_2:HCl mass ratios of ~4.9 - ~5.8; consistent with the active degasing of a basaltic volcano (Francis et al., 1995). I have derived a high SO_2:HCl mass ratio of ~7.4 for analyses carried out at the Bocca Nuova on 25/9/04 in thick cloud. This is much higher than the ratios estimated by Pennisi and Le Cloarec (1998); ~2.5 - ~3 and ~3.4 - ~3.8 for filter analyses conducted in July 1994 and September 1995 respectively. In Section 5.3.4, I suggest that this high gas ratio was possibly caused by heavy cloud scavenging ~50% of the HCl in the plume; thus altering the initial SO_2:HCl mass ratio from ~3.5 to ~7.8. The accurate use of open-path data for soluble gas species, such as HCl and HF, therefore depends on the analyses being conducted in fine weather as water, either as rain or as clouds can remove significant proportions of analyte from the gas plume.

Analysis of CO_2, CO and N_2O

I have detected CO_2, CO and N_2O in IR spectra collected in September 1994. Next to H_2O, CO_2 has the highest atmospheric background concentration of an IR-active gas, ~355 ppmv. This causes the total attenuation of the fundamental absorbance peak, ~2300 - 2400 cm^{-1}, over long path lengths. Mori et al. (1997) used a much less intense absorbance peak at 2077 cm^{-1} to quantify the CO_2 in IR spectra collected at Aso volcano, Japan in 1996. My preliminary investigations into using this absorbance peak have shown that CO_2 may be present at the Bocca Nuova in concentrations of up to 20,000 ppmv.m over a 900 m optical path, equivalent to ~22 ppmv above background levels. By contrast, at the NE Crater, I only estimated CO_2 concentrations of up to ~8000 ppmv.m over a similar path length. I observed only a weak correlation between SO_2 and CO_2 concentrations on 25/9/94 and none at the NE Crater, see **figure 5.9**.

Allard et al. (1991) measured SO_2 and CO_2 concentrations at Mt. Etna over the period 1975 to 1989, using a combination of COSPEC, gas chromatography and IR spectrometry. For this period they estimated average SO_2 and CO_2 fluxes of ~4000 ± 800 and 35,000 ± 7000 t/d respectively. From their data I have derived an average CO_2:SO_2 mass ratio of ~12. Their reported CO_2:SO_2 mass ratios varied from ~26 (low activity, i.e. no ejecta) to ~8-9 (medium-high activity, i.e. mild to intense strombolian activity).

I estimated a CO_2:SO_2 mass ratio of ~17.5 for part of the 25/9/94 OP-FTIR data-set collected at the Bocca Nuova, see **figure 5.9**, during a period of quiet degassing (low activity). This ratio lies mid-way between the average and "low activity" values of Allard et al. (1991), supporting its validity. The large variation I encountered in the OP-FTIR data may be due to our ground-based technique detecting the large quantities of soil-gas emitted from the flanks of the volcano. Allard et al. (1991) reported that at heights of ~1.5 m above ground-level, CO_2 concentrations may be ~20 - 100 ppm above the atmospheric background level. Wind turbulence will chaotically mix emitted soil gases with the atmosphere, thus producing a wide range in the CO_2 concentrations detected and in the ensuing CO_2:SO_2 ratios.

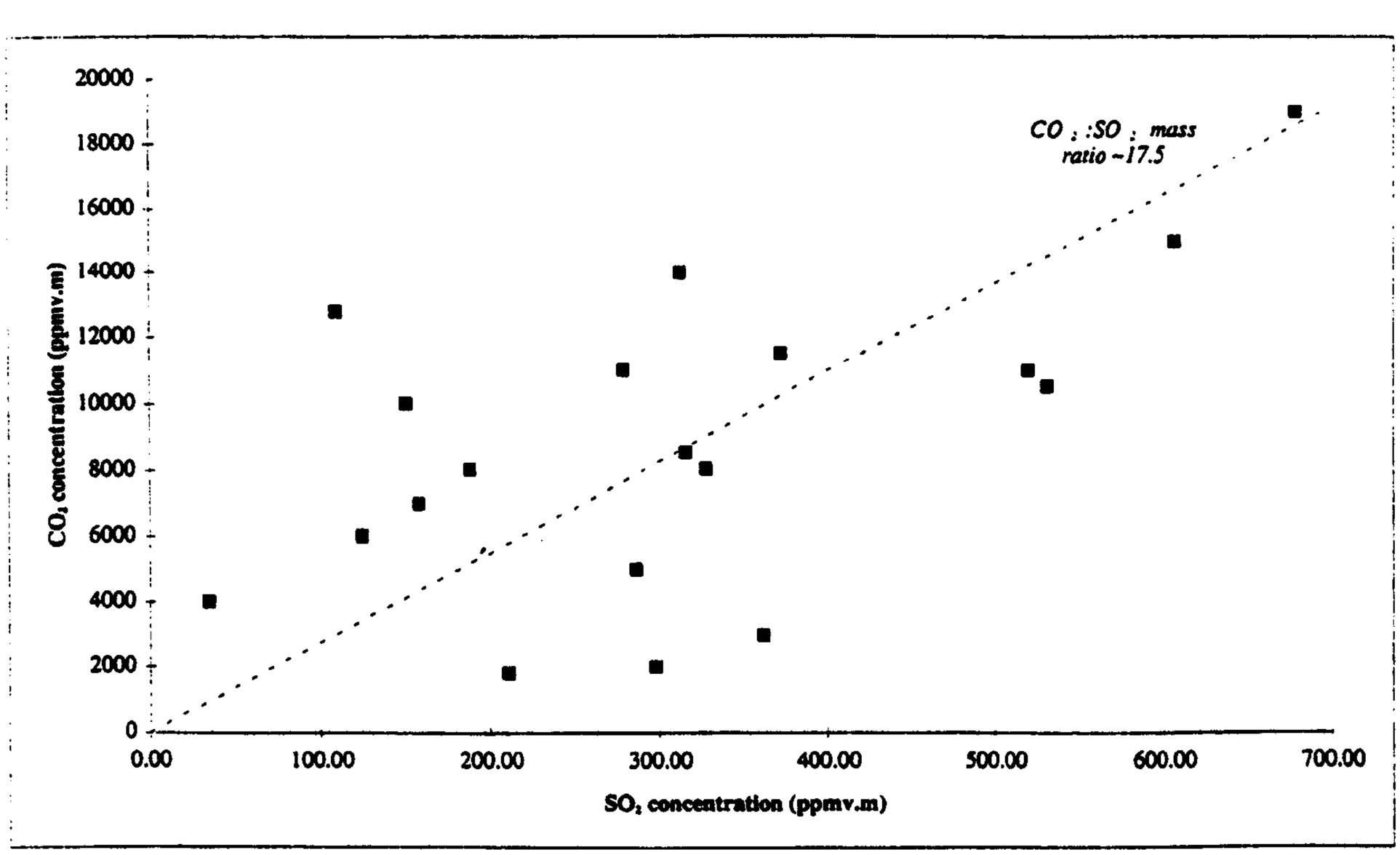

***Figure 5.9.** Plot showing relationship between CO_2 and SO_2 detected using OP-FTIR at Pizzi Deneri on 22/9/94. From the data I have derived a CO_2:SO_2 mass ratio of 17.5.*

I have also detected CO and N_2O in a few of the IR spectra we collected at Mt. Etna. N_2O is a constituent of the atmosphere and is normally present a very low levels, ~312 ppb

(Badr & Probert, 1990). For gases to be detected in absorbance spectra there has to be a difference in the concentrations of the background and sample spectra. N_2O and CO_2 should be homogenised throughout the atmosphere so any variations detected must either be of volcanic origin or from a local source, such as fires, exhausts or agriculture. On La Fossa, Vulcano, see Chapter 4, I attributed N_2O to an anthropogenic source, possibly industry or brush fires. The same may be true at Mt. Etna, although the analyses were carried out at much higher altitudes and at greater distances away from urban and vegetated/forested areas. I estimated the levels of N_2O and CO, where detected, to be very low, <70 ppb and <30 ppb respectively. Andres & Rose (1995) estimated CO concentrations in a diluted volcanic plume to be <20 ppb; similar to concentrations I have estimated using OP-FTIR. It is also possible that some of the exhaust fumes from either our Land-Rover or from passing tour-buses may have contaminated the optical path.

The detection of volcanic SiF_4

C. Chaffin, one of our co-workers, discovered the presence of SiF_4 in the volcanic plume at Mt. Etna (Chaffin et al., 1995, Francis et al., 1995 & 1996). Symonds et al. (1992) had previously estimated a concentration of SiF_4 in gases from Mt. Augustine, based on thermochemical calculations, and suggested it to be the 10th most abundant volcanic gas. SiF_4 is a common by-product of the reaction of volcanic HF with sample tubes and glassware used to collect volcanic gases; and had therefore never before been measured at a volcano. However, by using a remote-sensing technique, we were the first to directly measure the gas in a volcanic plume. I developed a technique for using HCl, HF and SiF_4 to estimate the equilibrium temperature of gases emitted from the La Fossa fumarole fields (Francis et al., 1996; Maciejewski et al., 1996), based on the relationships in Rosenberg (1973). I have applied this technique to the data we obtained from Mt. Etna in Section 5.3.5.

5.3.4 Discussion of results and observations

The variation in the SO_2:HCl mass ratios for the active OP-FTIR analyses at Mt. Etna are shown in **figure 5.10A**, which represents an approximate time-series throughout the sampling period. I have used 10-point moving averages to smooth out noise and to highlight the general trends in the data. For the 21/9/94 data-set there are too few data to determine anything more than a general downwards trend. The wide variation in mass ratios, ~2 - 6, might be caused by atmospheric effects or due to the mixing of gases from other craters. The larger data-set collected on 22/9/94 shows a much slower change in SO_2:HCl mass ratios; which vary between ~4.4 - 6.7. The fair weather on this day and gradual rate of change suggests that the changing ratios are a product of magmatic, rather than atmospheric, processes. Such a process may be the slow convective overturn of magma within the conduit, with cooler, degassed (and therefore denser) magma being replaced by more volatile rich material. It may also have been possible for gases from one of the other craters upwind, the Bocca Nuova or La Voragine, to have become incorporated into the optical path, thus subtly changing the gas ratios determined.

Figure 5.10A shows that OP-FTIR data collected on 25/9/94 exhibit a far wider range in gas ratios, <1 to >10. The concentrations of SO_2 and HCl are plotted against order of spectra collection in **figure 5.10B**. This shows that during periods of thick cloud and/or condensed plume, the HCl concentrations were much lower; giving higher SO_2:HCl mass ratios. The low concentrations recorded for spectra numbers 330 and over, coincided with a re-adjustment of the OP-FTIR set-up. The IR spectra collected during the cloud-free periods, spectra numbers ~220 - ~240, coincide with a maximum concentration of HCl and an approximate SO_2:HCl mass ratios of ~5.0; similar to ratios I derived for gases emitted from the NE Crater. In chapter 4, I attributed the higher SO_2:HCl ratios at La Fossa to the preferential solution of HCl in the hydrothermal system. Here I suggest the presence of thick cloud has caused HCl, which is ~10^6 times as soluble in H_2O as SO_2, to be dissolved and not detected by OP-FTIR; this is discussed below.

Atmospheric effects on gas ratios

The removal of SO_2 from volcanic plumes by the formation of SO_3 and SO_4^{2-} aerosols may have severe implications for those techniques, such as OP-FTIR and COSPEC that determine the concentrations of SO_2 at some distance away from the vent. Edner et al. (1994) reported that scavenging rates of SO_2 from Mt. Etna's plume were ~10^{-4} - $10^{-5}s^{-1}$, see Section 5.1.3. The removal of SO_2 can occur in several ways; I have highlighted three which can occur: photochemically in air; on the surface of dust particles; and in water droplets, **equations 5.2** to **5.4** respectively (after Möller, 1980).

$$SO_2 + 2O_2 \overset{+ hv}{\rightleftharpoons} SO_3 + O_3 \text{ } (SO_4 \text{ as intermediate}) \qquad \textbf{(5.2)}$$

$$SO_2 + 2{\bullet}OH \rightleftharpoons (HO)_2SO_2 \rightleftharpoons SO_4^{2+} + 2H^- \qquad \textbf{(5.3)}$$

$$SO_2 + 2H_2O \rightleftharpoons HSO_3^- + H_3O^+ \qquad \textbf{(5.4)}$$

HCl is ~10^6 times more soluble in H_2O than SO_2 at ambient temperatures and will therefore preferentially partition into any water droplets present in the volcanic plume or cloud, as described by **equation 5.5** (CRC, 1992). This results in the significant reduction of HCl concentrations detected during cloudy periods, see **figure 5.11B**.

$$HCl_{(g)} + nH_2O_{(l)} \rightleftharpoons HCl{\bullet}[H_2O]_{n\,(aq)} \qquad \textbf{(5.5)}$$

I have used the results of Fenton et al. (1980) and **equation 5.6** to estimate rates of wash-out of HCl from the plume; these are ~10^{-3} - $10^{-4}s^{-1}$, an order of magnitude faster than rates of SO_2 removal.

$$\Lambda = 5.15\times10^{-5} \times M^{-0.176} \times R^{0.773} \qquad \textbf{(5.6)}$$

where Λ= rate of HCl scavenging (s^{-1}), M= concentration of HCl (g/m^3) and R= precipitation rate (mm/h) (Fenton et al., 1980). The above scavenging rates are based on the effects of rainfall, rather than thick cloud. Scavenging in clouds will be more rapid, due to the greatly increased surface area:volume ratio of the many small droplets, which will facilitate HCl solution (Fenton et al., 1980).

I have attempted to estimate the amounts of HCl scavenging by approximating the density of drifting cloud droplets to a rainfall rate, based on volume of water passing a fixed point. For this I assumed: a starting HCl concentration of ~76 ppmv.m, see **table 5.5**; a cloud density of ten 0.1 mm droplets/cm^3; and 5.1 m/s wind speed; - estimations based on my personal observations at the Bocca Nuova on 25/9/94; general parameters in Fenton et al. (1980) and the wind measurements of Caltabiano (pers. com.). Using these parameters and **equation 5.6**, I derived an estimated scavenging rate, Λ, of ~$2 \times 10^{-3} s^{-1}$. Over distances of ~900 m, the OP-FTIR path length used, this suggests the removal ~40 - 50 % of HCl from the plume; similar to my estimate based on differences in SO_2:HCl mass ratio. **Table 5.6** shows how variations in the wind speed, cloud particle abundance (particles/cm^3) and particle size affect the estimates of amount of scavenged HCl; with scavenging increased with higher numbers of larger particles.

Factor	Factor varied:						
	Wind speed			Droplet size		Droplet density	
Wind speed (m/s)	**2.5**	**5.1**	**7.6**	5.1	5.1	5.1	5.1
Particle abundance (cm^{-3})	10	10	10	100	100	**100**	**1000**
Particle diameter (mm)	0.1	0.1	0.1	**0.1**	**0.05**	**0.01**	0.01
Λ = solution rate (s^{-1})	$2x10^{-3}$	$3x10^{-3}$	$3x10^{-3}$	$2x10^{-3}$	$3x10^{-3}$	$7x10^{-5}$	$4x10^{-4}$
HCl loss (%)	~40	~36	~33	~93	~41	~1	~7

***Table 5.6**. This illustrates how atmospheric factors, i.e: cloud particle size, particle abundance and wind speed can affect the rates of HCl scavenging by clouds; based on **equation 5.6** and HCl loss = $X_t = X_v \times e^{(-\Lambda \times t)}$; where X_t= HCl concentration at time t; X_i = HCl concentration at vent; Λ= scavenging rate; and t= time taken for plume to drift ~900 m, the OP-FTIR path length, (after Fenton et al., 1980; Oppenheimer et al., 1998 -in prep.). Numbers in **bold** show variations.*

For the 25/9/94 data-set I derived an average SO_2:HCl mass ratio of ~7.4; ignoring a scattering of data points that lay away from this value, see **figure 5.8C**. These had a much lower ratio of ~3.5 and related to the only cloud-free period. If it is correct to assume that the cloud-free period enabled us to collect the most representative data relating to unaltered gas ratios, the SO_2:HCl ratio is actually much lower, ~3.5, see **figure 5.8C**. This implies that ~50% of the HCl has been removed from the gas plume by the thick cloud within ~1 km of the vent.

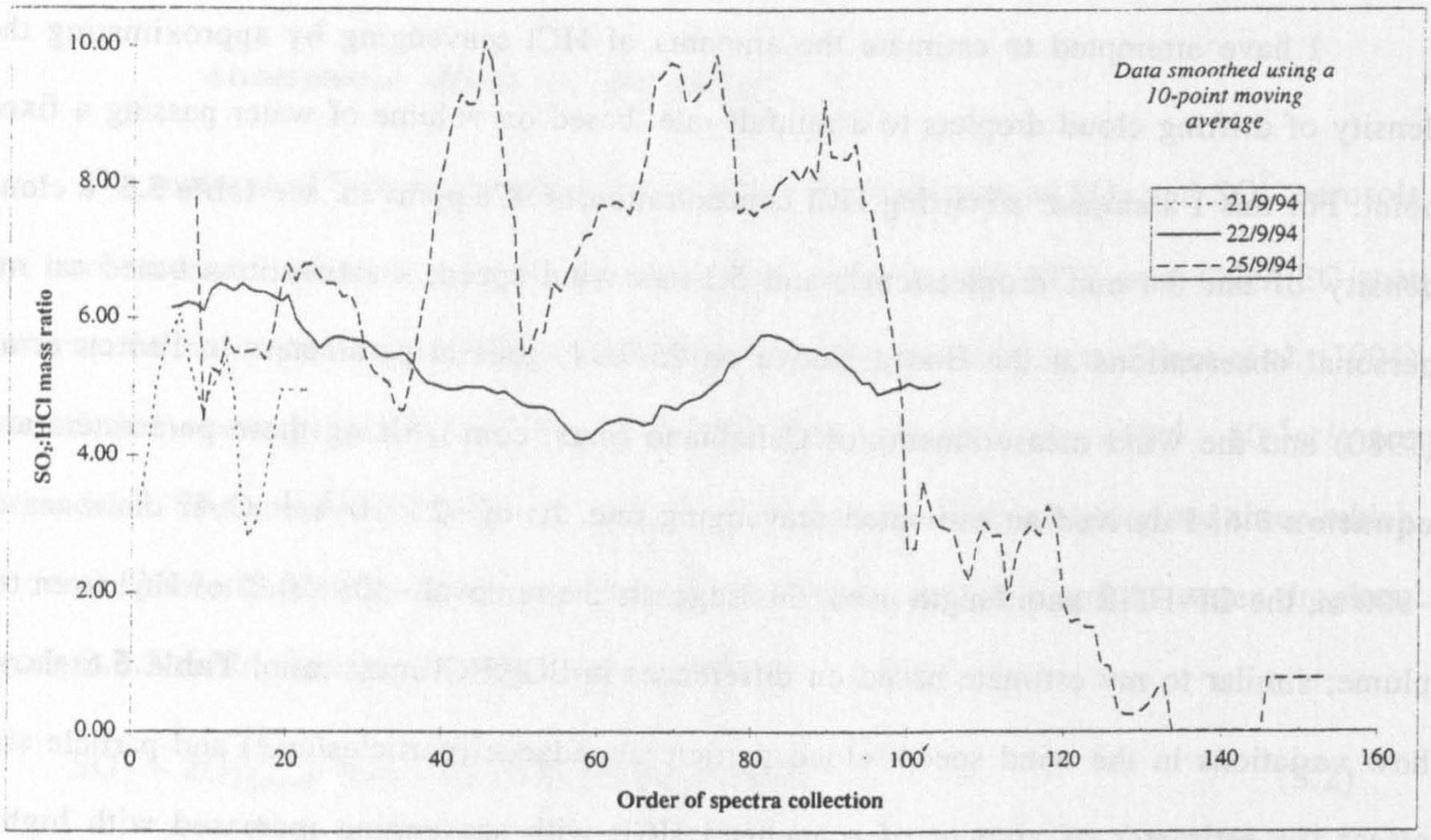

***Figure 5.10. A**. Plot showing variation in SO_2:HCl mass ratios with sample number. Data have been smoothed with a 10-point moving average to highlight major trends. The small but gradual variation with time of the 22/9/94 fine-weather data-set can be seen. The cloudy 25/9/94 data-set by comparison has a much wider variation in gas ratios possibly due to scavenging of HCl by water droplets - see text for discussion.*

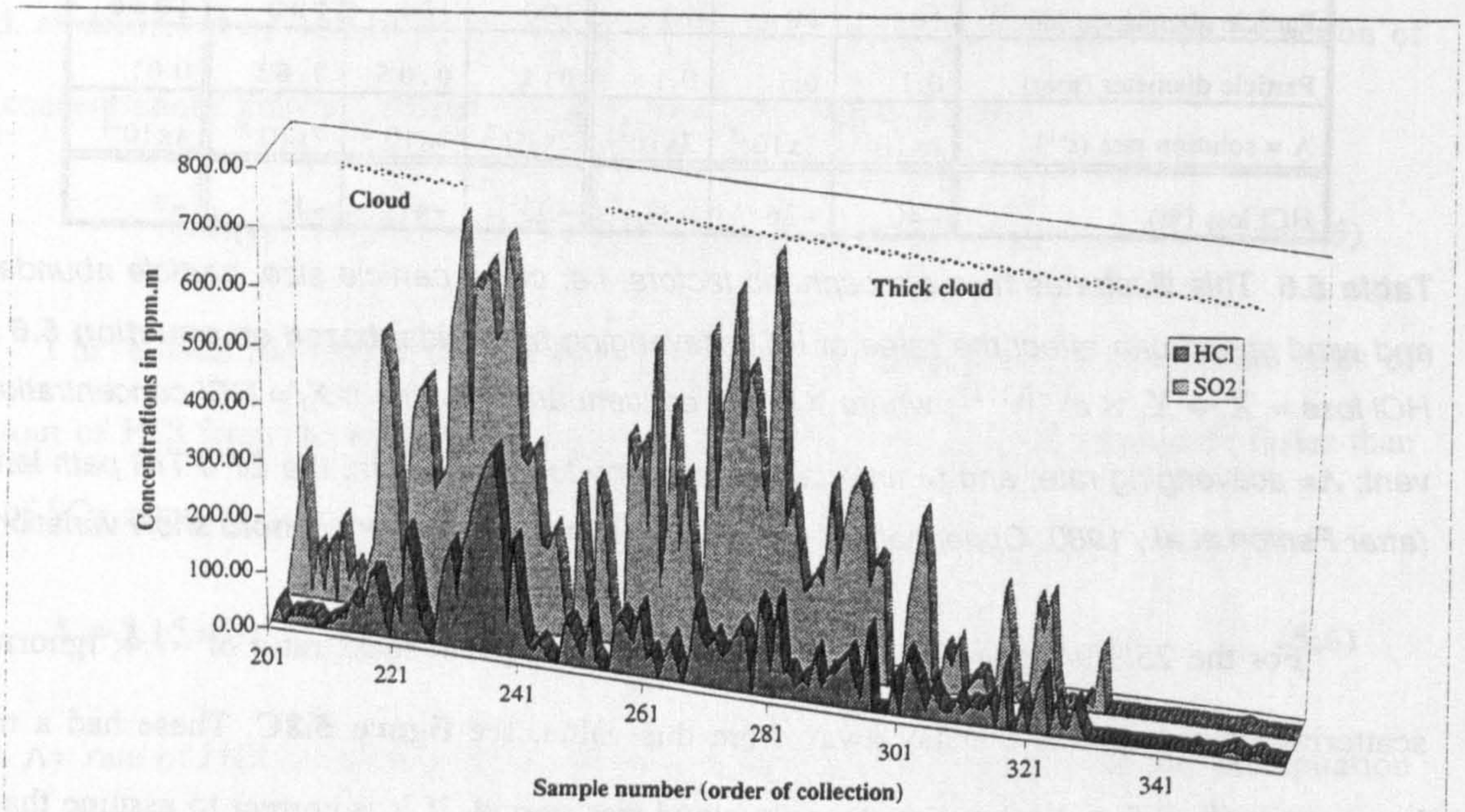

***Figure 5.10. B**. Variation in the concentrations of SO_2 and HCl against sample number. The variation of both analytes in concert relates to changes in the amount of plume passing through the optical path. Changes in only one analyte relate to the atmospheric effects, i.e. oxidation and solution. Note that the highest HCl concentrations coincide with a relatively cloud-free period.*

Our cloud-free OP-FTIR-derived SO_2:HCl mass ratio of ~3.5 agrees well with the filter data of Pennisi & Le Cloarec (1998); ~4.4 - 5.3 for the period 18/6/94 - 23/6/94.

Differentiating between the two opposing mechanisms of SO_2 and HCl removal with our OP-FTIR data is difficult. Using the arguments of Fenton et al. (1980) pertaining to the solution and scavenging of HCl in clouds, and the much higher solubility of HCl relative to SO_2, I infer that a significant proportion of the 25/9/94 OP-FTIR data-set has been affected by HCl solution. These results suggest that other data-sets, collected using remote techniques during periods of heavy cloud, may also contain discrepancies in gas ratios of possibly over 50%. This could have serious implications for the accurate monitoring of volcanoes using a remote technique where the target gas is highly soluble, i.e. HF or HCl.

5.3.5 SiF_4 on Mt. Etna: Its use in telethermometry

I have developed and refined a method of using OP-FTIR-derived molar HF:SiF_4 ratios to estimate the equilibrium temperatures of emitted gases (Francis et al., 1996). This enables an average temperature to be estimated from a safe distance, rather than by using temperature probes or a line-of-sight radiometer. The main arguments regarding the technique were discussed in Section 4.2.5 for estimations of gas temperatures from the fumarole field at La Fossa di Vulcano (Francis et al., 1996). I will therefore summarise the main points for the technique pertinent to Mt. Etna below.

A method for remote thermometry

We detected very low concentrations, <0.5 ppmv.m, of SiF_4 at Mt. Etna using the OP-FTIR technique. This is due to the dissipation of volcanic gases into the atmosphere and the inverse relationship between temperature and the concentration of SiF_4. The concentrations of SiF_4 and HF are related by the position of equilibrium in **equation 5.7** (Rosenberg, 1973):

$$SiO_2 + 4HF \rightleftharpoons SiF_4 + 2H_2O \qquad \textbf{(5.7)}$$

The equilibrium constant, K_{eq}, governs the rate at which HF reacts to form SiF_4. As discussed in Section 4.2.5, it is the change in K_{eq} with temperature, rather than the equilibrium position of **equation 5.7**, that controls the HF:SiF_4 ratio (Morgan, pers. com.). Honda & Mizutani, (1988) reported that at higher temperatures the rate of reaction is far slower; with K_{eq} ~1×10^2 at 600°C but ~1×10^{11} at 100°C, see Section 4.2.5.

Rosenberg (1973) suggested that the equilibrium temperature, T_{eq}, of the HF–SiF_4 system can be determined if the molar SiF_4:HF ratio; HF fugacity (fHF) and pressure are known. For a system such as Mt. Etna where there is an open conduit I have assumed that equilibrium is attained soon after leaving the magma surface; i.e. close to atmospheric pressures (Stevenson, 1993).

We could not measure HF concentrations in 1994 as we had not calibrated our OP-FTIR system to detect HF which has its fundamental absorbances at very high wavenumbers, >4200 cm^{-1}. I have therefore used HCl as a proxy for HF as we collected a large number of HCl concentration data. HCl, although less soluble in magma than HF, will behave chemically in a similar enough manner to be used as a proxy. I have derived molar F:Cl ratios from data reported by Carbonelle et al. (1982); Metrich et al. (1993); and Andres et al. (1993); these range between ~0.14 and ~0.47. Francis, Oppenheimer and Burton (pers. com.) collected OP-FTIR HF data on a return trip to Mt. Etna in October 1997 using an InSb IR detector. They derived HF:HCl volume ratios of ~0.20 - 0.24; similar to the average HF:HCl ratio of 0.29 I derived from other techniques. I combined the OP-FTIR-derived molar HCl:SiF_4 ratios of Francis et al. (1995) with HF:HCl ratios, to estimate the molar HF:SiF_4 ratios required to derive T_{eq}.

Carbonelle et al. (1982) reported an HF fugacity, or fHF, of 0.05 wt%; equivalent to log fHF = ~3.3. Andres et al. (1993) reported a similar HF fugacity of ~1200 ppm, or log fHF = ~2.9, derived from particulate analyses. Symonds et al. (1988) estimated an HF fugacity of log fHF = -3.3, equivalent to ~500 ppm or a partial pressure of 5×10^{-4} atm. **Figure 5.11** shows the variation of T_{eq} within a range of log fHF values and the relationship between HF/SiF_4 and T_{eq}. I have calculated T_{eq} using the exponential **equations 5.8, 5.9** and **5.10** relating to log fHF.= -2, -3 and -4 respectively; with results summarised in **table 5.7**.

$$T_{eq} = 205.53 \times e^{\left(0.2459 \times \log\left(\frac{HF}{SiF_4}\right)\right)} \quad \textbf{(5.8)}$$

$$T_{eq} = 149.03 \times e^{\left(0.1908 \times \log\left(\frac{HF}{SiF_4}\right)\right)} \quad \textbf{(5.9)}$$

$$T_{eq} = 102.12 \times e^{\left(0.1736 \times \log\left(\frac{HF}{SiF_4}\right)\right)} \quad \textbf{(5.10)}$$

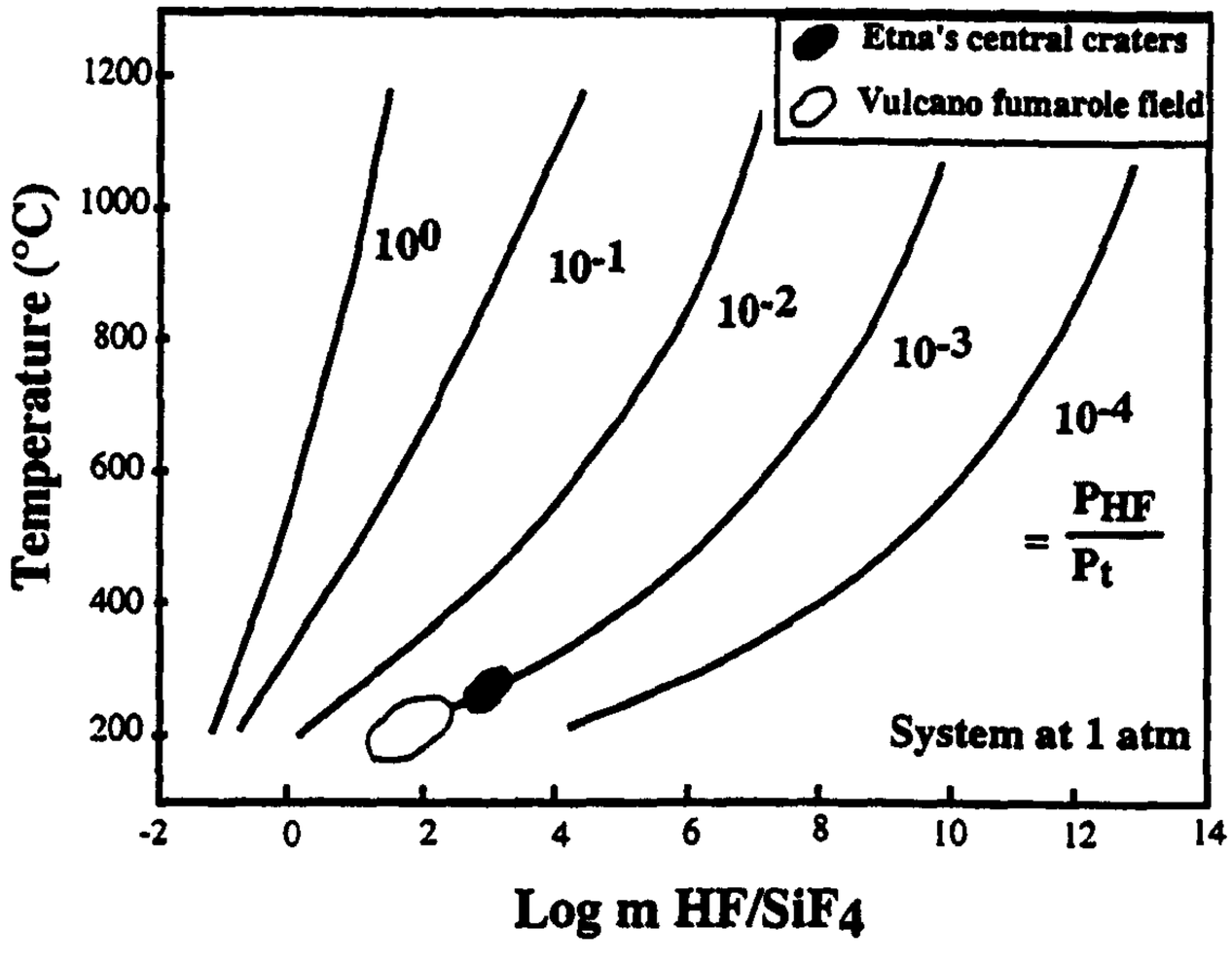

Figure 5.11. *Plot showing the relationship between HF fugacity; HF:SiF_4 molar ratio and temperature at 1 atmosphere pressure (after Rosenberg, 1973). The field for OP-FTIR analyses conducted on 22/9/94 and 25/9/94 are shown; as is the field I have estimated for La Fossa di Vulcano for comparison. The low T_{eq} of 25/9/94, <300°C, may be due to removal of a large proportion of the HCl by clouds thus reducing the estimated HF:SiF_4 ratio.*

Discussion of results

The results of the author's investigation into T_{eq} for the NE Crater and Bocca Nuova gave temperatures ~20 - 50°C above those measured by Oppenheimer (pers. com.) and Harris (pers. com.) in 1994. Recalculation of temperature data to account for ~50% HCl removal on 25/5/94 gave a higher temperature of ~290°C. The equilibrium temperatures in **table 5.7** are far below the magmatic temperatures. Volatiles which leave the magma surface within the conduit undergo re-equilibration as they cool and rise towards the vent. The temperatures calculated correspond to the final equilibrium temperature before the gas is emitted; which may be hotter than the gas temperatures measured at the surface. Carapezza et al. (1981) and

Tedesco et al. (1991) noted a similar disparity between the calculated equilibrium temperatures and those measured at La Fossa di Vulcano, see Section 4.2.6.

OP-FTIR observations			Equilibrium temperature			Temperatures measured using a radiometer on:		
			$fHF = 10^{-4}$	10^{-3}	10^{-2}	25/9/94	14/10/94	
Date	Location	Path (m)	Minimum	Expected	Maximum	Max.	Min.	Max.
22/9/94	NE Crater	900	180	290	460	–	39	246
25/9/94	Bocca Nuova	900	160	250	390	~212	47	173
Recalculated - assuming ~50% loss in HCl - see earlier								
25/9/94	Bocca Nuova	900	180	290	460	~212	47	173

Table 5.7. *Summary of results of the attempt to calculate T_{eq} from average HCl and SiF_4 data collected on 22/9/94 and 25/9/94 at Pizzi Deneri and the Bocca Nuova respectively, see* ***table 5.5****. An HF fugacity (fHF) of ~10^{-3} is expected from an open volcanic system (Symonds et al., 1988). Indications show that the system in the NE Crater is possibly hotter than the Bocca Nuova; this is corroborated by temperature measurements taken by Harris (pers. com.)on 14/10/94 at the craters.*

The inverse relationship between SiF_4 concentration and T_{eq} cause the hottest gases to have SiF_4 concentrations close to, or below the detection limits of the OP-FTIR system. Rosenberg (1973) reported that HF:SiF_4 molar ratios of a fumarole at ~400°C are ~1×10^4 times greater than an equivalent fumarole at ~200°C. The relatively high SiF_4 concentrations emitted from low temperature fumaroles/vents will therefore effectively drown out any high temperature HF:SiF_4 ratios; thus estimated temperatures tend to reflect the cooler gases. A reduction in the levels of SiF_4, effectively an increase in HF:SiF_4 ratio, will reflect the increase in temperature of the fumarole or vent. The HF–SiF_4 equilibrium system can therefore be used alongside OP-FTIR to remotely monitor temperature changes. Indeed, Love et al. (1998) used the OP-FTIR technique in 1997 to measure and derive temperatures from SiF_4 for eruptions at Popocatepetl, Mexico.

HCl, CO_2 and SiF_4 fluxes determined from OP-FTIR data

Caltabiano used COSPEC to measure SO_2 fluxes at Mt. Etna during the period of our OP-FTIR analyses; these were 6742 t/d and 5404 t/d for 22/9/94 and 23/9/94 respectively. This is higher than the 20 year average SO_2 flux of 4762 t/d as calculated from published data by Maciejewski et al. (1996). I have estimated the fluxes of HCl, CO_2 and SiF_4 by combining COSPEC SO_2 flux data with simultaneous OP-FTIR-derived gas mass ratios, see **table 5.7**. The large variation in HCl fluxes as observed at the Bocca Nuova on 25/9/94 is due to the uncertainty in the true SO_2:HCl ratio; due to heavy cloud scavenging HCl from the plume. The CO_2 flux data has been estimated from a small portion of the 22/9/94 data-set which gave a usable CO_2:SO_2 mass ratio of ~17.5, see Section 5.3.3.

I have estimated an annual HCl flux of $\sim 3.7 \times 10^5$ t/y using the 20-year average annual SO_2 flux reported in Maciejewski et al. (1996), 4762 t/d, and the average SO_2:HCl mass ratio, ~4.7. This is >3% of the global volcanic chlorine flux and ~20% of the global anthropogenic flux (after Andres et al., 1993) and therefore considerably affects the background levels in the local atmosphere. The HCl fluxes in **table 5.7** are lower than those of Francis et al. (1995). This is due to Francis et al. (1995) incorrectly using gas volume ratios, rather than mass ratios when deriving fluxes from COSPEC data.

Date	Location	SO_2 flux t(/d)	CO_2 flux (t/d)	HCl flux (t/d)	SiF_4 flux (t/d)
21/9/94	Pizzi Deneri	~*6000	#nd	~1220	#nd
22/9/94	Pizzi Deneri	~6742	§~118,000	~1250	~1.6
25/9/94	Bocca Nuova	~*6000	#nd	~810 - ~1800	~7.5

Table 5.8. *Flux data calculated using COSPEC derived SO_2 fluxes and OP-FTIR-derived mass ratios (Caltabiano, pers. com.). #nd = not determined, *estimated SO_2 flux.; §estimated from a small portion of the 22/9/94 data-set.*

Andres et al. (1993) estimated the flux of all fluorine species to be 160 t/d. Unpublished 1997 OP-FTIR data, provided by Francis, Oppenheimer and Burton (pers. com.), give average SO_2:HF mass ratios of ~38 - 50. Combining these ratios with the SO_2 flux in **table 5.8** gives an HF flux of ~135 - 177 t/d; similar to the total fluorine flux of Andres et al. (1993). I have estimated that SiF_4 comprises only a small percentage, <2%, of the total

fluorine flux; equivalent to ~0.03% of the global anthropogenic flux (after Andres et al., 1993).

Summary of OP-FTIR results

The use of OP-FTIR at Mt. Etna by Francis et al. (1995 & 1996) and the author has enabled us to estimate SO_2:HCl mass ratios of gases exsolved from the magma beneath the summit craters. These ratios ranged between ~3.5 - ~7.4 and depended on both climate and crater. I determined SO_2:HCl ratios for gases emitted from the NE Crater of ~4.9 - 5.8, which, according to Pennisi & Le Cloarec (1998), relates to a combination of deep and shallow degassing. The SO_2:HCl mass ratios I estimated for 25/9/94 at the Bocca Nuova are harder to interpret. It is possible ~50% of the HCl was scavenged from the plume by the thick cloud present during the analyses.

I have used molar HF:SiF_4 ratios to estimate equilibrium temperatures for volcanic gases. Francis et al. (1995) did not collect any HF concentration data in 1994 and so I have used HCl as a proxy for HF and derived an average HF:HCl molar ratio of ~0.29 from published data. OP-FTIR investigations by Francis, Oppenheimer and Burton (pers. com.) in 1997 have since validated this technique by deriving a molar HF:HCl ratio of ~0.20 - 0.24. I estimated equilibrium temperatures to range between ~250 and ~290°C for the Bocca Nuova and NE craters respectively; compared to maximum temperatures measured by Harris (pers. com.) of 173 and 246°C respectively. Recalculating T_{eq} assuming a loss of ~50% HCl for 25/9/94 gave a higher temperature of ~290°C. The disparity between T_{eq} and measured temperatures can be explained by further cooling after the last re-equilibration of the emitted gases.

I estimated fluxes of HCl and SiF_4 of ~800 - 1250 t/d and 2 - 8 t/d respectively, using simultaneous COSPEC and OP-FTIR data. By using the average annual SO_2 flux reported in Maciejewski et al. (1996) I estimated an annual HCl flux of ~3.7×10^5 t/y, equivalent to ~20% of the global anthropogenic chlorine flux.

5.4 Conclusions

5.4.1 Technical aspects

A number of remote sensing techniques have been used on Mt. Etna, including: COSPEC, DIAL, DOAS and OP-FTIR. The bulkiness and limited applicability of the DOAS and DIAL techniques as they stand have resulted in their being of limited use for investigating volcanic gases. COSPEC, although only being able to measure SO_2 is a simple and portable system. Variations in cloud-cover and wind speed can give rise to errors of up to ~45% in COSPEC-derived SO_2 fluxes.

OP-FTIR simultaneously measures a wide range of IR frequencies and is best used for determining gas ratios as these are generally independent of the effects of plume dilution and atmospheric conditions. I have shown, however, that the measurement of highly soluble gases, such as HF and HCl, can be affected by rain and/or cloud. Such gases are rapidly taken out of the gas phase into solution and therefore will not contribute to the gas-phase HCl absorption of IR radiation detected by the OP-FTIR technique. Other atmospheric effects include the oxidation of gases and the formation of aerosols, either photochemically, or on dust or water particles. The rates of atmospheric-plume interactions vary from $<10^{-3}$ s^{-1} for HCl solution (Fenton et al., 1980) to $>10^{-5}$ s^{-1} for SO_2 oxidation (Edner et al. 1994).

A variety of natural IR sources were used for OP-FTIR analyses. Low temperature sources, such as sun-heated ash and fumarolic ground proved too cool to emit enough the high frequency radiation required for analysis of HCl. The portable 1275°C artificial IR source was therefore used for ~300 active analyses. The use of solar and sky backgrounds also proved problematic due to emission bands which prevented data being readily analysed. We used an MCT detector in 1994 which has a peak sensitivity at ~770 cm^{-1}. and was not calibrated to detect HF. A later investigation in 1997 by Francis, Oppenheimer and Burton (pers. com.) detected HF using an InSb detector; which has a peak sensitivity at ~2130 cm^{-1}.

The technical aspects of this chapter can therefore be summarised as:

- OP-FTIR and COSPEC are the two techniques most suited to volcanological applications due to their portability, ease of use and, for OP-FTIR, the wide range of gases that can be analysed simultaneously.
- The use of natural IR sources for passive OP-FTIR analyses is entirely dependant on their temperature. If the IR source is too cool it will not radiate enough high frequency radiation to enable lighter gases, such as HCl and HF, to be detected.
- OP-FTIR analyses of soluble gases cannot be performed during periods of heavy cloud or rain as these analytes are rapidly scavenged from the plume.
- The simultaneous use of COSPEC and OP-FTIR enables fluxes for a range of analytes to be estimated.

5.4.2 Scientific implications

High gas emission rates have been linked to periods of eruptive activity by several authors. To study this, I compared COSPEC-derived SO_2 fluxes with those I calculated from effusion-rate data for the 1991 - 1993 eruption. In my calculations I have assumed a constant amount of sulphur is degassed per unit volume of magma throughout the eruption. Generally the two sets of data, measured and calculated, match well; indicating that the total gas flux is proportional to the amount of lava erupted. I observed differences between the measured and calculated fluxes at the beginning and end of the first and last magma pulses reported by Bruno et al. (1994); the second pulse being missed due to paucity of effusion rate data. I have inferred that at the end of each magma pulse, the drainage of degassed magma from the summit areas into the eruptive fissure led to a higher calculated gas flux as degassed material was erupted. The lowering of the magma levels also coincided with periods of crater collapses. As a new magma pulse rose up into the system, it expelled any degassed magma still residing in the system. This was accompanied by increases in summit activity and ground deformation

but little change in gas flux. Only once the new magma had begun to be erupted did the measured gas fluxes reflect the ones I had calculated.

Pennisi & Le Cloarec (1998) proposed a two-stage degassing model. Low SO_2:HCl mass ratios, <1, related to the deep degassing, >4 km depth, of mainly chlorine, H_2O and CO_2 during non-eruptive periods. Shallow degassing during eruptive periods represents the exsolution of remaining H_2O and most of the SO_2; giving a higher SO_2:HCl mass ratio of ~10. The collection of filter data has indicated a general increase in S:Cl ratio of gases emitted from the summit craters since 1993. This is indicative of the reactivation of the volcano after the 1991 - 1993 eruption. The different composition of gases emitted from each of the summit craters relates to their different plumbing systems. Studies using short-lived isotopes have indicated that the SE Crater has no direct link to the magma chamber but lies along the Southern rift zone. It therefore does not emit gases exsolved during deep degassing, and receives only material that has first passed through the summit chambers and thus is partially degassed. Consequently gas ratios measured at the SE Crater are somewhere between the ratios associated with the deep and shallow degassing processes.

I have used OP-FTIR to investigate the SO_2:HCl mass ratios in gases emitted from the Bocca Nuova and NE Crater. Gas ratios at the NE Crater varied little during periods of fair weather, generally ranging between ~4.4 and 6.7. During periods of intermittent plume the spread of data increased to ~3 - 6. I propose that the analyses conducted through heavy cloud at the Bocca Nuova have lost ~50% of the emitted HCl by solution into water droplets. I have estimated a solution rate for HCl of $\Lambda \approx 10^{-2}\ s^{-1}$ based on the equations of Fenton et al. (1980); relating to a loss of ~50% HCl over ~1 km, similar to that I estimated from gas ratio data. I have estimated a minimum fine-weather SO_2:HCl mass ratio of ~3.5 which is in keeping with the OP-FTIR data from the NE Crater.

I have used the presence of SiF_4 in the gas plume to estimate an equilibrium temperature of the emitted gases. This is ~290°C for both the NE Crater and Bocca Nuova, assuming the loss of ~50% HCl. This estimate is higher than the measured surface temperatures indicating that the equilibrium is frozen into the gases before being vented into the atmosphere. This temperature is a minimum estimate as the hotter gases cannot be

analysed for SiF_4 as it is present at concentrations too low to be detected using the OP-FTIR technique.

I have used the simultaneous COSPEC and OP-FTIR analyses on 22/9/94 to estimate fluxes of CO_2, SO_2, HCl and SiF_4; these were: ~128,000, 6742, ~1250, and ~1.6 t/d respectively. The high HCl flux is ~20% of the annual anthropogenic chlorine flux; based on a 20-year average SO_2 flux of 4762 t/d (Maciejewski et al., 1996).

The scientific aspects of this chapter can be summarised as follows:

- COSPEC analyses conducted during periods of lava effusion can be used to monitor the passage of volatile and degassed magma through the magmatic system.
- Inclusion data, filter analyses and our OP-FTIR analyses all support the two-stage degassing model of Pennisi & Le Cloarec (1998); which suggests that chlorine is principally exsolved at >4 km during deep degassing, whilst SO_2 is exsolved much closer to the surface during shallow degassing. The non-eruptive/background gas flux is provided by deep degassing with shallow degassing occurring during eruptive periods.
- Average OP-FTIR-derived SO_2:HCl mass ratios are ~4.9 - 5.8 at the NE Crater. Heavy cloud removed ~50% of the HCl from the Bocca Nuova's plume giving a higher ratio of ~7.4; an estimated original gas ratio being ~3.5. The lower ratio at the Bocca Nuova is consistent with gases being primarily sourced from deep degassing.
- The use of the SiF_4–HF system for telethermometry gave an estimated equilibrium temperature of ~290°C at both the Bocca Nuova and NE Crater. This is higher than vent temperatures recorded by radiometer indicating that the gas equilibrium is set before the gas has been vented.

Chapter 6.

The Soufrière Hills volcano, Montserrat, W.I.

6.1 Introduction

6.1.1 Introduction to chapter

This chapter describes the methodology and problems associated with two terrestrial remote-sensing techniques: Correlation Spectroscopy (COSPEC) and Open-path Fourier Transform Infrared Spectroscopy (OP-FTIR). These were used by the author to monitor the activity at Soufrière Hills volcano, Montserrat, during the period 6/5/96 - 6/6/96. I will discuss COSPEC and OP-FTIR data from this period, as well as that collected by the Montserrat Volcano Observatory (MVO) between July 1995 and December 1997, with the aim of establishing a relationship between rates of gas emission and lava effusion. The chapter is divided into five main sections:

6.1. An introduction to Montserrat, volcanic history of the island and review of the current eruption, with a general description of the monitoring effort. I shall also review the initial activity at Mt. Unzen as this has been used as an analogue for the current Soufrière Hills eruption by the MVO.

6.2. The use of COSPEC on Montserrat as part of the monitoring effort. The background, analysis techniques and results will be discussed, as will the data's relevance to the Mt. Unzen analogue.

6.3. The use of OP-FTIR as an experimental technique for determining plume compositions. I will discuss the methodology and results and whether gas compositions can be related to those at Mt. Unzen.

6.4. COSPEC and OP-FTIR observations will be combined with the results of geophysical and petrologiocal investigations by MVO scientists to produce a general model of the magmatic processes ongoing at Soufrière Hills volcano. I also propose that South Soufrière Hills may be a more accurate magmatic analogue to the current eruption than Mt. Unzen.

6.5. Conclusions to chapter. These can be summarised as:

- OP-FTIR derived SO_2:HCl ratios of $<0.5 \pm 0.2$ were much lower than at other volcanoes discussed in this thesis. High errors are due to the very low levels of analyte gases detected; although these low values may be partially due to removal of SO_2 by oxidation to SO_4. The low COSPEC-derived SO_2 flux during early - mid 1996 also supports the view that the magma was partially degassed.

- Petrological investigations indicate that magma resided at ~7 - 15 km depth and cooled, giving >35% phenocrysts. Reactivation by a basaltic magma has lead to this being erupted at the present time.

- Discrepancies between SO_2 flux, analysed magmatic volatiles and effusion rate have led the author to propose that a significant proportion (~50%) of the sulphur degassed must come from the deeper basaltic magma, rather than the erupted andesite.

6.1.2 Remote-sensing of gaseous emissions from Soufrière Hills volcano

The use of the OP-FTIR system on Montserrat was funded by the Overseas Development Administration (ODA) to complement the COSPEC investigations being conducted by the MVO as part of the general monitoring effort. The use of the technique on an inaccessible volcano capable of generating pyroclastic flows was experimental and the mixed results of the investigation bear this out, see Section 6.3. The author also conducted COSPEC analyses for ~3 weeks as part of MVO's "Team COSPEC" during late May and early June 1996. Using the results from the COSPEC and OP-FTIR investigations, I have elucidated

some of the fundamental characteristics of the degassing and magmatic processes at Soufrière Hills volcano; these are discussed in Section 6.4.

6.1.3 Geological background to the Soufrière Hills volcanic crisis

General geology

The volcanic island of Montserrat, one of the Leeward Islands, lies within the northern part of the Lesser Antilles island chain. Montserrat is composed of a series of volcanic centres of andesitic composition, the only exception being South Soufrière Hills which contains both basaltic and andesitic lavas (Rea, 1974). The active volcanic centres have generally moved from the northern to the southern part of the island, with the current activity centred at Soufrière Hills, see **figure 6.1A**. The main volcanic centres, in stratigraphic order are:

The Bugby Hole - Harris Centre: This is the oldest volcanic centre dated, ~4.31 ± 0.22 Ma (Rea, 1974), and is composed of two-pyroxene andesitic lava, agglomerates and pumice fall deposits.

Silver Hill Centre: Rea (1974) reported that the complex had been dated at ~1.55 Ma and has experienced a high degree of erosion (Wadge & Isaacs, 1988; Shepherd et al., 1971). Petrologically it is composed of two-pyroxene andesitic tuffs and agglomerates (Shepherd et al., 1971).

Centre Hills: Shepherd et al. (1971) reported an age for this complex of ~4.3 ± 0.3 Ma; although this age may actually relate to the Bugby Hole Centre. It is also substantially eroded; the petrology of the complex being two-pyroxene andesite tuffs and agglomerates. Garibaldi Hill is a small, undated, volcanic dome with a similar composition to the Centre Hills and thus may have been a parasitic vent linked to Centre Hills (Rea, 1974).

South Soufrière Hills: The southern part of Montserrat is the only part of the island to have erupted olivine-basalt lavas and pyroclastics (Shepherd et al., 1971), see Section 6.4.2. Within the mainly andesitic complex there are at least two series of basaltic lava flows; one of which has been suggested by Rea (1974) to possibly be contemporaneous with the middle

zone of the White River Pyroclast fall series. This series is initially andesitic, being composed of block falls; andesite-based lahars and ash and lapilli falls; and basic-andesite rock falls. The series then conformably grades up into basaltic scoriae and basaltic cinder beds, possibly associated with basaltic lava flows (Rea, 1974). Rea (1974) interpreted this sequence as the progressive emptying of a fractionated magma chamber. Deposits within South Soufrière Hills have been dated at ~0.9 - 1.8 Ma (Wadge & Isaacs, 1988).

Soufrière Hills Complex: This is the highest and youngest volcanic complex on the island and is the site of the current volcanic activity. The complex is composed of a number of andesitic domes with associated andesitic block and ash flows; pyroclastic surges; and lahars mantling its flanks (Chiodini et al., 1996). Three compositional variations were reported by Rea (1974): two-pyroxene andesite - the domes of Gage's and Perche's Mountains; hypersthene-hornblende andesite - the domes of Chance's Peak and Galway's Mountain; and hornblende-hypersthene andesite - the Castle Peak dome. The similarity between the hypersthene-hornblende andesitic pumices of St. George's Hill and those on Soufrière Hills has led Rea (1974) to suggested that the St. George's Hill was a late-stage parasitic centre of the larger Soufrière Hills complex.

The effect of regional structure on volcanism

The alignment of the most recent volcanic centres: Raspberry Hill (South Soufrière Hills); Garibaldi Hill; St. George's Hill; Gage's Mt., Perche's Mt., Chance's Peak, Galway's Mt and Castle Peak domes form a narrow, ~2 km, ESE - WNW band across the southern part of Montserrat. Sparks (MVO report, 1996) has interpreted this to be a zone of preferential magma transport. Davies & Rymer (1998, in prep) have attributed Bouger gravity anomalies across this narrow zone to the presence of a half graben. Graben formation may reflect the transtensive environment as hypothesised by Sparks (MVO report, 1996) and Aspinall et al. (1998, in press). It is within this graben, oriented ~SE - NW, as inferred from the SE - NW alignment of the volcanic centres, that the current Soufrière Hills eruption is located.

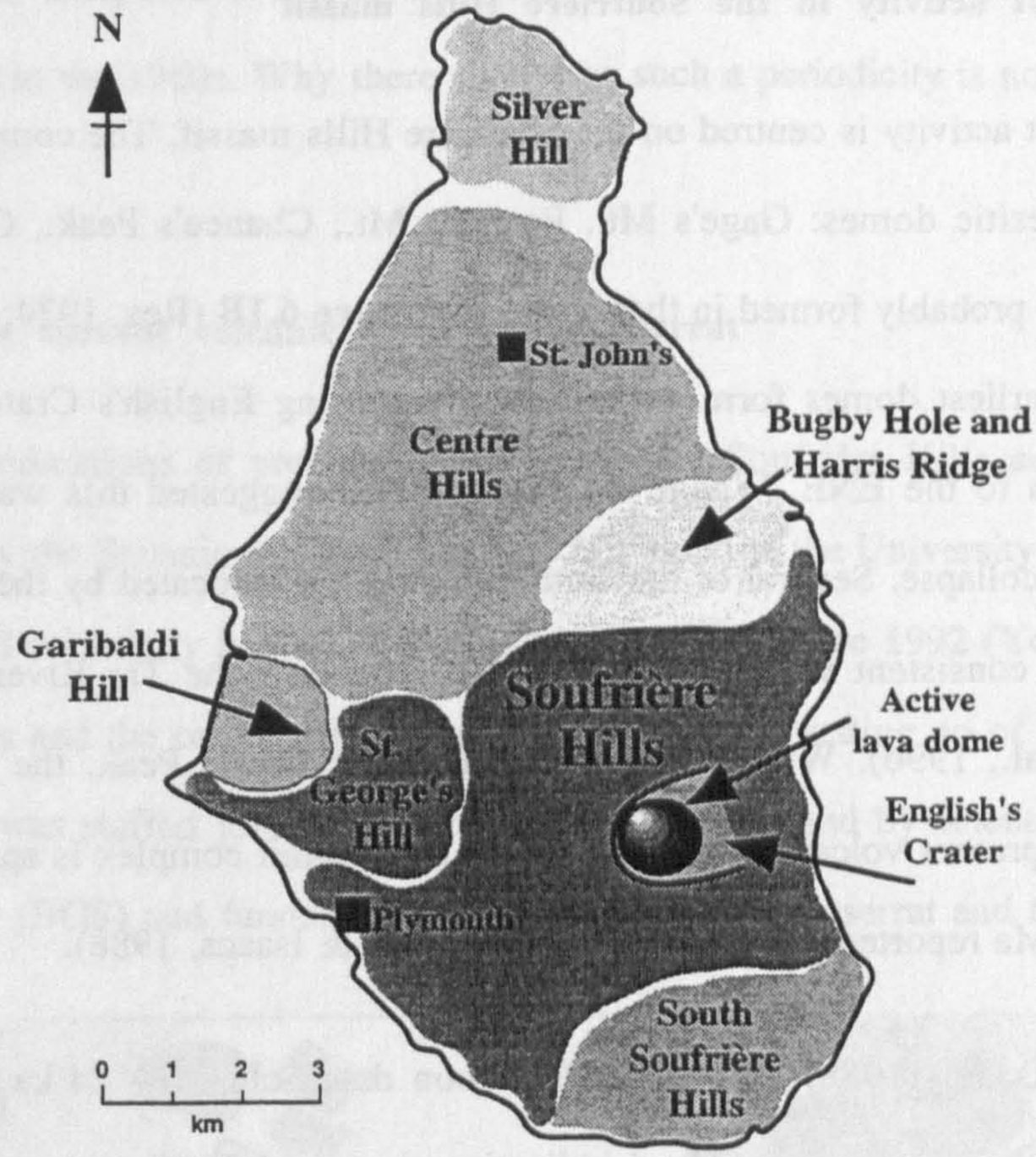

***Figure 6.1. A**. Map of the island of Montserrat showing the volcanic centres that have formed through time. The pre-existing domes of Soufrière Hills volcano are also shown as is the position of the current active dome (after Wadge & Isaacs, 1988).*

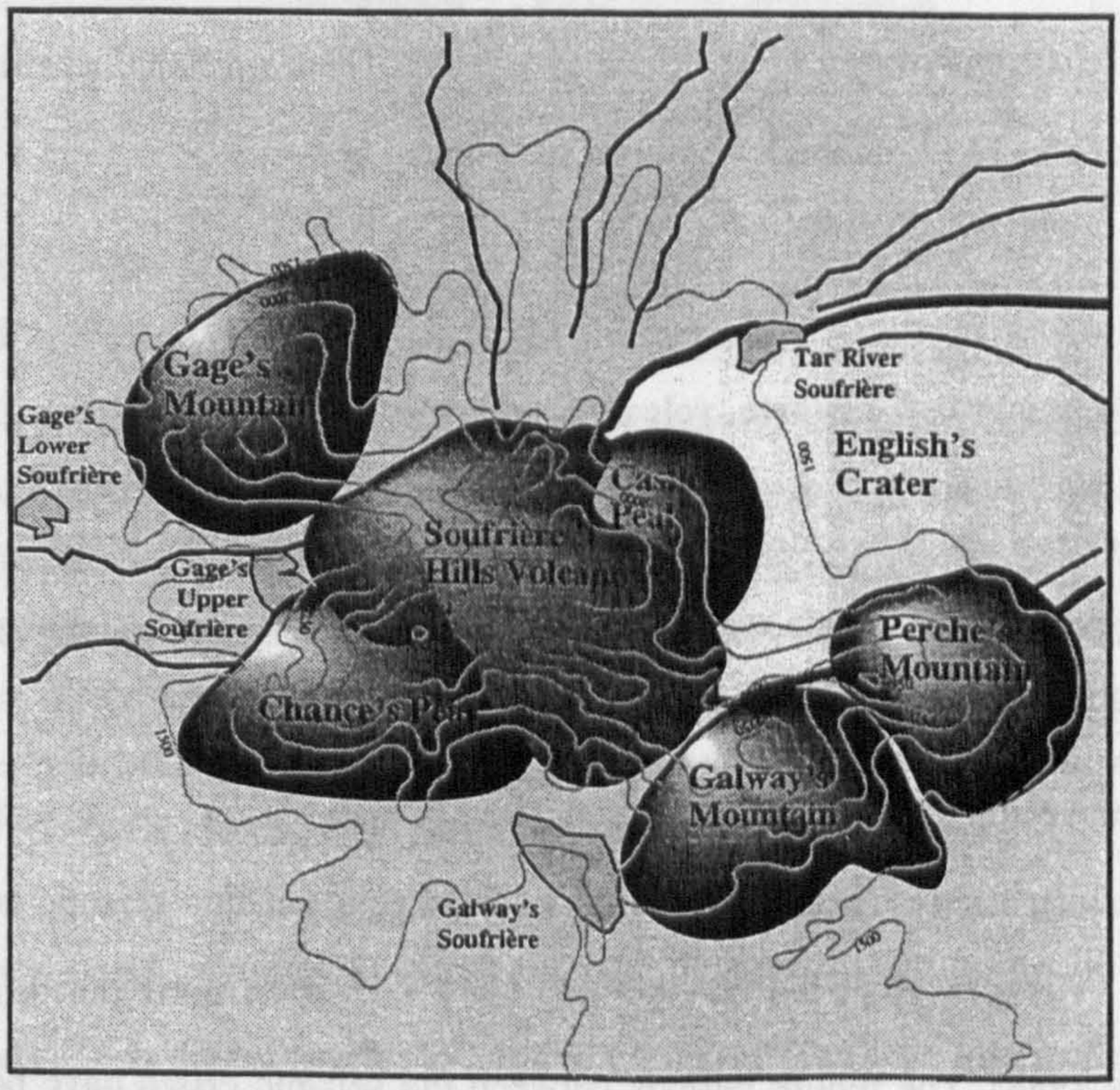

***Figure 6.1. B**. Enlargement of **A** showing the active dome and the area around English's Crater.*

Past activity in the Soufrière Hills massif

The current activity is centred on the Soufrière Hills massif. The complex consists of a series of five andesitic domes: Gage's Mt., Perche's Mt., Chance's Peak., Galway's Mt. and Castle Peak, which probably formed in that order, see **figure 6.1B** (Rea, 1974; Wadge & Isaacs, 1988). The four earliest domes form a horse-shoe enclosing English's Crater, a large crater ~1 km across open to the ENE. Wadge & Isaacs (1988) suggested this was the result of a Bezymmiany-type collapse. Several of the summit domes are truncated by the crater walls and hummocky terrain consistent with a collapse can be found in the Tar River - Spring Ghaut area (Chiodini et al., 1996). Within English's Crater lies Castle Peak, the last dome to be erupted before the present volcanic crisis. Dating of the summit complex is sparse with a K-Ar date of 1.1 ± 0.25 Ma reported for Chances Peak (Wadge & Isaacs, 1988).

Wadge & Isaacs (1988) reported radiocarbon dates of ~16 - 24 ka for near-surface outcrops in the southern half of the island indicating a period of volcanic activity occurred at this time. Weakly developed soil horizons between some of the fall deposits indicate that during this period eruptive activity was intermittent rather than continuous (Wadge & Isaacs, 1988). The most recent radiocarbon date reported by Tomblin (1966: in Rea 1974) was 1646 ± 54 A.D. from below the Castle Peak dome. This relates to the last period of eruptive activity and the extrusion of the Castle Peak lava dome. This probably predated the earliest settlers, who landed in 1632, as there was no record of the eruption.

Summary of historic volcanic activity

In comparison to the long and well documented eruptive history of the Italian volcanoes, that of Soufrière Hills volcano is very short; Montserrat having been settled by Europeans in 1632. It is likely that the last eruption of Castle Peak, dated at 384 ± 54 years ago, was just before the island was colonised (Rea, 1974). No eruptive activity has been documented in historic times. There have, however, been four volcano-seismic crises in the last 100 years: 1897 - ~1898; 1933 - 1937; 1966 - 1967 and 1994 until the eruption in 1995 (Wadge & Isaacs, 1988). The repose periods between the seismic crises have been 36, 33 and

28 years. Perret (in: Shepherd et al., 1971) correctly predicted in 1939 that the next seismic crises would occur in the 1960s. Why there should be such a periodicity is not yet known.

The current volcanic crisis on Montserrat

The first indications of precursory activity in the Soufrière Hills area were noted in November 1994, by the Seismic Research Unit (SRU), based at the University of West Indies in Trinidad; increased seismicity had been recorded by the SRU since 1992 (Young, pers. com.). Phreatic explosions and the onset of the eruption prompted the setting up of the MVO in mid-July 1995, which was staffed jointly by members of the SRU and by scientists of the British Geological Survey (BGS) and funded by the government of Montserrat and the ODA.

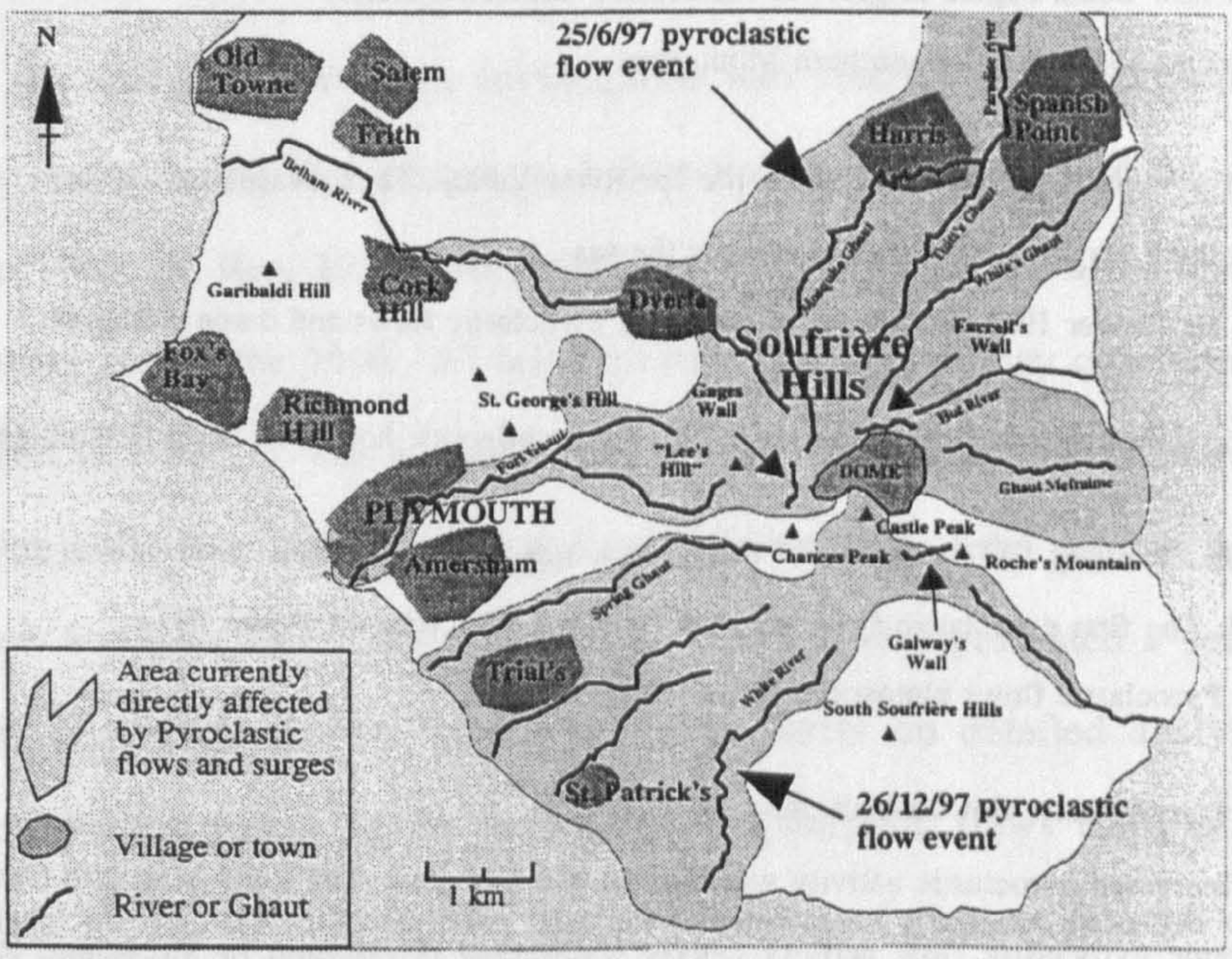

Figure 6.2. *Map of the southern half of Montserrat showing the areas affected by pyroclastic flows and surges. The confinement of flows to topographic lows such as valleys and ghauts has lead to much of the material being channelled along the Belham, Paradise and Tar Rivers to the north and east and the White River to the south. Heavy rains during the hurricane seasons have caused mud flows to fill many of the minor ghauts. Those ghauts and valleys used by pyroclastic flows have gradually been infilled and the topography smoothed. This has enabled later flows to achieve a greater run-out distance, even reaching the sea.*

The current crisis is probably one of the best documented eruptions in the world, with daily updates and reports freely available over the Internet (at URL: http://www.geo.mtu.edu/volcanoes/west.indies/soufriere/govt/). A summary of the eruptive activity at Soufrière Hills can

also be found at this site; the main events are outlined below and show the gradual escalation in level of activity (MVO report, 1997):

Stage	Description of eruptive events
1	January 1992: Start of earthquake swarms below southern Montserrat June 1994: Large precursory earthquake swarm.
2	18/7/95: Initial steam and ash venting from English's Crater. 21/8/95: Large phreatic eruption and first evacuation of surrounding villages and Plymouth.
3	September 1995: First indication of dome growth and the appearance of a small spine in crater. 30/10/95: Another large phreatic eruption.
4	14/11/95: A new dome begins to grow in the 18/7/95 explosion crater. 1/12/95: Second evacuation of southern Montserrat.
5	3/4/96: First pyroclastic flows travel down the Tar River Valley. Third evacuation initiated. 12/5/96: Mothers Day pyroclastic flow reaches the sea. August and September 1996: increase in numbers of pyroclastic flows and dome collapses.
6	17 - 18/9/96: First magmatic explosion caused by dome collapses; houses in Long Ground destroyed.
7	October 1996 - January 1997: A series of new domes appeared on 1/10/96, 11/12/96 and 20/1/97. March 1997: The first pyroclastic flows overtop Galway's Wall into the White River. April 1997: Pyroclastic flows almost reach the sea at O'Garras.
8	29/5/97: First pyroclastic flows travel down Tuit's Ghaut. June 1997: Increased pyroclastic activity with flows travelling down Tuit's and Mosquito Ghauts. 25/6/97: Major pyroclastic flow activity causes widespread devastation in Streatham, Riley's, Harris, Windy Hill, Bramble, Bethel, Spanish Point, Trant's and Farm's. Pyroclastic flows travel down Belham River valley to Cork Hill, see **figure 6.2**. First recorded fatalities of current crisis. 1/7/97: Pyroclastic flows reach as far as the Catholic church in Plymouth .
9	3 - 4/8/97: Major pyroclastic flows in central Plymouth. Explosive venting of ash and pumice. 5 - 8/8/97: Series of large explosions associated with collapse of convective column.
10	August 1997: Continued dome growth.
11	21/8/97: Major dome collapse lead to pyroclastic flows covering the area between Trant's and White's. 22/9/97 - 21/10/97: A series of Vulcanian eruptions caused pyroclastic flows to travel down all six major ghauts on the volcano: Tar River, Tuits, Mosquito, Tyre's, Gages and the White River.

1 2 22/10/97: A new dome begins to rapidly grow on south side of main dome complex.

2/11/97: Galway's Wall begins to crack and be displaced.

6/11/97: Dome collapse caused pyroclastic flows to travel to the sea down the White River Valley.

1 3 November - December 1997: Low activity but continued growth of Galway's lobe on 22/10/97 dome.

26/12/97: Major collapse of Galway's lobe triggered large pyroclastic flows and a lateral blast; ~64 × 10^6 m^3 of debris added to the White River pyroclastic fan, see **figure 6.2**, ~1 m tsunami formed.

January - February 1998: Steady growth of a new dome in the 26/12/97 collapse scar.

6.1.4 Previous work and the MVO monitoring activity at Soufrière Hills volcano

Previous work on Montserrat

Before the volcanic crisis, little investigation into volcanism on Montserrat had been reported. Some early dating and petrological investigations were carried by a number of authors prior to 1960 (in: Rea, 1974). Shepherd et al. (1971) conducted a limited seismic and deformation survey during the 1966 - 67 seismic crisis from which they concluded that if any magma had been intruded, it was a small volume located at depths of greater than 10 km beneath Soufrière Hills. Rea (1974) conducted a detailed survey of the geology and petrology of Soufrière and South Soufrière Hills. Wadge & Isaacs (1988) presented a detailed hazard map and likely course for the next eruption; based partly on detailed analyses of older pyroclastic deposits and partly on the modelling of pyroclastic flows using a DEM. Their models were used by the MVO to initially predict the areas of greatest risk and create hazard zonation maps for the island's authorities. Chiodini et al (1996) investigated the fluid geochemistry of the various soufrières on Montserrat during March 1991 and September 1992. They summarised that there was strong isotopic evidence for the incorporation of an "andesite-type" magmatic component in the geothermal fluids analysed.

MVO monitoring

The monitoring effort conducted by the MVO has concentrated mainly on using geophysical techniques although other techniques have also been used. These include:

- EDM (Electronic Distance Measurement), which has been used for measuring ground deformation and monitoring the growth of the dome.

- Fixed-point photo-trigonometric methods, which were used in the earlier days to determine dome growth. These have since been superseded by a combination of kinematic GPS (Global Positioning Satellite) and laser-ranging binoculars to allow a much more accurate estimate of extrusion rates.

- GPS and wet/dry tilt stations, which were used to determine ground deformation. In places where fissures have opened up, such as at Gage's Wall, strain gages have been used to determine deformation rates.

- Both short and long period (broadband) seismometers, which have been used to monitor magma and gas movement.

- Gravity and microgravity, which have been used to elucidate further changes in the state of the magma system.

- COSPEC and OP-FTIR, which have been used to investigate the rate of degassing and the composition of the gas plume.

- Environmental investigations into the ash and rainwater chemistry, including: the monitoring of drinking water; levels of airborne particulates; and background SO_2 levels to determine environmental effects of the eruption.

The techniques used have depended on the level of activity and access to the volcano. Over the course of the volcanic crisis the escalation in number and run-out distances of pyroclastic flows has prevented a number of the techniques, including GPS, EDM and COSPEC being carried out close to the volcano. The burial of the roads skirting Soufrière Hills has affected COSPEC most of all. Analyses are sporadically conducted from a Montserrat Police boat, although poor reliability of both the instrument and the boat has introduced large gaps into the data collected. Poor weather is still the main cause for the lack of observations on dome growth, eruption rate and changes in loci of activity. This is due to the persistent clouds which cap the Soufrière Hills massif, obscuring the dome.

Comparison of the Soufrière Hills eruption with that of Mt. Unzen

MVO scientists have compared gas, seismic and geophysical data for Soufrière Hills with data collected at Mt. Unzen, Japan, in an attempt to use Mt. Unzen as an analogue for the current eruption to model and predict pyroclastic flows and explosive activity. I shall briefly review the initial stages of activity at Mt Unzen in 1991, as reported by Nakado & Fujii (1993), so that the two eruptive crises may be compared.

The activity at Unzen volcano was initially phreatic, the first explosions reported on 12/2/91, following a series of shallow earthquakes. On 13/5/91 shallow earthquakes coincided with a period of summit inflation and the opening up of several NW trending fissure centred on one of the phreatic craters. On 20/5/91 a lava spine was seen growing in the Jigokuato crater. By the 21/5/91 a small lava dome had formed. This had filled the crater by 23/5/91 and dome debris had begun to run down the steep outer slope of the crater. The first pyroclastic flows were produced on 24/5/91. The first major pyroclastic flow occurred on 26/5/91 and travelled 3 km down the Oshigadani valley after a partial dome collapse. Renewed growth extended the dome eastwards out of Jigokuato crater. On 3/6/91, 13 days after the first extrusion of material, a series of major pyroclastic flows, caused by collapse of half of the dome, carried ~0.6×10^6 m^3 of material down the Mizunashi River valley killing forty three people. Further dome growth lead to larger pyroclastic flows on 8/6/91 coupled with an explosive phase. Vulcanian eruptions on 11/6/91 ejected breadcrust bombs to distances of >3 km before activity returned to a period of sustained dome growth.

There are several similarities between the eruptions of Mt Unzen and Soufrière Hills. Both extrude andesitic magma and have formed large domes which have sporadically collapsed, forming pyroclastic flows. Similar extrusion rates, of ~1 - 3 m^3/s, have also been measured at both volcanoes during the earlier stages of the eruptions (MVO reports; Hirabayashi et al., 1995). The MVO therefore concluded that the Mt. Unzen eruption could be used as an advanced analogue, indicating how the eruptive activity at Soufrière Hills volcano may change as the eruption proceeded. One startling difference between the two volcanoes was the time taken from onset of dome extrusion to pyroclastic flow formation.

This was only four days at Mt. Unzen, compared to over six months at Soufrière Hills; the difference probably being the eruption within the deep English's Crater, rather than on a steep sided summit as at Mt. Unzen. The validity of using Mt. Unzen as an analogue for Soufrière Hills will be discussed later.

6.2 Use of COSPEC to monitor volcanic activity at Soufrière Hills

6.2.1 Introduction to COSPEC analyses on Montserrat

The correlation spectrometer (COSPEC) has been used to monitor the SO_2 flux at a large number of volcanoes throughout the world since the early 1970's. The remote technique can be done easily from a vehicle or a boat and provides a simple method of recording the gas output of a volcano. Many authors, including: Malinconico (1987); Bruno et al. (1994); and Hirabayashi et al. (1995), have shown that the level of SO_2 flux from an individual volcano correlates with the levels of eruptive activity and lava effusion rate. COSPEC has therefore been used by "Team COSPEC" on Montserrat as part of the overall monitoring effort.

The high turnover of staff and equipment within the MVO has meant that the conditions under which COSPEC analyses have been collected, and the data derived, have changed on a frequent basis. Individual scientists within "Team COSPEC" have used their own methods of deriving flux-values from chart print-outs or computer readouts. This, coupled with their individual techniques for collecting the data and wind speeds, will introduce a margin of error into the final values when considering the changes in SO_2 flux with time. At least four different COSPEC instruments have been used on Montserrat since eruptive activity first started in 1995: one owned by the United States Geological Survey (USGS) (29/7/95 - 28/8/95); one by the University of Montreal (28/4/96 - 21/7/96); the MVO mini-COSPEC (22/7/96 onwards); and one loaned by the USGS for a short period in 1996 as a replacement. Large gaps in the COSPEC data-series are due to the instrument being inoperative or to prolonged periods of inclement weather. The instrument-platform used to conduct the analyses has also varied; vehicles, boats and helicopters all being used at different times to collect the data.

6.2.2 Techniques of COSPEC analysis on Montserrat

General COSPEC instrumentation

The techniques for using COSPEC tend to be specific to each volcano. I shall therefore briefly review the general COSPEC technique before discussing details relating specifically to my use of COSPEC on Montserrat. A broader overview of the instrumentation and technique appears in Section 2.3.

COSPEC determines the mass of SO_2 in the optical path. This is usually a vertical air column situated between the detector and direct/indirect UV light sources; mainly sun, clouds and light-scattering particles. Solar radiation passes through the gas plume and enters the COSPEC via a telescope. A right-angled extension to the telescope enables UV radiation to be captured from vertically above the instrument when using a vehicle or aircraft. Once inside the instrument, the light is focused on to a diffraction grating which separates the beam into individual wavelengths. These are then focused onto a rotating correlator disc in which slits have been etched to allow the passage of specific sets of UV spectral bands (Stoiber et al., 1983). One of the spectral bands used corresponds to a wavelength of SO_2 absorption at ~300 nm; the other to a similar frequency where no SO_2 absorption takes place. Modulated radiation passing through the correlator disc is converted into two voltages by a photomultiplier tube and processed by the instrument's electronics. The output from the COSPEC is a voltage proportional to the concentration of SO_2 in the optical path. This is recorded either on a simple chart recorder or, by using an analogue-to-digital converter, inputted directly into a computer.

Calibration of the instrument is achieved by positioning one of two internal gas calibration cells with known concentrations of SO_2 into the instrument's optical path when this is directed away from the volcanic plume into clean air. For the particular instrument I used on Montserrat, the calibration concentrations, CAL1 and CAL2, were: 339.2 ppm.m and 64 ppm.m respectively.

Using a road vehicle for COSPEC monitoring

I was able to conduct COSPEC analyses in Montserrat from a vehicle during May and June 1996 due to the lower level of volcanic activity at the time. The prevailing winds at Montserrat carry the volcanic plume almost due west over the capital, Plymouth. I analysed the gas plume by driving beneath it along the road between St. Patrick's and Cork Hill, see **figure 6.3**. The area was quite built-up and had a well maintained road; which ran from Old Fort Point at the southern end of the island in a NW direction to Plymouth from where the road headed due north inland. Nearly all of this area has now been affected by pyroclastic flow activity, lahar and debris avalanches preventing further COSPEC analyses along this route.

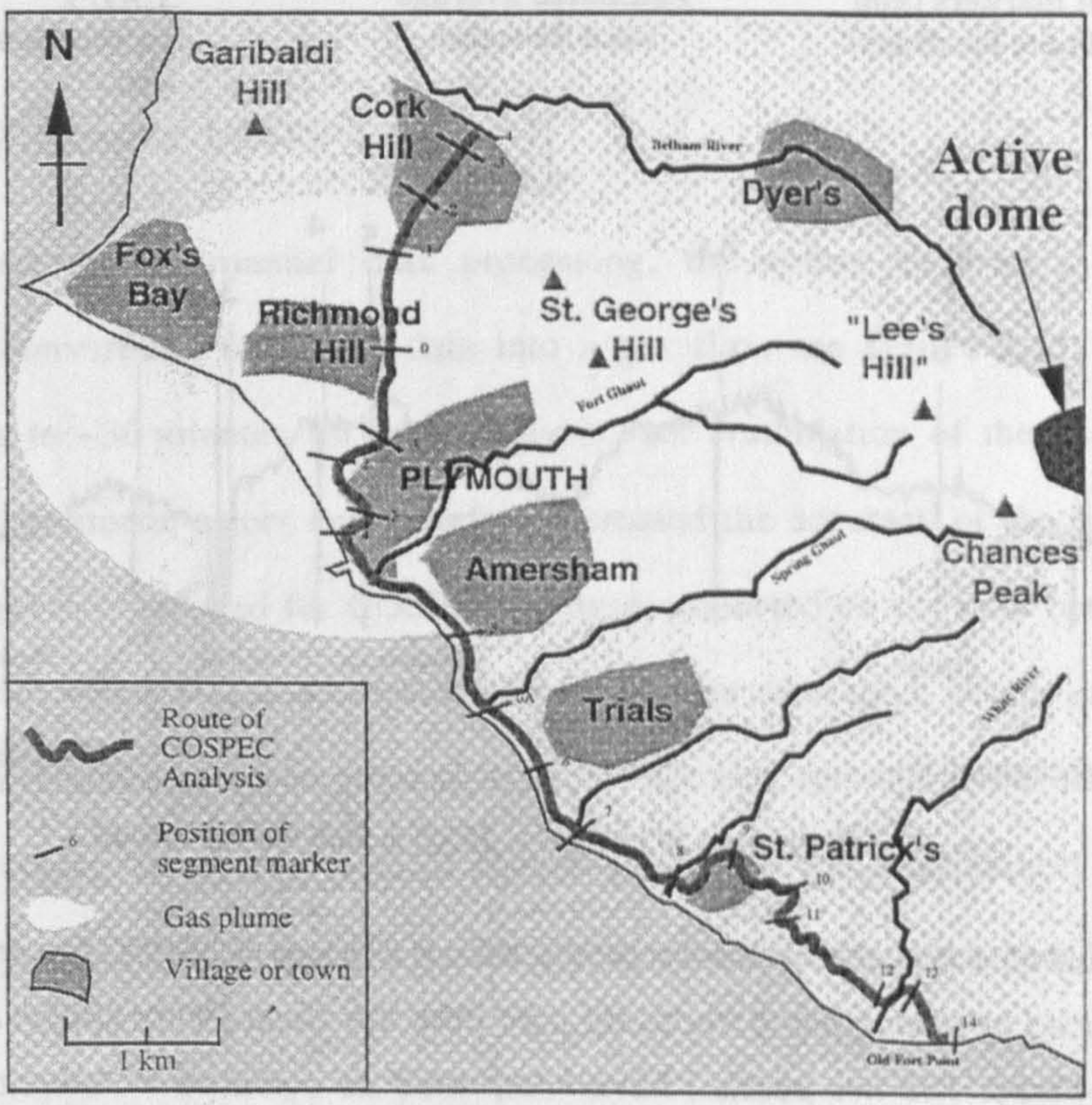

***Figure 6.3**. Map of the route along the coast road used by the author and Team COSPEC for COSPEC analyses. The breaks marking each road section are shown, as is a typical footprint for the gas plume.*

The COSPEC was strapped into the front passenger seat so that the right-angled telescope projected out of the window and pointed vertically upwards. The analogue output from the COSPEC was recorded using a chart-recorder; both the chart recorder and the COSPEC being powered from the vehicle's main battery. The wide and mainly treeless route

used was almost ideal for conducting COSPEC analyses. The few overhanging trees had to be avoided whilst collecting COSPEC data as the blockage of light into the instrument resulted in loss of data. Any data loss was corrected by extrapolation of the good data to either side of the affected area.

The total length of the route used for COSPEC analyses was ~8.8 km. During periods with higher wind speeds, the narrower gas plume allowed only part of the route to be used for analyses. The COSPEC route passed along roads with a variety of orientations, see **figure 6.3.** Ideally the COSPEC traverse should be at 90° to the wind direction to allow the plume to be sampled evenly. For those road segments not at 90°, this can be corrected by taking the Sine of the acute angle between the wind direction and the road segment.

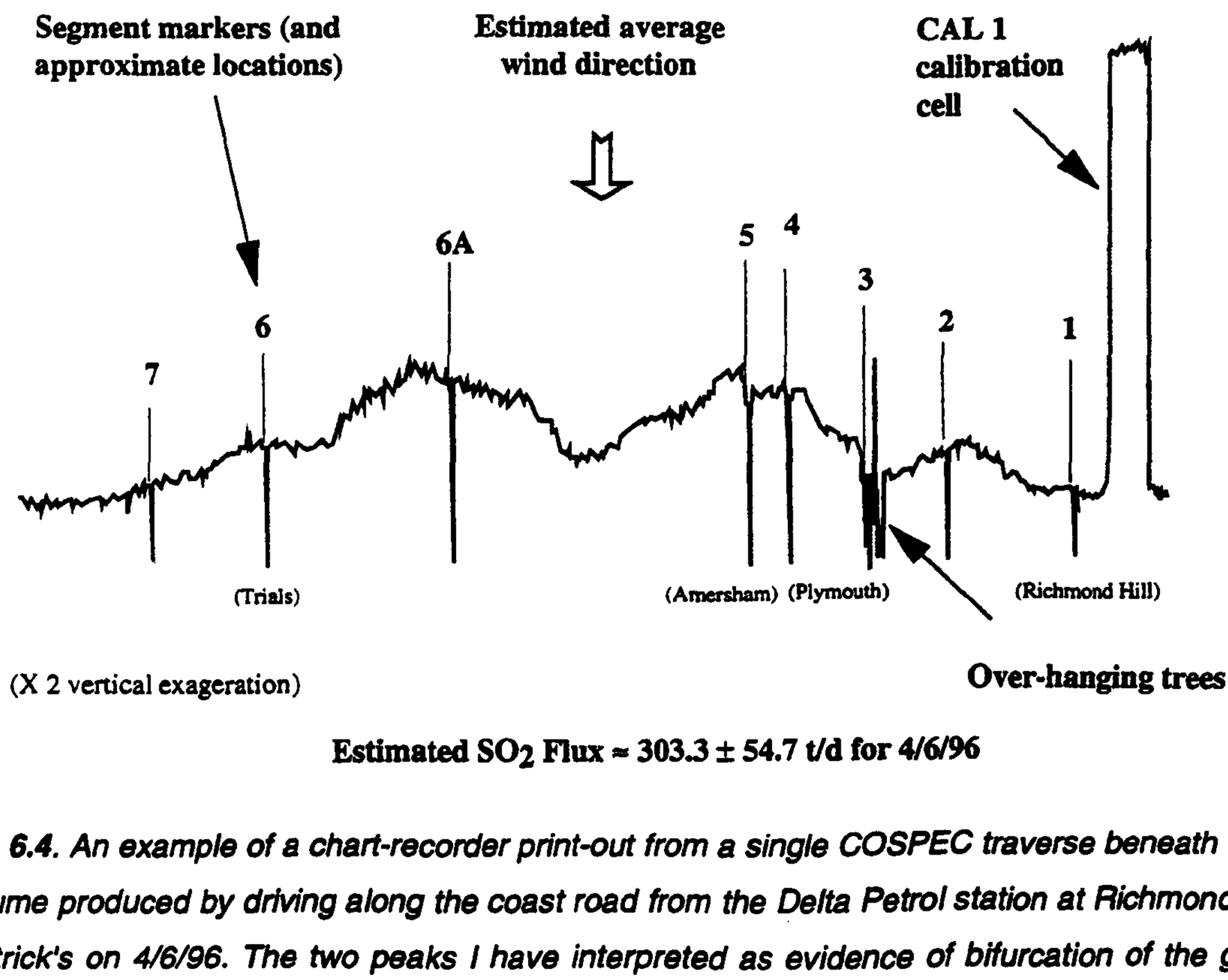

Figure 6.4. *An example of a chart-recorder print-out from a single COSPEC traverse beneath the gas plume produced by driving along the coast road from the Delta Petrol station at Richmond to St. Patrick's on 4/6/96. The two peaks I have interpreted as evidence of bifurcation of the gas plume; with each half separated by ~1.2 km. The disruption of data caused by passing beneath overhanging trees is also shown. The segment markers (numbered circles and lines) correspond to those marked in* ***figure 6.3*** *and indicate where there is a change in the general direction of travel (COSPEC data from MVO).*

To make the calculations of SO_2 flux as accurate as possible, MVO's Team COSPEC had divided the COSPEC route into 18 segments, each with an average length and direction; these were individually adjusted for their orientation with respect to wind direction before

being used to derive the gas flux. During the analysis runs, as the vehicle passed the location of the segment break, the new section was marked on the chart output; thus enabling each segment to be corrected afterwards during data processing, see Section 2.3.2.

Uniform sampling across the plume was aided by maintaining a constant vehicle speed of 20 kph during analysis runs. This particular speed was chosen as it was easy to maintain on winding roads and aided the negotiating of slow moving dock traffic and the Police road block at Richmond. The collection of COSPEC data was limited to two time periods each day, ~09:30 - 11:30 and ~12:30 - 15:30. Outside of these times the sun was either too low to provide a good UV source or shone directly into the telescope, saturating the detector and producing a series of sharp positive and negative peaks with consequent loss of data.

Processing COSPEC data

To speed up the manual data processing, the author devised a simple Excel spreadsheet to convert the raw chart data into a gas flux, see **figure 2.11**. This reduced processing time to ~30 minutes for each analysis run. Automation of the calculations also reduced simple arithmetic errors and therefore increased the accuracy of the final value. The spreadsheet could only be used for COSPEC analyses collected on the road between Shooters Hill and Cork Hill which was downwind of the volcano for most days. Winds originating from the SE or south required using an alternative COSPEC route running across the centre of the island through Gages, Dyers and towards Harris. This route was considerably more tortuous and tree lined, producing consequently poorer quality data (Watson, pers. com.).

Measurement of wind speeds

I collected five one-minute wind speed measurements before and after each day's COSPEC analyses, using a precision Davis ball-bearing air-flow meter. This was done from exactly the same position at the top of Windy Hill in an attempt to keep the data as consistent as possible. The wind speeds should ideally be measured at the same height as the volcanic plume; and at a height of 10 m above ground level and at a distance downwind of 10 × the

height of the nearest building or hill (Williams-Jones et al., 1998). This however was not possible on Montserrat and so the measured wind speeds are only an estimate. To try and reduce the effect of ground friction on the wind speed, the air-flow meter was held above the head for each measurement. The standard deviation of the five wind speeds was used, both by the author and the MVO, as the COSPEC error when reporting the gas flux. Due to the time taken to drive to Windy Hill, the location for measuring wind speeds was moved to the top of St. George's Hill in August 1996. Oppenheimer and Francis (pers. com., 1996) conducted a short trial in late July 1996 in which they measured winds regularly at both Windy Hill and St. George's Hill. They observed that average wind speeds were ~50% higher at the St. George's Hill location. To keep the data-set consistent, I have converted all the SO_2 fluxes recorded prior to August 1996, and based on wind speeds from Windy Hill, by recalculating the flux as if based on wind speeds measured at St. George's Hill. The large local variations and uncertainties in the measured wind speeds are the main cause of errors within the COSPEC technique; these are discussed in more detail in Sections 2.3 and 6.2.5.

6.2.3 Results of COSPEC analysis on Montserrat

The results from COSPEC investigations at Soufrière Hills volcano will be divided into two parts: the data gathered by the author; and the data gathered by MVO's Team COSPEC. As previously discussed, the MVO have used the eruption at Mt. Unzen as an analogue for the Soufrière Hills eruption. I shall therefore also discuss the MVO COSPEC results in relation to those reported by Hirabayashi et al. (1995) for Mt. Unzen. In the following sections I have used the daily SO_2 flux averaged over a month to highlight the major trends in eruptive activity. Monthly averages are summarised in **table 6.1**.

COSPEC data collected by A. Maciejewski (25/5/96 - 4/6/96)

I collected data from 30 traverses beneath the plume during the period 25/5/96 - 4/6/96 whilst in Montserrat conducting OP-FTIR investigations. The errors in **figure 6.6** are calculated as the standard deviation of the measured wind speeds, with an average variation of ~10%. As will be discussed later, the true level of the error associated with COSPEC analyses is

much higher, ~16 - 45%, and relates mainly to variable wind speeds and the presence of ash and cloud.

I derived an average SO_2 flux of ~157 t/d for the data I collected. This is similar to the monthly averages of May and June, of ~182 and 189 t/d respectively (MVO Scientific reports), see **table 6.1**. The large daily variation in flux values in **figure 6.5** prevent any real trends being identified over such a short period. Much of this variation may possibly be attributed to differences in cloud cover and amounts of airborne ash; which can produce combined errors of >30%, see Section 6.2.4. The effects of clouds could be clearly seen during calibration of the COSPEC outside the plume; as small clouds passed over the instrument, the baseline would vary by ~5 ppm.m.

Figure 6.5 shows that pyroclastic flows occurred on the days immediately after I measured local SO_2 flux maxima. Assuming these are real, rather than atmospheric, variations, I have interpreted these as the rise of gases through the volcanic system ahead of small pulses of magma. When the pulses reach the base of the lava dome, they cause inflation, steepening and destabilising the dome; the ensuing increase in rockfalls can then trigger a larger collapse - forming a pyroclastic flow.

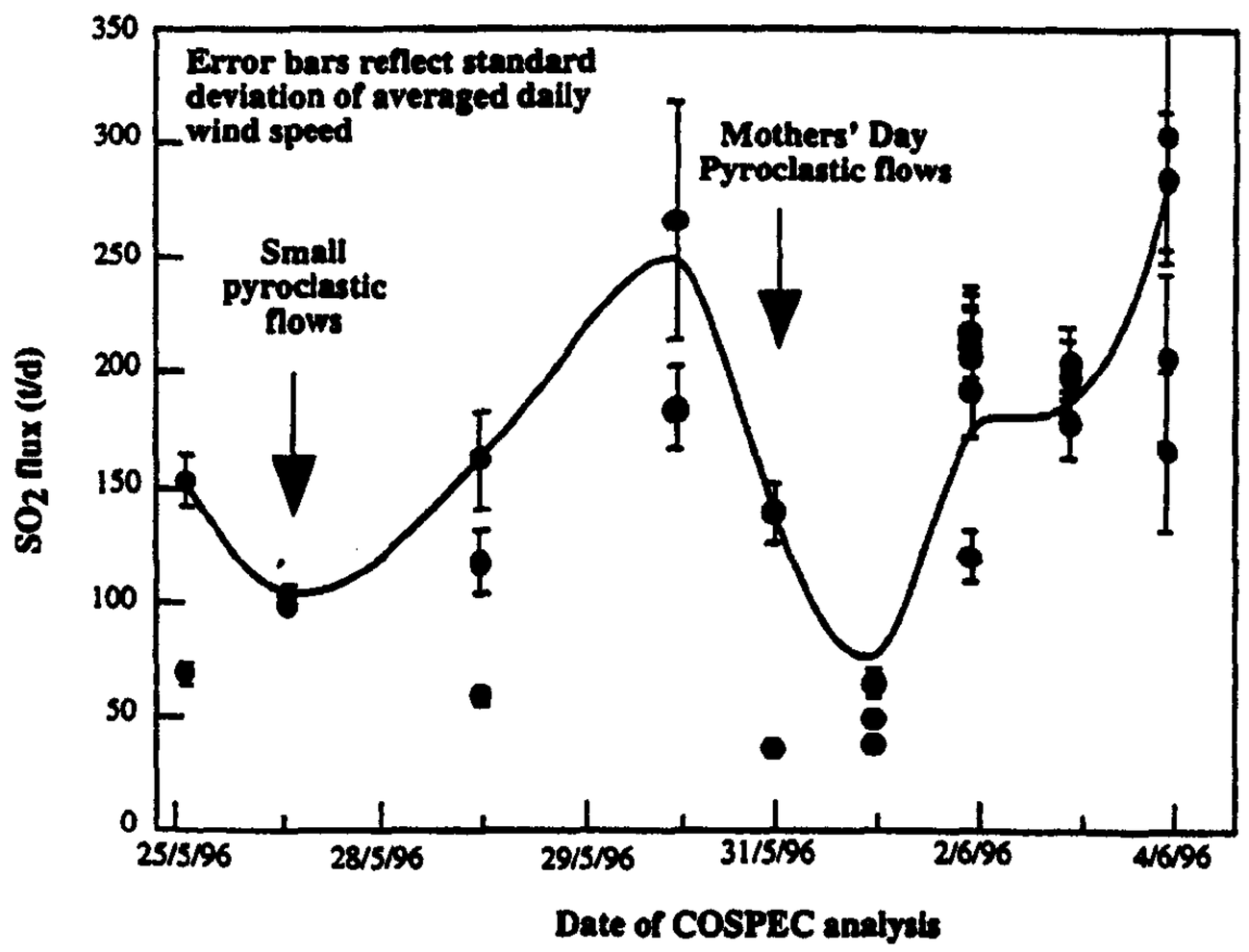

Figure 6.5. *Results of COSPEC analyses conducted by the author on Montserrat along the SW coast between Cork Hill and Shooters Hill between 25/5/96 and 4/6/96. The line relates to a smoothed curve through the data to show the general changes. Data are shown with error bars relating solely to the standard deviation in recorded wind speeds.*

COSPEC data collected by the USGS and the MVO (29/7/95 - 1/1/98)

The USGS and the MVO's "Team COSPEC" have both measured the SO_2 flux from Soufrière Hills volcano sporadically since July 1995. Large gaps in the SO_2 flux time-series exist; mainly due to the unavailability or failure of a COSPEC, bad weather and elevated pyroclastic flow activity. The MVO data-set can be seen in **figure 6.6**, which summarises the results of all COSPEC investigations from July 1995 onwards. As previously mentioned, the data-set is not wholly internally consistent due to the use of several different COSPEC systems by different scientists using a variety of techniques. I have therefore assumed that only the larger variations are significant of changing volcanic conditions.

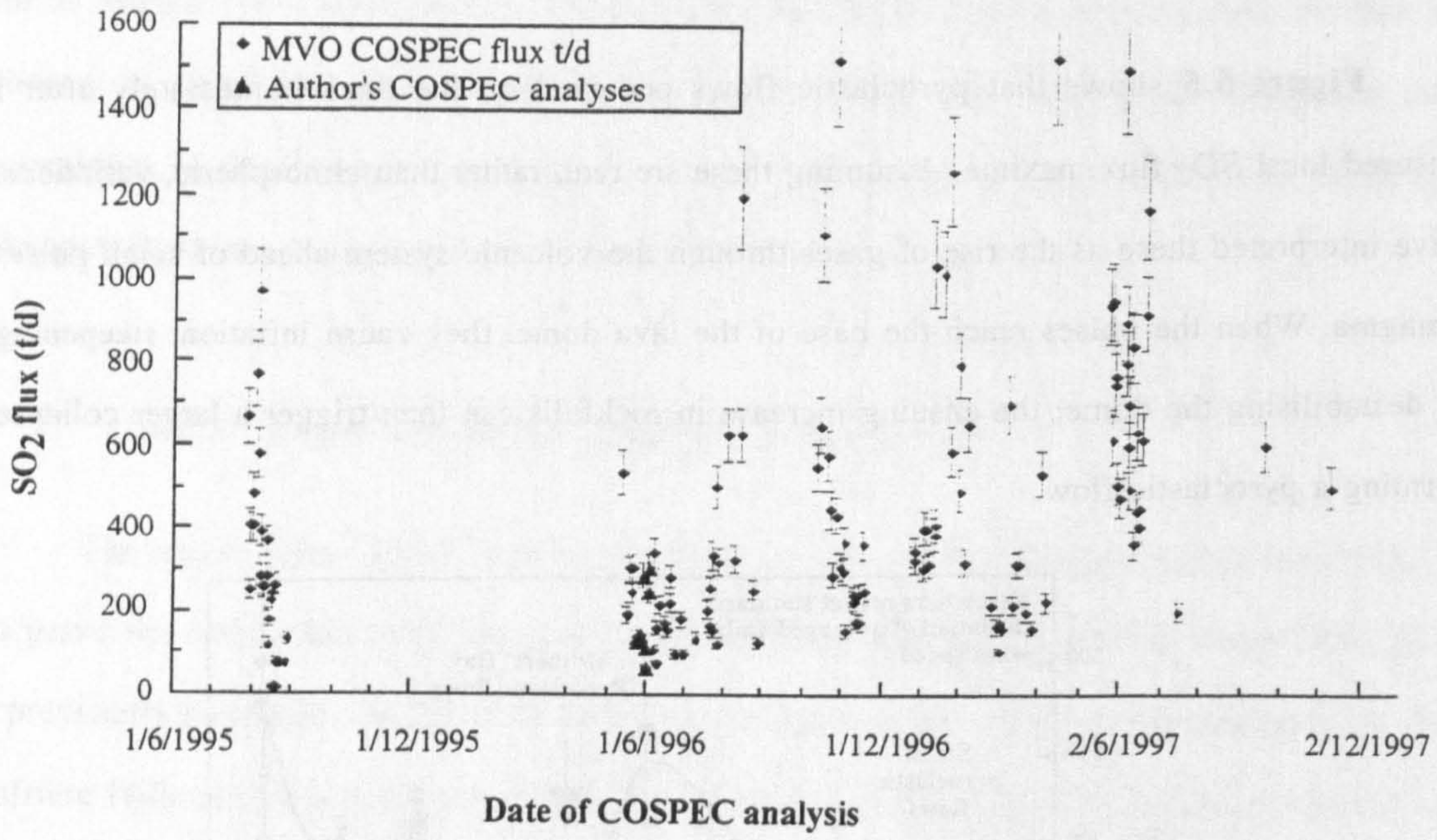

***Figure 6.6**. Results of the USGS and MVO COSPEC monitoring campaign for the period 29/7/95 to 1/1/98 presented as daily averages (MVO Scientific and Daily reports, Team COSPEC, pers. com). Numerous gaps in the data relate to periods of bad weather, equipment failure or hazardous volcanic conditions. Triangles indicate the author's own analyses, see **figure 6.5**.*

COSPEC monitoring by the USGS (29/7/95 - 28/8/95)

During the early phreatic phase of the eruption, July - August 1995, the USGS measured a relatively high SO_2 flux; monthly averages of ~300 and 440 t/d being estimated for July and August respectively. I have inferred from the rapid decline in SO_2 flux, see

figure 6.6, that the energetic gas venting acted to release gases trapped at a shallow level. Unfortunately, a gap of almost nine month separates these observations from the start of the MVO monitoring campaign and so the evolution of the magmatic system during this period cannot be elucidated.

COSPEC monitoring by the MVO (~13/5/96 onwards)

The earliest SO_2 fluxes recorded by MVO's Team COSPEC were consistently lower than those from the phreatic phase; with average monthly fluxes of ~180 - 290 t/d for May - July. During late June 1996 a sudden rise in gas fluxes occurred immediately prior to a period of increased dome growth, with effusion rates of ~8 m^3/s, associated with dome collapses and

Month	Average SO_2 flux (td)	Number of days with COSPEC analyses
July 1995	441	3
August 1995	304	28
May 1996	182	11
June 1996	189	17
July 1996	289	9
August 1996	963	6
October 1996	655	9
November 1996	250	10
December 1996	337	2
January 1997	619	12
February 1997	397	3
March 1997	251	10
April 1997	761	3
May 1997	756	9
June 1997	704	17
July 1997	647	1
September 1997	600	1

Table 6.1. *The average monthly SO_2 flux, as determined using COSPEC, at Soufrière Hills volcano, Montserrat (after: MVO reports). As can be seen the record is incomplete and some monthly averages are the product of only a few days analyses.*

pyroclastic flows. The averaged SO_2 flux for early August, ~963 t/d, reflected this increased activity, before COSPEC analyses were halted due to instrument failure. COSPEC analyses restarted in mid October, after the appearance of the 1/10/96 dome; the initially high effusion rates in October gave a month-averaged SO_2 flux of ~655 t/d. The decrease in volcanic activity, marked by lower lava extrusion rates, during November and December was reflected in the lower monthly-averaged SO_2 fluxes of ~250 and ~337 t/d respectively, see **table 6.1** and **figure 6.7**. No COSPEC analyses were taken during the period of growth of the 11/12/96 dome during which dome growth was relatively rapid, ~8.5 m^3/s.

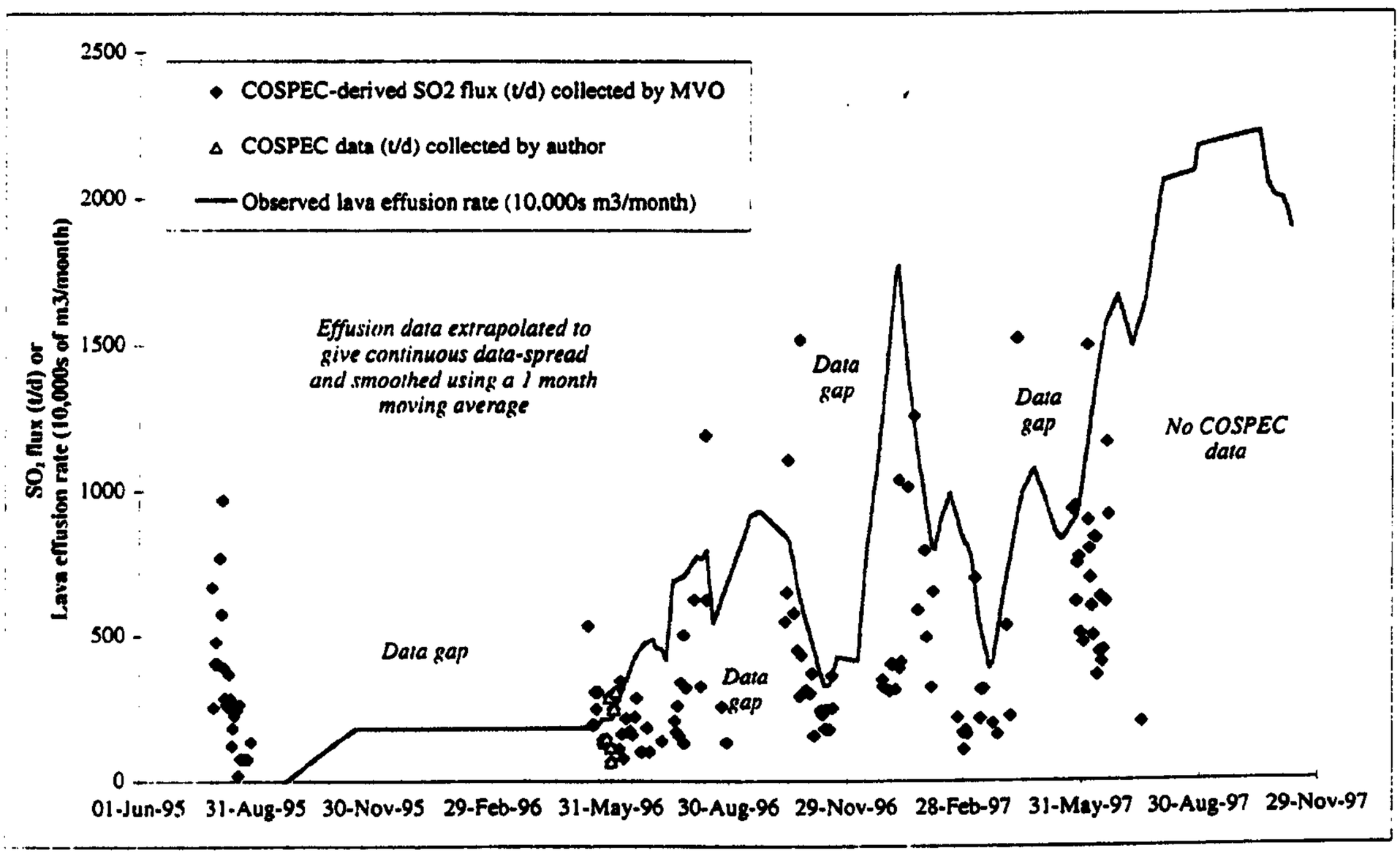

Figure 6.7. *Results of the MVO COSPEC monitoring campaign for the period 13/5/96 to 1/1/98 (MVO Scientific and Daily reports, Team COSPEC, pers. com). Numerous gaps in the data relate to periods of bad weather, equipment failure or hazardous volcanic conditions. I have smoothed the data with a one month moving average to eliminate noise due to weather and ash clouds. Also included are the results of the MVO "Team volume" campaign to monitor rates of dome growth (MVO Scientific reports). This has also been smoothed with a one month moving average to counter the paucity of effusion data. The two data -sets follow the same trends - both gradually increasing with time as the volcanic crisis has continued.*

SO_2 flux measurements during January 1997 increased rapidly with a maximum of ~1250 t/d, measured on 21/1/97, coinciding with growth of the 20/1/97 dome. February and March, a period of relatively slow dome growth, had correspondingly low SO_2 fluxes of 397

and 251 t/d respectively. Early April 1997 was marked by a rapid rise in the flux of SO_2, with a maximum of ~1524 t/d recorded on 11/4/97. This corresponded to an increase in the effusion rate and the beginning of a series of pyroclastic flow events which travelled down the White River. No data were recorded in the second half of April and most of May as the Mini-COSPEC was unavailable.

Recommencement of COSPEC analyses on 24/5/97 initially showed a slow decrease in the SO_2 flux, relating to a decrease in effusion rate from ~4.6 to ~3 m^3/s. On ~1/6/97 this suddenly increased, coinciding with an increase in effusion rate and the beginning of a period of elevated pyroclastic flow activity; due to the actively growing area switching from the south to north side of the dome. The high monthly averages for May and June, ~756 and ~704 t/d, reflected the high, ~9 m^3/s, lava effusion rates; with >1100 t/d measured on 20/6/97; the last date analyses could be safely conducted due to the danger of pyroclastic flows. On 25/6/97 a series of major pyroclastic flows devastated the NE, NW and western parts of the volcano.

Collection of COSPEC data after the 25/6/97 activity has been exceedingly sporadic, using either a Montserrat Police boat or a static method; the only data reported being ~200 t/d on 17/7/97 and ~600 t/d on 20/9/97. The low flux recorded on 17/7/97 corresponded to a period with lower rate of lava effusion.

There appears to be a good relationship between the SO_2 flux and lava effusion rate, see **figure 6.7**. However, the local maxima for gas emission seem to lag behind those for lava effusion. This may possibly be an artefact of the high effusion rates, causing pyroclastic flows and ash clouds and thus preventing the safe use of COSPEC during these periods; measurements only being possible at a later date. Alternatively rising magma may displace the material above it, thus increasing effusion rates. Only once the new magma reaches shallower depths can it degas fully, thus increasing the measured gas fluxes. This is contrary to the interpretation I used for the smaller May - June 1996 COSPEC data-set; for which I suggested that the gas was emitted prior to the increase in effusion rates. The paucity of COSPEC data immediately prior to a major increase in effusion rate makes it difficult to determine the exact relationship between gas flux and lava effusion at Soufrière Hills.

Observations drawn from COSPEC monitoring: A comparison of Soufrière Hills and Mt. Unzen volcanoes

The SO_2 fluxes initially measured by MVO were lower than observed at other, erupting volcanoes discussed in this thesis. Fluxes of SO_2 at Stromboli and Mt. Etna, both basaltic volcanoes, range from <300 - >1400 and <1000 - >6,000 *t/d* respectively for periods without active lava effusion (Allard et al., 1996). The apparent deficit in SO_2 emission at Soufrière Hills may be explained by the different sulphur concentrations in various magma types. Giggenbach (1996) reported that sulphur concentrations in andesitic and rhyolitic melts tended to be much lower than in basaltic melts, see **table 1.1**. The low COSPEC-derived SO_2 fluxes reported by Hirabayashi et al. (1995) for the andesite-dome eruption at Mt. Unzen support this; average SO_2 fluxes ranging between ~40 and 220 t/d for the period 18/6/91 to 10/5/94. For the same period, the effusion rate at Mt. Unzen was consistently lower than at Soufrière Hills; average effusion rates being ~1.5 and ~3.6 m^3/s respectively (Hirabayashi et al., 1995: MVO Scientific reports).

I compare the relationship between SO_2 flux and effusion rate for Mt. Unzen and Soufrière Hills volcano in **figure 6.8**. At Mt. Unzen, the data show that both gas emission and lava effusion rates are comparatively low. This contrasts sharply with the Soufrière Hills data; which I have divided into two fields, based on the level of explosive activity and numbers of pyroclastic flows reported at the time of data collection (MVO evening and scientific reports), see **figure 6.8**. These are:

A. Periods of slow to intermediate levels of dome growth and small collapses triggering minor pyroclastic flows.

B. Periods of accelerated dome growth associated with major dome collapses, increased pyroclastic flow activity and explosive activity.

Figure 6.9 shows that eruptive activity at Mt. Unzen can be best compared with periods at Soufrière Hills volcano characterised by explosive episodes and pyroclastic flow formation. Activity at Mt. Unzen, however, is accompanied by very low emission of gas. This concurs with the general observations of Hirabayashi et al. (1995) on the activity of Mt. Unzen. Activity represented by field A of **figure 6.7**, with high gas emission and little or

no pyroclastic flow activity, has not been reported for Mt. Unzen and suggests that the mechanisms behind the degassing of the two volcanoes may be different.

Barclay et al. (1996) reported an initial magmatic sulphur content of <150 ppm for the lava erupted from Soufrière Hills volcano. The maximum gas flux due to the loss of this amount of sulphur is denoted in **figure 6.8** by a dashed line. Much of the Soufrière Hills data exhibit higher apparent magmatic sulphur concentrations than have been analysed, see Section 6.4. In order to generate the measured SO_2 flux, magma must therefore either be being intruded after degassing, or magma with a higher sulphur concentration than that analysed lies below Soufrière Hills volcano and contributes to the SO_2 flux measured. This will be discussed in Section 6.4.

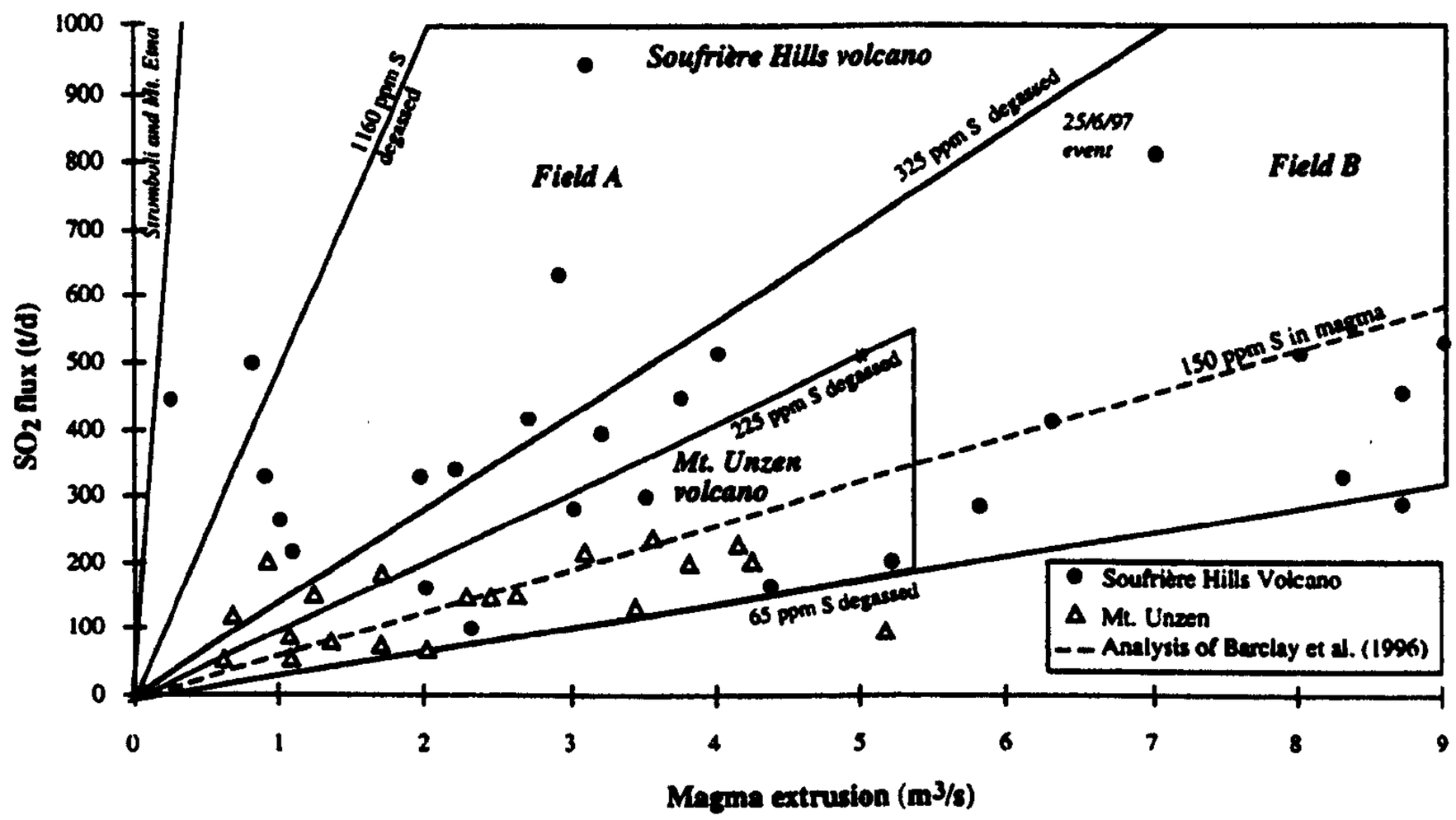

Figure 6.8. *The relationship between SO_2 flux and magma effusion rate for Mt. Unzen and Soufrière Hills volcanoes (after Hirabayashi et al., 1995; MVO Scientific reports). The field boundaries for the data indicate approximate minimum and maximum concentrations of degassed sulphur, assuming sulphur is degassed only from erupted lava. The Mt. Unzen data show a continuous decrease in extrusion rate, with a fairly constant SO_2 flux. The Soufrière Hills data can be divided into two fields relating to: A. Periods of slow to intermediate rates of dome growth and small collapses; B. Periods of major collapses and increased pyroclastic flow activity and explosive activity. The dashed line marks the analysis of Barclay et al. (1996) who reported a magmatic sulphur concentration of <150 ppm for Soufrière Hills lavas.*

6.2.4 *The scavenging of SO_2 from the gas plume: implications for COSPEC monitoring*

The use of a Montserrat Police launch has enabled the MVO to obtain COSPEC analyses of the plume at differing distances downwind from the volcano for three different days, 29/7/96, 8/8/96 and 16/1/97 (MVO reports; Oppenheimer et al., 1998 - in prep.). The SO_2 fluxes, see **table 6.2**, were derived for traverses beneath the plume at ranges of between 4.3 and 12.8 km from the dome. It can be clearly seen that the SO_2 fluxes decrease substantially with increasing distance from the dome, see **figure 6.9**. Möller (1980) and Edner et al. (1994) have suggested this is due to the oxidation of SO_2 to SO_4^{2-} which is not detected using COSPEC.

Date	Boat run 1		Boat run 2		Boat run 3		Calculated data		
	distance (km)	SO_2 (t/d)	distance (km)	SO_2 (t/d)	distance (km)	SO_2 (t/d)	initial SO_2 (t/d)	K_1	wind (m/s)
29/7/96	5.3	228	6.3	133	7.2	81	3710	0.0054	10.1
8/8/96	6.5	2514	9.0	1546	12.7	959	7040	0.0015	9.3
16/1/97	*4.3	*~2000	9.8	344	12.8	233	5480	0.0017	~7.3

Table 6.2 *Results of COSPEC traverses across the plume at different distances from dome on 29/7/96 and 8/8/96 (Oppenheimer et al., 1998 - in prep.) and16/1/97. (MVO report). Wind speeds for the first two days were measured from Windy Hill. The wind speed for 16/1/97 was estimated at 7.3 m/s, the average wind speed at 5000 feet as recorded by V.C. Bird Airport on Antigua for the period 28/4/96 - 21/5/96. The average surface wind speed for the same period was 7.0 m/s. The initial SO_2 flux on effusion from the dome has calculated by using the value of k_1 derived using* ***equation 6.1*** *(after Oppenheimer et al., 1998 - in prep.). * Vehicular flux-estimate based on a half-width plume of ~1000 t/d.*

The SO_2 to sulphate mechanism has been previously suggested by Malinconico (1979) and Martin et al. (in Edner et al., 1994) for the removal of SO_2 from Mt. Etna's plume; caused by SO_2 being adsorbed onto the surface of water droplets and ash particles (Möller, 1980; Oppenheimer, pers. com.). Edner et al. (1994) reported that rates of SO_2 decrease (k) at

Mt. Etna were ~10^{-4} - 10^{-5} s^{-1}. The scavenging of SO_2 from the plume has serious implications for SO_2 monitoring now that data collection cannot be done using road vehicles in the Plymouth - St. Patrick's area. The only possible way to continue using COSPEC on a regular basis is by boat; although this is dependent on the availability of boat and COSPEC and also calm sea conditions.

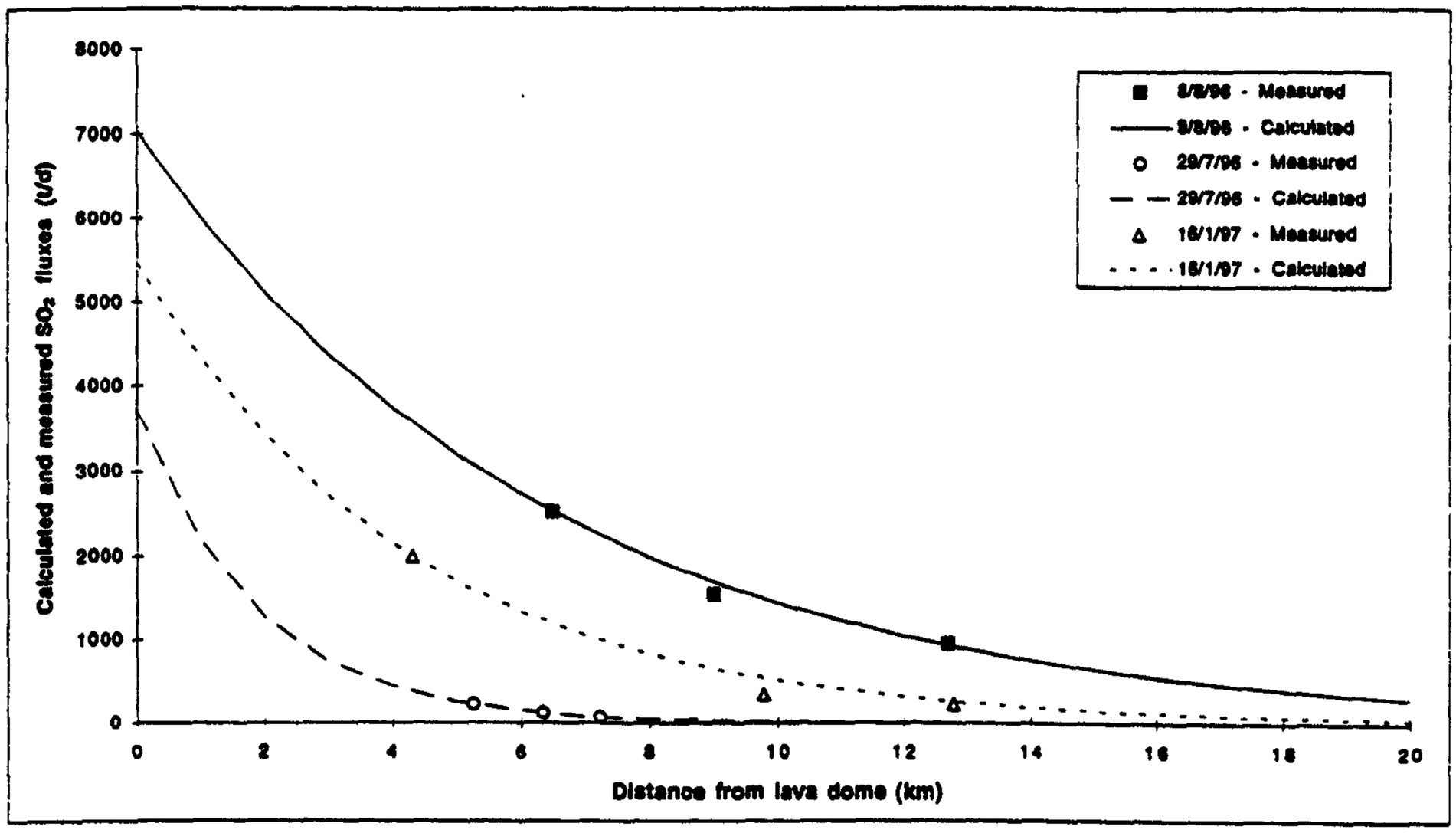

***Figure 6.9** This shows the exponential decrease in measured SO_2 flux (symbols), reported by the MVO and Oppenheimer et al. (1998, in prep.), for three days when COSPEC analyses were conducted off the western coast of Montserrat. I have calculated first-order exponential decreases using **equation 6.2** (after Oppenheimer et al., 1998 - in prep.) to give the calculated curves (lines) representing the theoretical SO_2 fluxes downwind of the dome as a function of time. Extrapolating back to a zero distance (zero travel time) I have estimated the initial SO_2 fluxes before scavenging took place, see **table 6.2**.*

The removal of SO_2 can be fitted to a simple exponential curve, as suggested by Oppenheimer et al. (1998, in prep.), see **equation 6.2**. The resulting decay rate, and therefore initial SO_2 flux, can however only be estimated as SO_2 fluxes for each day were only recorded at three distances away from the dome making it difficult to fit an accurate curve to the data. I have determined SO_2 removal rates, using **equation 6.2**, of k_1 = 0.0015, 0.0017 and 0.0054.

$$\Phi_1 = \Phi_2 e^{k_1(t_2 - t_1)} \qquad \text{(Oppenheimer et al., 1998 - in prep.)} \qquad (6.2)$$

where Φ_1 and Φ_2 are initial and observed (reduced) fluxes, k_1 is the SO_2 removal rate, t_1 and t_2 being initial and observed plume travel-times. The highest value of k, ~0.0054, was calculated using the lowest concentration SO_2 data with the lowest inter-analysis spacing, <1 km. This has introduced errors into the value of k, which may actually be closer to the other k values of <0.0020. These values are themselves only estimates as the error on COSPEC flux values is up to ~45%, see Section 6.2.5.

This limited study is only an indication of the actual amount of scavenging. A far more detailed study is required to accurately constrain the rates of SO_2 removal. It can, however, be seen that in order to make comparable measurements, COSPEC analyses must consistently be made at a set distance from the dome, relating to plume travel-time. This should be undertaken as close to the volcano as is safe to measure the highest SO_2 concentrations, thus reducing the errors on the results.

6.2.5 Errors associated with COSPEC analyses

COSPEC data can only be used within the limits set by the accuracy of the technique. Correlation spectrometry is susceptible to the scattering of light by airborne ash, clouds and aerosols within the atmosphere; these can all act to alter the amount of SO_2 apparently detected, see Section 2.3.4. The generation of an SO_2 flux is, in principle, a simple procedure; requiring only the wind speed data and the integrated absorbance of SO_2 across the plume. I have attempted to identify and quantify various types of errors associated with the SO_2 fluxes I collected at Soufrière Hills volcano; these are summarised in **table 6.3** and lie between ~16 and ~45%. I have divided the errors into three groups. These are:

A). Data processing errors.

B). Instrumental errors.

C). Natural errors, i.e. atmospheric and volcanic.

A - Data processing errors

These mainly concern the integration of the area beneath the chart recorder's plotted line and are principally simple arithmetic errors. Data processing consists of counting the squares for each segment of the COSPEC route. Each column of squares counted is generally rounded to the nearest half square; thus giving a ~2 - 10% error for each column counted. These errors relate to the recorded lengths of each road-segment (SEG), see **table 6.3**; the average area beneath the plotted line in each segment (AREA); and the height of the calibration peak (CAL1) which also is recorded on the print-out. The wind direction (AZM), see **table 6.3,** is taken as being the orientation of the line from the dome to the point within a road-segment corresponding to the maximum SO_2 peak on the plotted chart. For bifurcated plumes the wind direction was taken as being mid-way between the two plume peaks. The lengths of each road segment (ROAD) were measured using either a vehicle odometer or the published 1:50,000 scale Montserrat map. The road segment-length was corrected to give its aspect relative to the wind direction by using **equation 6.1**.

$$\text{Segment length} = \text{Sin}\left(\begin{array}{l}\text{accute intersection between}\\ \text{road orientation and wind}\\ \text{direction}\end{array}\right) \times \left(\text{length of road segment}\right) \qquad \textbf{(6.1)}$$

B - Instrumental errors

Instrumental errors associated with the COSPEC are hard to detect in the field unless the instrument is malfunctioning badly. Errors may come from several sources including: instrumental drift, due to temperature changes; supply voltage variation; and vehicle vibrations, which affect the rotation of the correlator disc. These can all contribute to small variations in the instrument's output voltage. The other main source of instrumental error comes from the measurement of speeds of the relatively constant trade-winds (WINMES), see **table 6.3**. A Davis ball-bearing wind flow-meter was used to collect wind speeds in feet/minute. Errors may arise from the conversion of speeds into metres per second and from adding on the manufacturers own error corrections. To reduce the effect of the ground on wind speed, the author held the instrument above the head whilst another person timed the 1 minute

measuring runs. Five runs were collected in each session and the average and standard deviation used to derive the fluxes and errors reported by the MVO.

C - Natural errors

Variation in wind speed is the main source of error in COSPEC analyses. Analyses were carried out downwind of the volcano where there is most disruption to the air-flow, caused by the volcanic edifice creating large eddy currents. Wind speed measurements on Montserrat were conducted outside the edifice's wind-shadow and at as high an altitude as possible. Inaccuracies were introduced into the derived gas flux by measuring the wind speed at ground-level - actually the top of a ~200 m high bluff facing into the wind, rather than at the altitude of the plume, ~900 m. The error introduced into the wind speed measurements due to convection and air turbulence is highly variable. I have therefore incorporated it into the general variation in wind speed (WINVAR), see **table 6.3**.

Wind speeds for COSPEC analyses were measured before the first and after the last run each day. Any major variation during the collection period may therefore not be detected. Collection of wind speed data was taken over several 1 minute periods; the average value taken as being representative for the entire day. Variation in wind direction at different altitudes can also introduce errors into the final flux estimate. The author observed low, <1000 m, wind-blown ash clouds diverging at angles of ~30° during May and June, 1996. I suggest this variation to be the cause of the plume bifurcation recorded in the COSPEC analyses, see **figure 6.4**. A comparison between the wind speeds measured at Windy Hill by the author and those recorded by D.C. Bird airport (Antigua) at 5000 feet showed the higher altitude winds were ~4% faster; I have called this error WINALT, see **table 6.3**.

Ash, clouds and condensation within the plume cause significant variations in the amount of SO_2 detected during traverses beneath the plume, see Section 2.3.4. Millán (1980) reported that scattering effects can increase the measured amount of SO_2 by ~10% in the centre of the plume, but will cause a similar decrease at its margins. Ash, cloud and condensation all act to enhance diffraction which, if the COSPEC is directly beneath the plume, can produce a total increase in the measured SO_2 of up to 30%.

Summary of COSPEC errors

The total errors in **table 6.3**, ~16 - 45%, are similar to those estimated by Stoiber et al. (1983). The variation in the wind speed and presence of clouds are the major sources of error. These may be comparable to errors associated with the scavenging of SO_2 from the plume by oxidation to sulphate and aerosol formation, see Section 6.2.4 and below. I summarised the data relating to plume scavenging in Section 6.2.4; the effects of which may reduce the observed flux by >50%.

Error type	Origin of Error (see text)	Units	Best error %	Average error %	Worst error %
A	CAL 1	0.5 squares	1	2	2
A	AREA	0.5 squares	5	9	11
A	SEG	0.5 squares	2	3	4
A	AZM	2 degrees	1	1	1
A	ROAD	2 percent	2	3	5
B	*INST	2 percent	2	2	2
B	WINMES	2 percent	1	2	2
C	WINVAR	variable	14	21	29
C	§WINALT (wind at 5000 ft)	4 percent	4	4	4
C	#Ash	variable	0	5	10
C	*Clouds	variable	0	15	30
Total error		percent	~16	~29	~45

Table 6.3. *Errors associated with COSPEC analyses at Soufrière Hills volcano, Montserrat. The errors are: CAL1. height of CAL1 calibration peak; AREA. segment area; SEG. segment length; AZM. wind direction; ROAD. actual length of each segment; INST. calibration cell concentrations; WINMES. measuring the wind speed; WINVAR. variation in wind speed; WINALT. variation of wind speed with altitude; Ash and Clouds. UV scattering due to ash and clouds. Errors have been calculated/estimated by using COSPEC data collected on 2/6/96. Percentages recorded relate to changes in the total SO_2 flux. Total error percentages are calculated as $\sqrt{\Sigma(E^2)}$ where E are the individual error values (after Stoiber et al., 1983). *Millán (1980), #Delmelle (pers. com.), §D. C. Bird International Airport, Antigua.*

6.2.6 General COSPEC summary

The major COSPEC errors have been summarised in **table 6.3**. Although cumulative errors range between ~16 and 45%, and can be larger in adverse situations, the system is a quick and convenient method to make semi-quantitative estimates of the SO_2 output of a volcano. The removal of SO_2 from the gas plume by oxidation and aerosol formation requires that the distance between plume source and route of COSPEC analyses must remain constant to accurately compare data.

Small-scale daily fluctuations in the data are probably due to changes in wind speed, and the presence of clouds and ash. Larger-scale fluctuations can, however, be correlated with changes in the rates of lava effusion. **Figure 6.7**, showed that increases in SO_2 flux seem to lag behind changes in effusion rate - thus preventing COSPEC being used as a predictive tool for short-term changes in the rates of dome growth and associated pyroclastic flow activity. However, the paucity of COSPEC data during times of rapid changes in the effusion rate makes the exact relationship between the two difficult to interpret.

The SO_2 fluxes and effusion rates at Soufrière Hills are generally higher than those reported for Mt. Unzen, used by the MVO as an advanced analogue for Soufrière Hills. The wider variation in SO_2 flux at Soufrière Hills has enabled the author to divide the SO_2 flux and lava effusion data into two fields: passive dome growth with high flux and low effusion rates; and active dome growth with lower flux and high effusion rates. The periods of major pyroclastic flow activity and explosive eruptions all occur within the active dome growth field; as does the gas flux and lava effusion data for Mt. Unzen. This suggests that Mt. Unzen, compared to Soufrière Hills, is relatively gas deficient. The levels of SO_2 flux at Soufrière Hills volcano are far too high to be supplied a magmatic sulphur content of <150 ppm (Barclay et al., 1996) suggesting that either a large proportion of degassed magma is intruded or extra sulphur is being degassed from another source; this is discussed later.

6.3 The use of OP-FTIR on Montserrat

6.3.1 Introduction to OP-FTIR on Montserrat

The OP-FTIR technique had only been used previously by the author in an experimental role, the volcanoes studied having been chosen for ease of access and suitability. Factors relating to this include: good weather and visibility; low-level dense volcanic plume; and the accessibility of the summit area. Soufrière Hills volcano was chosen to determine how the system would work under difficult operating circumstances and non-ideal conditions. Analysis of the Soufrière Hills gas plume was the first time that the OP-FTIR technique had been used as part of a multi-disciplinary approach reacting to a volcanic crises.

6.3.2 OP-FTIR technique used on Montserrat

The Midac AMS™ OP-FTIR system was first used on Montserrat by the author and Peter Francis (Open University) with the help of MVO staff. The eruption of Soufrière Hills volcano provided the opportunity to fully test the OP-FTIR technique during an actual volcanic crisis. The system had previously been used on Mt. Etna and Vulcano in 1994 (Chaffin et al., 1995; Francis et al., 1996); see Chapters 4 and 5.

The OP-FTIR system comprised of an IR spectrometer with liquid-nitrogen cooled MCT (Hg-Cd-Te) detector, housed in a rigid casing, mounted piggy-back on top of a 10" (25.4 cm) diameter telescope on a heavy-duty Quickset™ tripod. Control of the detector and data retrieval were controlled by a 586 75 MHz "Colossus" portable computer, using Spectacle™ software (LabControl GmbH) for data manipulation. A 1275°C artificial IR source mounted in a 20" (50.8 cm) parabolic reflector completed the set up used for "active" analyses; "passive" analyses utilised a natural IR source e.g. the hot lava dome. The IR source, detector and computer were all powered using either 12V D.C. car batteries or a 240 A.C. portable petrol generator. A more detailed description of the OP-FTIR system can be found in Section 2.2.

The author's previous experience of using the OP-FTIR system on Mt. Etna and Vulcano had shown that optimum results were achieved when the IR source and spectrometer were positioned within the volcanic plume at distances of ~400 - 1800 m apart. At Soufrière Hills volcano there was no access to the dome or the gas plume due to danger of rock falls, pyroclastic flows and the rugged topography. The author therefore had to devise alternative methods to analyse the plum's composition. The new OP-FTIR methodology was broadly divided into four styles; these were:

1). The spectrometer was positioned at a distances of ~2000 - 3000 m from the dome, which was used as a passive IR source.

2). The spectrometer and portable IR source were situated downwind of the dome using path lengths of ~500 - 1500 m.

3). The spectrometer and portable IR source were used over path lengths of <400 m in habitated areas to provide environmental data on background levels of volcanic gases.

4). The telescope and spectrometer were mounted in the MVO helicopter which flew close to the up-wind side of the dome which was used as an IR source.

Most of these methods were, to a large extent, experimental and only intended to show whether they were suitable for use in circumstances where there was no direct access to the volcanic plume. As anticipated, several methods provided little or no usable data.

Methods and problems experienced with OP-FTIR investigations

Below I have described the OP-FTIR methods I used at each location during the period 15/5/96 - 4/6/96, see **figure 6.10**, and the problems encountered:

15/5/96. The spectrometer was located at Harris school playing-field and the NE side of the dome used as a passive IR source, giving a path length of ~2900 m. Thick cloud prevented any useful IR signal being detected. The easterly wind ensured that only a fraction

The author's previous experience of using the OP-FTIR system on Mt. Etna and Vulcano had shown that optimum results were achieved when the IR source and spectrometer were positioned within the volcanic plume at distances of ~400 - 1800 m apart. At Soufrière Hills volcano there was no access to the dome or the gas plume due to danger of rock falls, pyroclastic flows and the rugged topography. The author therefore had to devise alternative methods to analyse the plum's composition. The new OP-FTIR methodology was broadly divided into four styles; these were:

1). The spectrometer was positioned at a distances of ~2000 - 3000 m from the dome, which was used as a passive IR source.

2). The spectrometer and portable IR source were situated downwind of the dome using path lengths of ~500 - 1500 m.

3). The spectrometer and portable IR source were used over path lengths of <400 m in habitated areas to provide environmental data on background levels of volcanic gases.

4). The telescope and spectrometer were mounted in the MVO helicopter which flew close to the up-wind side of the dome which was used as an IR source.

Most of these methods were, to a large extent, experimental and only intended to show whether they were suitable for use in circumstances where there was no direct access to the volcanic plume. As anticipated, several methods provided little or no usable data.

Methods and problems experienced with OP-FTIR investigations

Below I have described the OP-FTIR methods I used at each location during the period 15/5/96 - 4/6/96, see **figure 6.10**, and the problems encountered:

15/5/96. The spectrometer was located at Harris school playing-field and the NE side of the dome used as a passive IR source, giving a path length of ~2900 m. Thick cloud prevented any useful IR signal being detected. The easterly wind ensured that only a fraction

The author's previous experience of using the OP-FTIR system on Mt. Etna and Vulcano had shown that optimum results were achieved when the IR source and spectrometer were positioned within the volcanic plume at distances of ~400 - 1800 m apart. At Soufrière Hills volcano there was no access to the dome or the gas plume due to danger of rock falls, pyroclastic flows and the rugged topography. The author therefore had to devise alternative methods to analyse the plum's composition. The new OP-FTIR methodology was broadly divided into four styles; these were:

1). The spectrometer was positioned at a distances of ~2000 - 3000 m from the dome, which was used as a passive IR source.

2). The spectrometer and portable IR source were situated downwind of the dome using path lengths of ~500 - 1500 m.

3). The spectrometer and portable IR source were used over path lengths of <400 m in habitated areas to provide environmental data on background levels of volcanic gases.

4). The telescope and spectrometer were mounted in the MVO helicopter which flew close to the up-wind side of the dome which was used as an IR source.

Most of these methods were, to a large extent, experimental and only intended to show whether they were suitable for use in circumstances where there was no direct access to the volcanic plume. As anticipated, several methods provided little or no usable data.

Methods and problems experienced with OP-FTIR investigations

Below I have described the OP-FTIR methods I used at each location during the period 15/5/96 - 4/6/96, see **figure 6.10**, and the problems encountered:

15/5/96. The spectrometer was located at Harris school playing-field and the NE side of the dome used as a passive IR source, giving a path length of ~2900 m. Thick cloud prevented any useful IR signal being detected. The easterly wind ensured that only a fraction

of the N-S optical path contained volcanic gas. This was a similar technique to that used successfully by Mori et al. (1993) at Mt. Unzen in 1992. see Section 6.3.4.

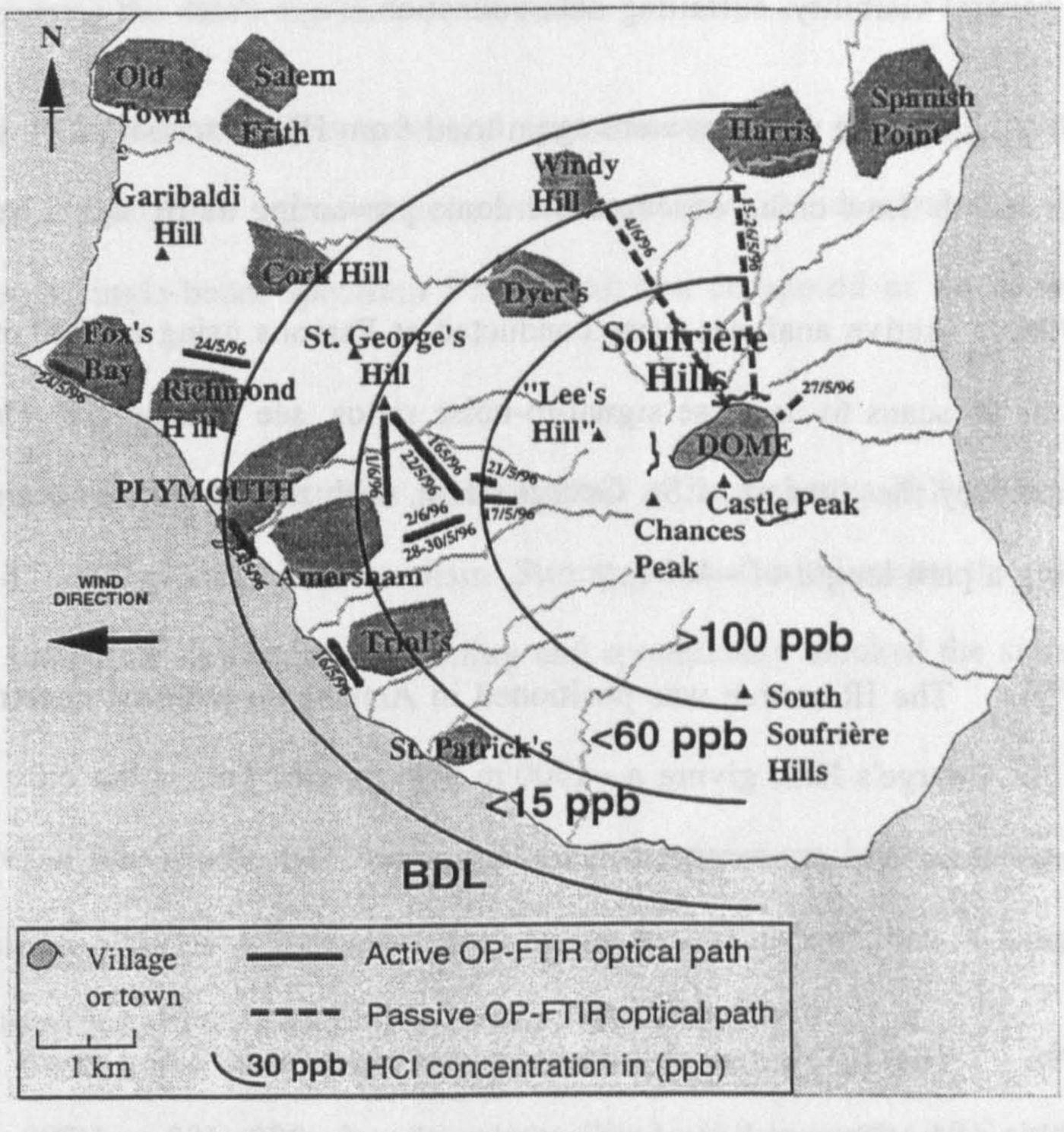

***Figure 6.10**. Map showing sample localities for passive and active OP-FTIR analyses on Montserrat. All the locations used, with the exception of St. George's Hill, have subsequently been affected by pyroclastic flow activity. The figure shows the a crude concentration gradient with the coastal areas having a lower HCl concentration relative to the areas directly downwind of the dome; BDL = below detection limits. The concentrations were measured over three weeks, during a period with different wind directions and levels of dome activity, and so can only give an estimate of the actual geographic variability of HCl downwind of Soufrière Hills volcano.*

16/5/96. The spectrometer was located at the top of St. George's Hill with the portable IR source positioned in Upper Amersham, giving an path length of ~1500 m. Difficulties in accurately aiming the telescope were due to the high gearing on the Quickset™ tripods. Later analyses on the coast road at Kinsale used paths lengths of ~150 - ~500 m.

17/5/96. Active analyses in Upper Amersham required a <200 m path length due to paucity of flat open ground. Sporadic ash falls coated optics on both IR source and telescope and reduced general visibility, curtailing data collection.

18/5/96. Passive analyses were again tried from Harris school playing-fields, using a ~2900 m path length. Low cloud obscured the dome preventing its IR signal being detected.

21/5/96. Active analyses were conducted at Parsons using a ~200 m path length. I co-added 32 or 48 scans to increase signal-to-noise ratios, see Section 2.2. The spectrometer was also situated by the old fort at St. George's Hill, with the IR source located by the wind turbines, giving a path length of ~400 m.

22/5/96. The IR source was positioned in Amersham with the spectrometer located at the top of St. George's Hill, giving a ~1500 m path length. This is the only data-set which contained detectable SO_2 concentrations, <40 ppmv.m. High winds and heavy rain stopped data collection.

24/5/96. The IR source and spectrometer were used along roads in Fox's Bay, Richmond Hill and by Plymouth dock at path lengths of ~380, 400 and 280 m respectively. Dry conditions and light winds provided excellent conditions for data collection.

26/5/96. Passive data were again collected from Harris school using a ~2900 m path length. Although cloud-free, persistent rockfalls generated ash that periodically obscured the dome. Again the sidewind meant that very little volcanic gas filled the optical path.

27/5/96. The telescope and spectrometer were securely tied into the MVO Jet-Ranger helicopter so that the telescope pointed out the starboard door. The helicopter hovered sideways ~50 m upwind of the dome. Only 10 scans were co-added to provide rapid data collection, sampling taking ~44 seconds, due to the danger from rock falls and pyroclastic flows. Aircraft vibration, turbulence and drift meant that the area of dome targeted was constantly changing; resulting in very low signal-to-noise ratios and poor quality data.

28/5/96. The portable IR source and spectrometer were located above Amersham, giving a ~325 m path length. Each single-beam spectrum I collected was composed of 32 co-added scans to increase the data's signal-to-noise ratio.

30/5/96. The portable IR source and spectrometer were positioned ~350 m apart above Amersham. To improve signal-to-noise ratios and thus the detectability of very low level analytes, each single-beam spectrum I collected was composed of 48 or 64 co-added scans.

1/6/96. The spectrometer was again located at St. George's Hill with the portable IR source located ~1500 m away in Amersham. Strong gusts of wind meant the telescope had to be repeatedly realigned. Ash reduced visibility and sporadically blocked the signal from the IR source.

2/6/96. The portable IR source and spectrometer were located along a track in Amersham, giving a ~350 m path length. High winds provided problems in keeping the IR source and spectrometer aligned, leading to erratic data collection.

4/6/96. The spectrometer was located on Windy Hill to use the NW side of the lava dome as a passive IR source. Intermittent ash and rain showers meant few spectra were obtained.

Derivation of gas concentrations

I derived gas concentrations from the OP-FTIR data by determining which spectrum in each data-set had the least volcanic analyte and using this as a background to create absorbance spectra from the single-beam data collected, see Section 2.2. Analytes were then manually subtracted, on screen, from the absorbance spectrum, using laboratory reference spectra, until they could no longer be observed. The product of the analyte's multiplication factor, needed to remove all the observed analyte from the sample spectrum, and the concentration of the analyte's laboratory reference spectrum gave the analyte's measured concentration above background. This is a slow way to analyse data, but is useful as the human eye can ignore spectral defects due to H_2O and spectral shifts caused by instrumental

errors. The nature of the data processing favours the accurate quantification of analytes with sharp, pronounced spectral features, such as HCl, HF and N_2O. Analytes with less pronounced, broader fundamentals, such as SO_2 and SiF_4, were harder to quantify at very low concentrations, see Section 2.2.

6.3.3 Results of OP-FTIR analysis on Montserrat

General Results

Table 6.4 summarises the results of the OP-FTIR study carried out principally by the author for the period 15/5/96 - 4/6/96. It is evident that gas concentrations are very low; SO_2 being below or at the instrument's detection limits. Only analyses conducted by the author on 22/5/96 using a 1500 m optical path between the top of St. George's Hill and Amersham produced SO_2 data. SO_2 concentrations determined close to the limit of detection, ~10 ppm.m. I determined only 10 SO_2:HCl ratios from the entire Montserrat OP-FTIR data-set. These were not enough to statistically analyse for temporal or source variations.

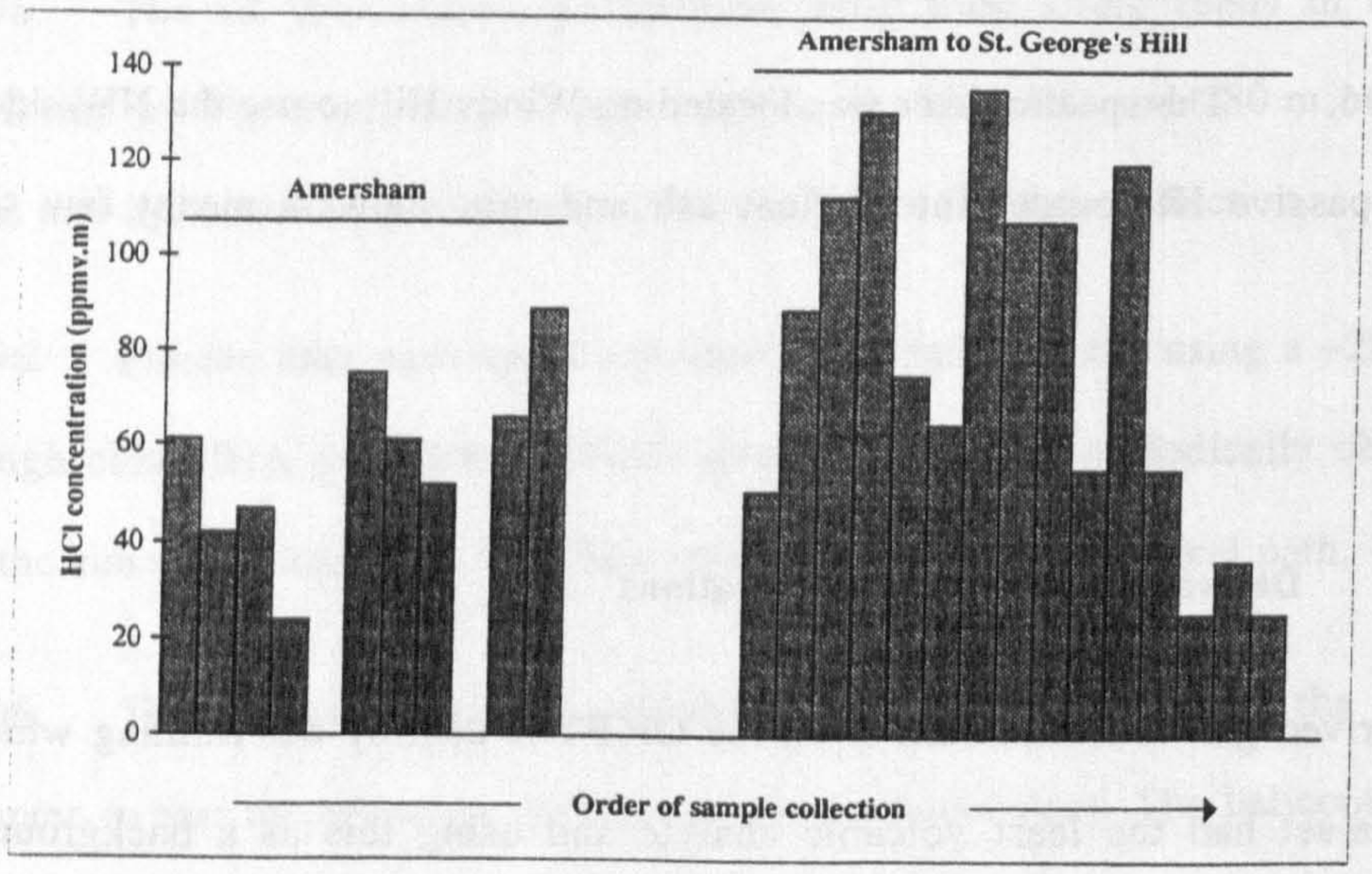

***Figure 6.11**. This shows the variation in HCl concentrations, measured using OP-FTIR on 17/4/96 and 22/4/96 at Montserrat. The variation in concentrations relate to a time-span of ~1 hour at each location. This may be due to eddy currents or real variations, possibly caused by puffing.*

The SO_2 concentrations were at the limits of detection, consequently the errors on the gas ratios are large, $<0.5 \pm 0.2$. SO_2 concentrations were below the limit of detection for the rest of the data-set and therefore support the very low SO_2:HCl ratio of emitted gases. My

results are consistent with a follow-up investigation in August 1996 by Oppenheimer et al. (1998) who estimated the SO_2:HCl mass ratio was <0.1. In Section 6.4.2 I interpret this low SO_2:HCl ratio as possibly relating to the deep degassing of a basaltic magma body beneath Soufrière Hills.

The average SO_2:HCl ratio of $<0.5 \pm 0.2$ was far lower than gas ratios determined by the author at either Vulcano or Mt. Etna (Chapters 4 and 5). I have interpreted this to reflect the differences in style of volcanic activity and volatile compositions that exist between basaltic and andesitic systems. This is supported by Giggenbach (1996) who reported much lower average S:Cl ratios in andesitic volatiles, ~0.07, compared to basaltic compositions, ~10.1.

Date	Location	Path length	HCl ppmv.m	SO_2 ppmv.m	$\frac{SO_2}{HCl}$ mass ratio
15/5/96	Harris school field at dome	2900 - P	BDL	BDL	na
16/5/96	Amersham to St. George's Hill	1500-A	BDL	BDL	na
16/5/96	Kinsale shore road	150 - 500 A	~7 ± 3	BDL	na
17/5/96	Upper Amersham	200 - A	57 ± 19	BDL	na
18/5/96	Harris school field at dome	2900 - P	BDL	BDL	na
21/5/96	Parsons Estate	200 - A	14 ± 7	BDL	na
21/5/96	St. George's Hill	400 - A	na	na	na
22/5/96	Amersham to St. George's Hill	1500 - A	80 ± 38	~24 ± 12	<0.5 ± 0.2
24/5/96	Plymouth docks	275 - A	14 ± 4	BDL	na
24/5/96	Fox's Bay (Bransby Pt.)	380 - A	BDL	BDL	na
24/5/96	Richmond Hill (Elberton)	400 - A	BDL	BDL	na
26/5/96	Harris school field at dome	1500 - P	BDL	BDL	na
27/5/96	Helicopter-mounted near dome	50 - 300 - P	BDL	BDL	na
28/5/96	Amersham	325 - A	18 ± 6	ND	na
30/5/96	Amersham	350 - A	17 ± 6	BDL	na
1/6/96	Amersham to St. George's Hill	1500 - A	BDL	BDL	na
2/6/96	Amersham	350 - A	~15	BDL	na
4/6/96	Windy Hill at dome	~2000 - P	ND	ND	na

Table 6.4. *Results of the author's OP-FTIR investigation of the gas plume on Montserrat during May and June 1996. BDL = below detection limit or due to poor data/low signal-to-noise/bad background; na = not applicable; A = artificial IR source, P = natural IR source - the active dome. OP-FTIR locations are shown in* ***figure 6.10.***

The OP-FTIR data-set I collected consists of small numbers of samples collected at several localities over a period of three weeks. It has not been possible to determine the variation of HCl due to differences in wind direction, eddy currents, and the techniques used. However, the two days when larger data sets were collected, 17/5/96 and 22/5/96, at Upper Amersham and Amersham to St. George's Hill respectively, showed a marked variation through the sample set, see **figure 6.11**. This may be due to eddy currents or real differences in the composition of the plume, caused by puffing or exsolution of volatiles from different pockets of magma.

Detection of other/non-volcanic gases.

During the analysis of the OP-FTIR data-set, the author identified three other gases species using OP-FTIR: CO_2, CO and N_2O. All three gases have a number of natural and anthropogenic sources, but principally relate to the combustion of organic material, i.e. wood, grass or oil/petrol; CO_2 is also a major component of volcanic emissions. I identified CO_2 in many IR spectra; however, due to its high ambient concentration, ~355 ppmv, it could not be quantified.

I only positively identified CO at one location, the main coast road adjacent to Plymouth dock, with CO concentrations of <75 ppmv.m being measured, see **figure 6.12A**. Several of the analyses runs I conducted here had to be redone due to vehicle traffic blocking the IR signal from the portable IR source. It is therefore likely the CO signature results from combustion of diesel fuel by dock traffic.

I detected N_2O at very low concentrations in several data-sets by the author, see **figure 6.12B**. These were collected in Plymouth, Upper Amersham and in an Amersham - St. George's Hill long-path analysis. N_2O, like CO and CO_2, is quite distinctive and easily identified by its numerous sharp peaks and has been identified at Mt. Etna and Vulcano by the author. Ambient levels of N_2O are ~312 ppbv (Badr & Probert, 1990). Any N_2O from a distant source should be homogenised throughout the atmosphere and therefore not detected in absorbance spectra. The N_2O must therefore originate from a local source. Two possible

sources may therefore be the petrol generator or jeep used to power the detector or portable IR source, or burning vegetation ignited or buried by rock falls and pyroclastic flows.

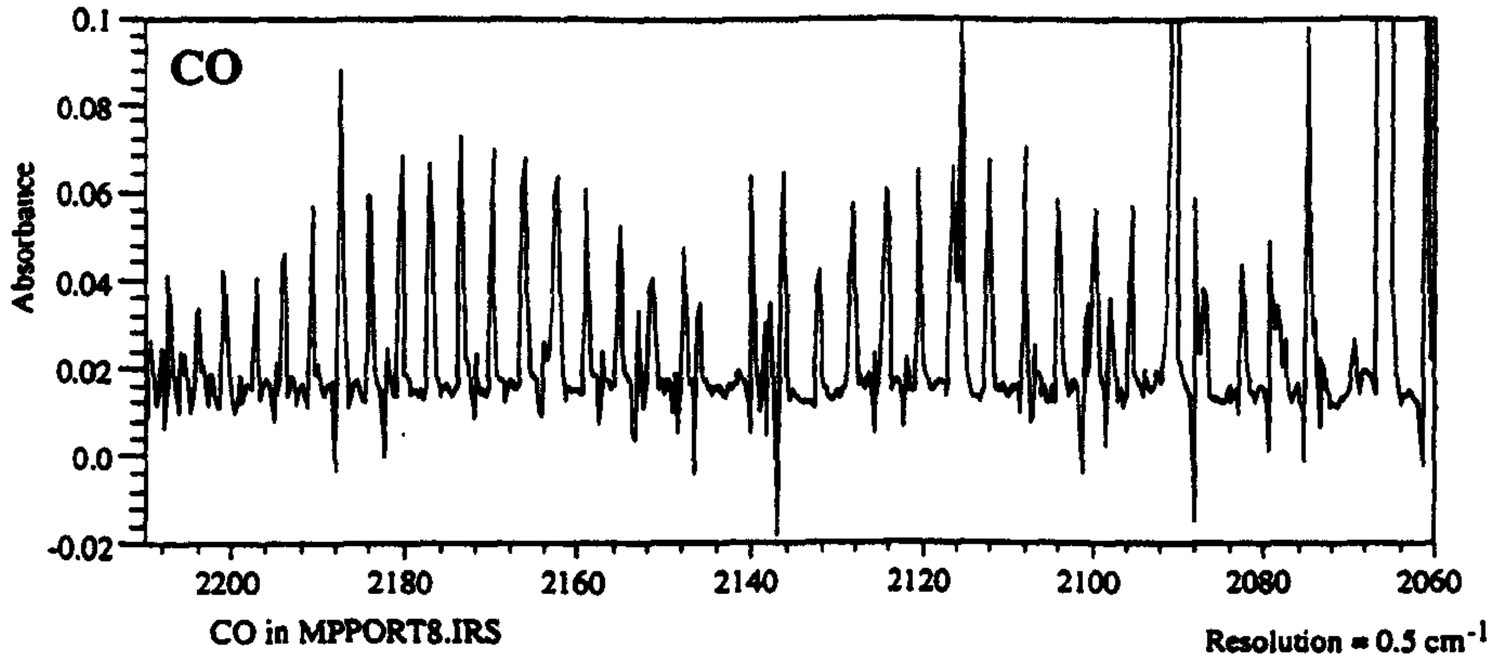

Figure 6.12. A OP-FTIR spectrum of CO collected along the docks road in Plymouth on Montserrat in May 1996.

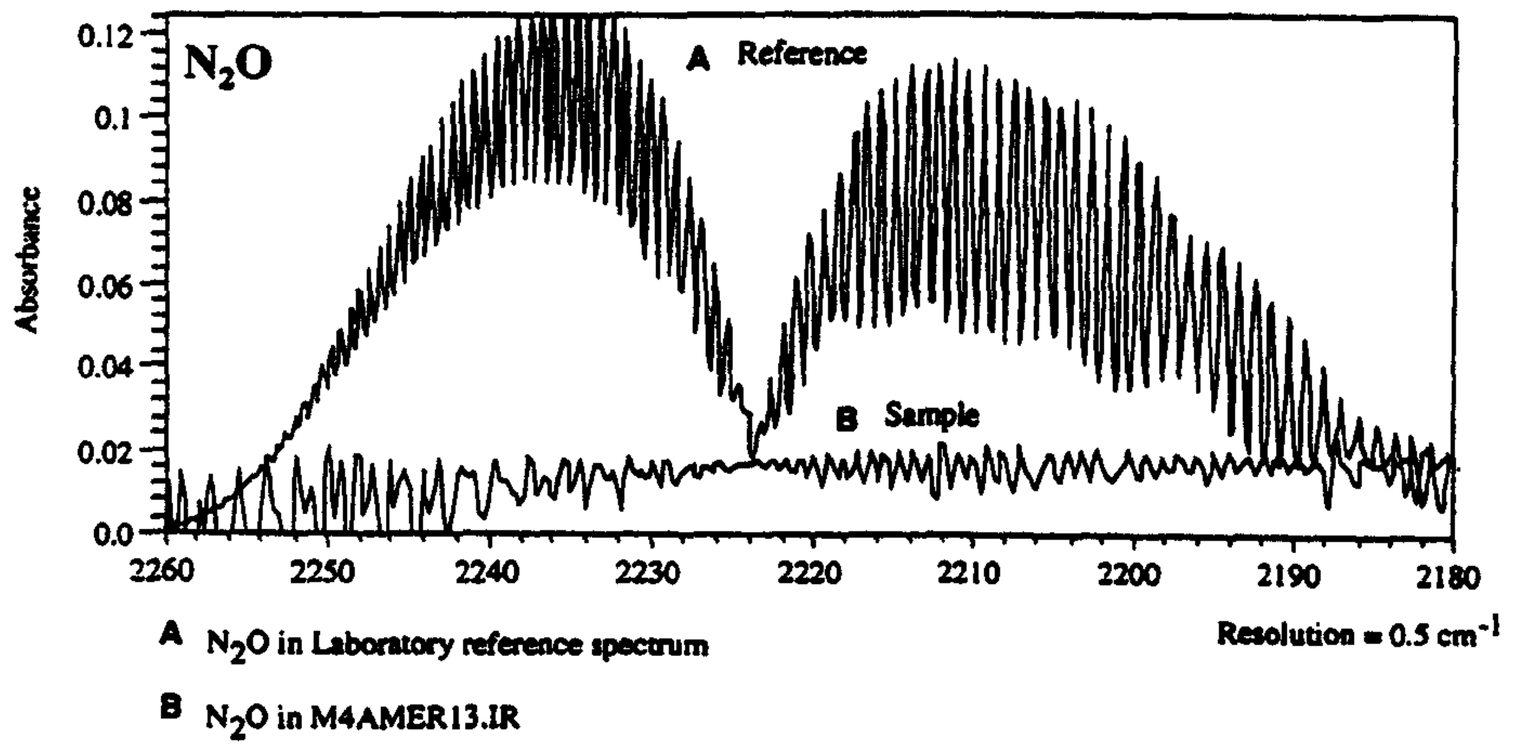

Figure 6.12. B. OP-FTIR spectrum of N_2O (with reference spectrum), collected above Amersham, Montserrat in May 1996.

Problems associated with the collection and interpretation of Soufrière Hills OP-FTIR data

Accessibility of dome and plume

Collection of OP-FTIR data at Soufrière Hills was severely hampered by the volcano's inaccessibility. Apart from whilst airborne, it was not possible to get closer than ~2500 m from the lava dome and ~800 m vertically from the gas plume. Any volcanic gases therefore

detected had already undergone considerable atmospheric mixing and dilution, as well as solution and oxidation, to alter the original degassed composition to that measured.

I have already demonstrated in Chapters 4 and 5 the optimum OP-FTIR set-up requires the plume to pass through the optical path. This can be achieved by either positioning the IR source and/or spectrometer within the gas plume or be using a solar source, see Section 2.2. On Montserrat the author had to rely on eddy currents downwind of the volcano to bring plume gases closer to the ground. This was only partially successful in that only very low analyte concentrations were measured.

Temperatures of natural IR sources

I used the lava dome as an IR source in an attempt to incorporate volcanic gases into the optical path. The dome could only be seen up-close from locations at right angles to the wind direction, thus most of the optical path was devoid of plume gas. Persistent cloud cover and ash clouds also markedly reduced the intensity of IR signal detected. Collection of passive IR data was further hindered by the low surface temperature of the lava dome. The author assisted Donelly (1996) in conducting an airborne dome-temperature survey on 27/5/96 from the MVO helicopter. The results of this showed that although incandescent material was visible at night, the surface temperatures, measured using a Minolta/Land Compaq 3 radiometer, were quite low, ~100 - 360°C. As discussed in Section 2.2, low IR source temperatures, <400°C, do not provide the high energy IR radiation required to conduct accurate HCl analyses.

The effect of atmospheric removal of analytes

The removal of SO_2 from the plume by oxidation and aerosol formation was discussed in Section 6.2.5. Most of the OP-FTIR analyses were conducted close to the dome and should have only been slightly affected by SO_2 scavenging. The active dome was almost constantly hidden behind thick cloud during late May and June 1996, the period of OP-FTIR investigation by the author. During such periods, HCl will be removed preferentially from the

plume, due to its greater solubility in water. The measured SO_2:HCl ratios should therefore be higher than those taken during fairer weather. Oppenheimer et al (1998) reported lower SO_2:HCl mass ratios of <0.1 during a relatively cloud-free period in August 1996; possibly suggesting the scavenging of HCl during the author's period of analyses. I have therefore concluded that the low SO_2:HCl ratio estimated is not only due to atmospheric interaction but relates to the original, degassed, composition of the plume.

Errors associated with OP-FTIR investigations on Montserrat

The levels of analyte detected on Montserrat are much lower than on other volcanoes where OP-FTIR analyses have been carried out by the author; namely Vulcano and Mt. Etna (Chapters 4 and 5; Francis et al., 1995 and 1996). The limit of detection for SO_2 is quite

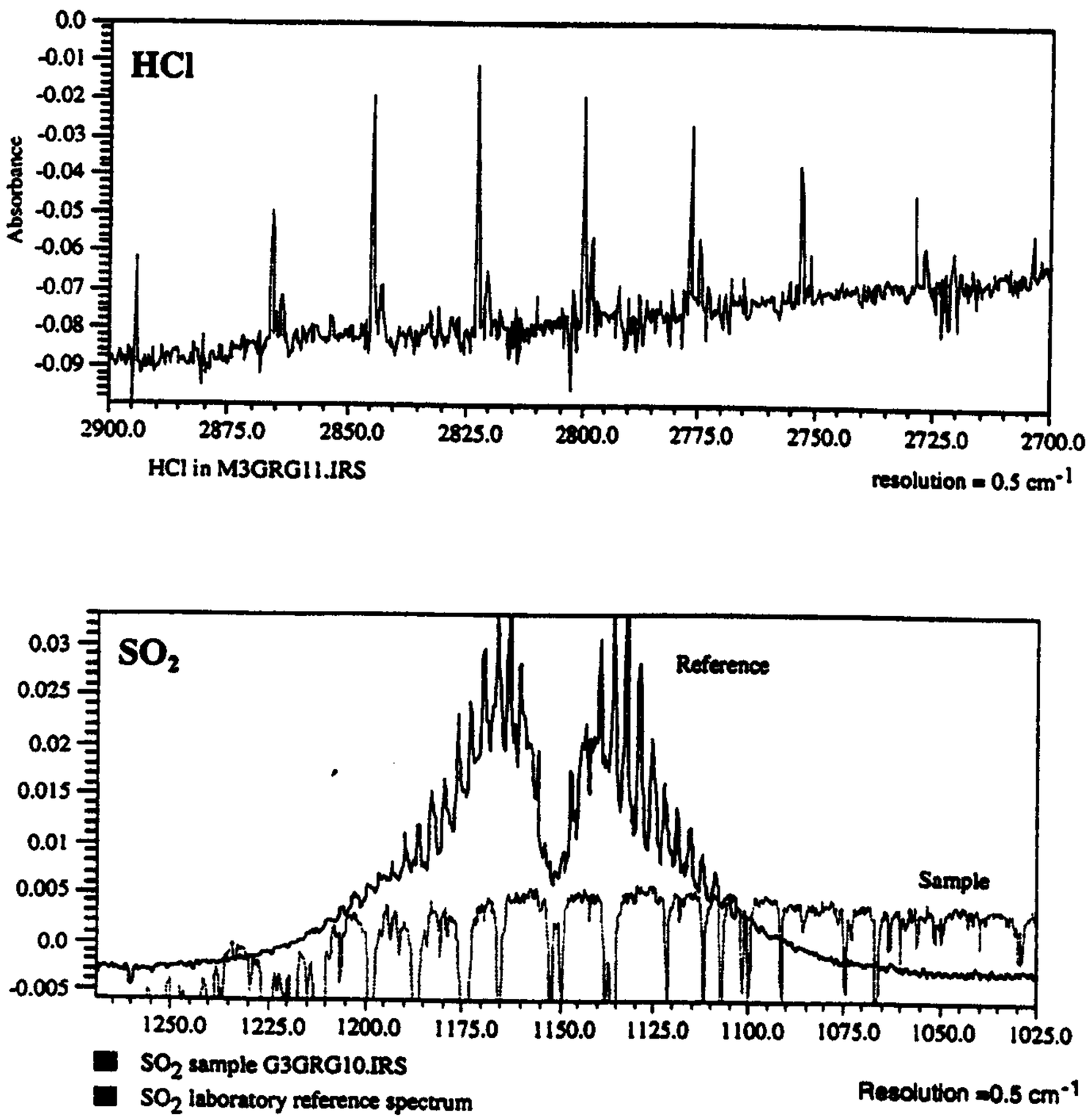

***Figure 6.13** A comparison of HCl and SO_2 fundamentals as determined on Montserrat. I have also shown the SO_2 laboratory reference spectrum, as the fundamental for sampled SO_2 is absent; due to its low concentration and low absorptivity coefficient.*

different to that of HCl. This is due to the higher absorptivity and much sharper fundamental of HCl, giving it a larger, easily identifiable peak, see **figure 6.13** and Section 2.2. The smaller broader SO_2 peak is extremely difficult to detect at very low concentrations, <50 ppmv.m. The error on the SO_2 concentrations measured, being close to the limit of detection are thus extremely high, >50%. The magnitudes of some of the data processing errors associated with OP-FTIR investigations on Montserrat are summarised in **table 6.5**. Other errors, mainly instrumental and atmospheric, are discussed in Section 2.2.

Analyte	Generally	Worst	Detection limits
SO_2	~25%	>50%	~10 ppmv.m
HCl	~10%	>25%	<5 ppmv.m

Table 6.5 *Summary of OP-FTIR errors as estimated for analyses collected on Montserrat by the author during May and June 1996. The higher errors of SO_2 reflect its lower concentration and the broader, less prominent shape of its fundamental absorbance peak.*

6.3.4 Comparison of OP-FTIR data for Soufrière Hills and Mt. Unzen volcanoes.

Mori et al. (1993) analysed gas emissions from Mt. Unzen volcano in March and July 1992 using a Bomem FTIR spectrometer, with an MCT detector, and telescope. They analysed gases ~1300 m away from the spectrometer; first using a cloud of volcanic gases and then a block of hot lava on the andesitic dome as their source of IR radiation. The lack of emission lines in their IR data indicate that the gas cloud was not hot, probably close to ambient temperatures; Mori et al. (1993) used a temperature of ~15°C in their HITRAN calculations, see Section 2.2.2. Their data consisted of sets of 100 co-added scans, collected at a lower resolution of 1 cm^{-1}. They used the HITRAN data-base to artificially generate a background atmospheric spectrum, against which the sample spectra were compared. Differences between the two spectra related to varying amounts of volcanic gases, which were determined using a least squares fit to the HITRAN-generated spectrum.

Mori et al. (1993) estimated SO_2:HCl mass ratios of ~1.2 - 2.8 and 1.8 - 3.2 for March and July 1992 respectively. These ratios are much higher than those determined by the author and Oppenheimer et al. (1998) at Soufrière Hills; with mass ratios consistently being

<0.5. The SO_2 concentrations of Mori et al. (1993) ranged from ~300 - 940 ppmv.m - two orders of magnitude greater than those I measured at Montserrat, <40 ppmv.m.

Conventional absorbance spectra are the log of the ratio between sample and background spectra, hence only analytes above the background level can be detected, see Section 2.2.2. Artificial backgrounds generated using the HITRAN database, however, enable lower, absolute, concentrations of analyte to be detected, thus increasing the sensitivity of the technique. I investigated HCl and SO_2 fundamentals in single-beam spectra from the Montserrat data-set to determine whether a high background analyte level was the cause of the low analyte concentrations in the calculated absorbance spectra. Compared to the Mori et al. (1995) data-set, the author's single-beam spectra show very few spectral features consistent with IR absorbance by HCl and SO_2. The lack of HCl and SO_2 absorbance peaks in the Soufrière Hills single-beam data indicate that analyte gas concentrations were genuinely low and not a product of the data reduction. I therefore suggest the main cause of differences between my results and those of Mori et al. (1993) was the much lower concentrations of analyte present at Soufrière Hills volcano.

6.3.5 Summary of OP-FTIR investigations on Montserrat

OP-FTIR was used on Montserrat to determine how the technique would perform under non-ideal situations. The use of the dome as a passive IR source proved unsuccessful, due to the low surface temperature of the dome lava and that only a small fraction of optical path that was filled with gas. This was compounded by the dome being obscured by thick cloud and ash from frequent rockfalls. The high altitude of the gas plume and inaccessibility of the volcano prevented the author from analysing higher concentration plume gases. Instead, only very low concentration gases, brought close to the ground by eddies, were analysed. Only 10 spectra had SO_2 concentrations above the limit of detection, ~10 ppmv.m. For these I estimated an SO_2:HCl mass ratio of $<0.5 \pm 0.2$. Later OP-FTIR studies by Oppenheimer et al. (1998) support this very low ratio. The low SO_2 concentrations concur with the low SO_2 fluxes I measured using COSPEC. I measured HCl concentrations at several points around the western flank of Soufrière Hills volcano. The highest concentrations were

measured during analyses conducted from the summit of St. George's Hill, possibly through the lower parts of the plume. The lowest concentrations were measured in the sampling locations furthest from the volcano, Fox's Bay and Richmond Hill, which were still populated at the time.

6.4 The magmatic system beneath Soufrière Hills volcano

The work of the MVO has mainly been concerned with monitoring the current eruption. To understand this better, MVO scientists have investigated the chemistry and petrography of the extruded lava as well as the volatile contents of glasses and melt inclusions. The results from some of these studies, along with observations drawn from the author's own gas investigations, are combined to propose a model for the magmatic activity at Soufrière Hills volcano and suggest an alternative analogue to Mt. Unzen.

6.4.1 Investigation of the magmatic system at Soufrière Hills using petrologic and geophysical data

Magma chamber depth

Murphy et al. (1996) and Devine et al. (1996) have used the presence of reaction rims around hornblende phenocrysts in the andesite lava to estimate the depth of the magma chamber and period of ascent to be >6 km and ~30 days respectively. This is supported by the work of Barclay et al. (1996) who have experimentally reproduced the dome phenocryst assemblage at pressures of ~150 - 175 MPa, ~6 - 7 km, and modelled volatile compositions at pressures of ~100 - 125 kbar, ~4 - 5 km. Wadge (MVO report, 1996), based on seismic evidence, inferred a maximum depth of ~15 km for the magma chamber. The magma chamber can therefore be constrained to depths of between ~4 and ~15 km.

Origin of magma

Murphy et al. (1996) undertook a comparative studies of the whole-rock and mineral chemistry of recent dome rock and 16 - 24 ka volcaniclastic deposits from Soufrière Hills. They concluded that the current andesitic magma was emplaced >24 ka ago and formed Chance's, Galway's and Castle Peak lava domes. The magma had been resting at a shallow level, below 7 km, beneath Soufrière Hills until its reactivation in 1995. Continued cooling over time has caused significant amounts of crystallisation, ~35% in early dome lavas. Murphy

et al. (1996) inferred from geothermometry that the andesite was initially at ~800 - 875°C before being reheated by a mafic magma at a temperature of >1050°C. Evidence of a mafic magma comes from ellipsoidal inclusions/autoliths which range in composition from basalt to basaltic andesite, 51 - 55 wt% SiO_2. Intrusion into the cooler andesite is supported by the quench textures and chilled margins of the autoliths (Murphy et al., 1996). Murphy et al. (1996) also reported mafic inclusions in older deposits; suggesting episodic magma mixing has occurred over the last ~24 ka.

Volatile contents of andesitic magma

Barclay et al. (1996) analysed melt inclusions in quartz crystals from the pumice and pyroclastic flow deposits of the 17/9/96 explosion. These had sulphur and chlorine concentrations of <150 and 2400 wt% respectively; giving an S:Cl mass ratio of ~0.06. This is similar to the average S:Cl ratio, ~0.07, reported by Giggenbach (1996) from analyses on several andesitic volcanoes, see **table 1.1**. The low magmatic sulphur content measured thus explains the low SO_2:HCl ratios determined using OP-FTIR and the low SO_2 fluxes measured using COSPEC during 1996.

Barclay et al. (1996) reported a magmatic sulphur concentration of <150 ppmm. To determine how much sulphur is required to degas to provide the observed COSPEC-derived SO_2 flux, I have used two methods.

1). In **figure 6.14**, I compared the observed lava effusion rate (taken from MVO Scientific reports) with an effusion rate I have estimated from daily COSPEC-derived SO_2 fluxes, using **equation 6.3**. I have smoothed both sets of data, using a one-month moving average, to overcome the paucity of COSPEC and effusion data.

$$\Phi_{\text{lava}} = \left(\frac{\Phi_{SO_2}}{2 \times X_S \times \rho \times k} \right) \qquad \textbf{(6.3)}$$

where: Φ_{lava} = calculated lava effusion rate (m^3/s); Φ_{SO_2} = SO_2 flux (t/d); k = constant of proportionality (86400); X_S = concentration of magmatic sulphur

degassed (ppm); and ρ = lava density (2.4 t/m^3). The calculated data is fitted to the observed data using a least squares fit, varying X_S. This gave an exsolved sulphur concentration of ~330 ppmm.

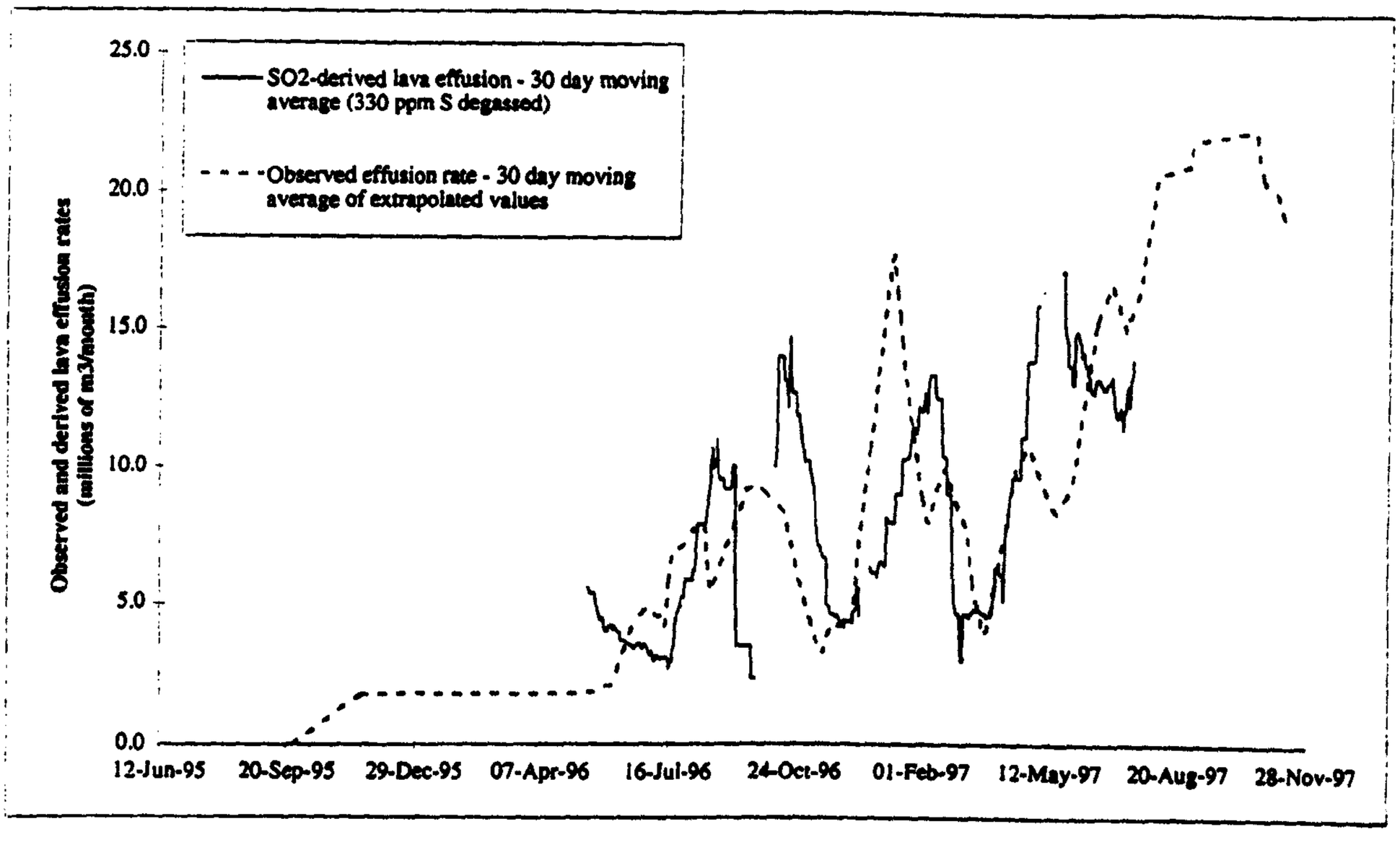

Figure 6.14. *Comparison between the observed lava effusion rate and that derived from SO_2 fluxes. Both data-sets have been smoothed using a one month moving average. I have estimated that the concentrations of sulphur degassed is ~330 ppmm.*

2). In **figure 6.15**, I compare cumulative lava effusion, as observed by the MVO, with cumulative effusion rates based on the reported-COSPEC derived SO_2 fluxes; again using **equation 6.3**. I have again used a least squares approach to determine the value of X_S which gives the best of calculated to observed data. This gave an exsolved sulphur concentration of ~270 ppmm.

For **figures 6.14** and **6.15** the degassed sulphur concentrations were ~330 and 270 ppmm respectively. When a degassed sulphur concentration of 330 ppmm was used for **figure 6.15** the total erupted volume derived from SO_2 flux was ~50% that of the observed volume, ~2.32×10^8 m^3 in December 1997 (MVO Scientific report N°. 80). I believe this shortfall may be due to the paucity of COSPEC data, especially in the latter half of 1997. I have therefore assumed that the concentrations of sulphur required to be degassed from the lava to provide the observed SO_2 flux lie between ~270 and 330 ppmm.

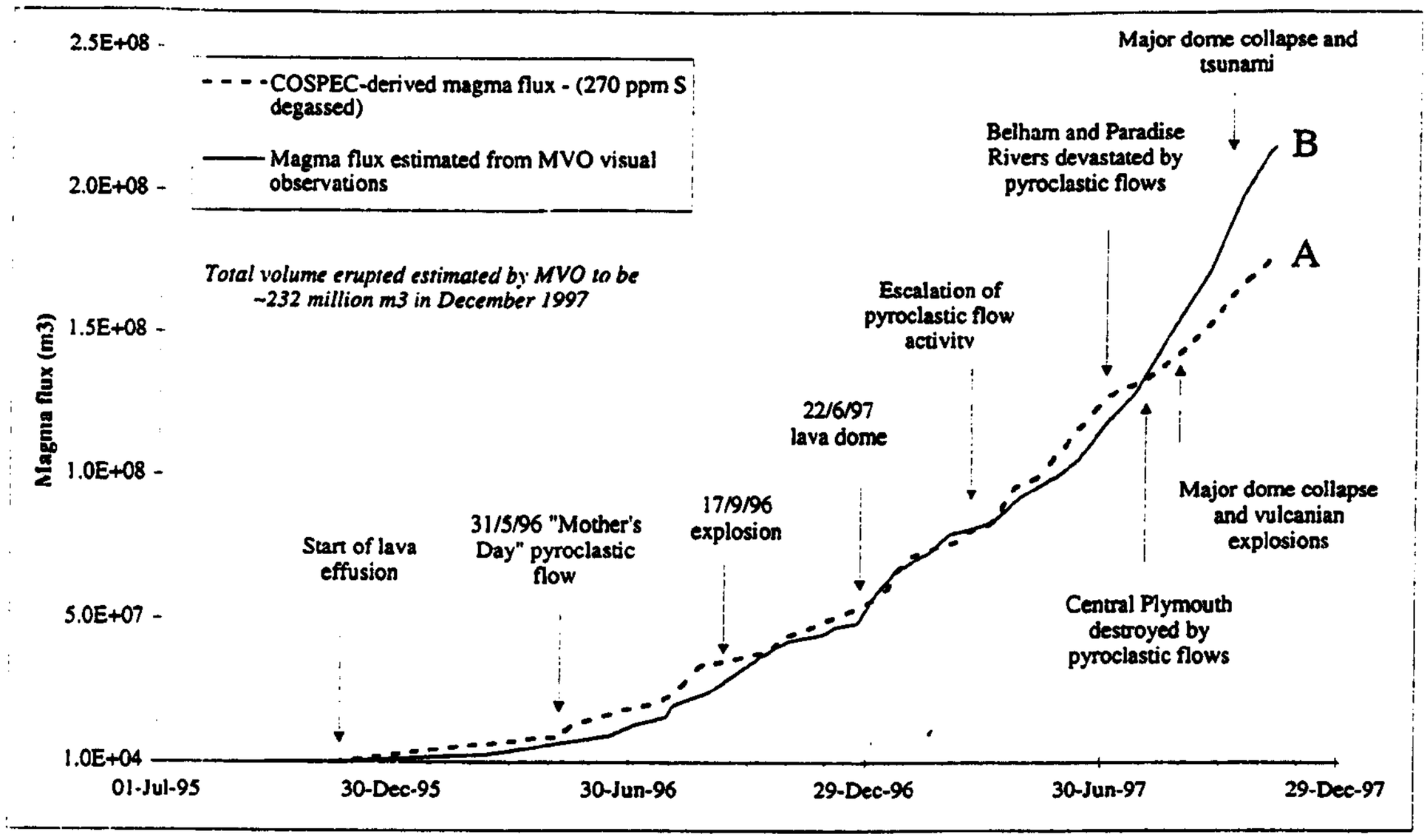

Figure 6.15. *Comparison between the cumulative effusion rates as determined from:* ***A.*** *SO_2-derived degassing volumes;* ***B.*** *Observed lava effusion rate (MVO Scientific reports). The close similarity between the two curves was the result of a least squares fit to the data giving a degassed sulphur concentration of ~270 ppmm.*

Using the analysed sulphur concentration of Barclay et al. (1996), <150 ppmm, to derive cumulative volumes of lava degassed, see **figure 6.15**, I estimated the total volume erupted to be $>3.2 \times 10^8$ m^3. Only ~70% of this volume has been observed to erupt (MVO Scientific report N°. 80). Ground deformation attributable to $\sim 1 \times 10^8$ m^3 of intruded magma has not been observed using either EDM (Shepherd, 1996), GPS (MVO Team Deform, 1996) or by gravity measurements (Davies, pers. com.); the only deformation observed being due to the dome forcing outwards the upper parts of English's Crater (MVO Team Deform, 1996).

The good correlation between the observed and calculated cumulative effusion rates suggests that the concentration of sulphur degassed from the magma has remained fairly constant at ~270 ppmm, approximately double the magmatic concentration of Barclay et al. (1996). There are several possible explanations for this disparity. These include:

- The original analyses of Barclay et al. (1996) were inaccurate, only detecting ~50% of sulphur present in the samples from the 17/9/96 explosive event.

- The sample analysed by Barclay et al. (1996) was uncharacteristically low in volatiles, the melt having partially degassed prior to being trapped as fluid inclusions.

- Degassing occurring from deeper within the andesitic magma, chamber, the lavas erupted in the earlier parts of the eruption being from a partially degassed upper layer in the chamber.

- The andesitic lava does contain a low sulphur content of <150 ppmm; the gas flux being supplemented by the degassing of a more basic magma beneath Soufrière Hills.

I cannot comment on the accuracy of the analyses of Barclay et al. (1996), having only the final data, apart from to note that their concentration data appear consistently low. It is quite possible that the upper parts of the andesitic magma were partially degassed prior to eruption, the main gas exsolution taking place at deeper levels. It is also possible that gases may be exsolved from the mafic magma that has been suggested by Murphy et al. (1996) to lie beneath Soufrière Hills volcano; thus giving the excess SO_2 emissions in field A of **figure 6.8**. I discuss the implications for the presence of a mafic magma beneath Soufrière Hills in the next section.

6.4.2 South Soufrière Hills: a possible analogue for the current Soufrière Hills eruption?

Geophysical evidence precludes the intrusion of a large volume of magma. Petrological investigations by Barclay et al. (1996) suggest more magma is required to degas than is observed. I therefore propose that additional sulphur fluids from another, deeper magmatic source contribute >150 ppmm of sulphur towards the measured SO_2 flux. I suggest this to be a basaltic magma, as evidenced by the numerous mafic autoliths/inclusions in the erupted lava (Murphy et al., 1996). I have interpreted the very low SO_2:HCl mass ratios, <0.1, measured using OP-FTIR, as possibly relating to the deep degassing of such a basaltic body.

The presence of mafic magma beneath Montserrat is probably not unusual. The basaltic lava flows in South Soufrière Hills are testament to their presence. Here, the extensive White River Pyroclastic Fall Series grades up from andesitic block falls, through lahars, andesitic lapilli and ash flows into basaltic-andesite lapilli and then welded basaltic scoriae and basaltic lava flows (Rea, 1974). Rea interpreted this sequence as the emptying of a stratified/fractionated magma chamber; based on chemistry and the occurrence of ultrabasic cumulates within some of the andesitic horizons.

I have re-interpreted the White River Fall Series in terms of the interaction of andesitic and basaltic magma. I suggest that the observed stratigraphic sequence was produced by the reactivation of an andesitic magma chamber by an influx of basaltic magma. Initial phreatic activity would produce block falls of andesitic magma during the initial reactivation and formation of a conduit. The eruption of lava and formation of a dome would generate pyroclastic flows. More vigorous vulcanian eruptions would then occur as volatiles from the mafic magma exsolved and pressurised the lava dome. As the mafic magma nears the surface strombolian explosions would produce welded basaltic scoriae and then finally the effusion of basaltic lavas as the mafic magma reached the surface. During the current volcanic crisis, eruptive activity has been constrained to phreatic and vulcanian explosions, the extrusion of the andesitic dome, and pyroclastic flow activity. The eruption of basaltic lavas from within English's Crater or the current dome may not possible due to the density contrast between the basaltic and andesitic magmas. The locations of basaltic lava flows at the southern tip of Montserrat suggests that magma by-passed the less dense andesitic rocks rather than rise up through them (Wadge, pers. com). The ongoing eruption at Soufrière Hills may therefore "stall" once the basaltic magma body reaches a level of neutral buoyancy. Further activity will result only from heat either being lost by convection into the andesite or by more buoyant magmatic fluids rising to the surface.

Basaltic lavas are found only in South Soufrière Hills, dated at ~1.6 ± 0.25 and 0.96 ± 0.25 Ma , suggesting that elsewhere mafic magmas do reach a shallow enough level to be erupted. If the contribution of mafic volatiles to those exsolved from the andesite is the cause of excess sulphur degassing, as I have demonstrated exists for the current Soufrière Hills eruption, then the basaltic magma must be at a shallow enough level to reactivate the andesitic

lava and exsolve its volatiles. The low SO_2:HCl ratios are characteristic of the deep degassing of a basalt, as defined by the two-stage degassing model of Pennisi & Le Cloarec (1998). This proposes that volatiles exsolved at depth (>4 km) have a SO_2:HCl mass ratios of <1, whilst shallow degassing (<4 km) results in a gas mass ratio of ~10. Based on the seismic investigations Wadge (MVO report, 1996), petrology (Murphy et al., 1996; Devine et al., 1996) and volatile pressures in melt inclusions (Barclay et al., 1996), coupled with the low gas ratios, I suggest the basaltic magma must be at a depth of at least 4 km, and probably >7 km. Based on the gas emissions and styles of eruptive activity, I therefore propose that South Soufrière Hills may be a more accurate analogue to the current eruption than Mt. Unzen.

6.5 Conclusions

The study of the volatiles and gases of the Soufrière Hills volcano using COSPEC and OP-FTIR techniques has enabled the following conclusions to be drawn about the gas and magmatic system and also about the above techniques.

6.5.1 Technical aspects

The main drawback suffered by both COSPEC and OP-FTIR was the ability to work from only downwind of the volcano during relatively good, ash-free, weather. The ability of the COSPEC system to analyse the volcanic gas plume as it passes ~1 km above the sampling route was a major advantage over the OP-FTIR system which only sampled the diluted plume gases at ground level. At certain volcanoes, such as Mt. Etna and Vulcano, it is possible to place the IR source and/or spectrometer within the plume due to accessibility to the crater areas, areas of high ground downwind of the volcano and a level of predictability to the volcanic activity. The situation at Soufrière Hills was such that almost continuous rock falls, some of which generated pyroclastic flows, meant that a wide exclusion zone was in place. The inaccessibility of the dome coupled with the gas plume being blown straight out to sea at an altitude of ~1000 m and no suitable locations for placing the detector within the plume meant high concentration data collection was not possible. The technical aspects can be summarised for COSPEC and OP-FTIR as below.

COSPEC

- I have estimated total errors for COSPEC analyses. These range from ~16 - 29% with a worst case of ~45% and are similar to estimates by Stoiber et al. (1983). The main sources of error are the variability in the wind speed and inability to measure it at the height of the plume, and the presence of ash and clouds which scatter UV radiation.

- The escalation in pyroclastic flow activity in 1997 prevented the COSPEC being used on roads skirting the volcano. COSPEC can now only safely be used from a boat; although this exacerbates the problems due to SO_2 scavenging which reduces the measured gas flux.

- I have demonstrated that COSPEC can be used as a proxy for the rate of lava effusion. Large deviations between observed and calculated effusion rates indicate changes in the magmatic volatile content which may herald periods of increased or reduced volcanic activity.

OP-FTIR

- OP-FTIR analyses were hampered by the inability to directly sample the gas plume, the optical paths between artificial IR source and detector being ~1000 m beneath the plume.

- Owing to the broad shape of the SO_2 IR fundamental absorbance and the low concentrations present, SO_2 was only detected in a 10 spectra. I estimated detection limits for SO_2 and HCl of ~10 and <5 ppm.m respectively. Only one data-set contained SO_2:HCl gas ratio data; high errors being were due to the SO_2 levels being close to detection limits.

- The day-to-day use of the OP-FTIR technique would not aid the monitoring effort; however a monthly investigation of the SO_2:HCl ratios may indicate changes in gas composition due to degassing of more volatile-rich magma.

6.5.2 Scientific aspects

The MVO have used Mt. Unzen as an advanced analogue for the Soufrière Hills eruption. I have compared the SO_2 fluxes and lava effusion rates of the two volcanoes and have shown that, apart from the physical processes involved with pyroclastic flow activity, the levels of degassing and dome growth at Soufrière Hills bear little resemblance to those at

Mt. Unzen. Degassing and lava effusion rates at Soufrière Hills volcano are generally higher and show much more variability. I have used OP-FTIR to estimate the SO_2:HCl ratios of emitted gases; these were $<0.5 \pm 0.3$ during May - June 1996 and reflect the andesitic composition of the parent magma.

My comparison of the melt inclusion analyses of Barclay et al. (1996) with the estimated magmatic sulphur concentrations required to provide the measured gas flux indicate that the dome rocks of the current eruption are strongly deficient in sulphur. I propose that the additional SO_2, >150 ppm, is provided by a volatile-rich source beneath the volcano rather than by intrusion of the andesite. The presence of basaltic-andesite autoliths/inclusions within extruded dome lava indicate the presence of basaltic magma; which have far higher concentrations of dissolved SO_2 and CO_2 (Giggenbach, 1996). Basaltic lavas in South Soufrière Hills have been interpreted by Rea (1974) as being the final cap on an andesite - basalt transitional series caused by the emptying of a fractionated magma chamber.

I have interpreted the four seismic crises over the last 100 years as being caused by the gradual migration of a mafic magma up into the andesitic magma chamber beneath Soufrière Hills, gradually reactivating the parent body responsible for the of the ~350 year old Castle Peak andesite. This was itself intruded ~16 - 24 ka ago and formed Chance's and Galway's domes. The high proportions of phenocrysts, ~35% (Wadge & Woods, 1996, pers. com.) and quench textures on mafic inclusions support the interpretation that the andesite has been reactivated and reheated by a mafic intrusion. I have interpreted the escalation in lava effusion levels and rates of SO_2 degassing as evidence of the increasing proximity of this mafic magma to the surface.

The main scientific aspects are summarised below:

- The andesitic magma beneath Soufrière Hills was intruded ~16 - 24 ka ago and formed Castle Peak during the last eruptive episode in ~1646 ± 54 A.D. Reactivation by a basaltic magma has caused a phenocryst-rich lava to be extruded.

- The initially low gas fluxes and lava effusion rates have gradually escalated as the eruption has progressed. Increasing volcanic activity has been marked by increasing numbers and volumes of pyroclastic flows and the occurrence of vulcanian explosive eruptions.

- The analysed magmatic sulphur content, <150 ppm is not sufficient to account for the measured SO_2 flux, assuming no magma is intruded as is suggested by geophysical data. I have suggested that the extra sulphur is sourced from the basaltic magma that has reactivated the andesite beneath Soufrière Hills and lies at a depth of >4 km.

- The removal of SO_2 from the gas plume by oxidation to sulphate has been shown (Oppenheimer et al., 1998 in prep) to remove ~50% of SO_2 from the plume by ~12 km from the dome. This therefore has implications for the methodology of monitoring levels of volcanic/degassing activity, especially where gas plumes can only be analysed at long distances, >10 km, downwind of the vent.

Chapter 7.

Remote measurements of volcanic gases: General conclusions

7.1 The beginning of the end

The previous chapters gave a diverse view of four very different volcanoes: the heavily degassing basaltic Masaya Volcanic Complex; the fumarolic trachytic-latitic La Fossa di Vulcano; the hawaiite composite cone of mighty Mt. Etna; and the andesitic Soufrière Hills volcano with its pyroclastic flows. I discussed the issues relating to gas composition, gas flux and the relationship between gas and magma flux for each of these. Much of the data I used was collected by other authors using a variety of techniques. I therefore included a chapter in which I described the more widely reported techniques and discussed their merits and disadvantages. In the following sections I first summarise my findings relating to gas analysis techniques and then my scientific findings which I present as a general summary of the geological principles which link each of the chapters.

7.2 Synthesis of technique aspects

I have described a number of different techniques for analysing a range of volcanic gases, including: H_2O, CO_2, SO_2, HCl, HF, SiF_4, CO and ^3He. Most of these originated from the chemist's laboratory or from the field of environmental science; and thus the techniques have had to be adapted for investigating volcanic emissions. The suitability of an individual technique depends greatly on the type of gas to be measured; the location of vent or fumarole; the level of volcanic activity; the environment in which data are collected; the duration over which data are collected and the purpose behind the data collection. I have divided the techniques described into two general groups: remote-sensing and direct- or grab-sampling.

gases, such as HF and HCl, may be compromised during periods of thick cloud or rain as the soluble gases are rapidly taken into solution and hence removed from the gas plume. Other atmospheric effects include the oxidation of gases and the formation of aerosols, either photochemically, or on dust or water particles. The detectability of a gas using OP-FTIR is dependent on the shape and size of the fundamental absorbance peak. The limit of detection of SO_2 is ~10 ppmv.m due to the broad shape IR fundamental. This contrasts with HCl which was the detected at concentrations of <5 ppmv.m due to the sharp peaks and high absorptivity coefficient (ε) of its fundamental absorbance.

I used both artificial and natural sources of IR radiation for OP-FTIR investigations of volcanic gases. Neither sun-heated or warm fumarolic ground provided sufficient intensity of radiation for analysis of lighter gases, such as HCl and HF. Passive analyses on Vulcano were only possible using the hottest central crater fumaroles, <540°C, as an IR source. The 1275°C artificial IR source, however, enabled high quality data to be collected at path lengths of up to 1875 m. Optimal OP-FTIR results are achieved when volcanic gas totally fills the optical path, requiring the IR source and/or detector being in the plume. Inaccessible gas plumes can be analysed using a solar IR source. This approach was successfully demonstrated recently by Love et al. (1998), at Popocatepetl, Mexico, and Burton & Horrocks (pers. com.), at Masaya, Nicaragua. The use of airborne OP-FTIR has yet to be perfected. A hot natural IR source must be targeted from a stationary (hovering) aircraft. This requires the co-operation and understanding of the aircrew and the correct volcanic and atmospheric conditions.

7.2.2 Direct-sampling techniques

These rely on the gas being trapped, dissolved or adsorbed before being analysed by more traditional methods of analysis; generally within a laboratory setting. The capture of gases is best achieved as close to the gas source as possible to avoid loss of analyte by atmospheric processes. This increases the risk to the operator, and will depend greatly on the accessibility of the gas source and level of volcanic hazard. The physical interaction of gases with collection vessels and instrument can lead to contamination and formation of secondary reactions; thus affecting the results of the analysis. The errors due to such problems may,

however, be relatively minor when compared with the errors caused by changing climatic conditions, as experienced by remote-sensing techniques. Direct-sampling techniques, although independent of climatic conditions, are, however, extremely labour intensive and, although capable of collecting a wide variety of gases and isotopes, are only capable of generating a relatively small amount of data.

7.3 Synopsis of geological principles covered in thesis

The study of volcanic gases has furthered the understanding of processes relating to magma convection and volatile exsolution within volcanoes. It has also highlighted the role of atmospheric processes which act to reduce the concentration of gases in the distal portions of volcanic plume. In the following sections I summarise the general findings from my research.

Gas analyses rely on the exsolution of volatiles from the magma. This occurs at different depths and is governed by the solubilities and initial concentrations of the volatiles within the melt. Generally CO_2 and H_2O exsolve at greater depths than sulphur, chlorine and fluorine. At depth, chlorine combines with alkali metals to form compounds that are relatively insoluble in magma. However, at shallower levels, <4 km, chlorine combines with hydrogen to form HCl which is highly soluble in magma and water. Pennisi & Le Cloarec (1998) proposed a two-stage degassing model, based on chorine's differential solubilities. "Deep" degassing produced gases with low SO_2:HCl mass ratios of ~1 whilst "shallow" degassing produced higher SO_2:HCl mass ratios of ~10.

I have measured SO_2:HCl mass ratios at several volcanoes using the OP-FTIR technique to investigate the ongoing magmatic processes relating to degassing and convection, and to try and elucidate the degassing history of the magma. Secondary processes, both within the volcanic hydrothermal system and in the atmosphere have acted to modify the original composition of the magmatic gases. Beneath the La Fossa di Vulcano cone, an established hydrothermal system interacts with the majority of magmatic volatiles that rise to the surface. The marine-hydrothermal and meteoric reservoirs scavenges soluble gases, such as HCl and HF, thus increasing the measured SO_2:HCl ratios. Only through the blocked central conduit,

where temperatures are too high for fluids to be present, can gas percolate up to reach the surface relatively unchanged. The separation of different fluid reservoirs beneath La Fossa is due to the precipitation of impermeable calcite and sulphate layers. Only during periods of increased seismicity, when new fractures develop, do reservoirs mix and fumarole chemistries change rapidly.

As gases percolate up through the volcanic system to the surface they gradually cool and re-establish their chemical equilibria. Venting of gases "freezes in" their equilibria; which can be measured to investigate the temperatures within the volcanic pile. The development of a new equilibrium system, HF–SiF_4, using OP-FTIR spectroscopy has had mixed results when used on Vulcano and Mt. Etna. This was mainly due to the equilibrium system strongly biasing the measurement of warm, rather than hot fumaroles. The higher equilibrium temperatures estimated for Mt. Etna are consistent with the active degassing from an open conduit. SO_2:HCl mass ratios measured in Mt. Etna's plume indicated that, at the time of analysis, the volcano was in a state of magma replenishment, gas ratios being halfway between "deep" and "shallow" degassing values. The S:Cl ratios had decreased markedly after the long-lived 1991 - 1993 effusive eruption. Since 1993, however, S:Cl ratios of emitted gasses have slowly risen (Pennisi & Le Cloarec, 1998); suggesting the refilling of the magma system beneath the summit. This culminated in the eruption from the SE Crater in late 1997.

During the 1991 - 1993 eruption at Mt. Etna, Bruno et al. (1994) measured the gas flux using a COSPEC. By comparing the differences between the observed lava effusion data of Calvari et al. (1994) with those I derived from the levels of SO_2 degassing, I was able to track the passage of two magma pulses relating to the eruption through the volcano's plumbing system. I was also able to link the decreases in effusion rate with drainage of the summit system and collapses of the summit craters and low periods in the measured gas flux.

The presence of atmospheric oxygen can cause the spontaneous oxidation of high temperature reduced gases, such as H_2, H_2S and S upon emission from the fumarole/vent. At La Fossa I observed blue sulphur flames within the hotter fumaroles, showing this to be the case. Problems can arise once the volcanic gases have left the vent as atmospheric processes take hold. Clouds and precipitation can rapidly remove the more soluble gases, HCl and HF,

from the plume. This was most noticeable on Mt. Etna during OP-FTIR analyses I conducted in periods of heavy cloud when SO_2:HCl ratios were markedly different to analyses taken during drier periods. Solar UV radiation, ash particles and water droplets can all act to initiate the oxidation of SO_2 to SO_3 and sulphate. The effects of aerosol formation on the plume concentrations of SO_2 have been noted at Mt. Etna, the Masaya Volcanic Complex and Soufrière Hills volcano.

At Soufrière Hills volcano, COSPEC measurements taken at different distances from the vent have indicated that the SO_2 content of the plume decreases exponentially with distance from the dome due to the scavenging of the gas. Since the escalation in eruptive activity prevented the use of vehicle-based COSPEC, analyses have to be done from off-shore, thus increasing the distance between vent and instrument and thus increasing the susceptibility of the plume to scavenging.

I have shown for both Mt. Etna and Soufrière Hills volcanoes that SO_2 can be used as a proxy to estimate lava effusion. At Soufrière Hills I have proposed that there is more gas emitted than can be accounted for, based on rates of lava effusion. No evidence for deformation related to intrusion of magma has been reported. I therefore suggested that the additional volatiles were sourced from degassing of deeper basaltic magma. Evidence for this comes from the numerous inclusions and presence of basaltic flows in the nearby South Soufrière Hills complex.

At Santiago Crater in the Masaya Volcanic Complex SO_2 is presently emitted at levels similar to Mt. Etna, <7000 t/d, but with the almost total absence of erupted material. Santiago Crater has undergone several degassing episodes over the last ~150 years. For this period I estimated ~10 - 20 km^3 of magma may have been degassed with little evidence for any shallow magmatic intrusions. To explain this I proposed that magma is convected up from a deeper chamber, degasses and sinks to either be recycled or intruded at depth; the sporadic nature of the degasing episodes being linked to the time required to refill a deeper chamber before the destabilisation of the system and ensuing convective overturn.

Thesis references

Allard P. Magma degassing budget of Etna volcano, 1975 - 1995. In: EC RDT Programme "Environment" - Natural Hazards: European Volcano-Laboratories. Contract EV5V-CT91-0177: Etna's volatiles, Final Scientific Report (01.05.93-30.11.95). Vol. 1, pt. 2, p. 7 - 11, 1996.

Allard P., Carbonelle J., Dajlevic D., Le Bronec J., Morel P., Robe M., Maurenas J., Faivre-Pierret R., Martin D., Sabroux J. and Zettwoog P. Eruptive and diffuse emissions of CO_2 from Mount Etna. Nature. Vol. 351, p. 387 - 391. 1991.

Allard P., Loyer H., Lefol N. and Pinte R. Airborne gas flux measurements and magma degassing budget. In: EC RDT Programme "Environment" - Natural Hazards: European Volcano-Laboratories. Contract EV5V-CT91-0177: Etna's volatiles, Final Scientific Report (01.05.93-30.11.95). Vol. 1, pt. 2, p. 1 - 6, 1996.

Andres R. J., Kyle P. R. Chuan R. L. Sulphur dioxide, particle and elemental emissions from Mount Etna, Italy during July 1987. Geoligische Rundschau. Vol. 82, p.687 - 695, 1993.

Andres R. J., Rose W. I., Kyle P. R., de Silva S., Francis P. W., Gardeweg M. and Moreno Roa H. Excessive sulfur dioxide emissions from Chilean volcanoes. Journal of Volcanology and Geothermal Research. Vol. 46, p. 323 - 329, 1991.

Armienti P., Clocchiatti R., D'Orazio M., Innocenti F., Petrini R., Pompillio M., Tonarini S. and Villari l. The long-standing 1991 - 1993 Mount Etna eruption: petrography and geochemistry of lavas. Acta Vulcanologica. Vol. 4, p. 15 - 28, 1994.

Aspinall W. P., Miller A. D., Ambeh W. B., Lynch L. L., Latcham J. L., Stewart R. C., White R. A., Power J. A. and Montserrat Volcano Observatory staff. Soufrière Hills eruption, Montserrat, 1995 - 1997: Volcanic earthquake locations and fault plane solutions. Geophysical Research Letters. (in press) 1998.

Badalamenti B., Calderone L. and Di Gangi F. Vulcano island: continuous monitoring (temperature, reducing capacity, CO_2 in soil gases). Acta Vulcanologica. Vol. 8, N°. 2, p.. 200 - 202, 1996.

Badr O. and Probert S. D. Sources of atmospheric nitrous oxide. Applied Energy. Vol. 42, p. 129 - 176, 1992.

Barberi F. and Villari L. Volcano monitoring and civil protection problems during the 1991 - 1993 Etna eruption. Acta Vulcanologica. Vol. 4, p. 157 - 165, 1994.

Barclay J., Murphy M. D., Carroll M. R., Sparks R. S. J., Le Jeune A.-M., Toothill J. and MacDonald R. Pre-eruptive volatiles and experimentally determined phase equilbria of the Soufrière Hills volcano: Implications for magma storage and degassing. Conference abstracts from: The Soufrière Hills Eruption, Montserrat. The Geological Society, Burlington House, London, 27 November 1996. Wadge G. (ed.). 1996.

Baubron J. C., Allard P. and Toutain J. P. Diffuse volcanic emissions of carbon dioxide from Vulcano Island, Italy. Nature. Vol. 344, p. 52 - 53, 1990.

Baubron J. C., Allard P. and Toutain J. P. Gas hazard on Vulcano Island, Italy. Nature. Vol. 350, p. 26 - 27, 1991.

Bice D. C. Quaternary stratigraphy of Managua, Nicaragua: Correlation and source assignment for multiple overlapping plinian deposits. Geological Society of America Bulletin. Vol. 96, p. 533 - 566, April 1985.

Bice D. C. Tephra stratigraphy and recent aspects of volcanism near Managua, Nicaragua. Ph. D. thesis, University of California, Berkely, California . 422 pp. 1980.

Bluth G. J. S., Casadevall T. J., Schneltzer C.C., Doiron S. D., Walter L.S., Krueger A. M. and Badruddin M. Evaluation of sulfur dioxide emissions from explosive volcanism: the 1982 - 1983 eruption of Galunggung, Java, Indonesia. Journal of Volcanology and Geothermal Research. Vol. 63, p. 243 - 256, 1994.

Bolognesi L Comment on "Origin of the fumarolic fluids of Vulcano Island, Italy and implications for volcanic surveillance" by G. Chiodini, R. Cioni, L. Marini and C. Panichi. Bulletin of Volcanology. Vol. 58, p. 319 - 320, 1996.

Bolognesi L. and D'Amore F. Isotopic variation in the hydrothermal system on Vulcano Island, Italy. Geochimica et Cosmochimica Acta. Vol. 57, p. 2069 - 2082, 1992.

Bruno N., Caltabiano T., Grasso M., Porto M. and Romano R. SO_2 flux from Mt. Etna volcano during the 1991 - 1993 eruption: correlations and considerations. Acta Vulcanologica. Vol. 4, p. 143 - 147, 1994.

Burt M. L., Wadge G. and Scott W. A. Simple stochastic modelling of the eruption history of a basaltic volcano: Nyamuragira, Zaire. Bulletin of Volcanology. Vol. 56, p. 87 - 97, 1994.

Calanchi N., Rossi P. L., Sanmarchi F and Tranne C. A. Guida Excursionistico Vulcanologica delle Isole Eolie. Dipartimento di Scienze della Terra e Geologico-Ambientali Università di Bologna: Centro studi e richerche di storia e promblemi Eoliani. Union Printing S.p.A. - Viterbo, Italia. 1996.

Caltabiano T., Romano R. and Budetta G. SO_2 flux measurements at Mt. Etna (Sicily). Journal of Geophysical Research. Vol. 99, N°. D6, p. 12809 - 12819, 1994.

Calvari S. and Groppelli G. The Chiancone volcaniclastic deposit and its relationship to the formation of the Valle del Bové, Mount Etna. In: Etna: fifteen years on. Gravestock P. J. & McGuire W. J. (ed.s). Proceedings of conference held at C&GCHE, Cheltenham on 12/2/96. p. 11 - 15, 1996.

Calvari S., Coltelli M., Müller W., Pompillo M., Scribano V. Eruptive history of South-Eastern Crater of Mount Etna, from 1971 to 1994. Acta Vulcanologica. Vol. 5, p. 11 - 14, 1994.

Calvari S., Coltelli M., Neri M., Pompillo M., Scribano V. The 1991 - 1993 Etna eruption: chronology and lava flow-field evolution. Acta Vulcanologica. Vol. 4, p. 1 - 14, 1994.

Capasso G., Dongarrà G., Favara R., Hauser S. and Valenza M. Isotope composition of rain water, well water and fumarole steam on the Island of Vulcano, and their implications for volcanic surveillance. Journal of Volcanology and Geothermal Research. Vol. 49, p. 147 - 155, 1992.

Capasso G., Inguaggiato S., Nuccio P. M., Pecoraino G. and Sortini F. Change in composition of La Fossa crater fumaroles, Acta Vulcanologica. Vol. 8, N°. 2, p208 - 209, 1996.

Carapezza M., Nuccio P. M. and Valenza M. Genesis and evolution of the fumaroles of Vulcano (Aeolian Islands, Italy): a geochemical model. Bulletin of Volcanology, Vol. 44-3, p. 546 - 563, 1981.

Carbonelle J., Dajlevic D., Zettwoog P. and Sabroux J. C. Gas output from an active volcano. Bulletin of Volcanology. Vol. 45, N°. 2, p. 267 - 268, 1982.

Carr M. J. Symmetrical and segmented variation of physical and geochemical characteristics of the Central American Volcanic Front. Journal of Volcanology and Geophysical Research. Vol. 20, p. 231 - 252, 1984.

Carroll M. R. and Webster J. D. Solubilities of sulfur, noble gases, nitrogen, chlorine and fluorine in magmas. In: Volatiles in Magmas. Carroll M. R. and Holloway J. R. (eds.). Reviews in Mineralogy. Vol. 30, Ch. 7, p. 231 - 279, 1994.

Chaffin C. T., Marshall T. L., Fately W. G. and Hammaker R. M. Infrared analysis of volcanic plumes: A case study in the application of open-path FTIR monitoring techniques. Spectroscopy Europe. Vol. 7. N°. 3, p. 18 - 24, 1995.

Chester D. K., Duncan A. M., Guest J. E. and Kilburn C. R. J. Mount Etna: The anatomy of a volcano. University Press, Cambridge. pp 404, 1985.

Chiodini G., Cioni R., Frullani A., Guidi M., Marini L., Prati F. and Raco B. Fluid geochemistry of Montserrat Island, West Indies. Bulletin of Volcanology. Vol. 58, p. 380 - 392, 1996.

Chiodini G., Cioni R., Marini L., and Panichi C. Origin of the fumarolic fluids of Vulcano Island, Italy and the implications for volcanic surveillance. Bulletin of Volcanology Vol. 57, p. 99 - 110, 1995.

Chiodini G., Frondini F., Raco B. Diffuse emission of CO_2 from the Fossa crater, Vulcano Island (Italy). Bulletin of Volcanology. Vol. 58, p. 41 - 50, 1996.

Cioni R. and Corazza E. Medium-temperature fumarolic gas sampling. Bulletin of Volcanology. Vol. 44, N°. 1, p 23 - 30, 1981.

Cioni R. and D'Amore F. D. A genetic model for the crater fumaroles of Vulcano island (Sicily, Italy). Geothermics. Vol. 13, N°. 4, p. 375 - 384, 1984.

Clocchiatti R. Volatile abundance and behaviour in Etna magma: fluid and melt inclusions in phenocrysts in lavas. In: EC RDT Programme "Environment" - Natural Hazards: European Volcano-Laboratories. Contract EV5V-CT91-0177: Etna's volatiles, Final Scientific Report (01.05.93-30.11.95). Vol. 1, pt. 1, 1996.

Clocchiatti R., Gioncada A., Mosbah M. and Sbrana A. Possible deep origin of sulphur output at Vulcano (Southern Italy) in the light of melt inclusion studies. Acta Vulcanologica. Vol. 5, p. 49 - 53, 1994.

Condomines M., Tanguy J - C. and Michaud V. Magma dynamics at Mt. Etna: Constraints from U-Th-Ra-Pb radioactive disequilibria and Sr isotopes in historical lavas. Earth and Planetary Science Letters. Vol. 132, p. 24 - 41, 1995.

Connor C. B. and Williams S. N. Interpretation of gravity anomalies, Masaya Caldera Complex, Nicaragua. Preprint-Transactions of the 13th Caribbean conference St Croix. 1990.

Coradossi N., Garavelli A., Salamida M. and Vurro F. Evolution of Br/Cl ratios in fumarolic salammoniac from Vulcano (Aeolian Islands, Italy). Bulletin of Volcanology. Vol. 58, p. 310 - 316, 1996.

Cortecci G. Ferrara G. and Dinelli E. Isotopic time-variations and variety of sources for sulfur in fumaroles at Vulcano island, Aeolian archipelago, Italy. Acta Vulcanologica. Vol. 8, N°. 2, p. 147 - 160, 1996.

CRC (The Chemical Rubber Company). Handbook of Chemistry and Physics. Lide D. R. (ed.) 72nd edition 1991 - 1992 - Special student edition. CRC Press Inc. 1992. ISBN 0-8493-0565-9.

Crenshaw W. B., Williams S. N. and Stoiber R. E. Fault location by radon and mercury detection at an active volcano in Nicaragua. Nature. Vol. 300, p. 345 - 346, November, 1982.

Davies M. A. and Rymer H. Static and dynamic gravity surveys on Montserrat, 1995 to 1997. 1998 (In prep.).

Donnelly L. J. Non-contact temperature measurements of the Soufrière Hills volcanic dome, Montserrat, West Indies, using portable infra-red thermometers. British Geological Survey Technical Report N°. WN/96/25. pp. 9, 1996.

7.2.1 Remote-sensing techniques

Remote-sensing techniques are optical techniques, relying on the specific, characteristic absorbances of IR or UV radiation by different gases. The radiation absorbed is provided either by a natural source, such as the sun or hot ground, or by an artificial source, such as a portable IR lamp or UV laser. The long range of these techniques facilitates the detection of gases in inaccessible and hazardous areas. As the instruments do not interact with the analysed gases, there is no contamination, condensation or secondary reactions. The high degree of automation and rates of data acquisition in the field enable large quantities of data to be collected in a relatively short time. Remote-sensing techniques are susceptible to the effects of wind, rain and clouds, including: dilution of the plume; mixing of gases from different craters/fumaroles; and removal of gases by solution and oxidation processes. The instruments also tend to be heavy, expensive, and complex to operate.

The two techniques most suited to volcanological applications are OP-FTIR and COSPEC owing to their portability, ease of use and, for OP-FTIR, the wide range of gases that can be analysed simultaneously. The simultaneous use of COSPEC and OP-FTIR enables fluxes for a range of analytes to be estimated. Other remote sensing techniques have been used in volcanology include the DIAL and DOAS systems. The bulkiness and limited applicability of these techniques as they stand have resulted in their being of limited use for investigating volcanic gases, with short studies being conducted at only a few volcanoes.

The COSPEC technique has been used to measure volcanic SO_2 world-wide since the early 1970s. I estimated total errors for COSPEC analyses to range from ~16 - 29% with a worst case of ~45%; these values are similar to estimates by Stoiber et al. (1983). The main sources of error are: variability in the wind speed; inability to measure it at the height of the plume; and the presence of ash and clouds which scatter UV radiation.

The OP-FTIR technique simultaneously measures a wide range of IR frequencies and is best used for determining gas ratios; these being generally independent of the effects of plume dilution but not atmospheric conditions. The accurate measurement of highly soluble

Duncan A. M. and Guest J. E. Etna volcano: Internal plumbing 15 years on. In: Etna: fifteen years on. Gravestock P. J. & McGuire W. J. (ed.s). Proceedings of conference held at C&GCHE, Cheltenham on 12/2/96. p. 4 - 10, 1996.

Edner H., Ragnarson P., Svanberg S., Wallinder E., Ferrara R., Cioni R., Raco B. and Taddeucci G. Total fluxes of SO_2 from the Italian volcanoes Etna, Stromboli and Vulcano measured by differential absorption LIDAR and passive differential optical absorption spectroscopy. Journal of Geophysical Research. Vol. 99, N°. D9, p. 18827 - 18838, 1994.

Elming S. Å. and Fonseca A. Preliminary interpretation of gravimetric and magnetic measurements within the Nicaraguan Traverse. Swedish geological, Upsala, Sweden. 1986.

Faivre-Pierret R., Guelff C. and Sestier-Carlin R. Estimation du débit de SO_2, HCl et HF émis par le volcan Vulcano (Italie). Bulletin Volcanologique. Vol. 4, N°. 3, p. 279 - 281, 1982.

Fenton D. L., Purcell R. Y., Hrdina D. and Knutson E. O. The washout of combustion generated hydrogen chloride. Atmospheric Environment. Vol. 14, p. 1055 - 1062, 1980.

Ferrara G., Garavelli A., Pinarelli L., and Vurro F. Lead isotope composition of the sublimates from the fumaroles of Vulcano (Aeolian Islands, Italy): inferences of the deep fluid circulation. Bulletin of Volcanology. Vol. 56, p. 621 - 625. 1995.

Flynn L., Mouginis-Mark P., Gradie J. and Lucey P. Radiative temperature at Kupaianaha Lava lake, Kilauea volcano, Hawaii. Journal of Geophysical Research. Vol. 98, N°. B4, p. 6461 - 6476, April 1993.

Francis P. W. and Oppenheimer C. M. M. Remote measurement of volcanic gases at Mt. Etna In: EC RDT Programme "Environment" - Natural Hazards: European Volcano-Laboratories. Contract EV5V-CT91-0177: Etna's volatiles, Final Scientific Report (01.05.93-30.11.95). Vol. 1, pt. 2, 1996.

Francis P. W. and Oppenheimer C. Persistent magmatic activity: evidence for the cryptic growth of volcanoes. Pre-print 1993.

Francis P. W., Chaffin C. T., Maciejewski A. J. H. and Oppenheimer C. Remote determination of SiF_4 in volcanic plumes: A new tool for volcano monitoring. Geophysical Research Letters. Vol. 23, N°. 3, p. 249 - 252, 1996.

Francis P. W., Maciejewski A. J. H., Oppenheimer C. and Chaffin C. T. New methods make volcanology less hazardous. EOS Transactions. Vol. 77, N°. 41, 1996b.

Francis P. W., Maciejewski A. J. H., Oppenheimer C., Chaffin C. T. and Caltabiano T. SO_2:HCl ratios in the plumes from Mt. Etna and Vulcano determined by Fourier transform spectroscopy. Geophysical Research Letters. Vol. 22, N°. 13, p 1717 - 1721, (1995).

Frazzetta G., Gillot P. Y., La Volpe L. and Sheridan M. F. Volcanic hazards at Fossa of Vulcano: Data from the last 6000 Years. Bulletin Volcanologique. Vol. 47, N°. 1, p. 105 - 124, 1984.

Gerlach T. M and Graeber E. J. Volatile budget of Kilauea volcano. Nature. Vol. 313, p. 273 - 277, 1985.

Giggenbach W. F. Chemical compositions of volcanic gases. In: Monitoring and Mitigation of Volcanic Hazards. Springer-Verlag (pub.), Scarpa R. and Tilling R. I. (eds.), pp.221 - 256, 1996.

Gioncada A. and Sbrana A. "La Fossa caldera", Vulcano: inferences from deep drillings. Acta Vulcanologica. Vol. 1, p. 115 - 125, 1991.

Gosz J., Moore D., Dahm C. and Hofstadler S. Field testing long-path Fourier Transform Infrared (FTIR) Spectroscopy for measurements of atmospheric gas concentrations. Remote Sensing of the Environment. Vol. 32, p. 103 - 110, 1990.

Grant W. B., Kagann R. H. and McClenny W. A. Optical remote measurement of toxic gases. Journal of the Air and Waste Management Association. Vol. 42, N°. 1, p. 18 - 30, 1992.

Griffiths P. Chemical Infrared Fourier Transform Spectroscopy. In: Chemical Analysis, Vol. 43. Elving P., Winefordner J. and Kolthoff I. (eds.) Wiley Interscience (publ.). p. 340, 1975.

Guest J. E. The summit of Mount Etna prior to the 1971 eruptions. Philosophical Transactions of the Royal Society of London. Vol. 274, p. 63 -78, 1973.

GVN. Smithsonian Institution, Bulletin of the Global Volcanism Network, Vol. 22, N°. 10, October, 1997.

Hanst P. L. Analysing air from a single-beam spectrum. Spectroscopy Europe. Vol. 8, N°. 9, p. 44 - 49, 1993.

Hanst P. L. and Hanst S. T. Gas measurement in the fundamental infrared region. In: Air monitoring by Spectroscopic Techniques. Sigcrist M. W. (ed.) Wiley Interscience. Ch. 6, p. 335 - 470, 1994.

Harris A. J. L and Stevenson D. S. Thermal observations of degassing open conduits and fumaroles at Stromboli and Vulcano using remotely sensed data. Journal of Volcanology and Geothermal Research. Vol. 76, p. 175 - 198, 1997.

Harris A. J. L. Low spatial resolution thermal monitoring of volcanoes from space. Ph. D. thesis (Open University) pp. 127, 1996.

Harris A. J. L. Low spatial resolution thermal monitoring of volcanoes from space. Unpublished Ph.D. thesis, Department of Earth Sciences, The Open University, UK. 1996.

Harris A. J. L., Blake S., Rothery D. A. and Stevens N. F. A chronology of the 1991-1993 eruption at Mt. Etna using data from the Advanced Very High Resolution Radiometer. Journal of Geophysical Research. Vol. 102, p. 7985 - 8003, 1997.

Harris A. J. L., Stevens N. F., Maciejewski A. J. H. and Röllin P. J. Thermal evidence for linked vents at Stromboli. Acta Vulcanologica. Vol. 8, N°. 1, p. 57 - 61, 1996.

Haulet R., Zettwoog P. and Sabroux J. Sulphur dioxide discharge from Mount Etna. Nature. Vol. 268, p. 715 - 717, 1977.

Herget W. and Brasher J. Remote measurement of gaseous pollutant concentrations using a mobile Fourier transform interferometer system. Applied Optics. Vol. 18, N°. 20, p. 3404 - 3420, 1979.

Hirabayashi J.-I, Ohba T. and Nogami K. Discharge rate of SO_2 from Unzen volcano, Kyushu, Japan. Geophysical Research Letters. Vol. 22, N°. 13, p. 1709 - 1712, 1995.

Hollas J. M. Modern Spectroscopy. John Wiley & Sons Ltd. (publ.). p. 45, 1987.

Honda F. and Mizutani Y. Silicon content of fumarolic gases and the formation of a siliceous sublimate. Geochemical Journal of Japan. Vol. 2, p. 1 - 9, 1968.

INETER. Desplazamiento de actividades volcanicas durante el Terciaro y le relacion entre paleo-arcos volcanicos y depositos de minerales en Nicaragua. INETER report (Spanish version) June, 1983.

Italiano F. and Nuccio P. M. Gas/steam ratios and thermal energy release measured at the gaseous emissions of the Baia di Levante of Vulcano Island, Italy. Acta Vulcanologica. Vol. 5, p. 89 - 94, 1994.

Jaupart C. and Vergniolle S. The generation and collapse of a foam layer at the roof of a basaltic magma chamber. Journal of Fluid Mechanics. Vol. 203, p. 347 - 380, 1989.

Johnson M. C, Anderson A. T. Jnr. and Rutherford M. J. Pre-eruptive volatile contents of magmas. In: Volatiles in magmas. Carroll M. R. and Holloway J. R. (eds.). Reviews in Mineralogy. Vol. 30, Ch. 8, p. 281 - 330, 1994.

Kazahaya K, Shinohara H. and Saito G. Excessive degassing of Izu-Oshima volcano: magma convection in a conduit. Bulletin of Volcanology. Vol. 56, p. 207 - 216, 1994.

Kearey P. and Vine F. J. Global Tectonics. Blackwell Scientific Publications, London (pub.) pp. 302, 1990.

Krueger A. J., Walter L. S., Schneltzer C.C. and Doiron S. D. TOMS measurement of the sulfur dioxide emitted during the 1985 Nevado del Ruiz eruptions. Journal of Volcanology and Geothermal Research. Vol. 41, p. 7 - 15, 1990.

Kyle P. R., Meeker K and Finnegan D. Emission rates of sulfur dioxide, trace gases and metals from Mount Erebus, Antarctica. Geophysical Research Letters. Vol. 17, N°. 2, p. 2125 - 2128, 1990.

Le Cloarec M. F., Pennisi M. and Corazza E. Radioactive, minor and trace elements in the plume of Mount Etna. In: EC RDT Programme "Environment" - Natural Hazards: European Volcano-Laboratories.

Contract EV5V-CT91-0177: Etna's volatiles, Final Scientific Report (01.05.93-30.11.95). Vol. 1, pt. 2, 1996.

Le Cloarec M. F., Pennisi M., Ardouin B., Le Roulley J. C. and Lambert G. Relationship between gases and volcanic activity of Mount Etna in 1986. Journal of Geophysical Research. Vol. 93, N°. B3, p. 4477 - 4484, 1988.

Le Guern F. and Faivre-Pierret R. Différenciation de l'emanation magmatique: réactions H_2S+SO_2 dans les gaz volcaniques. Vulcano (Italie), 1923 - 1979. Bulletin Vulcanologique. Vol. 45, N°. 3, p. 169 - 190, 1982.

Love S. P., Counce D., Goff F., Seibe C. and Delgado H. Quantitative passive Infrared Remote-Sensing of Gaseous Emissions at Popocatepetl Volcano, Mexico. Abstracts in the Proceedings Volume of the Associated Geophysical Union (AGU) meeting in San Francisco, December 1997. Session V32E N°. 6, p. F799, 1997.

Maciejewski A. J. H., Harris A. J. L. and Francis P. W. Mt Etna's plume: The view from below. In: Etna: Fifteen years on. Gravestock P. J. & McGuire W. J. (ed.s). Proceedings of conference held at C&GCHE, Cheltenham on 12/2/96. p. 47, 1996.

Maciejewski A. J. H. and van Wyk de Vries B. Morphological Evolution of the Masaya Volcanic Complex, Nicaragua. Volcanic & Magmatic Studies Group annual meeting, poster-session. 7 - 8/1/98, University of Leicester, 1998.

Malinconico L. Jnr. On the variation of SO_2 emission from volcanoes. Journal of Volcanology and Geothermal Research. Vol. 33, p. 231 - 237, 1987.

Malinconico L. L. Jnr. Fluctuations in SO_2 emission during recent eruption of Etna. Nature. Vol. 278, p. 43 - 45, 1979.

Martini M. Variations in surface manifestations at Vulcano (Aeolian Islands, Italy) as a possible evidence of deep processes. Bulletin of Volcanology. Vol. 46, N°. 1, p. 83 - 86, 1983.

Martini M., Gianni L. and Capaccioni B. Geochemical and seismic precursors of volcanic activity. Acta Vulcanologica. Vol. 1, p. 7 - 11, 1991.

Martini M., Gianni L. and Capaccioni B. The influence of water on chemical changes of fumarolic gases: Different characters and their implications in forecasting volcanic activity. Acta Vulcanologica. Vol. 1, p. 13 - 16, 1991b.

Martini M., Piccardi G. and Cellini Legittimo P. The effect of variations in rainfall on the chemical composition of Vulcano fumaroles (Italy). Bulletin of Volcanology. Vol. 44, N°. 1, p. 109 - 113, 1981.

Mason B. H. and Moore C. B. Principles of Geochemistry, 2nd edition. John Wiley and Sons (publ.). pp. 345, 1982.

McBirney A. R. The Nicaraguan volcano Masaya and its caldera. EOS, Transactions of the American Geophysical Union. Vol. 37, N°. 1, p. 83 - 96, 1956.

McGuire W. J. Dome collapse and explosive eruption at Soufrière Hills volcano, Montserrat, September 17 - 18 1996: An overview and chronology of events. Conference abstracts from: The Soufrière Hills Eruption, Montserrat. The Geological Society, Burlington House, London, 27 November 1996. Wadge G. (ed.). 1996.

McGuire W. J., Moss J. L., Saunders S. J. and Stewart I. S. Dyke induced rifting and edifice instability at Mount Etna. In: Etna: fifteen years on. Gravestock P. J. & McGuire W. J. (ed.s). Proceedings of conference held at C&GCHE, Cheltenham on 12/2/96. p. 20 - 24, 1996.

Metaxian J.-P. Etude seismologique et gravimetrique d'un volcan actif: Dynamisme intense et structure de la Caldeira Masaya, Nicaragua. Unpublished Ph. D. thesis, Laboratoire D'Instrumentation Geophysique, Universite de Savoie, 1994.

Metrich N. Chlorine and fluorine in tholeiitic and alkaline lavas of Etna (Sicily). Journal of Volcanology and Geothermal research. Vol. 40, p. 133 - 148, 1990.

Metrich N., Clocchiatti R., Mosbah M. and Chaussidon M. The 1989 - 1990 activity of Etna magma mingling and ascent of H_2O-Cl-S-rich basaltic magma. Evidence from melt inclusions. Journal of Volcanology and Geothermal research. Vol. 59, p. 131 - 144, 1993.

Millán M. M. & Hoff R. M. Remote sensing of air pollutants by Correlation Spectroscopy - instrumental response characteristics. Atmospheric Environment. Vol. 12, p. 853 - 864, 1978.

Millán M. M. & Hoff R. M. Technical Note: How to minimalise the baseline drift in a COSPEC remote sensor. Atmospheric Environment. Vol. 11, p. 857 - 860, 1977.

Millán M. M. Remote sensing of air pollutants: A study of some atmospheric scattering effects. Atmospheric Environment. Vol. 14, p. 1241 - 1253, 1980.

Millán M. M., Gallant A. J., Chung Y-S. and Fanaki F. COSPEC observation of Mt. St. Helens volcanic SO_2 eruption cloud of 18 may 1980 over southern Ontario. Atmospheric Environment. Vol. 19, p. 255 - 263, 1985.

Miller A. D. and MVO "Team Seismic". MVO seismic terminology and a summary of dome-related seismicity: August 1997. MVO meeting at BGS Keyworth, May 1997.

Minakami T. Seismology of volcanoes in Japan. The Earthquake Research Institute, Japan (pub.), 1960.

Möller D. Kinetic model of atmospheric SO_2 oxidation based on published data. Atmospheric Environment. Vol. 14, p. 1067 - 1076, 1980.

Montalto A. Seismic events at Vulcano (Italy) during 1988 - 1992. Journal of Volcanology and Geothermal Research. Vol. 60, p. 193 - 206, 1994.

Mori T. and Notsu K. Remote CO, COS, CO_2, SO_2, HCl detection and temperature estimation of volcanic gas. Geophysical Research Letters. Vol. 24, p. 2047 - 2050, 1997.

Mori T. and Notsu K. Remote detection of CO, COS, CO_2, SO_2 and HCl in volcanic gas: Application for remote temperature estimation of volcanic gas. Preprint 1997.

Mori T., Notsu K., Tohjima Y. and Wakita H. Remote detection of HCl and SO_2 in volcanic gas from Unzen volcano, Japan. Geophysical Research Letters. Vol. 20, N°. 13, p. 1355 - 1358, 1993.

Mori T., Notsu K., Tohjima Y., Wakita H. Nuccio P. M. and Italiano F. Remote detection of fumarolic gas chemistry at Vulcano, Italy, using a FTIR spectral radiometer. Earth and Planetary Science Letters. Nos. 1-2, p. 219 - 225, 1995.

Mueller R. F. Energetics of HCl and HF in volcanic emanations. Geochimica et Cosmochimica Acta. Vol. 34, p. 737 - 744, 1970.

Murphy M. D., Barclay J., MacDonald R., Sparks R. S. J. and Carroll M. R. Petrology and geochemistry of the Soufrière Hills volcano, Montserrat. Conference abstracts from: The Soufrière Hills Eruption, Montserrat. The Geological Society, Burlington House, London, 27 November 1996. Wadge G. (ed.). 1996.

Murray J. B. Elastic Model of the actively intruded dyke feeding the 1991 - 1993 eruption of Mt. Etna, derived from ground deformation measurements. Acta Vulcanologica. Vol. 4, p 97 - 100, 1994.

MVO Team Deform: Jackson P., Shepherd J. B., Robertson R., Skerrit G., Sol S., Herd R., Norton . E., Cole P. D., Devine J., Silcott D. and Young S. R. Twelve months of ground deformation surveys using the Electronic Distance Measurement technique at Soufrière Hills volcano, Montserrat. Conference abstracts from: The Soufrière Hills Eruption, Montserrat. The Geological Society, Burlington House, London, 27 November 1996. Wadge G. (ed.). 1996.

Nakada S. and Fujii T. Preliminary report on the activity at Unzen volcano (Japan), November 1990 - November 1991 - dacite lava flows and pyroclastic flows. Journal of Volcanology and Geothermal Research. Vol. 54, N°. 3 - 4, p. 319 - 333, 1993.

Neuville D. R., Le Jeune A.-M., Linard Y. and Sparks R. S. J. Viscosity of Montserrat lavas. Conference abstracts from: The Soufrière Hills Eruption, Montserrat. The Geological Society, Burlington House, London, 27 November 1996. Wadge G. (ed.). 1996.

Notsu K., Mori T., Igarashi G., Tohjima Y., Tohjima Y. and Wakita. Infrared spectral radiometer: A new tool for remote measurement of SO_2 of volcanic gas. Geochemical Journal. Vol. 27, p. 361 - 366, 1993.

Oppenheimer C. and Francis P. W. Rapid depletion of SO_2 in tropospheric plume of Soufrière Hills volcano, Montserrat and its implications. 1998, in prep.

Oppenheimer C., Francis P. and Maciejewski A. Volcanic gas measurements by helicopter-borne Fourier transform spectroscopy. International Journal of Remote Sensing. Vol. 19, N°. 2, p. 373 - 379, 1998.

Oppenheimer C. Volcanology from space: Applications of infrared remote sensing. Unpublished Ph.D. thesis. Department of Earth Sciences, The Open University, UK, 1991.

Pennisi M. and Le Cloarec M. F. Time-series variations of Cl, F and S in Mt. Etna's plume (Italy) between 1992 and 1995. Journal of Geophysical Research. Vol. 103, N°. B3, p. 5061 - 5066, 1998.

Rea W. J. The volcanic geology and petrology of Montserrat, West Indies. Journal of the Geological Society of London. Vol. 130, p. 341 - 366, 1974.

Realmuto V. J., Abrams M. J., Buongiorno M. F. and Pieri D. C. The use of multispectral thermal infrared image data to estimate the sulfur dioxide flux from volcanoes: A case study from Mount Etna, Sicily, July 29, 1986. Journal of Geophysical Research. Vol. 99, N°. B1, p. 481 - 488, 1994.

Realmuto V. J., Sutton A. J. and Elias T. Multispectral thermal infrared mapping of sulfur dioxide plumes: A case study from the East Rift Zone of Kilauea volcano, Hawaii. Journal of Geophysical Research. Vol. 102, N°. B7, p. 15,057 - 15,072, 1997.

Röllin P. J. Geophysical models of Mount Etna, Sicily: its structural evolution and implications for slope stability. Unpublished Ph.D. thesis, Department of Earth Sciences, The Open University, Milton Keynes, 1996.

Romano R. and Struriale G. The historical eruptions of Mt. Etna (Volcanological data). Mem. Soc. Geol. It. Vol. 23, p. 75 - 97, 1982.

Rosenberg P. E. HF/SiF_4 ratios in volcanic and magmatic gases. Geochimica et Cosmochimica Acta. Vol. 37, p. 109 - 112, 1973.

Rothman L. S., Gamache R. R., Tipping R. H., Rinsland C. P., Smith M. A. H, Benner D. C., Malathy Devi V., Flaud J.-M., Camy-Peyret C., Perrin A., Goldman A., Massie S. T., Brown L. R. and Toth R. A. The HITRAN molecular database: Editions of 1991 and 1992. Journal of Quantitative Spectroscopy and Radiative Transfer. Vol. 48, N°. 5/6, p. 469 - 507, 1992.

Rymer H., Brown G. C., Ferrucci F. and Murray J. B. Dyke intrusion mechanisms on Etna 1989 - 1993 and microgravity precursors to eruption. Acta Vulcanologica. Vol. 4, p. 109 - 114, 1994.

Rymer H., Cassidy J., Locke C. A. and Murray J. B. Magma movements in Etna volcano associated with the major 1991 - 1993 lava eruption: Evidence from gravity and deformation. Bulletin of Volcanology. Vol. 57, p. 451 - 461, 1995.

Rymer H., Murray J. B., Brown G. C., Ferrucci F. and. McGuire W. J. Mechanisms of magma eruption and emplacement at Mt. Etna between 1989 and 1992. Nature. Vol. 361, p. 439 - 441, 1993.

Rymer H.. van Wyk de Vries B., Stix J. and Williams-Jones G. Pit-crater structure and processes governing persistent activity at Masaya Volcano, Nicaragua. Bulletin of Volcanology. Vol. 59, p. 345 - 355, 1998.

Sabroux J. C. Measurements of the gas discharge at Vulcano (Italy). Bulletin of Volcanology. Vol. 3, N°. 3, p. 277 - 278, 1982.

Sato H., Fujii T. and Nakada S. Crumbling of dacite dome lava and generation of pyroclastic flows at Unzen volcano. Nature. Vol. 360, N°. 6405, p. 664 - 666, 1992.

Schiff H. I. Ground based measurements of atmospheric gases by spectroscopic methods. Ber. Bunsenges Phys. Chem. Vol. 96, N°. 3, p. 296 - 306, 1992.

Schneltzer C. C., Doiron S. D., Walter L. S. and Krueger A. J. Satellite measurement of sulfur dioxide from the Redoubt eruptions of 1989 - 1990. Journal of Volcanology and Geothermal Research. Vol. 62, p. 353 - 357, 1994.

Sharp A. G. Inorganic Chemistry, 2nd edition. Longman Scientific & Technical (publ.). pp. 696, 1986.

Shepherd J. B. GPS measurements at the Soufrière Hills volcano, Montserrat, April - November 1996. Conference abstracts from: The Soufrière Hills Eruption, Montserrat. The Geological Society, Burlington House, London, 27 November 1996. Wadge G. (ed.). 1996.

Shepherd J. B., Tomblin J. F. and Wood D. F. Volcanoseismic crisis in Montserrat, West Indies. Bulletin Volcanologique. Vol. 35, p. 143 - 163, 1971.

Smithsonian Institute. Global Volcanism Network. Bulletins from 1991 - 1997.

Solomons T. W. G. Organic Chemistry. 4th Edition. J. Wiley & Sons, Inc (publ.) pp. 568, 1976.

Sparks R. S. J. The dynamics of bubble formation and growth in magmas: A review and analysis. Journal of Volcanology and Geothermal Research. Vol 3, p. 1 - 37, 1978.

Sparks R. S. J. Structural Control on the Soufrière Hills Volcano. MVO report. 1996.

Stevens N. F., Murray J. B. and Wadge G. The volume and shape of the 1991-1993 lava flow field at Mount Etna, Sicily. Bulletin of Volcanology. Vol. 58, p. 449 - 454, 1997.

Stevenson D. S. Physical models of fumarolic flow. Journal of Volcanology and Geothermal Research. Vol. 57, p. 139 - 156, 1993.

Stoiber R. E. and Jepsen A. Sulfur Dioxide contributions to the Atmosphere by Volcanoes. Science. Vol. 182, p. 577 - 578, 1973.

Stoiber R. E. and Williams S. N. Sulphur and halogen at Masaya Caldera Complex, Nicaragua: Total flux and variation with time. Journal of Geophysical Research. Vol. 91, N°. B12, p. 12215 - 12231, 1986.

Stoiber R. E., Malinconico L. L. Jnr. and Williams S. N. Use of Correlation Spectrometer at volcanoes. In Developments in Volcanology 1: Forecasting Volcanic Events. Tazieff H. and Sabroux J.-C. (eds.). Elsevier Press. Ch. 29, p.425 - 444, 1983.

Symonds R. B. & Reed M. H. Calculation of multi-component chemical equilibria in gas-solid-liquid systems: calculation methods, thermochemical data and applications to studies of high temperature volcanic gases with examples from Mount St. Helens. American Journal of Science. Vol. 293, p. 758 - 864, 1993.

Symonds R. B., Reed M. H. and Rose W. I. Origin, speciation, and fluxes of trace-element gases at Augustine volcano, Alaska: Insights into magma degassing and fumarolic processes. Geochimica et Cosmochimica Acta. Vol. 56, p. 633 - 657, 1992.

Symonds R. B., Rose W. I. and Reed M. H. Contribution of Cl- and F-bearing gases to the atmosphere by volcanoes. Nature. Vol. 334, N°. 4, p. 415 - 418, 1988.

Symonds R. B., Rose W. I., Bluth G. J. S. and Gerlach T. M. Volcanic gas studies: methods, results and applications. In: Volatiles in Magmas. Carroll M. R. and Holloway J. R. (eds.). Reviews in Mineralogy. Vol. 30, Ch. 1, p. 1 - 66, 1994.

Symonds R., Reed M. and Rose W. Origin, speciation and fluxes of trace-element gases at Augustine volcano, Alaska: Insights into magma degassing and fumarolic processes. Geochimica et Cosmochimica Acta. Vol. 56, p. 633 - 657, 1992.

Talena H., Lugo C., Buitrago N. and Membreño O. Muestreo Quimico de gases temperaturas y acidez en Cratère Santiago. INETER report (unpubl.), 1994.

Tedesco D. Fluid geochemistry at Vulcano Island: a change in the volcanic regime or continuous fluctuations in mixing of different systems? Journal of Geophysical Research. Vol. 100, N°. B3, p. 4157 - 4167, 1995.

Tedesco D., Miele G., Sano Y. and Toutain J. P. Helium isotopic ratio in Vulcano island fumaroles: temporal variations in shallow level mixing and deep magmatic supply. Journal of Volcanology and Geothermal Research. Vol. 64, p. 117 - 128, 1995.

Tedesco D., Toutain J. P., Allard P. and Losno R. Chemical variations in fumarolic gases at Vulcano Island (Southern Italy): seasonal and volcanic effects. Journal of Volcanology and Geothermal Research. Vol. 45, p. 325 - 334, 1991.

Tilling R. I and Dvorak J. J. Anatomy of a basaltic volcano. Nature. Vol. 363, p. 125 - 133, 1993.

Tratt D. M. and Menzies R. T. Evolution of the Pinotubo volcanic aerosol column above Pasadena, California observed with a mid-infrared backscatter lidar. Geophysical Research Letters. Vol. 22, N°. 7, p. 807 - 810, 1995.

Vagelli G., Giacobbe A. De Vivo B. Silicate melt inclusions in clinopyroxenes from "prehistoric" transitional to alkaline Etnean lavas: inferences on magma evolution processes. Acta Vulcanologica. Vol. 8, N°. 1, p. 99 - 106, 1996.

van Wyk de Vries B. Tectonics and magma evolution of Nicaraguan volcanic systems. Unpublished Ph. D. thesis, The Open University, Milton Keynes, UK. 1993

Ventura G. Tectonics, structural evolution and caldera formation on Vulcano Island (Aeolian Archipelago, southern Tyrrhenian Sea). Journal of Volcanology and Geothermal Research. Vol. 60, p. 207 - 224, 1994.

Villasenor A., Benz H. M. and Power J. A. Three dimensional P-wave velocity model for Soufrière Hills volcano, Montserrat, W.I. Conference abstracts from: The Soufrière Hills Eruption, Montserrat. The Geological Society, Burlington House, London, 27 November 1996. Wadge G. (ed.). 1996.

Voltaggio M., Barbieri M., Branca M., Castorina F., Taddeucci A., Tecce F., Tuccimei P., Turi B. and Vesica P. Calcite in fractures in a volcanic environment (Vulcano Island, Italy): contribution of geochronological and isotopic studies to volcanotectonics. Journal of Volcanological and Geothermal Research. Vol. 75, p. 271 - 282, 1997.

Wadge G. and Isaacs M. C. Mapping of the volcanic hazards from Soufrière Hills volcano, Montserrat, West Indies using an image processor. Journal of the Geological Society. Vol. 145, p. 541 - 551, 1988.

Wadge G. and Woods A. W. Volcano model for subsurface activity at Soufrière Hills, Montserrat. MVO report. May 1996.

Walker G. P. L. Basaltic volcano systems. From H. M. Prichard et al. (eds.) Magmatic Processes and plate tectonics. Geological Society Special Publications. N°. 76, p. 3 - 38, 1993.

Walker G. P. L. Coherent intrusion complexes in large basaltic volcanoes- a new structural model. Journal of Volcanology and Geothermal Research. Vol. 50, p. 41 - 54, 1992.

Walker G. P. L. Gravitational (density) controls on volcanism, magma chambers and intrusions. Australian Journal of Earth Sciences. Vol. 36, p. 149 - 165, 1989.

Walker G. P. L. Re-evaluation of inclined intrusive sheets and dykes in the Cuillins volcano, Isle of Skye. Geological Society of London. 1993b.

Walker J. A. Williams S. N., Kalamarides R. I. and Feigenson M. D. Shallow open-system evolution of basaltic magma beneath a subduction zone volcano: the Masaya Caldera Complex, Nicaragua. Journal of Volcanology and Geothermal Research. Vol. 56, p. 379 - 400, 1993

Wallace P. J. and Gerlach T. M. Magmatic vapour source for sulfur dioxide released during volcanic eruptions: Evidence from Mount Pinatubo. Science. Vol. 265, p. 497 - 499, 22 July 1994.

White A. F and Hochella M. F. Surface chemistry associated with the cooling and subaerial weathering of recent basalt flows. Geochimica et Cosmochimica Acta. Vol. 65, p. 3711 - 3721, 1992.

Williams S. N. Geology and eruptive mechanisms of Masaya Caldera Complex, Nicaragua. Unpublished Ph. D. thesis, Dartmouth College, Hanover, NH. 169 pp, 1983.

Williams S. N. Plinian airfall deposits of basaltic composition. Geology. Vol. 11, p. 211 - 214, April, 1983.

Williams-Jones G., Stix J. and Hickson C. Provisional manuscript of: "The COSPEC Cookbook: Using the COSPEC in the field". To be submitted for publication in 1998.

Wooster M. J. and Rothery D. A. Thermal monitoring of Lascar Volcano, Chile, using infrared data from the along-track scanning radiometer: a 1992-1995 time series. Bulletin of Volcanology. Vol. 58, p. 566 - 579, 1997.

Young S. R., Ambeh W. B., Miller A. D., Lynch L., Robertson R., Jackson P., Mattioli G., Smith A., Devine J., Shepherd J. B. and Aspinall W. Eruptive activity at Soufrière Hills volcano, Montserrat July 1995 to June 1996. 1998 (1998 - in prep)

Young S. R., Francis P. W., Barclay J., Casadevall T. J., Gardner C. A., Daroux B., Davies M. A., Dellmelle P., Norton G. E., Maciejewski A. J. H., Oppenheimer C. M. M., Stix J. and Watson I. M. Monitoring SO_2 emissions at the Soufrière Hills volcano: Implications for changes in eruptive conditions. Accepted for publication in Geophysical Research Letters, summer 1998

Appendix

Glossary of acronyms and units

Acronyms

AMS	Midac™ Air Monitoring System.
COSPEC	Correlation spectroscopy.
DGTS	Deuterated triglycerine sulphate used in making a photosensitive cell for detecting IR radiation.
DIAL	Differential absorption LIDAR.
DOAS	Differential absorption spectroscopy.
EDM	Electronic distance measurement using a laser and reflector.
FOV	Field of view.
GPS	Global positioning satellite system for accurately determining a point on the earth's surface.
HITRAN	HIgh TRANsmittence high resolution spectral database covering UV and IR parts of the spectrum.
INAA	Instrumental neutron activation analysis.
InSb	Indium Antimonide photosensitive cell used to detect IR radiation.
IR	Infra-red radiation
LIDAR	Light detection and ranging.
MCT	Mercury cadmium telluride photosensitive cell used to detect IR radiation.
MVC	Masaya Volcanic Complex.
MVO	Montserrat Volcano Observatory.
ODA	Overseas Development Administration (UK government).
OP-FTIR	Open-path Fourier transform infra-red spectroscopy.
SNR	Signal-to-noise ratio.
USGS	United States Geological Survey.
UV	Ultra-violet radiation.
YAG	Yttrium-aluminium-garnet laser.

Units

Bar	1×10^5 Pa, or ~1 atm.
Dry gas	Mass or weight % of gases derived assuming H_2O is absent.
Exsolved ppm	The amount (by mass) of a gas exsolved from a unit mass of magma. Defined as the difference in the volatile concentration of an undegassed and fully degassed sample of lava.
mg/kg.bar	The solubility (by mass) of a volatile in relation to the confining pressure.
mol%	Percentage of total number of atoms/molecules of a gas in a fixed volume - synonymous to vol% assuming an ideal gas.
ppmm	Concentration recorded as parts per million by mass.
ppmm.m	Concentration measured as parts per million (by mass) per metre of optical path length.
ppmv	Concentration recorded as parts per million by volume
ppmv.m	Concentration measured as parts per million (by volume) per metre of optical path length.
SO_2 t/d	Flux of SO_2 gas estimated using the COSPEC technique as the average amount of gas detected in a vertical column of air which transects the gas plume at perpendicular to the wind direction. This is then multiplied by the estimated wind speed to give the final value. Other gas fluxes are derived by combining the SO_2:other gas mass ratio and the SO_2 flux.
vol%	Percentage of atoms/molecules of a gas in a fixed volume.
Wet gas	Mass or weight % of gases derived assuming H_2O is present.
Wt%	Percentage of gases as defined by mass of sample gas/total mass of all gases.
$\mu g/m^3$	Mass of gas per unit volume.